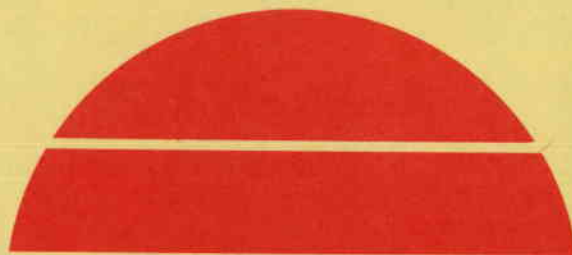CONCEPTUAL DESIGN OF ADVANCED CENTRAL RECEIVER POWER
SYSTEMS SODIUM-COOLED RECEIVER CONCEPT

Final Report. Volume 2, Book 1. Commercial Plant Conceptual Design

March 1979

Rockwell International
Energy Systems Group
Canoga Park, California

U.S. Department of Energy

Solar Energy

CONCEPTUAL DESIGN
OF
ADVANCED CENTRAL RECEIVER POWER SYSTEMS
SODIUM-COOLED RECEIVER CONCEPT
FINAL REPORT

VOLUME II
BOOK 1
COMMERCIAL PLANT CONCEPTUAL DESIGN

MARCH 1979

PREPARED FOR THE
U.S. DEPARTMENT OF ENERGY
AS PART OF
CONTRACT NO. EG-77-C-03-1483

Rockwell International
Energy Systems Group

UNIVERSITY OF HOUSTON Founded 1927

MCDONNELL DOUGLAS CORPORATION

Salt River Project
WATER ◆ POWER

Stearns-Roger

CONTENTS

CONTENTS

CONTENTS

CONTENTS

CONTENTS

TABLES

TABLES

TABLES

TABLES

FIGURES

FIGURES

FIGURES

FIGURES

FIGURES

FIGURES

PREFACE

This report is submitted by the Energy Systems Group to the Department of Energy under Contract EG-77-03-1483 as final documentation. This Conceptual Design Report summarizes the analyses, design, planning, and cost efforts performed between October 1, 1977, and September 1, 1978. The report is submitted in four volumes, as follows:

Volume I   Executive Summary

Volume II   Book 1, Commercial Plant Conceptual Design

                   Book 2, Appendices

Volume III   Development Plan and Pilot Plant Description

Volume IV   Commercial and Pilot Plant Cost Data

The principal contractors supporting the Rockwell International Energy Systems Group, in this conceptual design effort, together with the main areas of responsibility, included McDonnell Douglas Aircraft Corporation as responsible for the Collector and Master Control Subsystem; Stearns-Roger Services, Inc. as responsible for Electric Power Generating Subsystem, Tower Design and Civil Engineering; and Salt River Project as the Utility Consultant. The University of Houston supported McDonnell Douglas in the Collector Field Studies. Personnel contributing to this design program and to the final report included:

Rockwell International, Energy Systems Group

T. H. Springer, Project Manager

T. L. Johnson, Project Engineer

W. B. Thomson, Lead Engineer, Receiver

L. E. Glasgow, Lead Engineer, Receiver Subsystem

A. Z. Frangos, Lead Engineer, Thermal Storage

McDonnell Douglas Aircraft Corporation

G. C. Coleman, Project Manager

J. E. Raetz, Lead Engineer, Collector Subsystem

D. W. Pearson, Lead Engineer, Master Control Subsystem

J. H. Nourse, Lead Engineer, Cost Analysis

University of Houston

L. L. Vant-Hull, Associate Director, Solar Energy Laboratory

Stearns-Roger Services, Inc.

W. R. Lang, Project Manager

A. W. McKenzie, Principal Author

Salt River Project

S. M. Chalmers, Director, Engineering Services

R. F. Durning, Staff Consultant, Engineering Services

D. R. Squire, Supervisor, Power Plant Engineering

R. M. Hayslip, Manager, Corporate Planning

1.0 INTRODUCTION

The conceptual design of an Advanced Central Receiver Power System using liquid sodium as a heat transport medium has been completed by a team consisting of the Rockwell International Energy Systems Group (prime contractor), McDonnell Douglas, Stearns-Roger, The University of Houston, and Salt River Project. The purpose of this study was to determine the technical and economic advantages of this concept for commercial-scale power plants. The concept is similar to that being studied on the water-steam programs, except that liquid sodium cools the receiver instead of water.

The Advanced Central Receiver System is composed of subsystems as pictorially shown in Figure 1-1. The basic area of responsibility of the team members is:

ESG	-	Overall System
	-	Receiver Subsystem
	-	Thermal Storage Subsystem
MDAC		Collector Subsystem with U of H as a Subcontractor
	-	Master Control Subsystem
Stearns-Roger		Electric Power Generating Subsystem Receiver Tower
Salt River	-	Project Utility Consultants for Operations, Design, and Cost

This final report covers all tasks of Contract EG-77-C-03-1483. These tasks were as follows:

Task 1 - Review and Analysis of Preliminary Specification
Task 2 - Parametric Analysis
Task 3 - Select Commercial Configuration
Task 4 - Commercial Plant Conceptual Design
Task 5 - Assessment of Commercial Plant
Task 6 - Advanced Central Power System Development Plan
Task 7 - Program Plan
Task 8 - Reports and Data
Task 9 - Program Management
Task 10 - Safety Analysis
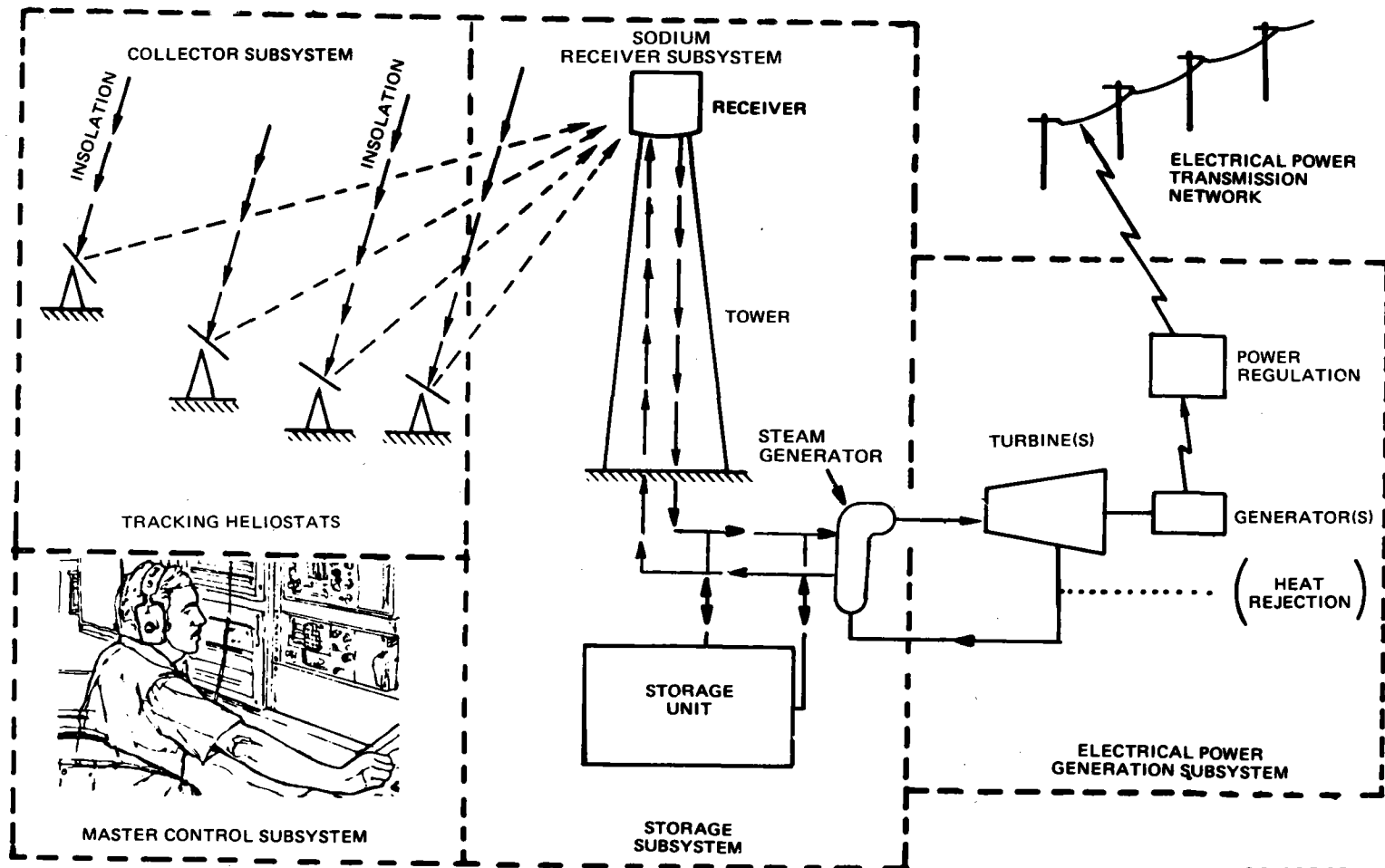
00-103431B

Figure 1-1. Advanced Central Receiver Subsystems

1.1 BASELINE CONFIGURATION

The baseline configuration is depicted in Figure 1-2. In this particular arrangement, sodium is pumped up to the top of a tall tower where the receiver is located. The sodium is heated in the receiver and then flows down the tower, through a pressure reducing device, and thence into a large, hot storage tank which is located at ground level and whose size is made to meet a specific thermal energy storage capacity requirement. From this tank, the sodium is pumped by a separate pump, through a system of sodium-to-water steam generators. The steam generator system consists of a separate superheater and reheater operating in parallel and an evaporator unit operating in series with the other two units. The sodium flowing from the evaporator unit is piped to a cold storage tank. From the cold storage tank, sodium is then pumped up to the tip of the tower to complete the cycle. The steam generated in the steam generators is fed to a conventional "off-the-shelf," high-efficiency turbine. The steam loop operates in a conventional rankine cycle with the steam generators serving the same purpose as a conventional boiler and water being fed to the evaporator with conventional feedwater pumps. The pressure reducing device (a standard drag valve, for example) serves to mitigate the pressure caused by the static head of sodium and thus allows the large tanks to operate at ambient pressure conditions.

There are several advantages to the sodium-cooled system. One of these is that the heat transport fluid remains in the liquid state at all times; therefore, the control of the system is simpler, and there is not a large density change between inlet and outlet. A second advantage is that liquid sodium is a very good heat transfer material; consequently, the receiver can be made smaller and the heat flux can be substantially higher. A third advantage is that the heat transport fluid can also serve as the heat storage material in some considerations, and operation from storage can be accomplished under the same thermodynamic conditions as would exist when operating directly from the receiver. In addition, the receiver, which is subject to varying heat input, can be totally decoupled from the power cycle. Finally, the sodium system is capable of providing steam to a turbine at temperatures and pressures commensurate with or exceeding modern steam plant requirements and can conventiently incorporate a reheat cycle. These advantages are offset, to some extent, by the need for some additional pieces of

RECEIVER

24 PANELS

PRESSURE REDUCING STATION

HOT STORAGE

PUMP

COLD STORAGE

PUMP

PURIFICATION SYSTEM

REACTION PRODUCTS TANK

EVAPORATOR

SODIUM SYSTEM

STEAM SYSTEM

HIGH-PRESSURE TURBINE

INTERMEDIATE-PRESSURE TURBINE

LOW-PRESSURE TURBINE

GENER-ATOR

REHEAT

SUPERHEAT

DEAERATOR

CON-DENSER

COOLING TOWER

AIR

WET COOLING SYSTEM

CONDENSATE PUMP

FEEDWATER HEATERS

42400-1096C

Figure 1-2. Sodium Cooled Advanced Central Receiver System

equipment not necessarily required by a water-steam system. However, the cost of these additional items is more th~n compensated by the substantial increase in system efficiency.

The technical approach that was adopted on this program was to establish a reference baseline configuration and then to perform various subsystem and system-level trade studies and parametric analysis in order to evaluate various potential improvements. As superior subsystems are identified on the basis of cost, performance, and operating characteristics, the reference baseline configuration is updated. In this way, a preferred commercial system configuration can be developed, designed, and evaluated on the basis of economic merit.

Some of the performance data for the reference baseline configuration that was used to initiate this program are delineated in the column labeled "baseline configuration - 6 hours" in Table 1-1. This reference baseline was adopted on the basis of a study conducted by The University of Houston, McDonnell Douglas, and Atomics International under a grant made in 1976 to The University of Houston (see Semiannual Review Reports SAND 77-8011 and SAND 77-8513).

Two major changes in this reference configuration were required in the light of the specifications provided by DOE and were made during the first few weeks of the program. The changes consisted of a reduction of the solar multiple from 1.66 to 1.5 and a storage time of only 3 h instead of 6. The new conditions are delineated in the column in Table 1-1 labeled "advanced baseline." This is the reference configuration against which parametric analyses were initially compared on the program.

After the Task 2 parametric studies, and the Task 3 effort to select the commercial configuration, the baseline commercial configuration was established as summarized in the column on the far right of Table 1-1.

1.2 POTENTIAL IMPROVEMENTS

Potential improvements are identified as an increase in plant size to 281 MWe which reduces Nth plant capital costs to $1,089/kWe as compared to $1,240/kWe for

TABLE 1-1
ADVANCED CENTRAL RECEIVER BASELINE DATA SUMMARY

System	Parameter	Units	Configuration		
			U of H	Initial Advanced Baseline	Revised Advanced Baseline
Electric	Net Power	MWe	100	100	100
	Gross Power	MWe	113	113	112
	Cycle Efficiency	%	39.5	39.5	43.1
Receiver	Solar Multiplier		1.66	1.50	1.50
	Nominal Thermal Power	MWt	286	286	260
	Maximum Thermal Power	MWt	474.9	429	390
	Receiver Temperature - In	°C (°F)	288 (550)	288 (550)	288 (550)
	Receiver Temperature - Out	°C (°F)	593 (1,100)	593 (1,100)	593 (1,100)
	Flow	10^6 kg/h (10^6 lb/h)	4.47 (9.83)	4.03 (8.88)	3.66 (8.07)
	Receiver Midpoint EL in (ft)		258 (846)	258 (846)	174 (571)
Storage (100% Power)	Operating Time	h	6	3	3
	Energy	MWt-h	1,610*	805*	812.5
	Quantity	10^5 kg (10^6 lb)	15.3 (33.6)	7.6 (16.8)	7.6 (16.8)
	Volume	10^3 m^3 (10^3 ft^3)	19 (68)	9.6 (340)	9.5 (340)
EPG	Turbine in Pressure	MN/m^2 (psig)	13.8 (2,000)	13.8 (2,000)	12.4 (1,800)
	Superheater Temperature	°C (°F)	538 (1,000)	538 (1,000)	538 (1,000)
	Reheater Temperature	°C (°F)	538 (1,000)	538 (1,000)	538 (1,100)
Collector	Mirror Area	km^2 (ft^2)	0.781 (8.40 x 10^6)	0.705 (7.59 x 10^6)	0.692 (7.44 x 10^6)
	Number of Heliostats		20,580	18,596	14,100

*Includes reduction in night parasitic power of 6 MWe, plus 62.5 MWt for startup and shutdown.

the 100-MWe baseline size. At the same storage capacity, bus bar energy costs (BBEC) are reduced by 15% with the large 281-MWe facility. The capital cost improvement is due effects of scale on component cost and the collector field optimization at about 1100 MWt. BBEC is improved for the larger plant by the reduced operating expenses (on a per kilowatt basis). The larger plant configuration is identical to that of the baseline plant with the exception that two evaporator units are operated in parallel and steam conditions are 2400 psig rather than 1800 psig. An additional low pressure feedwater heater is used to increase the total number of heater units from six to seven.

A longer-than-3-h storage capacity is a potential improvement that can lower bus bar energy costs for a given plant electrical output. The storage capacity study showed a reduction in BBEC of 17% by increasing storage capacity from 3 h to 13.4 h due to the increase in yearly operating hours. Solar multiple (thermal power) required increases in order to supply the thermal energy to the storage system. At about 13.4 h of storage capacity, 24-h-a-day operation is reached in the summer months, and plant yearly operating hours accumulate less rapidly than plant capital cost, giving increasing BBEC. The minimum BBEC is at 13.4 h of storage capacity. (Refer to Figure 9-8 together with Figure 9-6 which shows the relationship between solar multiple and average storage capacity.) The usefulness of this added capacity to a utility, both with regard to plant size and storage capacity, was not evaluated. Plant integration studies into a utility network was beyond the scope of this study.

The air-rock storage concept is a potential improvement in that lower-cost storage could be provided for storage durations greater than about 6-h capacity. A plant configuration, presented in Section 9, would include about one-half hour of all sodium storage in order to obtain 100% buffering between the receiver and steam generators. At a 13.4-h storage capacity, the cost of the storage and storage-related equipment is reduced from $37.46/kW-h for all sodium storage to $21.4/kW-h for the air-rocks concept.

Added storage capacity was examined from the viewpoint of operating all night at reduced power level of 20% in order to avoid daily starts and stops of the steam turbine and, hence, improve turbine life and reliability. The minimum

storage capacity to accomplish this operation is 4.4 h with an increase in solar multiplier to 2.05. BBEC increases about 4% with this configuration. This solar multiplier can support a storage capacity of 7.2 h to give a more effective configuration that reduces BBEC by 5.6%. The baseline configuration retains the daily start and stop cycle on the basis that the effect on turbine life is uncertain since predicted cooldown is less than the maximum allowed for hot start. With these conditions, the manufacturer's predicted turbine life meets the design goal. However, if a utility establishes a need for added energy, the added storage capacity is cost effective in terms of lower BBEC.

1.3 SUMMARY AND RECOMMENDATION

The subject study shows that on the conceptual level, plants with power levels greater than 100 MWe and storage durations greater than 3 hours can yield significant reductions in BBEC. However, the incremental development of plant size has proven effective in the past for new technologies, and the 100-MWe plant size is considered to be appropriate for a first commercial demonstration plant. A plant of this size is a significant power level for many utilities and yet small enough to be integrated into a utility network with a minimum of disturbance due to plant operating uncertainties. The 100-MWe plant capital costs are well within magnitude of capital expenditures typically experienced by utilities for new plant additions (though the cost per kilowatt is higher). The actual commercial plant characteristics will depend on site specific considerations and new work integration studies.

2.0 SYSTEM DESCRIPTION AND ANALYSIS

2.1 REQUIREMENTS

The general system requirement for the Advanced Central Receivers are located in Table 2-1. These requirements are derived from the preliminary specification, Reference 1. The preliminary specification was supplied as part of the Request for Proposal. Task 1 of the subject study was to review and comment on the preliminary specification. This task was accomplished within the first 3 weeks of the program. A revised specification was received and comments on this revision were also submitted. The current revision of the preliminary specification, Reference 1, was subsequently received. The requirements of this specification identify nominal values for the power level, solar multiplier, and storage duration at 100% power as shown in Table 2-1. A plant configuration meeting these requirements is to be established and costs developed. However, the specification does permit variations in the above parameters in order to provide a more cost-effective alternative plant configuration.

The reference site is established as Barstow, California, with a design life of 30 years. Wet cooling is specified. The seismic environment is given as Zone 3 with a survival ground acceleration of 0.25 g in both the horizontal and vertical direction.

The system is to have the capability of operation from storage at the 100% power level.

The heat transfer fluid and the power conversion system is not specified. The Energy Systems Group has selected a sodium-cooled receiver system with a Rankine cycle power conversion system as the configuration with the promise of substantially improving system performance and reducing costs of producing electricity compared to current water-steam systems.

TABLE 2-1

ADVANCED CENTRAL RECEIVER
SYSTEM REQUIREMENTS

Design Point Power Levels	
During Receiver Operation (MWe, net)	100
Operation Exclusively from Thermal Storage (MWe, net)	100
Solar Multiple (SM)	1.5
Storage Capacity (h)	3
Design Insolation (W/m^2)	950
Heat Rejection	Wet Cooling
Wet Bulb Temperature [^{o}C (^{o}F)]	23 (74)
Dry Bulb Temperature [^{o}C (^{o}F)]	28 (82.6)
Nominal Design Wind* [m/s (mph)]	3.5 (8)
Maximum Operating Wind (including gusts)* [m/s (mph)]	16 (36)
Maximum Survival Wind (including gusts)* [m/s (mph)]	40 (90)
Seismic Environment	Zone 3 (not near a great fault)
Survival Earthquake Horizontal and Vertical (g)	0.25
Availability (Exclusive of Sunshine)	0.9
Lifetime (years)	30

*At reference height of 10 m (32.8 ft)

2.2 SYSTEM CONCEPTUAL DESIGN

The baseline advanced central receiver configuration, shown in Figure 2-1 with the performance characteristics summarized on the system Design Data Sheets of Table 2-2, meets the performance requirements given in Table 2-1. The system incorporates an external cylindrical receiver concept on a single tower 174 m (571 ft) to the receiver centerline and an all-sodium, two-tank thermal storage system. The collector field consisting of 14,106 heliostats surrounds the tower with the tower located to the south of the field center (north biased field). Net power output is 100 MWe with a daytime parasitic power requirement of 12 MWe, which reduces to 6 MWe during storage only operation, since neither the collector

RECEIVER

24 PANELS

PRESSURE REDUCING STATION

HOT STORAGE

PUMP

COLD STORAGE

PUMP

PURIFICATION SYSTEM

REACTION PRODUCTS TANK

EVAPORATOR

SUPERHEAT

REHEAT

SODIUM SYSTEM   STEAM SYSTEM

HIGH-PRESSURE TURBINE

INTERMEDIATE-PRESSURE TURBINE

LOW-PRESSURE TURBINE

GENER-ATOR

CON-DENSER   COOLING TOWER

AIR

WET COOLING SYSTEM

DEAERATOR

FEEDWATER HEATERS

CONDENSATE PUMP
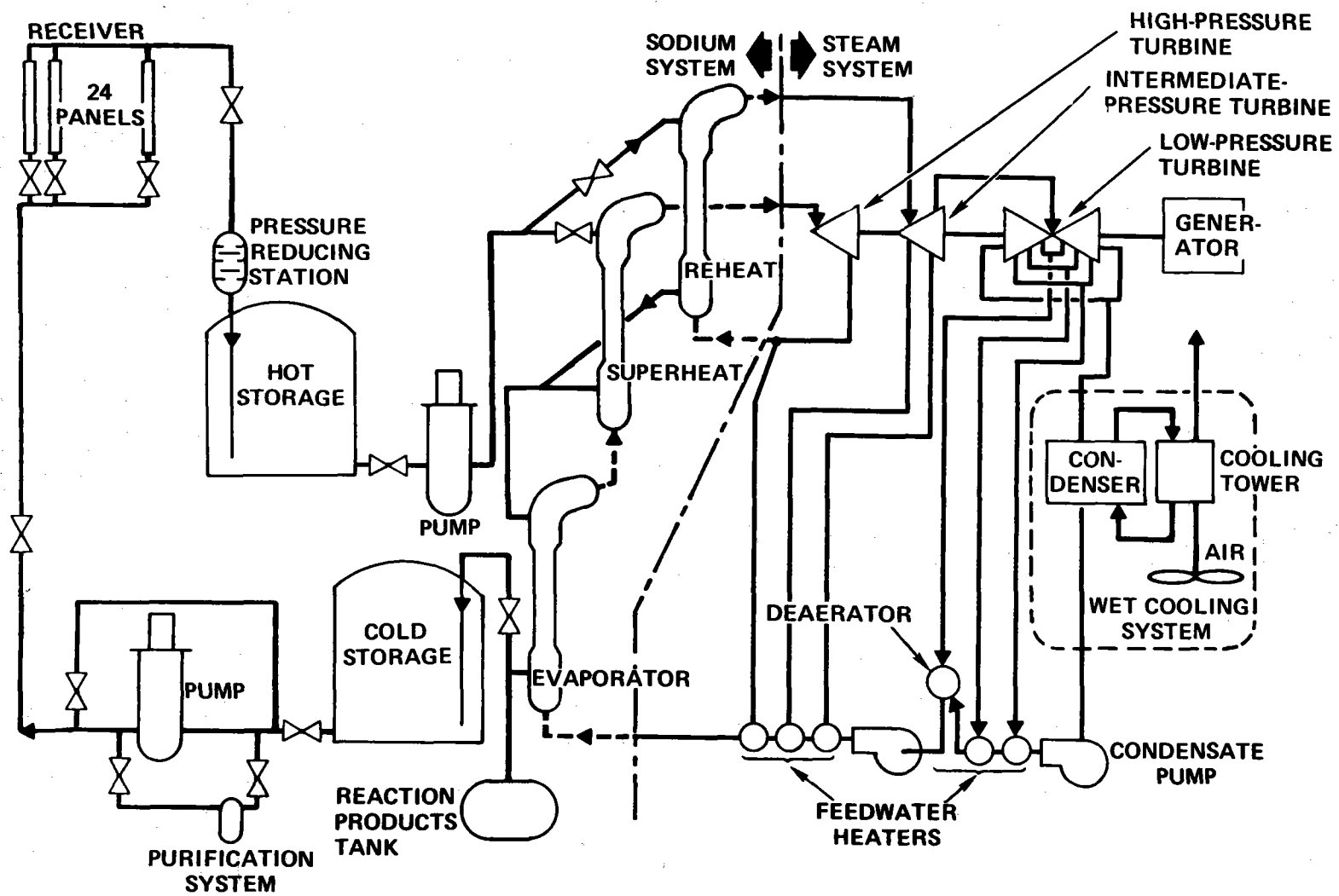
42400-1096C

Figure 2-1. Sodium Cooled Advanced Central Receiver System

TABLE 2-2

ADVANCED CENTRAL RECEIVER
SYSTEM SUMMARY DATA

New Electrical Power (MWe)	100
Parasitic Power (MWe)	
Daytime	12
Nighttime	6
Insolation (W/m^2)	950
Maximum Solar Power Absorbed (MWt)	390
Nominal Solar Power Absorbed for Direct Operating (MWt)	260
Plant Net Efficiency (%)	24.5
Collector Field Configuration	Single 360°, North Biased
Solar Multiple, Equinox Noon	1.5
Number of Heliostats	14,106 (Inverted)
Heliostat Shape and Size [m (ft)]	~Square, 7.38 x 7.42 (24.2 x 24.3)
Number of Towers/Receivers	1
Receiver Midpoint Elevation [m (ft)]	174 (571)
Receiver Configuration	External Cylinder
Number of Receiver Panels	24
Receiver Height and Diameter [m (ft)]	16.1 x 16.1 (52.8 x 52.8)
Receiver Maximum Heat Flux (MW/m^2)	1.53
Sodium Temperatures [^{o}C (^{o}F)]	288/593 (500/1100)
Receiver Sodium Flow Rate [kg/h (lb/h)]	3.66×10^6 (8.07×10^6)
Steam Generator Sodium Flow Rate (Direct Operation) [kg/h (lb/h)]	2.45×10^6 (5.36×10^6)
Thermal Storage Capacity (MWt-h)	805
Total Sodium Inventory [kg (lb)]	7.6×10^6 (16.8×10^6)
Steam Generator and Reheater Type	Modular Steam Generator
Steam Conditions [MN/m^2, ^{o}C (psia, ^{o}F)]	
Initial	12.51, 538 (1815, 1000)
Reheated	2.72, 538 (394, 1000)
Steam Flow Rate [kg/h (lb/h)]	
Daytime	3.32×10^5 (7.32×10^5)
Nighttime	3.15×10^5 (6.95×10^5)
TSS Sodium Flow Rate [kg/h (lb/h)]	2.31×10^6 (5.09×10^6)
Feedwater Temperature [^{o}C (^{o}F)]	234 (453)
Turbine Back Pressure [MN/m^2 (in. Hg)]	0.007 (2.0)
Heat Rejection [MW (Btu/h)]	
Daytime	158 (540×10^6)
Nighttime	150 (511×10^6)

field nor the receiver feed pump are required. Based on insolation of 950 W/m^2, the collector field mirror area is 692,000 m^2 (7.45 x 10^6 ft^2) with a total incident power of 657 MWt. The total incident power required for direct operation at 100 MWe is 409 MWt which gives a plant net efficiency of 24.5%.

The receiver consists of 24 flat panels arranged to form a right circular cylinder with a diameter of 1.61 m and a height of 16.1 m.

Liquid sodium from the cold storage tank at 288°C (550°F) is pumped by the receiver feed pump through the receiver where the sodium is heated to 593°C (1100°F). The sodium flows from the receiver down the tower through a pressure reducing valve to the hot storage tank. The pressure reducing device reduces the tower static head to that the storage tank operates at atmospheric pressure with an inert cover gas such as argon. The sodium in the hot storage tank is pumped by the steam generator supply pump to the steam generator units where steam at 538°C (1000°F) and 12.4 MPa (1800 psig) turbine inlet pressure is produced. The steam generator units consist of an evaporator, a superheater, and reheater units. Sodium from the evaporator returns to the cold storage tank, completing the circuit.

The electric power generating subsystem is a conventional system with a tandem compound, double-flow turbine with reheat, wet cooling system with forced draft cooling towers, and six feedwater heaters using turbine extraction flow. The cycle efficiency is 43.1% with 7.0 KPa (2.0 in. Hg) condenser back pressure. A steam drum is between the evaporator unit and the superheater to insure that dry steam enters the superheater. Maximum guaranteed generator output is 112,000 kW and, at the VWO rated conditions, the generator output is 116,741 kW.

System Power Flow - 100-MWe Plant

A system power flow chart is shown in Figure 2-2 for the 100 MWe net system; with 3 h of storage for equinox noon. The incident power required for direct operation at 100-MWe net is 437 MWt. The overall plant efficiency is 22.9%.
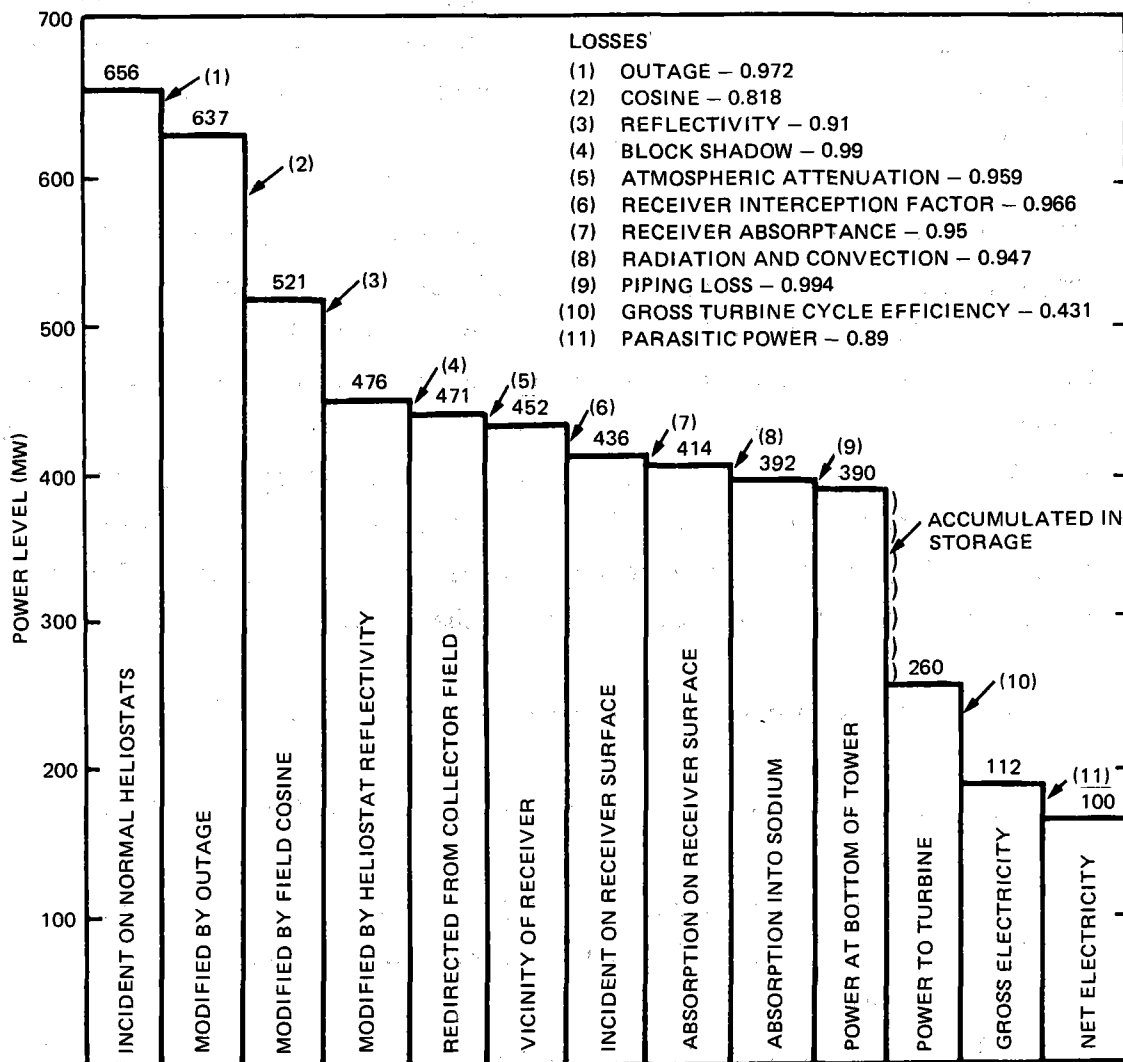
Figure 2-2. System Power Flow (Equinox Noon)

2.3 SYSTEM ANALYSIS

For establishing the performance characteristics of the total system, the performance of the power conversion system is established first. These performance characteristics then establish the requirements on the receiver, thermal storage, and collector subsystems. Thus, the system performance characteristics are established at the system output end (turbine-generator) and worked forward to the system input end (collector field).

The thirteen turbine-generator configurations that are discussed in Section 7 are compared in Figure 2-3 with the cost effectiveness slope for the collector, receiver, and storage subsystems. This comparison indicates that Cases 2, 6, 9, and 10 have effective cost-vs-efficiency characteristics and were, therefore, developed in greater detail as is also presented in the section discussing the EPG system. This data was then used in an optimization study to select the steam generator arrangement and the turbine cycle that will give the most cost-effective arrangement and cycle for the advanced central receiver system. The steam generator information of Appendix E was also used in the study.

The possible steam generator arrangements included:

1) Once-through unit without reheat, Type 316 stainless steel construction.

2) Separate evaporator and superheat units without reheat. Evaporator constructed of 2-1/4 Cr - 1 Mo, superheater of Type 316 stainless steel.

3) Separate evaporator, superheater, and reheater units. Evaporator constructed of 2-1/4 Cr - 1 Mo, superheater and reheater of Type 316 stainless steel.

The latter two units require a steam separator drum to ensure that water does not enter the superheater. The cost of these units, including the drum, is shown in Figure 2-4 as a function of steam throttle pressure. This figure shows the considerable cost associated with the reheat unit. However, the added cost of the reheat unit is shown in later discussions to be more than offset by the 2.35 point improvement in cycle efficiency.
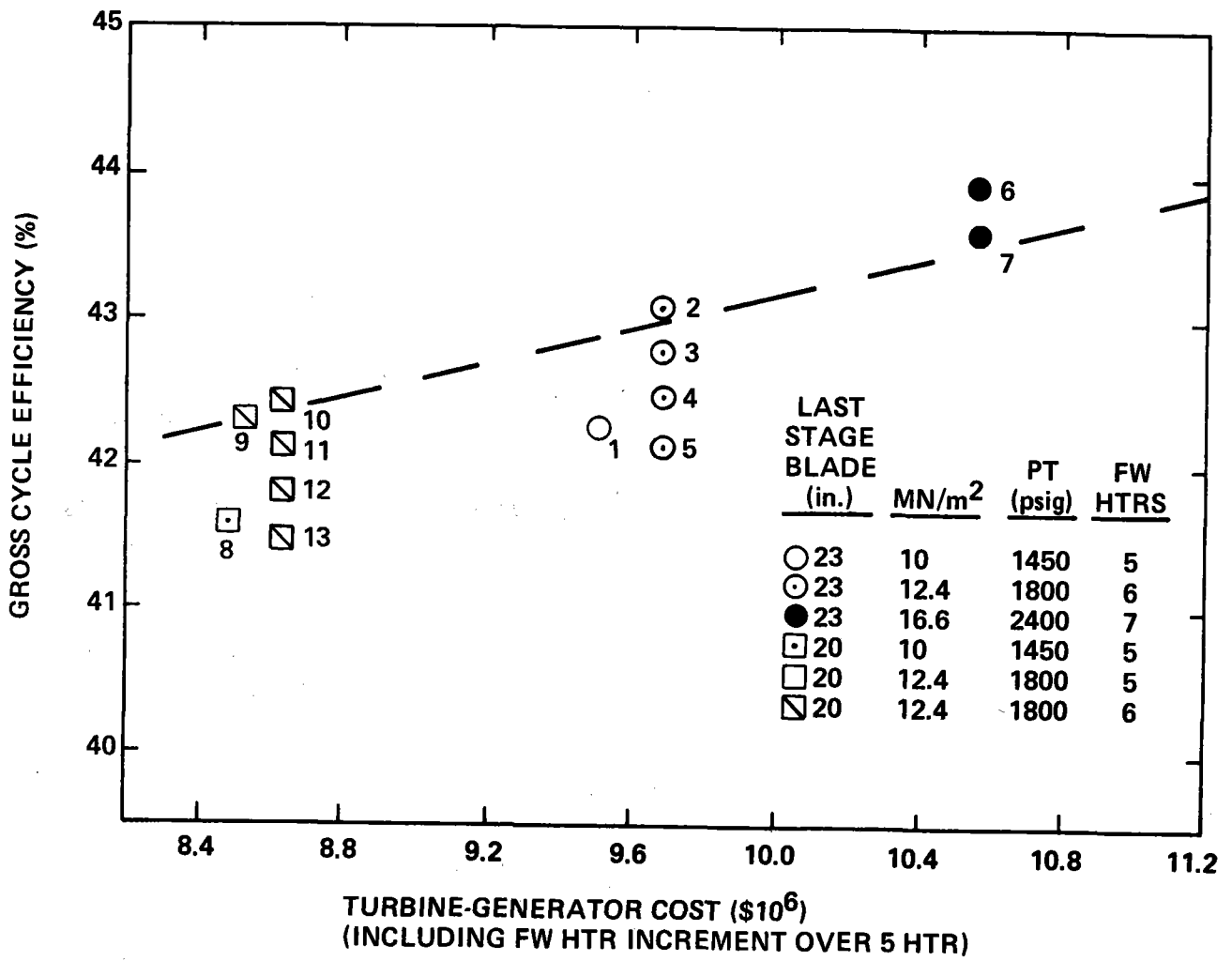
Figure 2-3. Electric Power Generating Subsystem — Gross Cycle
Efficiency vs Turbine-Generator Cost

79-MA21-46-1A
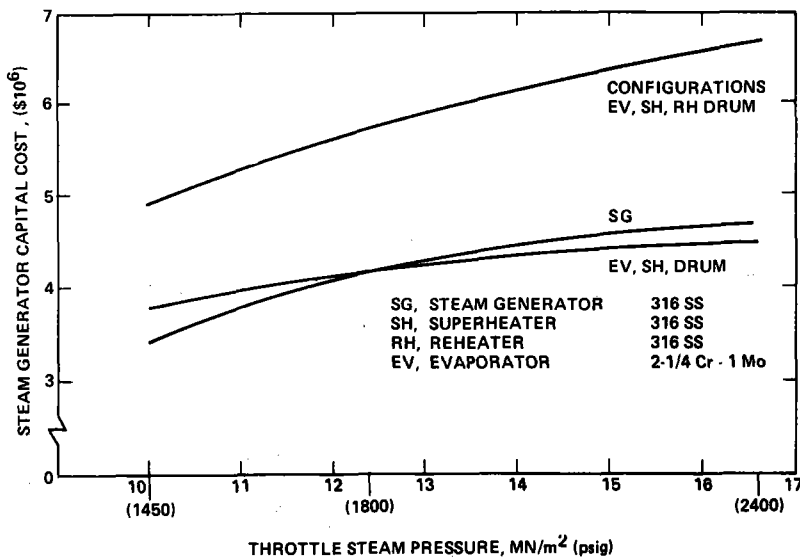
Figure 2-4. Steam Generator
Arrangement Costs

The graph axes and labels:

STEAM GENERATOR CAPITAL COST, ($10^6)

CONFIGURATIONS
EV, SH, RH DRUM

SG

EV, SH, DRUM

SG, STEAM GENERATOR	316 SS
SH, SUPERHEATER	316 SS
RH, REHEATER	316 SS
EV, EVAPORATOR	2-1/4 Cr - 1 Mo

THROTTLE STEAM PRESSURE, MN/m^2 (psig)

79-MA21-46-6

Figure 2-5 shows the variation of plant capital cost increment with gross cycle efficiency referenced to the initial baseline value of 39.5%. The symbols shown on this figure are efficiency values for the four cases selected above for more detailed consideration. Other plant capital cost increments used in this study are shown in Figures 2-6 and 2-7. In general, plant equipment and hardware costs are assumed to vary with size (P) as $(P_i/P_o)^{0.8}$ and cycle efficiency and, of course, auxiliary power can be interpreted as a plant size variation. Variation of the sodium loop temperature difference (ΔT) (Figure 2-7) determines the quantity of sodium in the all-sodium storage system and the sodium flow rates to transport the thermal energy from the receiver and through the steam generator units. The flow rate is inversely proportional to the loop ΔT, hence, as ΔT decreases, the pump power increases because of the increased flow rate (Q) and pump head ($\sim Q^2$).

Steam generator cost increments as a function of sodium loop ΔT are shown in Figure 2-8, as derived from the data of Appendix D. These costs increase rapidly due to the heat transfer area increase resulting from the small pinch point temperature difference as the sodium loop ΔT increases.

The turbine-generator variation in the EPG Section of this report are for a number of different combinations of pressures, temperatures, feedwater heaters, and last stage blade length. Additional information was received from Stearns-Roger for nonreheat turbines. Incremental cost and efficiency values for these
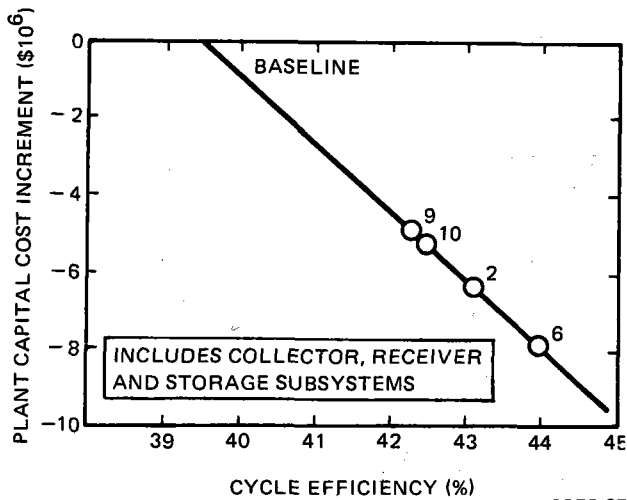
Figure 2-5. Variation of System
Costs With Gross Rankine
Cycle Efficiency

BASELINE

INCLUDES COLLECTOR, RECEIVER
AND STORAGE SUBSYSTEMS

9272-35

Figure 2-6. Variation of System
Cost With Auxiliary Electrical
Power Requirements

BASELINE
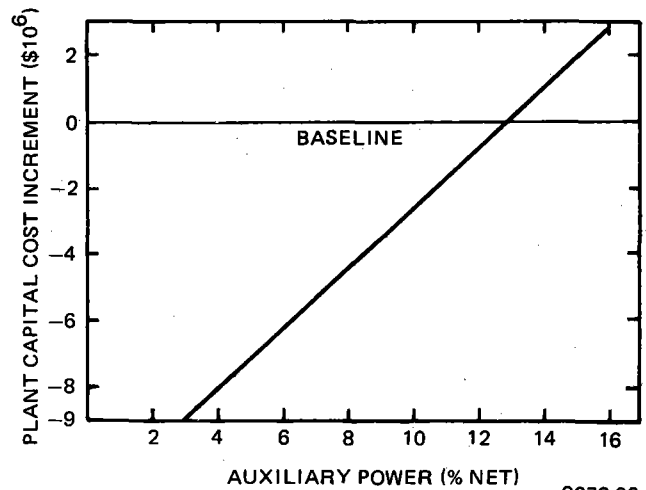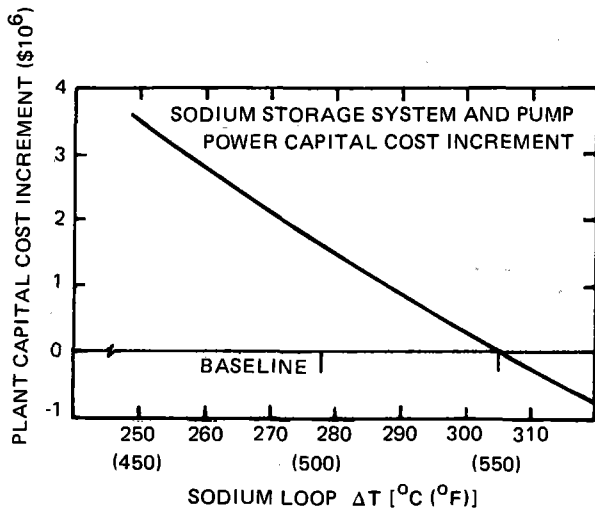
9272-36

Figure 2-7. Effect of Sodium Loop
ΔT on Steam Generator Thermal
Storage, and Pump Costs

SODIUM STORAGE SYSTEM AND PUMP
POWER CAPITAL COST INCREMENT

BASELINE

9272-37
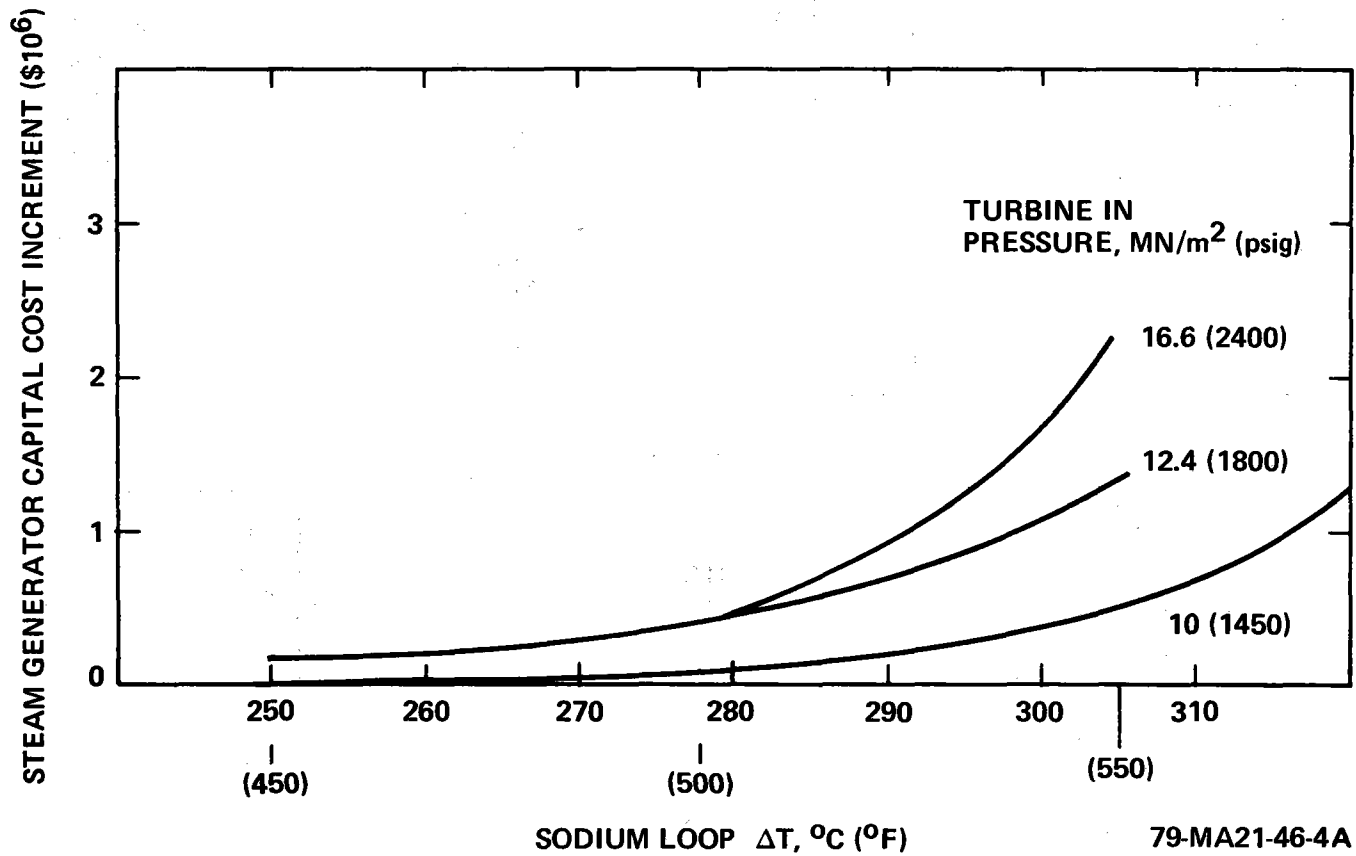
Figure 2-8.   Capital Cost Increment for Superheater, Reheater, Evaporator

parameters are shown in Table 2-3. This table, together with Figures 2-4 through 2-8, allow various basic system parameters such as reheat, steam pressure, and temperature and sodium ΔT to be evaluated as to cost effectiveness. The relationship of these parameters to plant cost is indicated by the logic sequence in Figure 2-9.

Two plant cost comparisons are shown in Figures 2-10 and 2-11, with the detailed input to these figures given in Tables 2-4 and 2-5, respectively. Figure 2-10 shows the influence of steam pressure and steam generator configuration on plant cost. A reheat configuration shows a cost advantage of about 10^6 with a steam throttle pressure in the range of 10 to 12.4 MN/m^2 (1450 to 1800 psig) for minimum plant cost. The sodium system ΔT is a constant 306°C (550°F) for this figure.

Figure 2-11 presents the influence of sodium ΔT on plant costs for a reheat configuration at three steam pressure levels. While the cost differences are not large for the various conditions, the minimum condition is for a 12.4 MN/m^2 (1800 psig) turbine in-pressure with a sodium ΔT of 306°C (550°F).

A reheat configuration operating at turbine inlet pressures of 12.4 MN/m^2 (1800 psig) with a sodium system ΔT is recommended as the revised baseline condition. The only difference, as compared to the previous baseline condition, is to reduce turbine in-pressure from 1505 to 12.4 MN/m^2 (2000 to 1800 psig). Reheat and a sodium ΔT of 306°C (550°F) were already part of the advanced central receiver concept, but without the technical background contained herein. Qualitative considerations supporting the selection of the 12.4 MN/m^2 (1800 psig) turbine in-pressure level are as follows:

1) Availability data presented in the section for the EPG Subsystem indicated that plant availability significantly decreased at pressures above 12.4 MN/m^2 (1800 psig).

2) Steam generator tube size and wall thickness combinations at high pressures tend to fall outside ESG's range of experience in performing tube-to-tubesheet welds, Appendix E.

TABLE 2-3
TURBINE EFFICIENCY COMPARISONS

Parameter	Case	Last Stage Blade (in.)	Press/SH/RH (psig/°F/°F)	Feedwater Heaters	Heat Rate (Btu/kW-h)	η	Δη	Correction To Constant Feedwater Heaters	Δη	Cost (10^6)
Reheat	-	23	1450/1000/-	5	8550	39.9 ⎫	2.35	-	2.35	2.223
	1	23	1450/1000/1000	5	8077	42.25 ⎭				
	-	23	1800/1000/-	6	8314*	41.06 ⎫	2.03*	-	2.03*	1.611
	2	23	1800/1000/1000	6	7919	43.09 ⎭				
Feedwater Heaters	9	20	1800/1000/1000	5	8069	42.29 ⎫	0.11	-	0.11	0.10
	10	20	1800/1000/1000	6	8048	42.40 ⎭				
Pressure	1	23	1450/1000/1000	5	8077	42.25 ⎫	0.86	-0.11	0.75	0.33
	2	23	1800/1000/1000	6	7919	43.09 ⎭				
	8	20	1450/1000/1000	5	8219	41.53 ⎫	0.76	-	0.76	0.35
	9	20	1800/1000/1000	5	8069	42.29 ⎭				
	2	23	1800/1000/1000	6	7919	43.09 ⎫	0.85	-0.11	0.74	1.40
	6	23	2400/1000/1000	7	7766	43.94 ⎭				
Blade Length	1-8	(23)-(20)		5, 5			0.72	-	0.72	1.0
	2-10	(23)-(20)		6, 6			0.69	-	0.69	1.02
Temperature Superheat	SR		1800/ΔT50/1000				0.70	-	0.70	0.15
			2400/ΔT50/1000				0.80	-	0.80	0.15
Temperature Reheat	SR		1800/1000/ΔT50				0.80	-	0.80	0.50
			2400/1000/ΔT50				0.80	-	0.80	0.50

*Estimated
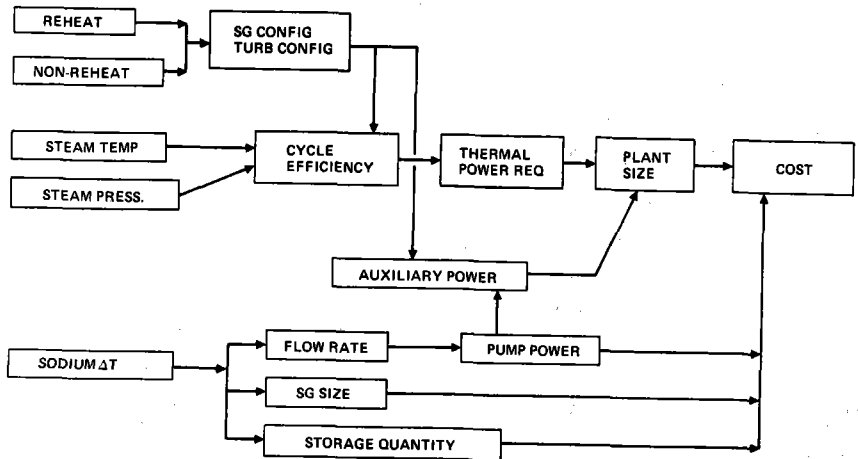
79-MA21-46-2

Figure 2-9. System Cost Considerations
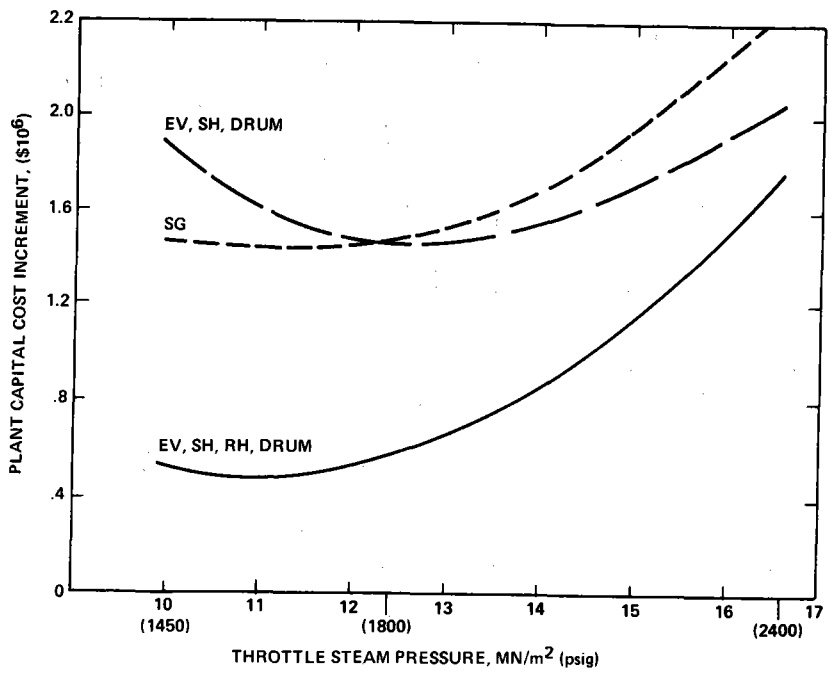
79-MA21-46-5

Figure 2-10. Plant Capital Cost Increment for
Various Steam Generator Configurations

TABLE 2-4

STEAM GENERATOR ARRANGEMENT COST COMPARISON
AT ΔT = 305°C (550°F)

System	Pressure (psi)	Steam Generator Cost (10^6)	Drum 10^6	$\Delta\eta$ (%)
1. EV, SH, RH	1450	4.6	0.3	2.35
	1800	5.36	0.37	3.09
	2400	6.20	0.50	3.83
2. EV, SH	1450	3.50	0.3	0.0
	1800	3.80	0.37	0.74
	2400	4.00	0.50	1.48
3. Once Through Steam Generator	1450	3.40	N/A	0.0
	1800	4.20		0.74
	2400	4.70		1.48

System	Cost Due to $\Delta\eta$ (10^6)	Equalize Size Due to Plant Efficiency (10^6)	Turbine ΔCost (10^6)	Summation (10^6)
1. EV. SH, RH	-3.94	-	-0.43	0.53
	-5.17	-	0.0	0.54
	-6.42	-	1.50	1.76
2. EV. SH	0.0	0.119	-2.04	1.88
	-1.24	0.129	-1.61	1.45
	-2.48	0.136	-0.114	2.04
3. Once Through Steam Generator	0.0	0.115	-2.04	1.47
	-1.24	0.142	-1.611	1.49
	-2.48	0.159	-0.114	2.26

TABLE 2-5
SUMMARY OF TURBINE CYCLE
COST IMPACT (10^6)

ΔT	A SG ΔCost			B Loop ΔT	C Turbine Efficiency (η), TC2F-23		
	1,450	1,800	2,400		1,450	1,800	2,400
450	0.3	0.45	0.58	3.46	-4.60	-6.03	-7.46
500	0.42	0.68	0.80	1.64	-4.60	-6.03	-7.46
520	0.52	0.89	1.22	0.95	-4.60	-6.03	-7.46
535	0.65	1.15	1.68	0.45	-4.60	-6.03	-7.46
550	0.77	1.57	2.54	0.0	-4.60	-6.03	-7.46
580	1.83	-	-	-0.8	-4.60	-6.03	-7.46

ΔT	D Turbine Cost Δ, TC2F-23			Summary A + B + C + D		
	1,450	1,800	2,400	1,450	1,800	2,400
450	0.712	1.14	2.64	-0.13	-0.98	-0.78
500	0.712	1.14	2.64	-1.83	-2.57	-2.38
520	0.712	1.14	2.64	-2.42	-3.05	-2.65
535	0.712	1.14	2.64	-2.79	-3.29	-2.69
550	0.712	1.14	2.64	-3.12	-3.32	-2.28
580	0.712	1.14	2.64	-2.86	-	-
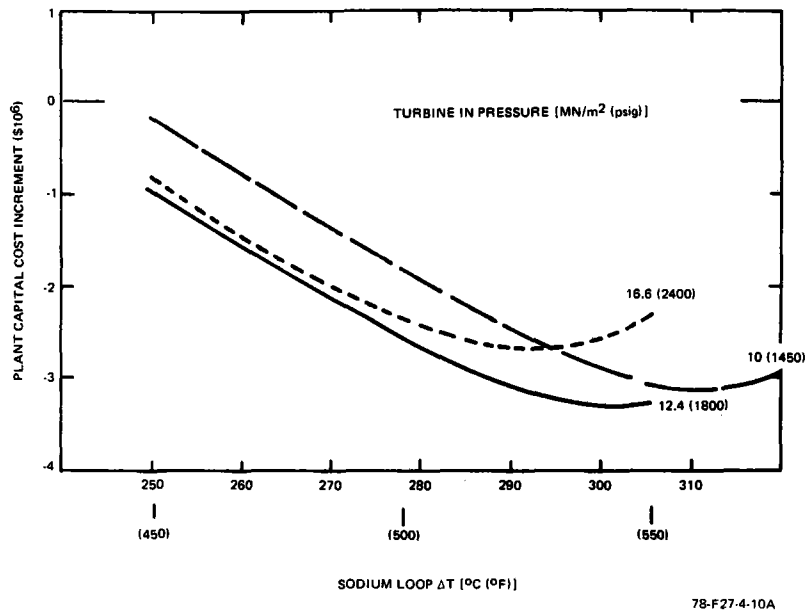
Figure 2-11. Summation of Plant Capital Cost Increments

3) Higher pressures tend to reduce the tube thermal stresses due to DNB (Departure from Nucleate Boiling), which would tend to support the selection of the 12.4 MN/m^2 (1800 psig) level over the 10 MN/m^3 (1450 psig) level.

Hence, the 12.4 MN/m^2 (1800 psig) turbine in-pressure is seen as a satisfactory compromise for the three qualitative items presented above.

2.4 SYSTEM DESCRIPTION AND ANALYSIS, RECEIVER DYNAMIC MODEL

A mathematical model, describing the dynamic behavior of the receiver sodium system, was written and used to verify the receiver control methodology and simulate the receiver system under various transients of interest.

A schematic of the model is shown in Figure 2-12. The components included in the model are the cold tank, receiver pump, riser piping and check valve, panel control valves, individual panels, panel flow controllers, receiver surge tank, downcomer piping, drag valve and controller, and the hot tank. The steam generator

100-Mile Solar Plant

(Dwg N272000001)

ESG-79-2, Vol II, Book 2

A-41
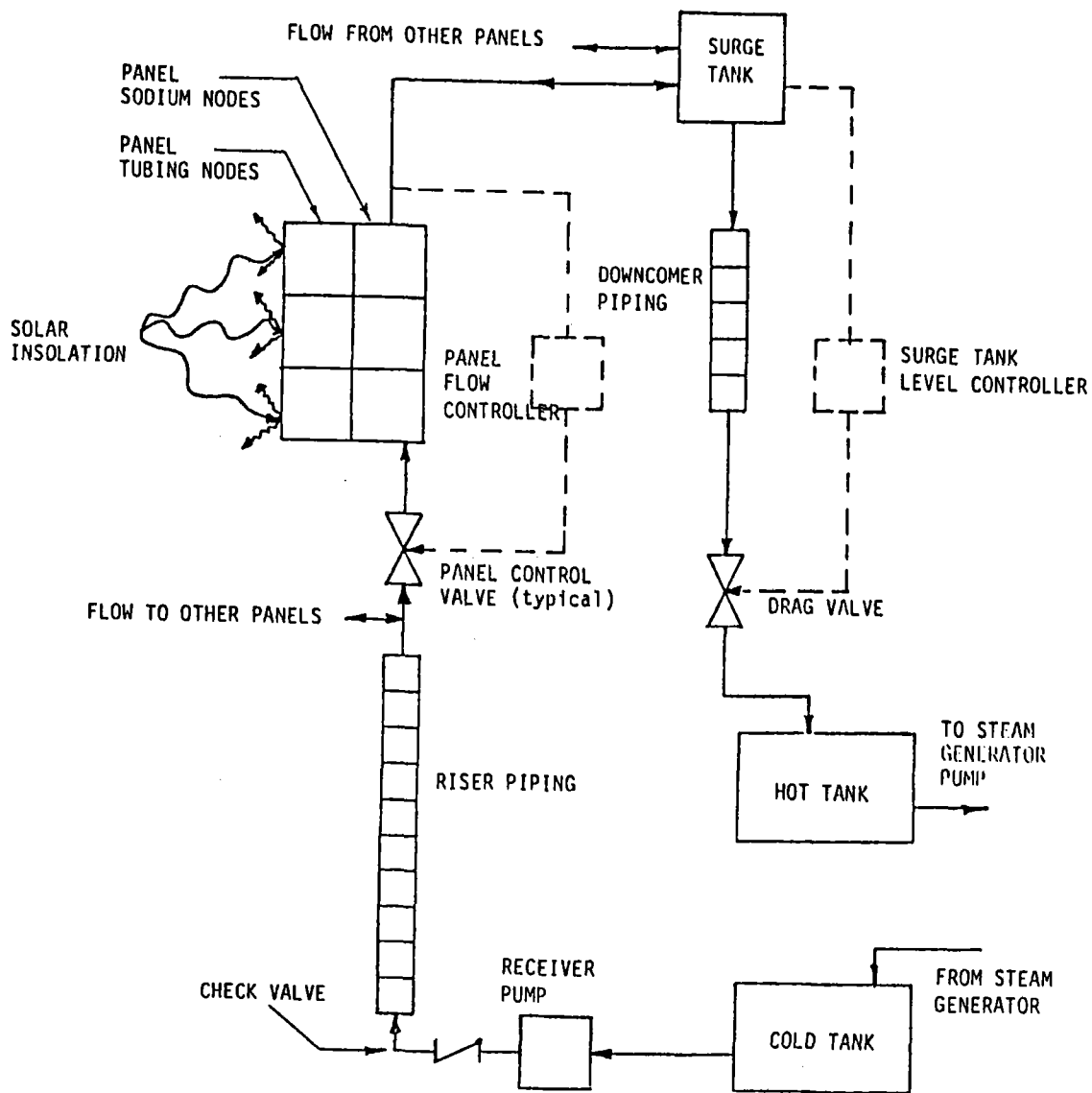
Figure 2-12. Schematic of Advanced Central
Receiver Transient Model

pump, evaporator, superheater, and reheater are not included due to the large mass capacity of the hot and cold tanks. These mass capacities provide a natural boundary for the model since their conditions change slowly in relation to other components.

Model capabilities include: an extensive data input routine which easily accommodates design or initial condition changes, arbitrary flux distribution input (each panel can be independently perturbed), full 24-panel simulation which can accommodate panel interaction and reverse panel flow, straightforward relatively simple heat transfer and hydraulics algorithms which facilitate rapid computer solutions, and 3-mode controller simulation.

Numerical methods are employed to solve the coupled, time-dependent, differential equations which describe the sodium flow and heat transfer in each component. The specific program used is entitled "Continuous System Modeling Program" (CSMP) Version III. CSMP translates inputted differential equations, initial and boundary conditions and constants into an equivalent FORTRAN subroutine named UPDATE. It then alters between UPDATE and a central, user-specified integration routine in a time-stepwise manner to find the time domain solution to the equations.

In some cases, the lumped parameters associated with a component are so large, in relation to other components, that numerical instabilities would result upon treating the component as single entities. This problem is handled by distributing these parameters to an integral number of nodes, which then represent the component, and writing coupled differential equations for each mode. Each receiver panel is divided into three axial nodes for the tubing and sodium, respectively. The receiver riser piping has been divided into 10 axial nodes and the downcomer piping into 5. All other components are treated as single entities.

The fundamental equation describing the temperature change of a given axial tube node is derived from an energy balance around the node and is of the form:

$$\frac{d}{dt}(TRWIi) = (QAIi - HIi \times A(TRWIi - TNRIi)/MCPTW \qquad ...(1)$$

where

> TRWIi = temperature of receiver wall panel I, axial node i (F)
>
> QAIi = heat absorbed by receiver wall panel I, axial node i (Btu/s)
>
> HIi = sodium film coefficient, inside tubes, panel I axial node i (Btu/ft^2-F-s)
>
> TRNIi = bulk sodium temperature, panel I, axial node i (F)
>
> A = tube inside heat transfer area/node (ft^2)
>
> MCPTW = tube mass heat capacity product/node (Btu/F)

QAIi is determined by subtracting reflective, reraditive, and convective heat losses from the incident solar insolation. Provision has been made for varying the convective loss circumferentially, if necessary. The sodium film coefficient is determined from the Seban-Shinosoky correlation for liquid metals.

Similarly, the relation describing the change in sodium bulk temperature was derived. It is

$$d/dt(TRNIi) = (HIi \times A(TRWIi - TRNIi) - WNRAI \times CPIi \times (TRNIi - TNR(I-1)i))/(NVOL \times RHOIi \times CPIi) \qquad ...(2)$$

where

> WNRAI = absolute value of sodium flow in panel I (lb/s)
>
> CPIi = sodium heat capacity panel I, axial node i (Btu/lb-F)
>
> TNR(I-1)i = upstream bulk sodium temperature (F)
>
> NVOL = sodium volume/node (ft^3)
>
> RHOIi = sodium density panel I, axial node i (lb/ft^3)

TNRIi, HIi, A, and TRWIi are as in Equation 1. Both density and heat capacity vary with bulk sodium temperature. TNR(I-1)i changes when the panel flow reverses.

The piping heat transfer simulation methodology only accounts for one dimensional axial transportation lag. Piping heat loss to the environment has been ignored due to its relatively small magnitude. A typical equation describing a piping node is:

$$\frac{d}{dt}(TNRPi) = KLNR(TNRP(i-1) - TNRPi) \qquad \ldots(3)$$

where

$$TNRPI = \text{bulk sodium temperature piping node I}$$
$$KLNR = \text{inverse variable piping time constant/node } (\sec^{-1})$$
$$= \text{flow/mass per node}$$
$$TNRP(i-1) = \text{upstream sodium node temperature (F)}$$

All tanks were assumed to behave as well-mixed single nodes. The equation for the cold tank is typical:

$$\frac{d}{dt}(TNCT) = (WCTI * TNCTI - WCT\emptyset * TNCT - DMNCT \times TNCT)/MCPCT \qquad \ldots(4)$$

where

$$WCTI = \text{sodium tank inflow (lb/s)}$$
$$TNCTI = \text{sodium inlet temperature (F)}$$
$$WCT\emptyset = \text{sodium outflow (lb/sec)}$$
$$TNCT = \text{sodium temperature (F)}$$
$$DMNCT = \text{change in tank inventory (lb/s)}$$
$$MCPCT = \text{mass heat capacity product of sodium in tank (Btu/F)}$$

Thermal energy added to the sodium due to pump viscous heating is described by:

$$TNRPU\emptyset = TNRPUI - HRP \times HRPO \times 144/778/RHOCT/CPCT \times (1 - 1/ETARP) \qquad \ldots(5)$$

where

TNRPUØ = pump sodium outlet temperature (F)
TNRPUI = pump sodium inlet temperature (F)
 RHDCT = cold tank sodium density (lb/cu-ft)
  CPCT = cold tank sodium heat capacity (Btu/lb-F)
 ETARP = receiver pump efficiency (fractional)
   HRP = normalized pump head
  HRPO = steady-state pump head (psi)

This equation assumes that the heat addition to the sodium is very nearly instantaneous in relation to other time-varying quantities.

The time varying change in flow of each receiver panel, derived from a force balance taken from the common entrance to exit of each panel is:

$$d/dt \, (WNRI) = (PIR - POR - FHI - DPCVI - SH)/IRI \qquad \ldots(6)$$

where

  WNRI = normalized flow in panel I
   PIR = common total inlet pressure (psia)
   PØR = common total outlet pressure (psia)
   FHI = friction head in panel I (psia)
 DPCVI = control valve pressure drop in panel I
    SH = static head (psia)
   IRI = inertia term in panel I (psia-s)
       = $\dot{W}_o \times L/g \times A$
  $\dot{W}$o = panel I reference flow (lb/s)
     L = panel length (ft)
     g = acceleration due to gravity 32.2 ft lbm/lbf s^2
     A = panel flow area (in.^{2})

The panel outlet pressure is easily determined from the level in the receiver outlet tank. In determining the receiver inlet pressure, the effect of inertia in

both the panels and riser piping was considered. The effect of the inertia of the riser piping is significant. The equation for the receiver inlet pressure is derived from the first derivative of the continuity equation:

$$dWN/dt = \Sigma d/dt \ (WNRI * WNRRI) \qquad \qquad ...(7)$$

where

$$WN = \text{riser sodium flow (lb/s)}$$
$$WNRI = \text{normalized flow in panel I}$$
$$WNRRI = \text{reference flow in panel I (lb/s)}$$

Since the expressions for d/dt(WN) and d/dt(WNRI * WNRRI) both include PIR, Equation 6 can be solved for PIR

$$
\begin{aligned}
PIR = \ &(24(P\emptyset R) + TSH + TFHR + TFHCV)/PL\emptyset GA + (P\emptyset CT \\
&+ (LNACT - LRI) \times (RHOCT + SNARII)/2/SINSFT \\
&- WN \times WNA \times KFHRP/WNO + HRP \times HRPO)/L\emptyset GAR)/(24/PLOGA \\
&+ 1/LOGAR)
\end{aligned}
\qquad ...(8)
$$

where

PIR, PØR are as in Equation 6

$$TSH = \text{total receiver static heat (psia)}$$
$$TFHR = \text{total friction head of the receiver (psia)}$$
$$= \Sigma FHI$$
$$TFHCV = \text{total friction head of the control valves (psia)}$$
$$= \Sigma DPCVI$$
$$PL\emptyset GA = \text{receiver panel length divided by g and panel flow area}$$
$$P\emptyset CT = \text{pressure over the cold tank (psia)}$$
$$LNACT = \text{level of sodium in the cold tank (ft)}$$
$$LRI = \text{elevation of the receiver inlet (ft)}$$
$$RH\emptyset CT = \text{sodium cold tank density (lb/ft}^3)$$

SNARII = sodium receiver inlet density (lb/ft^3)

SINSFT = 144 in.^{2}/ft^2

WN&WNO = See Equation 5

WNA = absolute value of riser flow (lb/sec)

KFHRP = reference riser friction head (psia)

HRPO = reference receiver pump head (psia)

HRP = normalized receiver pump head

LOGAR = riser piping L over gA (see Equation 6)

The equation describing the change in downcomer flow is similar to Equation 6. While these equations do not describe the total model, they give an adequate representation of the major model characteristics. A complete, detailed model description and results presentation is given in Volume II, Book 2, Appendix L.

The optimum control configuration was determined to be proportional + integral + derivative (PID). Proportional control gave adequate response but unacceptable offset. Proportional + integral had acceptable offset but sluggish response.

The overall system response to the transients examined using the model are shown in Figure 2-13a-g. The transients include: 10% step flux change, cloud cover, 25% step changes, pump trip, drag valve failures, and emergency shutdown. Each of the CRT (Cathode Ray Tube) graphs shown in Figure 2-13 depicts the time varying incident and absorbed power, total receiver flow, and receiver outlet tank temperature.

During the 10% step change transient, the receiver outlet tank temperature varied less than 8°F, verifying the acceptable response of the system to a standard perturbation. During the cloud cover transient, the tank temperature varied less than 5°F. During the 25% step changes, the tank temperature varied a maximum of 7°F. It was concluded that for these normal transients, the system response was acceptable.

During the pump trip transient, it was assumed that the heliostats would freeze and that the only defocusing would be due to the solar image drift-off. As shown in Figure 2-13d, this is inadequate. The receiver outlet tank temperature

RUN 04-04 100 SEC, 100 STEP FLUX DECREASE AT 5 SEC., PID
QI - TOTAL INCIDENT SOLAR POWER (MWT)
QA - TOTAL ABSORBED SOLAR POWER (MWT)
WN - TOTAL RECEIVER FLOW (LB/SEC)
TNRO - TEMPERATURE OF SODIUM RECEIVER OUTLET TANK (F)

°071796301
050378 0002

QI VS TIME

QA VS TIME

WN VS TIME

TNRO VS TIME
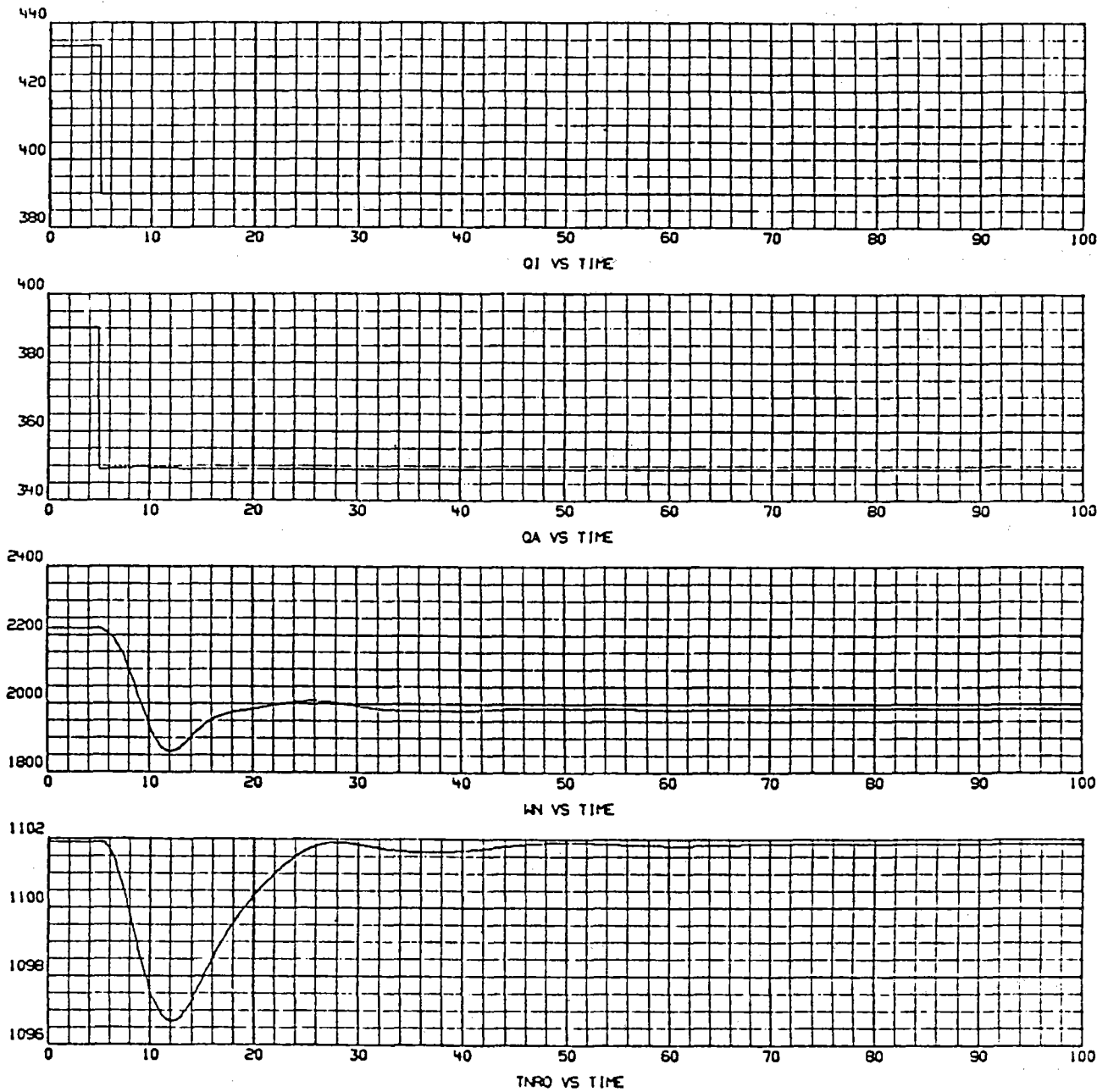
Figure 2-13a.   Overall System Response to the Transients Using Model
(Sheet 1 of 7)
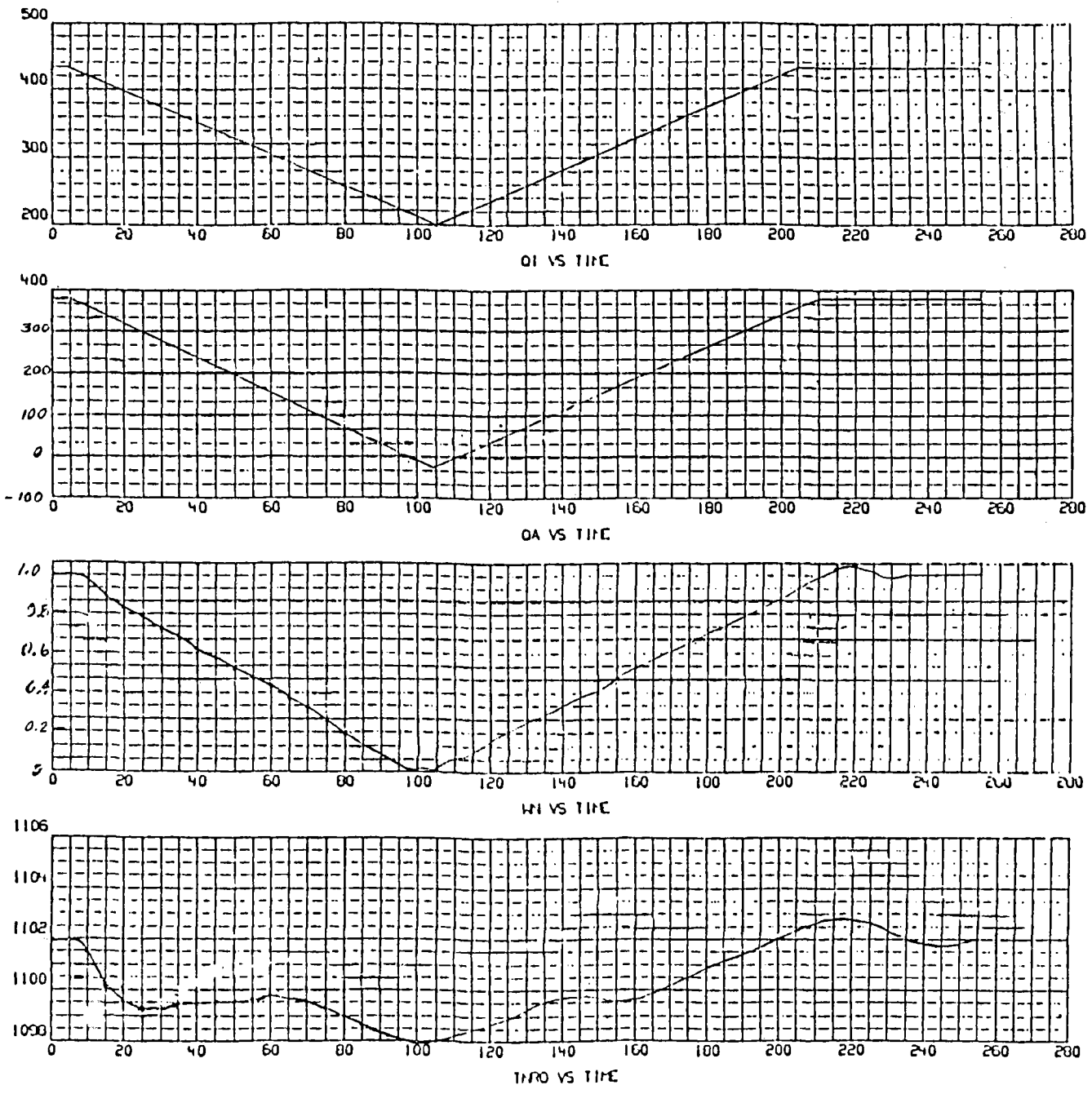
Figure 2-13b.   Overall System Response to the Transients Using Model
(Sheet 2 of 7)

RUN 04-07 25 PERCENT STEP CHANGES, AUGUST 9, 1978
   QI - TOTAL INCIDENT SOLAR POWER (MWT)
   OA - TOTAL ABSORBED SOLAR POWER (MWT)
   WN - TOTAL RECEIVER FLOW (LB/SEC)
   TNRO - TEMPERATURE OF SODIUM RECEIVER OUTLET TANK (F)

*071752301
081078 0002

QI VS TIME

OA VS TIME

WN VS TIME

TNRO VS TIME
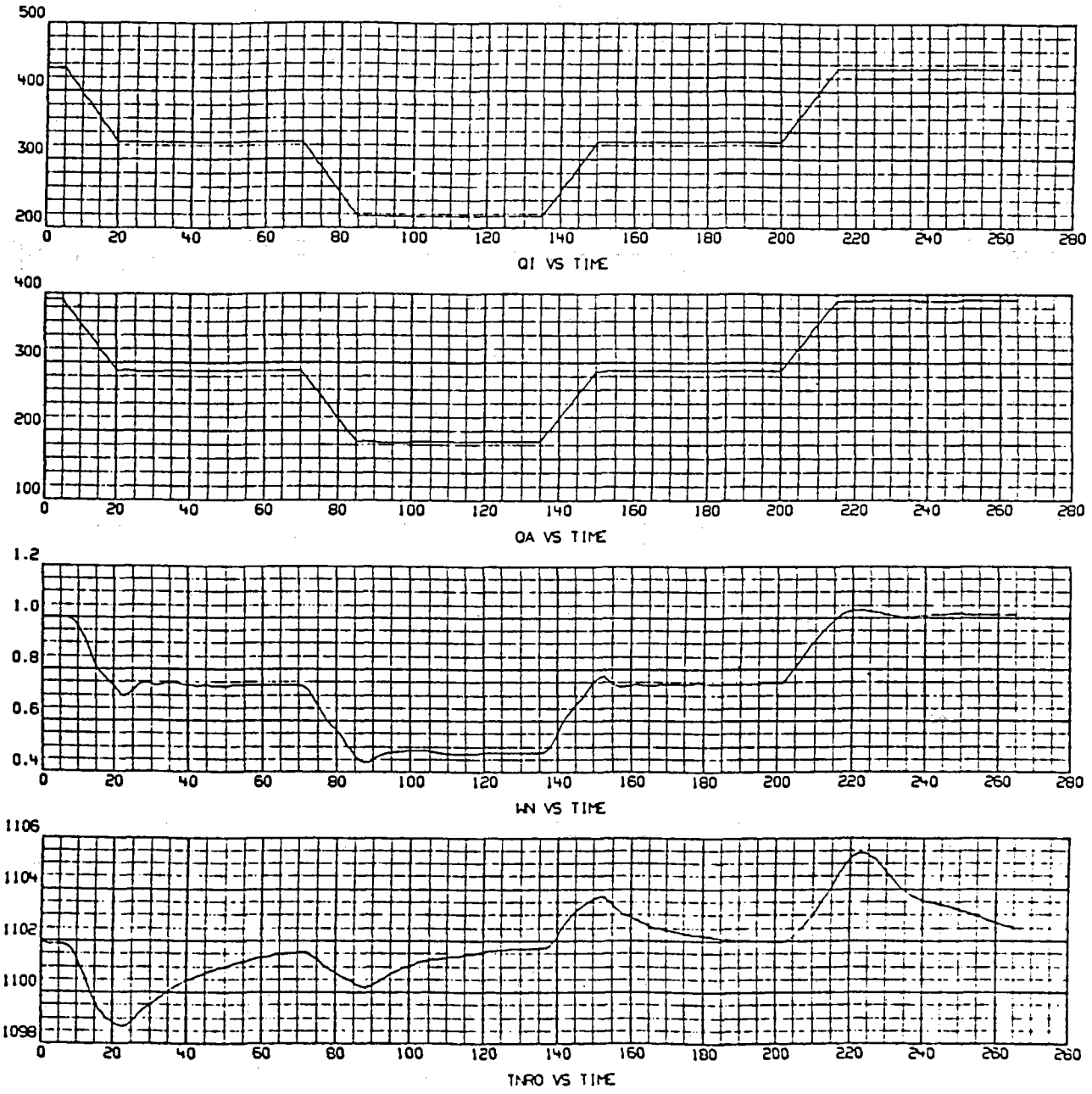
Figure 2-13c.   Overall System Response to the Transients Using Model
(Sheet 3 of 7)

RUN 04-038 PUMP TRIP, DEFOCUS, RUNDOWN INC, 7-13-78
QI - TOTAL INCIDENT SOLAR POWER (MWT)
QA - TOTAL ABSORBED SOLAR POWER (MWT)
WN - TOTAL RECEIVER FLOW (LB/SEC)
TNRO - TEMPERATURE OF SODIUM RECEIVER OUTLET TANK (F)

*071759301
071378 0002
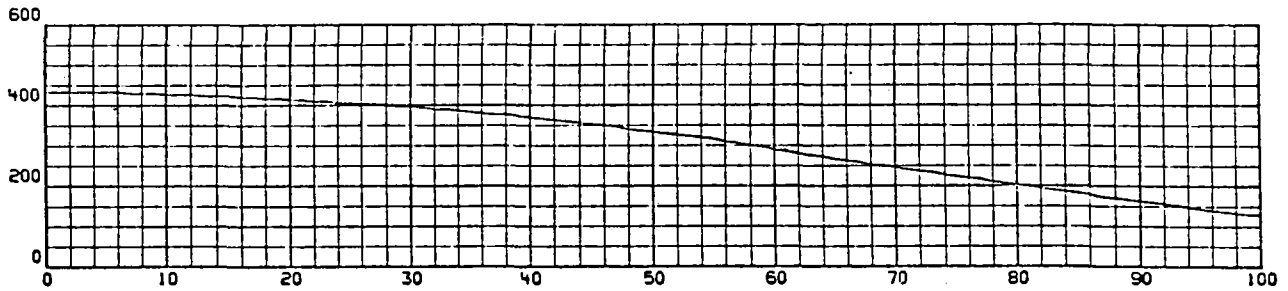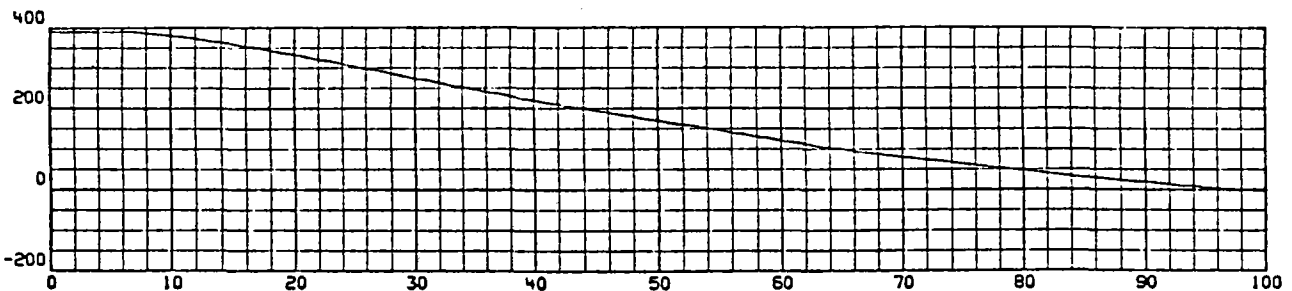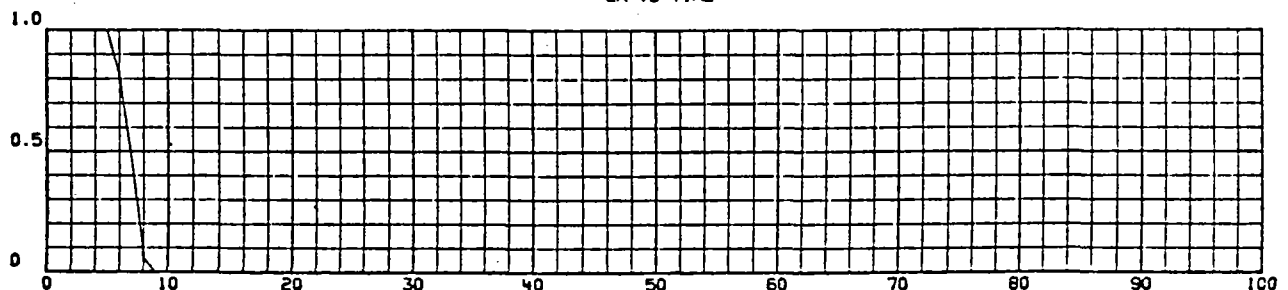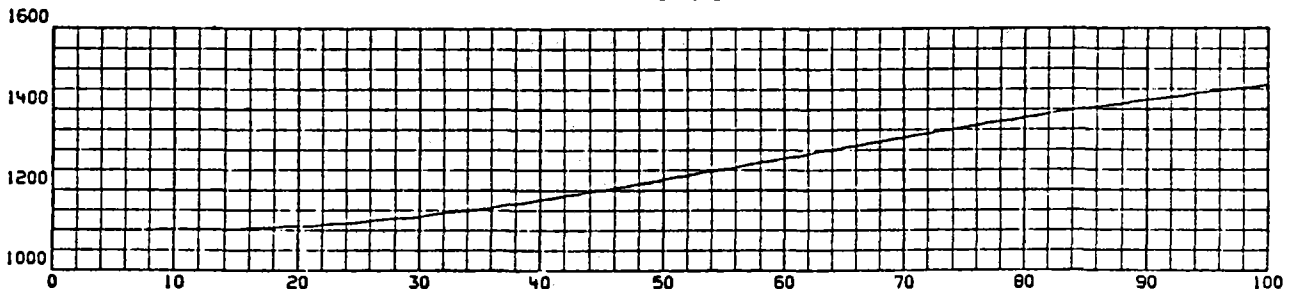
Figure 2-13d.   Overall System Response to the Transients Using Model
(Sheet 4 of 7)

ESG-79-2, Vol II, Book 1
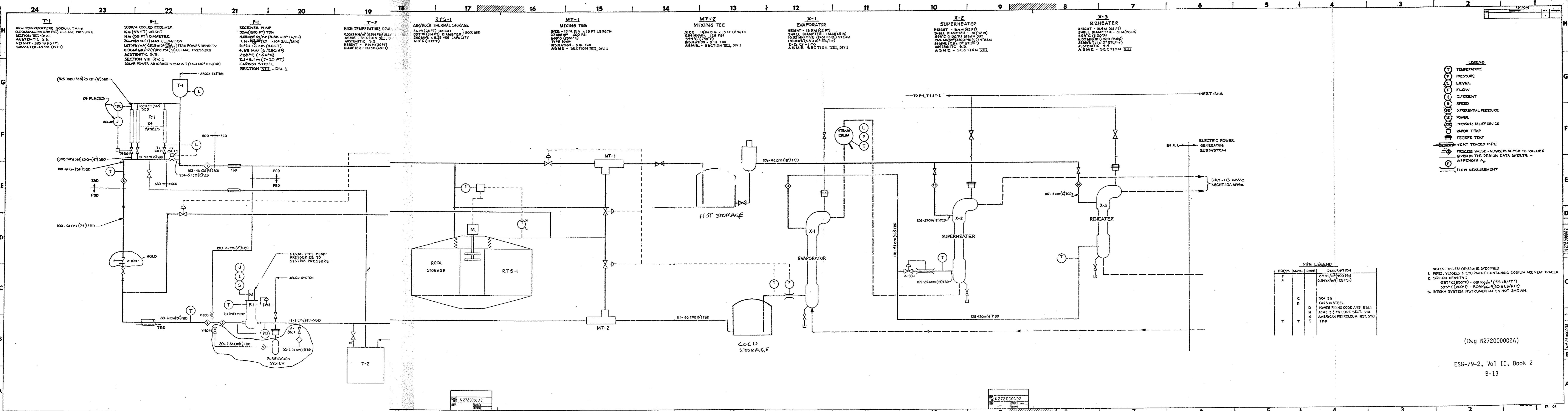
T-1
HIGH TEMPERATURE SODIUM TANK
0.00kN/m²(0.01 PSI) ULLAGE PRESSURE
SECTION VIII - DIV 1
AUSTENITIC S.S.
HEIGHT - 305 M (100 FT)
DIAMETER - 4.57 M (15 FT)

R-1
SODIUM COOLED RECEIVER
16 M (55 FT) HEIGHT
16.4 M (55 FT) DIAMETER
2.64 M (874 FT) MAX ELEVATION
1.47 MW/m² (1.3 x 10⁵ BTU/hr) PEAK POWER DENSITY
0.006 kN/m²(0.1 PSI(g)) ULLAGE PRESSURE
AUSTENITIC S.S.
SECTION VIII DIV 1
SOLAR POWER ABSORBED 4.13 MW/T (1.44 x 10⁸ BTU/hr)

P-1
RECEIVER PUMP
78 m³(900 FT³) TON
4.03 x 10⁶ kg/hr (8.88 x 10⁶ lb/hr)
1.28 m³/s (10 x 10⁶ GAL./MIN)
INLET 12.2 M (40 FT)
4.6 M MW (6,780 HP)
288°C (550°F)
Z.J=6.1 M (7 x 20 FT²)
CARBON STEEL
SECTION VIII - DIV 1

T-2
HIGH TEMPERATURE DRAIN
0.006 kN/m²(0.01 PSI) ULLAGE
55.7 M (234 FT) DIAMETER) ROCK BED
250 MW x 2.29 HRS CAPACITY
815°C (1135°F)

RTS-1
AIR/ROCK THERMAL STORAGE
7.C M (23 FT) WEIGHT

MT-1
MIXING TEE
0.54 M (21 IN DIA X 19 FT LENGTH
27 M (90 FT) 400 FW
399°C (730°F)
INSULATION - 8 IN THK
ASME - SECTION VIII, DIV 1

MT-2
MIXING TEE
SIZE - 18 IN DIA. x 18 FT LENGTH
0.54 M (90) 225 PSI
399°C (750°F)
INSULATION - 5 IN THK
ASME - SECTION VIII, DIV 1

X-1
EVAPORATOR
HEIGHT - 18.9 M (62 FT)
SHELL DIAMETER - 1.14 M (45 IN)
16.55 MW/m²(D (2400 PSIG) STEAM
170 MWt (5.8 x 10⁵ BTU/hr)
E.S C²= 1.00
ASME SECTION VIII, DIV 1

X-2
SUPERHEATER
HEIGHT - 18.9 M (62 FT)
SHELL DIAMETER - 80 (32 IN)
399°C (100) STEAM OUT
15.6 MW/m²(D (2100 PSIG) STEAM
84 MWt (2.8 x 10⁵ BTU/hr)
AUSTENITIC S.S.
ASME - SECTION VIII

X-3
REHEATER
HEIGHT - 18.9 M (62 FT)
SHELL DIAMETER - 80 (30 IN)
393°C (100°F)
6.99 MW/m²(D (1000 PSIG)
30 MWt (1.0 x 10⁵ BTU/hr)
AUSTENITIC S.S.
ASME - SECTION VIII

HOT STORAGE

ROCK STORAGE
RTS-1

COLD STORAGE

EVAPORATOR

SUPERHEATER

REHEATER

STEAM DRUM

MT-1

MT-2

X-1

X-2

X-3

TO P-1, T-1 & T-2

INERT GAS

ELECTRIC POWER GENERATING SUBSYSTEM

DAY-113 MWe
NIGHT-106 MWe

BY A.I.

HOLD

V-100

RECEIVER PUMP

PURIFICATION SYSTEM

FERMI TYPE PUMP PRESSURIZED TO SYSTEM PRESSURE

ARGON SYSTEM

T-1

T-2

LEGEND
- T TEMPERATURE
- P PRESSURE
- L LEVEL
- F FLOW
- I CURRENT
- S SPEED
- D DIFFERENTIAL PRESSURE
- E POWER
- PRESSURE RELIEF DEVICE
- VAPOR TRAP
- FREEZE TRAP
- HEAT TRACED PIPE
- PROCESS VALUE - NUMBERS REFER TO VALUES GIVEN IN THE DESIGN DATA SHEETS - APPENDIX A
- P FLOW MEASUREMENT

PIPE LEGEND
PRESS	MATL.	CODE	DESCRIPTION
F	N		2.7 kN/m²(400 PSI)
			0.84 kN/m²(125 PSI)
	C	B	304 S.S
			CARBON STEEL
H	K	T	POWER PIPING CODE ANSI B31.1
			ASME B & P.V CODE SECT. VIII
			AMERICAN PETROLEUM INST. STD.
	T		TBD

NOTES: UNLESS OTHERWISE SPECIFIED
1. PIPES, VESSELS & EQUIPMENT CONTAINING SODIUM ARE HEAT TRACED.
2. SODIUM DENSITY:
   288°C (550°F) - 881 kg/m³ (55 LB/FT³)
   593°C (1100°F) - 809 kg/m³ (50.6 LB/FT³)
3. STEAM SYSTEM INSTRUMENTATION NOT SHOWN.

ESG-79-2, Vol II, Book 2
B-13

(Dwg N272000002A)

N272000002

RUN 04-04 DRAG VALVE FAILS OPEN, NO DEFOCUS, 7-03-78
QI - TOTAL INCIDENT SOLAR POWER (MWT)
QA - TOTAL ABSORPED SOLAR POWER (MWT)
WN - TOTAL RECEIVER FLOW (LB/SEC)
TNRO - TEMPERATURE OF SODIUM RECEIVER OUTLET TANK (F)

QI VS TIME

OA VS TIME

WN VS TIME

TNRO VS TIME

Figure 2-13e.   Overall System Response to the Transients Using Model
(Sheet 5 of 7)

ESG-79-2, Vol II, Book 1

RUN 04-05 DRAG VALVE FAILS CLOSED, NO DEFOCUS, 7-03-78
QI   - TOTAL INCIDENT SOLAR POWER (MWT)
QA   - TOTAL ABSORBED SOLAR POWER (MWT)
WN   - TOTAL RECEIVER FLOW (LB/SEC)
TNRO - TEMPERATURE OF SODIUM RECEIVER OUTLET TANK (F)

•071758301
070678 0002

QI VS TIME

QA VS TIME

WN VS TIME

TNRO VS TIME
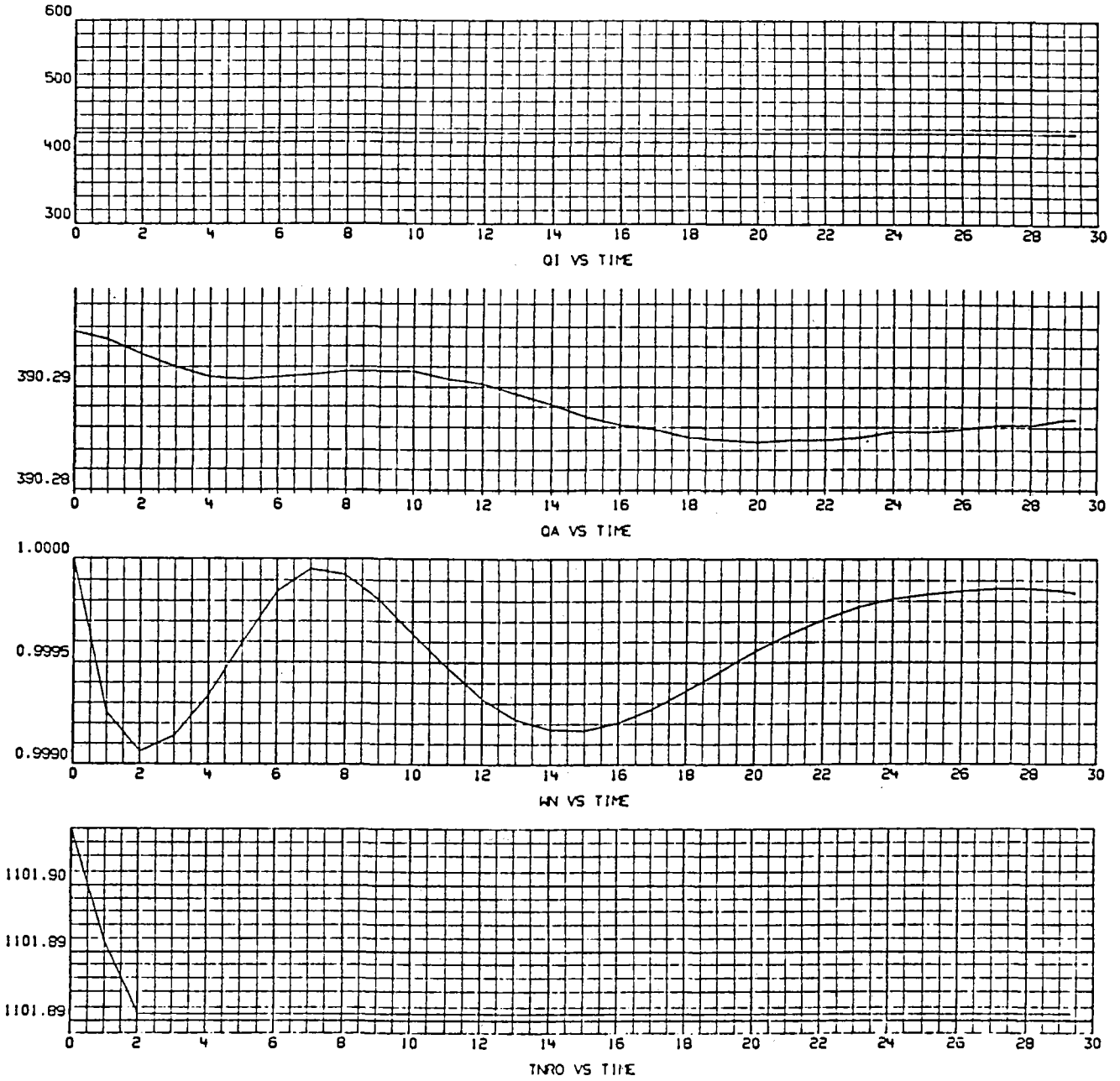
Figure 2-13f. Overall System Response to the Transients Using Model
(Sheet 6 of 7)

ESG-79-2, Vol II, Book 1

2-30

RUN 04-10 EMERGENCY SHUTDOWN, 08-09-78
QI - TOTAL INCIDENT SOLAR POWER (MWT)
QA - TOTAL ABSORBED SOLAR POWER (MWT)
WN - TOTAL RECEIVER FLOW (LB/SEC)
TNRO - TEMPERATURE OF SODIUM RECEIVER OUTLET TANK (F)

QI VS TIME

QA VS TIME

WN VS TIME

TNRO VS TIME
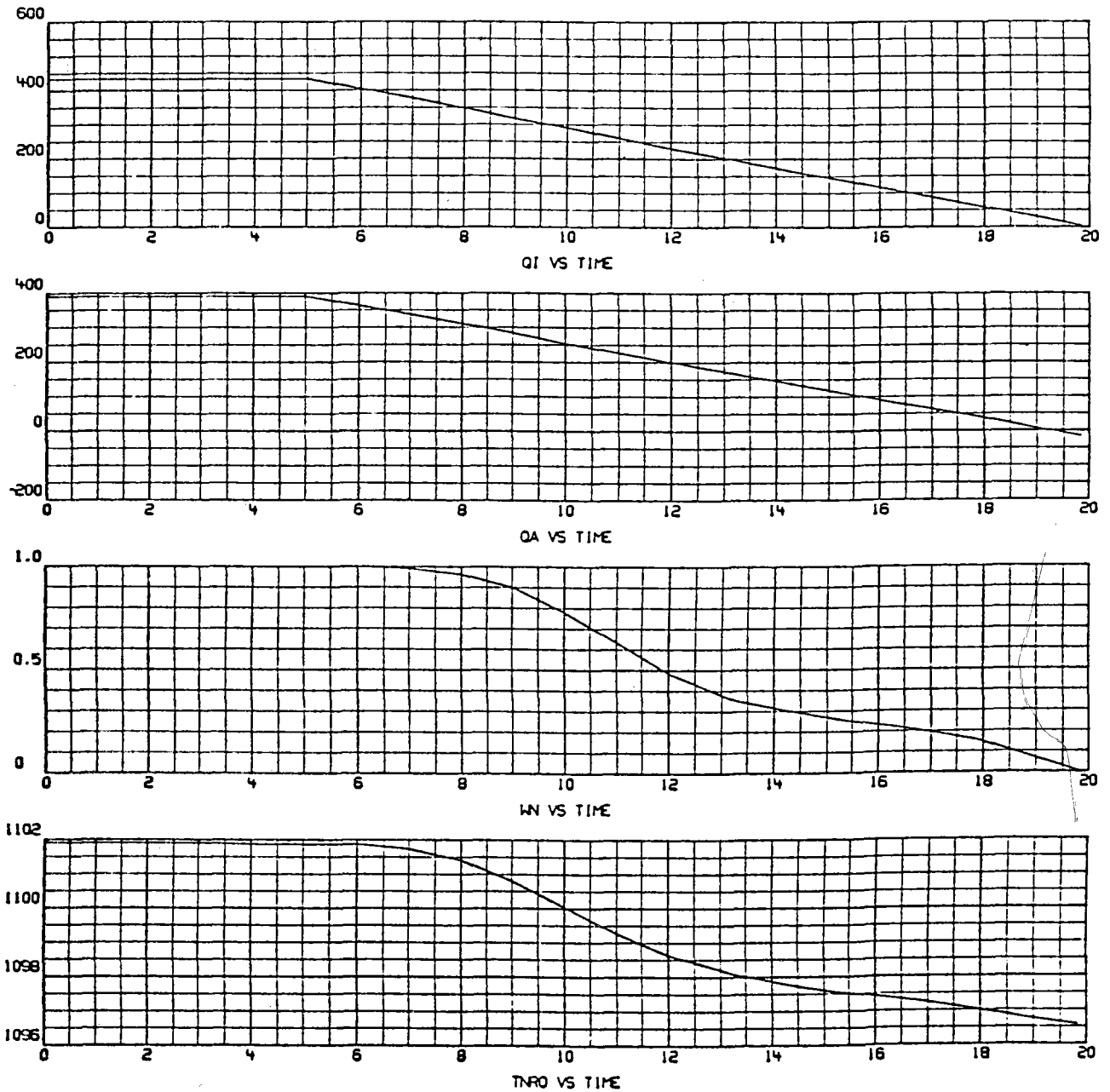
Figure 2-13g.   Overall System Response to the Transients Using Model
(Sheet 7 of 7)

ESG-79-2, Vol II, Book 1

exceeds 1500°F and several of the north panels vaporize sodium. It was concluded from this run that active heliostat steer-off is required to protect the receiver following a pump trip.

During the drag valve failure simulation, two cases were considered: failed open and closed. In both cases, the receiver outlet tank temperature variation was insignificant. During the failed open case, the tank drains down to the 1-ft level after 100 seconds. This is satisfactory so long as the opening of the drag valve is not followed by a pump trip. However, if the valve fails closed, the tank will fill in about 25 seconds. Active steer-off and subsequential pump trip will be required during this time to prevent receiver flow stoppage.

The final transient examined was an emergency shutdown in which active heliostat steer-off is employed. In this run, the outlet tank temperature varied <6°F.

A summary of the significant parameters of all runs is shown in Table 2-6.

From these studies, it is concluded that the conceptual control scheme as included in the current design is acceptable. However, active defocus of the collector field is required to prevent overheating of the north side receiver panels following a pump trip.

2.5 UTILITY COMMENTS ON SODIUM-COOLED ACR SYSTEM

This section is primarily directed toward utility viewpoints on the sodium-cooled solar central receiver concept. A 1-day meeting was held in Phoenix on March 10, 1978, to review a number of operational, costing, and sodium-use aspects of the program. Also, a 1-day tour and briefing was held at the Energy Systems Group on May 18, 1978, to review the state of the art of sodium technology and to observe the status of large-scale sodium systems. Salt River Project (SRP) had representatives from management, engineering, operations, generation planning,

TABLE 2-6

TRANSIENT PARAMETER SUMMARY

Transient	10% Step	Cloud Cover	25% Step	Pump[†] Trip	Drag Valve Failure	Emergency Shutdown
Receiver Outlet Variation ($^\circ$F)	6	5	6	>400	NA	8
Panel Outlet Variation ($^\circ$F)	12	NA	25	>500	NA	12
Tube Ramp* ($^\circ$F/s)	8	NA	20	>160	NA	5
Maximum Receiver Inlet Pressure (psia)	100	NA	150	70	70	170
Receiver Outlet Tank Level Variation ± ft	0.4	NA	2.5	0.2	5	1
Minimum Receiver to Inlet Pressure (psia)	70	70	70	33	70	70

*All controlled tube ramps lasted less than 100°F.
†Uncontrolled transient.

and safety present at these meetings. Some of the key questions posed and answered at these sessions were as follows:

Engineering:

1) What method of economic analysis is used by SRP for tradeoff studies, equipment selection, etc.? SRP uses the present worth of revenue requirements approach for most evaluations of this type.

2) What is the tradeoff between capital investment and one operator? For a 30-year plant life and SRP revenue requirements, the capital value of an operator is about $600,000. Using private utility financial parameters, this value would drop to $300,000 to $400,000.

3) A discussion was held on the use of stainless steel in the steam cycle. SRP opined that there is no particular concern if metals are properly applied and correct water chemistry control is adhered to.

4) On questions relating to initial steam temperatures and pressures, SRP believes that the selection of 1800 psig, 1000°F, 1000°F for

the conceptual design is very appropriate for this size and class of plant. Final design selection does involve an economic trade-off study, but from an operational standpoint these conditions have the best experience record.

Operations:

1) What is the minimum staff for a late shift? Per our practice, one would require three people for the turbine-generator and steam portion of the plant.

2) What is the minimum load for a 100 MW plant? For SRP, the minimum load for 100 MW units is about 19 MW's, using full arc admission on the turbine.

3) What is SRP's overhaul schedules? SRP schedules a major overhaul after approximately 26,000 operating hours, and this overhaul would be for about 6 weeks. Every year we have a 2-week minor overhaul.

4) What are the emergency power requirements for a 100 MW plant? Generally, the requirements would be in the order of 200 to 300 hp. Also, an engine-driven fire pump is commonly required.

5) Considerable discussion was held on daily cycling. Particularly with 1800 psig, $1000^\circ F/1000^\circ F$ class machines, SRP has avoided this type of operation. It is pretty well established that standard steam turbines are not capable of cycling daily without risking very high maintenance costs due to thermal cycle fatigue and corrosion. Hence, the all-night plant would be SRP's preference. However, the total economics, including reliability and availability considerations, would need to be reviewed in order to make a final decision.

6) What are startup times for a 100 MW turbine-generator? For a cold turbine, it would require 2 h to synchronize, and another hour to reach full load. For a hot turbine, if heat source is not constrained, it takes about 5 min to resynchronize and 15 to 30 min to full load. For an overnight shutdown, with unconstrained heat source, it takes 0.5 h to synchronize and 1.16 h to full load.

7) Other factors such as spare parts inventory require-
ments, effects of lightning storms, etc., were
discussed.

Generation Planning:

Discussions in this category dealt with how a solar plant would fit into the
SRP system, viz, for base load, intermediate, or peaking service. Also, the
economics of heat storage were discussed. For the most part, these questions
went unanswered since quite detailed computer-aided studies would be required.
SRP is preparing a requirements document and time schedule to describe this work.

Safety:

The ESG was concerned about SRP's acceptance of sodium as a heat transfer
medium from both a safety and operational standpoint. The ESG showed movies on
these matters at the March 10th meeting. Detailed discussions were held at the
ESG on May 18, 1978.

The enclosed internal memo from SRP indicates that they would have no funda-
mental concern with the use of liquid sodium as a heat transfer fluid in a utility
power plant.

AVOID VERBAL ORDERS
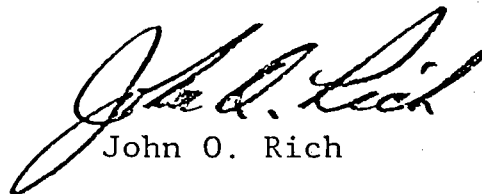
Date __May 26, 1978__

FROM __John O. Rich, Assistant General Manager - Power Operations__

TO __S. M. Chalmers, Director of Engineering - Power Engineering__

SUBJECT: __Atomics International Solar Energy Project and Acceptability__
__of Sodium as a Heat Transfer Fluid for Electric Utility__
Operation

Our review of pure metallic sodium as a heat transfer fluid shows that
it is acceptable for use in a power plant fluid cycle. This response
assumes that the design, construction, operation and maintenance ac-
tions are specially designed to eliminate the several negative fea-
tures of a sodium heat transfer fluid.

We have seen a number of techniques in the solar plant design and at
the Atomics International liquid metal test site in the Santa Susana
Mountains which appear to solve the problems of toxicity, flammability,
and corrosiveness. Further knowledge of those techniques will be re-
quired before completion of the final design.

Specific construction, operation and maintenance procedures must be
developed for any sodium system used in electric utility power plants.
At this time, we see no problems which cannot be managed without
reasonable design criteria and work procedures.

John O. Rich

DRS/pd

cc: R. E. Ayers
     Power Operations File
     Steam File

XC: R F Durning

3.0 RECEIVER

3.1 RECEIVER REQUIREMENTS

The receiver type selected for the reference plant is an external configuration. Studies made comparing cavity with external receivers showed that the latter led to lower capital costs and cost of power. The maximum absorbed thermal power is 390 MWt while the thermal power absorbed to generate 100 MWe is now 260 MWt during daylight.

The design lifetime of the receiver is 30 years although it is anticipated that panels may be replaced from time to time. The average maximum temperature reached by the receiver panels is 608°C (1125°F) when sodium storage is used. The flow rate is 3.66 x 10^6 kg/h (8.05 x 10^6 lb/h) with sodium storage.

The plant will be in Seismic Zone III. Both horizontal and vertical ground accelerations will be about 0.25 g. The nominal design wind at the receiver is 5.4 m/s (12.0 mph) while the maximum operating wind is 24.5 m/s (55 mph). The maximum survival wind velocity is 61.2 m/s (137 mph).

The receiver will be exposed to ambient temperatures in the range of -30°C (-22°F) to +50°C (122°F). The plan is to drain the receiver each night to prevent sodium freeze-up which occurs at 90°C (208°F). The receiver requirements are summarized in Table 3-1.

3.2 RECEIVER DESIGN CONSIDERATIONS

The receiver is a critical component in the ACR plant as it is the interface between the collector and the heat transport subsystems. The receiver is exposed to a heat flux in excess of 1000 suns. At any given instant the heat flux on the receiver varies by at least a factor of 30 at different locations. During the course of a day a typical point on the receiver will have an incident flux that varies by at least a factor of 4. The temperature difference across the tube wall receiving the greatest flux may be up to 100°C (180°F) while on the rear half of the same tube there will be little or no thermal gradient.

TABLE 3-1

RECEIVER REQUIREMENTS

Configuration	External
Maximum Thermal Power (MWt)	390
Nominal Thermal Power (MWt)	260
Lifetime (yr)	30
Maximum Temperature ($^\circ$C)	608
Startup Sodium Temperature ($^\circ$C)	150
Maximum Flow Rate (10^6 kg/h)	3.66
Seismic Environment (g)	0.25/0.25
Winds at Receiver (m/s)	
Nominal	5.4
Maximum Operating	24.5
Survival	61.2
Ambient Temperature Range ($^\circ$C)	-30 to +50
Thermal Control	Nighttime Drain

The heat flux on the receiver is such that a loss of coolant can cause severe overheating in a matter of seconds. The heat flux pattern on a panel varies in space and time such that the thermal stresses in a rigid panel can lead to deformation and failure. About 10% of the incident radiation will be lost to the surroundings, while about 5% of the arriving energy misses the receiver altogether. If the receiver is made smaller to reduce the heat losses, then the interception loss will increase; or if the receiver is made large to intercept more radiation, then the thermal losses will increase.

If a gap between receiver tubes occurs then the incident heat flux can seriously overheat any structures behind the tubes. Any uncooled strip of metal exposed to the heat flux has a chance of being overheated. Structures such as the tower top and receiver roof are vulnerable to stray radiation.

The receiver is exposed to all the elements such as rain, snow, hail, wind, lightning, and earthquake. It is in a relatively inaccessible location so that maintenance will be limited. While the receiver spends half the time exposed to a variable and intense heat flux, the rest of the time it is in darkness and is inactive. If hot sodium is circulated through the receiver at night, many operational problems are eased but the thermal losses become high. A thermal shroud can be used on the receiver at night but is a cumbersome and costly component. If the sodium circulation is stopped at night and no thermal shroud is used, the sodium will freeze in the receiver. While this is a feasible approach, it does make for a complex startup procedure each morning.

While a sodium-cooled receiver has many problems, it also has many favorable features. The sodium has a high heat transfer capability and can accept very high heat fluxes without causing excessive temperatures. The sodium is well below its normal boiling point (882°C or 1620°F) so remains as a dense liquid. The pressure of sodium in the receiver is only that due to gravity, so it reaches only 200 kPa (30 psi) at the base of the receiver where the sodium is relatively cool. Since the pressure and corrosion problems are minimal, the receiver walls can be relatively thin which reduces thermal stresses, thermal losses, and material costs.

3.3 CAVITY VS EXTERNAL RECEIVERS

At the initiation of this program, the baseline receiver configuration was the external type. The cavity receiver is an alternate approach that has certain advantages. One of the advantages of the cavity receiver is that it can capture the incident radiation more efficiently than the external receiver. Another is that it offers better thermal control and protection from the elements.

Trade studies of cavity and external receivers were made at both the system and component levels. The system comparison involves such factors as the receiver view factor, the size, shape, and orientation of the collector, spillage, atmospheric attenuation and tower height. The component comparison considers receiver size, weight, complexity, and cost.

19.00 M (62 ft-4 in.)
APERTURE

30 M (98.4 ft)

INLET HEADERS

UPPER TUBE BANK

SUPPORT/SNUBBER
(THERMAL EXPANSION)

SIDE TUBE BANK

OUTLET HEADERS

28.2 M
(92.5 ft)

19.00 M (62 ft-4 in.)
APERTURE

INLET HEADER

LOWER TUBE BANK

18 in. DOWNCOMER

24 in. RISER
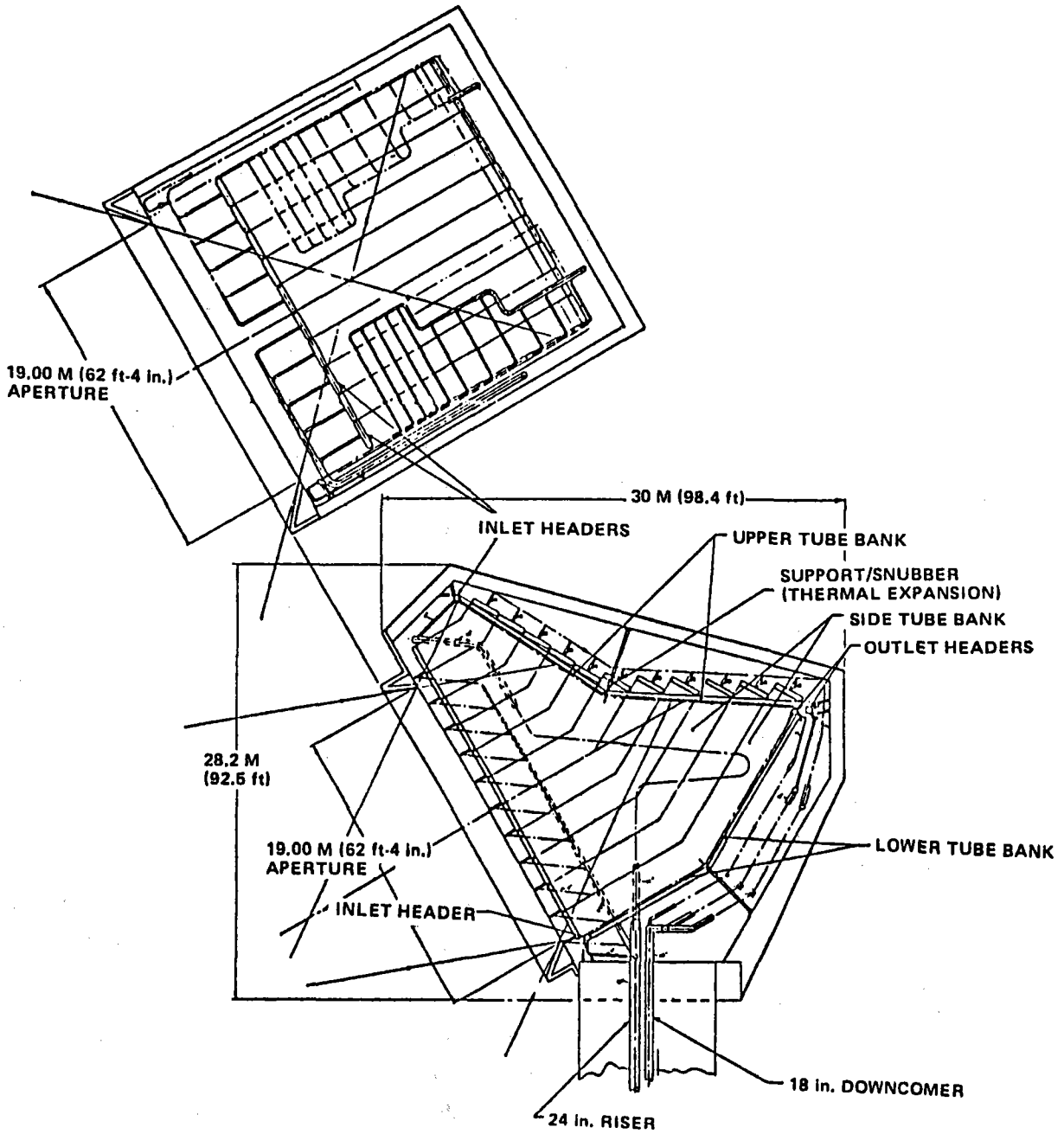
9272-39

Figure 3-1.   Cavity Receiver Concept Sodium Cooled
100-MWe Solar Plant

Since a baseline receiver was already in existence, comparable cavity receivers were designed. Consideration was first given to downward-facing receivers and one layout was made. The downward-facing receiver had a poor view factor which required an unreasonably high tower to capture the heat flux from the collector. There was some compensation in that the heliostat density could be fairly high. Another problem arising in downward-facing cavity designs is that there is interference between the incoming heat flux and the receiver support structure.

North-facing cavity receivers appear to be much more effective. Figure 3-1 shows one such design. Data from the University of Houston indicated that a receiver having a 30^0 downward tilt and a square aperture 19 m x 19 m would be satisfactory. It was decided to have the rear panels be oblique with respect to the incoming rays to keep the heat flux at the surface below the limit of 1.7 MWt/m^2. The receiver floor was originally intended to be uncooled as the incident flux would be reduced by the slant angle. However, there were heat losses involved such that the floor equilibrium temperatures were considerably hotter than the panels themselves. It was decided that cooling of the floor was the better approach. It was observed in this design that the 19 m x 19 m aperture was greater than the 16 m x 16 m dimensions of the baseline receiver. This was a result of the greater average distance of the heliostats and the inferior view factor of easterly and westerly heliostats.

The receiver in Figure 3-1 has a panel area of 1400 m^2 compared with 800 m^2 in the baseline external receiver. Even so, the thermal loss objective of 5.2% was not achieved. This was a result of the shallow depth of the receiver. Consequently, a second design was prepared which had a better capture capability. A layout of this design is shown in Figure 3-2, and its installation on a tower is shown in Figure 3-3. This receiver is box-shaped having a height of 24 m, a width of 24 m, and a depth of 16 m. This receiver traps the incident radiation more effectively and approaches the design goal of 5.2% loss.

This receiver has a total of 33 panels - six on the top, bottom, left side and right side, and nine on the rear face. All panels are identical having a
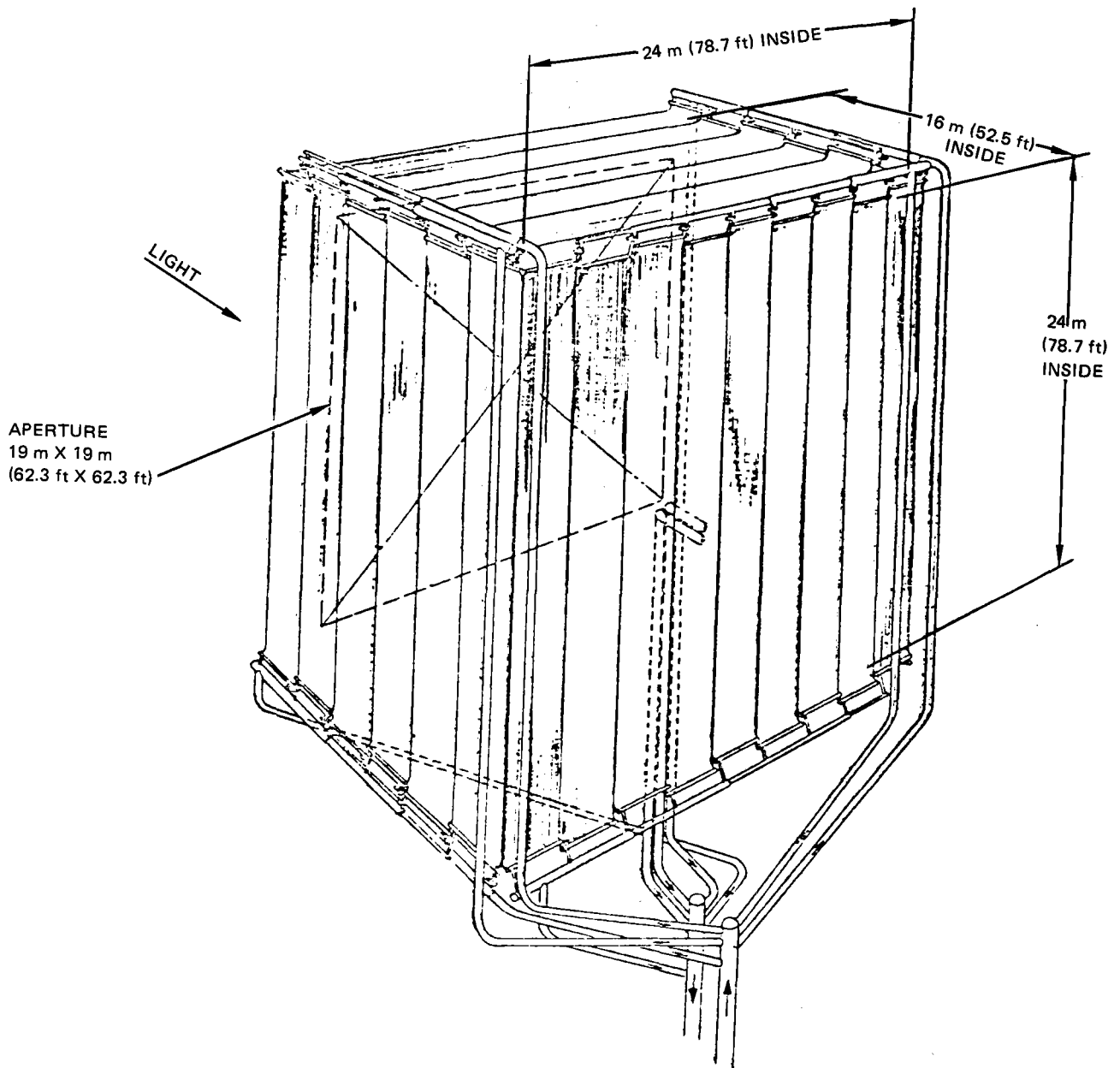
Figure 3-2. Cavity Receiver Concept

130 FT

WEATHER PROOF COVER

62.3 FT^2 APERTURE

$15°$

110 FT

75 FT DIA

879 FT

840 FT

SCALE: 1 in. = 100 ft

150 FT DIA

9272-41
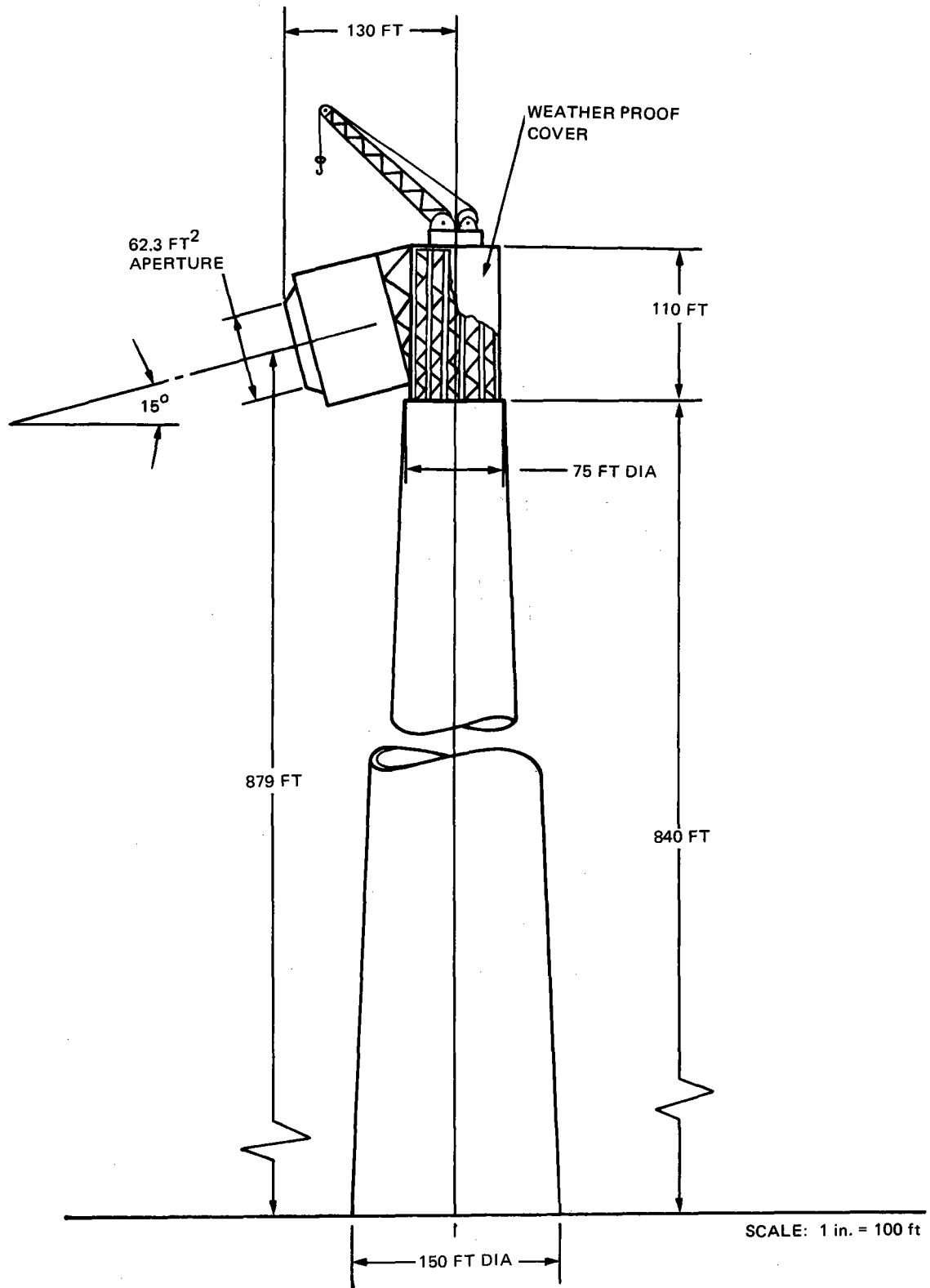
Figure 3-3. Cavity Receiver-Tower

length of 24 m (78.7 ft) and a width of 2.7 m (8.75 ft). The tubes are 1.91 cm (0.75 in.) OD with a 0.125 cm (0.049 in.) wall, there being 140 tubes per panel. The total panel area in this design is 2100 m^2 compared with 1400 m^2 in the previous concept and 800 m^2 in the baseline external receiver. The additional area and other complexity adds about $5 million to the cost of the receiver relative to the external receiver. However, the cavity design captures up to six percent more of the incident energy. Table 3-2 compares the larger cavity receiver with the baseline external receiver at the time the study was made.

TABLE 3-2

RECEIVER COMPARISON

	Cavity	External
Maximum/Normal Thermal Power (MWt/MWt)	390/260	390/260
Sodium Inlet Temperature ($^{\circ}$C)	288	288
Sodium Outlet Temperature ($^{\circ}$C)	593	593
Sodium Maximum Flow Rate (10^6 kg/h)	3.66	3.66
Aperture Size (m)	19 x 19	-
Tube Array Dimensions (m)	16 x 24 x 24	D = 16 H = 16
Tube Heated Area (m^2)	2112	804
Average Heat Flux (390 MWt), MWt/m^2	0.18	0.48
Peak Tube Wall Temperature ($^{\circ}$C)	612	635
Dry Weight (kg)	520,000	275,500
Thermal Loss (260 MWt, std. Wind, %)	5.2	10.9

Cavity receivers have better thermal control characteristics and tend to protect the panels from the elements — wind, rain, snow, hail, low temperatures, etc. However, to take full advantage of its enclosed configuration, a cavity receiver would require some form of closure for the large aperture. As presently envisioned, an external receiver would be drained to the tower-receiver interface to provide thermal control at night. It is not clear that the cavity receiver has a marked advantage in regard to thermal control.

The external receiver has several overall plant advantages. One is that for a given power the tower is shorter and less expensive. Another is that the average distance of the heliostats is less. This leads to less atmospheric absorption, less shading and blocking, and less spillage of collected energy. The external receiver was selected as the baseline for the remainder of the program chiefly because of these overall plant advantages, but also because it is a smaller, simpler, and lower-cost receiver.

3.4 RECEIVER PANEL THERMAL ANALYSIS

A preliminary thermal analysis of the baseline receiver sodium cooled panels has been performed. The incident heat flux was obtained from the University of Houston for the case of equinox noon. These data plotted in normalized form are shown in Figure 3-4 for the north, east-west, and south panels.
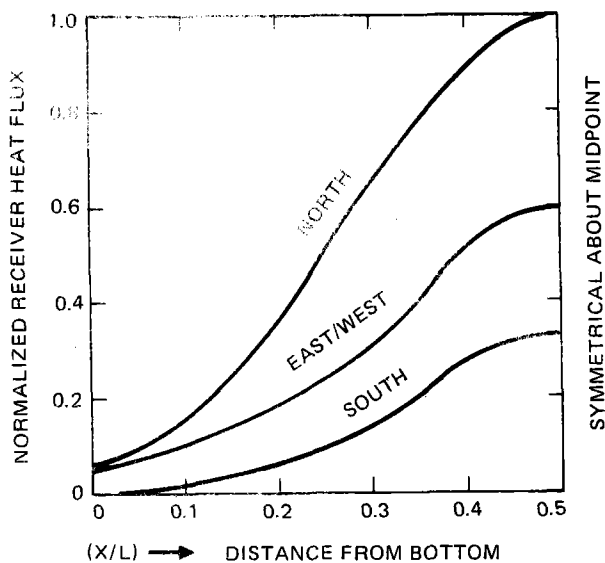
Figure 3-4. Normalized Receiver Heat Flux Profiles Based on Equinox Noon

9272-42

The baseline power at the time of the analysis was 429 MWt. The sodium inlet and outlet temperatures were 288°C (550°F) and 594°C (1100°F), respectively. The receiver flow rate at this maximum power condition was 3,975,000 kg/h (8,744,500 lb/h).

The receiver had 24 panels, each consisting of 110 tubes, there being 2640 tubes in all. Each tube had an outside diameter of 0.75 in. and a wall thickness of 0.049 in. These tubes were made of Type 304 stainless steel.

The receiver was divided into four quadrants - north, east, west, and south. At equinox noon, the characteristics of the east and west quadrants were identical. Each of the four quadrants was analyzed on the basis of its average properties. Table 3-3 shows the flow fraction, flow rate, and heat input for each quadrant.

TABLE 3-3

RECEIVER QUADRANT FLOW AND HEAT INPUT

Quadrant	Flow Fraction	Flow Rate (kg/h)	Heat Input (MWt)
North	0.425	1.69×10^6	182
East	0.235	0.93×10^6	101
West	0.235	0.93×10^6	101
South	0.105	0.42×10^6	45

where (in consistent units)

$Nu = hD/K_w$

$Pr = C_p u/K_w$, the Prandtl Number

$Re = D\rho V/u$, the Reynolds Number

h = sodium heat transfer coefficient

D = tube diameter

Cp = specific heat of sodium

μ = viscosity of sodium

K_w = thermal conductivity of sodium

ρ = sodium density

V = sodium velocity

The heat transfer correlation for sodium flowing in tubes was:

$$Nu = 7.0 + 0.025 \ (PrRe)^{0.8*},$$

Each panel will have the flow metered by the panel control valves so that the outlet temperature is very nearly a constant. Thus, the flow velocity will vary among the panels from 0.933 m/s (3.06 f/s) in the south quadrant to 4.05 m/s (13.3 f/s) in the north quadrant. Because of the temperature and velocity variations, the sodium heat transfer coefficient will range from 30260 W/m^2-K (5337 Btu/h-ft^2-^{0}F) at the hot end of the south quadrant to 52170 W/m^2-K (9201 Btu/h-ft^2-^{0}F) at the cool end of the north quadrant.

K_w varies from about 18.2 W/m-K (10.5 Btu/h-ft-^{0}F) to 22.3 W/m-K (12.9 Btu/h-ft-^{0}F) from the cool inlet of the receiver to the hot exit. The conductance across the wall thickness is K_w/x, where K_w is the thermal conductivity of the wall and x is the wall thickness.

The overall heat transfer coefficient, U, is:

$$U = \cfrac{1}{\cfrac{x}{K_w} + \cfrac{1}{h}} \ .$$

This coefficient is controlled more by the wall conductance than it is by the sodium conductance. Values of U range from 9871 W/m^2-K (1741 Btu/h-ft^2-^{0}F) at the cold end of the south quadrant to 12179 W/m^2-K (2148 Btu/h-ft^2-^{0}F).

The ΔT between the outer tube surface and the bulk sodium was calculated assuming that one-half of each tube surface is available for heat transfer and using the values of U at each point on the receiver. The maximum ΔT's ranged from 35.3^{0}C (63.6^{0}F) at the midpoint of the south quadrant to 96.3^{0}C (173.4^{0}F) in the north quadrant. Figure 3-5 shows the ΔT's at various points on the baseline receiver. When these ΔT's are added to the local sodium temperatures, then the

---

*W. H. McAdams, "Heat Transmission," Third Edition (1954), McGraw-Hill, p. 213

peak metal temperatures at all points on the receiver are obtained. Figure 3-6 shows these temperatures.
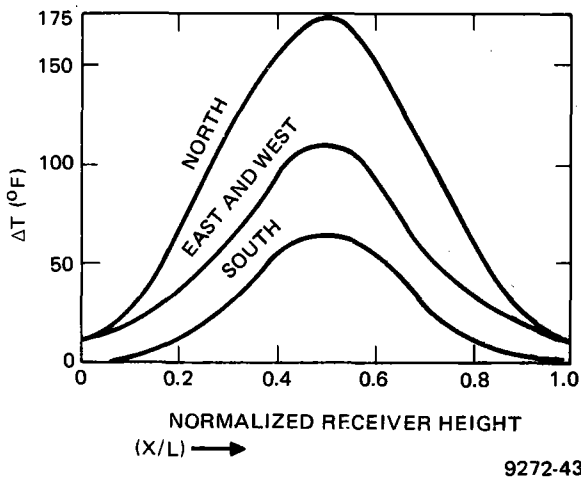
Figure 3-5. ΔT Through Tube Wall and Sodium Film

9272-43

Since this analysis was performed, the maximum receiver power has been reduced from 429 to 390 MWt. On the other hand, since the temperatures of the north quadrant represent an average case, the peak temperature in that quadrant will be somewhat greater. The current peak ΔT is estimated to be $119^{\circ}C$ ($214^{\circ}F$), and the peak metal temperature will be $618^{\circ}C$ ($1144^{\circ}F$) instead of the $608^{\circ}C$ ($1125^{\circ}F$) shown in Figure 3-6.

3.5 EXTERNAL RECEIVER THERMAL LOSSES

A study was made of the thermal losses that occur in an external receiver. This effort was part of the comparison being made of cavity and external receiver performance characteristics. Table 3-4 lists the assumptions used in this study. Figure 3-4 shows the equinox noon receiver incident power distribution which was adapted to the current baseline 16 by 16-in. receiver. The receiver model was divided into eighty small sections, each of which was losing heat to the surroundings by reflection, radiation, and convection.
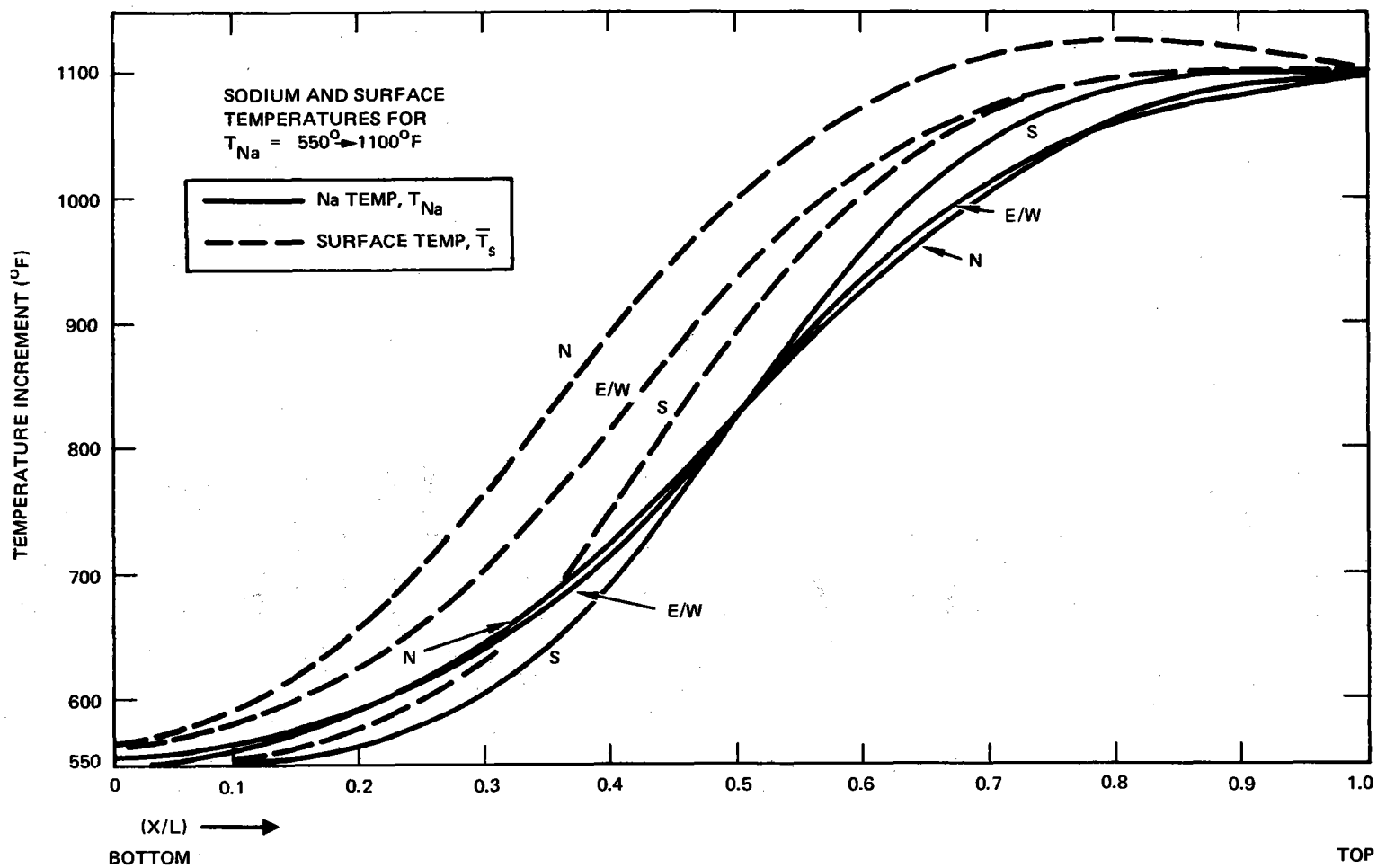
Figure 3-6.   Axial Temperature Distribution on Solar Panel Tubes

TABLE 3-4

ASSUMPTIONS FOR THERMAL LOSS STUDY

Equinox, Noon Incident Power Distribution

$288^{O}C$ Sodium In, $593^{O}C$ Sodium Out

Four Azimuthal Quadrants

Twenty Vertical Sections

Solar Absorptance in Pyromark = 0.95

Emittance = 0.90 Effective

Roughness of Cylinder = 60×10^{-5}

Achenbach Heat Transfer Correlation Plus Natural Convection

Winds from 0 to 16 m/s (36 mps)

The radiation emittance chosen was 0.90, which is somewhat conservative. For the convection heat transfer, the correlation of Achenbach was used. The Achenbach experiments were performed at a high Reynolds number, but not quite as high as the value of 10^{7} that could be reached by an external receiver in a high wind. The effects of natural convection were added to the forced convection value.

Figure 3-7 shows the thermal losses as a percent of the incident power for the design wind condition of 3.5 m/s at 10 m or 5.7 m/s at the receiver elevation. At the yearly average incident thermal power of about 325 MWt, the total loss is about 10.1%. The part contributed by the convection process is about 1.3%. Figure 3-8 shows the thermal losses at a wind velocity of 7 m/s at 10 m (11 m/s at the receiver). The total loss at 325 MWt is 10.7% of which convection is 2.0%.

Figure 3-9 shows the effect of receiver wind velocity on thermal losses for various receiver absorbed thermal power levels. Finally, in Figure 3-10, thermal losses are shown as a function of the wind frequency probability as taken from the program specifications. As can be seen, high wind losses occur only a small fraction of the time. At low wind velocities ($\leq$4 m/sec), which occur almost 50%
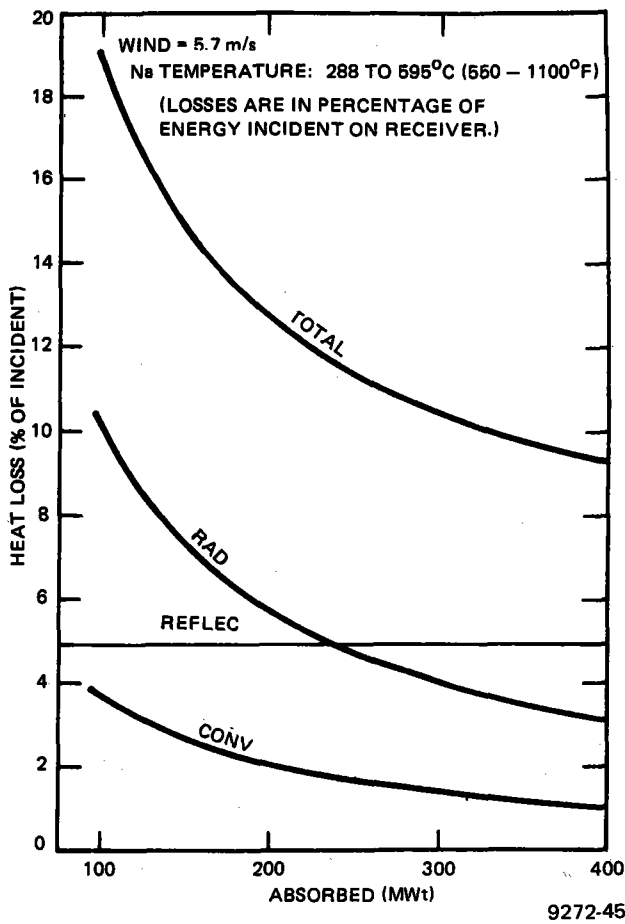
Figure 3-7. Heat Losses
From Receiver
(Wind = 5.7 m/s)

Figure 3-8. Heat Losses
From Receiver
(Wind = 11.0 m/s)
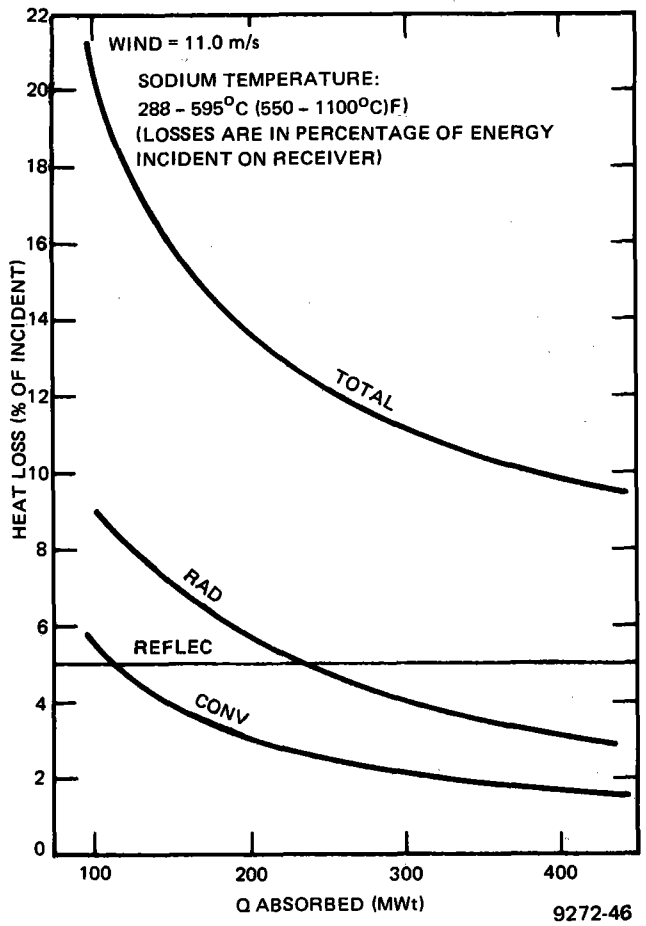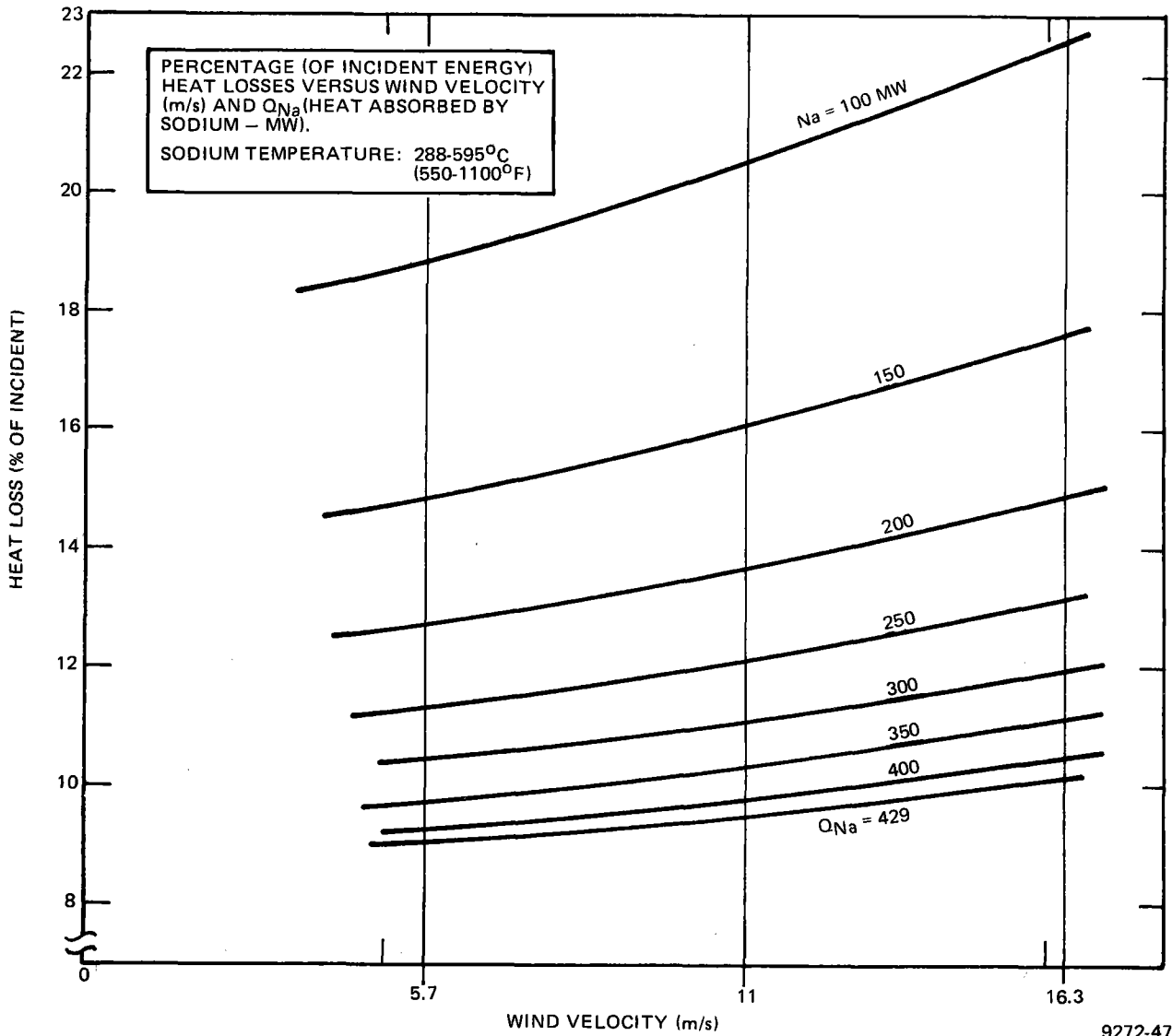
Figure 3-9. Heat Losses From Receiver (As a function of wind velocity)
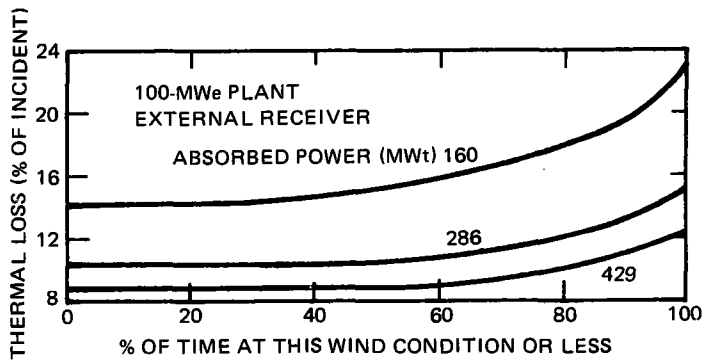
Figure 3-10. Thermal Loss as Affected by Specification Wing Velocity Frequency

of the time, the convective heat transfer is very nearly controlled by natural convection processes. Further studies of thermal losses are planned as optimization of the receiver proceeds.

3.6 EFFECT OF LIGHT LEAKAGE BETWEEN TUBES

The baseline receiver panel uses seamless tubing to absorb the incident energy, although other panel configurations are being studied. One problem associated with tubes is the possibility that the tubes may separate. The incident heat flux may enter through gaps between tubes and damage structures within the receiver.

An analysis has been performed to determine the heating that can occur when such gaps are present. Figure 3-11 shows the normalized heat flux that will reach the midpoint of a north panel at equinox noon. Also shown is the heat flux integrated with respect to the incident angle. The actual heat is 1.7 MWt/m^2. Later in the program, the heat flux was determined to be only 1.40 MWt/m^2. Figure 3-12 shows the tube geometry which is set by three dimensions - the tube diameter, the gap between tubes, and the distance to the structure in question. It was assumed that the structure radiated heat to the surroundings but that thermal conduction did not occur.
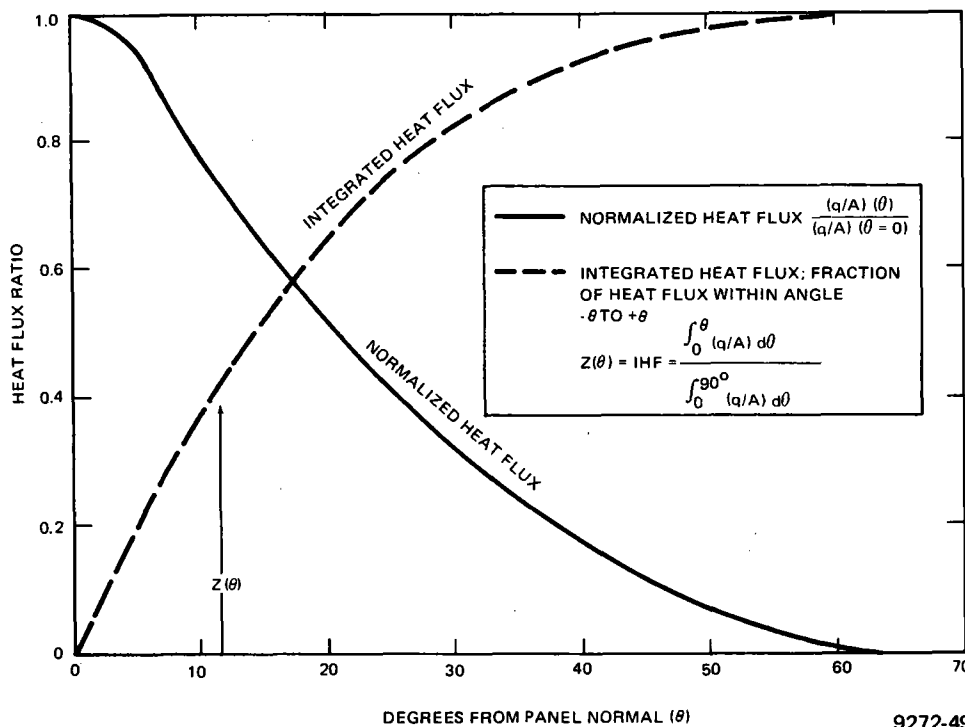
Figure 3-11. Heat Flux Distribution and Integrated Heat Flux

9272-49
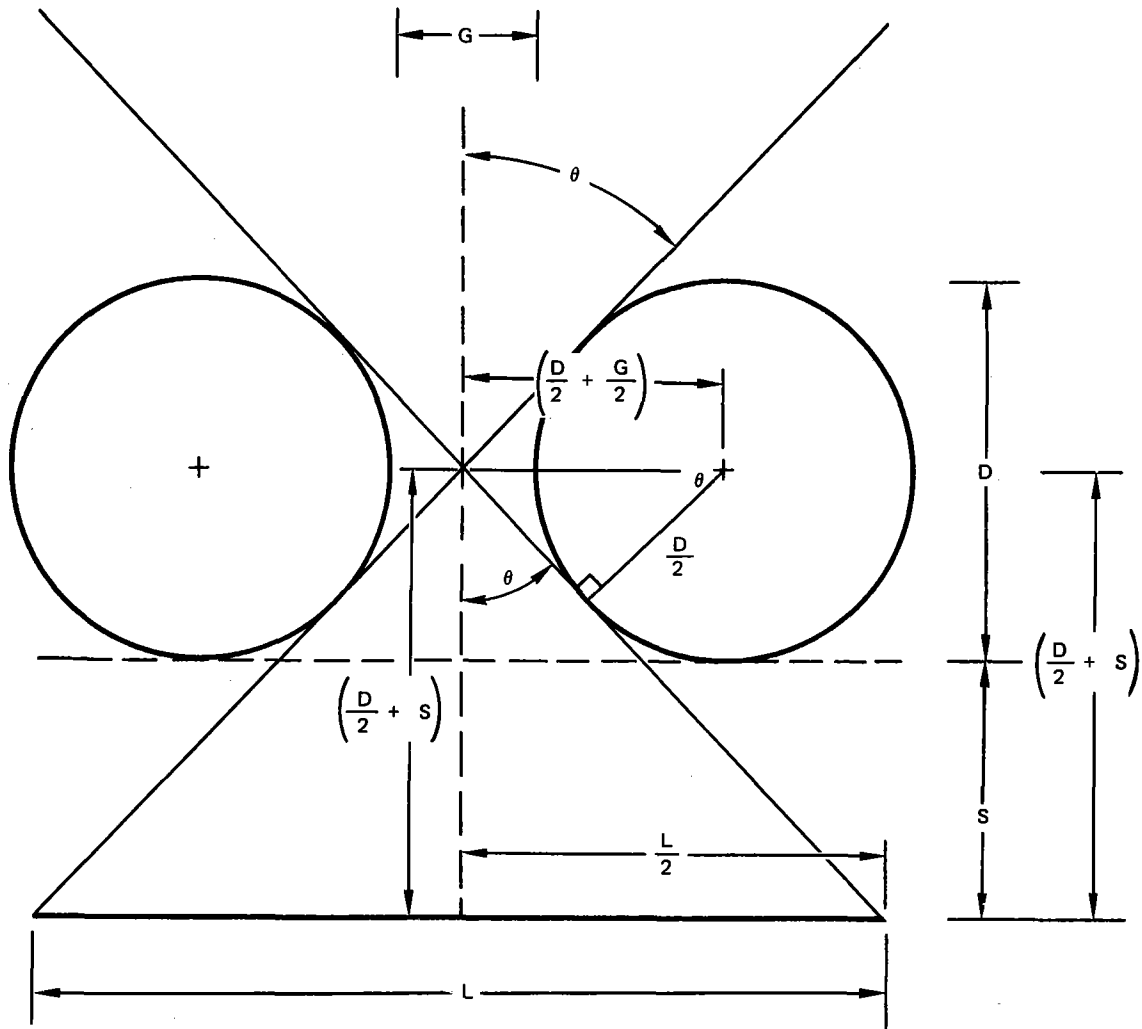
$$\cos \theta = \frac{D}{D+G} \quad \tan \theta = \frac{L}{D+2S} = \frac{\sqrt{(D+G)^2 - D^2}}{D}$$

$$\theta \text{ (HALF ANGLE)} = \cos^{-1}\left(\frac{D}{D+G}\right) = \tan^{-1}\left(\frac{\sqrt{(D+G)^2 - D^2}}{D}\right)$$

$$L = (D+2S)\tan\theta = (D+2S)\frac{\sqrt{(D+G)^2 - D^2}}{D}$$

9272-50

Figure 3-12. Tube-Gap Geometry, Basic Equations

Figure 3-13 shows the result of calculating the heat flux incident on structures at various distances from the tubes and for various gaps between tubes. The structure was assumed to radiate into one hemisphere with a sink temperature of 482°C (900°F). The structure equilibrium temperatures shown in Figure 3-13 show that large gaps (such as 1/4-in.) can lead to overheating, while even narrow gaps (such as 10 mils) may overheat nearby structure. If heat fluxes lower than the 1.7 MWt/m^2 used in this study were assumed, and if thermal conduction in the structure were considered, the results would be more favorable. Nevertheless, this study shows a light-tight receiver should be a design goal to avoid overheating of structures.
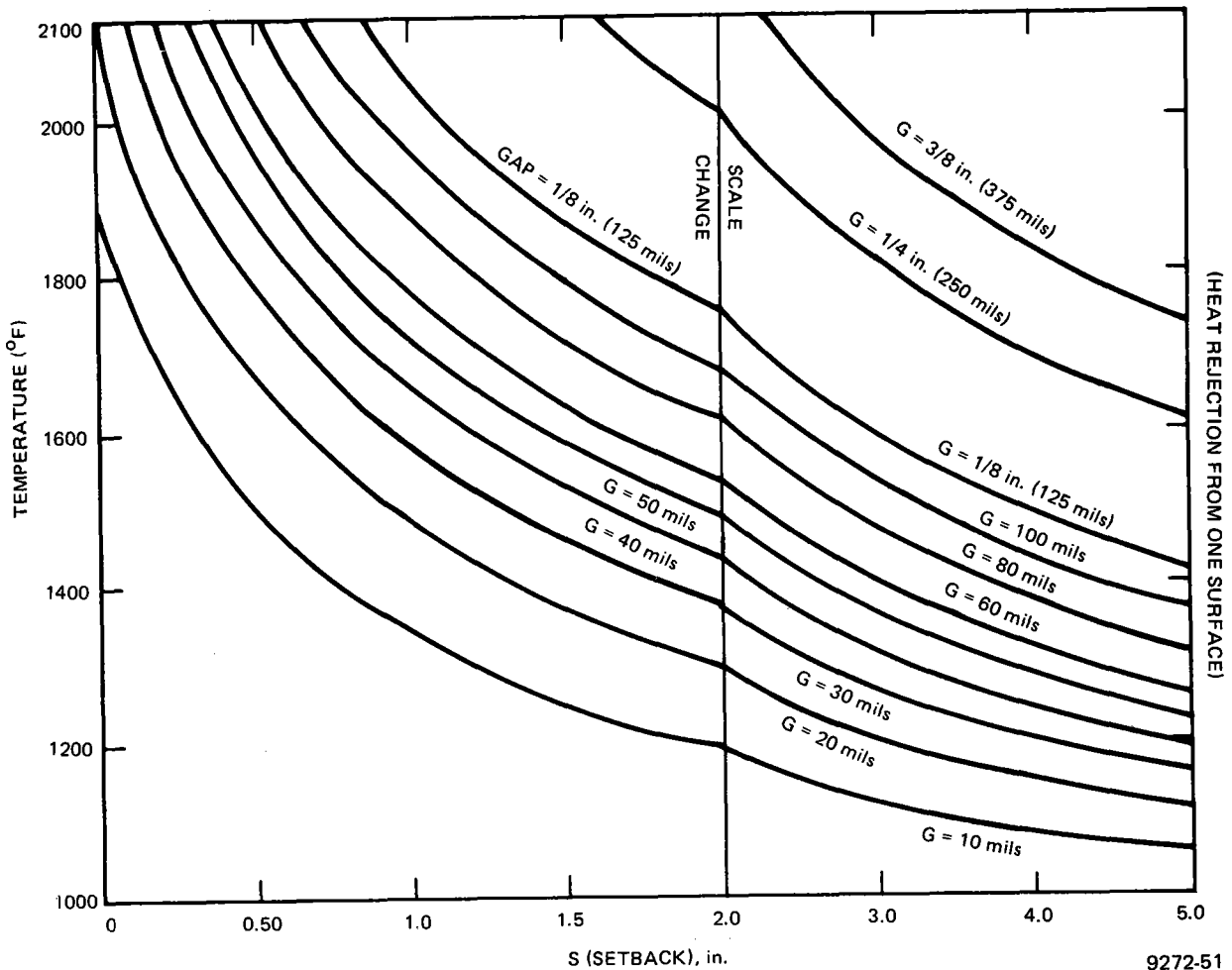
Figure 3-13. Equilibrium Temperature vs Setback and Gap Size
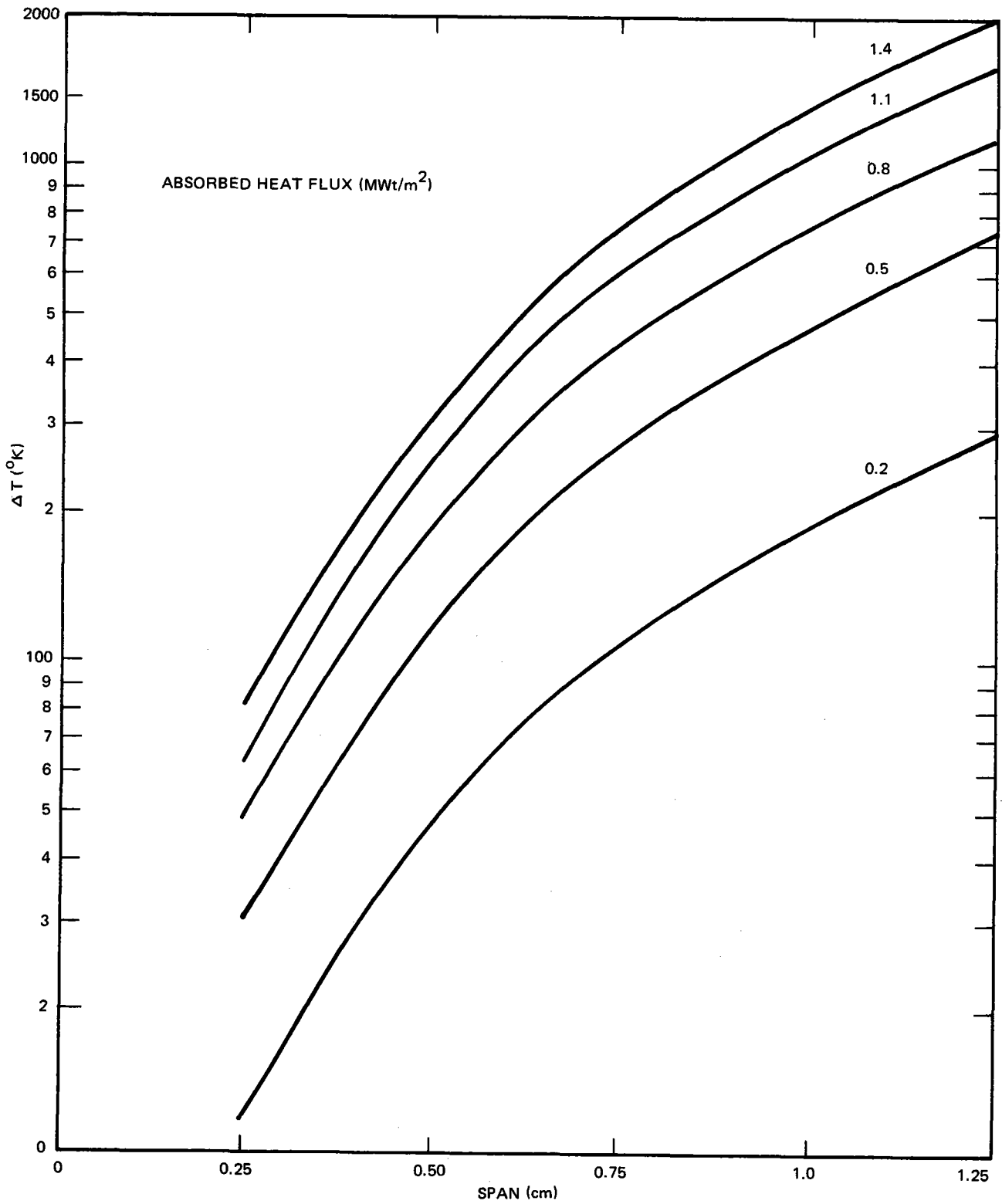
Figure 3-14.   Temperature Rise in Span Cooled at One Edge

3.7 OVERHEATING OF UNCOOLED SURFACES

In the receiver design there is the possibility that there will be some uncooled metal exposed to the incident heat flux. This could occur if there are gaps between tubes, if the tubes are connected by uncooled fins, or if there is uncooled metal at the edges of panels. An analysis was performed to determine the temperature rise that will occur in a metal strip that is exposed to the heat flux on the flat side and cooled only at one edge.

The following equation gives the ΔT that exists between the cooled and uncooled edges of such strips:

$$\Delta T = \frac{8990 \ Fx^2}{Kt}, \ ^\circ C$$

F = MWt/m^2, heat flux absorbed by the fin

x = cm, span of fin

K = W/m-K, thermal conductivity of fin material

t = cm, thickness of fin

This approximate analysis assumes that the span-thickness ratio is large and that thermal radiation can be ignored. More exact analysis shows that the above equation is reasonably accurate.

This equation shows that the temperature rise is proportional to the absorbed heat flux and the square of the fin width. The ΔT is inversely proportional to the metal thermal conductivity and the fin thickness. Figure 3-14 shows the results of this study for K = 21 W/m-K and t = 0.25 cm. It can be seen that even short spans of 0.75 cm can lead to a ΔT of 600°F or so. If there are uncooled structures that will receive incident radiation, it will be necessary to minimize the strip span, minimize the surface absorptivity, maximize the thickness of material, and (if practicable) maximize the material thermal conductivity.

In the future, additional studies of uncooled structures will be made to identify possible problems of overheating and thermal stress due to receiver spillage. Such structures include the receiver support structure and covering, the tower, and the receiver crane.

3.8 ENHANCED RADIATION CAPTURE

The heat losses from an external-type central receiver of a solar power plant include the following:

1) Heat radiated to space by virtue of the receiver surface temperature
2) The fraction of the incident energy reflected to space
3) Heat lost by convection to the atmosphere
4) Conduction to the tower.

A study has been initiated to determine the extent to which losses due to Items 1 and 2 could be reduced by use of surfaces whose configurations are such that some of the energy radiated and reflected from the receiver surface will be directed to another part of the receiver surface rather than all of it being directed out to space and lost as is the case for a smooth cylindrical surface.

The results of the initial study, namely, a comparison between the saw-toothed surface and the plane surface for radiant heat transfer when the surfaces are both diffuse and gray, are presented in this report.

The assumptions made in the analysis include the following:

1) The surfaces are gray.
2) The surfaces emit and reflect diffusely.
3) The radiation received by the receiver is diffuse. (The results would be essentially the same if the radiation were assumed to be unidirectional.)
4) The dimensions of the grooves in the saw-toothed surface are large compared to the wave length of the incident radiation.
5) Convective heat transfer to the atmosphere is not considered.

The comparison between the saw-toothed surface and the plane surface was made for the following specific set of conditions:

1) The receiver wall is Type 304 stainless steel and its thickness is 0.05 in.
2) The receiver is cooled by sodium and the sodium heat transfer coefficient is 8480 Btu/h-ft^2-^{o}F.
3) The sodium temperature is the same for both surfaces and such that the temperature of the plane surface is always 1000°F.

Calculations were made for surface reflectivities of 0.05, 0.10, and 0.15, and incident radiation fluxes of 1.7, 0.5, and 0.2 MW/m^2. The results are plotted in Figure 3-15. Figure 3-15 shows the ratio of the net radiant heat absorbed by the saw-toothed surface per unit projected area to the net radiant heat absorbed by the plane surface per unit area. It is seen that this ratio is greater than unity and increases with decrease in the opening angle (θ) and with increase in the reflectivity (P). It is also seen that this ratio is quite insensitive to the flux (B) of the incident radiation.

The radiation incident on the central receiver is neither diffuse nor uni-directional but has an angular distribution. It is anticipated that there will be little difference between the present results and the results which take into account the actual angular distribution of the incident flux, for opening angle θ greater than about 60°.

3.9 RECEIVER DESIGN

Figure 3-16 shows a conceptual sketch of the receiver mounted on the tower. A crane mounted at the top is shown lifting a panel and its support structure into position. Vertical I-beams and associated trusses provide the main receiver structure.

Figure 3-17 shows some of the structural details of the receiver. The panel and panel structure are supported by the main structure. Sodium piping with
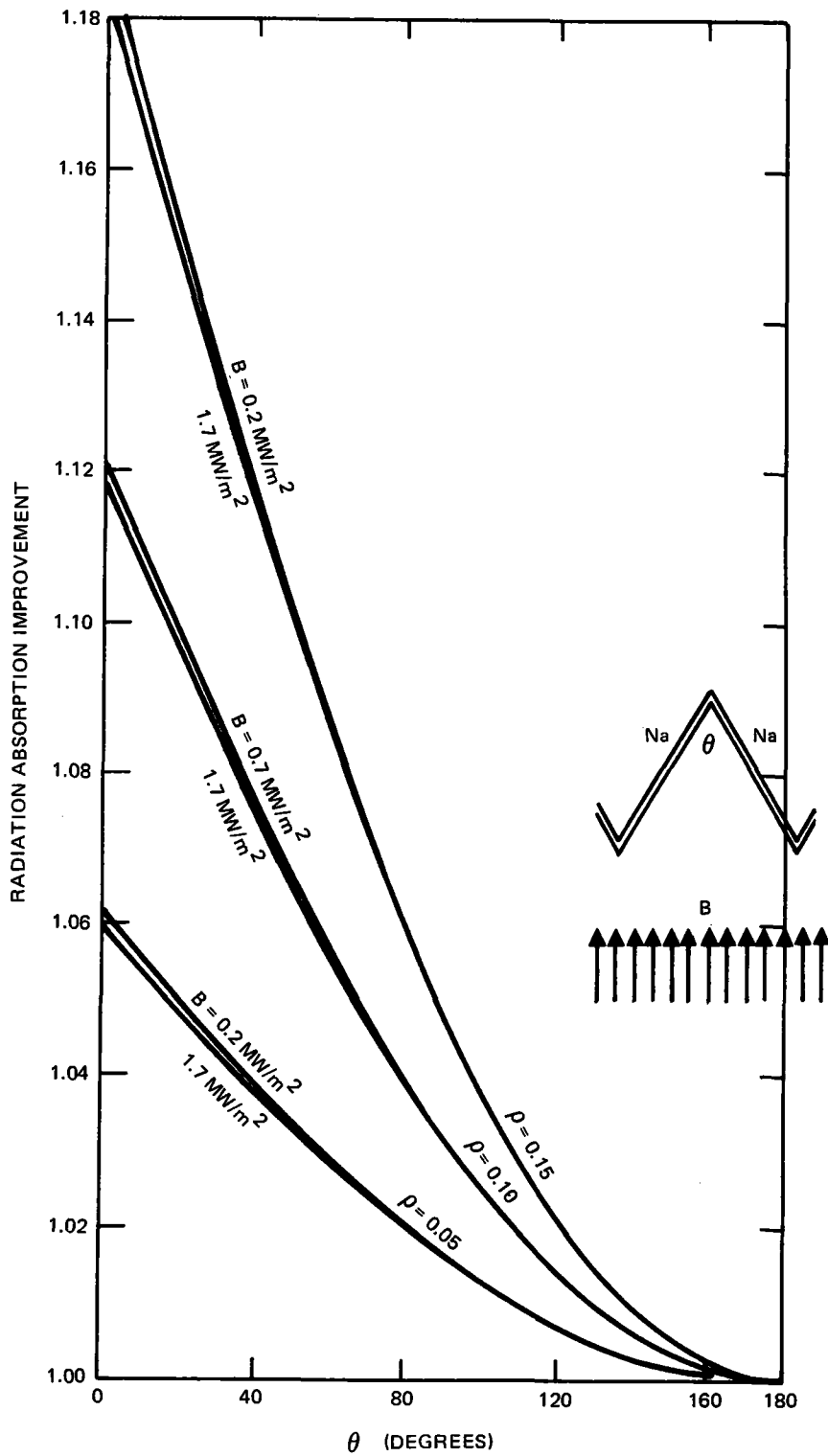
Figure 3-15. Heat Transfer Performance of Saw-Toothed
Surface Relative to Plane Surface

9272-53
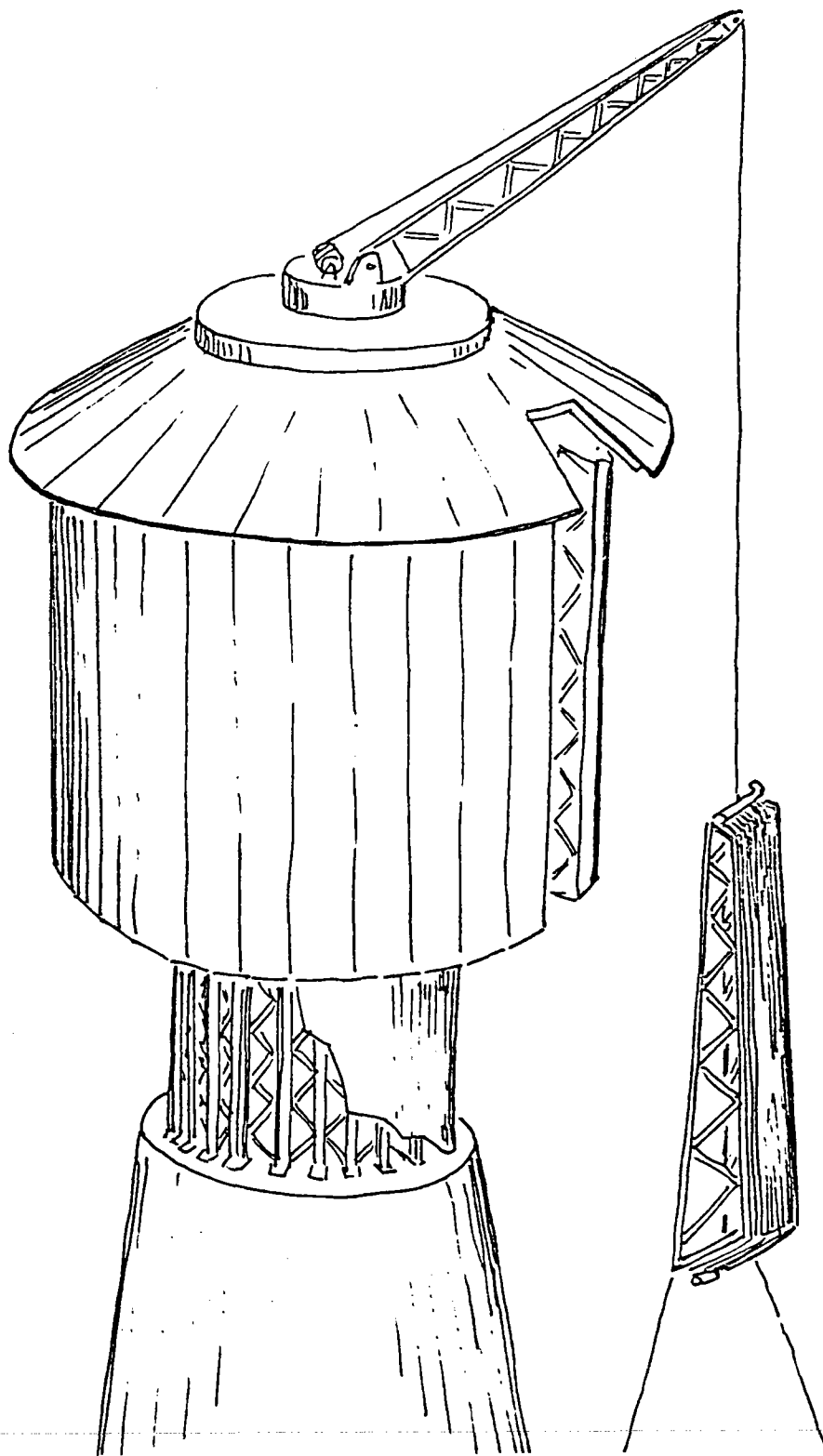
Figure 3-16.   External Receiver Concept
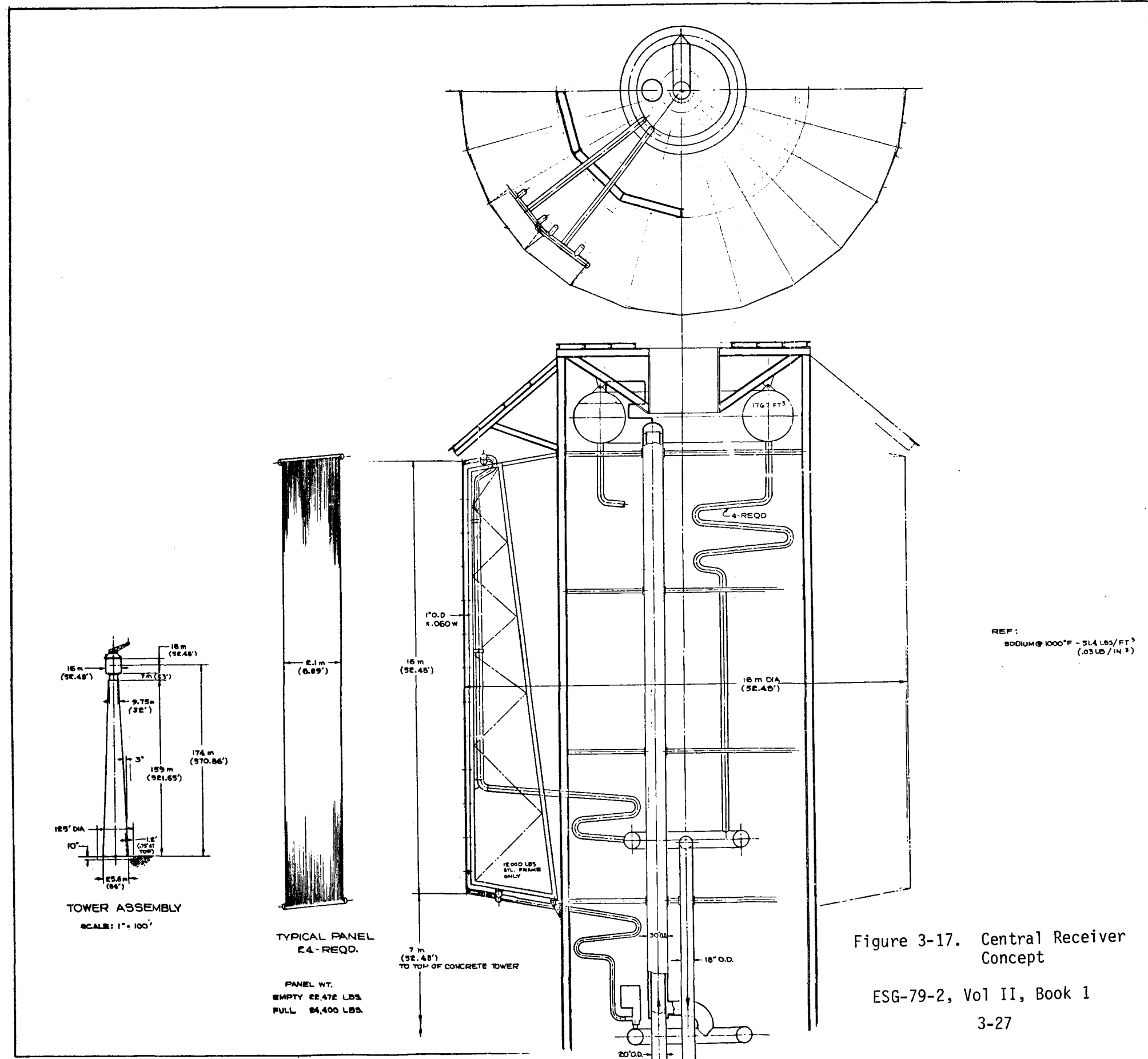
Figure 3-17. Central Receiver
Concept

bends to allow for thermal expansion connect the panels to the riser and downcomer. The riser is higher than the upper edge of the panels and acts as a standpipe to provide sodium to the panels in case of pump and/or check valve failure. The sodium expansion tank is a hexagonal toroid and is located near the top of the receiver.

The baseline receiver is of the external type and it is 16.1 m (52.8 ft) in diameter and 16.1 m in height. It consists of 24 separate vertical panels – each panel being constructed of 110 stainless steel tubes. Each tube has a diameter of 1.91 cm (0.75 in.) and a wall thickness of 0.124 cm (0.049 in.). See Figure 3-18.

The panel tubes are tangent to one another forming a flat panel 209.6 cm (82.5 in.) wide. The tubes are held mechanically in this position. The tubes are anchored to the support structure at the panel base and are permitted to grow vertically – the maximum growth being in the neighborhood of 15 cm (7 in.). The tubes are supported every 1.2 m (4.0 ft) by a pin and bracket arrangement which firmly mounts the tubes to the support structure while permitting thermal expansion.

The tubes enter manifolds at the top and bottom of the panels. The manifolds are constructed of 20 cm (8 in.) pipe with a 0.277 cm (0.109 in.) wall, and extend the width of the panel. The manifold at the bottom is connected to the main sodium riser pipe by means of a circuitous 20 cm (8 in.) pipe. The analogous pipe at the upper manifold doubles back parallel to the panel and for about 2/3 of the panel length. Thus, the growth of the panel is compensated by the reverse growth of this pipe, minimizing the pipe stress.

Each panel is supported by a full-length strong-back that is constructed of 15 cm (6 in.) box beams having a steel thickness of 0.953 cm (0.375 in.). Each strong-back is bolted to the vertical I-beam structure that is attached to the top of the tower. Behind each panel is a thin stainless steel thermal shield that serves to intercept any stray light beams that may enter between tubes. There is also thermal insulation between the panels and internal structure to prevent overheating of structures and reduce heat losses.

20 cm OD x 0.28 cm W 304 CRES
(TOP AND BOTTOM)

1.91 cm OD x 0.124 W
304 CRES TUBING
(INDEPENDENTLY
SUPPORTED)

2.1 m

15 cm OD x 0.28 cm W 304 CRES
(2 BRANCHES, TOP AND
BOTTOM)

0.75 m

608°C
(MAX METAL)

SLIDE

20 cm OD x 0.28 cm W
304 CRES

75% UP — 608°C

11.9 m

50% UP — 540°C

14.3 m

SLIDING
@ 1.2 m CTRS.

25% UP — 377°C

608°C
(MAX METAL)

FIXED

1.2 m

277°C
(MAX METAL)

1.07 m

9272-54
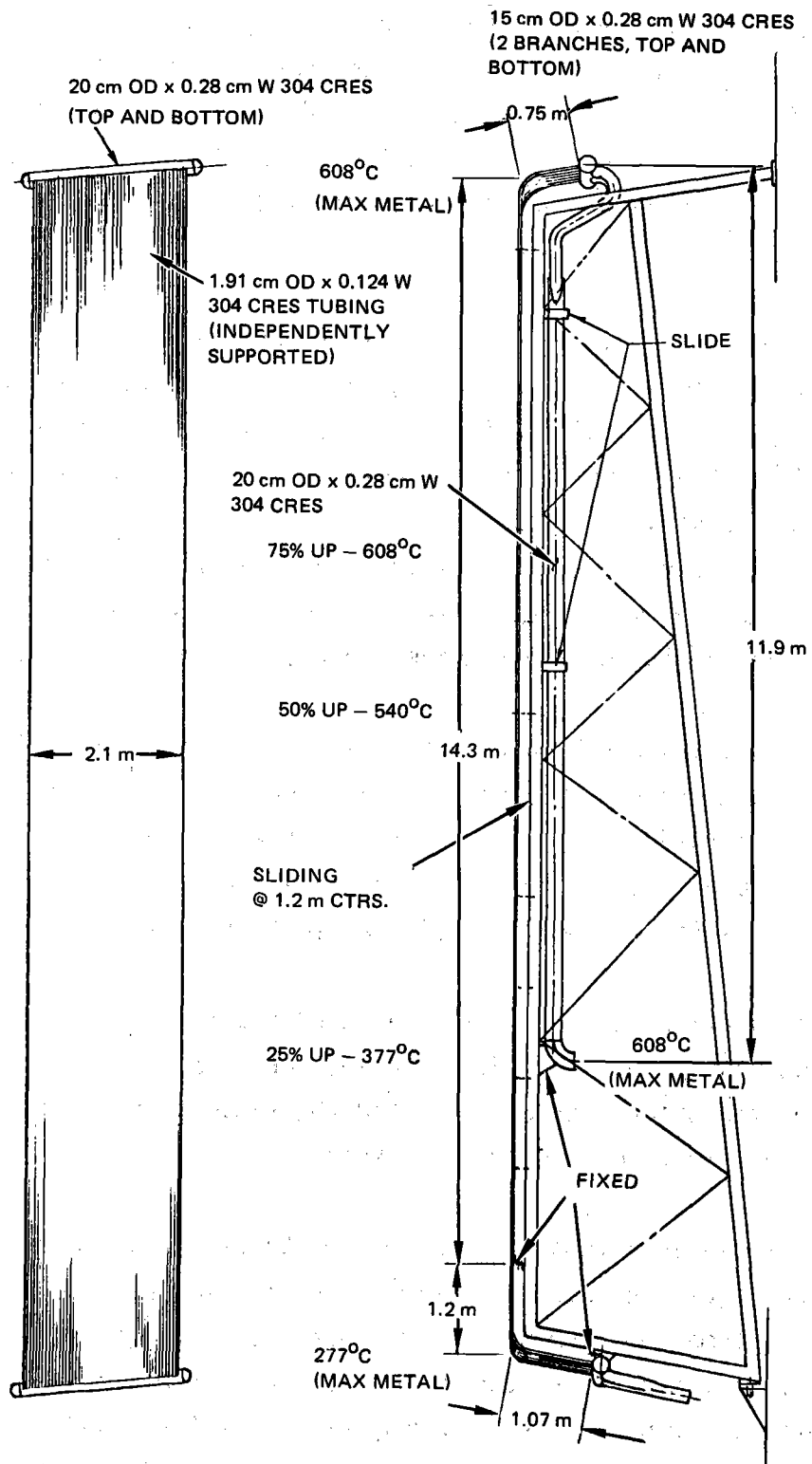
Figure 3-18.   Panel Concept

The riser pipe is connected to an anti-siphon pipe which extends from a point below the panel base to well above the panels — a distance of 33 m (72 ft). It consists of an inner 51 cm (20 in.) pipe and an outer concentric 76 cm (30 in.) pipe. Sodium from the riser travels up the inner pipe then returns down the outer annulus delivering sodium to the toroidal distribution ring at the base of the receiver.

An expansion tank is located near the top of the anti-siphon pipe and above the panels and manifolds. It is a hexagonal torus measuring 8 m (26 ft) across the flat diameter and is constructed of six mitered pipes each having a diameter of 1.8 m (6 ft). The expansion tank accommodates the effect of temperature changes in the sodium and the piping of the receiver loop. A crane hoist will be placed on top of the receiver to lift the panel and strong-back assemblies into position and remove them during maintenance periods. A circular shed roof is installed around the top of the receiver to protect against rain, snow, etc.

In Figure 3-19, a panel made up of small equilateral triangles is shown. This shape could increase performance by 3% over a flat surface. The panel is made by brazing a folded 0.060 in. sheet to a flat 0.060 in. sheet. Metal shims are placed at the points of contact to ensure a strong brazed point. At the end of each panel, the folded sheet is roll-welded to the flat sheet.

The configuration in Figure 3-19 has good thermal performance and would be a relatively low-cost panel. The disadvantages are the relatively high stresses in the corners of the triangular passages and the rigid construction of the panel which could generate severe thermal stresses.

Figure 3-20 is an attempt to remove one objection to the previous design. The coolant passages are made of square tubing formed into a diamond shape, having a good thermal performance. Each tube has fittings brazed to it so that the tube may be attached to a supporting framework by means of pins. The pins allow the tubes to grow axially with respect to the frame and also rotate on the pin. This design retains the potential stress problem in the tube corners.

ROLL RESISTANCE WELD

5 × SIZE
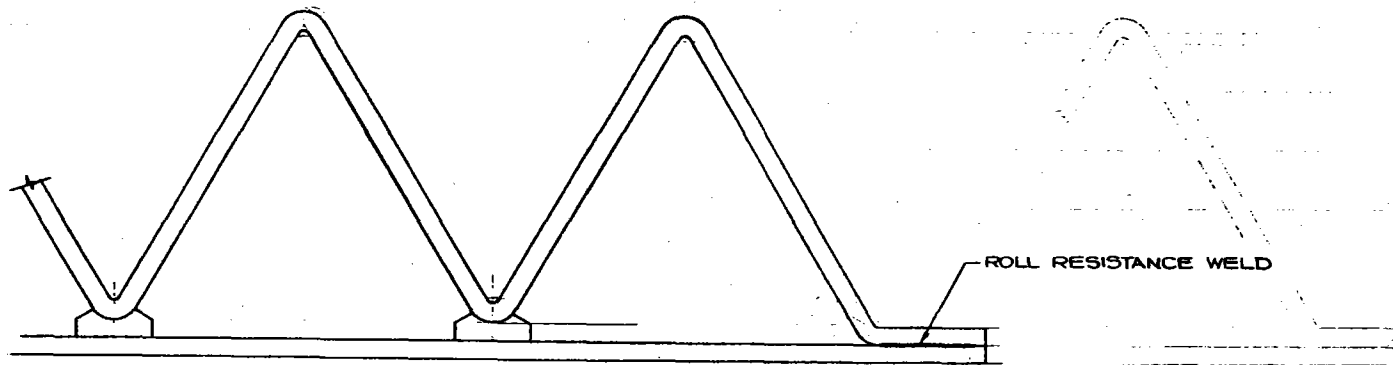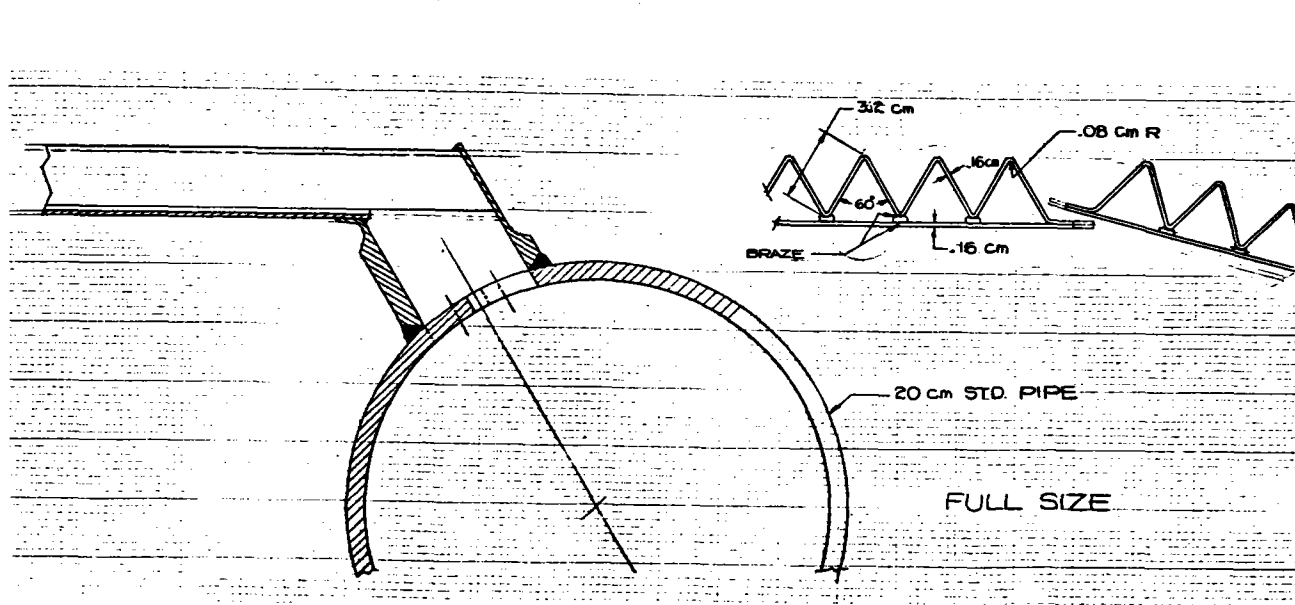
MATL:
304 CRES

REF. ONLY
112 TUBES
67 TRIANGLES
.75 cm EXP (WIDTH) EACH
SIDE OF PANEL

3.2 cm

.08 cm R

.16 cm

60°

BRAZE

.16 cm

20 cm STD. PIPE

FULL SIZE

Figure 3-19.   Receiver Panel Concept Showing Brazed Assembly
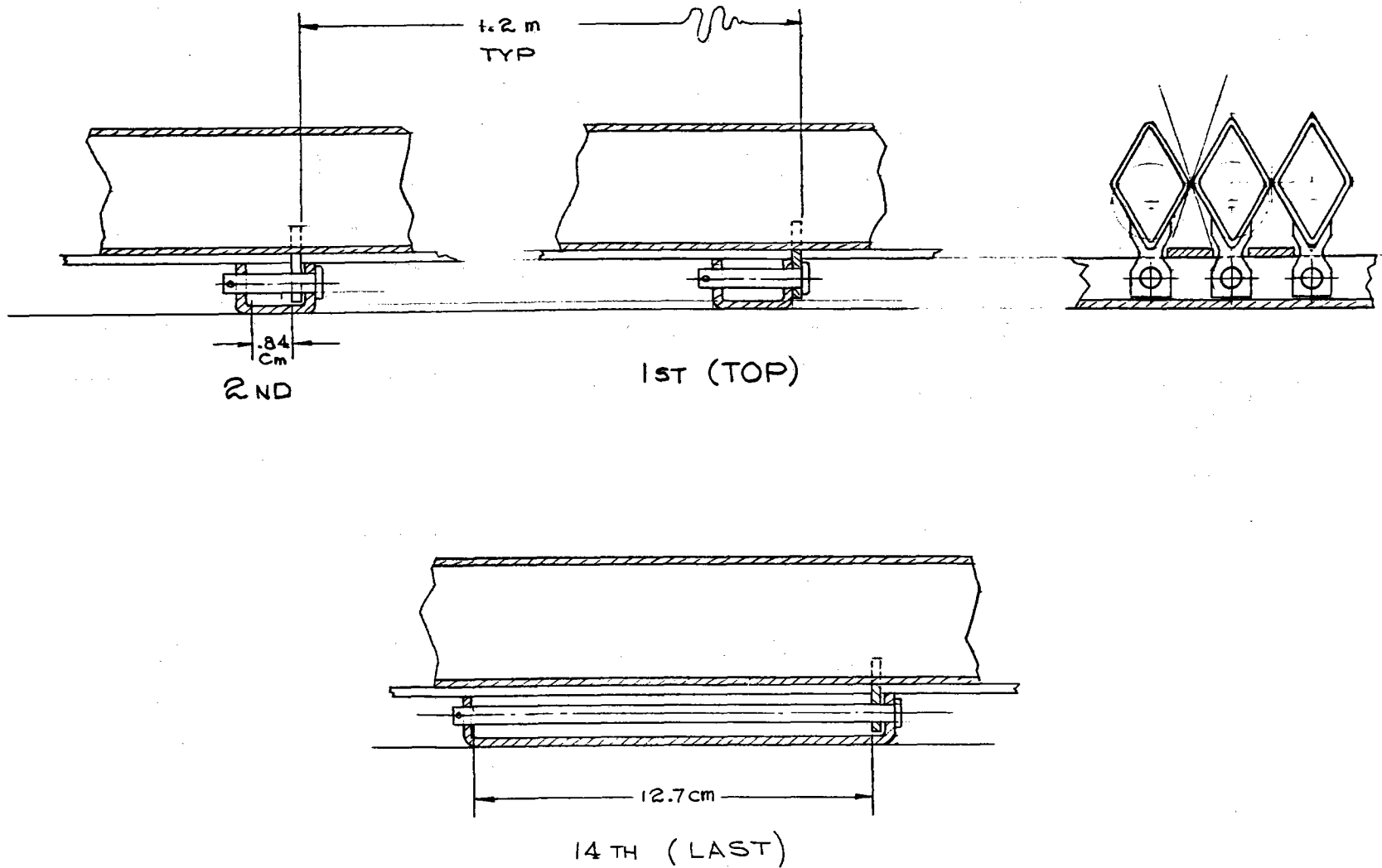
Figure 3-20. Receiver Panel Concept Showing Formed Tube Pin Mounting Arrangement
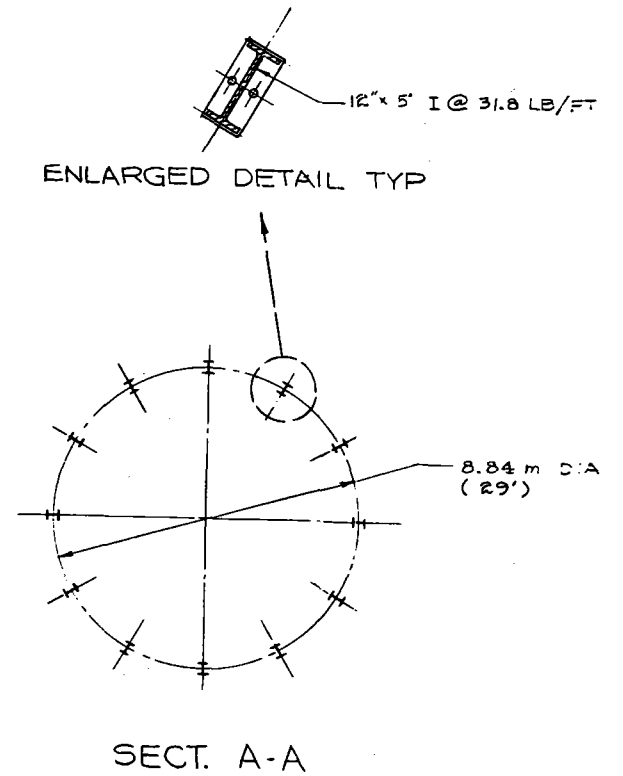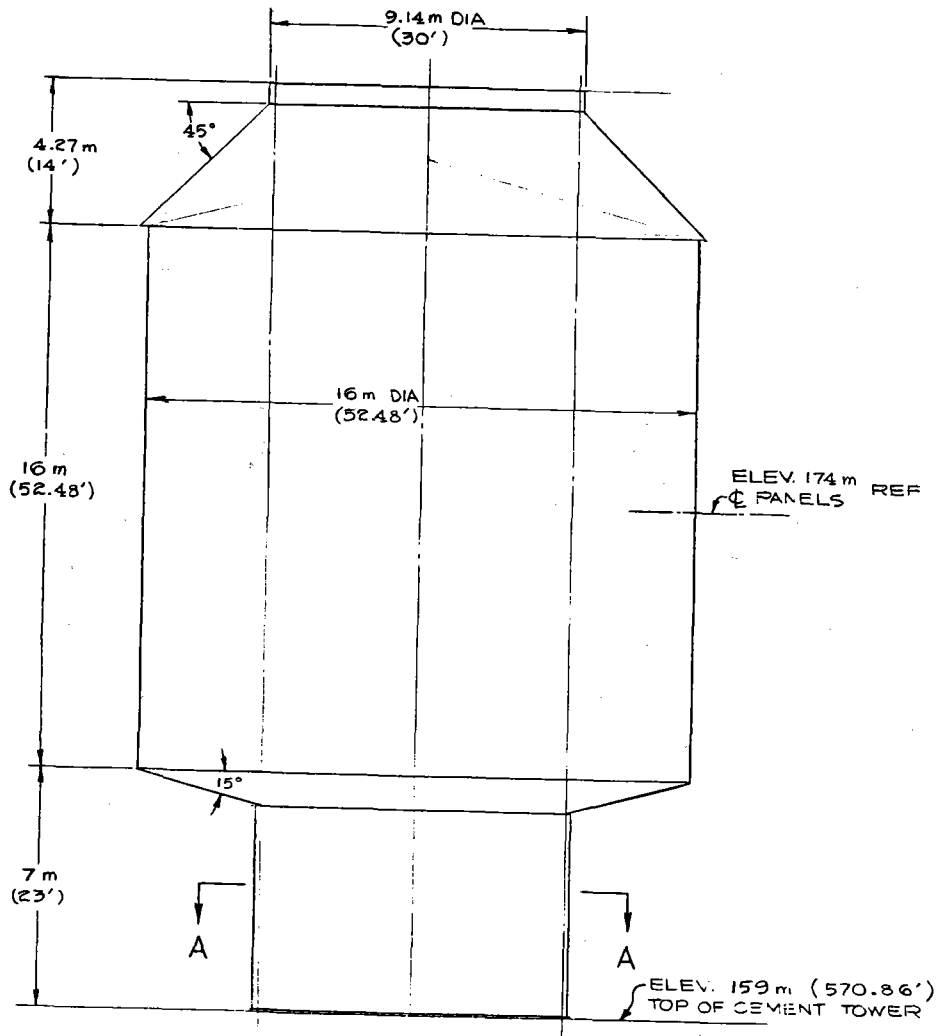
Figure 3-21. Central Solar Receiver Tower Concept

Other radiation capture surfaces have been studied, but no really attractive design has been achieved to date.

3.10 RECEIVER-TOWER INTEGRATION

Figure 3-21 was generated to show an envelope of the baseline receiver. The receiver and support structure (but without crane hoist) stands 27.3 m (89.5 ft) above the tower top. The active surface of the receiver is a cylinder 16 m high and 16 m in diameter. The receiver is attached to the tower by twelve I-beams which form a circle 8.84 m (29.0 ft) in diameter. The tower height is 167.3 m (548.9 ft).

3.11 RECEIVER STRUCTURAL ANALYSIS

3.11.1 Receiver Subsystem Conceptual Design

The solar receiver concept considered in the conceptual design analyses is shown in Figure 3-17. The panel consists of 110 Type 304 stainless steel seamless tubes, each 1.91 cm (0.75 in.) OD with 0.124 cm (0.049 in.) wall thickness. The tubes are independently supported at every 1.22 m (4.0 ft) to restrain motions transverse to the tube centerline, but permit thermal rotations and axial growth. Additionally, all tubes are rigidly anchored at a location 1.52 m (5.0 ft) from the bottom of the tube panel. The tubes are bent on 0.305 m (1.0 ft) radii at their ends and connected to inlet and outlet manifolds 16.08 m (52.75 ft) apart. This provides each solar panel with a planar area of 14.9 m (49 ft) times 2.1 m (6.89 ft) or 31.29 m^2 (337.6 ft^2). See Figure 3-18.

The inlet and outlet manifolds are Type 304 stainless steel tubing with 20.32 cm (8.0 in.) OD and 0.277 cm (0.109 in.) wall thickness. They are angled slightly to the horizontal to provide free-draining through the inlet plumbing. The inlet manifold is anchored to the supporting structure, whereas the outlet manifold is free-floating and connected to the downcomer through 15.24 cm (6.0 in.) and 20.32 cm (8.0 in.) OD outlet piping. The 15.24 cm outlet piping has two 22.86 cm (9.0 in.) radii to absorb thermal expansion mismatch between the tube

panel and the 20.32 cm outlet piping. This thermal expansion mismatch has been minimized for steady-state thermal profiles in the solar panel and outlet piping by the judicious selection of the tubing and piping anchor points.

3.11.2 Structural Analyses

Structural analyses of the receiver subsystem were confined to those sub-components most influenced by solar flux changes during service, i.e., the solar panel tubing, manifolds, and outlet piping. A piping flexibility-stress analysis was performed using an in-house, finite-element computer code, DRIPS* to predict deadweight and thermal expansion stresses in the solar panel tubing and outlet piping. The thermal inputs to this analysis were based on tubing cross-section temperature distributions for the conceptual receiver design at the north side - Equinox noon. Thermal gradient stress analyses were performed based on closed-form cylinder equations with the same thermal inputs as used in the piping flexibility-stress analysis. Evaluations of predicted results were performed utilizing ASME B&PV Code criteria and material data generated to support develop-ment of ASME rules for construction of nuclear pressure vessel components in elevated temperature service. Conclusions were reached as to the feasibility of the receiver conceptual design and areas of future design activities were identi-fied which can improve the design's structural adequacy. The following paragraphs provide a more detailed summary of these conceptual design activities and results.

3.11.3 Thermal Inputs

Both the piping flexibility-stress analysis and thermal gradient stress analysis required a detailed definition of thermal profiles in the solar panel tubes at all locations along the length of the tubes. The north side tube panel was selected as the reference case since the highest solar flux exists at this location, and therefore the highest thermal stresses will also occur here. Conceptual thermal analyses were performed which resulted in predicted tube (hot-side) outside temperatures and sodium temperatures at this location as a function of axial location in the receiver. Figure 3-6 presents these results. Detailed

---

*Dynamic Response in Piping Systems (Rockwell proprietary computer code).

thermal flux analyses have been performed which predicted tube cross-section thermal profiles for various flux levels. Figure 3-22 is a typical predicted thermal profile. An equivalent tube (hot-side) outside temperature was developed for these various profiles and equations established which could relate key temperature values and gradients in the tube cross-section to the difference between outside tube temperature and sodium temperature. Thus, utilizing these equations, the key temperature values and gradients for the conceptual design could be determined. Figure 3-23 presents these equations and temperature definitions while Table 3-5 summarizes the results of this effort.

3.11.4 Piping Flexibility-Stress Analysis

Figure 3-24 is the model of the solar panel tubes and outlet piping employed in the DRIPS flexibility-stress analysis. Hand calculations were utilized to determine an optimum location of anchor points to minimize the stresses at the outlet piping bends. Basically, the axial thermal expansion of the solar panel tubes away from the lower axial support was matched to the axial thermal expansion of the outlet piping away from its axial support location. By inputting the linearized across-the-tube temperature gradients (ΔT_1) and bulk metal temperatures (T) for the solar panel tubing, the program could compute thermal induced moments at all nodal locations along the computer model. ASME Code B31.1 stress intensification factors were then used to calculate stresses at all piping locations.

Stresses due to weight and pressure loadings were calculated using DRIPS computed moments and conventional ASME Code B31.1 design procedures.

The results of these analytical efforts are summarized in Table 3-6. Figure 3-25 is a computer plot of exaggerated piping displacements due to the thermal loadings. Note that the utilization of solar panel tube supports on 1.22 m (4.0 ft) centers essentially provides full restraint of the across-the-tube thermal moments as evidenced by minimal bowing of the tubes between support locations. This is important with respect to gapping considerations that exist when an individual tube concept is employed versus alternate integral tube wall concepts.

```
1185
          1161
1114
        1095        1093
1038
        1025    1042
  957
     950     987
                            989
        929         960
              930
           898

              864   867   869   870

              864   867   869   870

              864   867   869   870

           860
              861
      860         861
                     861
     860     860
860
       860     860
860
       860        860
860
         860
860
```
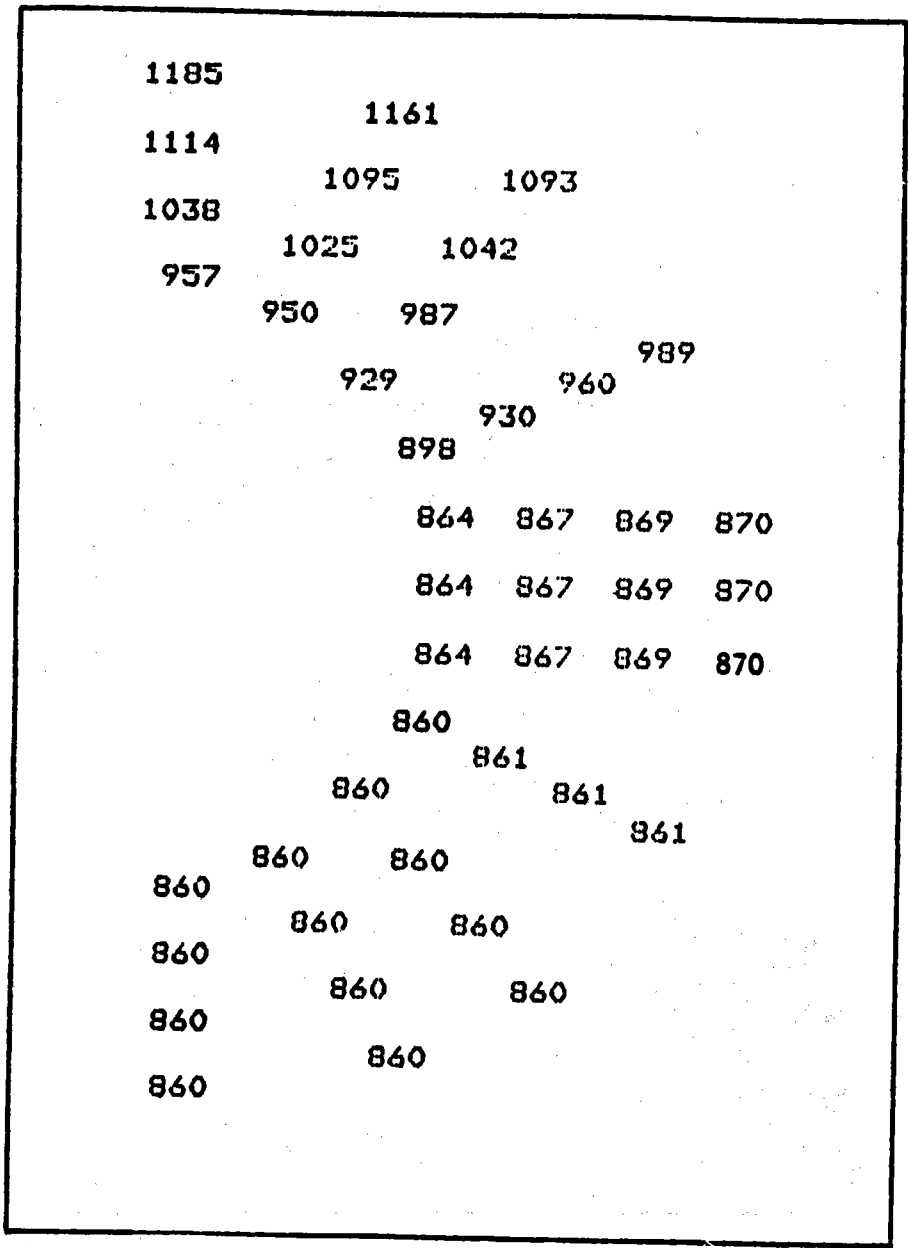
(Temperatures in °F)

Figure 3-22. Advanced Receiver Tube Temperature Profile
Equinox Noon - North Side
(1.9 cm (3/4 in.) OD, 0.127 cm. (0.05 in.) Wall
Elevation 8.5 m, Heat Flux at Crown 2.15 MW/M^2.
One-Point Aim Strategy, 15 m Receiver,
CRES 304 Tubes)
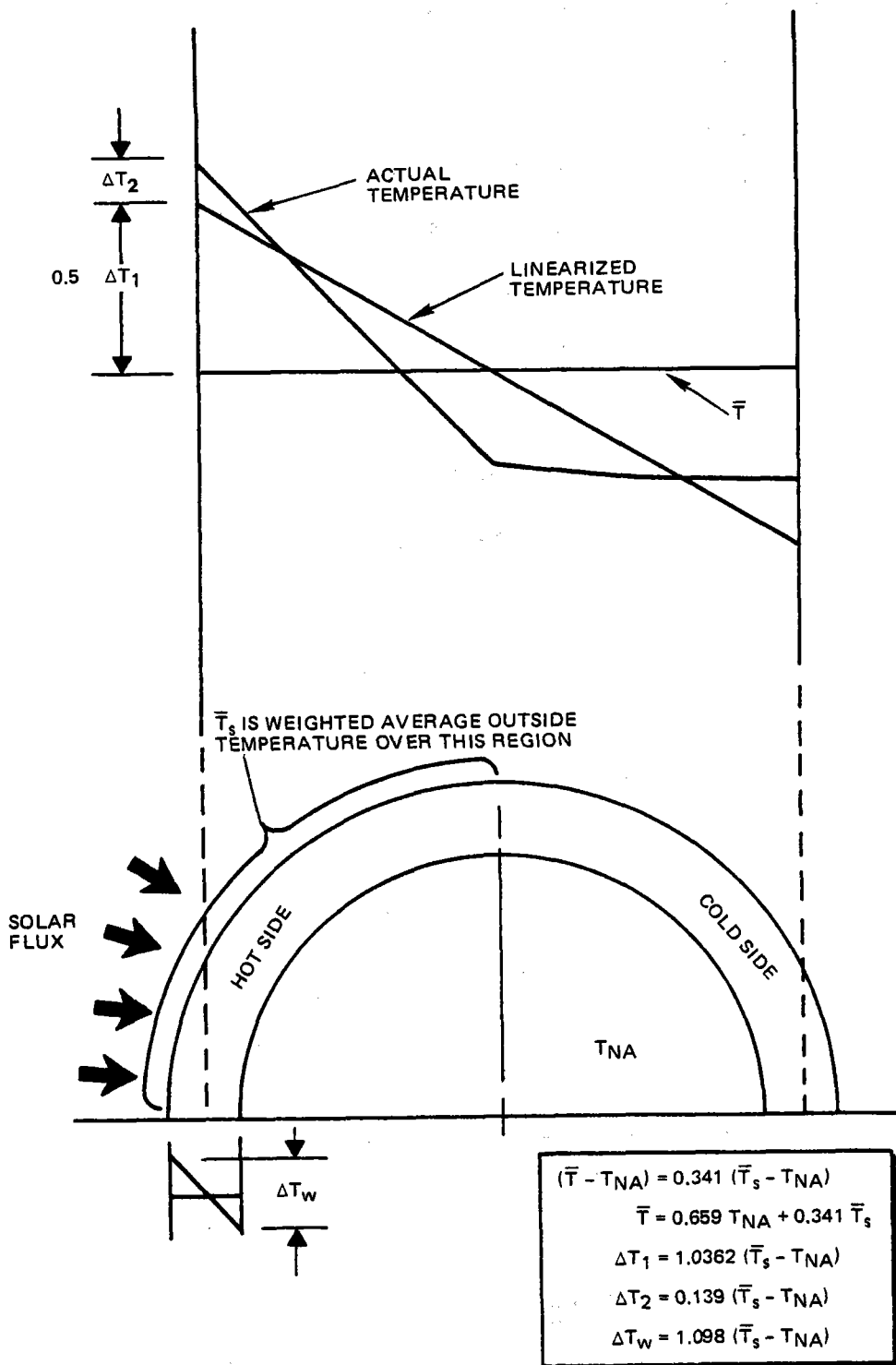
Figure 3-23.   Derived Temperature Relationships

TABLE 3-5

DERIVED TEMPERATURE VALUES IN SOLAR PANEL

X/L*	T_{Na} ($^{\circ}$F)	T_s ($^{\circ}$F)	$\bar{T}$ ($^{\circ}$F)	ΔT_1 ($^{\circ}$F)	ΔT_2 ($^{\circ}$F)	ΔT_w ($^{\circ}$F)
0	550	562	554.1	12.4	1.7	13.2
0.033	550	571	557.2	21.7	2.9	23.1
0.066	554	580	562.9	27.0	3.6	28.5
0.106	561	595	572.6	35.3	4.7	37.3
0.146	572	617	587.3	46.6	6.3	49.4
0.187	583	647	604.8	66.3	8.9	70.3
0.227	601	683	629.0	85.0	11.4	90.0
0.268	622	725	657.1	106.7	14.3	113.1
0.308	648	770	689.6	126.3	17.0	134.0
0.348	678	819	726.1	146.1	19.6	154.8
0.389	713	870	766.5	162.6	21.8	172.4
0.329	751	920	808.6	175.0	23.5	185.6
0.470	793	970	853.4	183.4	24.6	194.3
0.510	834	1010	894.0	182.4	24.5	193.2
0.550	877	1040	932.6	168.8	22.7	179.0
0.591	918	1065	968.1	152.3	20.4	161.4
0.631	952	1088	998.4	140.9	18.9	149.3
0.672	985	1106	1026.3	125.3	16.8	132.9
0.712	1015	1116	1049.4	104.6	14.0	110.9
0.752	1041	1122	1068.6	83.9	11.3	88.9
0.793	1061	1124	1082.5	65.2	8.8	69.2
0.833	1073	1123	1090.1	51.8	6.9	54.9
0.873	1084	1120	1096.3	37.3	5.0	39.5
0.914	1091	1118	1100.2	28.0	3.8	29.6
0.954	1096	1114	1102.1	18.6	2.5	19.8
0.977	1098	1111	1102.4	13.4	1.8	14.3
1.000	1100	1108	1102.7	8.3	1.1	8.8

*X/L denotes the vertical location along the receiver solar panel as a fraction of the panel height.
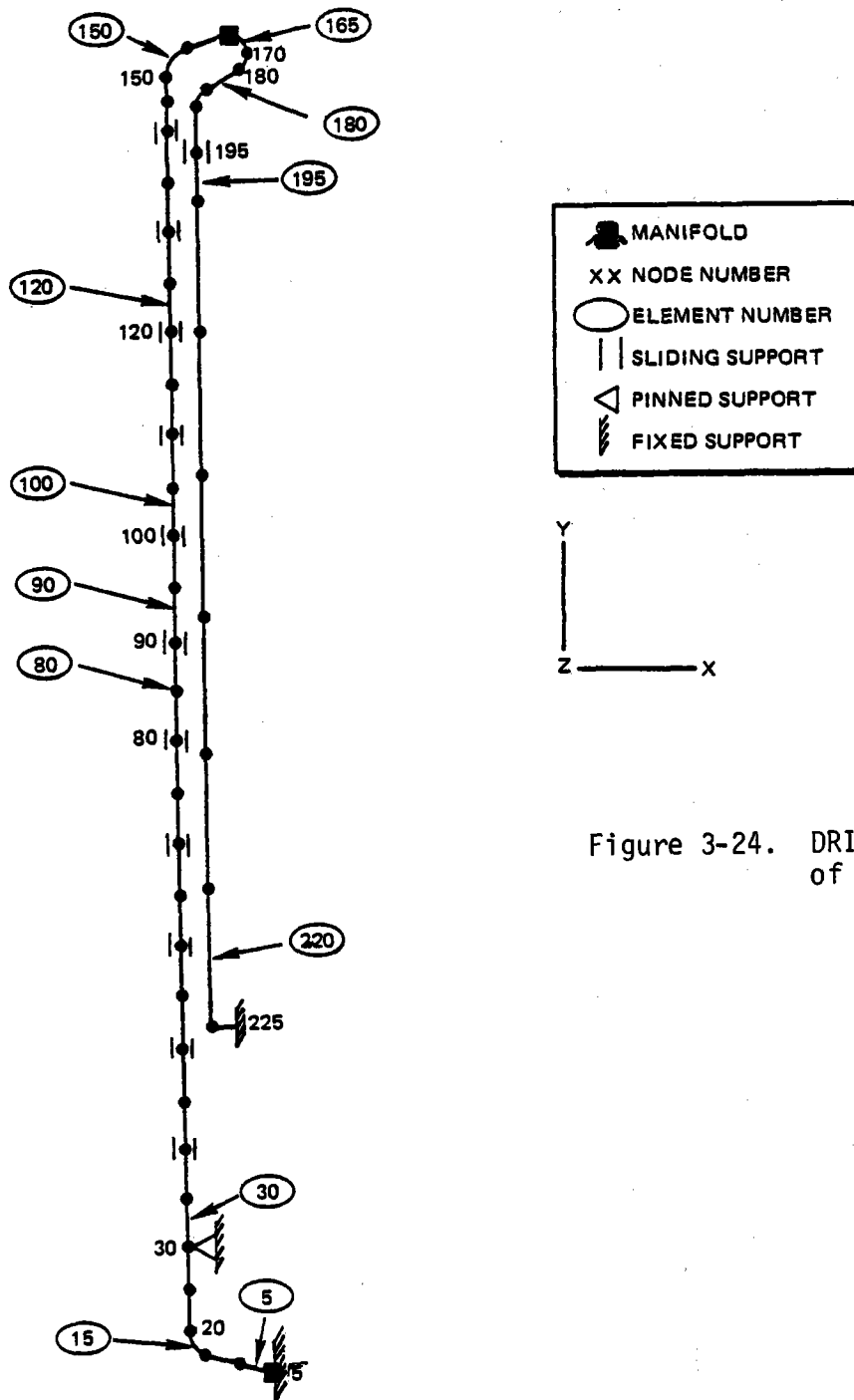
Figure 3-24. DRIPS Computer Model
of Solar Receiver
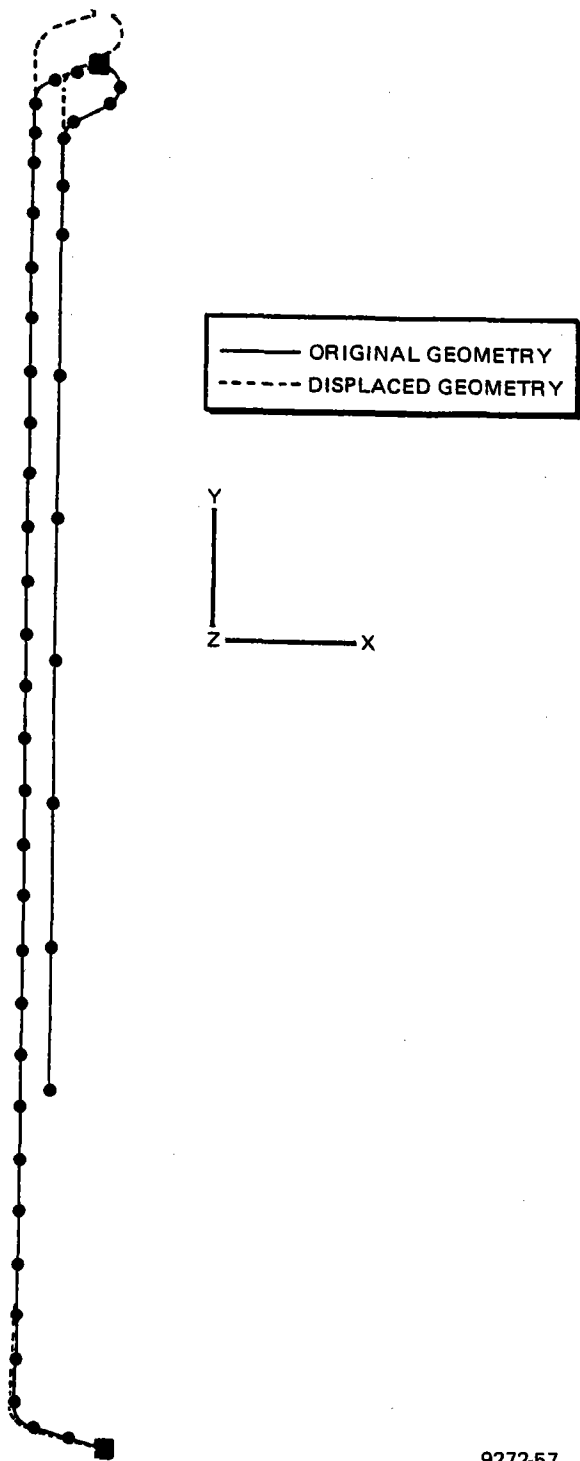
Figure 3-25. DRIPS Predicted Thermal
Displacements
(Exaggerated)

9272-57

TABLE 3-6
DRIPS PREDICTED STRESSES (psi)

Element	Node	σ_z Pressure Membrane	σ_z Weight Membrane	σ_z Weight Bending	σ_z Thermal Membrane	σ_z Thermal Bending	* Combined Stress
5	5	125.0	-0.9	-277.2	-118.2	-10720	11000.2
15	20	122.1	5.1	-112.1	-136.4	6231	6123.5
30	30	116.7	-218.4	37.2	61.5	-8379	8328.8
80	80	82.9	-122.9	0.1	61.5	-22353	22364.9
90	90	76.3	-103.8	-0.7	61.5	-20470	20487.4
100	100	69.6	-84.7	2.6	61.5	-16947	16968.5
120	120	56.3	-46.5	36.2	61.5	-7931	7931.7
150	150	39.2	-2.7	-120.0	59.2	-2662	2831.2
165	170	138.3	-102.9	-3421.6	-192.9	-15096	18438.9
180	180	147.4	-81.4	-2442.3	-77.6	-4373	6810.8
195	195	225.5	-291.4	451.6	-275.3	12	654.9
220	225	484.7	-590.6	0.5	-272.7	0	720.5

*Using Von Mises yield criterion

3.11.5 Thermal Gradient Analyses

Stresses due to linearized across-the-tube thermal gradients and overall thermal expansion were considered in the piping flexibility/stress analysis. This leaves only consideration of peak across-the-tube thermal gradients (ΔT_2) and through-the-wall thermal gradients (ΔT_w), to complete the thermal loading evaluation. This was done by assuming the maximum values of these gradients, located at the crown of the hot side of the tube, acted uniformly around the circumference of a cylinder. This assumption allowed utilization of classical cylinder thermal stress equations and resulted in the predicted stresses summarized in Table 3-7.

TABLE 3-7

COMPUTED THERMAL GRADIENT STRESSES

Element	Node	$\sigma_z{}^*$ ΔT_2 Bending	$\sigma_z{}^\dagger$ ΔT_w Bending
5	5	0	0
15	20	0	0
30	30	-817	-4661
80	80	-5584	-31777
90	90	-5153	-29274
100	100	-4290	-24417
120	120	-1998	-11317
150	150	-248	-1439
165	170	0	0
180	180	0	0
195	195	0	0
220	225	0	0

$^*\sigma_z = E\alpha\Delta T_2$ $^\dagger\sigma_z = \dfrac{E\alpha\Delta T_w}{2(1 - \nu)}$

3.11.6 Evaluation of Stress Results

Two approaches were taken to evaluate the predicted stresses: (1) utili-
zation of the damage definitions, criteria, and material allowables contained in
ASME Code B31.1, and (2) utilization of the creep-fatigue damage theories and
material test data which forms a basis for the design criteria in the ASME Nuclear
Code.

3.11.7 ASME Code B31.1 Evaluation

An ASME Code B31.1 design evaluation establishes acceptable stress levels dependent on the nature of loading, the material strength at temperature, and the type of stress field resulting from the loading. Cyclic loadings are addressed by a reduction factor, based on the number of service cycles, which is used to lower the allowable stresses. Many years of service experience in the power industry have demonstrated this design approach can result in reliable piping designs.

Table 3-8 which summarizes the results of the B31.1 evaluation, indicates the conceptual receiver design will satisfy the criteria at all locations except in the solar panel tubes local to the maximum flux location. Here, the cyclic thermal expansion stresses exceed the allowables, however, only by 5%. This indicates that any of the several design modifications available should result in easy satisfaction of the B31.1 criteria.

One shortcoming exists in applying the B31.1 criteria. It was developed for power piping which undergoes relatively mild transients; therefore, thermal gradient stresses are not addressed. In the solar receiver, the thermal gradient stresses are very large due to the heat flux entering on one side of the tubes only. Although across-the-tube thermal gradients were included in the evaluation to reflect the B31.1 philosophy to address thermal induced piping moments, through-the-wall thermal gradients were ignored. The implications of this is that the B31.1 design approach may fail to account for all of the critical cyclic stress mechanisms that can lead to fatigue cracking. Additionally, the use of a simple reduction factor for cyclic loading does not provide the designer with a quantitative feeling for the actual design margin against cyclic failures. This precipitated an effort to evaluate the total stress situation, including the potential for creep-fatigue interactions.

3.11.8 Solar Panel Relaxation-Fatigue Damage Evaluation

Over the past 6 to 8 years, considerable attention has been given to the cyclic behavior of metals subjected to temperatures where creep can be significant.

TABLE 3-8

SUMMARY OF B31.1 STRESS EVALUATION

Element	Node	Pressure Plus Weight Stress Evaluation			Thermal Stress Evaluation		
		Computed Stress (psi)	B31.3 Allowable (psi)	Design* Margin	Computed Stress (psi)	B31.3 Allowable (psi)	Design* Margin
5	5	333	15900	High	10720	21880	1.04
15	20	206	15900	High	6231	21880	2.51
30	30	145	15900	High	8379	21880	1.61
80	80	83	14060	High	22353	21512	-0.05†
90	90	77	12420	High	20470	21184	0.03
100	100	72	10280	High	16947	20756	0.22
120	120	83	8740	High	7931	20488	1.58
150	150	129	9380	High	2662	20576	6.73
165	170	2704	9700	2.59	15096	20640	0.37
180	180	1979	9700	3.90	4372	20640	3.66
195	195	564	9700	High	12	20640	High
220	225	485	9700	High	0	20640	High

*Design margin = $\dfrac{\text{Allowable stress}}{\text{Computed Stress}} - 1.0$

†The negative design margin is undesirable. However, with small design changes and with more refined calculations, it is felt that a positive design margin can be readily achieved.

This was the result of an observation that the introduction of slow cyclic rates or periods of sustained loading between cycles can reduce fatigue life below that of conventional continuous cycling test data. Although cyclic behavior at elevated temperature is complex and not completely understood, interim failure theories have been developed by the ASME Code committees which, with appropriate safety factors, provide an adequate design basis for nuclear power plant components.

In order to be applicable to a wide range of loading situations and geometries, the ASME Code design criteria contains various assumptions which increase the design conservatism as the sophistication of the design analysis decreases. Unfortunately, it was not possible to justify performing rigorous (inelastic) analyses for the receiver conceptual design effort whereby the less conservative design criteria could be employed. However, the material data base and failure theories forming the basis for the ASME design criteria, can be used to establish a "screening criteria" particular to the stress behavior and design confidence needs of the solar receiver.

A key observation supporting this effort was that the regions of maximum thermal gradient stresses (hot side of the tubes) would be subjected to compressive stresses at the hot end of the load cycle. Also, the tension stress field existing on the cold side of the tubes decreased in value going up the receiver from the maximum flux location so that at those locations where this region was hot enough to exhibit creep effects, the stresses were not extremely large. Finally, equilibrium (primary) stresses were small at the maximum gradient locations and the piping system was such that elastic followup should be minimal. This led to the conclusion that the critical regions would be governed largely by relaxation-fatigue with compressive hold periods. For Type 304 stainless steel, hold-time fatigue test data indicates this type of fatigue behavior is the least detrimental of the four basic cyclic stress mechanisms (tension vs. compressive hold periods-relaxation vs creep-fatigue interaction). In fact, only a minimal reduction in fatigue life is observed in the test data with respect to the continuous cycling fatigue curve.

For these reasons, it was felt a conceptual design level "screening criteria" could be used which employed the continuous cycling fatigue curves contained in the high-temperature ASME Code (Code Case 1592). Additionally, in light of the design confidence needs of a solar power plant, it was decided to adjust the curves to provide a safety factor of 1.5 on strain range and 10 on cycles rather than the implicit factors of 2 on strain range and 20 on cycles contained in the code. This would bring the safety factors more in line with design practices conventionally employed by high-reliability technologies such as that found in the aerospace industry.

The results of this evaluation are presented in Table 3-9 which indicates the design is adequate. However, at the maximum flux locations, calculated strain ranges approach limiting values. Several design modifications are available to increase design margins in these areas.

TABLE 3-9

RELAXATION-FATIGUE EVALUATION

Element	Node	Computed Strain Range (%)	Allowable Cycles	Design* Margin
30	30	0.036	$>10^6$	>100
80	80	0.263	10,000	0.00
90	90	0.248	12,800	0.28
100	100	0.211	26,000	1.63
120	120	0.099	$>10^6$	>100
150	150	0.020	$>10^6$	>100

$$*\text{Design margin} = \frac{1.0}{10,000/\text{Allowable cycles}} - 1.0$$

3.11.9 Conclusions

Based on the conceptual design calculations, the design of a structurally adequate receiver subsystem appears feasible.

3.11.10 Recommended Future Structural Design Activities

Due to the marginal nature of the conceptual design evaluations, the lack of rigorous detailed analyses, and in the interest of developing an optimum design, it is recommended three design options be further evaluated, each of which can significantly increase the receivers structural adequacy:

1) Reduction of solar panel tube thickness
2) Multipoint aiming techniques
3) Alternate materials (such as alloy 800H)

Obviously, more sophisticated thermal and structural evaluations need to be performed with particular emphasis placed on development of an appropriate design criteria. However, this is a natural occurrence in any design activity progressing out of the conceptual stage into preliminary design.

3.12 RECEIVER WEIGHT STUDY

The weights of the 100-MWe commercial plant, including the sodium, are given in Table 3-10.

3.13 LOSS OF RECEIVER FLOW INCIDENT

The dynamic studies of Section 2.4 and the collector field studies of Section 6.2.2 indicate that upon loss of flow in the receiver panels, the sodium in the north panels will boil and excessive panel temperatures will result before passive defocus due to the sun motion occurs. Complete passive defocus requires about 150 seconds. To avoid excessive panel temperatures, active defocus of the collector field in about 15 s is required. If electric power is available, this can readily

TABLE 3-10

ESTIMATED RECEIVER WEIGHTS

	100 MWe		281 MWe	
	(kg)	(lb)	(kg)	(lb)
Twenty-four Panels	39,300	86,500	91,400	201,000
Piping and Expansion Tank	20,900	46,000	58,600	129,000
Insulation	26,900	59,200	61,800	136,000
Structure	158,200	348,000	300,500	661,000
Roof	10,000	22,000	19,100	42,000
Crane	20,200	44,500	43,600	96,000
Dry Total	275,500	606,200	575,000	1,265,000
Sodium	66,400	146,000	186,400	410,000
Wet Total	341,900	752,200	761,400	1,675,000

be achieved; however, if loss of flow is due to loss of electric power, emergency direct current power for defocus would be required for the interval until the diesel-powered generators come on line. A heliostat modification to use a stored energy device (spring loaded tilt mechanism) to provide rapid defocus on each unit is considered too expensive. Alternate receiver protection schemes have been considered such as a gravity sodium flow system through the panels as a smoke-cloud generator to obscure the receiver.

An evaluation of the various options to accomplish receiver protection indicates that active defocus is the most cost effective including provision for a 600-kW dc emergency power supply. Such a supply is required for about 30 s at a cost of $200,000.

3.14 RECEIVER STUDY CONCLUSIONS

The conclusions drawn from the receiver studies made since the inception of the program are as follows:

1) External receivers are much superior to cavity receivers for this application.

2) The optimum receiver size for 100 MWe is 16 by 16 m (53 by 53 ft).

3) Round tubes are the best shape for receiver coolant passages.

4) Type 304 stainless steel has been selected for the receiver panels although there are promising alternate materials.

5) Panels should be joined mechanically rather than be welded or brazed as a unit.

6) Tubes may be welded in groups of three or so to simplify the structure.

7) Only small gaps between tubes [such as 0.025 cm (0.01 in.)] can be tolerated at high flux conditions.

8) Methods are available to perform detailed stress analysis of the receiver.

9) Some calculated stresses are high but not excessively so.

10) Ways to reduce the receiver stress problem, if needed, are to reduce the tube wall thickness, use a multipoint collector aim strategy, and use an alternate tube material such as Incoloy 800.

4.0 RECEIVER SUBSYSTEM

4.1 REQUIREMENTS

The Receiver Subsystem functional requirements are given in Table 4-1. These requirements are derived from the optimized performance characteristics of the EPG, collector, and master control subsystem, which in turn satisfy the requirements of the ACR Specification of Reference 1. There are additional operational and sodium system requirements as follows:

1) Transport up to 390 MWt to storage or 130 MWt to storage and 260 MWt to the steam generator simultaneously or 260 MWt from storage to the steam generator.

2) Provide for the control of the receiver outlet sodium temperature and the evaporator temperature.

3) Provide for anti-siphoning of the receiver sodium.

4) Provide protection against reverse flow through the receiver.

5) Provide for purging and filling and draining the system sodium for maintenance.

6) Provide for draining the receiver system on a daily basis.

7) Provide for maintaining the purity of the sodium below 15 ppm O_2 and 1 ppm H_2.

4.2 DESIGN CHARACTERISTICS (For detailed quantification, see Appendix A, Book 2.)

4.2.1 <u>Overall Features</u>

The reference design of the sodium heat transport system is schematically shown in Figure 4-1. The quantitative values of the process variables are given in Appendix A.

The system may be considered operating as two independent loops. The first loop transfers sodium from the cold storage tank, T-1, at about 288°C (550°F) through the receiver which heats it to ~593°C (1100°F). The sodium then flows

TABLE 4-1

ADVANCED CENTRAL RECEIVER —
SUBSYSTEM FUNCTIONAL REQUIREMENTS

Parameter	Requirement
Nominal Thermal Power (MWt)	260
Maximum Thermal Power (MWt)	390
Receiver Mid-Point Elevation [m (ft)]	174 (571)
Water-Steam Side	
Feedwater Temperature, In [$^\circ$C ($^\circ$F)]	234 (453)
Evaporator Temperature, Out [$^\circ$C ($^\circ$F)]	341 (646)
Steam Temperature, Out [$^\circ$C ($^\circ$F)]	538 (1000)
Reheat Temperature	
In [$^\circ$C ($^\circ$F)]	342 (647)
Out [$^\circ$C ($^\circ$F)]	538 (1000)
Reduced Power Operation (%)	10 - 100
Transient Operation (Power)	
10% to 100% or 100% to 10% (s)	90

by gravity through the drag valve to the hot storage tank, T-2. Nominal maximum flow rates are about 1.3 m^3/s (20,000) gpm. The second loop transports sodium from the hot storage tank through the sodium heated superheater and reheater, through the evaporator and then to the cold storage tank, T-1. The maximum nominal flow is about 1.0 m^3/s (15,000) gpm range.

Provided there is some reserve in Tank T-1, the first loop operates to transfer all of the energy received by the receiver to storage, independent of the steam generator power requirements. As the insolation varies, the flow is modulated to maintain a constant receiver outlet temperature. The second system, after some storage accumulation in Tank T-2, operates independently of the insolation. The storage tank being in series in the loop functions as thermal
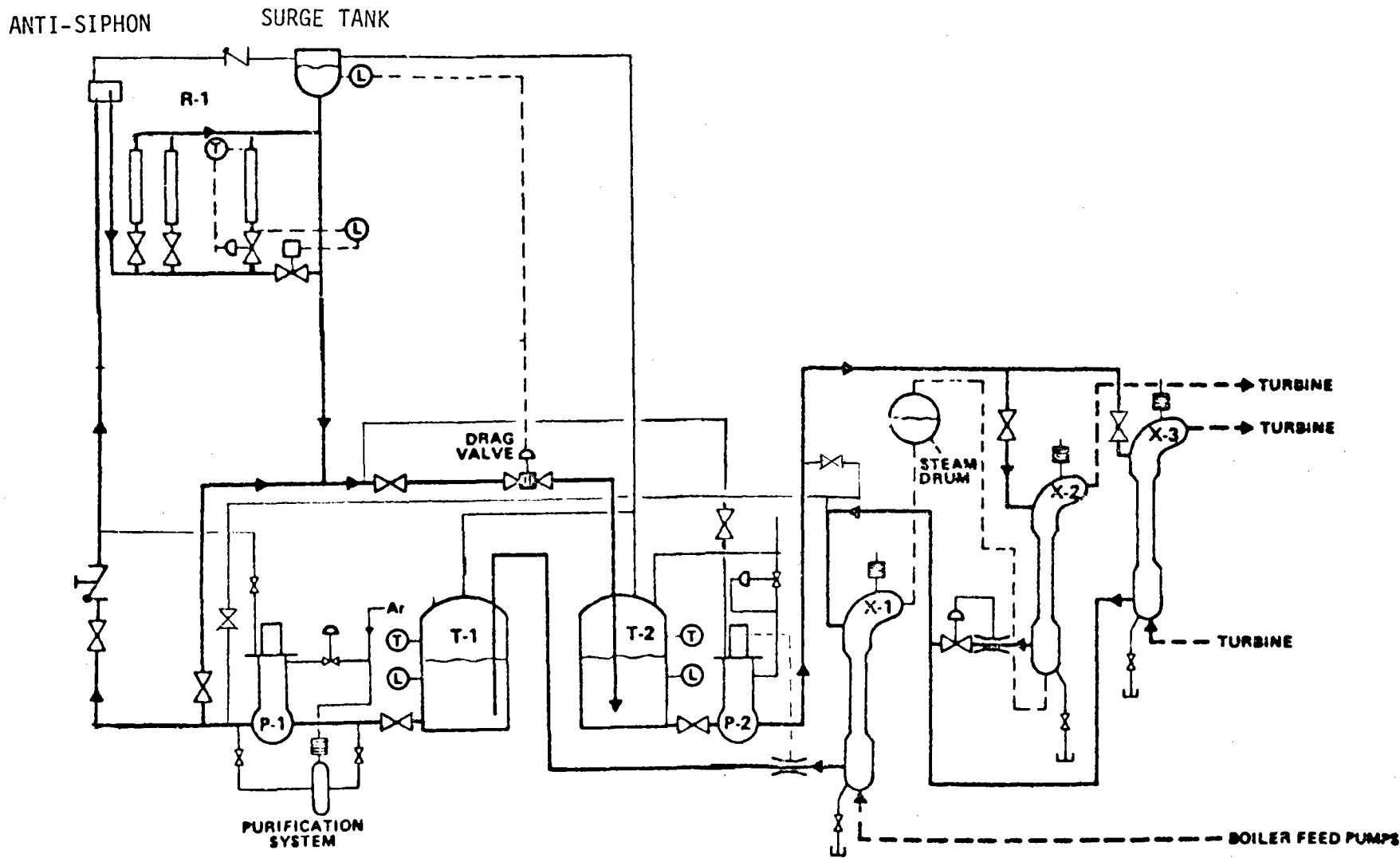
Figure 4-1.   Sodium Heat Transport System

inertia and thermal capacitance thus protecting the pumps and the steam generating equipment from thermal shocks from the sodium. The independence of the second loop permits level loading the power output which minimizes thermal cycling of the steam generators. The stored energy accumulates or is drawn upon automatically since it is simply the difference between the inflow and outflow of Tank T-1.

Sodium circulation is provided by means of the P-1 and P-2 pumps. These are free surface "Fermi" type pump centrifugal pumps. The P-1 pump is a high-head (~300 m (1000 ft) TDH) two-speed (full speed and 25% speed), single-stage centrifugal pump. The lower speed is only used at plant startup. The bearing flow at startup is provided by opening the block valve in the supply line to the pump bearing. Immediately after the pump starts the pump discharge pressure supplies the hydrostatic bearing. The large suction stop valve is required for maintenance. The free surface level is maintained by pressurizing the pump ullage with argon. The P-2 pump is a variable speed, single-stage pump of the same type as the P-1 pump. The speed control is a modified Kramer system which operates as a straight induction motor at full speed. Sodium is supplied to the pump hydrostatic bearing at startup by means of a line connected to the downcomer. The in-the-pump level is controlled by argon pressurization. The pumps are described in more detail in Section 4.6. Sodium flow through the receiver is modulated by the control valves on each panel to maintain the panel outlet temperature constant. The surge tank permits these fast acting valves to operate independently of the drag valve. The drag valve reduces the sodium pressure to near atmospheric pressure to match the pressure requirements of the storage tank. The flow in the downcomer line is modulated to maintain the sodium level in the surge tank fixed. The storage tanks and the drag valve are discussed in Section 5.

The sodium flow in the steam generator loop is set by the power requirements. It is planned to operate this system in a load forcing mode at various fixed power levels as required for the maximum utilization of the plant. The variable speed drive on the P-2 pump has a 5:1 turndown ratio which provides base flow settings. Trim control is provided by control valves in the supply and return lines of the steam generating modules.

The anti-siphon system and the surge tank operate to prevent the draining of the sodium from the receiver on loss of pump power. The anti-siphon device also prevents backflow in this event which would draw hot sodium into the cold header and riser.

4.2.2 Operations

Tentative operating sequence outlines, based on test experience with sodium systems, are presented in Tables 4-2 through 4-6. Outlines are as follows: (1) Table 4-2, Prestartup, gives the basic steps required for preparing the system to receive sodium; (2) Table 4-3, Initial Startup, gives the steps required for bringing the sodium systems up to cold leg temperature for the first time; (3) Table 4-4 gives the steps needed to bring the sodium and steam system to part load. The system is leveled at 1/2 full power to permit its characteristics to be examined before preceding to full power. Subsequent cold startups should be possible in 4 hours or less, depending on the starting temperature (never less than $300^{\circ}F$); (4) Table 4-5, Shutdown, gives the steps needed to secure the plant for an expeditious startup the following day; and (5) Table 4-6, provides the hot startup sequence for full power operation by 0815 mid-winter. The steam generator cooldown characteristics are given in Figure 4-2.

Because of the complete buffering action that is provided by the all-sodium storage system between the receiver and the steam generator system, low solar power operating conditions are accommodated by throttling the receiver independently of the steam generator and electric power generating system. Basically, if the energy input exceeds the turbine requirement, the storage system automatically accumulates the excess. If the turbine demands more energy than the receiver is collecting, the difference is automatically drawn from storage. The maximum stored energy is set by the preliminary specification at 3-1/4 hours of full-power operations.

4.3 SUBSYSTEM ANALYSIS

The dynamic analysis of the sodium subsystem is covered in Section 2.4.

TABLE 4-2
OPERATIONS PRE-STARTUP

Checkout Instrumentation

Preheat Sodium Systems to 150°C (300°F)

Purge with Argon

Heat Tank Car

Fill Storage Tank 210 Cars--100 Days*

---

*An alternate procedure is to fill 25% in 25 days,
start limited operations and complete filling as
required.

TABLE 4-3
OPERATIONS INITIAL STARTUP — FIRST DAY

	Clock Time
Sunrise	0730
Preheat Receiver - Solar - 200°C (400°F)	0800
Start P-1 Pump	
Fill Riser and Downcomer to Receiver Bypass Line	0830
Open Drag Valve Part Way	
Circulate Sodium - Bypass Steam Generator - 174°C (350°F)	
Fill Dry Steam Generator with Sodium and Circulate	0900
Close Receiver Bypass and Fill Receiver	0930
Raise Sodium Temperature to 270°C (525°F) with Solar Heating	1030
Circulate Sodium and Check Out the System	
Shut Down System - Drain Receiver to Standby	1600
Sundown	1645

TABLE 4-4
OPERATIONS STARTUP — SECOND DAY

	Clock Time
Heat Feedwater on Bypass Flow	0500
Pressurize Evaporator to ~6.89 MN/m^2 (1000 psi)	
Admit Water to Evaporator 260°C (500°F)	0600
Start Sodium Flow	0600
Flash Steam to S.H. and R.H. - Condenser	0615
Balance Water, Steam, and Sodium Temperature	0630
Stepwise Raise and Spread at Log Mean ΔT	
Roll Turbine (Min. - 40% Press. - 100°F.S.H.)	0715
Sunrise - Power to Grid	0730
Stepwise Increase Steam Temperature and Flow	
Level at 1/2 Power	0815

TABLE 4-5
OPERATIONS SHUTDOWN — SECOND DAY

	Clock Time
Reduce Load to 10%	1630
Collapse the Log Mean ΔT	
Trip Turbine - Dump to Condenser	1730
Bypass Evaporator - Na and H$_2$O - Evaporator Dry	
Isolate - Full Na - NO H$_2$O	1800

TABLE 4-6
OPERATIONS STARTUP — THIRD DAY

	Clock Time
Heat Feedwater on Bypass Flow	0500
Pressurize Evaporator to ~6.89 MN/m^2 (1000 psi)	
Admit Water to Evaporator 260°C (500°F)	0600
Start Sodium Flow <u>from Bypass Line</u>	0600
Flash Steam through S.H. and R.H. to Condenser	0615
Balance Water Steam and Sodium Temperatures	0630
Stepwise Raise and Spread Log Mean ΔT	
Close Bypass Line	0710
Roll Turbine	
Sunrise Power to Grid	0730
Fill Receiver and Circulate to Storage	0730
Stepwise Increase Steam Temperature and Flow and Power	
Level at Full Power	0800
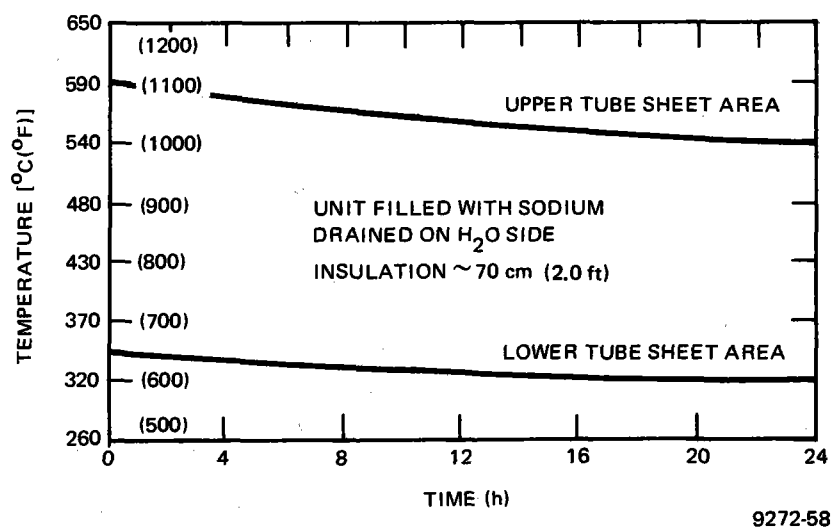
Figure 4-2. Superheater Cooldown

The drag valve description is covered in Subsection 5.4.3.

The energy represented by the elevation difference between the receiver and the hot storage tank is dissipated in the drag valve during operation. The idealized hydraulic energy converted into heat in the drag valve is ~2.2 MW. This energy is supplied by the Receiver Pump P-1 and represents about 18% of the hotel load or 2.2% of net plant output. It is desirable to recover this energy if it can be done in a cost effective way. All of this energy is not wasted since about 43% of it is converted back into electricity in the plant cycle. What remains to be recovered is 57% of 2.2 MW or 1.25 MW.

An earlier trade study examined the possibility of recovering the head by utilizing a high-pressure loop and a low-pressure loop thermally coupled by a heat exchanger (Figure 4-3). It was determined that the value of the power savings was less than the cost of the heat exchanger. This system was judged not cost effective. An additional eight other methods were examined. These schemes and their summary evaluations are as follows.

SUMMARY OF ALTERNATE SCHEMES

Scheme	Result
Elevated Hot Tank	Not cost effective
Elevated Cold Tank	Not cost effective
Parallel Storage Tanks	Not cost effective
Reduced Downcomer Diameter	Net savings 0.6×10^6
Sodium Turbo Pump Addition	Net savings 0.8×10^6
Jet Pump Addition	Net savings 0.85×10^6
Magnetohydrodynamic (MHD) Addition	Net savings 1.2×10^6
Helical Rotor Generator Addition	Net savings 1.2×10^6

A more detailed discussion of these alternatives is given in Appendix G.
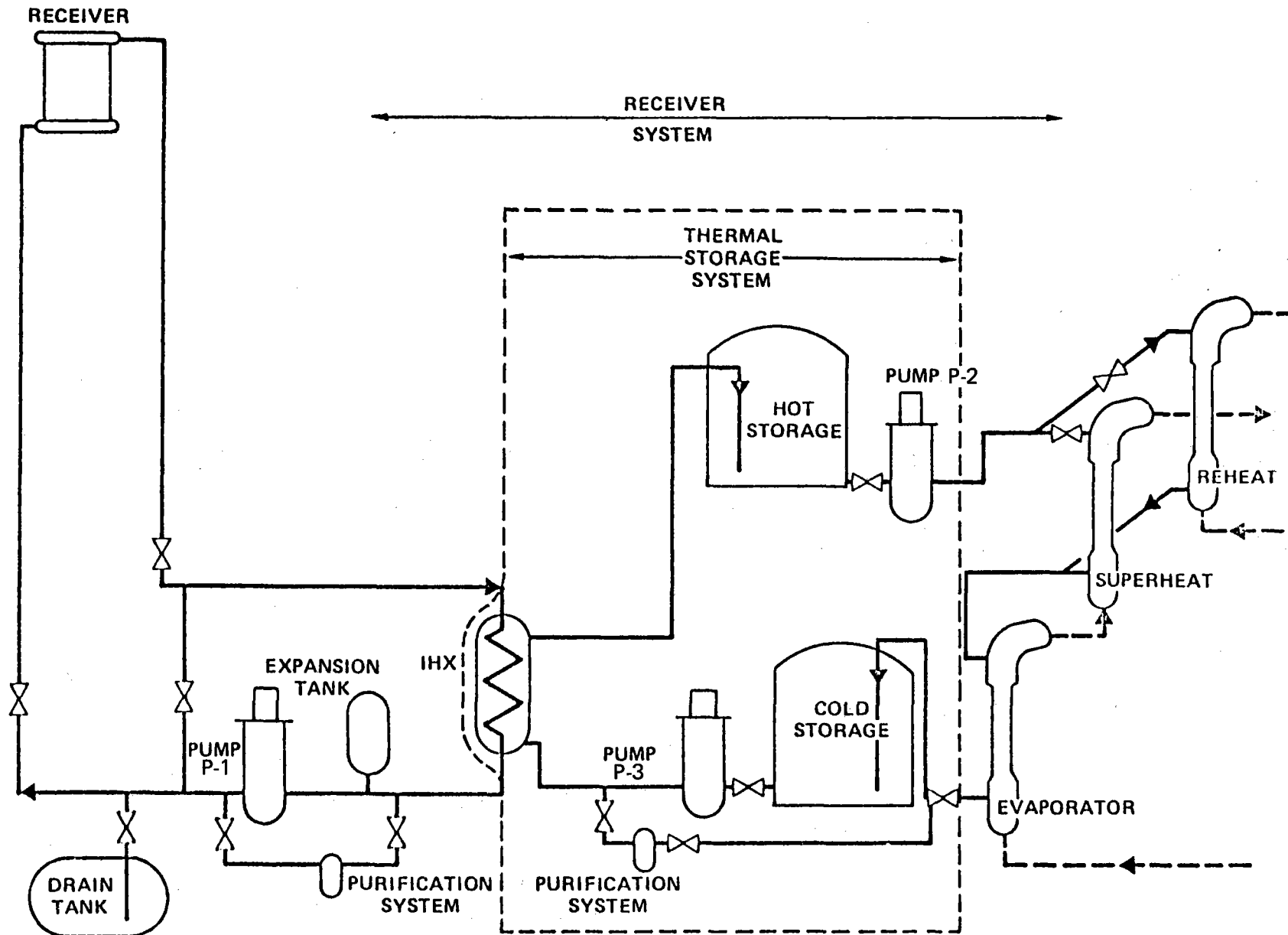
Figure 4-3. Two Loops With IHX

9272-59

4.4 TOWER DESIGN AND ANALYSIS

The tower must be designed to support the receiver, provide access for
maintenance and inspection of the receiver, instruments and controls, piping
and other equipment that may be located on the tower, and adequate provisions
must be made to insure crew safety at all times for required operations, inspec-
tion, maintenance and repair. With respect to earthquake environment, the tower
must survive an earthquake that would produce an acceleration of 0.20 g to
0.25 g horizontal and vertical ground accelerations and shaking intensity of
about VII to VIII on the Modified Mercalli Scale. The spectral data used are
presented in U.S. Atomic Energy Commission (Revision 1 dated December 1973)
Regulatory Guide 1.60. In addition, the plant must satisfy the requirements
specified for seismic zone 3 in the Uniform Building Code.

The conceptual design study for the tower has been completed along with a
sensitivity analysis to determine the effects of various tower height and receiver
weight combinations on tower cost.

The tower is reinforced, slip formed concrete design. The concrete tower
height is 159 m (516 ft) with a base diameter of 24 m (80 ft), top diameter of
9.1 m (30 ft)   The base wall thickness is 0.46 m (1.5 ft); top wall thickness
0.25 m (0.83 ft). The tower supports a total receiver subsystem weight of
224,500 kg (494,000 lb) and rests on a reinforced concrete mat 3 m (10 ft) thick
with an outside/inside diameter of 39.6/9.1 m (130/30 ft).

A sketch of the tower with receiver and receiver support is shown in
Figure 4-4.

Figure 4-5 identifies the various dimensins for the tower conceptual design
which were varied in the process of the tower cost sensitivity analysis.

Table 4-7 presents the dimensions for a tower of various heights from 100
to 400 m (328 to 1312 ft) supporting receiver assemblies of 0 to 3000 kips
(0 to 1.36×10^6 kg).

INPUT DATA

    SEISMIC   0.25g GROUND ACCEL
                (RESPONSE PER NRC REG. 1-60)

    WIND   40 M/S (90 MPH) @ 10m

    SOIL   478 kPa (10,000 LB/FT^2)
                (BARSTOW , CAL)

    TOWER HEIGHT (VARIABLE)
           100m (328 FT) 200m (656 FT)
           300m (984 FT) 400m (1312 FT)

    RECEIVER WEIGHT (VARIABLE)
           O kg (LB) 680,400 kg (1.5 x 10^6 LB)
           226,800 kg (500,000 LB) 1.36 x 10^6 kg
           (3.0 x 10^6 LB)

MODEL
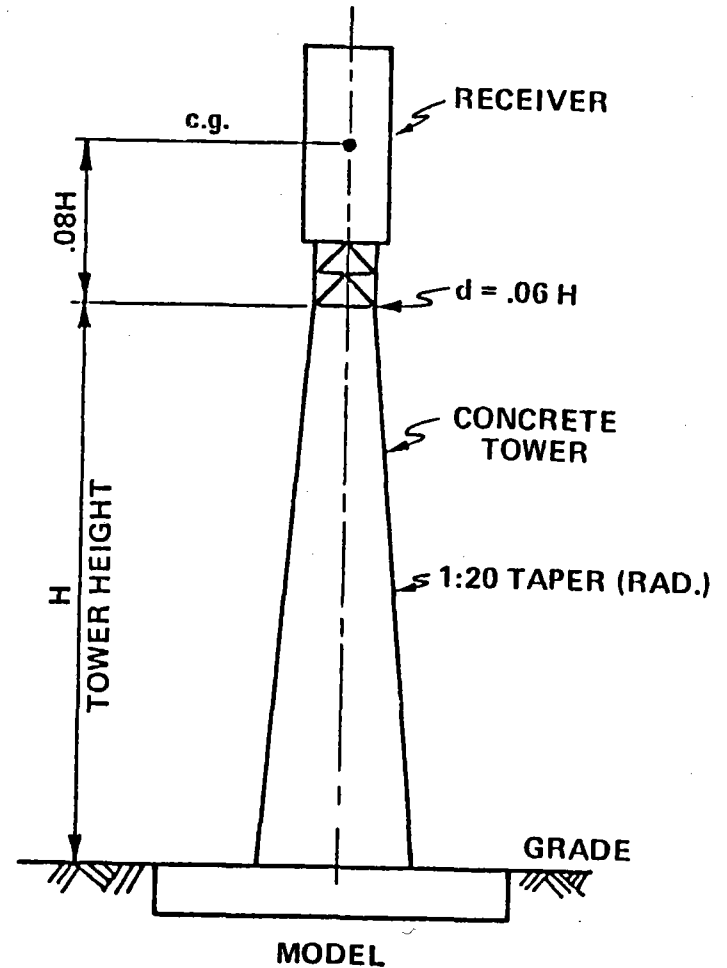
OUTPUT DATA
    PLOT OF TOWER COST VS. TOWER HEIGHT FOR VARIOUS RECEIVERS
    ACCELERATIONS AT RECEIVER C.G.
    DEFLECTIONS AT RECEIVER C.G.
    FUNDAMENTAL TOWER FREQUENCIES

9272-60

Figure 4-4. Receiver Tower Sensitivity Analysis
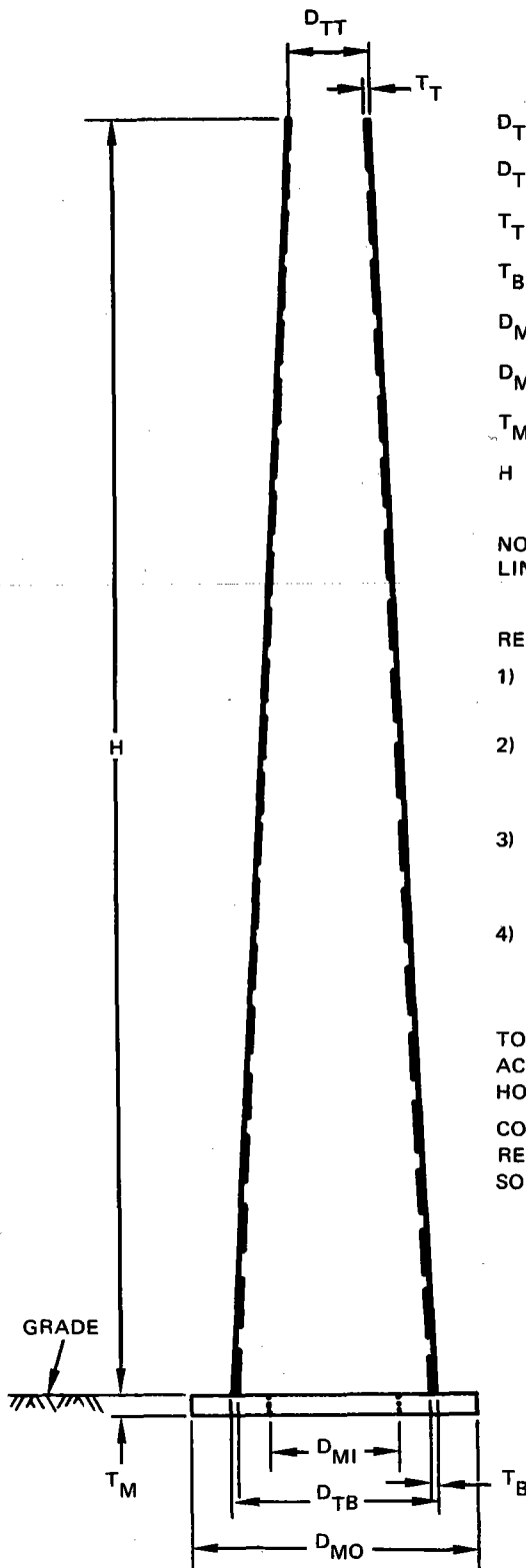
D_{TT} = OUTSIDE DIAMETER AT TOP OF TOWER

D_{TB} = OUTSIDE DIAMETER AT BOTTOM OF TOWER

T_T = TOWER WALL THICKNESS AT TOP

T_B = TOWER WALL THICKNESS AT BOTTOM

D_{MO} = OUTSIDE DIAMETER OF MAT

D_{MT} = INSIDE DIAMETER OF MAT

T_M = MAT THICKNESS

H = TOWER HEIGHT

NOTE: TOWER WALL THICKNESS VARIES
LINEARLY FROM TOP TO BOTTOM

REFERENCES:

1) " BUILDING CODE REQUIREMENTS FOR
REINFORCED CONCRETE" (ACI 318-71)

2) "SPECIFICATION FOR THE DESIGN AND
CONSTRUCTION OF REINFORCED
CONCRETE CHIMNEYS" (ACI 307-69)

3) "DESIGN RESPONSE SPECTRA FOR SEISMIC
DESIGN OF NUCLEAR POWER PLANTS"
(NRC REG. GUIDE 1.60)

4) "DAMPING VALUES FOR SEISMIC DESIGN
OF NUCLEAR POWER PLANTS"
(NRC REG. GUIDE 1.61)

TOWER DESIGN BASED ON 0.25 g MAXIMUM GROUND
ACCELERATION IN BOTH VERTICAL AND
HORIZONTAL DIRECTIONS WITH 7% DAMPING

CONCRETE f'c = 4 ksi
REBAR Fy - 60 ksi
SOIL BEARING PRESSURE = 10 ksf (ALLOW 1/3
INCREASE FOR SEISMIC)

9272-61

Figure 4-5. Receiver Tower Model

TABLE 4-7
ADVANCED CENTRAL RECEIVER —
TOWER AND MAT DIMENSIONS
(Job No. 20325)
STEARNS-ROGER
FEBRUARY 6, 1978

Height (m)	Dimensions (ft)*	Receiver Weight (kips)*			
		0	500	1500	3000
100	D_{TT}	20.0	20.0	20.0	20.0
	D_{TB}	53.0	53.0	53.0	53.0
	T_{TT}	0.5833	0.5833	0.8333	1.0
	T_{TB}	0.9167	0.9167	1.25	1.5
	D_{MO}	90.0	90.0	100.0	106.0
	D_{MI}	0.0	0.0	0.0	0.0
	T_M	0.0	8.0	9.0	10.0
200	D_{TT}	40.0	40.0	40.0	40.0
	D_{TB}	106.0	106.0	106.0	106.0
	T_{TT}	0.8333	0.8333	1.0	1.25
	T_{TB}	1.5	1.5	1.875	2.25
	D_{MO}	160.0	160.0	168.0	170.0
	D_{MI}	52.0	52.0	44.0	42.0
	T_M	11.0	11.0	11.0	14.0
300	D_{TT}	60.0	60.0	60.0	60.0
	D_{TB}	159.0	159.0	159.0	159.0
	T_{TT}	1.0	1.0	1.125	1.25
	T_{TB}	2.0	2.0	2.25	2.5
	D_{MO}	220.0	220.0	224.0	230.0
	D_{MI}	98.0	98.0	94.0	88.0
	T_T	15.0	15.0	15.0	15.0
400	D_{TT}	80.0	80.0	80.0	80.0
	D_{TB}	212.0	212.0	212.0	212.0
	T_{TT}	1.25	1.25	1.25	1.25
	T_{TB}	2.5833	2.5833	2.5833	2.5833
	D_{MO}	284.0	284.0	284.0	284.0
	D_{MI}	140.0	140.0	140.0	140.0
	T_M	15.0	15.0	15.0	15.0

*Refer to Figure 1-1

Table 4-8 shows the accelerations and deflections for the same combinations of tower height and receiver weight.

Figure 4-6 presents the final results of the cost vs tower height and receiver weight.

Appendix H presents the cost backup data for the Stearns-Roger ACR Central Receiver Tower Study.

4.5 STEAM GENERATOR

The reference design utilizes three steam generator units: an evaporator, a superheater, and a reheater. The evaporator is made of unstabilized 2-1/4 Cr - 1 Mo ferritic steel. This material was chosen because of its excellent resistance to chloride stress corrosion cracking in an aqueous environment, and the excellent and extensive field experience with it. The superheater and reheater units are Type 316 austenitic stainless steel. This material is used because its higher strength at the design temperature makes it cost effective compared to the 2-1/4 Cr - 1 Mo material. Chloride stress corrosion is only initiated in aqueous solution, thus if the bulk liquid is kept out of the stainless steel units chloride stress corrosion does not become a problem. To accomplish this, a combined steam drum and steam separator are installed between the evaporator and the superheater and reheater to assure that no bulk liquid is carried over to the stainless steel units. The units are shown mounted vertically to avoid problems which could arise due to temperature stratification on the sodium side.

The physical features of the evaporator unit are shown in Figure 4-7. The water and steam flow through the tubes because this is the high pressure side of the unit, and the sodium flows in the shell. The "hockey stick" configuration allows individual tubes to deflect during thermal transients, thus virtually eliminating axial tube stresses during thermal transient events. The sodium flow bypasses the bend section because the tubes are supported in the horizontal plane only in this region; elsewhere the tube support plates suppress any potential tube vibration due to flow. A unit, similar to the one shown, has been built and tested in sodium. A summary of the test results is given in Figure 4-8.

TABLE 4-8

ADVANCED CENTRAL RECEIVER —
DYNAMIC RESPONSE (SEISMIC)
(Job No. 20325)

STEARNS-ROGER
FEBRUARY 6, 1978

Height (m)	Parameter	Receiver Weight (kips)*			
		0	500	1500	3000
100	Fund. Hor. Freq., Hz	1.25	0.83	0.62	0.50
	Rcv. Hor. Accel., G's	1.35	0.73	0.49	0.39
	Rcv. Hor. Defl., In.	4.61	6.81	7.36	8.75
	Fund. Vert. Freq., Hz	10.49	8.77	7.34	6.23
	Rcv. Vert. Accel., G's	0.86	0.90	0.85	0.81
	Rcv. Vert. Defl., In.	0.07	0.11	0.14	0.19
200	Fund. Hor. Freq., Hz	0.65	0.59	0.53	0.47
	Rcv. Hor. Accel., G's	1.39	1.48	0.96	0.71
	Rcv. Hor. Defl., In.	10.43	12.29	12.71	13.30
	Fund. Vert. Freq., Hz	5.36	5.20	5.00	4.74
	Rcv. Vert. Accel., G's	1.08	1.09	1.10	1.09
	Rcv. Vert. Defl., In.	0.32	0.35	0.38	0.42
300	Fund. Hor. Freq., Hz	0.44	0.43	0.41	0.38
	Rcv. Hor. Accel., G's	1.26	1.89	1.38	1.03
	Rcv. Hor. Defl., In.	16.66	19.26	19.68	20.09
	Fund. Vert. Freq., Hz	3.63	3.59	3.53	3.45
	Rcv. Vert. Accel., G's	1.22	1.21	1.22	1.21
	Rcv. Vert. Defl., In.	0.77	0.79	0.83	0.86
400	Fund. Hor. Freq., Hz	0.34	0.33	0.32	0.31
	Rcv. Hor. Accel., G's	1.21	2.09	1.70	1.26
	Rcv. Hor. Defl., In.	23.41	26.87	27.21	27.61
	Fund. Vert. Freq., Hz	2.74	2.72	2.70	2.66
	Rcv. Vert. Accel., G's	1.10	1.08	1.08	1.08
	Rcv. Vert. Defl., In.	1.12	1.12	1.14	1.16

*Accelerations and deflections for "zero-weight" receiver are referred to top of tower. Accelerations and deflections for 500, 1500, and 3000 kip receivers are referred to receiver centroid, assumed 0.08H above top of tower.
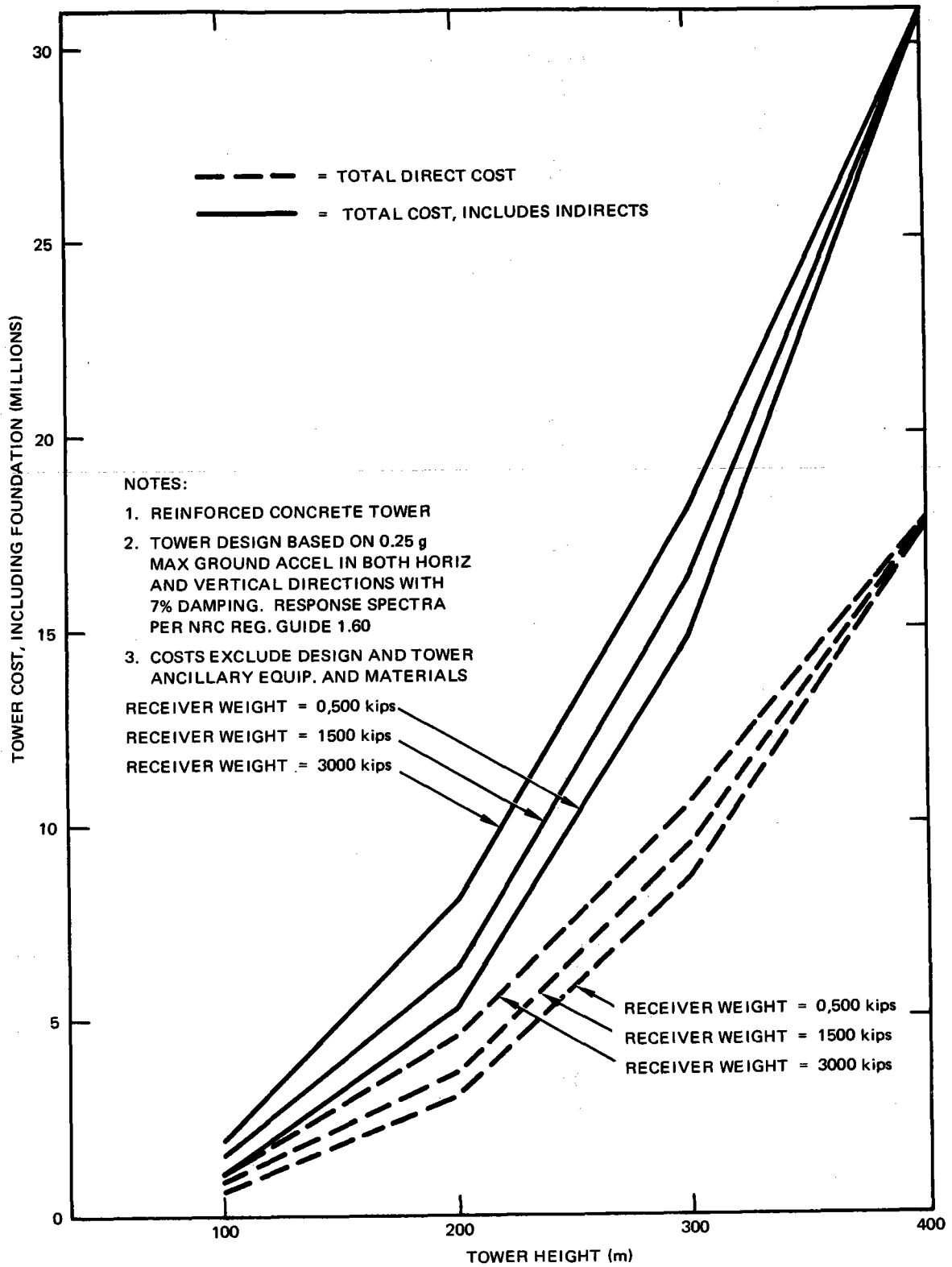
Figure 4-6.   Receiver Cost vs Tower Height and Weight
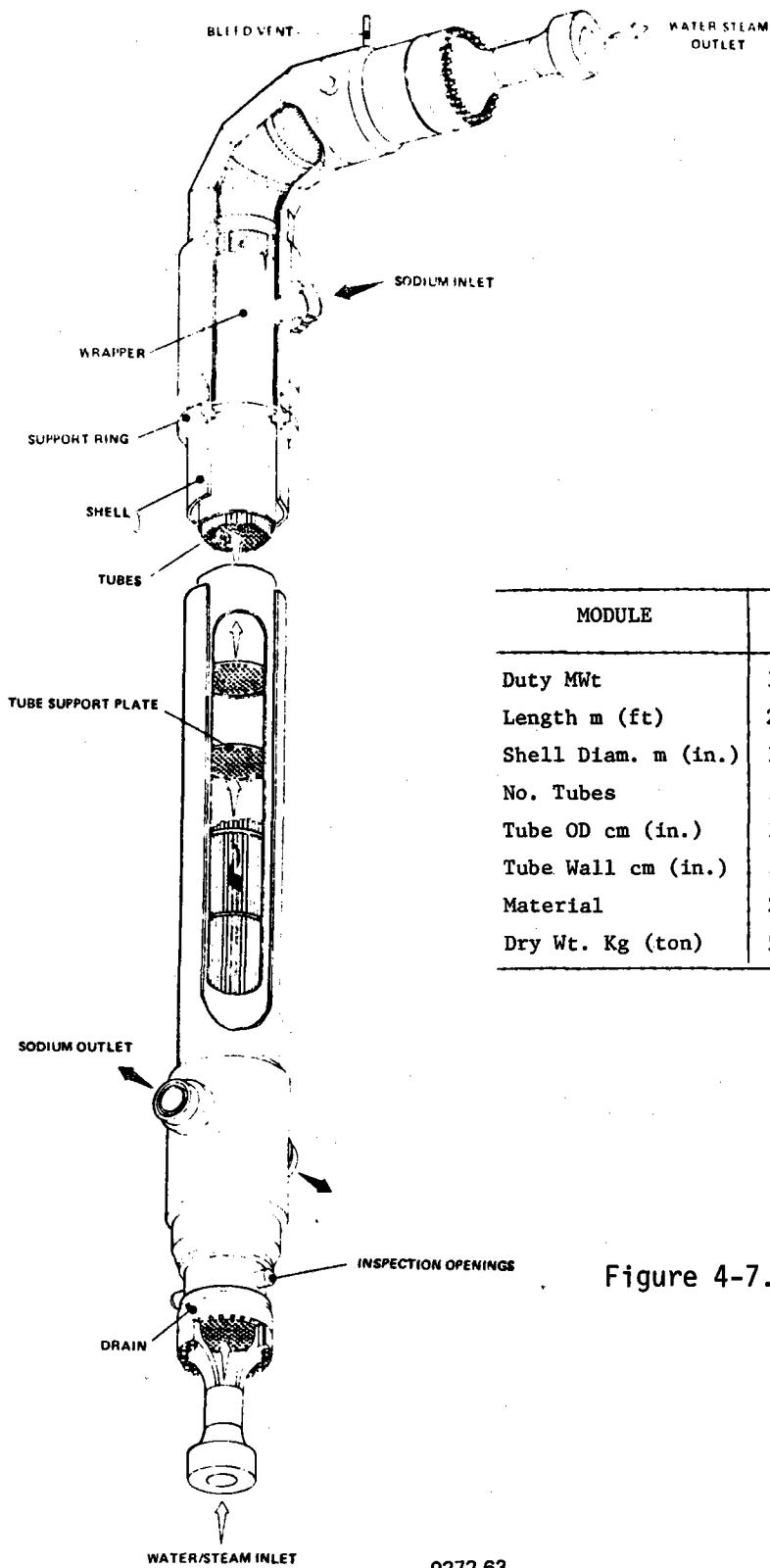
MODULE	EVAP	SH	RH
Duty MWt	148	76.1	35.3
Length m (ft)	29 (95)	27.7 (91)	20.1 (66)
Shell Diam. m (in.)	1.22 (48)	.76 (30)	.81 (32)
No. Tubes	1100	283	163
Tube OD cm (in.)	1.59 (5/8)	1.9 (3/4)	3.81 (1.5)
Tube Wall cm (in.)	.19 (.075)	.335 (.132)	.272 (.107)
Material	2-¼ Cr-1 Mo	316	316
Dry Wt. Kg (ton)	58,000 (64)	20,000 (22)	22,000 (24)

Figure 4-7. Steam Generator Modules

9272-63

62 ft 0 in.

9 ft 0 in.

STEAM OUTLET

DETAIL A

SODIUM INLET

158 TUBES – 5/8 in. OD x 0.109 in. WALL

BUTT WELD

BOSS ON TUBE SHEET

DETAIL A

TUBE-TUBE SHEET JOINT

18 in.

SODIUM OUTLET

26 in.

MATERIAL – 2-1/4 Cr · 1 Mo

DETAIL A
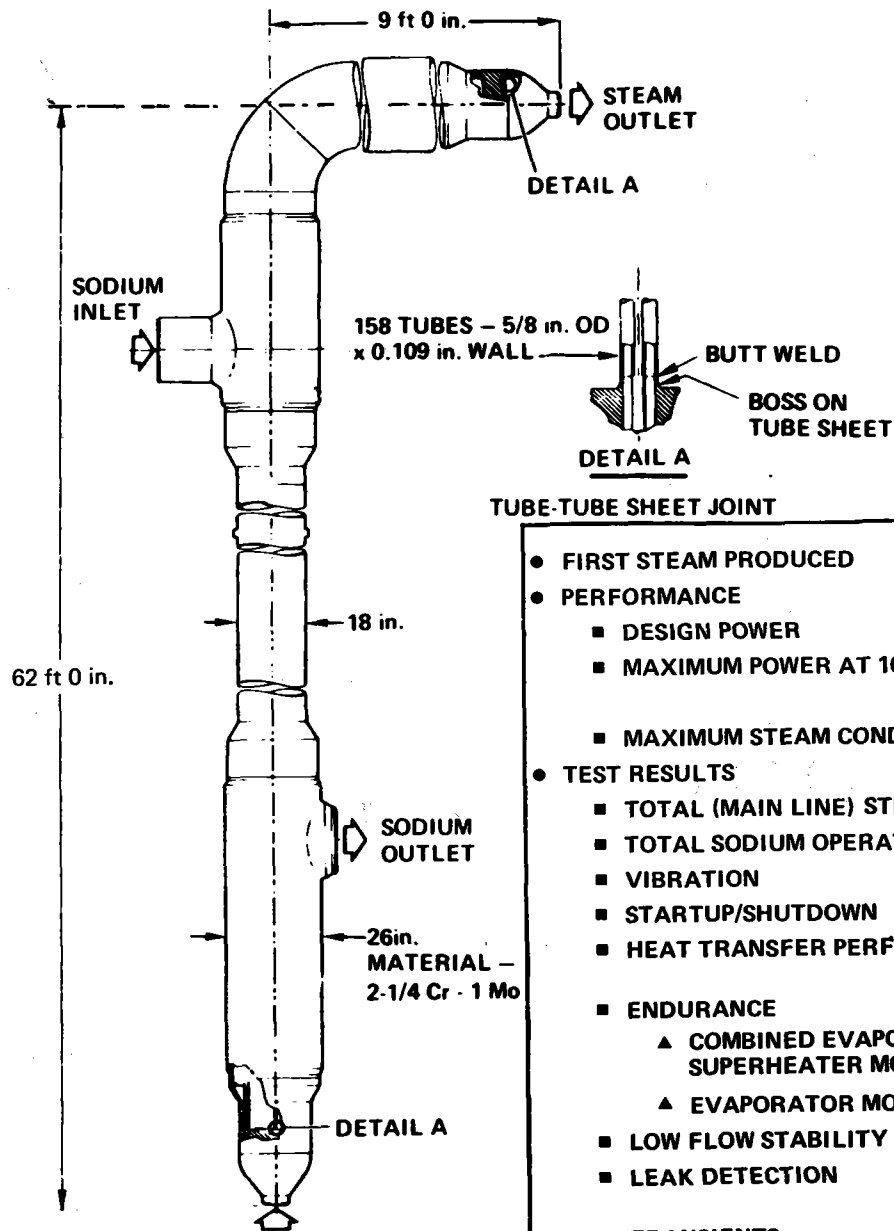
- **FIRST STEAM PRODUCED** — 7-9-72
- **PERFORMANCE**
  - **DESIGN POWER** — 28.4 Mwt
  - **MAXIMUM POWER AT 100% FLOW** — 32.1 Mwt (FOR 2400 psig STEAM)
    33.8 Mwt (FOR 1450 psig STEAM)
  - **MAXIMUM STEAM CONDITIONS** — 2430 psig/930°F
- **TEST RESULTS**
  - **TOTAL (MAIN LINE) STEAMING TIME** — 4015 hr
  - **TOTAL SODIUM OPERATING TIME** — 9305 hr
  - **VIBRATION** — LEVELS LOW, SAFE
  - **STARTUP/SHUTDOWN** — 37 CYCLES, STABLE
  - **HEAT TRANSFER PERFORMANCE** — PARAMETRIC DATA OBTAINED FROM 1450 TO 2450 psig
  - **ENDURANCE**
    - ▲ COMBINED EVAPORATOR/ SUPERHEATER MODE — 500 hr
    - ▲ EVAPORATOR MODE — 500 hr
  - **LOW FLOW STABILITY** — STABLE, ALL CONDITIONS OF INTEREST
  - **LEAK DETECTION** — DETECTABILITY OF 10^{-6} lb/sec H_2O DEMONSTRATION
  - **TRANSIENTS** — INTEGRITY MAINTAINED

74-M20-15-44

Figure 4-8. Highlights of LMEC-SCTI Test of ESG MSG

STEAM OUTLET

SODIUM INLET

SODIUM OUTLET

FEEDWATER INLET

STEAM PRESSURE
2450 psig

SUPERHEATED STEAM REGION

WATER/STEAM TEMPERATURE

FILM BOILING REGION

NUCLEATE BOILING REGION

PREHEAT REGION

IMPROVED CORRELATIONS FROM TEST

SODIUM TEMPERATURE PREDICTIONS –
ORIGINAL PROTOTYPE DESIGN

450 500 550 600 650 700 750 800 850 900 950

TEMPERATURE (°F)

73-J26-6-2
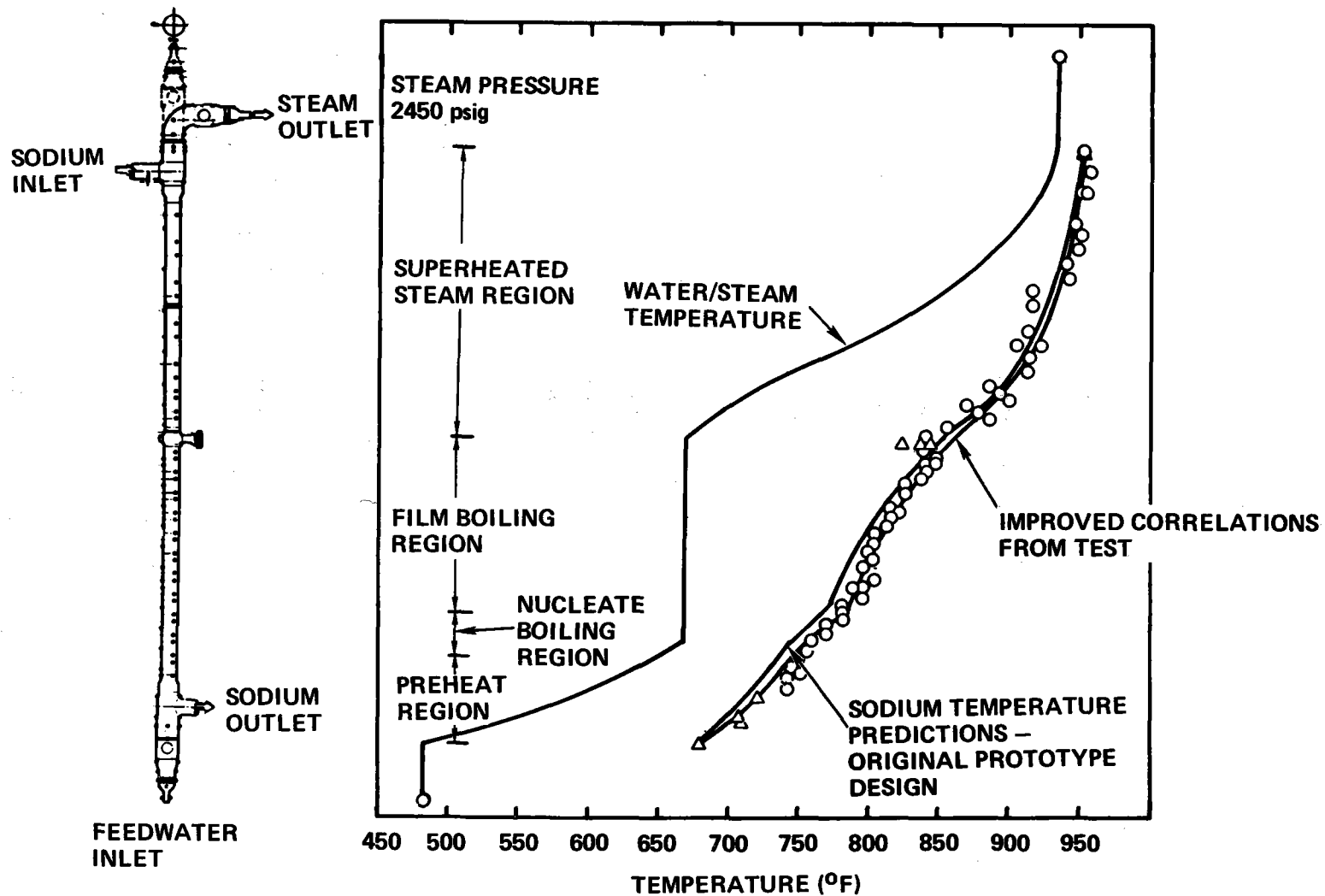
Figure 4-9.   Heat Transfer Results From LMEC-SCTI Test of ESG MSG
(100% Power in Combined Evaporator-Superheater Mode)

It is to be noted that the boss shown in Detail A in this figure is milled out of the solid tubesheet forging; thus, the autogeneous butt weld provides a tube-to-tubesheet weld that can be 100% x-rayed. The performance characteristics of these units correlate well with the engineering predictions. The correlations are shown in Figure 4-9.

4.6 PUMPS

The viable alternative sodium pumps for large-scale sodium systems appear to be alternating current electromagnetic induction pumps or centrifugal pumps. Electromagnetic induction pumps require no moving parts and no pressure boundary penetration for their operation. These excellent operational characteristics are offset by the difficulty in maintaining the pump in a shutdown condition. In addition, the pumping efficiency of these pumps is <50% which leads to an unacceptable economic penalty. A comparison of electromagnetic pumps vs mechanical pumps is given in Appendix J.

Free surface pumps for large-scale sodium service have already been developed for the Liquid Metal Fast Breeder Reactor Program. Two basic designs are available: the Hallam-type and the Fermi-type. The key differences are shown in Figure 4-10. For our purpose, the Fermi-type appears to be the better choice since it does not require the seal bypass overflow line; it has a higher efficiency; it is more tolerant of pipe reactions; it has lower pressure boundary stresses; and it is more fully developed than the Hallam-type. (The Fast Flux Test Facility and the Clinch River Breeder Reactor plants utilize a version of this concept.) The implementation of this pump type for the P-1 and P-2 pumps is shown schematically in Figure 4-11. The overall dimensions and hydraulic characteristics of these pumps is given in Appendix A "Design Data Sheets."

4.7 PIPE AND VALVES

The tower downcomer stainless steel piping expands approximately 102 in. during heatup from ambient to the receiver outlet temperature of 1100°F. The mild steel riser piping expands about one-half this amount in heating up to

HEIGHT OF SEAL
BYPASS SODIUM

SEAL
BYPASS
OVERFLOW
LINE

SEALS

BEARING
(HYDROSTATIC)

BEARING
SUPPLY

HIGH
PRESSURE

OUTLET

INLET

"HALLAM" TYPE

SHUTDOWN
FREE
SURFACE

OPERATING
FREE
SURFACE
(DRAWNDOWN)

BEARING
(HYDROSTATIC)
AND SEAL

BEARING
SUPPLY

SUBMERGENCE

LOW
PRESSURE

HIGH
PRESSURE

INLET   OUTLET

"FERMI" TYPE
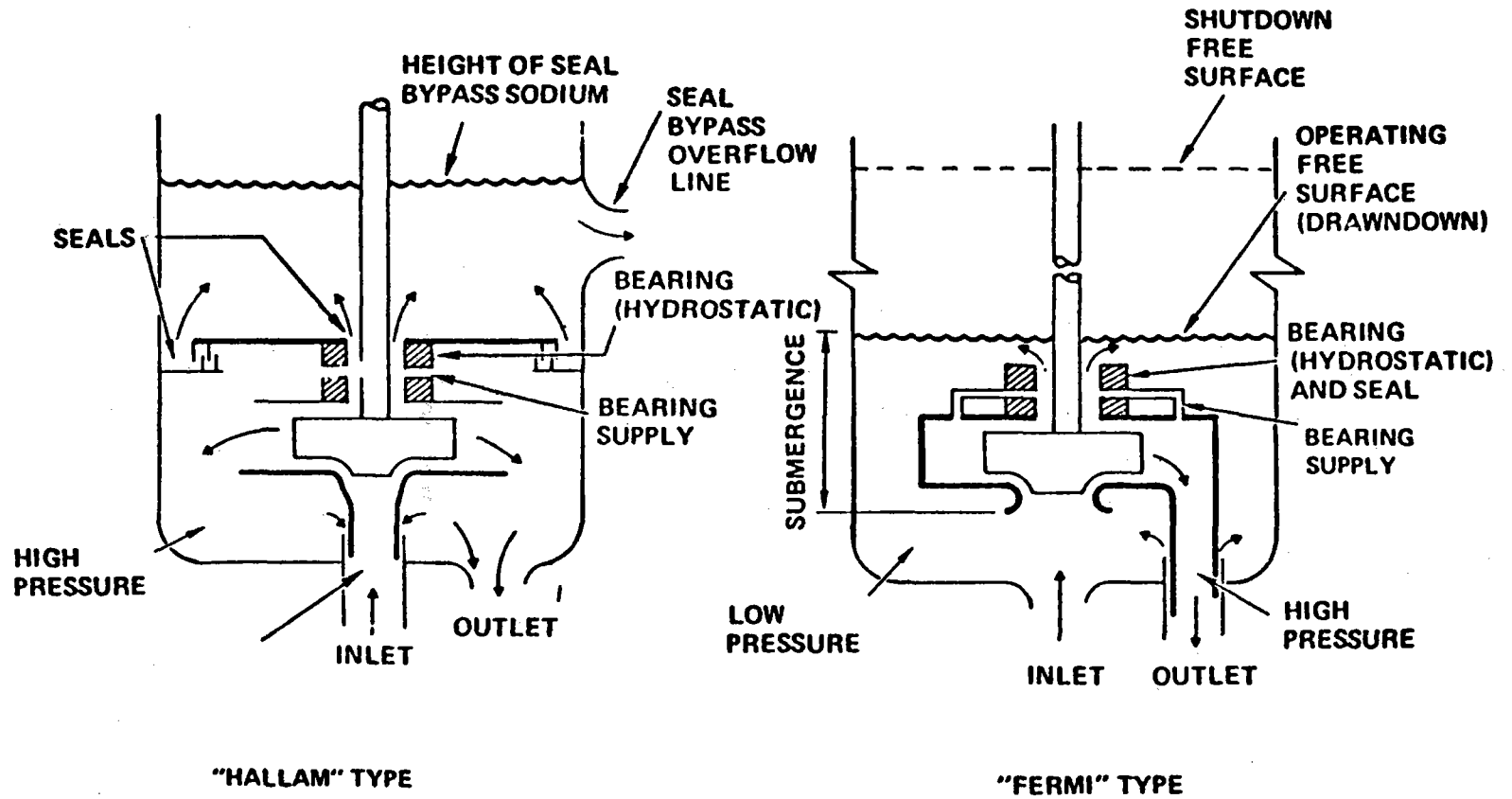
Figure 4-10.   Key Differences Between the Fermi and Hallam Pumps

Figure 4-11. Reference Pump

SUPPORT RING

96 in.

186 in.

THERMAL SHIELD

SODIUM LEVEL

HYDROSTATIC BEARINGS

DISCHARGE COLLECTOR

9272-64
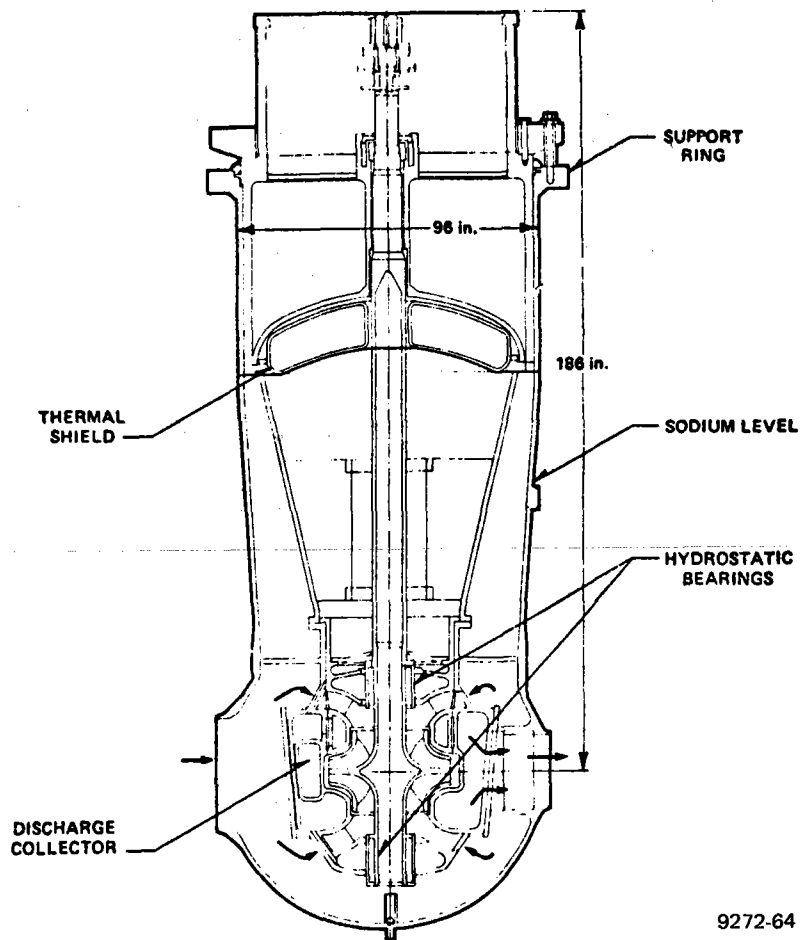
550°F. Two methods have been identified to accommodate the 102 in. of thermal expansion of the downcomer. The simplest pipe arrangement is to fix the down-comer at the receiver and storage tank ends and taking the expansion in a single plane with one 5D bend and a 235-ft horizontal run of pipe. Although this arrangement is geometrically simple, it complicates the pipe hanger requirements because of the large motions. An alternate arrangement utilizes ten expansion loops and ten anchor points on the tower. Each loop contains four 5D bends and 20 ft of straight pipe. The pipe hangers would be conventional rigid supports. This subject is discussed in more detail in Appendix K, Book 2. The reference design is designated as Type I in that appendix.

The drag valve is discussed in Subsection 5.4.3. The remaining valves will be similar to those developed for the Fast Flux Test Facility and the Clinch River Breeder Plant project. The small valves will be bellow seal valves, the larger valves may be freeze stem valves.

5.0 THERMAL STORAGE SUBSYSTEM

5.1 REQUIREMENTS

The thermal energy storage subsystem provides the means of storing energy which is available from the receiver; provides supplemental thermal energy when the thermal power from the receiver is less than that required for plant operation at nameplate electrical rating; provides all thermal energy for operation of the plant at nameplate electrical rating (for the specified time period); and reserves thermal energy for startup and shutdown.

In general, the thermal storage system must be designed to maximize the economic recovery of useful energy from storage and to minimize, with cost-effective considerations, energy storage losses during the various operating modes. Operation and maintenance requirements must be provided for in the design, and the thermal storage subsystem must be compatible with the other subsystem during normal, transient, and emergency operations. The thermal storage subsystem functional requirements are given in Table 5-1.

The thermal storage subsystem is required by the Reference 1 specification to charge at a maximum rate of 100% of receiver thermal power or 390 MWt. The maximum discharge rate is 250 MWt for electric power generation at 100 MWe net. While the all-sodium storage system inherently permits this operation without special design consideration on cost, the alternate air-rock bed storage system requires a special operating mode and a substantial increase in fan power in order to accomplish the maximum charging rate. The air handling system for the air-rock bed storage system presented here is sized for the maximum charge rate condition, but with added hardware costs and with an additional operating mode.

5.2 DESIGN CHARACTERISTICS

5.2.1 All-Sodium Storage

The all-sodium ARC concept is shown in Figure 1-2. The thermal storage subsystem contains the hot and cold storage liquid sodium tanks, the P-2 pump, a

TABLE 5-1

ADVANCED CENTRAL RECEIVER THERMAL STORAGE
SUBSYSTEM FUNCTIONAL REQUIREMENTS

Parameter	Requirement
Thermal Storage Capacity	
Capacity (MWt-h)	750
Additional Capacity for Shutdown, 12 hr Hold and Restart (MWt-h)	62.5
Total Capacity (MWt-h)	812.5
Maximum Charging Rate (MWt)	390
Maximum Extraction Rate (MWt)	250
Time at Maximum Extraction Rate (h)	3
Temperature Conditions	Generate Steam Including Reheat at $1000^\circ F^{+10}_{-50}$
Reduced Power Operation (%)	10 to 100
Transient Operation (Power)	
10% to 100% or 100% to 10% (s)	90
30% Charge to 100% Extraction or 100% Extraction to 30% Charge	2 min

pressure-reducing device, and interconnecting pipe. Liquid sodium from the receiver subsystem is stored in the hot storage tank at energy rates up to 390 MWt, which corresponds to a flow rate of 3.66×10^6 kg/h (8.07×10^6 lb/h). Sodium is drawn from the hot storage tank at energy rates of up to 250 MWt 2.34×10^6 kg/h (5.29×10^6 lb/h) to generate steam for the Electric Power Generating Subsystem. Sodium from the steam generator units flows to the cold storage tank. During the day, hot sodium is accumulated by the hot tank in a sufficient quantity to store up to 3.25 h of operation at 100% rated power. With this storage arrangement, plant operation is always from storage. The steam conditions provided are the same regardless of whether the receiver loop is operating or not.

The storage tanks are 30.5 m (100 ft) in diameter with a height of 13.6 m (45 ft) for the hot storage tank and 12.3 m (41 ft) for the cold. The hot tank

operating at 593°C (1100°F) is made of stainless steel; the cold tank at 288°C (550°F) is made of carbon steel. The tanks operate at static head pressures only in order to minimize cost. This requires a pressure-reducing device to dissipate the tower static head.

The pressure-reducing device for the baseline configuration consists of a nominal 18 in. drag valve. A steam generator pump in this system moves the hot sodium through the steam generator units to the cold storage tank. The receiver pump identified in the Receiver Subsystem description charges the hot storage tank. The steam generator pump is similar to the FFTF pump with approximately the same head and flow requirements. The developed head for this pump is 76 m (250 ft) at 0.95 m^3/s (15,000 gpm).

The thermal storage system functional requirements are presented in Table 5-1. The design characteristics of the all-sodium ACR Thermal Storage Subsystem are presented in the Design Data Sheets of Appendix A, Book 2. A layout drawing of the high temperature storage tank constructed with stainless steel is shown in Figure 5-1. The low-temperature tank is similar, only using carbon steel.

5.2.2 Alternate Air-Rock Bed Storage System

The ACR concept with the air-rocks thermal storage alternative is shown in Figure 5-2. Appendix B of Book 2 to this report presents the ACR-P&ID preliminary version for the Air-Rock Thermal Storage Alternative System (Drawing N272000002) along with a set of Design Data Sheets for this alternative.

In this arrangement, the thermal storage subsystem consists of the air-rock thermal storage unit with the air-sodium (or sodium-air) heat exchanger and the necessary interconnecting piping, valves, and associated instrumentation and control systems required for the proper integrated operation of the thermal storage subsystem with the remainder of the ACR plant.

The operational modes and control methodology unique to the air-rocks thermal storage subsystem alternative are discussed here with the position of

PLAN

ROOF PURLINS - 6" C FORM
MAKE FROM 1/2" x 12" x 30 TO 34 FT.

BEAM FLANGES - 1 R 1 1/2" x 10' x 36' (CUTS 8)
BEAM WEBS - 1 R 3/4" x 8.34' x 36' (CUTS 4)

CENTER ROOF PURLINS:
1 R 3/8" x 4' x 23' (CUTS 4)
1 R 3/8" x 4' x 15' (CUTS 4)
1 R 3/8" x 4' x 17' (CUTS 8)

25'-0
TYP

SUMP
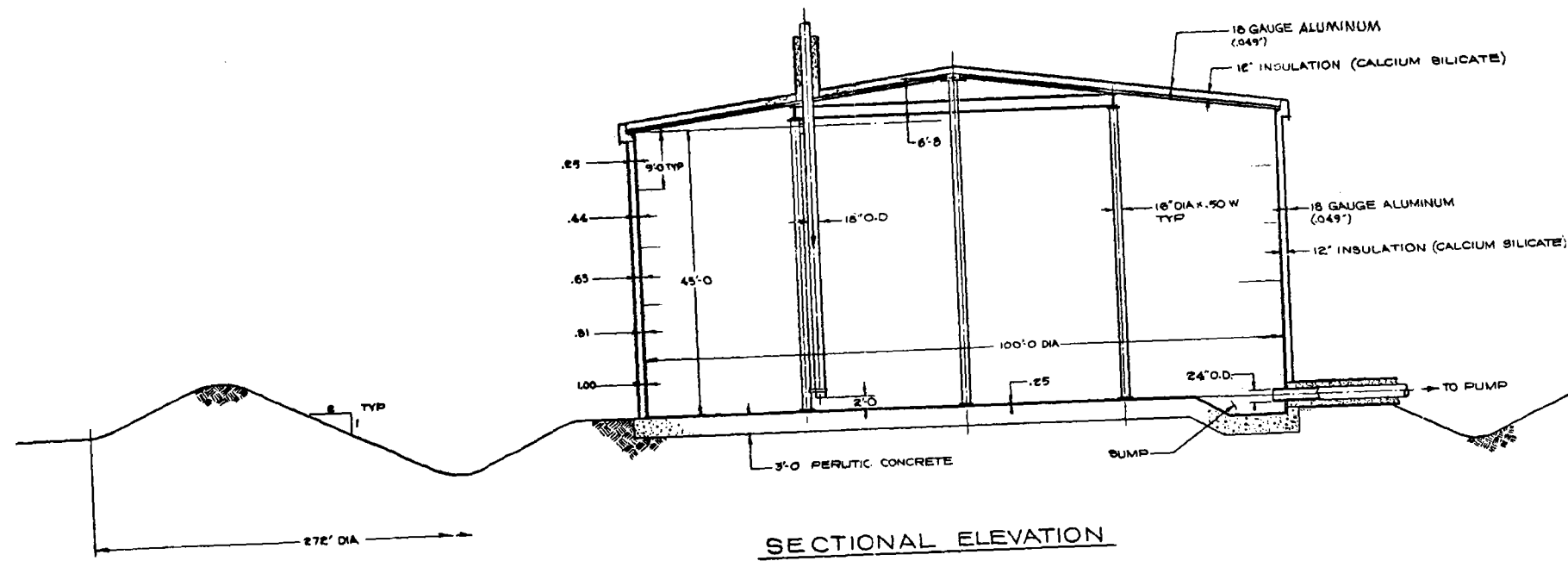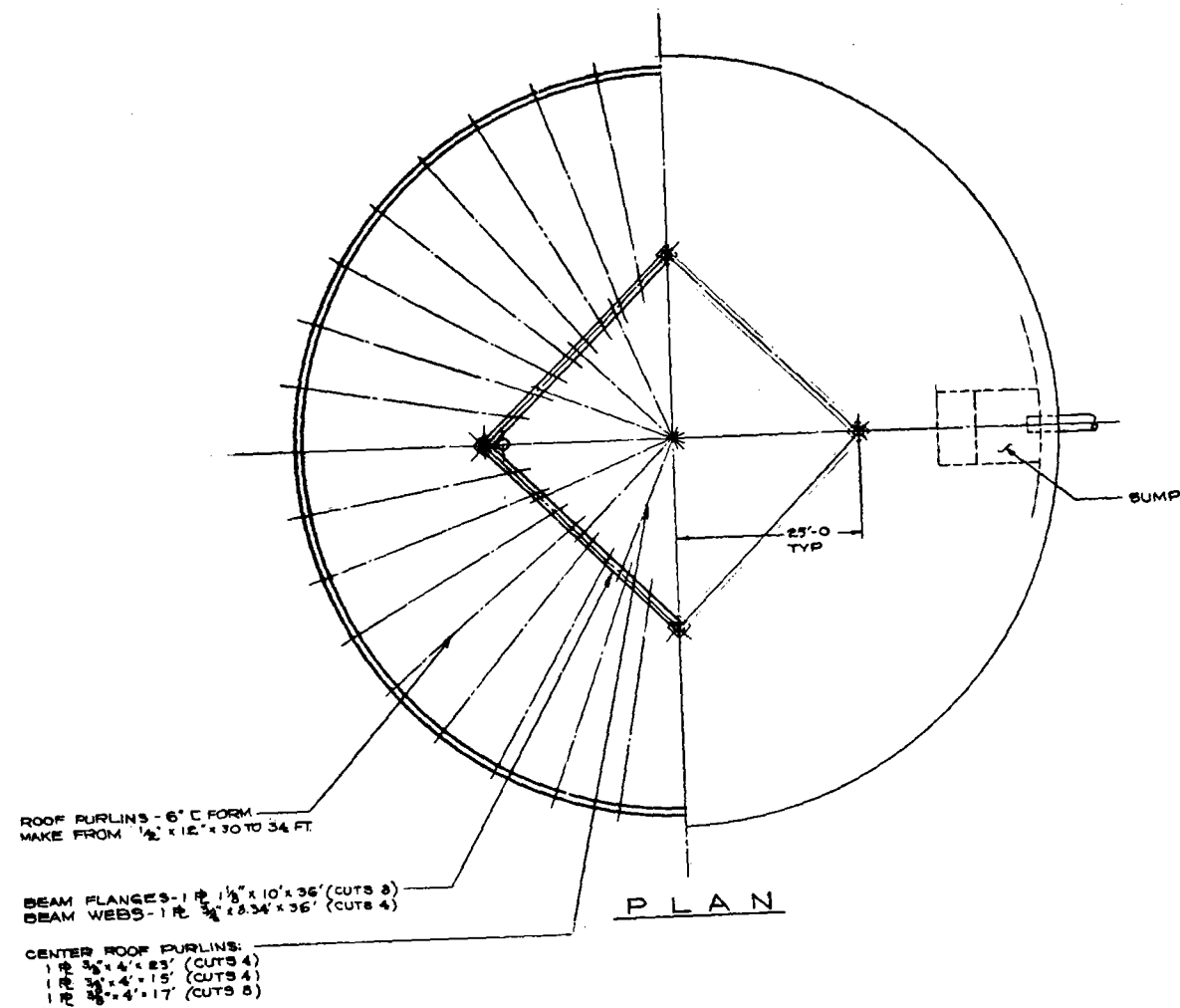
MAT'L. NOTE:
304 CRES EXCEPT AS
SHOWN OTHERWISE

18 GAUGE ALUMINUM
(.049')

12" INSULATION (CALCIUM SILICATE)

18"DIA x .50 W
TYP

18"O.D

6'-8

3'-0 TYP
.25

.44

.65

.81

1.00

45'-0

18" DIA x .50 W
TYP

18 GAUGE ALUMINUM
(.049')

12" INSULATION (CALCIUM SILICATE)

100'-0 DIA

24"O.D.

.25

2'-0

TO PUMP

8 TYP

3'-0 PERLITIC CONCRETE

SUMP

272' DIA

SECTIONAL ELEVATION

Figure 5-1. High Temperature
Sodium Tank Layout

ESG-79-2, Vol II, Book 1

5-5
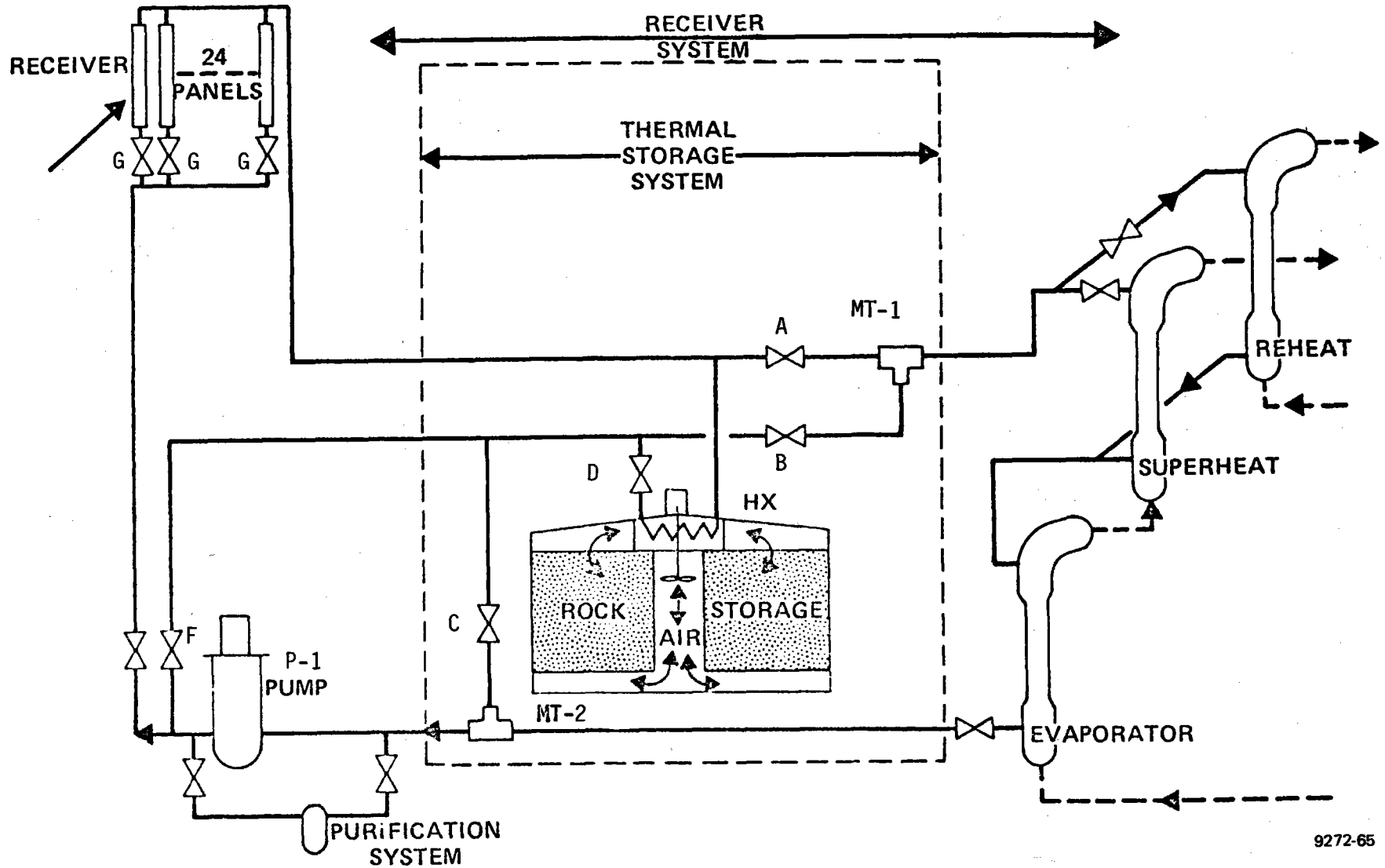
Figure 5-2. Advanced Central Receiver Hot Rocks and Air Thermal Storage

9272-65

TABLE 5-2

VALVE POSITIONS IN VARIOUS OPERATIONAL MODES

Mode	Valve Position						Remarks
	A	B	C	D	F	G	
Normal Solar Power	Open-Controlling	S.G.Na Temp Control	Open	Open-Controlling	Closed	Open-Controlling	Excess Receiver Output to Storage Fans and Air Flow Direction per Design
Low Solar Power	Open-Controlling	Closed	Closed	Open-Controlling	Open	Open-Controlling	Receiver Output Supplemented by Storage; Fans and Air Flow Reverse
Intermittent Cloud	Open-Controlling	Closed	Closed	Open-Controlling	Open	Open-Controlling	Receiver Output Supplemented by Storage; Fans and Air Flow Reverse
Operation from Storage	Open-Controlling	Closed	Closed	Open-Controlling	Open	Closed	All Power from Thermal Storage only. Fans and Air Flow Reverse
Thermal Storage Charging Only	Closed	Closed	Open	Open-Controlling	Closed	Open-Controlling	All Power to Thermal Storage; Air Flow and Fans Direction per Design

the valves identified in Figure 5-2 shown in Table 5-2. The thermal storage subsystem must be designed to operate in a stable manner for several different operating modes which can be described as follows.

5.2.2.1 <u>Normal Solar Power</u> (1.5 ≥ Effective Solar Multiple ≥ 1.0)

During the normal solar power operating mode, sodium is pumped to the receiver where it is raised to the peak operating temperature by the insolation energy focused on the receiver panels by the heliostat field. The heated sodium then flows by gravity to the thermal storage system and to the steam generating system. More sodium flows from the receiver than is required by the steam generating system. The excess sodium flows through the heat exchanger of the thermal storage system through Valves D and C and into Mixing Tee 2 where it is mixed with sodium returning from the steam generating system. From Mixing Tee 2, the sodium goes to the pump suction where the loop is completed. The air flow in the thermal storage unit is toroidal flowing upward through the center and across the heat exchanger, then downward through the rock bed heating and rock bed matrix from the top down. The thermal energy in the rock bed is later used to provide thermal energy required for sustained turbine operation (albeit for a specified limited time) when there is insufficient (or none at all) solar insolation. As the insolation changes, the sodium flow to the receiver is changed in proportion by control valves G to maintain constant sodium outlet temperature at the receiver. The excess sodium flow available to the thermal storage heat exchanger (and hence for the storage of thermal energy) is reduced accordingly, until, at some point, the insolation thermal energy rate corresponds to the plant nameplate electrical rating.

5.2.2.2 <u>Low Solar Power Mode</u> (1.0 ≥ Effective Solar Multiple ≥ 0.1)

When the thermal power insolation rate falls below that required for the nameplate rating electrical output, the system is described as operating in the Low Solar Power Mode. The sodium flow through the receiver is further reduced to maintain the design sodium outlet temperature at the receiver (and at the steam generator inlet). To maintain the required sodium flow through the steam

generator system, the receiver flow is supplemented by flow in the reverse direction through the thermal storage heat exchanger. Although the valve position table identifies Valves B and C as being closed during this mode, they are used to obtain temperature and flow control. Simultaneously, the fans and air flow direction are reversed in the air-rock thermal storage unit to discharge (or take heat from) the rock bed. The sodium flow and thermal energy from the thermal storage unit are used to maintain the required thermal energy flow to the steam generators. This supplemental flow is continued until the energy level in the thermal storage unit is reduced to a predetermined level set by the operational strategy. When this level is reached, the electric load is reduced, and the sodium and steam flow rates are reduced accordingly. Operating from the receiver supplemented by storage energy to supply a reduced electric load for a longer time is a variation of this operating mode. Obviously, it is not planned to store energy in this mode. The lowest operating level planned is at ~10% of full power.

5.2.2.3 Intermittent Cloud Operation (Short-Term Variations in Insolation. 1.5 ≥ Effective Solar Multiple ≥ 0.1)

The intermittent cloud case is in effect a combination of the Normal Solar Power mode and the Low Solar Power cases. Ordinarily, the flow bypassed to the thermal storage heat exchanger will be varied to insure that the required constant flow and temperature to the steam generator system is maintained. If the expected integral of the insolation is less than a full power typical day, the electrical output may be reduced. Normally, any energy not used (i.e., the integrated insolation greater than a solar multiple of 1.0 over the time period being considered) is stored in the thermal energy storage unit. On those occasions when the intermittent cloud cover is such as to reduce the effective solar multiplier below 1.0, or what is the same thing, when the insolation is below that required to provide the equivalent thermal energy corresponding to the nameplate electrical rating, it becomes necessary to supplement the energy rate from thermal storage. Since there is a finite time required for the fans to stop (estimated at from 30 to 45 s) and for them to reverse direction to provide adequate air flow (estimated at an additional 45 to 60 s), there is a time

period during which the thermal storage unit cannot provide the required supplementary energy. This "dead spot" problem is ameliorated by the fact that: (1) the rock bed temperature gradient is not reversed; and (2) the temperature gradient along the sodium to air heat exchanger is not reversed either. The top of the rock bed is always at the high temperature, and the bottom of the rock bed is at the cold temperature. The sodium to air heat exchanger is always hot at the outer diameter and colder at the inner diameter. The transient operating modes, one of which is represented by the intermittent cloud case, would normally have to contend with the long time constant of both the rock bed and the heat exchanger. This is fortunately not the case. For those cases where the intermittent cloud event occurs over a very short time period, it is best not to perturb the system and either reduce the electrical load or supplement it from other utility sources. For the intermittent cloud situation, some anticipatory action is required if transfer to the thermal energy storage discharge mode is required. Rather than require surveillance by an operator, some device such as a clear sky detector operating on the principle of a photocell or smoke detector could be aimed at various sky diameters from the heliostat field to give visual or audible warning of impending cloud interference. The operator could then make the decision whether the cloud formations are such as to require transfer to thermal storage supplemental operation, or take whatever more appropriate action is deemed necessary.

5.2.2.4 Extended Operation from Thermal Storage (Effective Solar Multiple = 0)

During the extended operation mode, the receiver is out of service (that is, no solar insolation-low sun angle, evening, or night, etc.) and the system is operating solely on thermal storage. In this mode, the plant can operate for 3 h at full power or for ~30 h at 10% power. Approximately 15 min at full thermal power is reserved for startup or shutdown. The control system allows operation at any thermal power level to the design limit. The integrated power vs time curve totals the energy storage used over a given time period.

5.2.2.5 Thermal Storage Charging Only (1.5 ≥ Effective Solar Multiple ≥ 0.1)

During this mode, the plant electrical output requirement is zero, such as for periodic maintenance, etc. Solar energy is still available, and the entire insolation energy to the extent possible is to be stored. Sodium is heated to operating temperature in the receiver and is directed to the air-rock thermal storage heat exchanger through Valve C and back to Pump P-1. The design characteristics of the ACR Thermal Storage Subsystem for the air-rocks alternative are presented in the Design Data Sheets of Appendix B in Book 2 of this report.

5.3 SUBSYSTEM DESIGN AND ANALYSIS STUDIES

5.3.1 All-Sodium System

The design and analysis studies in the area of thermal storage for the all-sodium system have been limited to the sizing and optimization of the single hot and single cold storage tanks, temperature-time decay for all sodium storage (shown in Figure 5-3), the drag valve sizing (discussed in Section 5.4.3), and pump trade studies (referenced in Section 5.4.2). In addition, a brief study has been made to determine whether significant thermal stratification of sodium would occur within the storage tank. The conclusion reached is that temperature stratification is minimized by the relatively low heat loss to heat content ratio, and the open circulation path in the tank interior. Buoyancy and natural convection circulation and the incoming sodium mixing velocity components minimize stratification to an estimated <0.5°F. Final design effort for the storage tanks and drag valve is not appropriate until the final decision is made on system concept. Cost Analyses for these components are based on the design data developed to this point.

Various trade studies have been made comparing the all-sodium baseline system with other systems such as:

1) Na Primary Loop; IHX; Draw Salt in Secondary Loop
2) Na in Primary Loop; IHX; Draw Salt in Secondary Loop with Draw Salt-Hot Rocks Thermocline Thermal Storage
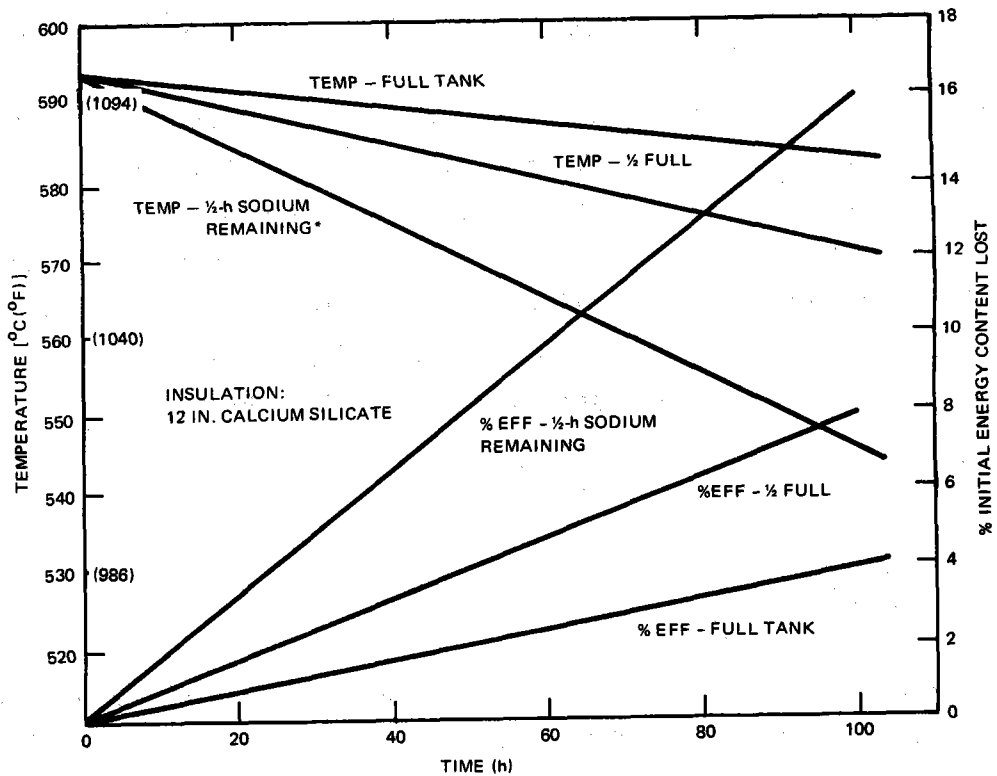
Figure 5-3. Temperature and Percent Heat Loss vs Time — All
Sodium Storage

3) Na in Primary Loop; Na-Air-Na Heat Exchanger; Air-Rocks Thermo-
cline for Thermal Storage

These analyses and subsystem cost comparisons are discussed here.

5.3.2 Air-Rock Thermal Storage

In this concept, heat absorbed in the sodium-cooled receiver is transferred
via a sodium-air heat exchanger to a rock bed through which air is circulated.
The basic idea is to use a low-cost rock bed to permit the storage of large
quantities of sensible heat. The use of such a storage system permits the
generation of $540^{\circ}C$ ($1000^{\circ}F$) steam when the power plant is operating on storage.
The temperature capabilities of sodium-cooled receivers are such as to permit
the temperature drops that occur when heat is transferred into and out from
storage.
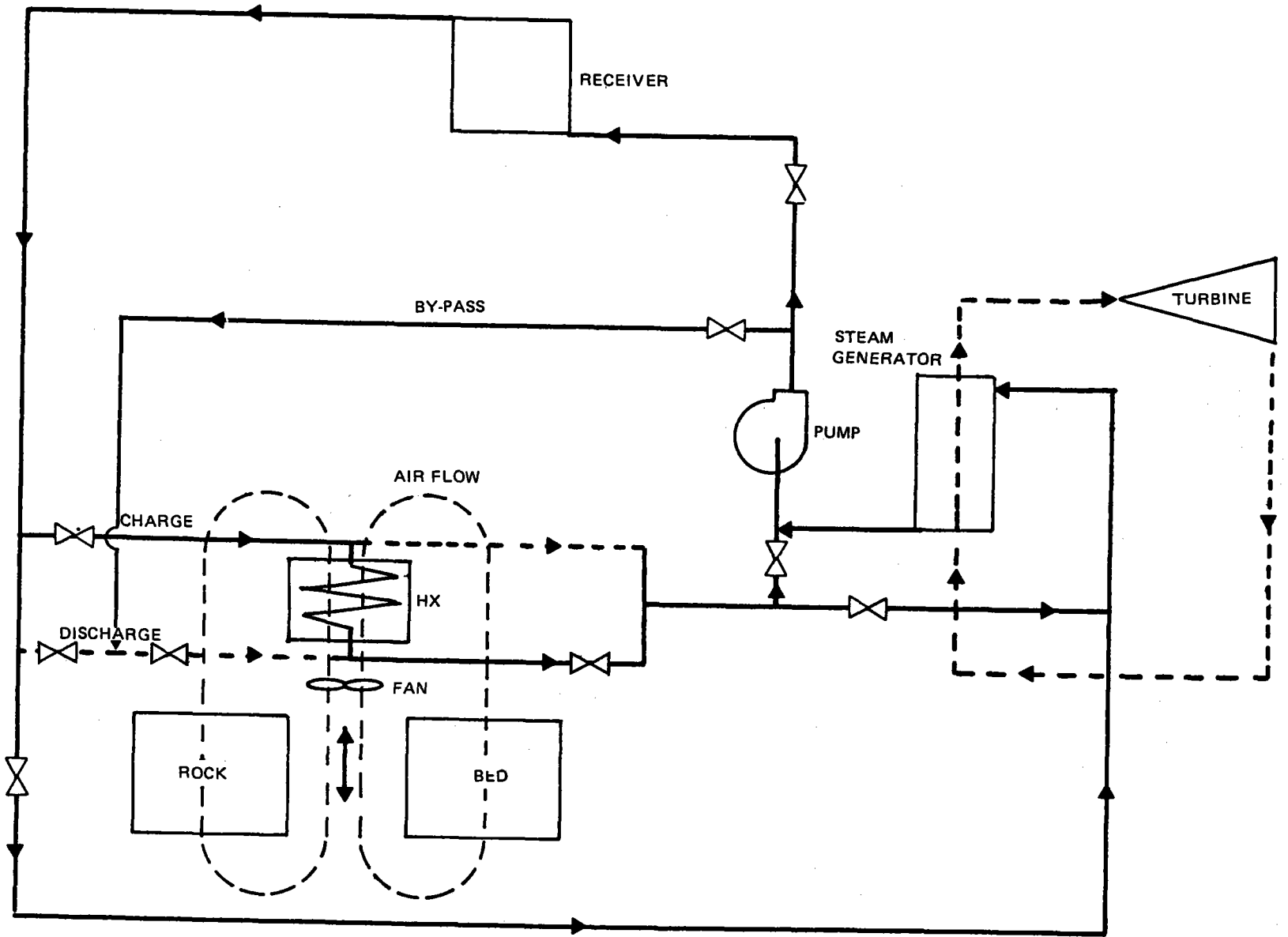
Figure 5-4. Air-Rock Storage System

9272-67

Air-rock thermal energy storage may be considered as the only storage subsystem in a solar power plant or it may be considered in combination with all-sodium storage. In either application, the structural and functional characteristics of air-rock storage are almost identical — the main difference being the speed with which the air-rock storage subsystem needs to respond to changes in plant operation. In the following then, either application can apply.

Figures 5-2, 5-4, and 5-5 show a schematic of a plant with air-rock storage. Hot sodium from the receiver can go directly to the steam generators or to storage or both. Hot sodium entering storage passes through a sodium-air heat exchanger which is cooled by a flow of air driven by fans. The cooled sodium continues on to either the steam generator or the receiver or both. The heated air is circulated downward in a rock bed, heating the rocks and thus charging the storage system.

When it is desired to operate the plant on storage, the sodium passes through the heat exchanger in the reverse direction as indicated in Figures 5-2, 5-4, and 5-5. At the same time, the fans drive the air in a reversed direction also. Thus, the stored heat in the rock bed heats the air which in turn heats the sodium in the heat exchanger. This hot sodium is circulated to the steam generator.

The arrangement shown in Figures 5-2, 5-4, and 5-5 allows the plant to operate in any of five modes, which are:

1) Direct (no storage involved)
2) Charge
3) Discharge
4) Direct Plus Charge
5) Direct Plus Discharge

During most of a typical day, the operation will be in Mode 4 which is Direct Plus Charge. Early or late in the day when the solar multiple is less than unity, the plant can be run in Mode 5, Direct Plus Discharge. In the
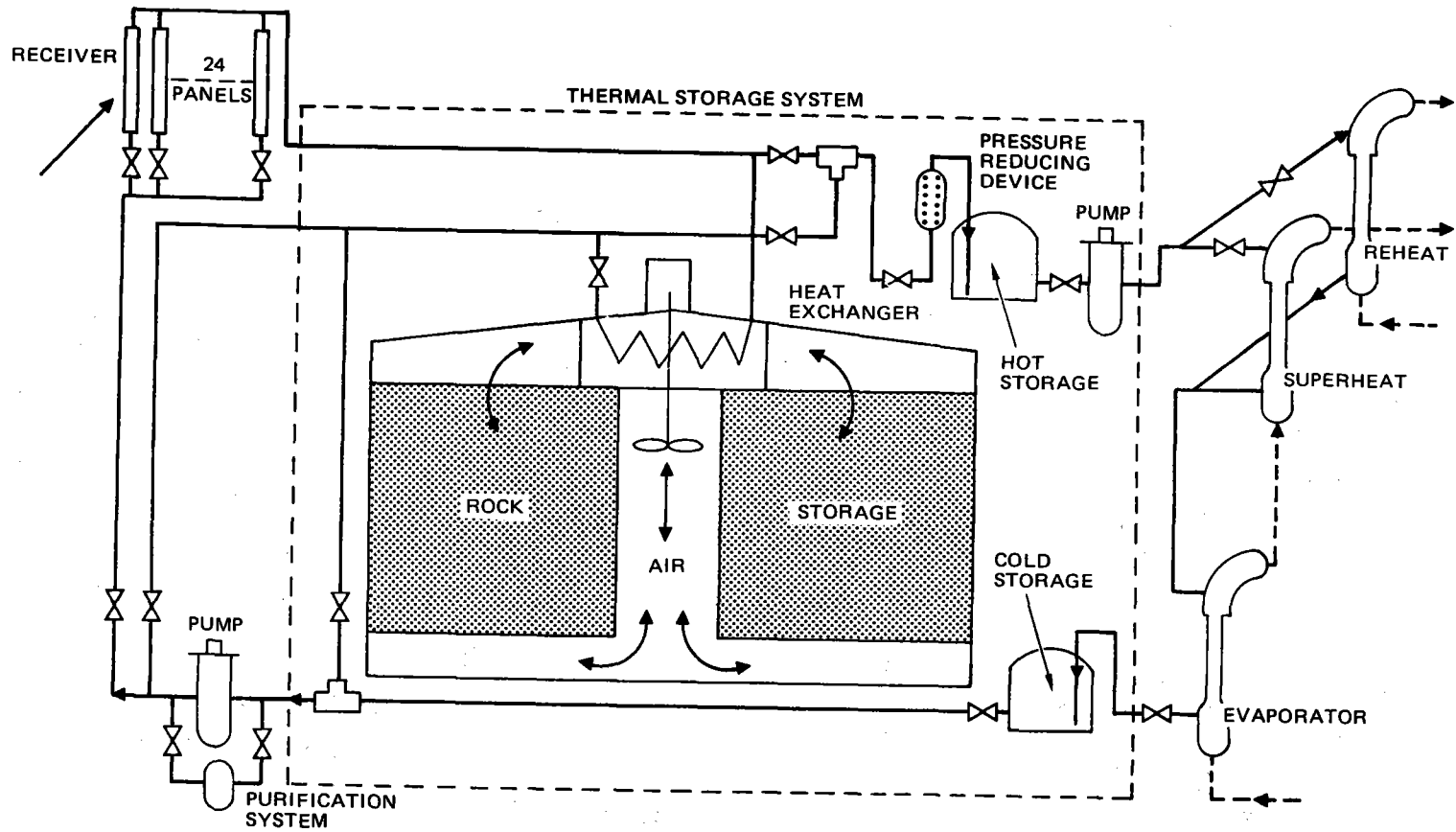
Figure 5-5.   Advanced Central Receiver Combined
Air-Rock and All-Sodium Storage

00-103853

morning, this mode would be associated with plant startup. At any time, the air-rock storage system can store the maximum receiver absorbed power of 390 MWt.

Analysis has shown that the piping arrangement in Figure 5-4 provides an adequate heat balance for all of these operating modes. What is not yet known is the rate that air-rock storage can shift from one mode to another and the consequent power and temperature transients. These transient effects depend on the design of the plant control system, the speed to which sodium valves can be adjusted, and the response of the air fans. For the above reasons, a plant combining air-rock with all-sodium storage may have the large storage capacity and low cost of air-rock storage plus the good response characteristics of all-sodium storage.

The objectives of air-rock storage are to employ low-cost materials and simple designs to achieve large storage capacities. Large storage capacity at a reasonable cost can be of great economic value to a plant. The following is a list of the reasons why adequate storage is of value:

1) Plant operation can be continued into the evening hours.
2) Insolation above a solar multiple of 1.0 can be stored rather than be wasted.
3) The plant can operate overnight at low power.
4) Plant startup can be facilitated in the morning.
5) Extended solar outages can be accommodated.
6) Unexpected demands for power can be accommodated.
7) Insolation can be stored during periods when the turbine is not operational.
8) Insolation can be stored when the demand for power is low.
9) There is room to store energy when for some reason the storage system is not empty at the start of a charge period.
10) In the case of sodium systems, storage provides a source of energy to keep the sodium warm.

EARTH FILL   HOT DUCT   MOTOR

ROCK   COOL DUCT   HX

SAND   STEEL ROOF   FAN   CONCRETE

10 m

GRADE

86 m

VERTICAL DUCTS

9272 ?8
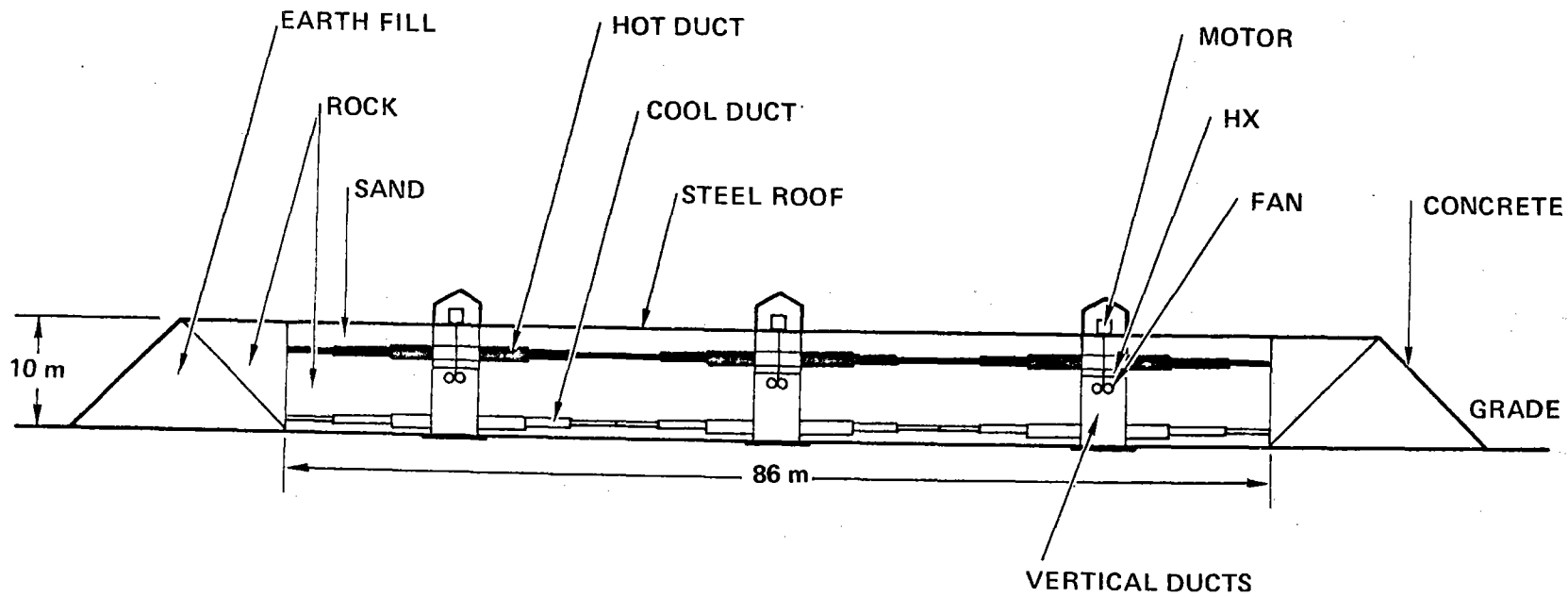
Figure 5-6. Air-Rock Storage System Schematic

Large storage capacity is generally associated with a large solar multiple. This combination leads to a reduction in the cost of power and to increased operational flexibility. However, merely increasing the storage capacity without increasing the solar multiple also accomplishes both of the above as is shown in the above list.

5.3.2.1 Air-Rock Storage System Construction

The construction of air-rock storage systems has recently been greatly simplified. It is now planned to build the storage system at grade level, thus eliminating the necessity for excavating and building a foundation. For the 100 MWe application, the area forming the storage region is surrounded by earth fill forming a square storage region 86 m (282 ft) on a side and about 11 m (36 ft) high. This earth could be obtained from other excavations and grading at the site.

This square region is divided into nine smaller squares each measuring 28.7 m (94.0 ft) on a side. The smaller squares each contain a row of six vertical concrete pipes that are 4 m (13 ft) OD. Cool air ducts branch out horizontally near the base of the vertical ducts, while hot air ducts branch out from a location near the top of the vertical ducts.

Figure 5-6 is a side view of a 100 MWe storage unit showing the location on the ground and the ducting arrangement. Figure 5-7 shows how the modular construction of this storage system can be used in power plants of various sizes without changing the basic design. The inner square, which has six vertical hot ducts, is about the correct size for a 10-MWe plant. When nine of these squares are used, as in Figure 5-6, the capacity is about that required for a 100-MWe plant. Finally, when 25 squares are used, the size matches that of a 281-MWe plant — a size which has been shown to be close to the optimum for minimum power costs.

Figure 5-8 shows how the horizontal ducts — both hot and cool — are connected to the vertical ducts. These ducts are stepped down in size to reduce

281 MWe
(25 MODULES)

100 MWe
(9 MODULES)

10 MWe
(1 MODULE)

86.4 m
(283 ft)

28.8 m
(94.5 ft)

144 m
(472 ft)

ALL MODULES ARE IDENTICAL, HAVING 6 Hx'S, 6 FANS,
6 VERTICAL DUCTS, 36 HOT DUCTS AND 36 COOL DUCTS
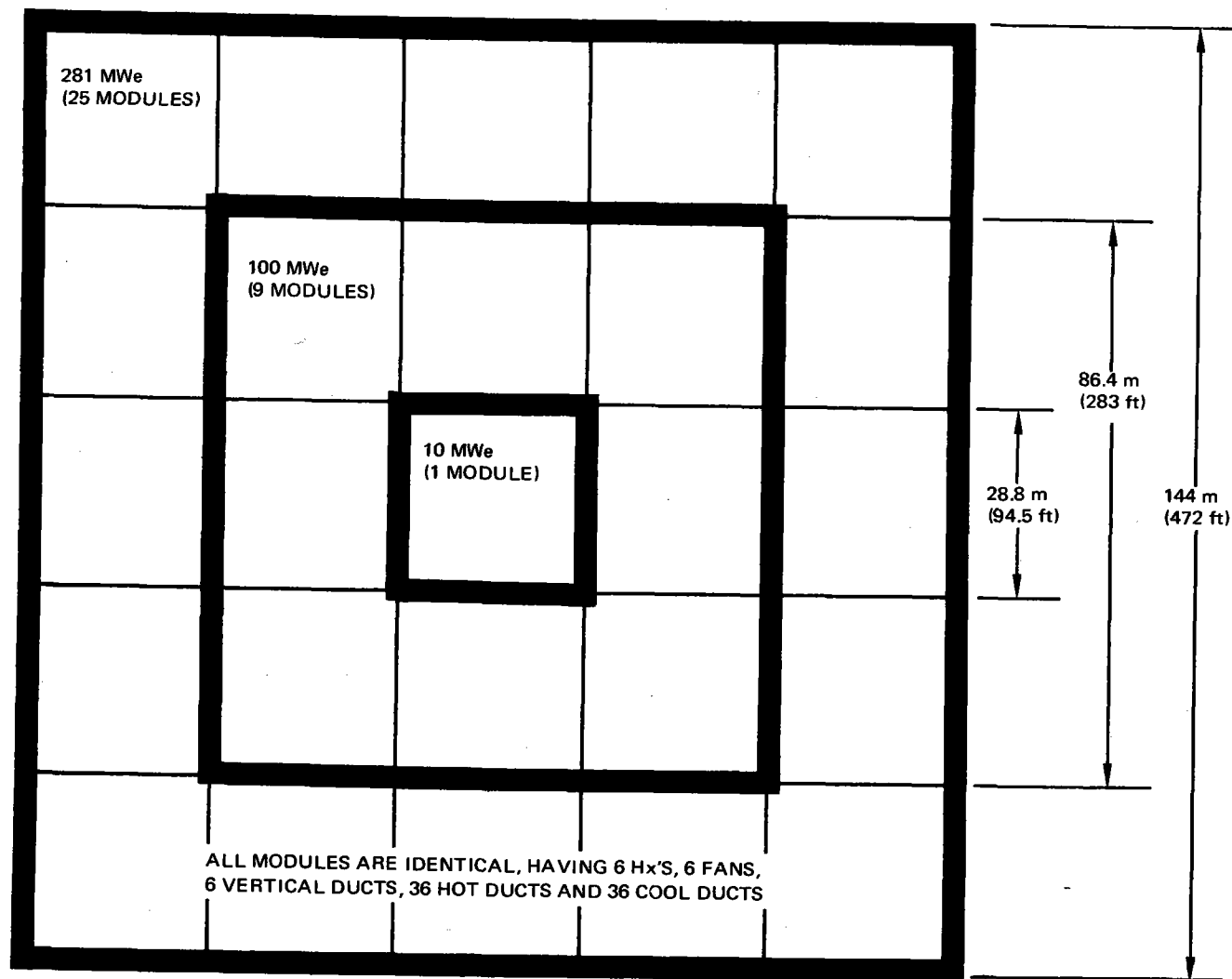
9272-26

Figure 5-7.   Outline of Three Air-Rock Storage Systems
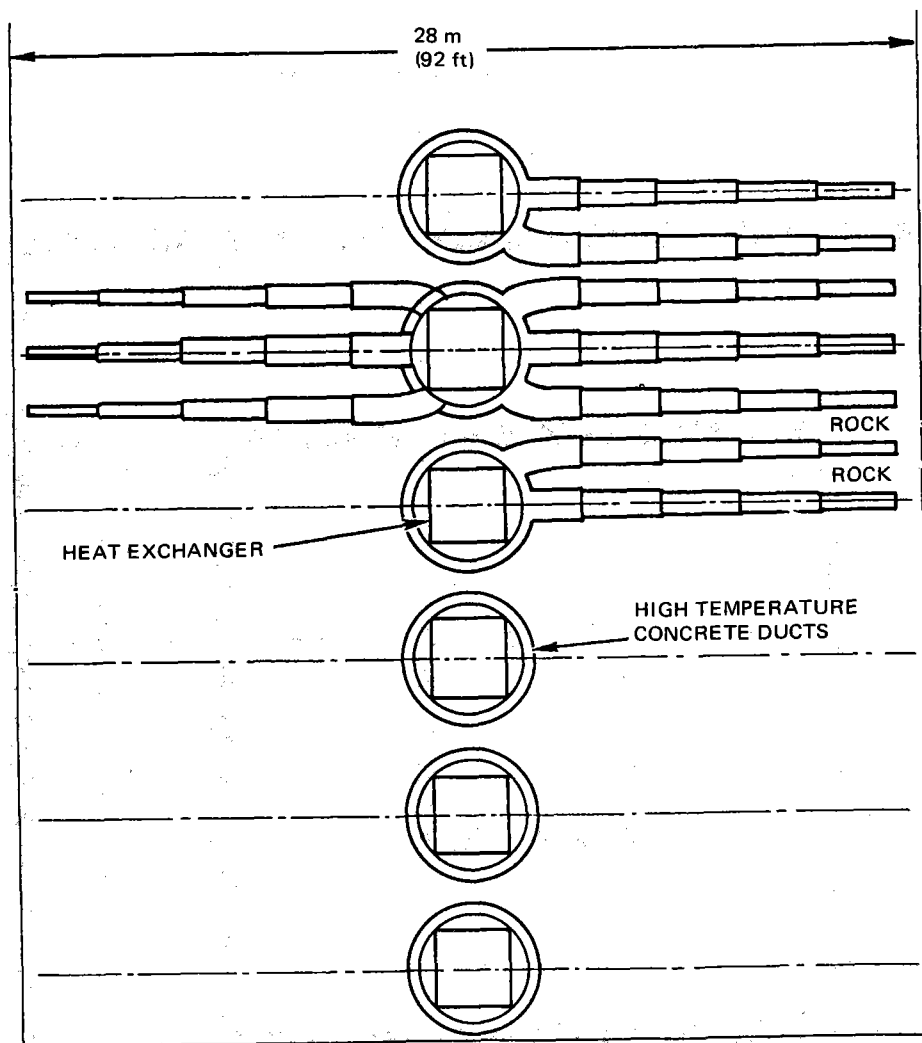
Figure 5-8. Air-Rock Storage System, Plan View
(1/9th of 100-MWe Storage System)
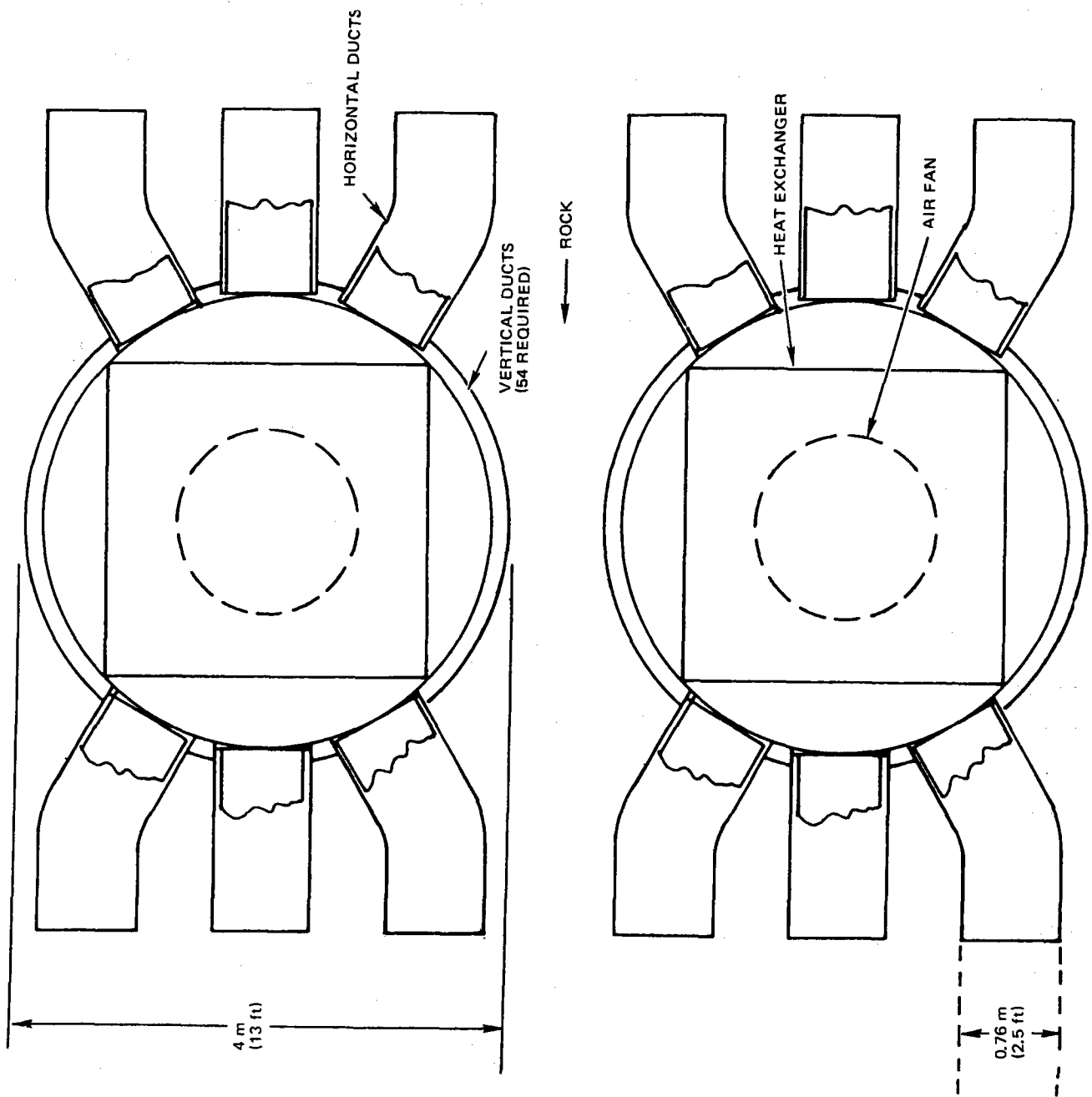
Figure 5-9. Air-Rock Storage System Details

9272-70

concrete costs. The outlines of the modular sodium-air heat exchangers are shown in the vertical ducts. Figure 5-9 shows more details of these ducts. Figure 5-10 shows how the heat exchangers and air fans are mounted in the vertical ducts. The fan motors are located so as to provide ease of maintenance. If necessary, each fan and heat exchanger can be removed from the storage system.

All of the air ducts are made of alumina-base high-temperature concrete. This concrete can be used to at least $1100^\circ C$ ($2000^\circ F$) which is well above the maximum design temperature of $650^\circ C$ ($1200^\circ F$). The stresses in this concrete are in the order of 1.0 MPa (145 psi) and are almost entirely compressive stresses. Vendors of high-temperature concrete have been consulted concerning this application.

The active rock bed storage medium lies between the upper (hot) ducts and the lower (cool) ducts — a depth of 6 m (20 ft). The rocks have a nominal diameter of 3 to 4 cm (1.2 to 1.6 in.) and are packed to a porosity of about 39%. During the charge mode, the air is forced upward in the vertical ducts, passes through the heat exchanger where it is heated, then travels downward in the rock bed where heat is transferred to the rocks. During the discharge mode, the air flow is reversed, and heat is transferred from the rock bed to the heat exchanger.

There is a 3 m (10 ft) layer of sand or dry soil above the upper (hot) horizontal ducts. This layer acts as effective and low-cost thermal insulation. The heat loss is reduced to roughly 0.30 MWt — a value which is subject to further optimization. Sand or dry soil is indicated for this layer to prevent natural convection air currents from creating a heat loss. A layer of gunite concrete is applied between this layer and the upper horizontal ducting to prevent sand from leaking down into the ducting and rock bed.

There is a layer of rock below the lower (cool) horizontal ducts. This layer serves to thermally insulate the storage region from the earth. It also provides room for dust and other fine rock particles to settle without blocking the active rock bed and the ducts.
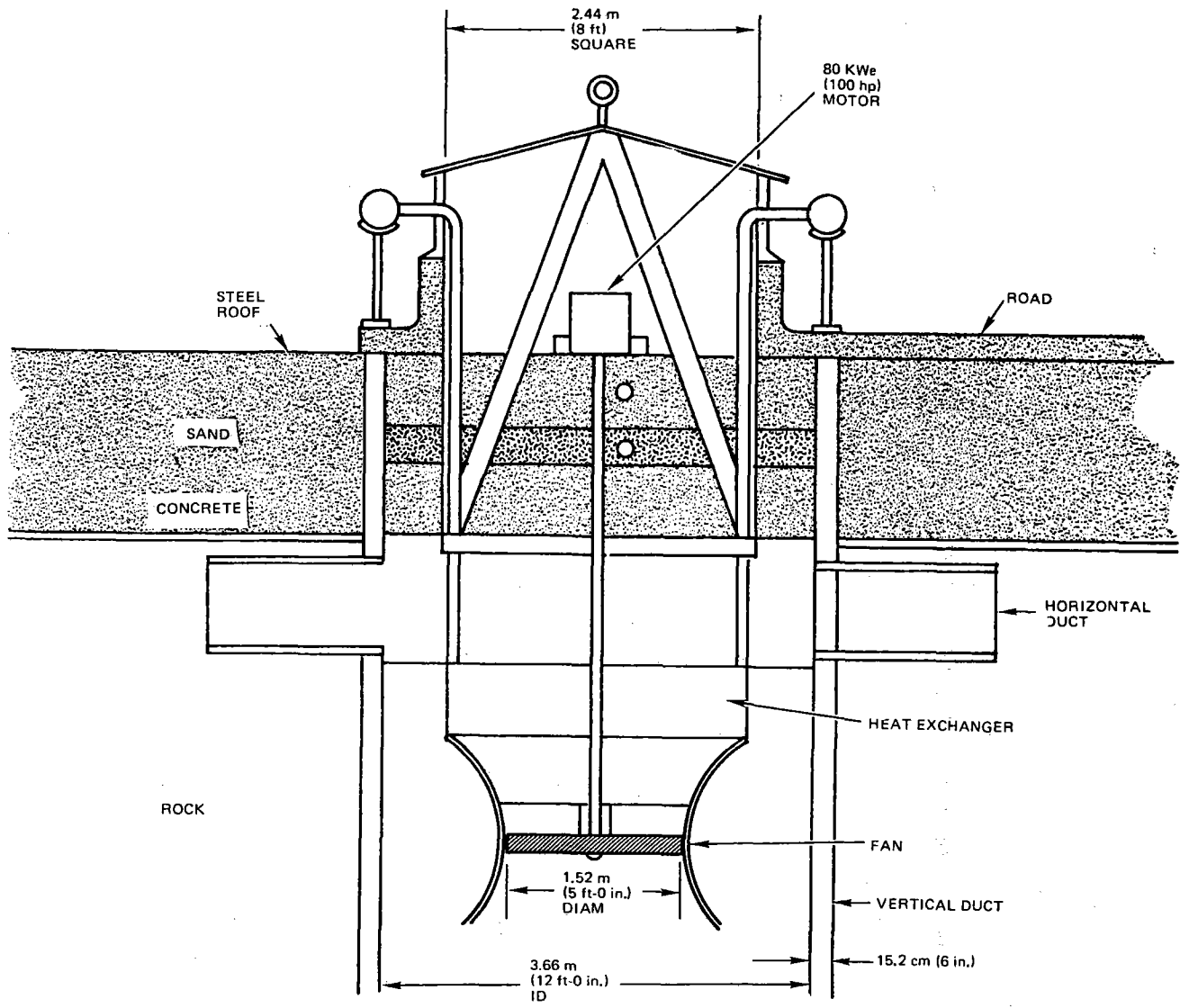
Figure 5-10. Heat Exchanger and Fan Assembly

9272-71

A study has been made of the heat transfer from the storage region into the earth. While the heat loss tends to be small (Q <0.10 MWt), the temperature of the earth will rise considerably. For example, the earth 20 m (65 ft) below the storage region will approach 100°C (212°F) after 30 years. Adequate drainage of the general storage area is required.

The storage system is covered by a galvanized, corrugated steel roof that rests on the sand insulating layer. Each of the three rows of fan access hatches has a concrete service road running the width of the storage region. The surrounding earth fill has a gunite concrete surface on the outer slope to shed water and prevent erosion.

Each of the fan-heat exchanger units is designed for easy access and for rapid replacement. The sodium lines to each unit have shutoff valves so that the lines can be cut and the heat exchanger removed.

5.3.2.2 Summary of Storage Construction Features

The following is a summary of the construction features of the most recent air-rock storage design.

1) The storage system is at ground level and surrounded by earth fill.
2) The region inside the earth fill is one large bed of rock.
3) The air duct array is made of high-temperature concrete pipe immersed in the rock bed.
4) The vertical ducts also support the fan and heat exchanger.
5) A thick layer of sand or soil insulates the top of the storage region.
6) The storage region is modular, having 54 fans and heat exchangers.
7) A steel roof resting on the sand protects the top of the storage system.

5.3.2.3 Rock Bed Characteristics

The following is a discussion of the characteristics and performance of the rock bed.

The 54 modules give the rock bed an effective planview area of 7,000 m^2 (75,000 ft^2) while the effective height of the active bed is 6.1 m (20 ft). The nominal rock size is 4.0 cm (1.5 in.), the sphericity is taken to be 0.80, and the porosity of the bed is 0.39.

It is important to size the rock bed so that the pressure drop and the fan power are reasonable at the maximum receiver absorbed power of 390 MWt. Using the methods described in Book 2, the air ΔP at 390 MWt and an air ΔT of 210°C (410°F) is estimated to be 0.64 KPa (0.0932 psi) and the resulting fan power is 2.57 MWe. Of course, a slight broadening and thinning of the bed will greatly reduce this power with only a very small reduction in rock bed heat transfer.

The fraction of time the storage system will be charged at 390 MWt is very small since the turbines would normally take 260 MWt of this amount. Therefore, the parasitic power drain is not a factor, but the capital costs of the fans are more significant. The most important power drain is during the discharge mode of 250 MWt. At this time, the air ΔP in the bed is 0.29 KPa (0.0427 psi) and the fan power is 0.881 MWe; however, if discharge occurs about 25% of the time, the effective parasitic power is 0.22 MWe due to the rock bed.

The rock sphericity is the area of a sphere having the volume of the rock divided by the actual surface area of the rock. The chosen sphericity of 0.80 is about that of a cube so the assumed rocks were far from being smooth spheres.

5.3.2.4 Storage Temperatures and Heat Exchanger Optimization

The heat exchanger is the most costly component in air-rock storage. Its cost is very nearly proportional to the air-side surface area. If the Hx log mean ΔT during discharge can be increased, then the costs can be reduced.

However, an increase in the log mean ΔT forces sodium temperatures up and/or the steam temperatures down — both of these having a penalty. If sodium temperatures are increased, then heavier piping may be indicated to compensate for reduced allowable stresses, increasing material costs. Also, the receiver stresses will become more significant. Reducing steam temperatures when on storage is the simplest solution. For example, if the steam temperature is reduced from 538°C (1000°F) to 482°C (900°F), the plant gross efficiency drops from 43.09% to 41.80%. If it is assumed that storage is in operation 25% of the time, then the average plant gross efficiency is 42.77%. The reduced cost of the Hx would far out-weigh the small drop in plant efficiency.

Another way to reduce the Hx cost is to expend more fan power to increase the overall heat transfer coefficient, U, in the heat exchanger and also to increase the average air temperature that heats the sodium.

Preliminary trade studies to reduce heat exchanger size based on the above ideas were initiated but were not completed. The following reference heat exchanger design has acceptable characteristics:

5.3.2.5 Reference Heat Exchanger

There are 54 heat exchangers mounted in the vertical concrete ducts. Each heat exchanger measures 2.44 m (8 ft) by 2.44 m (8 ft) by 0.85 m (2.8 ft). The heat exchanger is a tube-and-fin design with high-pressure sodium (1.38 MPa (200 psi)) in the tubes. The tubes have an OD of 2.60 cm (1.02 in.) and a wall thickness of 0.124 cm (0.049 in.). The fin thickness is 0.061 cm (0.024 in.), and the fin height is 0.91 cm (0.36 in.). The total air-side surface area is 52,800 m^2 (568,000 ft^2).

At the discharge power of 250 MWt, the air ΔP is 0.32 KPa (0.046 psi) and the resulting fan power is 0.843 MWe. At 390 MWt, the Hx fan power is 2.75 MWe. At 390 MWt, the combined rock bed and heat exchanger fan power is 5.32 MWe. This power, while seldom used, tends to determine the fan capital cost.

5.3.2.6 Bed Utilization

It will be shown in subsequent sections that the energy utilization of an air/rock bed depends on how much temperature degradation is permitted at the end of the charge and discharge cycle. If the degradation is permitted to be $28^\circ C$ ($50^\circ F$) at both ends of the bed, the performance remains good, but the utilization is only 15 or 20% for the reference air-rock design. That is, for a given amount of storage, the bed size must be large. On the other hand, if the temperature degradation is allowed to be $83^\circ C$ ($150^\circ F$), the utilization of the bed rises to 60 or 65% and the storage time increases to about 12 hours.

As the temperature in the bed degrades, the effective steam temperature (on storage operation) declines as does the cycle efficiency. Using cycle efficiency data provided by Stearns-Roger, the relative plant efficiency was plotted versus the hours of storage in the reference 100 MWe air-rock storage system. Figure 5-11 shows these results. One curve shows the drop in efficiency when operation on storage only is considered. The second curve shows the drop in average plant
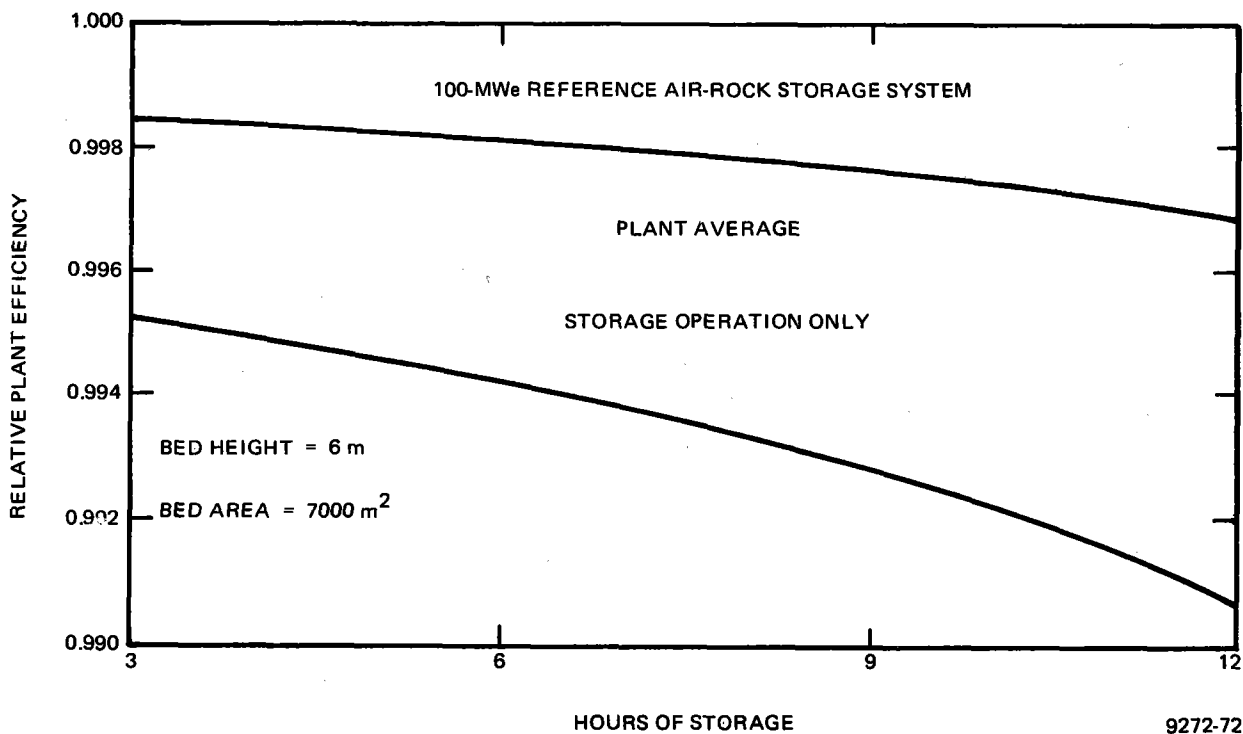
Figure 5-11. Relative Plant Efficiency vs Hours of Storage

efficiency assuming that operation on storage occurs one-third of the time. It can be seen that the loss in efficiency is small compared with the large increase in utilization and storage capacity. While the reference 100 MWe air-rock storage system was designed for 3 h of storage, it can actually store up to at least 12 h if some loss in performance is allowed. Thus, while the storage system may be normally exercised over a 3-h storage energy range most of the time, it is capable of either absorbing or delivering power over much larger times if the occasion demands. The economic value of this operational capability will significantly reduce the cost of power.

5.3.2.7 Larger Air-Rock Storage Systems

In a 3-h, 100-MWe air-rock storage system, most of the capital cost is in the heat exchanger and fans. The balance of the storage system which consists of rock, sand, concrete, earth, and some steel is relatively low in cost, especially when the construction techniques described above are used. In a plant having a given maximum absorbed thermal power, the heat exchanger and fan capital costs are fixed regardless of the storage energy capacity. On the other hand, the cost of the balance of the storage system (rocks, sand, etc.) is, at a given utilization, proportional to the storage capacity. Thus, the storage capacity can be increased a large amount for a small increase in the capital costs. Figure 5-12 shows the relative cost of a 100-MWe, 3-h storage system as a function of storage time.

In summary, the storage capacity can be increased by either taking a small performance penalty and increasing the utilization or by simply building a larger rock bed with fixed-size heat exchanger and fans.

5.3.2.8 Combined Air-Rock and All-Sodium Storage

It was shown in Figure 5-5 that air-rock storage can be combined with all-sodium storage. The reason for doing this is to combine the large storage capacity and low cost of air-rock storage with the response characteristics of all sodium. The amount of sodium storage to incorporate in such a combination

100-MWe PLANT
250-MWt DISCHARGE
CONSTANT UTILIZATION ≈ 20%

RELATIVE COST

ROCKS, SAND, CONCRETE, EARTH AND STEEL (INCREASED CAPACITY)

HEAT EXCHANGERS AND FANS (INCREASED POWER)

HOURS OF STORAGE

9272-73
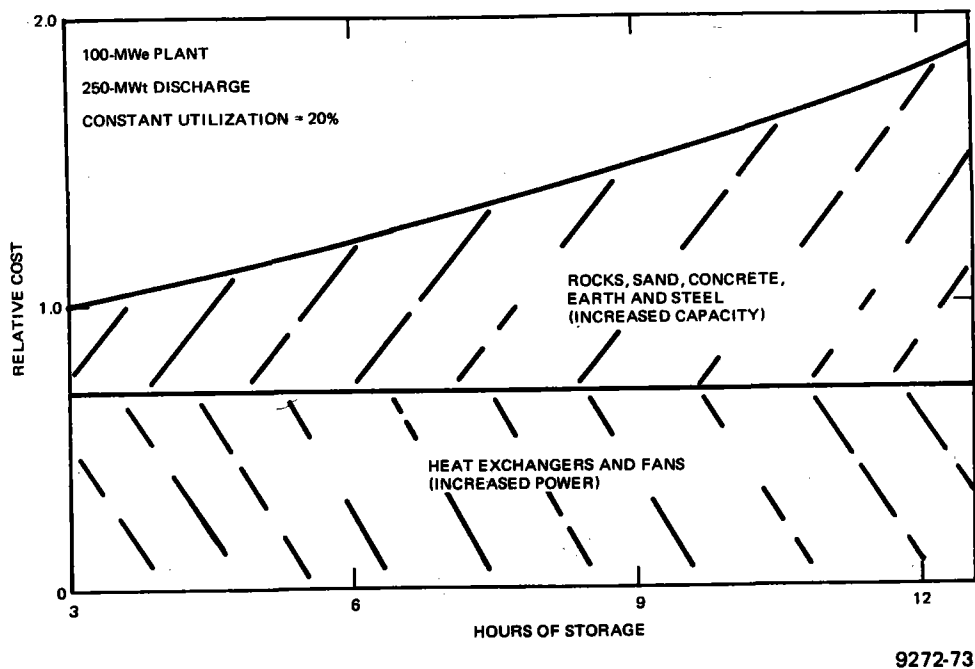
Figure 5-12.   Expected Cost of Air-Rock Storage vs Hours of Storage or Bed Size

is not known at this time. It depends on the rate at which the air-rock system can change operating modes — for example, from the Direct Plus Discharge to the Discharge mode. It also depends on the length of time any change of mode can be anticipated. A half-hour of all-sodium storage combined with a longer term air-rock storage is probably a conservative approach. It is expected that further study would greatly reduce this amount.

The amount of sodium storage greatly influences the sodium loop design. If the amount of sodium storage is large, then the drag valve would be retained to reduce the sodium pressure. The second sodium pump would also be retained, and the receiver sodium pump would require a 3.35-MWe pump to pump against the tower head — all characteristics of all-sodium storage. If the amount of stored sodium is small, then the two sodium tanks can be economically designed to withstand the tower sodium pressure. In such circumstances, the drag valve can be eliminated, the second (storage) sodium pump can also be eliminated, and the

main sodium pump can be 1.50 MWe — as in air-rock storage plant designs. Preliminary studies indicate that a half-hour of sodium storage is about at the cross-over point but more studies are needed.

In summary, in this hybrid storage system, a half-hour or less of sodium storage is probably sufficient. The most economical arrangement would then eliminate the drag valve and the second sodium pump, and the receiver pump would be 1.85 MWe smaller.

5.3.2.9 Air-Rock Thermodynamics

Calculations were made to determine heat transfer and pressure drop behavior of air flow through a rock pebble bed thermal storage device. The bed was assumed to be composed of a random packing of pebbles, with air flow through it. The thermal capacitance of the rocks (ρC_p) is employed to store heat in conjunction with a solar energy system. Parameters are identified in Table 5-3.

The bed is assumed to have a cylindrical configuration, height L and horizontal diameter, D. It is assumed that the bed is composed of uniform pebbles of diameter, d.

The following correlations have been developed:

1) Pressure Drop (Fan Power): The pressure drop correlation used is given by Kunni and Levenspiel (Reference 1, Page 67) with an upward adjustment (by a factor of 4/3) to bring it into closer agreement with Leva as shown in Perry, Fourth Edition.[2] The correlation used is:

$$\frac{\Delta p}{L} g_c = 200 \frac{(1 - \epsilon)^2}{\epsilon^3} \frac{\mu V_o}{(\emptyset d)^2} + 2.33 \frac{(1 - \epsilon)}{\epsilon^3} \frac{\rho V_o^2}{\emptyset d} \; .$$

The first term predominates at low velocities (laminar), and the second term takes over at high velocities (turbulent). Using the sum has the effect of giving a smooth transition with increasing velocity (or Reynolds Number).

TABLE 5-3

NOMENCLATURE FOR ROCK-AIR STORAGE SYSTEM

A_{Grss} = gross flow area $(A_{Grss} = \frac{\pi}{4} D^2)$ ft^2

A_{sur} = total pebble heat transfer surface area (ft^2)

C_p = specific heat $(Btu/lbm-^oF)$

d = pebble diameter (inch or feet) (The diameter a sphere would have if its volume were the same as the pebble's.)

D = bed diameter (ft)

eff = blower efficiency

ENG = total thermal energy capacity of bed (MW-days)

g_2 = gravitational constant $(lbm-ft/lbf-s^2$ or $lbm-ft/lbf-h^2)$

h = heat transfer coefficient $(Btu/h-ft^2-^oF)$

k = thermal conductivity $(Btu/h-ft-^oF)$

L = bed height (ft)

Nu = Nusselt Number [hd/k (based on pebble diameter)]

Δp = pressure drop (lbf/ft^2)

P_{fan} = fan pumping power (kWe)

POW = heat rate charging (or discharging) the bed (MWt)

Pr = Prandtl Number $(\mu C_p/k)$

Re = Reynolds Number $[(W/A_{Grss})$ $d/\mu]$ (based on pebble diameter and gross flow area)

T = temperature (^oF)

U = overall heat transfer coefficient $(Btu/h-ft^2-^oF)$

$\overline{UA}$ = heat transfer property of bed, average between hot and cold temperature $(Btu/h-^oF)$

Vo = superficial velocity (ft/s)

$\dot{W}$ = gas flow rate (lbm/h)

E = porosity of bed (void fraction)

μ = viscosity (lbm/ft-h)

ρ = density (lbm/ft^3)

$\emptyset$ = sphericity: For a pebble of a given volume:

$$\emptyset = \frac{\text{Surface area it would have if a sphere}}{\text{Actual surface area}}$$

The fan power required to overcome this pressure drop is:

$$P_{fan} = 3.77 \times 10^{-7} \frac{W \Delta p}{\rho (eff)}$$

2) Heat Transfer Coefficient: Several correlations[1,3-6] have been considered to determine the gas-to-particle heat transfer coefficient. While there are areas of reasonable agreement, there are also important differences between the references. The Nusselt number variation with Reynolds number shows reasonable agreement. However, there is disagreement with respect to the effect of porosity, sphericity, and particle diameter.

As a compromise, the following correlation is used:

$$Nu = 0.5 \ Re^{0.7}$$

The heat transfer coefficient, h, is calculated from this correlation. The overall heat transfer coefficient, U, is determined by:

$$U = \frac{1}{\frac{1}{h} + \frac{d}{7.7 \ k_{Rock}}}$$

This takes into account the thermal conductive resistance of the individual pebble — from its surface ot a "mean" interior location.

The average value of UA (i.e., $\overline{UA}$) is taken to be the arithmetic mean of the values of UA at the hot gas temperature and the cold gas temperature.

The rock and gas properties used in the calculations are given in Table 5-4. The rock properties are approximate values assumed for the calculation. The air properties are based on correlations from Reference 7. These fan power requirements and heat transfer characteristics based on correlations for pressure drop

<center>

TABLE 5-4

MATERIAL PROPERTIES

</center>

Rock

Specific Heat	$= C_p = 0.25$ Btu/lbm $^\circ$F
Density (No Voids)	$= \rho_s = 165$ lbm/ft^3
Thermal Conductivity	$= k = 1.0$ Btu/h-ft-$^\circ$F

Air

Specific Heat $= C_p = 0.239 + (0.90 \times 10^{-5}\ T) + (1.4 \times 10^{-7}\ T^2)$ Btu/lbm-$^\circ$F

Viscosity $= \mu = 0.02996 + (0.6336 \times 10^{-4}\ T) - (0.144 \times 10^{-7}\ T^2)$ lbm/ft-h

Thermal Conductivity $= k = 0.0133 + (0.026 \times 10^{-4}\ T) - (0.2 \times 10^{-8}\ T^2)$ Btu/m-ft-$^\circ$F

Density $= \rho = 39.65874/(T + 459.69)$ lbm/ft^3

Prandtl Number $= \mu C_p/k$

$(T = {}^\circ F)$

Air Properties

Hot	Cold	
1100.0	600.0	Temp:Air, $^\circ$F
0.265840	0.249440	Cp:Air Btu/lbm-$^\circ$F
0.092232	0.072792	Viscosity:Air lbm/h-ft
0.025427	0.037425	Density:Air lbm/ft^3
0.731036	0.728037	Prandtl:Air
0.900837	0.899603	PR**1/3
0.033540	0.024940	Conductivity:Air Btu/h-ft-$^\circ$F

Ave Air Cp = 0.0257057 Btu/lbm-$^\circ$F

---

and heat transfer film coefficients for air flow through rock pebble beds were developed for air-rock thermal storage system with storage capacities of 3 MW-h/MW and for larger capacity beds.

The detailed analysis for heat transfer and pressure drop correlations is presented in Appendix G, Book 2 of this report.

A typical performance map for a 190 MWt-day (theoretical maximum energy content for the specified delta temperature) air-rock thermal storage system is presented in Figure 5-13. This shows fan power vs overall heat transfer coefficient (i.e., UA product) for various bed diameters and rock size. Corresponding bed height, L, is also given. Computer runs for various combinations

ENG (THEO) = 190 MW DAYS

POWER = 286 MWt

$\epsilon = 0.39 \quad \emptyset = 0.80$

$T_{HOT} - T_{COLD} = 1100^{\circ} - 600^{\circ}F$

VOL = 1,237 x 10^6 ft^3

MASS = 62,253 tons

D (BED) (ft)	L (BED) (ft)
225	31.1
250	25.2
275	20.8
300	17.5
325	14.9

9272-74
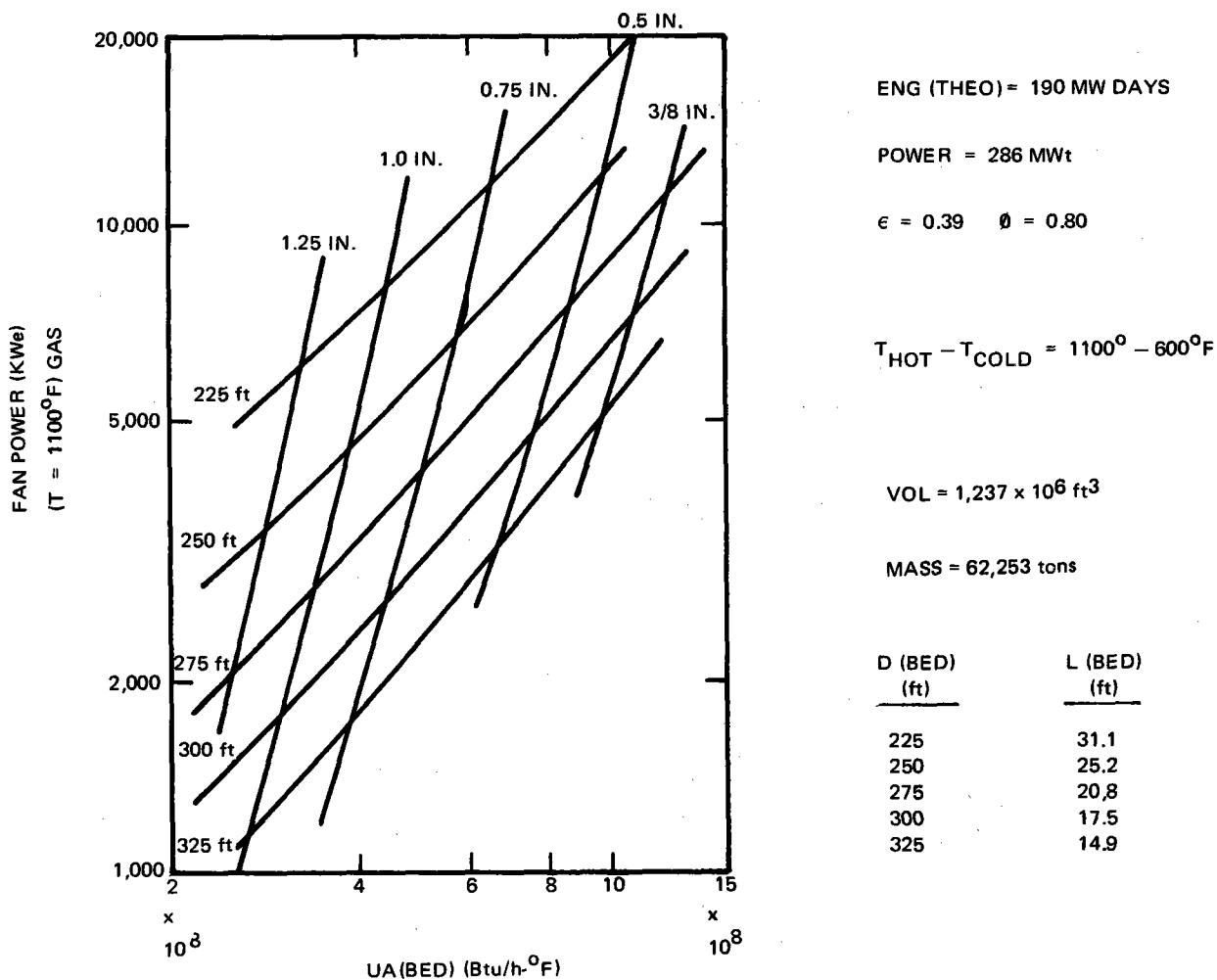
Figure 5-13. Typical Air-Rock Thermal Storage Performance Map

of bed diameter, bed height, and rock size indicate that cyclic performance
is approximately the same for any point on the map. Thus, the final design of
an air-rock thermal storage system can consider factors such as the most cost
effective bed-width-to-height-ratio, rock size, and construction constraints.

Figure 5-14 shows cyclic performance of a 190 MWt-day bed with the constraint
of 50°F (28°C) temperature change at both the inlet and outlet of the bed. The
bed starts out initially fully charged at 1100°F (593°C) and cools to the temper-
ature distribution identified as ΔT_1 in 12.85 h. The bed is subsequently heated
to the ΔT_2 temperature profile in an additional 8.38 h. The final stabilized
cyclic temperatures are identified, and the bed utilization is 20%. Bed utili-
zation is defined as the ratio of the effective bed energy output (or input) to
the maximum bed energy content if the entire bed could be cycled between the
maximum and minimum operating temperatures.
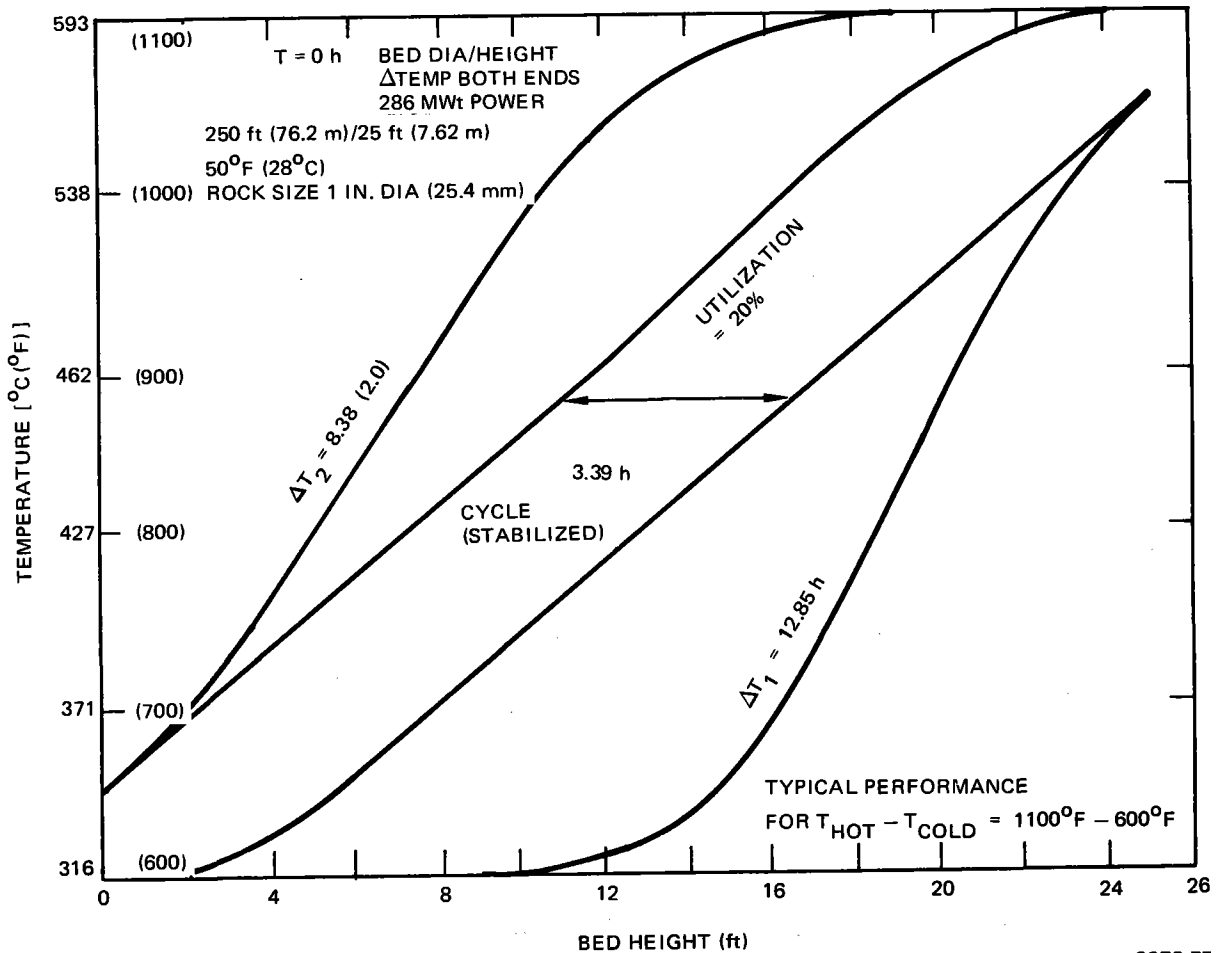
Figure 5-14. Air-Rock Thermal Storage — Cyclic Operation

ESG-79-2, Vol II, Book 1

Although the final design of an air-rock thermal storage system will consider factors such as the most cost-effective bed-width-to-height-ratio, rock size, and construction constraints, a typical air-rock bed configuration was selected to develop temperature profiles, operating criteria, and performance parameters based on realistic charging-discharging power levels.

Figure 5-15 shows typical diurnal variations in absorbed thermal power with nondimensional ordinate. Assuming a solar multiple of 1.5 with 390 MWt insolation, only the insolation at levels above 260 MWt is available for thermal storage input. (The 260 MWt is the updated thermal requirement to the steam generator when the receiver subsystem is operating.) Integrating the area under the equinox curve for insolation above 260 MWt ($07.35 \le t \le 16.70$) gives a Q available for storage of approximately 910.7 MW H (97.4 MWt average for 9.35 h). For the summer solstice, the time for insolation above 260 MWt with a solar multiple of 1.5 is 11.15 h ($06.40 \le t \le 17.55$). The Q available for storage increases to approximately 1013.2 MW h (90.87 MWt average for 11.15 h).

A 250 MWt discharge rate to the steam generators is used to simulate operation on thermal storage (receiver subsystem out of the loop as opposed to 260 MWt with receiver operating). To balance thermal storage system input and output, Table 5-5 can be constructed.

TABLE 5-5

THERMAL STORAGE ENERGY BALANCE

Season	Average Thermal Input Rate (MW)	Charge Period (h)	Q_{input} (MW-h)	Discharge Rate (MW)	Discharge Period (h)
Equinox	97.4	9.35	910.7	250	3.64
Summer Solstice	90.87	11.15	1013.2	250	4.05
Equinox	101.2	9	910.8	250	3.64

*Values used for bed cycling calculations.
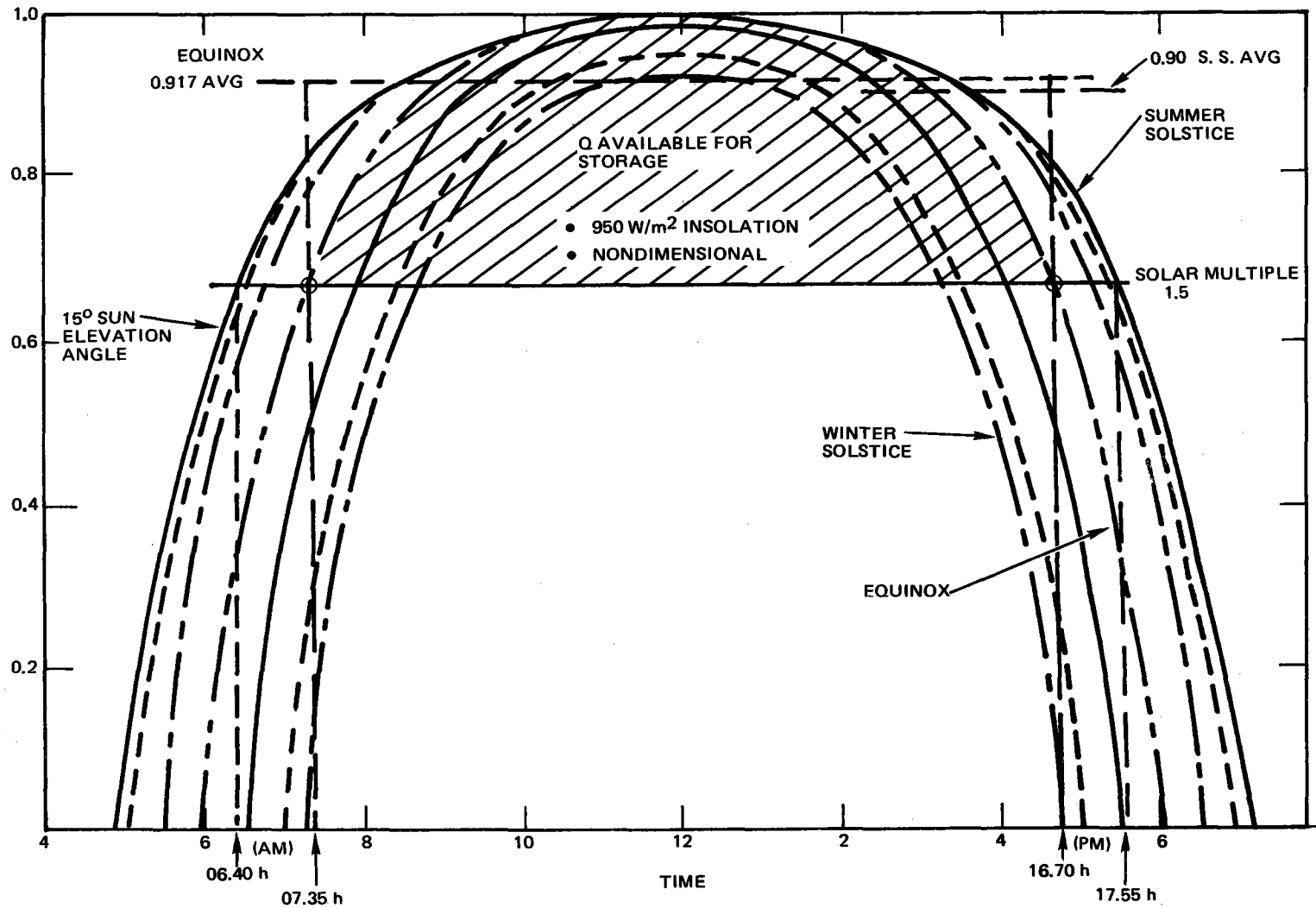
Figure 5-15. Diurnal Variations in Absorbed Thermal Power

9272-134

System integration studies have indicated that 4.5 h of storage capacity is a more reasonable design point. This larger storage capacity precludes any loss of insolation available for storage. For purposes of the initial computer runs, the bed was sized for 4.5 h storage at 250 MWt. This larger bed size (11% increase over the 4.05 h) will provide a higher average outlet air temperature for smaller discharge periods.

A typical air-rocks thermal storage unit to provide 250 MWt for 4.5 h with an assumed utilization of 15%, 1135°F and 675°F maximum and minimum air temperatures, and 1-in. diameter rocks (porosity = 0.39) has the following rock mass and gross volume:

$$M_{rocks} = \frac{Q \times h \times 3.413 \times 10^6}{C_p \times \Delta temp \times utilization}$$

Substituting,

$$M_{rocks} = \frac{250 \times 4.5 \times 3.413 \times 10^6}{0.24 \times (1135 - 675) \times 0.15} = \frac{2.319 \times 10^8 \text{ lb}}{115,931 \text{ tons}}$$

$$V_{rocks} = \frac{M_{rocks}}{(1 - \epsilon)\rho}$$

Substituting,

$$V_{rocks} = \frac{2.319 \times 10^8}{(1 - 0.39) \times 165} = 2.304 \times 10^6 \text{ ft}^3$$

Also,

$$V_{rocks} = \frac{\pi}{4}\left(D_0^2 - D_i^2\right) \times height$$

Assuming a height = 25 ft for the rock bed with a 40-ft diameter center hole,

$$D_0 = 345 \text{ ft}$$
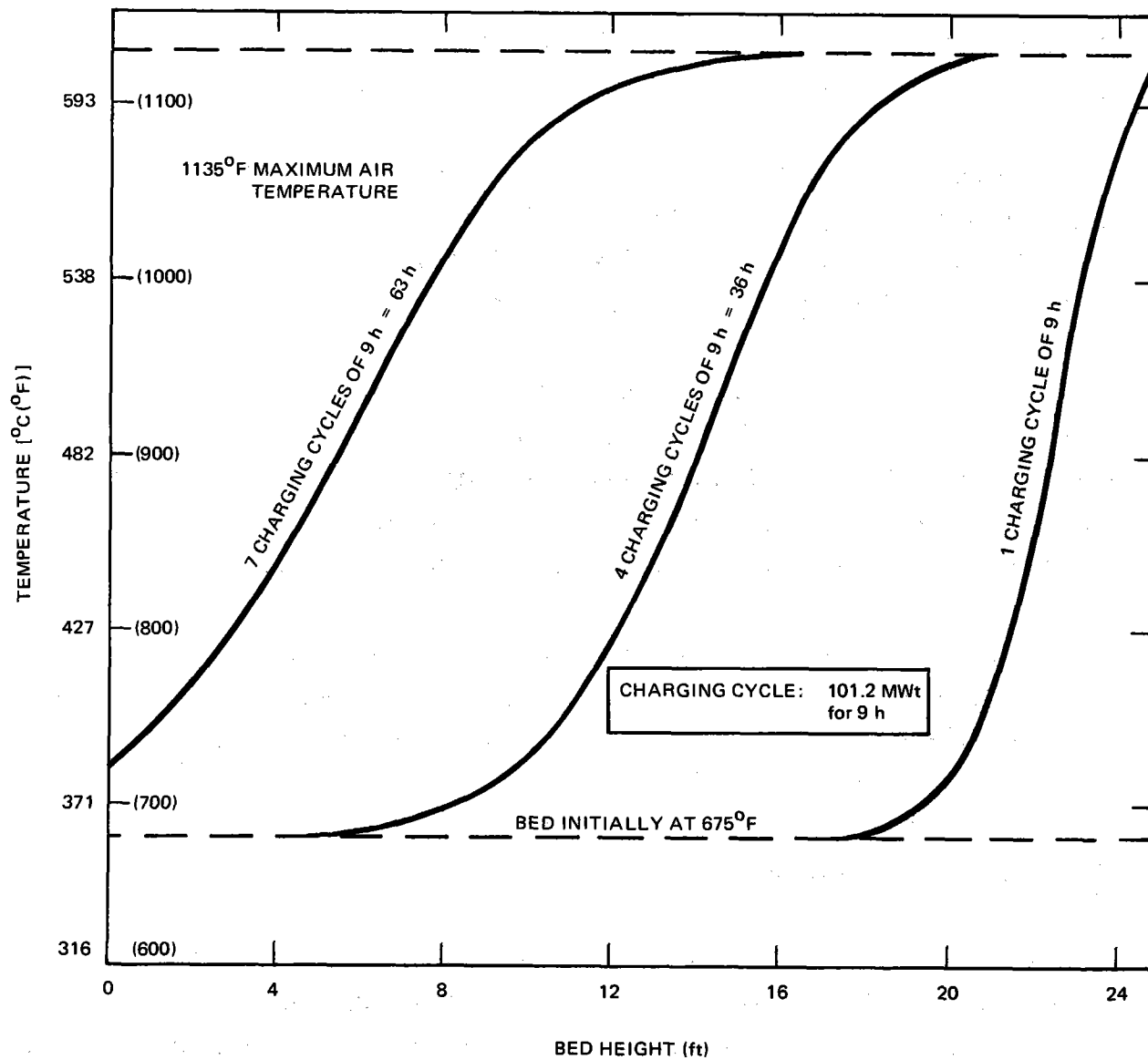
Figure 5-16. Air-Rock Thermal Storage System (Initial Charging Cycles)

For computer program input with $D_1 = 0$,

$$D_0' = 342.48 \text{ ft}$$

For the initial computer runs, the bed charging and discharging cycles (MW power, h) were taken at (101.2, 9) and (250, 3.65), respectively.

Figure 5-16 shows temperature profiles through the rock bed after 9, 36, and 63 h of charging at 101.2 MWt. The bed is initially assumed to be at 675°F throughout. Subsequent analyses will show temperature profiles vs time with the bed initially at ambient conditions.

Figure 5-17 shows temperature profiles for the first cooling cycle after 63 h of heating. As the bed is cycled in alternating heating (101.2 MW x 9 h) and cooling (250 MW x 3.65 h) cycles, the temperature profiles gradually assume the stabilized heating and cooling distribution shown. It should be noted that the temperature profiles shown are those obtained after about 40 cycles.

The bed utilization resulting from the cycling selected is ~11% (target at 15%). Figure 5-18 shows the air outlet temperature versus time for a stabilized bed cooling cycle, and shows a minimal drop in temperature over the discharge period.

5.3.2.10 Storage Integration Studies

A number of studies were performed to integrate thermal storage with plant operation. The first study was to determine the number of hours of storage required each day to handle the insolation absorbed over and above the power going to the steam generators for a solar multiple (SM) of 1.5. The results are shown in Figure 5-19. For 8 months of the year, 3 h of storage is insufficient to store the available insolation. This results in an annual energy loss of 8% even when completely empty storage is assumed at the start of each daily storing inverval. From Figure 5-19, it is seen that 4.5 h of storage is a more reasonable storage capacity.
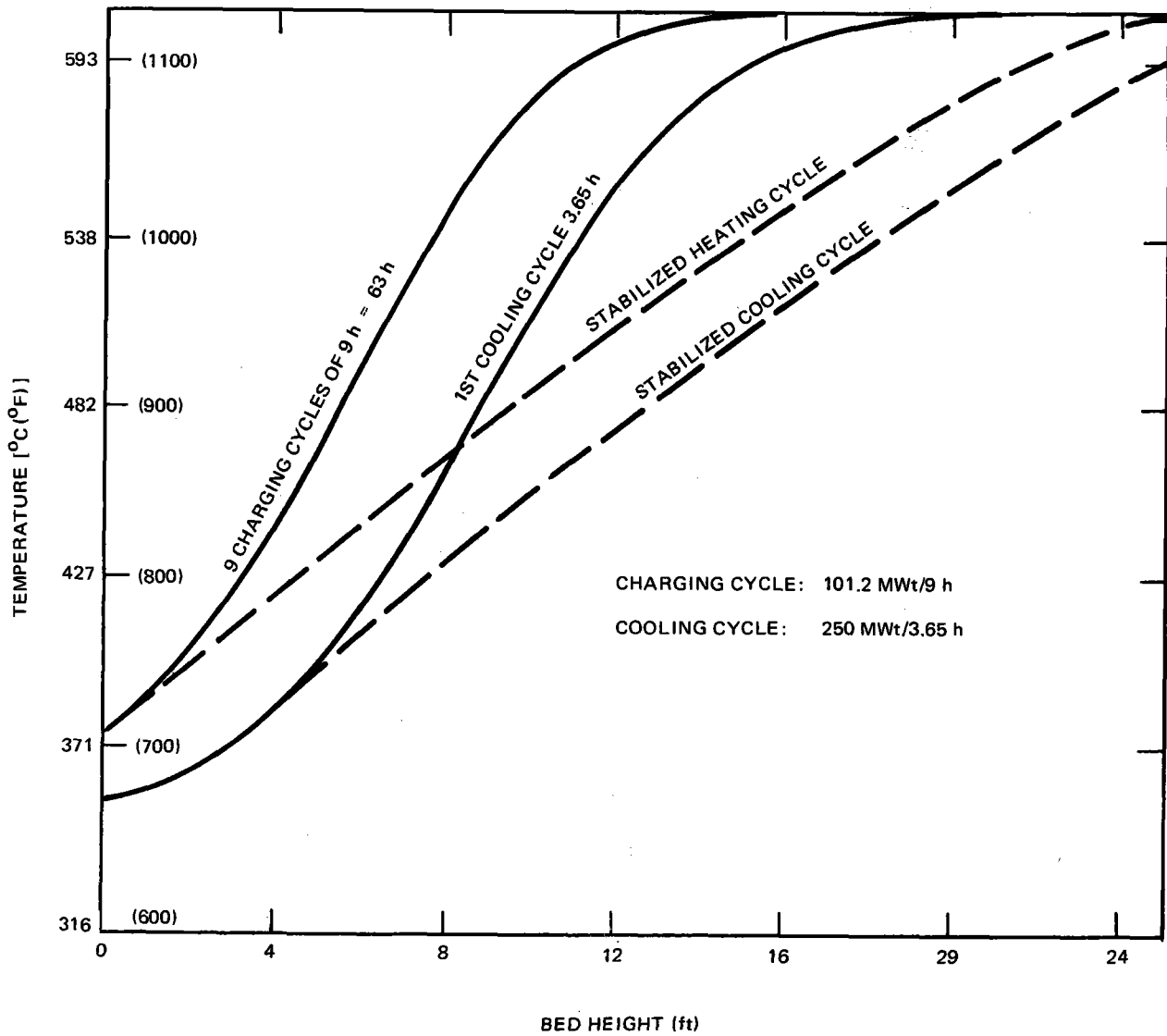
Figure 5-17. Air-Rock Thermal Storage System (Cyclic Operation)
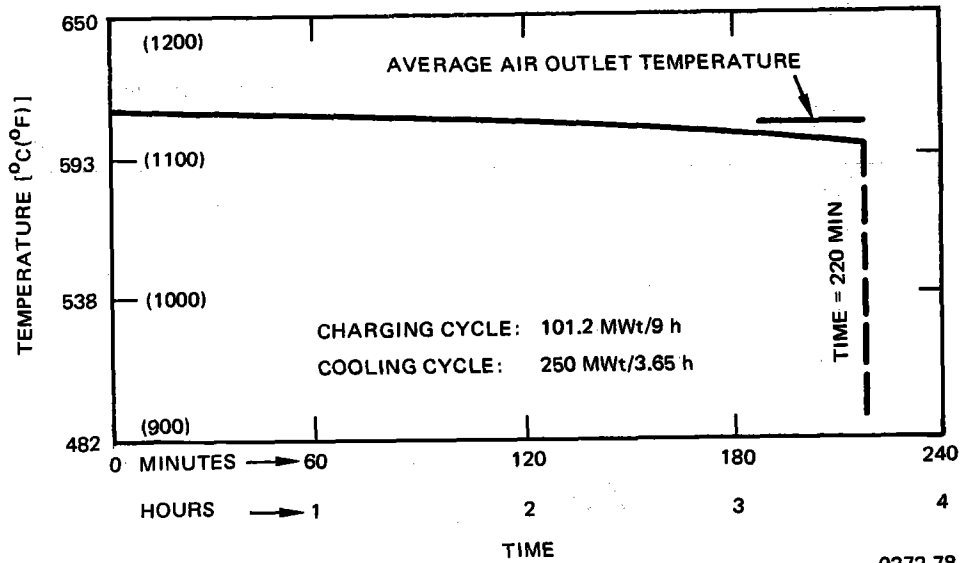
9272-76

Figure 5-18. Air-Rock Thermal Storage System Air
Outlet Temperature vs Time for Stabilized Bed
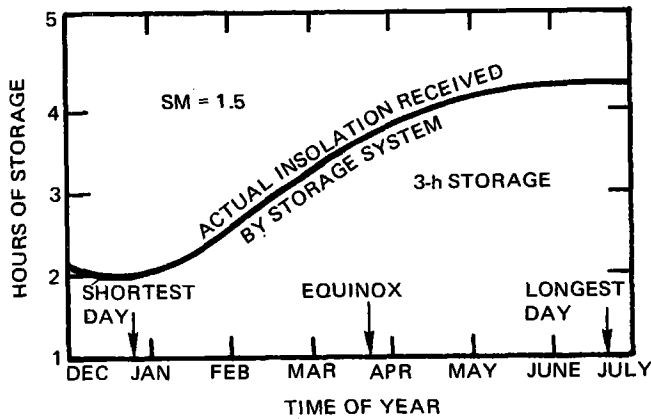
Figure 5-19. Insolation Available
for Storage
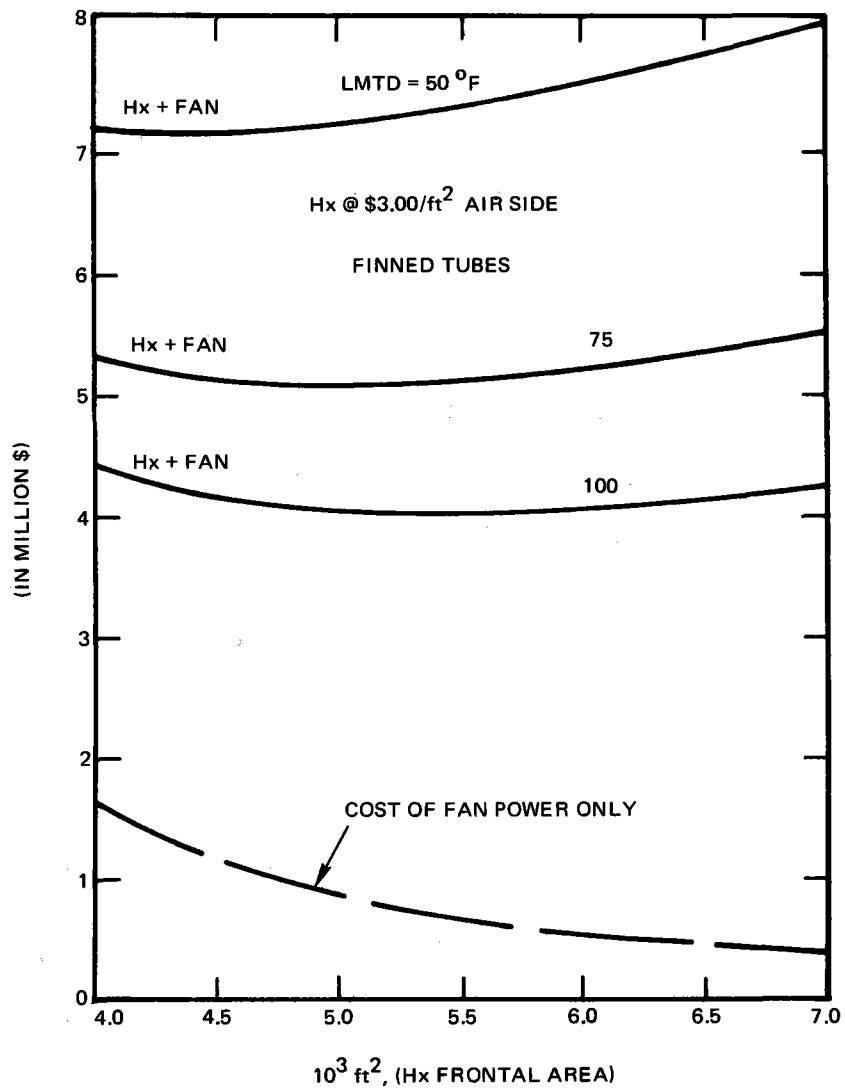
Figure 5-20. Cost of Rock Bed Heat Exchanger
Plus Cost of Fan Power

Optimization of the heat exchange of rock bed storage subsystems was conducted in conjunction with the fan power requirements to determine minimum cost conditions. The heat exchanger air frontal area was varied from 4000 to 7000 ft^2 with the lowest cost heat exchanger being at the smallest frontal area where the air velocity was highest; however, the pumping power increases with a small area so that in general there is a frontal area that minimizes the cost of heat exchanger plus fan power. The heat exchanger was assumed to cost $3.00/$ft^2$ based on the air-side area. The fan power cost was the daily average power times an assumed plant capital cost of $1.25 x 10^6/MWe. The results are shown in Figure 5-20.

A method was developed to calculate the sodium flow rates and temperatures in all major lines of a plant with rock bed storage. Figure 5-21 is a schematic diagram of the plant loop showing all flow rates and temperatures for the equinox noon condition when the receiver is absorbing 390 MWt, with 130 MWt going into storage and 260 MWt going to the steam generator. This analysis was extended to determine the storage and plant parameters from 7:30 a.m. when the insolation absorbed reaches 260 MWt to 4:30 p.m. when it finally drops below 260 MWt. These parameters include flow rates and temperatures in all lines, the ΔT between sodium and storage air coolant, the fan pumping power, and the receiver outlet temperature.

The above studies have permitted trades to be made between receiver outlet temperature and plant efficiency. As receiver outlet temperature is increased, the thermal losses increase which eventually offset any gains in heat exchanger performance and cycle efficiency.

Preliminary tests on air-rock systems to include thermal cycling and "long-term" heating have been performed in company-funded IR&D work. These thermal cycling tests have evaluated cracking, exfoliation (scaling or flaking), crumbling, or other dimensional instability of the rocks.

Thermal cycling tests of samples of river gravel have been completed to verify that rocks can tolerate temperature excursions over the range and rate anticipated in the event air-rocks are selected for the thermal storage application.
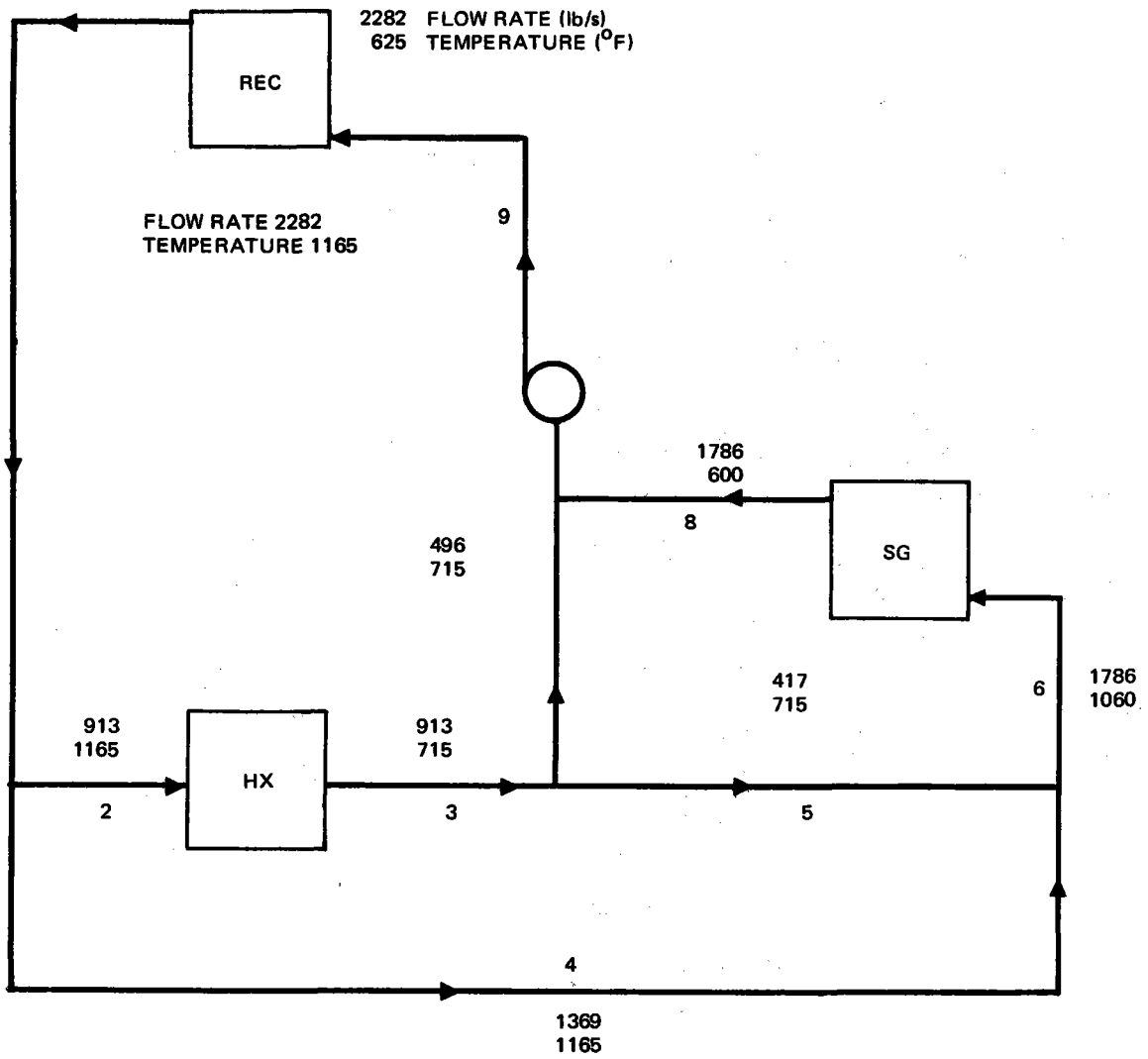
Figure 5-21. Air-Rock System at Equinox Noon

Figure 5-22 is a photograph of the rocks tested, particularly the one with the center and surface thermocouples. Random samples of Santa Clara River natural run granite rocks were subjected to thermal cycling, ambient to ~600°C (1112°F) followed by a 168-h heat soak at ~600°C (1112°F). The objectives of these tests were to determine if any dehydration or physical degradation occurred during the heat cycles. Twenty-one random rock samples were selected for the tests. The rocks were preheated to ~120°C (248°F) for a 48-h period to remove excess water of hydration (the rocks had been exposed to the seasonal rains). Pretest and post-test weight measurements were made of the specimens and are listed in Table 5-6. One rock was instrumented with a center and a surface chromel-alumel thermocouple to monitor temperatures.
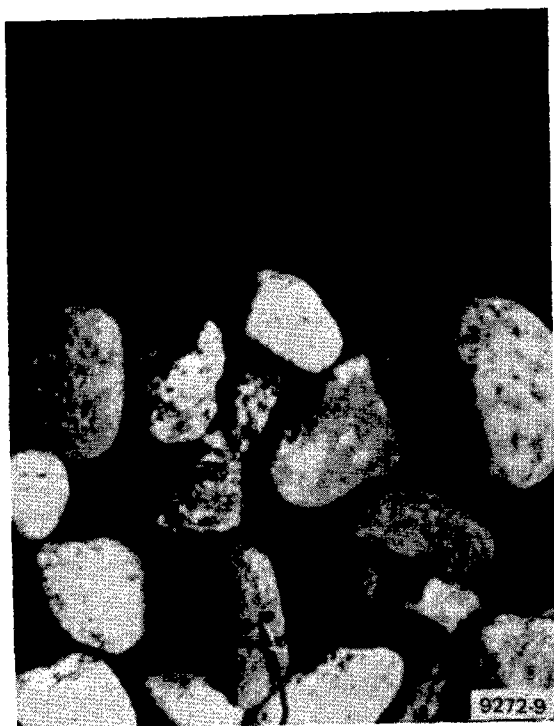
Figure 5-22. Rocks Tested — Instrumented Rock

For Phase 1, the rocks were subjected to eight thermal cycles where the temperature was increased from ambient to ~625°C (1157°F) then allowed to cool to ambient again. After each cycle, the rocks were observed for any degradation. The second phase of the tests required heating the rocks to 600°C (1112°F) and

TABLE 5-6

RIVER ROCK WEIGHT MEASUREMENT

Specimen No.	Pretest Weight (gm)	Post-Test Weight (gm)
1	17.382	17.328
2	24.777	24.754
3	45.366	45.303
4	11.955	11.688
5	11.787	11.764
6	10.151	10.030
7	12.055	11.818
8	30.970	30.592
9	31.430	31.052
10	24.873	24.826
11	11.940	11.815
12	18.337	18.291
13	24.419	24.273
14	11.738	11.714
15	14.966	14.950
16	10.515	1.0502
17	11.838	11.826
18	27.490	27.338
19	12.411	12.166
21*	4.008	3.689

*Sample was found broken on post-test examination.

maintaining that temperature for 168 hours. At the completion of this test, the rocks were again inspected. The third test phase again subjected the rocks to eight thermal cycles as in Phase 1.

A summary of the test observations and conditions are presented below.

1) Phase 1 - No apparent physical degradation was observed.

2) Phase 2 - No apparent physical degradation was observed.

3) Phase 3 - Specimens removed from test apparatus. One rock which had a high mica content was found broken into two parts. All other rocks showed no apparent signs of physical degradation except a distinct color change. All rocks exhibited a tan to brownish color upon removal.

4) Post-test weight measurements were made. The rocks showed an average weight loss of ~1.1%.

5) Temperature heat rate during tests - 840°C/h maximum (1512°F/h).

6) Temperature decay rate during tests - 560°C/h maximum (1008°F/h).

7) Peak temperature obtained during cycle tests — 550-630°C (1022-1166°F).

8) Steady-state temperature during soak tests — 580-600°C (1076-1112°F).

9) Three randomly selected samples were used to determine compression strength.

Sample	Pretest Compression (psi)	Post-Test Compression (psi)
1	2600	2100
2	2000	400
3	2600	2400

5.3.2.11 Rock Transient Temperature and Thermal Stress Analysis

Analytical predictions for air-rock thermal gradients are of interest. Thermal stress calculations based on resulting temperature gradients will allow

an evaluation of how critical thermal cycling (over the temperature range anticipated for the air-rocks thermal storage alternative) is with respect to rock bed thermophysical stability.

When spherical rocks at isothermal conditions are exposed to sudden changes in ambient temperature, resulting transient temperature profiles are a function of the Biot and Fourier Moduli. Graphical solutions to transient heat conduction in a sphere are presented in Eckert-Drake, Mass and Heat Transfer, 2nd Edition, McGraw-Hill, 1959, Page 85, Figure 4.8.

Fourier and Biot Moduli for rock sizes of interest (r_o = 0.25, 0.50, and 1.0 in.) can be calculated as follows:

$$\text{Fourier Modulus} = \frac{\alpha \tau}{r_o^2}$$

$$(\text{Biot Modulus})^{-1} = \frac{K}{h r_o}$$

where

$\alpha = K/\rho\, C_p$, thermal diffusivity

τ = time in hours

K and h = thermal conductivity and film coefficient, respectively.

For air-rock thermal storage system take

$K = 1.2\ (\text{Btu/h-ft}^o\text{F})$

$h = 4.0\ (\text{Btu/h-ft}^2\text{-}^o\text{F})$

$\rho = 165\ (\text{lb/ft}^3)$

$Cp = 0.24\ (\text{Btu/lb-}^o\text{F})$

$\alpha = 0.0303\ (\text{ft}^2\text{/h})$

Biot Modulus inverse and Fourier Modulus divided by time, τ, in hours, are given here for different rock sizes and for the application to air-rock storage with h = 4.0 (See Table 5-7.)

TABLE 5-7
BIOT AND FOURIER MODULI

Parameter	Rock Size, r_0 (in.)		
	0.25	0.50	1.0
1/Biot Modulus	14.4	7.2	3.6
Fourier Modulus/τ	69.81	17.45	4.36

To extend the solutions to the ranges of θ/θ_0 and Fourier Modulus of interest, semilog straight line equations can be developed. These equations facilitate calculations which are presented below: (Note that $\theta/\theta_0 = 1$ at FM = 0 for all cases.) See Table 5-8 for "B" values.

$$\theta/\theta_0 \simeq e^{-B \times FM}$$

where

$$\theta = t - t_f$$

$$\theta_0 = t_{initial} - t_f$$

$$t_f = t_{fluid} = t_{ambient\ air}$$

TABLE 5-8
TABLE OF "B" VALUES

	$r_0 = 0.25$ in.	$r_0 = 0.50$ in.	$r_0 = 1.0$ in.
Center of Rock $r/r_0 = 0$	0.10536	0.35668	0.71335
$r/r_0 = 0.4$	0.16252	0.43078	0.75502
Surface of Rock $r/r_0 = 1.0$	0.22314	0.5108	0.8675

Figure 5-23. Temperature Profiles, θ/θ_0 vs r/r_0
(for various times after sudden exposure)

Figure 5-24. Temperature Profiles, θ/θ_0 vs r/r_0
(for various times after sudden exposure)

The attached curves, Figures 5-23 through 5-25, present data for θ/θ_0 vs time (Table 5-9) and location in the rock. Temperature profiles vs time for various locations in the rock (center $r/r_0 = 0$, to the surface $r/r_0 = 1$) are determined by:

$$t \text{ (time, } r/r_0) = (\theta/\theta_0) \cdot \theta_0 + t_f$$

Temperature profiles for the rock center, surface, and $r/r_0 = 0.4$ are shown in Figure 5-26 for a 1-in. diameter ($r_0 = 0.5$ in.) rock initially at 675°F and suddenly exposed to air at 1135°F with an average film coefficient h = 4 Btu/h-ft^2-°F. This value of film coefficient is the expected value for the initial design air-rocks thermal storage unit and represents a discharge rate of 250 MWt. In the real situation, the rocks see a much lower temperature difference.

Figure 5-27 shows surface temperature vs time profiles for rocks of $r_0 = 0.25$ in., $r_0 = 0.5$ in., and $r_0 = 1.0$ in. The surface gradient is more severe for the rocks of smaller radius.

Thermal Stresses

For rocks, typical values for thermophysical properties of interest are as follows:

$E = 8 \times 10^6$ psi $\qquad$ $K = 1.2$ Btu/h-ft-°F

$r = 0.25$ $\qquad$ $C_p = 0.24$ Btu/lb-°F

$\alpha' = 4.5 \times 10^{-6}$ per °F $\qquad$ α = thermal diffusivity = 0.030 ft^2/h

Compressive strength $\simeq$ 12000 psi

Shear strength $\simeq$ 2400 psi

Tensile strength $\simeq$ 480 psi.

Roark, "Formulas for Stress and Strain," 4th Edition, McGraw-Hill, Page 378 gives the following formulae for thermal stresses in a sphere whose surface temperature is changed at the uniform rate of "m" degrees per unit time.
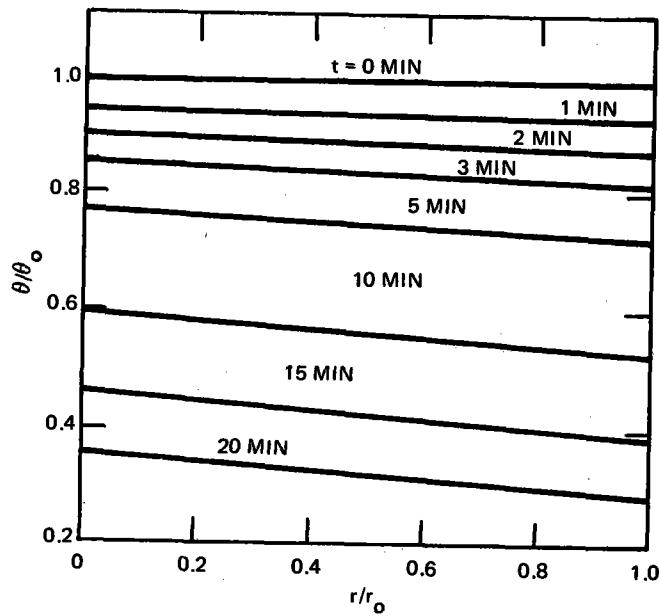
$$r_o = 1 \text{ IN.}$$

$$t = (\theta/\theta_o)\ \theta_o + t_f$$

$$\text{WHERE}\quad \theta = t - t_f$$

$$\theta_o = t_{INITIAL} - t_f$$

$$h = 4\ \text{Btu/h-ft}^2\text{-}{}^\circ\text{F}$$

9272-84

Figure 5-25. Temperature Profiles, θ/θ_o vs r/r_o
(for various times after sudden exposure)

TABLE 5-9

θ/θ_o vs TIME
(For "Spherical" Rock Exposed to Sudden Change in Ambient Temperature
with $h = 4$ BTu/h-ft^2-°F)

Time (Min)	$r/r_o = 0$			$r/r_o = 0.4$			$r/r_o = 1.0$		
	$r_o = 0.25$	$r_o = 0.5$	$r_o = 1.0$	$r_o = 0.25$	$r_o = 0.5$	$r_o = 1.0$	$r_o = 0.25$	$r_o = 0.5$	$r_o = 1.0$
0	1.000	1.000	1.000	1.000	1.000	1.000	1.000	1.000	1.000
1	0.885	0.901	0.949	0.828	0.882	0.947	0.771	0.862	0.939
2	0.783	0.813	0.902	0.685	0.778	0.896	0.595	0.743	0.882
3	0.692	0.733	0.856	0.567	0.687	0.848	0.459	0.640	0.828
5	0.542	0.595	0.772	0.389	0.534	0.760	0.273	0.476	0.730
10	0.294	0.354	0.595	0.151	0.286	0.578	0.075	0.226	0.532
15	0.159	0.211	0.460	0.059	0.153	0.439	0.020	0.108	0.388
20	0.086	0.126	0.355	0.023	0.082	0.334	0.006	0.051	0.283
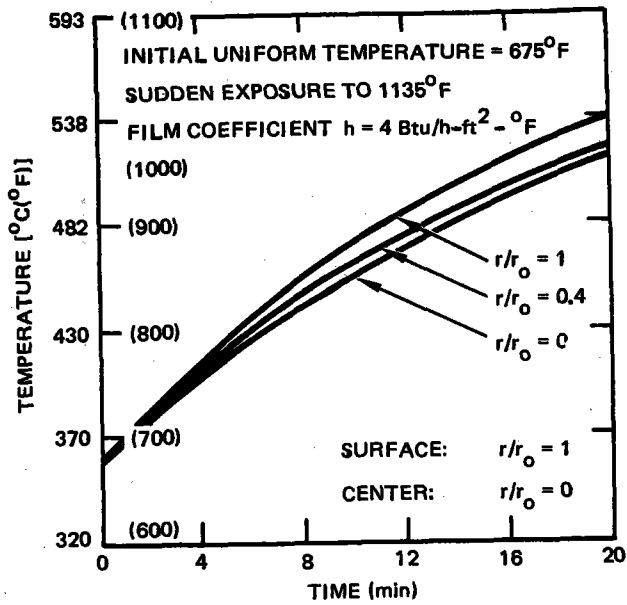
Figure 5-26. Temperature vs Time for 2 in. Diameter Rock

Figure 5-27. Surface Temperature vs Time
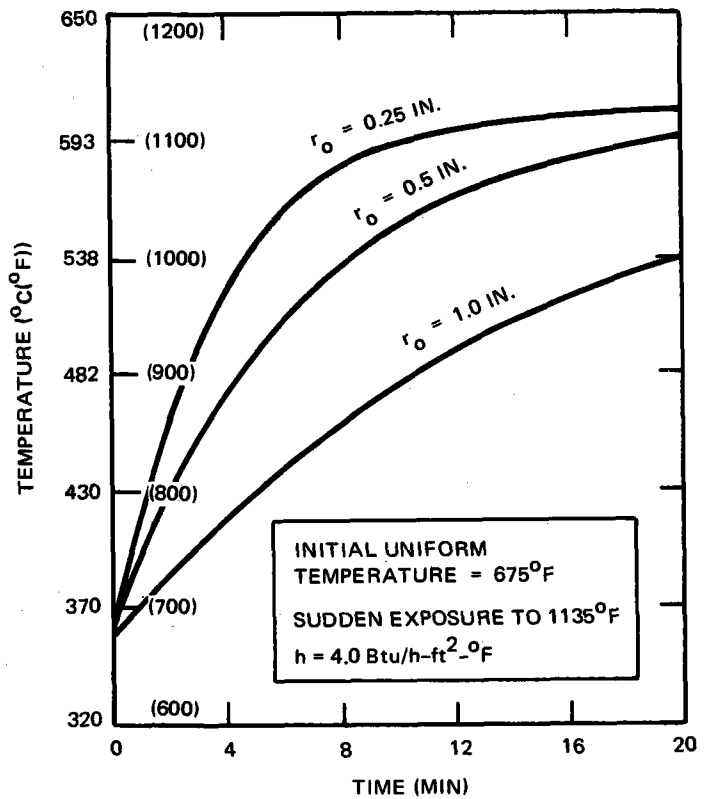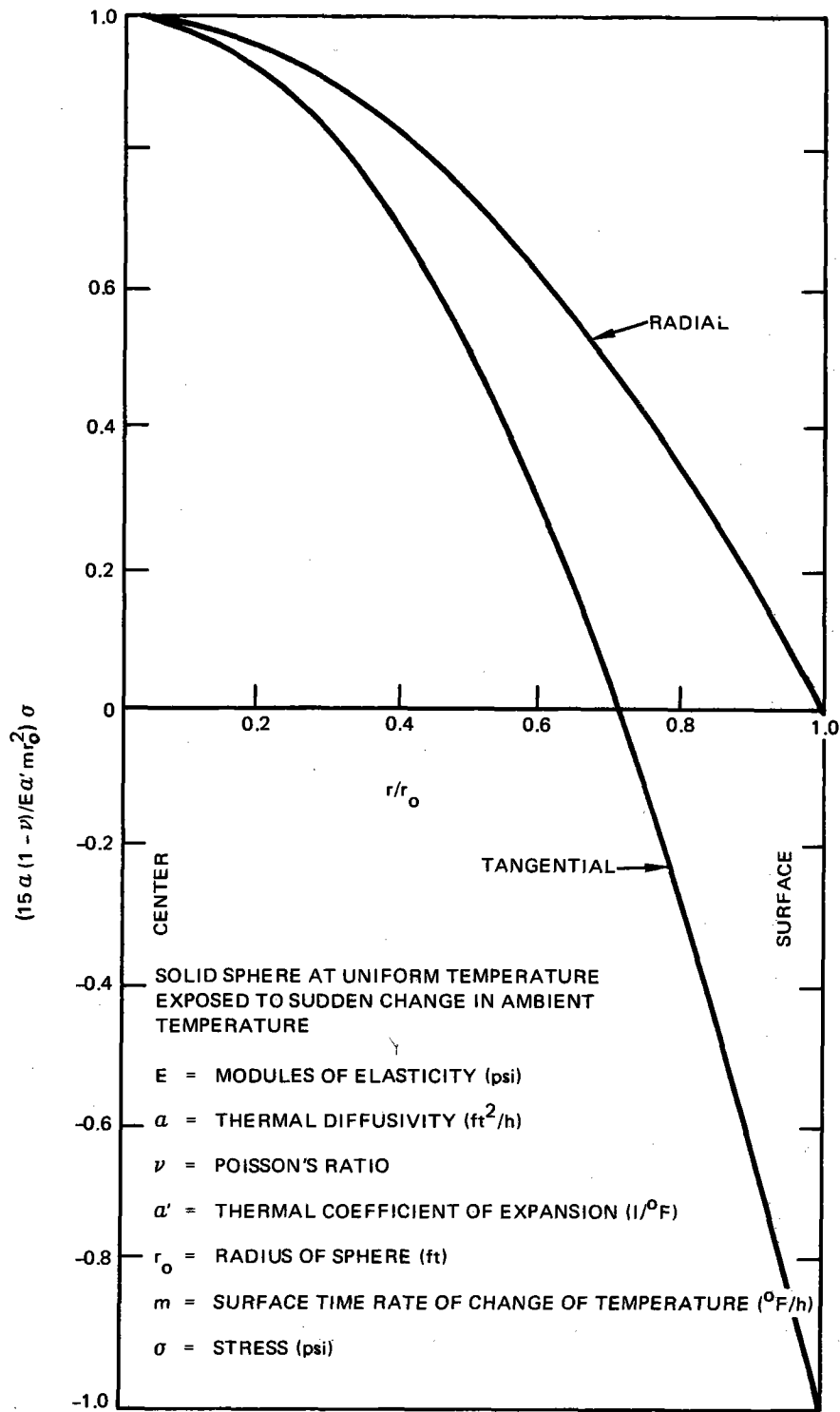
Figure 5-28.   Dimensionless Thermal Stress

$$\sigma_{radial} = \frac{E\alpha'm}{15\alpha(1-\nu)} (r_0^2 - r^2)$$

$$\sigma_{tangential} = \frac{E\alpha'm}{15\alpha(1-\nu)} (r_0^2 - 2r^2)$$

where

E = modulus of elasticity

α' = coefficient of thermal expansion

m = temperature rate of change at surface

α = thermal diffusivity

ν = Poisson's ratio

r_0 = sphere radius

r = radial distance from center of sphere.

The equations for radial and tangential stress can be rearranged as follows in dimensionless form:

$$\frac{15(1-\nu)}{E m r_0^2} \sigma_{radial} = 1 - (r/r_0)^2$$

$$\frac{15\alpha(1-\nu)}{E\alpha'm r_0^2} \sigma_{tangential} = 1 - 2(r/r_0)^2$$

Figure 5-28 shows plots of σ_{rad} and $\sigma_{tangential}$ in dimensionless parameters as a function of r/r_0. (Note that positive stresses are tensile; negative stresses are compressive.)

Examining the equations for σ_{rad} and σ_{tan} and the dimensionless plots of Figure 5-28 shows that $(\sigma_{radial})_{max}$ location is at r = 0 (center) and $(\sigma_{tangential})_{max}$ location is at r = 0 and r = r_0 (center and surface). The $\sigma_{tangential}$ = 0 at r = 0.707 r_0.

The maximum "m," or time rate of temperature change, occurs at the surface, and, further, occurs at time = 0 (when the system is exposed to the sudden change in ambient temperature).

$$m_{max} = \left(\frac{dt_s}{d\tau}\right)_{time=0}$$

$$\frac{dt_s}{d\tau} = \theta_0 \cdot \frac{d(\theta/\theta_0)_s}{d\tau}$$

but

$$\theta/\theta_0 = e^{-BxFM} = e^{-\frac{B\alpha}{r_0^2}\tau}$$

$$\frac{d(\theta/\theta_0)}{d\tau}_{max} = -\frac{B\alpha}{r_0^2}$$

$$\therefore m_{max} = -\frac{B\alpha}{r_0^2}\theta_0$$

Substituting for m_{max},

$$\sigma_{radial\ max} = \sigma_{tangential\ max} = -\frac{E\alpha'B\theta_0}{15\ (1 - \nu)}$$

It should be noted that when the rocks are exposed to an increase in ambient temperature, the sign of θ_0 is negative. The radial stress and tangential stress at the center of the rock are tensile. The tangential stress at the surface is compressive. If ambient temperature decreases, θ_0 is >0 and σ_{radial} is a compressive stress at the rock center. The tangential stress is a tensile stress and has a maximum at the rock surface.

From the standpoint of allowable stress, the tensile stress is controlling, and although the maximum tensile stress occurs at different locations and is in one case radial and in the other case tangential, both increasing or decreasing sudden changes in ambient temperature are equally important considerations.

Table 5-10 shows allowable sudden ambient temperature increases (or decreases) for different rock sizes for operation of air-rock beds with $h \simeq 4$ Btu/ h-ft^2-°F with $\sigma = 480$ psi tensile.

TABLE 5-10
ALLOWABLE ROCK TEMPERATURE INCREASES

Rock Size Diameter (in.)	Allowable Temperature	
	°F	°C
0.5	672	373
1.0	293	163
2.0	173	96

Results show that the larger rocks experience more inner temperature lag when exposed to sudden changes in ambient temperature. For a given change in ambient temperature, thermal stresses are greater for larger diameter rocks. Temperature increases or decreases are equally important since they result in equal levels of tensile stress although at different locations.

The analysis indicates that a 2-in. diameter rock can tolerate an ambient temperature increase of approximately 173°F without exceeding a maximum tensile stress of 480 psi; a 1-in. diameter rock can tolerate 293°F change. The 1/2-in. diameter "spherical" rock is least sensitive to sudden ambient temperature change, and can tolerate approximately 672°F ambient temperature change without exceeding 480 psi tensile stress.

The rocks as utilized in the air-rocks thermal storage concept can be brought to operating temperatures slowly to avoid thermal stress problems. Once the bed is stabilized, the actual temperature differences "seen" by the rocks (as the system will operate) are approximately 1/3 the magnitude which can be tolerated by rocks as large as 2-in. diameter.

Thermal cycling tests will continue for already available river gravel samples and other rocks which will be obtained and classified.
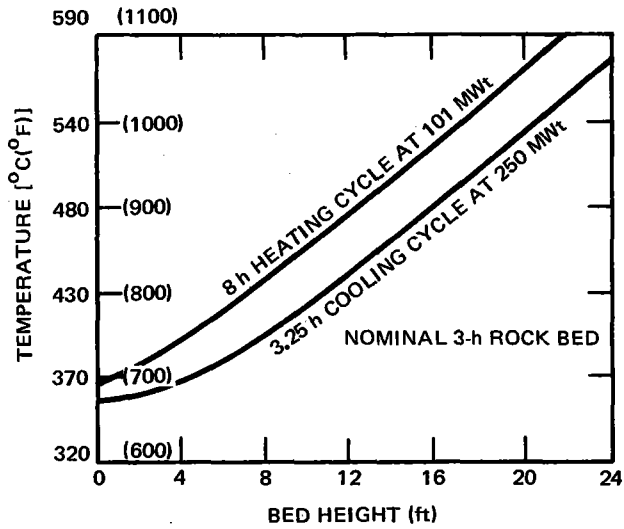
Figure 5-29. Air-Rock Thermal Storage —
Cyclic Operation Stabilized Bed
←——Temperature Profiles

9272-88

Figure 5-30. Average Bed Temperature
vs Number of Charging Cycles——→

9272-89
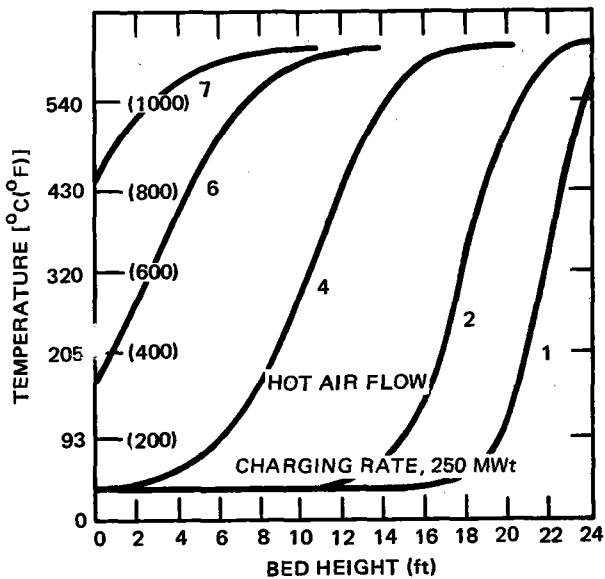
Figure 5-31. Temperature Profiles
←——for Various Charging Cycles

9272-90

The commercial plant-size air-rock thermal storage unit was cycled on the GE 440 Computer to obtain stabilized bed performance curves. These results are shown in Figure 5-29. Cases were also run to develop charging curves for the bed starting from ambient conditions of $26.7^{\circ}C$ ($80^{\circ}F$). These curves are shown in Figures 5-30 and 5-31 giving results in terms of average bed temperature and also temperature profiles after each identified charging cycle.

The solution to the basic heat transfer analysis for the thermocline can be examined in terms of the dimensionless parameters:

$$\pi = \frac{hS}{mc} \tau$$

$$= \frac{hS}{GC_p} L$$

and

$$U = \frac{\pi}{\Lambda}$$

where

h = surface heat transfer coefficient ($Btu/h\text{-}ft^2\text{-}^{\circ}F$)

S = heat transfer surface area (ft^2/ft^3)

m = bed matrix density

c = specific heat of matrix material ($Btu/lbm\text{-}^{\circ}F$)

τ = cycle cooling or heating period (h)

G = mass fluid velocity based on free flow area ($lbm/h\text{-}ft^2$)

C_p = fluid (air specific heat) ($Btu/lbm\text{-}^{\circ}F$)

L = bed height (ft)

π = dimensionless time period parameter

Λ = dimensionless length parameter

U = utilization factor

The utilization factor is a quantitative measure of how much of the maximum theoretical energy content of the bed is removed over a cycle of cooling and heating.

Substituting,

$$U = \frac{\pi}{\Lambda} = \frac{G \, C_p \, \tau}{mc \, L}$$

but

$$G = \frac{\dot{W}}{\alpha A}$$

where

$\dot{W}$ = air weight flow

A = matrix frontal area

α = porosity of rock bed matrix

$U = \dot{W} \, C_p \, \tau / \alpha mc \, AL$

(AL is the rock bed matrix volume.)

For a given thermal storage energy capacity requirement and power charge or discharge rate,

$$U = \text{constant} \times \tau$$

Therefore, the only approach to increasing bed utilization would appear to be increasing the charge or discharge period or, what is equivalent, undersizing the bed and allowing a greater outlet air temperature drop during the discharge cycle. Under the constraint of maintaining steam generator outlet temperature over the entire thermal storage discharge period, this approach is not viable.

To verify the conclusions regarding bed utilization, computer runs were made for the cases: (1) film coefficient values 2 x baseline; and (2) equivalent bed design with bed height 2 x baseline. The results are shown in Figures 5-32 and 5-33 with utilization factors noted.
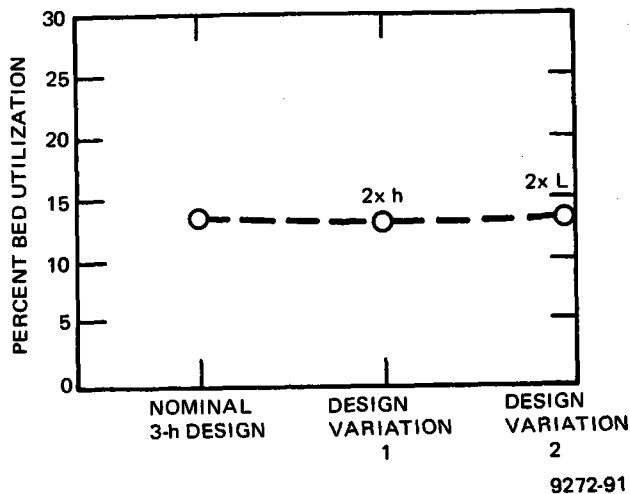
Figure 5-32. Air-Rock Thermal Storage Bed Utilization (as influenced by film coefficient and bed length)
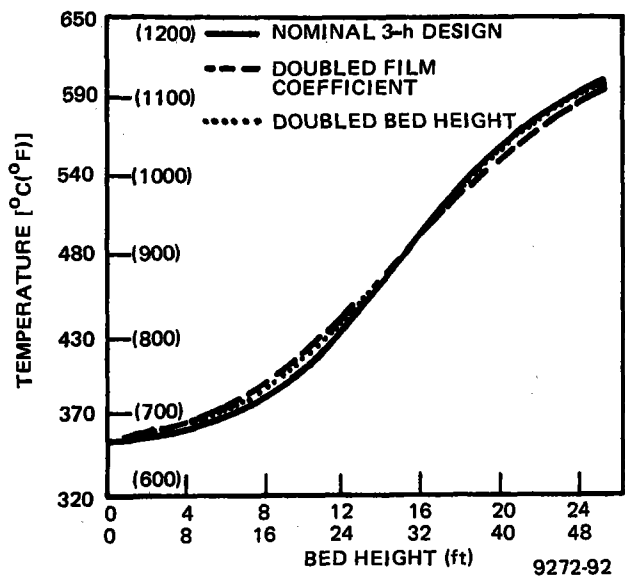
Figure 5-33. Stabilized Temperature Profile — Cooling Cycle

Summary of Air-Rock Operating Characteristics

The impact of bed utilization on the storage system design may be summarized as follows. The utilization of a bed depends on the amount of energy that is stored in or removed from the bed. If this amount of energy is relatively low, then the utilization is low, and the cycle temperature drop is small. Conversely, if the amount of energy is large, the utilization is high, but there is a small drop in cycle temperature and plant efficiency when operation is from storage.

The energy capacity of air-rock storage can be greatly increased by simply adding low-cost rock and concrete ducting. Therefore, an optimum storage system system would have an oversize rock bed. This bed would have relatively small amounts of energy added or extracted during normal daily operation, the utilization would be low, and the temperature fall-off would be small. During unusual operating conditions, much larger amounts of energy can enter or be removed from storage which will improve the operational flexibility and reduce the cost of power. Thus, the reference air-rock storage system has a nominal 3-h storage capacity but has an actual capacity of at least 12 hours.
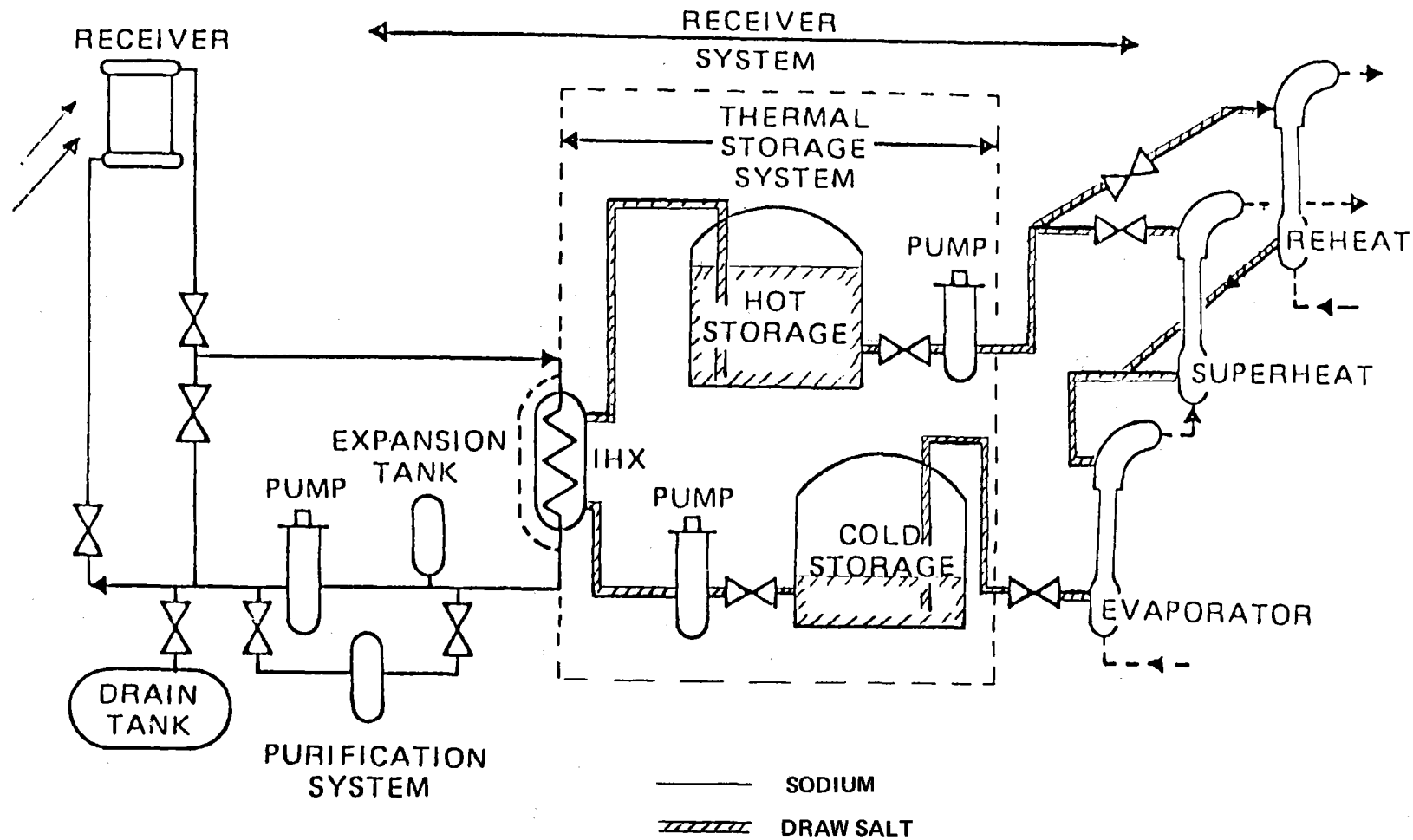
Figure 5-34.   System Modification Using Draw Salt Storage

9272-93

5.3.3 Draw Salt

5.3.3.1 Two-Loop Sodium-Draw Salt System

A brief investigation was performed to determine the delta costs associated with utilizing draw salt (45% $NaNO_3$, 55% KNO_3) in a two-loop system. The system schematic is shown in Figure 5-34. Sodium would be used in the primary loop with an intermediate sodium-to-draw salt heat exchanger (IHS). The draw salt would be used in a secondary loop which includes a hot and cold thermal storage system.

The results are presented in Table 5-11, and show a net additional cost increment of $5.68 x 10^6 for a 3-h storage capacity where the savings, which are realized by a reduced storage volume requirement and lesser cost of heat transfer storage medium, are more than offset by the cost of the IHX and added pump and the increased cost of the steam generator. The larger steam generator (1.4 area ratio) is required because of the poor heat transfer characteristics of the draw salt. For 6-h storage capacity the added cost drops to $2.6 x 10^6 since the savings in sodium costs tend to offset the IHX cost.

However, the use of sodium in a single loop system appears to be a better alternative to a two-loop system using molten draw salt in the secondary loop with a hot and cold storage tank system at least up to 6-h storage capacity.

5.3.3.2 Two-Loop - Sodium Primary; Draw Salt-Rock Thermocline

A two-loop system utilizing a thermocline thermal storage with draw salt (45% $NaNO_3$, 55% KNO_3) and rocks was investigated to determine delta costs when compared to the single-loop, all-sodium design baseline. The system schematic identifying the various operating modes and valve positions is shown in Figure 5-35. Sodium would be used in the primary loop with an intermediate sodium-to-draw salt heat exchanger (IHX). The draw salt in the secondary loop would function as the heat transfer fluid for the steam generators and as the thermal storage medium in a draw salt-rock thermocline-type thermal storage subsystem.

RECEIVER

PRIMARY
PUMP

EXPANSION
TANK

IHX'

DRAW SALT/
ROCKS STORAGE

A

B

C

REHEATER

SUPERHEATER

EVAPORATOR

SECONDARY PUMP

DRAIN TANK

PURIFICATION
SYSTEM

VALVE POSITION

MODE	A	B	C
Direct (no storage)	Open	Closed	Closed
Direct + Storage	Open	Closed	Open
Operation from Storage	Closed	Open	Closed

― ― ― ―	H₂O/STEAM
―――――	SODIUM
≠≠≠≠≠≠≠	DRAW SALT

H_2O/STEAM

SODIUM

DRAW SALT

9272-94
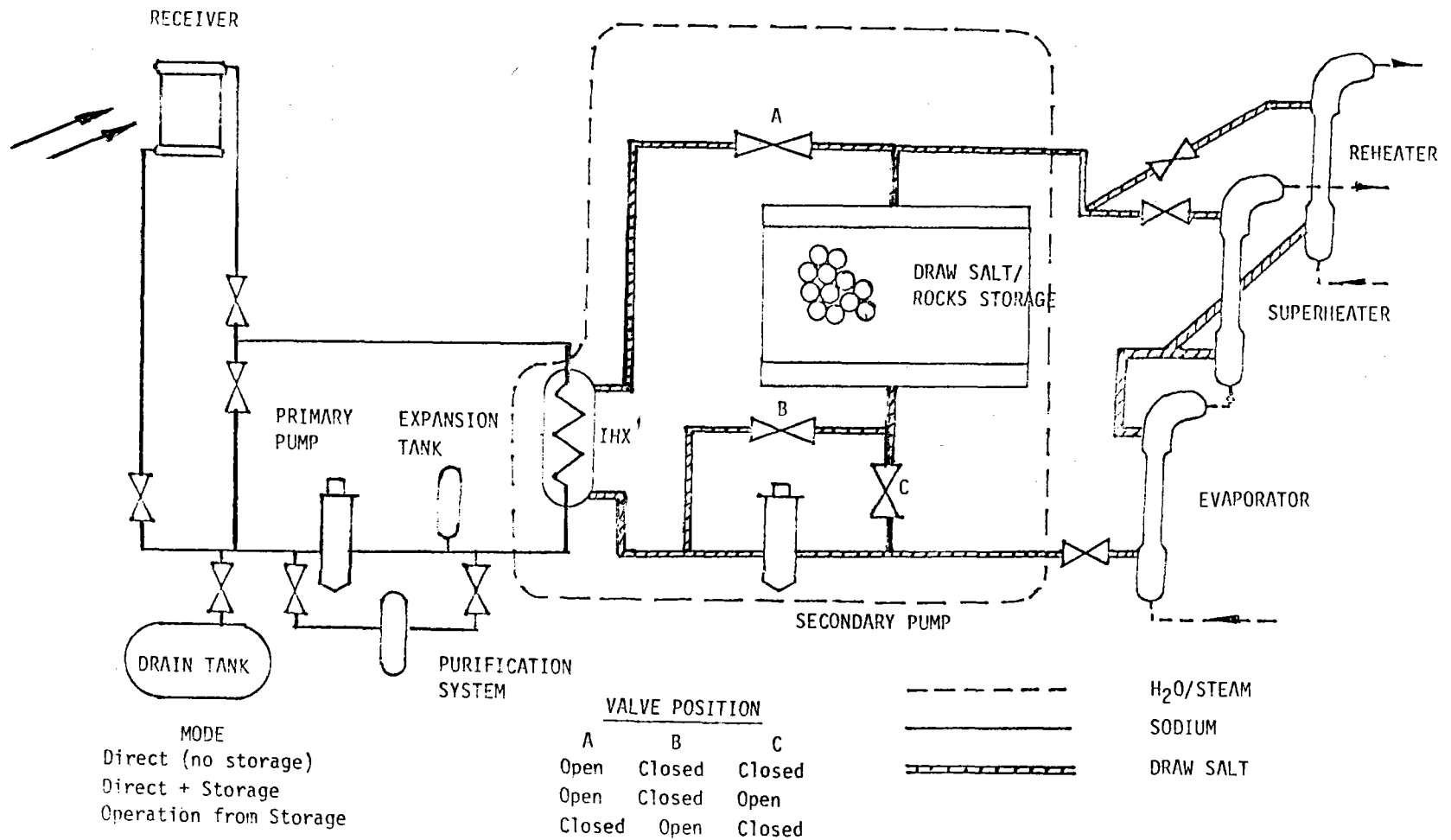
Figure 5-35.   System Modification Using Draw Salt-Rock Thermal Storage

TABLE 5-11
SODIUM IN PRIMARY LOOP, IHX, SALT IN SECONDARY LOOP
(3-h Storage Capacity)

| | Cost Increment (10^6F) | |
	Added	Reduced
Reduced Storage Tank Volume		2.08
Cost of IHX	7.10	
Added Pump	1.00	
Salt vs Sodium Thermal Storage		2.03
Steam Generator Cost (1.43 x A_{Na})*	1.69	
Drain Tank in Primary Loop	0.20	
Reduced Purification Requirements		0.20
Totals	9.99	4.31
Net +	5.68	

*A_{Na} = heat transfer area for sodium steam generator.

Figure 5-36 shows the normalized heating and cooling cycles temperature profiles vs normalized bed height for a stabilized condition draw salt-rocks thermal storage system. The curves drawn represent a utilization of ~60% for a 22% delta temperature drop.

Figure 5-37 presents cooling cycle outlet temperature vs normalized cooling period for the same draw salt-rock thermocline. The outlet temperature is expressed in percent of maximum delta temperature. The curve shows that although the maximum end temperature drop is about 24%, the time average outlet temperature is only 4% of the maximum delta temperature between hot and cold side.

Similar performance curves were generated for sodium-iron and draw salt-rock thermoclines to determine percent utilization for a range of allowable outlet temperature drop-off.
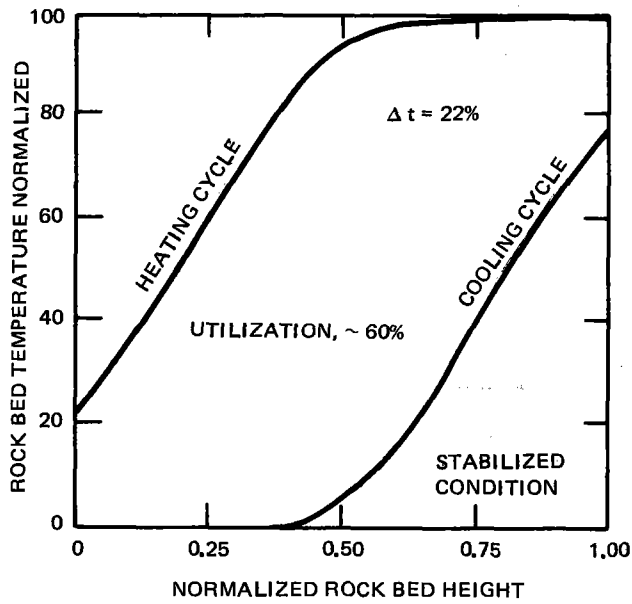
Figure 5-36. Draw Salt-Rock
Bed Cyclic Operation
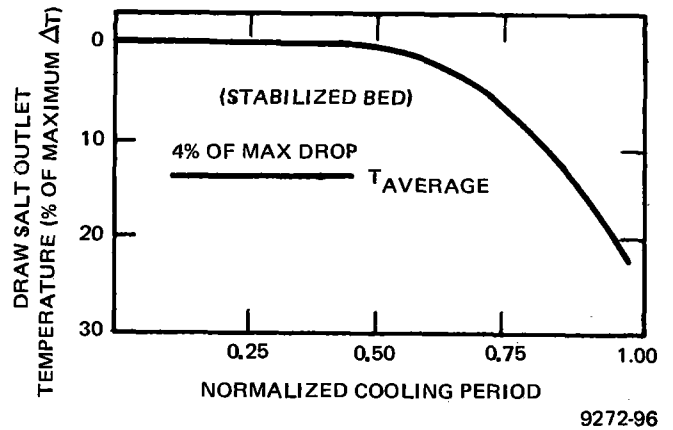
Figure 5-37. Draw Salt-Rock Thermal
Storage — Cooling Cycle
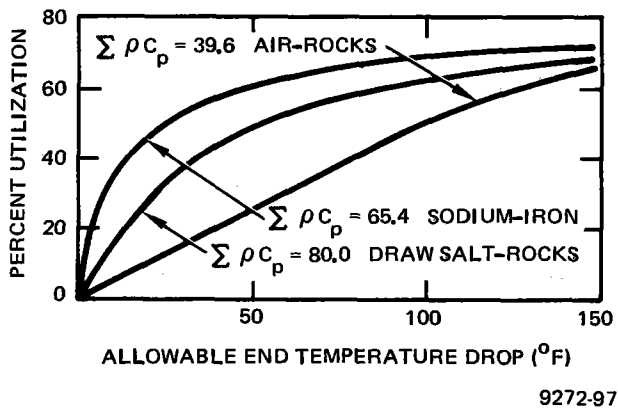
Figure 5-38. Thermocline Utilization
vs Allowable End Temperature
Drop
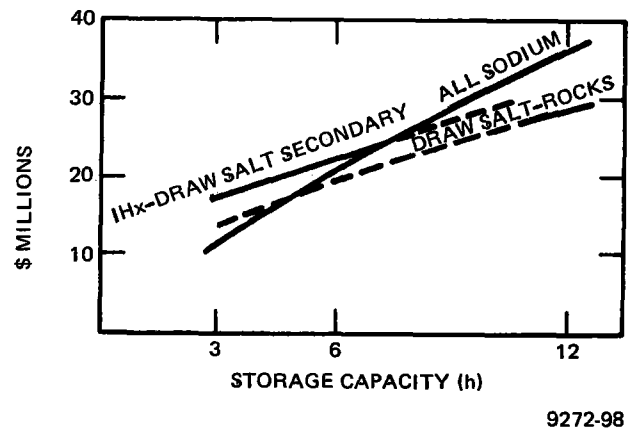
Figure 5-39. Storage Systems Costs —
250-MWt Discharge Rate

The resulting utilization curves vs allowable end temperature drop are shown on Figure 5-38 for various thermocline systems: sodium-iron; draw salt-rocks; and air-rocks.

For cost comparisons to be valid, thermocline sizing must be based on a common end temperature drop and the corresponding % utilization for the various thermocline system.

Tables 5-12 (3-h capacity) and 5-13 (6-h capacity) present thermocline sizing data for air-rocks, draw salt-rocks, and sodium-iron using 20, 50, and 60% utilizations, respectively.

Tables 5-14, 5-15, and 5-16 present costs of thermal storage for 3, 6, and 12 h capacity for all-sodium, sodium-iron thermocline, and draw salt-rock thermocline systems. The break-even point for the sodium-iron thermocline is the required maximum cost of the iron to result in sodium-iron thermocline costs equal to those for the all-sodium system.

Figure 5-39 shows storage system costs vs hours of storage capacity for all-sodium and the draw salt systems (both draw salt storage and draw salt-rock thermocline). The all-sodium system appears to be more cost effective than the draw salt alternatives for the 3-h storage capacity. Storage capacity requirements greater than ~5 h would appear to favor the draw salt-rocks thermocline, while the IHX-draw salt secondary shows an all-sodium crossover point at about 7-1/2 h storage capacity. The air-rock thermocline system costs are not shown in this comparison.

Table 5-17 presents some costs and comments concerning scrap iron for use in sodium-iron thermoclines. The cost for suitable (low carbon content) iron has to be reduced by about one-half for the sodium-iron thermocline to be competitive.

TABLE 5-12
SIZING THERMOCLINES FOR 250 MWt x 3 h = 750 MWt-h
(ΔT = 460°F)

	Air-Rocks	Draw Salt-Rocks	Sodium-Iron
Utilization (%)	20	50	60
End Temperature Drop (°F)	50	50	50
Bed Volume (ft^3)	1.15×10^6	0.279×10^6	0.257×10^6
Tons of Solid	57,949	14,051	38,461
Pounds of Fluid	Sodium	11.76×10^6	5.24×10^6

TABLE 5-13
SIZING THERMOCLINES FOR 250 MWt x 6 h = 1500 MWt-h
(ΔT = 460°F)

	Air Rocks	Draw Salt-Rocks	Sodium -Iron
Utilization (%)	20	50	60
End Temperature Drop (°F)	50	50	50
Bed Volume (ft^3)	2.30×10^6	0.558×10^6	0.514×10^6
Tons of Solid	115,898	28,102	76,922
Pounds of Fluid	Sodium	23.52×10^6	10.48×10^6

TABLE 5-14
4600 COST OF THERMAL STORAGE (3 h)
($000)

		All Sodium	Sodium-Iron	Draw Salt-Rocks
4610	Media Containment Equipment	4,000	2,890	3,007
4620	Media Circulation Equipment	0	0	0
4630	Working Fluid Circulation Equipment	688	1,688	2,688
4640	Discharging Heat Exchanger	0	0	0
4650	Charging Heat Exchanger	0	0	5,000
4660	Foundation	300	248	260
4670	Design and Engineering	0	0	0
4680	Media			
	Sodium (40¢/lb)	6,400	2,096	0
	Iron	0	4,466*	0
	Rocks (10$/ton)	0	0	141
	Draw Salt (22¢/lb)	0	0	2,587
		11,388	11,388	13,683

Sodium-Iron

4610: $2.40 \times 10^6 + (\$0.49 \times 10^6$ Drain Tank$) = \$2.89 \times 10^6$

4630: Includes Additional Valves and Manifold

*4680: Iron at $116.12/ton (5.8¢/lb) is Break-Even Point

Draw Salt-Iron

4610: $2.517 \times 10^6 + 0.490 \times 10^6$ Drain Tank $= \$3.007 \times 10^6$

4630: Includes 2×10^6 for Added Steam Generator Cost + Valves + Manifolding Less PRD

TABLE 5-15

		All Sodium	Sodium-Iron	Draw Salt-Rocks
4610	Media Containment Equipment	6,063	4,380	4,558
4620	Media Circulation Equipment	0	0	0
4630	Working Fluid Circulation Equipment	688	1,688	2,688
4640	Discharging Heat Exchanger	0	0	0
4650	Charging Heat Exchanger	0	0	6,000†
4660	Foundation	455	376	394
4670	Design and Engineering	0	0	0
4680	Media			
	Sodium (40¢/lb)	12,800	4,192	0
	Iron	0	9,370*	0
	Rocks (10$/ton)	0	0	282
	Draw Salt (22¢/lb)	0	0	5,174
		20,006	20,006	19,096

Sodium-Iron

*4680: Iron at $121.81/ton (6.09¢/lb) is Break-Even Point

Draw Salt-Iron

†4650: Larger IHX Required with Larger SM.

5.3.3.3 Draw Salt-Rock Thermal Storage – Material Costs Study

Costs for draw salt raw materials (KNO_3 and $NaNO_3$) were investigated to determine whether there was a substantial enough difference in cost between the finished product and the raw materials to warrant consideration of "making" draw salt rather than "buying" it.

Imported as well as domestic sources of the $NaNO_3$ were investigated. The 15% price difference between the domestic and imported $NaNO_3$ ($139/ton vs $118/ ton, Chemical Marketing Reporter 2/20/78) does not warrant the use of the Chilean

TABLE 5-16
4600 COST OF THERMAL STORAGE (12 h)
($000)

		All Sodium	Sodium-Iron	Draw Salt-Rocks
4610	Media Containment Equipment	9,190	6,639	6,908
4620	Media Circulation Equipment	0	0	0
4630	Working Fluid Circulation Equipment	688	1,688	2,688
4640	Discharging Heat Exchanger	0	0	0
4650	Charging Heat Exchanger	0	0	7,000[†]
4660	Foundation	690	569	597
4670	Design and Engineering	0	0	0
4680	Media			
	Sodium (40¢/lb)	25,600	8,384	0
	Iron	0	18,888[*]	0
	Rocks (10$/ton)	0	0	564
	Draw Salt (22¢/lb)	0	0	10,348
		36,168	36,168	28,105

Sodium-Iron

*4680: Iron at $122.77/ton (6.13¢/lb) is Break-Even Point.

Draw Salt-Iron

†4650: Larger IHX Required with Larger SM.

---

product. Table 5-18 presents a chemical analysis comparison of the domestic (Olin) vs imported (Chilean) material. Note, particularly, the NaCl content 0.12 vs 1.74%) and the H_2O content (0.02 vs 0.35%) of the domestic vs imported, respectively. Table 5-19 presents additional data on the Olin $NaNO_3$.

Discounting foreign sources for potassium nitrate (Israel and West Germany) as being too costly (~$500/ton), the sole U.S. source for KNO_3 is Vicksburg Chemical, Mississippi. Purchases made west of the Mississippi are through International Minerals Company (IMC), Boston, Massachusetts. The current price

TABLE 5-17

THERMAL CAPACITANCE MATERIALS FOR
ACR THERMAL STORAGE

Carbon transfer and diffusion rates from carbon to stainless steels are increased at the high temperatures planned for thermal storage systems (1100°F).

Carburization of stainless steels (receiver, tanks, etc.) may form low ductility surface layer and could initiate cracks under thermal cycling.

Railroad Wheels and Rails	0.55 to 0.85% Carbon	7¢/lb
Railroad Axles	0.40 to 0.55% Carbon	7¢/lb
Structural Steel - Scrap	0.20 to 0.25% Carbon	15 to 25¢/lb
Scrap Pipe	0.20 to 0.25% Carbon	15 to 25¢/lb
Steel Balls		70 to 94¢/lb

Only scrap pipe and structural steel can be considered and only after verifying carbon content.

---

is $316/ton, F.O.B. Vicksburg, Mississippi. Park Chemical Company, Detroit, Michigan, is the largest supplier of draw salts (3000 tons/year). Their best price quote 3/10/78 is 20-1/2¢/lb ($410/ton in the quantities required for the ACR thermal storage system.

Figure 5-40 summarizes the costs discussed above. Accordingly, for a Partherm 430 mixture of 55/45 KNO_3/$NaNO_3$ product, a raw material cost of 12.8¢/lb is indicated. This indicates that approximately 8¢ is available between the Park cost of 20-1/2¢ and the raw material costs to cover capital costs, labor, overhead, and profit. On the basis of these figures, it would not seem feasible to "make" the product, but a final decision would require a more detailed economic analysis beyond the present scope of work. The technology factor has not been considered although Park indicates there is an "art" involved.

TABLE 5-18

COMPARISON OF CHEMICAL ANALYSIS — DOMESTIC VS IMPORTED $NaHO_3$

Component	Olin				Chilean Product
	Old		New		
	Minimum	Maximum	Minimum	Maximum	
$NaNO_3$	99.4%		99.5%		97.14
$NaNO_2$		0.02%		0.25%	0.0036
NaCl		0.22		0.12	1.74
Na_2SO_4		0.35		0.30	0.56
SiO_2		0.004		0.0085	0.0111
CaO		0.03		0.03	0.006
MgO		0.002		0.002	0.464
Al_2O_3		0.001		0.001	0.0059
Mn		0.0001		0.0001	0.00007
Cu		0.0001		0.0001	0.00021
Hot Water Insolubles		0.01		0.03	0.045
I		0.0001		0.0001	—
Fe_2O_3		0.003		0.0025	0.0015
Total M.O. Akly.					
Na_2CO_3		0.20		0.04	0.162
H_2O		0.05		0.02	0.35
Total N	16.38		16.40		15.84
Breakage*		0.9		0.9	9.26 (gm of pressure breakage)

Sodium Nitrate
Product Specification Limits

*Breakage is a measure of how "dusty" the product is. Both products are prilled: both are technical grade.

TABLE 5-19

⊘lin

PRODUCT DATA

SODIUM NITRATE

Sodium Nitrate

Olin sodium nitrate, $NaNO_3$, is manufactured in Lake Charles, Louisiana and is guaranteed to contain 99.5% sodium nitrate. It is in the form of hard spherical pellets with a bulk density of 75 pounds per cubic foot and it is prilled to provide a uniformly free-flowing material with minimum dusting properties. These qualities are maintained over long periods of time in storage. Specifications for Olin sodium nitrate are given in Table 1.

Table 1
Specifications

Component	Shipping Limit (%)
$NaNO_3$, min.	99.5
$NaNO_2$, max.	.025
NaCl, max.	.12
Na_2SO_4, max.	.30
SiO_2, max.	.0085
CaO, max.	.03
MgO, max.	.002
Al_2O_3, max.	.001
Mn, max.	.0001
Cu, max.	.0001
I, max.	.0001
Fe_2O_3, max.	.0025
H_2O, max.	.02
Hot Water Insolubles, max.	.03
Total Methyl Orange Alkalinity as Na_2CO_3, max.	.04
Total N, min.	16.40

Principal Uses

Sodium nitrate is used in the manufacture of explosives, glass, ceramics, pyrotechnics, soaps and detergents, charcoal briquettes, pulp and paper and porcelain enamel. It is used as a fertilizer and in fertilizer mixtures and has a number of other chemical uses. Metallurgical industries use sodium nitrate as a flux, as an oxidizing agent and as a component in heat treating baths.

In bags coded food grade, Olin sodium nitrate is acceptable to the Meat Inspection Division of the United States Department of Agriculture as a color fixing agent in meat curing.

Table 2
Screen Analysis

U.S. Standard Screen	%
On 6 mesh, max	1
Thru 6, on 20 mesh, min	80
Thru 60, on 100 mesh, max	3
Thru 100 mesh, max	1.5

Shipping

Olin sodium nitrate is shipped in 50- and 100-pound, 5-ply, polyethylene-lined paper bags. Unitized bag shipments on disposable paper or wooden pallets are available. Bulk shipments are made in boxcars or hopper cars.

Technical Assistance

Technical assistance is available to facilitate your further investigation of Olin sodium nitrate. If you have a question or need more information, please call or write your nearest Olin Sales Office.

⊘lin CHEMICALS
120 Long Ridge Road, Stamford, Connecticut 06904

SODIUM NITRATE

DRAW SALT FINISHED PRODUCT (PARKE CHEMICAL CO.
BEST PRICE 3-10-78, F.O.B. DETROIT)

(DIFFERENCE BETWEEN PARKE QUOTE AND THE RAW MATERIAL COSTS
IS THE MARGIN FOR MIXING, PACKAGING, OVERHEAD, AND PROFIT)
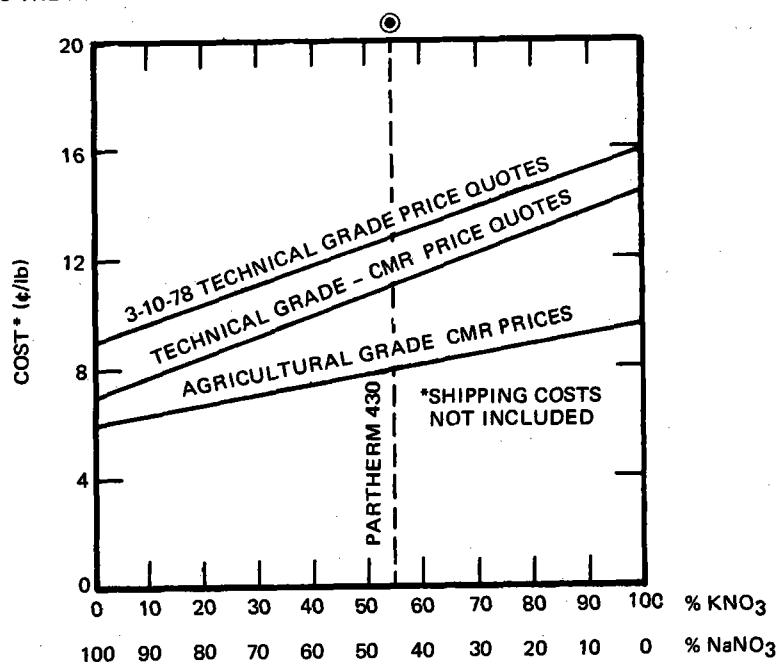
Figure 5-40. Cost of Raw
Materials for Draw Salt

9272-99

5.4 SUBSYSTEM COMPONENTS — ALL SODIUM

5.4.1 Sodium Storage Tanks

The storage subsystem is sized for a minimum net capacity of 3 MWe-h/MWe.
The all-sodium ACR concept with single hot and cold sodium storage tanks is
shown in Figure 1-2. The functional requirements and system design details for
the all-sodium storage system are given in the baseline design data sheets of
Book 2, Appendix A, along with a P&I diagram of the all-sodium concept.

The storage tanks are low-pressure tanks with a height about one-half the
diameter. The baseline design storage tanks are 30.5 m (100 ft) in diameter
with a height of 13.6 m (45 ft) for the hot storage tank and 12.3 m (41 ft) for
the cold. The hot tank operating at 593°C (1100°F) is made of stainless steel;
the cold tank at 288°C (550°F) is made of carbon steel. The tanks operate at

static head pressures only in order to minimize cost. This requires a pressure-reducing device to dissipate the tower static head. The pressure-reducing device for the baseline configuration consists of a nominal 18-in. drag valve.

Details of this drag valve are discussed in Section 5.4.3. Figure 5-1 shows a layout of the all-sodium system high-temperature (hot) tank. Although no sodium tanks of this size have been built, no particular difficulty is expected in their fabrication, installation, and operation. They will be designed in general compliance with API Standard 620, Recommended Rules for Design and Construction of Large Welded, Low-Pressure Storage Tanks. It should be noted that a major advantage of the all-sodium thermal storage is that the EPGS can operate independently of transient which may occur in the receiver system.

5.4.2 Pump

The discussion relating to the receiver pump, P-1, are applicable to the steam generator pump, P-2, which is included in the all-sodium thermal storage system. Pump discussion is contained in Section 4.6 of this report.

5.4.3 Drag Valve

In the all-sodium thermal storage system, a pressure reducing device is required to dissipate the tower (receiver) static head. This allows the all-sodium storage tanks to be designed for operation at atmospheric pressure. The argon cover gas pressure is very low 5 psi. Pressurized storage tanks of the large size required would be prohibitively expensive.

A drag valve has been tentatively selected for application as the pressure reducing device. The drag valve must pass ~20,000 gpm and dissipate the tower static head of 720 ft (maximum receiver elevation). At a sodium density of 50.69 lb/ft^3, this corresponds to a pressure of 253.4 psi.

The valve is sized with 18-in. nominal end connections for a line velocity of 24 ft/s. The drag valve utilizes velocity control elements to provide

system pressure and flow control. The valve also incorporates shutoff capability. The valve will be all stainless steel with Inconel control elements and can be provided with pneumatic or electro-hydraulic control-operator. Cost is estimated to be less than $300,000 with 18 to 24 months delivery.

The disk stack (Figure 5-41) consists of many disks, integrated together, and fitted with a plug for modulating flow. Each disk has a finite flow capacity which is dependent on the area and number of flow passages between the inside and outside of this disk. The required disk impedance is developed by a series of turns in the flow passages with the number of turns chosen to limit the fluid velocity to an acceptable level regardless of the pressure drop. Since each disk has a specific flow capacity, an appropriate number of them are used to meet the total flow requirement. Typical drag valve construction is shown in Figures 5-42 and 5-43.
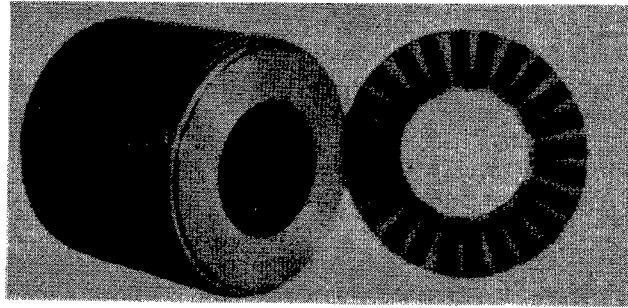
9272-100

Figure 5-41. Disk Stack With Single Disk
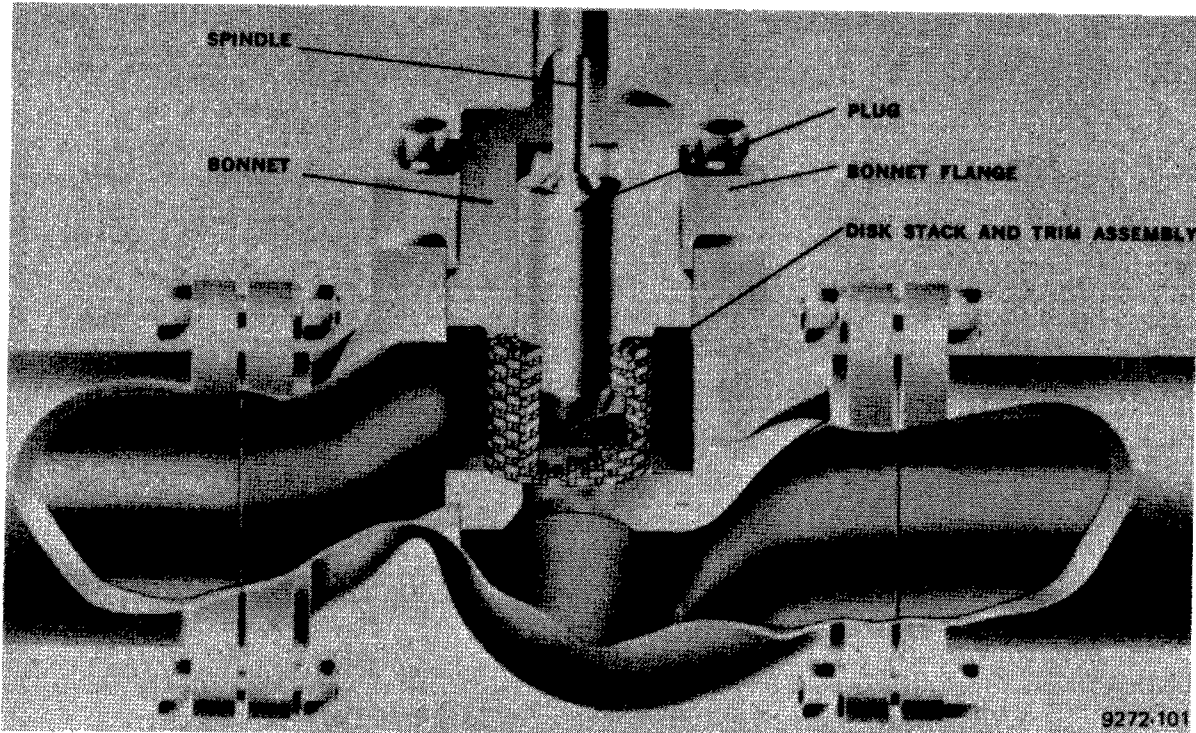
Figure 5-42. Self-Drag Velocity Control Element

GLAND
FLANGE

PACKING
FOLLOWER

YOKE
CLAMP

STEM
PACKING

BONNET

STEM

BONNET
FLANGE

BONNET
SEAL

PLUG
SEAL

PLUG
(DISK
STACK
ASSY)

FLEX
GASKET

SEAT
RING

BODY
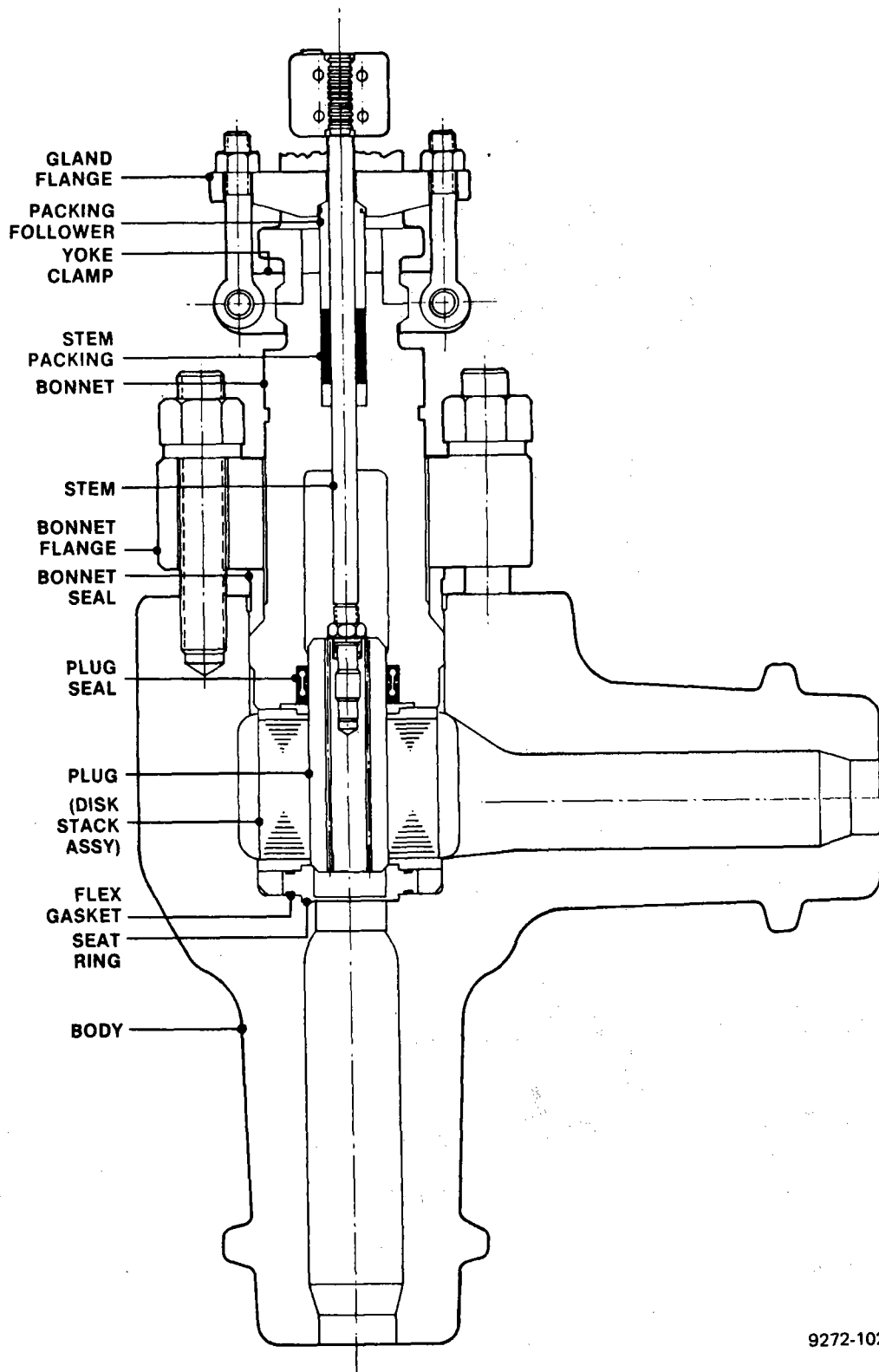
9272-102

Figure 5-43. Drag Valve Construction

6.0 COLLECTOR SUBSYSTEM

The collector subsystem includes the individual heliostats and all of the power distribution and control equipment necessary for their operation. Since the principal subsystem design requirements for the collector subsystem are set by the total power and peak heat flux delivered to the receiver, the analysis and definition of the collector subsystem are closely coupled to the receiver design parameters. In addition, because of the desire to minimize the cost of energy delivered to the system, the definition of the collector subsystem is also closely tied to the costs associated with the balance of the energy collection equipment (receiver, tower, sodium piping, and pump). These factors will all be treated in the subsystem analysis discussed in Section 6.2.

The information presented in this section will review the major requirements, discuss some of the significant optimization analyses, and finally present characteristics of the baseline collector subsystem design.

6.1 COLLECTOR SUBSYSTEM REQUIREMENTS

The principal subsystem design requirements are summarized in Table 6-1. They are divided into subsystem and individual heliostat requirements. From a subsystem standpoint, the collector field shall be designed to yield 390 MW of net absorbed power into the sodium at the best field performance (cosine plus blocking and shadowing considerations) with an insolation of 950 W/m^2. From a receiver design standpoint, the collector subsystem shall be designed and operated so that the peak receiver heat flux is <1.65 MW/m^2. In addition, because of cost considerations, it is necessary to design a subsystem with a long life and high availability.

For an individual heliostat, it is important to minimize reflected image size to maximize the high concentration ratio potential of the sodium system. As a result, it is desirable to have heliostats that can accommodate canted reflector panels and a tight constraint on reflector pointing and beam quality errors. These values must also be a result of cost effective heliostat design in order to

TABLE 6-1
COLLECTOR SUBSYSTEM DESIGN REQUIREMENTS

Subsystem	
Peak Absorbed Power (MWt) at 950 W/m^2)	390
Peak Incident Receiver Flux (MW/m^2)	<1.65
Field Design and Layout Criteria	Minimize Cost of Annual Energy
Time to Initiate Emergency Slew or Other Protective Action (s)	<0.5
Availability	>0.97
Lifetime (years)	30
Heliostat	
Reflector Configuration	Canted
Slew Rate (deg/min)	15
Reflector Pointing Error (mr)	1.5
Beam Quality Error (mr)	2.2
Aim Strategy	1 point (equator)
(Operation within Specification)	
Temperature [^{o}C (^{o}F)]	0 to 40 (32 to 104)
Wind Speed	
Sustained [m/s (mph)]	12.0 (26.8)
Gusting [m/s (mph)]	16 (36)
(Survive)	
Temperature [^{o}C (^{o}F)]	-30 to 50 (-20 to 120)
Dust Devil Wind Speed [m/s (mph)]	17 (40)
Wind Speed - Gusting [m/s (mph)]	
At Angle of Attack = ±10°	40 (90)
At Any Angle of Attack	25 (50)
Seismic Acceleration (g)	Zone 3, Uniform Building Code
Precipitation	
Rain	
(Average Annual [mm (in.)]	750 (30)
(Maximum 24-h Rate) [mm (in.)]	75 (3)
Snow Load [Pa (psf)]	250 (5)
Sleet Buildup [mm (in.)]	50 (2)
Hail (Special Gravity)	0.9
(Any Orientation) [mm (in.)] Diameter at a velocity [m/s (ft/s)]	20 (0.75) at 20 m/s (65 fps)
(Vertical Stowed Position [mm (in.)]	25 (1) at 23 m/s (75 fps)
Sand and Dust	Survive tests per MIL-STD-810B, Method 510

Reference: DOE Heliostat Specification 001, Solar Central Receiver Prototype Heliostat RFP, Number EG-77-R-03-1468, dated July 1977

ensure that the complete energy collection portion of the system, including the receiver, tower, etc., are cost effective. The heliostat requirements shown in Table 6-1 reflect extensive design and performance optimization analyses that have been carried out as part of the MDAC Prototype Heliostat contract.

The balance of the information represents environmental conditions to be used in the design of the subsystem equipment. The first portion of the data represents limits in which the heliostat equipment will operate within its design specification. The second portion represents environmental factors which the heliostat equipment must survive. Since the plant is not operating during these extreme conditions, no limit on reflected beam accuracy is imposed in conjunction with these survival conditions.

6.2 SUBSYSTEM DESIGN AND ANALYSIS STUDIES

A series of conceptual studies were carried out to aid in the definition of the commercial advanced sodium system. The most significant of these studies addressed the issues of single vs multiple collector fields, external vs cavity receiver configurations, optimum collector field capacity, and emergency heliostat defocus.

6.2.1 Conceptual Collector Field and Receiver Analysis

This analysis was designed to define the most cost effective collector field and receiver combination sized to absorb 429 MWt into the sodium at equinox noon with an insolation level of 950 W/m^2. The analysis investigated single and multiple fields with both external and cavity receivers.

In carrying out the optimization analysis, cost models were required for the energy collection hardware along with their sensitivity to power level and other critical sizing parameters. Eight cost factors were considered in the analysis which are listed below.

> Fixed Cost (independent of configuration)
> Heliostats

TABLE 6-2
COST MODELS USED IN THE OPTIMIZATION ANALYSIS

		Comment
Fixed	$4.97M	Based on water-steam contract
Heliostats	$101.25/m^2	Early commercial production
Land	$1.08/m^2 (4,370/acre)	
Wiring	Trenching $6.10/m	Relative cost burden per
	Data Cable $4.54/m	heliostat depends on helio-
	ac Power Cable $8.06/m	stat spacing
Receiver		
External	$10.4M (P/429 MWt)$^{0.8}$	From previous sodium study
Cavity	$16.0M (P/429 MWt)$^{0.8}(A/Ar)^{0.8}$	Precursor analysis
	P = thermal power	
	Ar = aperture area for average flux = 1.5 MW/m^2	
	A = actual aperature area	
Tower	$460.25 (H$_R$ - 26 m)$^{1.816}$	Concrete towers - based on
	H$_R$ = receiver centerline elevation	water-steam study
Piping Network		
Piping	74 · D (in.)	$/ft (stainless steel)
	45 · D (in.)	$/ft (carbon steel)
Valves	$2,000 · D (in.)	6-in. to 17 in. valves
	$3,000 · D (in.)	17-in. to 24-in. valves
Expansion and Bends	X (1.5)	Adjustment to pipe length
Vertical	$1 + \dfrac{H_R + 20 \text{ m}}{800}$	5% increase per 60 ft

Land

Wiring

Tower and Foundation

Vertical Piping

Horizontal Piping

The assumed cost factors or pertinent algorithms are listed in Table 6-2. Wherever possible, these costs or algorithms were taken from work developed on previous water-steam central receiver design contracts. Cost models for hardware that is unique to the advanced sodium system were developed as part of precursor analysis to this optimization effort.

Thermal loss models for the various receiver sizes and configurations were also required for the analysis. The thermal loss model assumed for the external receivers included consideration of surface absorption, radiation, anu convection losses combined to equal 22.1 MWt for a 16.15 m receiver (identical diameter and height). It was assumed that the loss is constant over all periods of energy collection and scales with surface area for smaller receivers. For cavity receivers, it was assumed that the absorption, radiation, and convection effects all combine to give a 5.2% loss during maximum power operating conditions. This was based on information published during water-steam contract work and is felt to be quite optimistic for the large aperture cavity receivers envisioned for the advanced system. However, in order to place the cavity in its best light, this optimistic assumption was retained in this analysis.

The results of the optimization analysis for 1 and 3 module* external receiver systems, which include receiver losses, are shown in Figure 6-1. The data are presented in a "layer cake" format which permits quick identification of major cost items. For each case, three separate bars are shown. The "nominal" data reflect results using the cost information given in Table 6-1. Those bars identified as (+20%) and (-20%) reflect the impact of increasing and decreasing the costs of the sodium elements (receiver and piping) by 20%. This sensitivity is included due to the relative uncertainty associated with sodium component costs

---

*A module includes a receiver and tower with a dedicated collector field. Multiple modules are piped together to satisfy the total design power requirement.
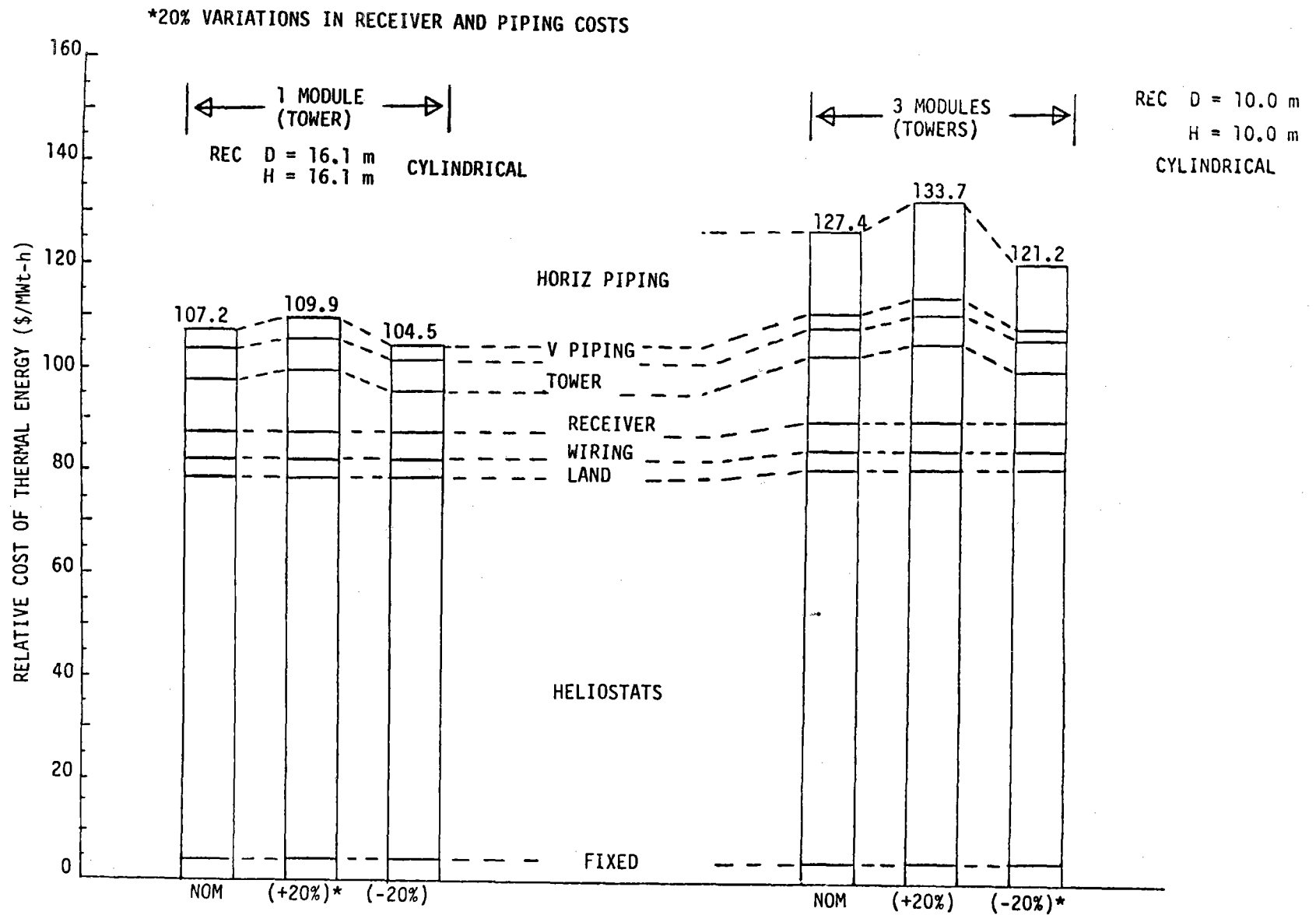
Figure 6-1. Comparison Between One and Three Module External Receiver Systems

that existed at that time. It is seen that the 20% variation has little impact when comparing the 1 and 3 module configurations. The 3-module configuration is clearly inferior because of the horizontal piping costs with less significant factors being the heliostat and receiver costs. These results were based on noncanted heliostats composed of flat panels, which were assumed for computational expediency. The impact of canting the heliostats would somewhat reduce the relative cost of energy estimates shown in Figure 6-1. The conclusions drawn from the figure, however, would be unchanged.

The results of the optimization study carried out for cavity systems are summarized in Figures 6-2 to 6-4. As in the case of the data for external receiver systems, these data show sensitivities to ±20% variations in sodium equipment costs. The data shown in Figure 6-2 are for a single module, cavity receiver systems in which the cavity is tipped downward 30° from pointing due north. The impact of varying aperture size is also depicted. It is seen that the smaller aperture system (17 x 17 m) requires a greater expenditure for heliostats because of greater energy spillage associated with the smaller aperture. By expanding the aperture, fewer heliostats are required as reflected in lower heliostat, land, and wiring costs. This cost benefit is offset by the increase in receiver costs resulting in a situation where no clearly superior configuration emerges. Due to the importance of the assumed cost models on this result, it would be necessary to refine these models before revised analysis could be carried out. However, in comparing these data to the costs expected for the external receiver, it appears that it would be impossible to define sufficient savings through cost refinements to cut the cost of energy by ~25% which would be necessary to compete against the external configuration.

Before a final comparison with the external receiver systems could be made, it was necessary to modify the assumption of flat heliostats. The data presented in Figure 6-2 were reevaluated for heliostats which are custom canted to their particular field location and while impractical from a production standpoint, represent the optimum limit to be derived through canting. These modified results for canted heliostats are shown in Figure 6-3 for the 19 and 21 m aperture cases. It is seen that only a minor change in the overall energy economics could be
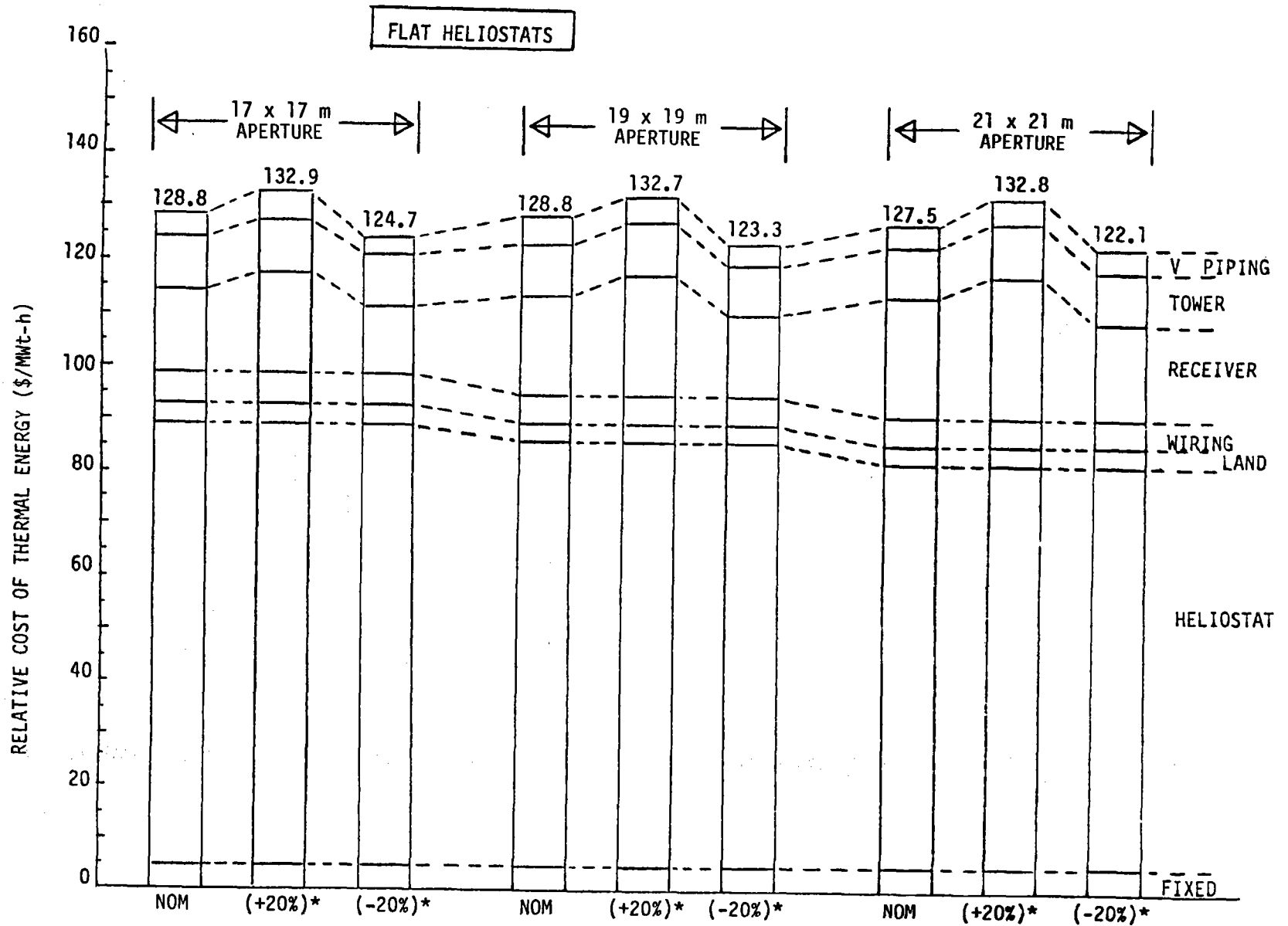
Figure 6-2. Economic Comparison of One Module Cavity Receiver System
(30° Downward Tilted Cavity)
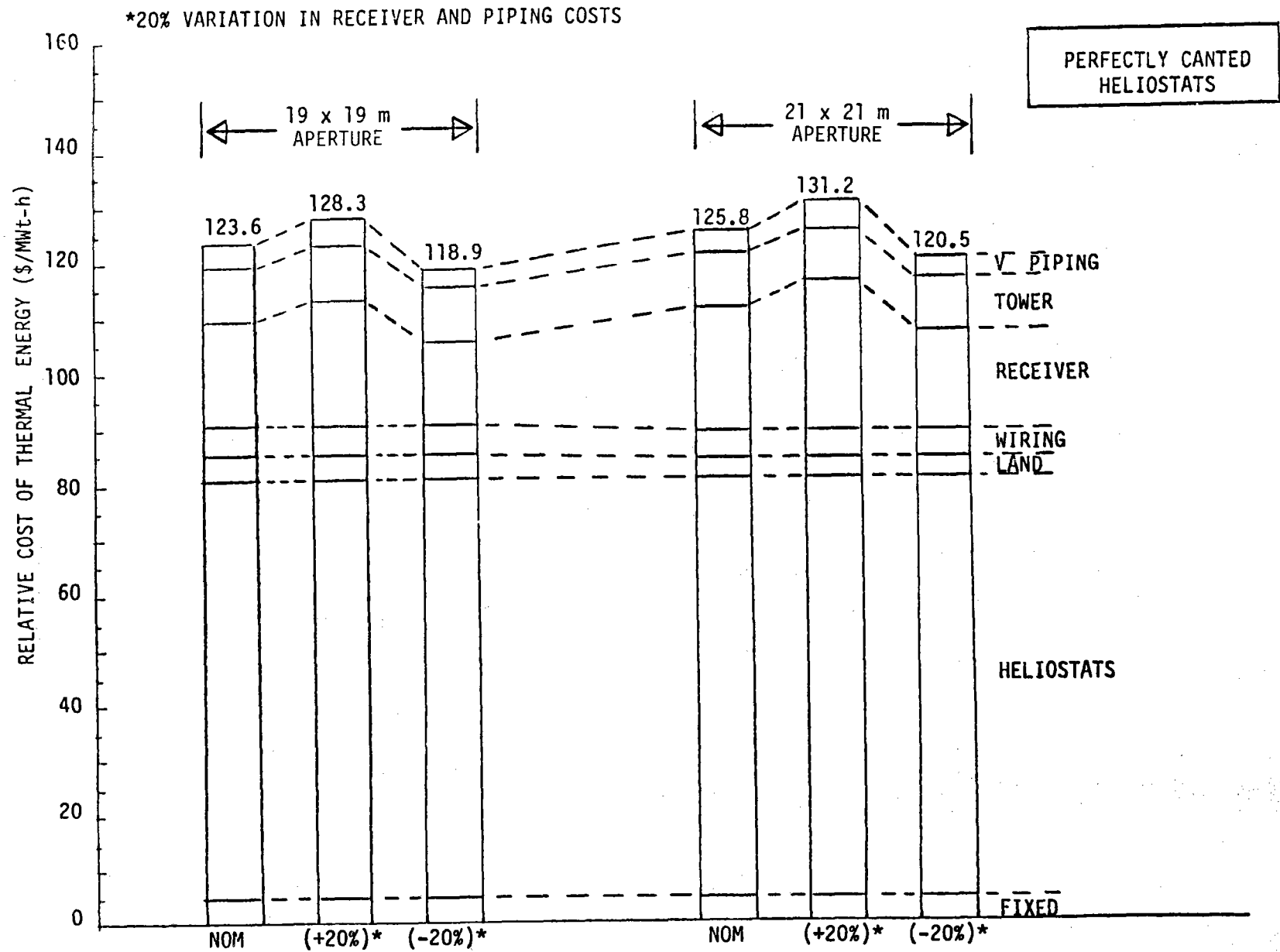
Figure 6-3. Economic Comparison of One Module Cavity Receiver System
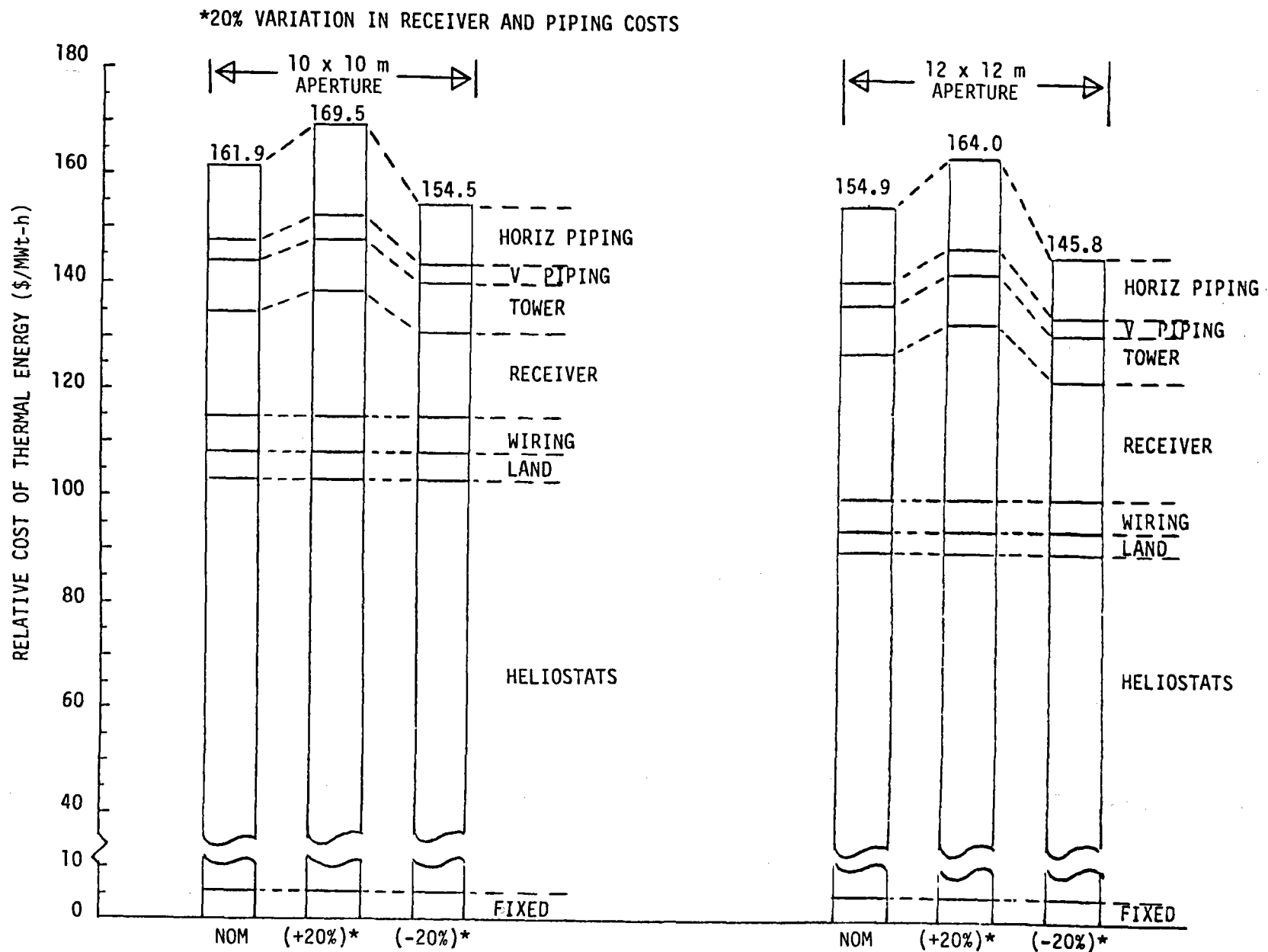
Figure 6-4. Economic Comparison of Three Module Cavity Receiver System

realized through canted heliostats (ignoring the cost of canting) which is clearly insufficient to make the cavity configuration superior to the external receiver configuration.

For the sake of completeness, three module cavity systems were also considered. The results are shown in Figure 6-4. Clearly this case suffers from the penalty characteristic of the cavity receiver with its limited field of view and the expensive horizontal piping network necessary to interconnect the three modules.

A tabular summary of the collector field and receiver configurations considered in the study are presented in Table 6-3. These results indicate the overall superiority of the single module, external receiver configuration from a cost of energy standpoint. The impact of ±20% cost variations in the sodium elements, as shown in Figures 6-1 to 6-4, will not affect the validity of these results.

TABLE 6-3

SUMMARY OF COLLECTOR FIELD-RECEIVER
ECONOMIC COMPARISON

Receiver Type and Size	Number of Modules	Heliostat Configuration	Cost of Energy* ($/MWt-h)
External/16.1 x 16.1 m	1	Noncanted	107.2
External/10 x 10 m	3	Noncanted	127.4
Aperture/17 x 17 m	1	Noncanted	128.8
19 x 19 m	1	Noncanted	128.8
19 x 19 m	1	Canted facets	123.6
21 x 21 m	1	Noncanted	127.4
21 x 21 m	1	Canted facets	125.8
Aperture/10 x 10 m	3	Noncanted	161.9
12 x 12 m	3	Noncanted	154.9

*Based on nominal cost assumptions

6.2.2 Emergency Heliostat Defocus

Because of the high concentrations of sunlight which impinge on the north facing receiver panels, it is important to analyze the situation where sodium flow to the receiver is interrupted because of a pumping, flow control, or electrical malfunction. The latter case is of greatest design concern since a loss of electrical power affects not only the sodium pumps but also operation of the heliostat field which is the source of the incident thermal power. In order to prevent damage to the receiver, sufficient uninterruptible power is required to reduce the incident power on the receiver surface to a sufficiently low level to prevent receiver damage.

Two separate analyses have been carried out to analyze this condition. The first analysis which will be discussed in this section, employs a transient thermal model of a typical tube and the contained sodium. The model assumes complete sodium stagnation and treats both the sensible temperature rise and boiling of the contained sodium. At all points during the boiling process, the model optimistically assumes nucleate boiling heat transfer until complete dryout occurs. Receiver radiation and convection losses are also included in the analysis.

The second analysis was carried out using the dynamic receiver simulation. This model allowed for internal circulation to occur within the receiver because of local differences in sodium density. Due to model limitations, the sodium boiling process was not simulated. A discussion of this analysis appears in Section 2.4.

Using the stagnant sodium model, a series of cases were analyzed which represent the permitted range of receiver heat flux decay conditions. The two limiting heat flux decay profiles are shown in Figure 6-5. For the case where heliostat slew occurs on a simultaneous basis for all heliostats, a rapid decay in incident flux is experienced with the composite image clearing the receiver surface in slightly more than 5 s. If the heliostat orientation remains constant, the incident heat flux decays over a period of ~180 s due to the apparent motion of the sun.
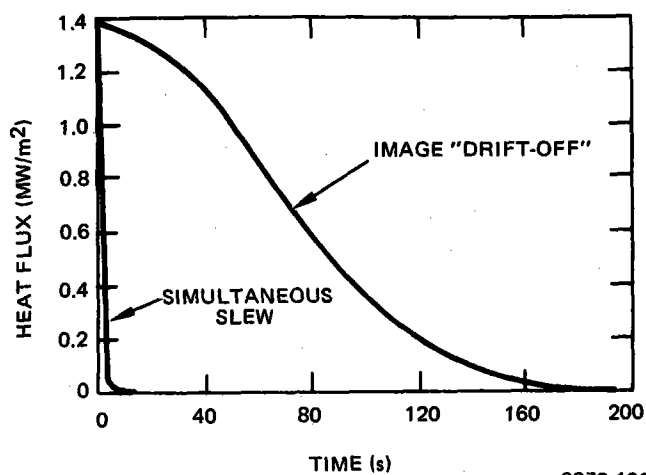
Figure 6-5. Receiver Heat Flux Decay

From the standpoint of uninterruptible power, this latter case represents the condition of minimum power requirement. As the heat flux decay period is shortened due to active heliostat slewing, the power requirements increase in inverse proportion to the time required for defocus with the costs of the power supply increasing in a corresponding fashion. As a result, it is desirable to lengthen the slew period to a maximum value without creating a thermal situation which can damage the receiver surface.

Typical histories for the sodium and wall temperatures are shown in Figures 6-6 through 6-9 for a variety of assumed slew-off times. The "20-s" case shown in Figure 6-8 produces a condition where the sodium boiling point is just reached as the flux decays to zero. The case for a 25-s slew-off shown on the same figure indicates that boiling is experienced in the tubes and a vapor fraction of 9.3% is reached late in the slew-off period. The longer slew rates depicted in Figure 6-9 produce ever increasing quantities of vapor.

The sodium and tube wall temperature histories for the case of no active slew (sun image drift-off) are shown in Figure 6-10. For the time interval shown, the incident heat flux decays to ~1.0 MW/m^2. During this period, the
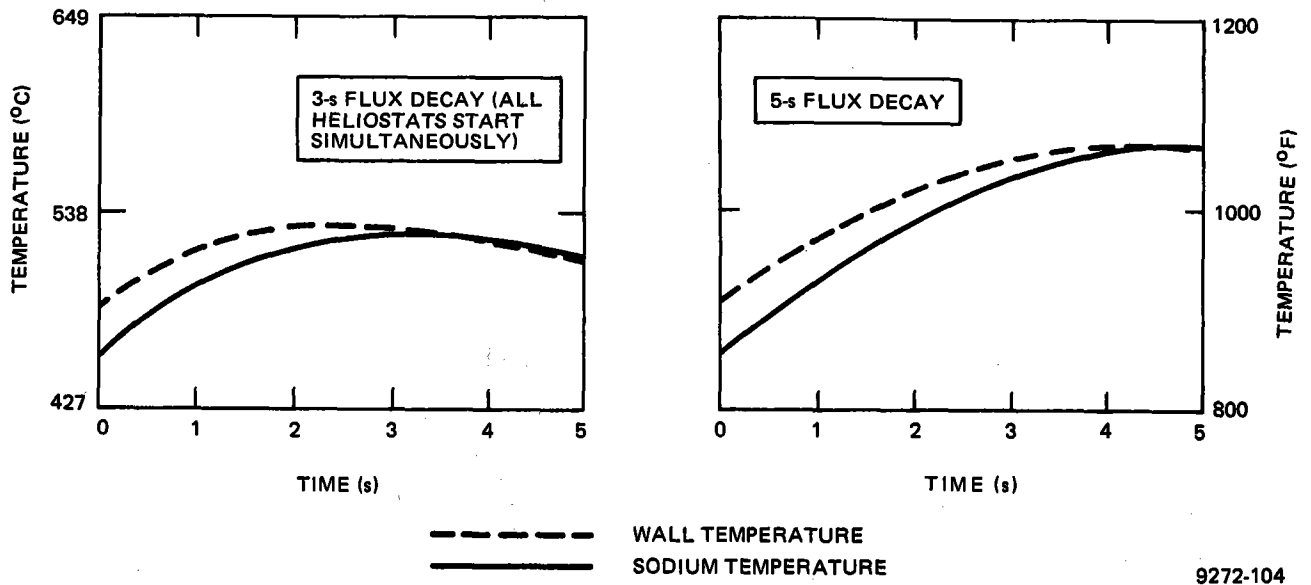
Figure 6-6. Receiver Temperature History During Emergency Defocus-1
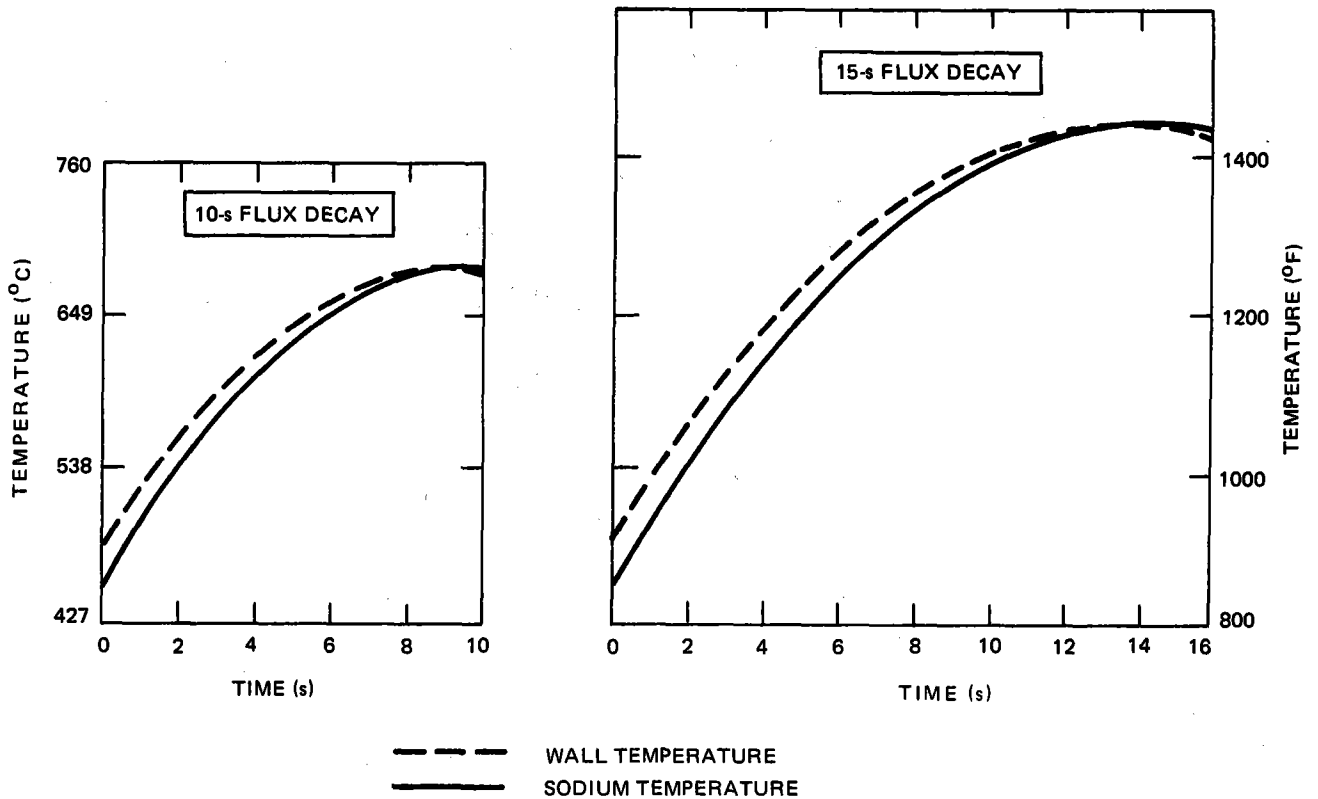
Figure 6-7. Receiver Temperature History During Emergency Defocus-2

ESG-79-2, Vol II, Book 1
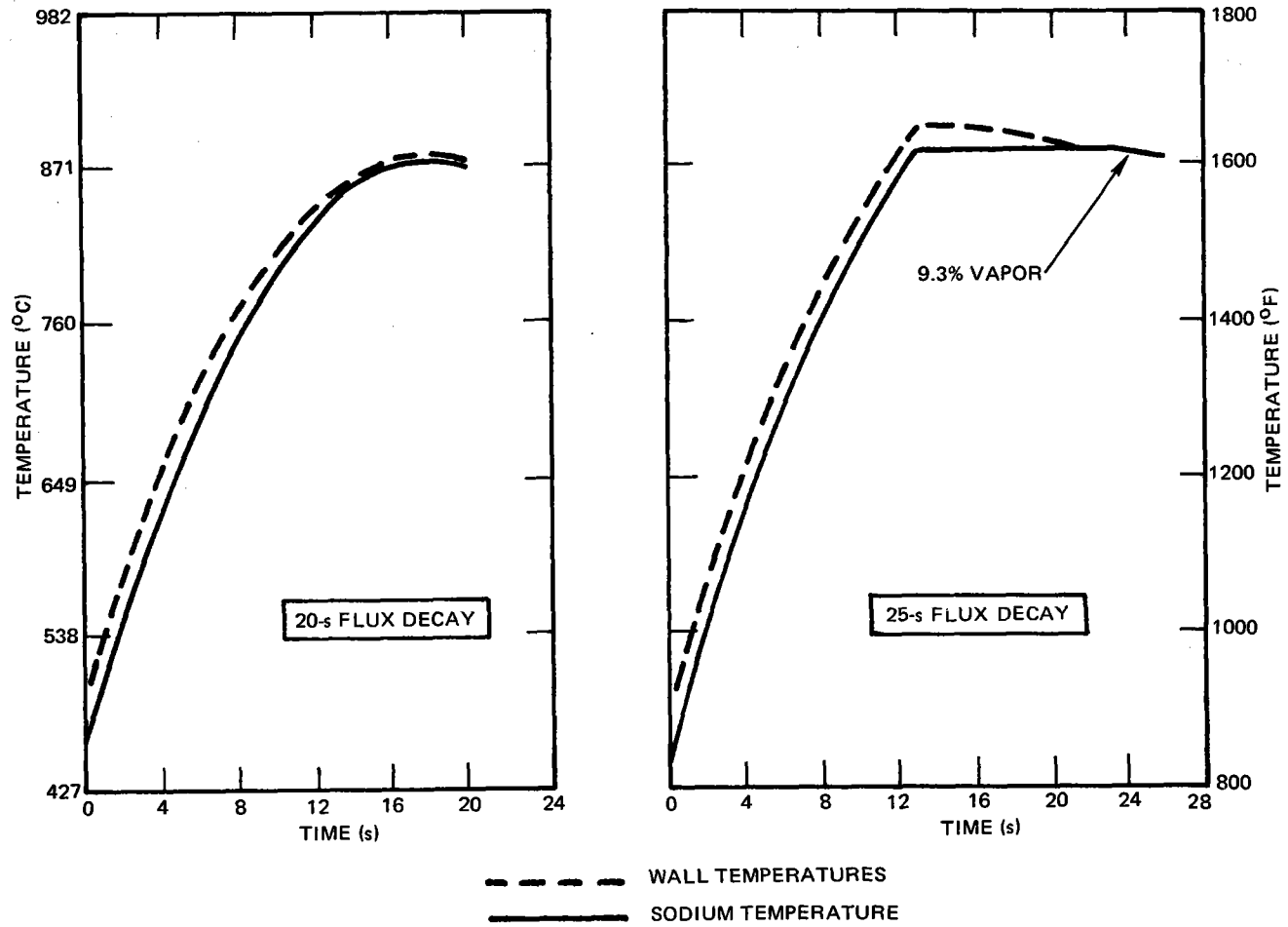
Figure 6-8. Receiver Temperature History During Emergency Defocus-3
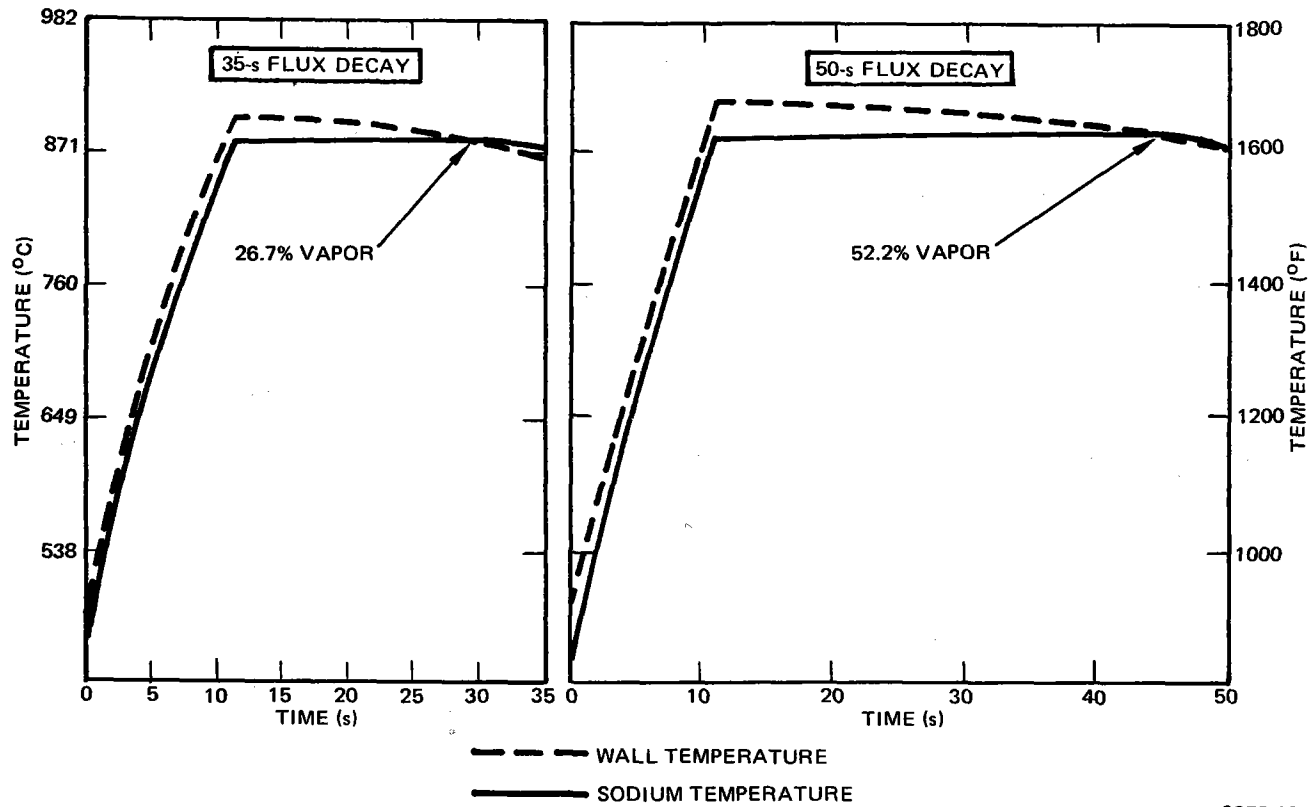
Figure 6-9.   Receiver Temperature History During Emergency Defocus-4
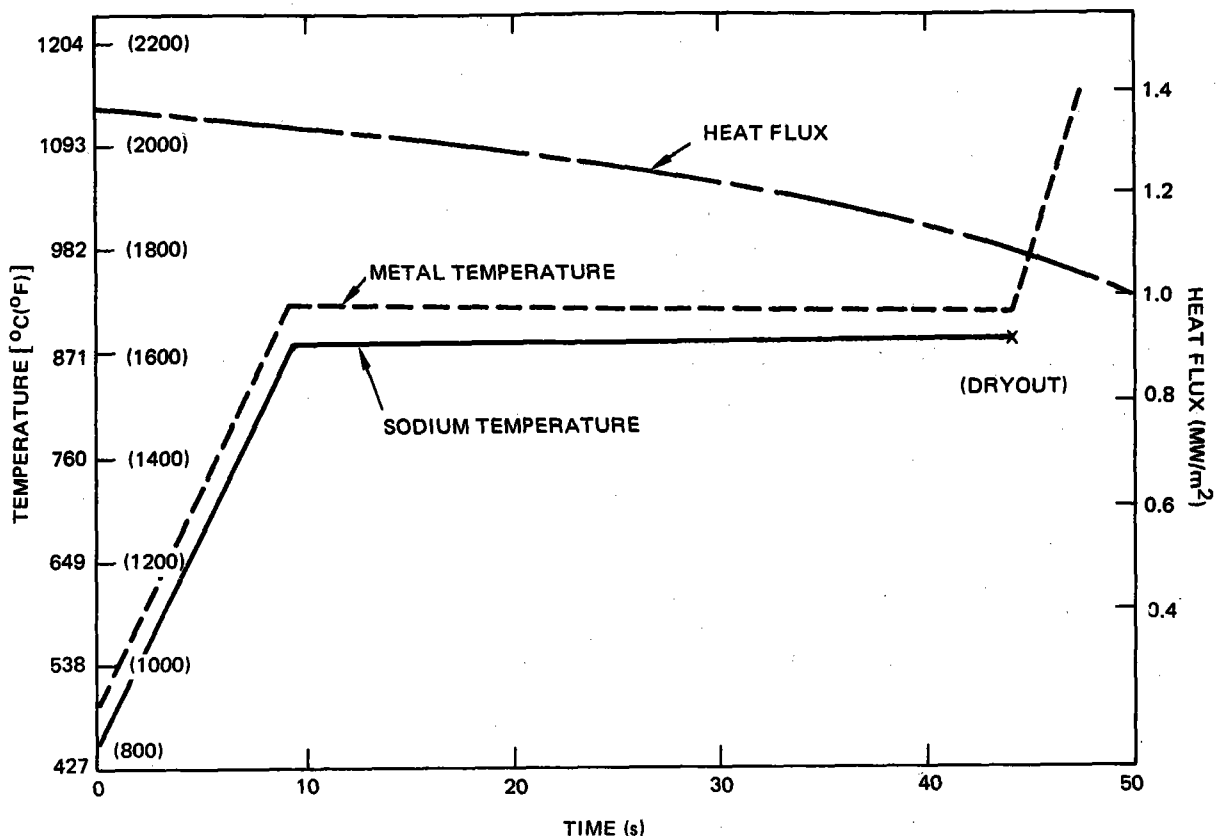
Figure 6-10. Temperature History During Image "Drift-Off"

sodium sensibly heats to the boiling point and is completely boiled away. The metal temperature closely tracks the sodium temperature until dryout occurs, at which point, the temperature rises rapidly until burnout occurs.

Based on these results, it is concluded that any emergency defocus of the receiver images must occur within ~25 s from the time of loss of sodium flow. Over this time period, little if any boiling would occur, especially if effects of internal recirculation were considered. In order to accommodate this slew condition, an uninterruptible power source rated at ~600 kW would be required. This would enable 8 sections of the field to each be run for a duration of ~3 s in a sequential fashion. During this 25-s interval, all heliostat electronics would be maintained in a "hot" condition with the total energy consumption being

~4.2 kWe-h. This electrical energy would be provided by batteries. After the 25-s period, it is assumed that backup diesel power would be available to complete the heliostat slew to achieve a safe stow position.

6.2.3 Heliostat Slew Procedure

Because of the high concentrations of sunlight which impinge on the north facing receiver panels (~1.37 MW/m^2 peak), it is important to analyze the case where sodium flow is lost to the receiver to determine collector field control and slew requirements as well as the potential damage environment for the receiver panels.

A study was carried out to determine the preferred heliostat slew procedure. The rate of slew-off from the receiver was determined for the cases of an azimuth drive command only and an elevation drive command only. It was determined that either technique would work equally as well, except for the south field heliostats. For these heliostats, slew-in elevation is generally preferred since for nearly horizontal heliostats, an azimuthal slew produces little or no image movement on the receiver. Heliostats which are not approximately horizontal can be slewed in either direction.

The impact of a divided azimuth slew (half of the images moving to the left and half moving to the right) on the peak north side incident heat flux is shown in Figure 6-11. It is seen that a rapid falloff in flux occurs once heliostat motion is initiated and the heat flux on the northern panel is zero shortly after 3 s of slew.

A transient thermal analysis of the receiver tubes was next considered to determine the impact of this heat flux characteristic on the receiver temperature during slew. The results of the two cases studied are shown in Figure 6-12. In both cases, slew was initiated when the metal temperature had risen to 761°C (1400°F) from its assumed original value of 649°C (1200°F). For the case where the tube is filled with sodium ~26 s are required for the surface temperature to rise to the slew initiation temperature. Once the slew is initiated, virtually no additional temperature rise occurs in the tube. For the case where the tube
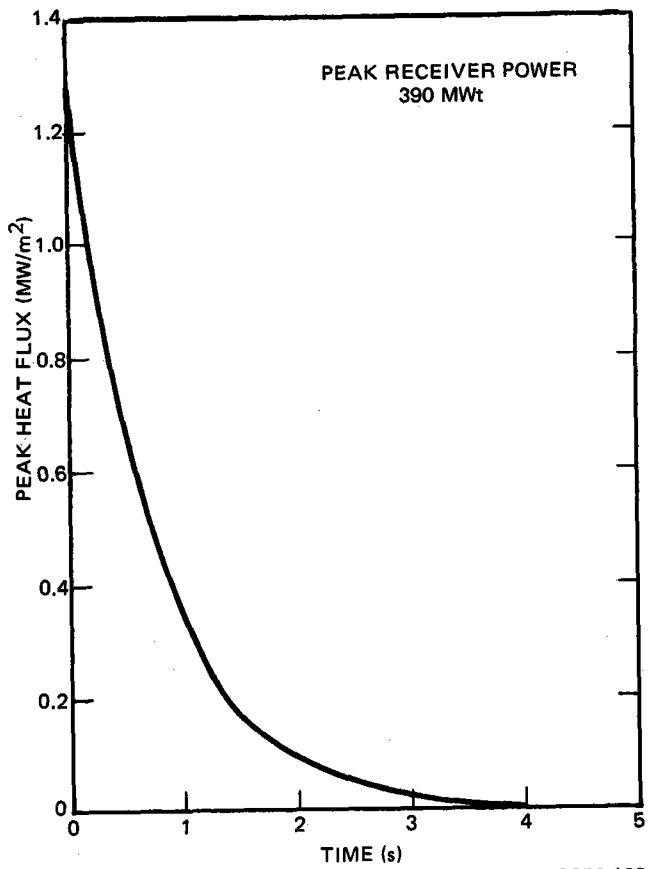
Figure 6-11. Decay in Peak Heat Flux During Emergency Collector Field Slew

9272-109
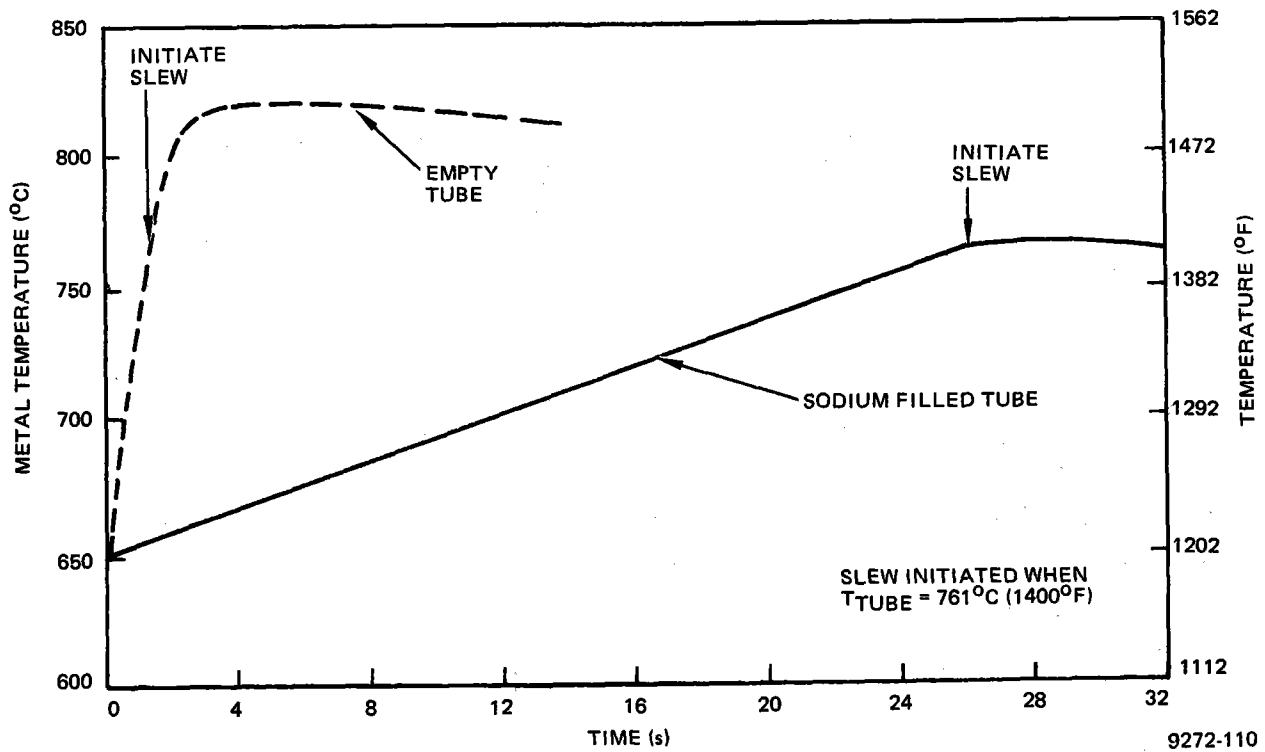
Figure 6-12. Receiver Tube Temperature History During Emergency Slew

9272-110

is empty, it is seen that a rapid temperature rise occurs. Even when the slew is initiated, a significant temperature rise rate continues until the heat flux is essentially off the receiver tube. At that point, the temperature curve falls off due to radiation effects. For this case, a peak temperature of 820°C (1508°F) would be anticipated.

In order to execute an emergency slew of the type described above, it is necessary to have instrumentation and sensors dedicated to measuring surface temperature anomalies. In addition, to prevent an overload of the collector electrical network, the heliostats must be started sequentially. This will prevent the individual motor surge currents from occurring simultaneously. Due to the short duration of these surge currents, the complete field can be in a slew mode 0.33 s after the initial slew command is given. This delay factor is included in the data presented in Figures 6-11 and 6-12.

In the event of a general power failure which would disrupt electrical power to both the sodium pumps and the collector field, sufficient emergency power must be available to carry out an emergency slew off the receiver. An analysis of the 390 MWt collector field indicates that ~10 MW of power would be required. Since the duration of the slew is quite short, the estimated energy consumption is only 12.7 kWh. Since the receiver over-temperature problem occurs in a matter of seconds, it is necessary to have this backup power available immediately or to momentarily cool the external surface of the receiver such as with spray water until the emergency slew can be initiated, or the natural motion of the sun causes the reflected images to move off the receiver.

6.3 COLLECTOR SUBSYSTEM DESIGN CHARACTERISTICS

The Collector Subsystem is composed of a field array of heliostats; the heliostat field electronics consists of primary and secondary power and data wiring, field transformers, distribution panels and data distribution interfaces; and the heliostat array controller which is located in the Plant Control Room and interfaces with the Master Control Subsystem. The heliostat field surrounds the receiver tower and reflects solar radiation onto the elevated receiver in a manner which satisfies system power requirements.

6.3.1 Collector Field

The baseline collector field (including the tower and receiver geometric characteristics) was determined as a result of a well established optimization procedure subject to constraints on the total receiver power (390 MWt net on the best cosine day at 950 W/m^2) and the peak incident heat flux (1.7 MW/m^2). The major characteristics of the resulting collector field are summarized in Table 6-4.

TABLE 6-4
COLLECTOR FIELD CHARACTERISTICS

Heliostat Size	49.05 m^2
Configuration	Canted
Number of Heliostats	14,100
Total Reflector Area	0.692 km^2
Receiver Size (Cylindrical)	
Height	16.15 m
Diameter	16.15 m
Receiver Centerline Elevation	174 m
Land Area (Excluding Central Exclusion)	3.06 km^2
Central Exclusion Area	0.10 km^2
Glass Coverage Density	22.6%
Layout Arrangement	Radial-Stagger

The collector field is defined on the basis of a cell-by-cell analysis with each computational cell being a square 147.2 by 147.2 m. The initial cell matrix is composed of 15 such cells in the east-west direction by 14 cells in the north-south direction. As a result of the optimization procedure, complete cells or fractions therof are trimmed from the field since the placement of heliostats in these locations is not cost effective. The resulting field shape relative to the cell matrix is shown in Figure 6-13. Instead of the irregular trim line illustrated in this figure, the actual heliostat layout would be arranged along a continuous arc through the sawtooth outline.

N ↑

T = TOWER

CELL SIZE
147.2 x 147.2 m

FIELD
TRIM
LINE

T

1215 m

700 m

994 m
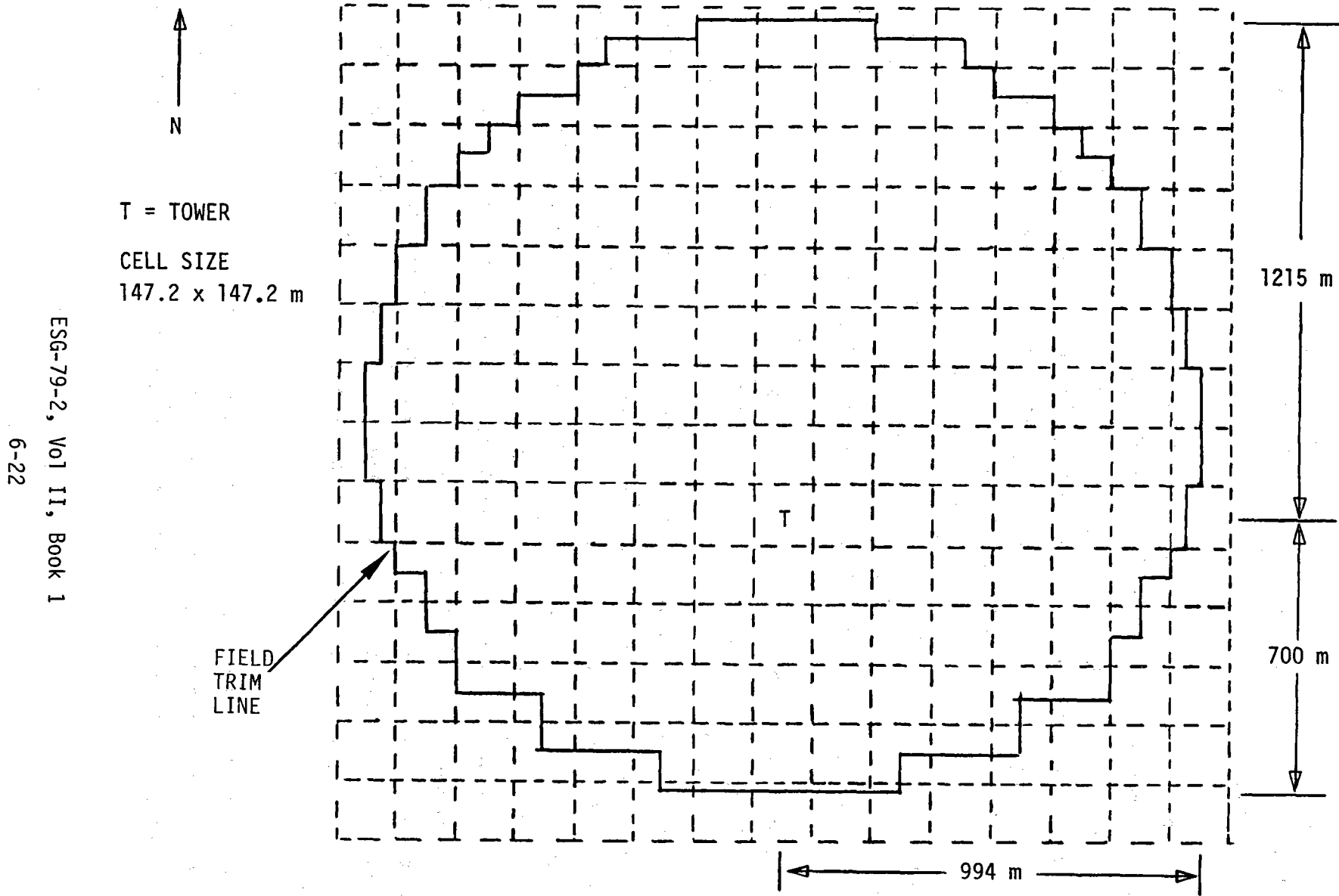
Figure 6-13. Baseline Collector Field Defined in Terms of Computational Cells

The actual number of heliostats contained in each of the cells is shown in Table 6-5. The location of the tower is in cell 8, 9 (measured from north-west) as indicated on the table. Cells to the top of the table represent cells located to the north of the tower.

The heliostat spacing information for each cell is contained in a nondimensional form in Tables 6-6 and 6-7. Table 6-6 shows the radial spacing data along a line which is normal to the ray extending from the tower. For clarity, Figure 6-14 shows how these data are applied to cells immediately northeast and southeast of the tower. Each of these tables represents the eastern half of the field with the tower located along the left edge of the table. Because of east-west symmetry, the mirror image of these data holds for the west side of the collector field. A constant (7.39773 m) should be multiplied times each of the tabular values (in Tables 6-5 and 6-6) to arrive at the appropriate dimensional spacing. This value corresponds to a characteristic heliostat dimension.

The performance characteristics for the collector field are summarized in Figure 6-15 for a complete year. The plot of subsystem efficiency versus sun azimuth angle includes the performance factors listed in the upper right-hand portion of the figure. These factors include all losses from the point where the sun is incident on the field to the energy intercepted by the receiver. The field layout factor represents a penalty that occurs when the cell-by-cell spacing ratio information is converted to actual heliostat coordinates. This occurs because heliostats along one cell boundary may physically interfere with boundary heliostats in an adjacent cell. Therefore, it is necessary when moving from one cell to another during the actual layout operation to locally compromise the placement of these heliostats. Other factors such as roads to the central exclusion or slip planes within the heliostat field also contribute to this factor. Previous analysis indicates that a value of 0.98 is appropriate for this factor.

The dashed lines which define the extremes of the performance correspond to the sun's motion on summer and winter solstice. It is seen that a reasonably high level of performance is maintained during most of the useful sunshine hours

N ↑

Table 6-5
NUMBER OF HELIOSTATS PER CELL

0.	0.	0.	0.	13.	26.	40.	41.	40.	26.	13.	0.	0.	0.	0.
0.	0.	0.	27.	57.	60.	61.	62.	61.	60.	57.	27.	0.	0.	0.
0.	0.	42.	60.	65.	69.	71.	72.	71.	69.	65.	60.	42.	0.	0.
0.	28.	61.	68.	74.	80.	85.	86.	85.	80.	74.	68.	61.	28.	0.
0.	60.	68.	77.	86.	96.	103.	106.	103.	96.	86.	77.	68.	60.	0.
14.	65.	74.	86.	100.	116.	129.	134.	129.	116.	100.	86.	74.	65.	14.
30.	69.	80.	96.	116.	140.	162.	171.	162.	140.	116.	96.	80.	69.	30.
31.	71.	85.	103.	129.	162.	189.	94.	189.	162.	129.	103.	85.	71.	31.
16.	72.	86.	106.	134.	171.	189.	TOWER	189.	171.	134.	106.	86.	72.	16.
0.	54.	85.	103.	129.	162.	189.	189.	189.	162.	129.	103.	85.	54.	0.
0.	17.	80.	96.	116.	140.	162.	171.	162.	140.	116.	96.	80.	17.	0.
0.	0.	37.	65.	100.	116.	129.	134.	129.	116.	100.	65.	37.	0.	0.
0.	0.	0.	19.	43.	72.	103.	106.	103.	72.	43.	19.	0.	0.	0.
0.	0.	0.	0.	0.	20.	21.	22.	21.	20.	0.	0.	0.	0.	0.

TABLE 6-6
NONDIMENSIONAL* RADIAL SPACING

N

↑

[CELL-BY-CELL

EAST HALF ONLY]

6.945	7.011	7.202	7.476	7.866	8.394	9.033	9.692
6.061	6.094	6.302	6.616	7.042	7.562	8.181	8.958
5.163	5.255	5.487	5.786	6.252	6.799	7.465	8.195
4.339	4.455	4.703	5.034	5.541	6.142	6.824	7.603
3.566	3.664	3.923	4.345	4.906	5.530	6.269	7.078
2.821	2.932	3.237	3.771	4.383	5.056	5.862	6.678
2.068	2.258	2.675	3.265	3.967	4.694	5.548	6.398
1.679	1.891	2.222	2.899	3.688	4.511	5.352	6.212
TOWER	1.778	2.061	2.811	3.612	4.403	5.241	6.165
1.697	1.744	2.274	2.997	3.739	4.509	5.330	6.253
2.417	2.447	2.706	3.301	3.993	4.752	5.558	6.444
2.788	2.990	3.316	3.817	4.458	5.137	5.962	6.841
3.531	3.643	3.976	4.454	5.021	5.721	6.477	7.356
4.396	4.473	4.724	5.154	5.699	6.369	7.110	7.847

*DIMENSIONAL VALUE = (NONDIMENSIONAL VALUE) (7.39773 m)

Table 6-7
NONDIMENSIONAL* AZIMUTHAL SPACING
$$\begin{bmatrix} \text{CELL-BY-CELL} \\ \text{EAST HALF ONLY} \end{bmatrix}$$

N ↑

2.125	2.127	2.135	2.147	2.163	2.206	2.323	2.540
2.105	2.086	2.094	2.109	2.127	2.149	2.198	2.651
2.061	2.065	2.076	2.070	2.092	2.117	2.168	2.221
2.041	2.045	2.057	2.054	2.079	2.108	2.140	2.196
2.027	2.031	2.042	2.041	2.068	2.079	2.114	2.150
2.063	2.060	2.040	2.056	2.062	2.076	2.115	2.131
2.155	2.117	2.069	2.061	2.063	2.057	2.098	2.117
2.378	2.213	2.161	2.081	2.073	2.066	2.087	2.108
TOWER	2.304	2.177	2.084	2.070	2.062	2.083	2.127
2.451	2.637	2.161	2.081	2.073	2.088	2.109	2.153
1.935	1.923	2.132	2.124	2.106	2.100	2.120	2.162
2.168	2.123	2.124	2.140	2.148	2.142	2.181	2.245
2.281	2.221	2.191	2.170	2.177	2.212	2.271	2.402
2.363	2.303	2.295	2.273	2.256	2.332	2.458	2.473

*DIMENSIONAL VALUE = (NONDIMENSIONAL VALUE) (7.39773 m)
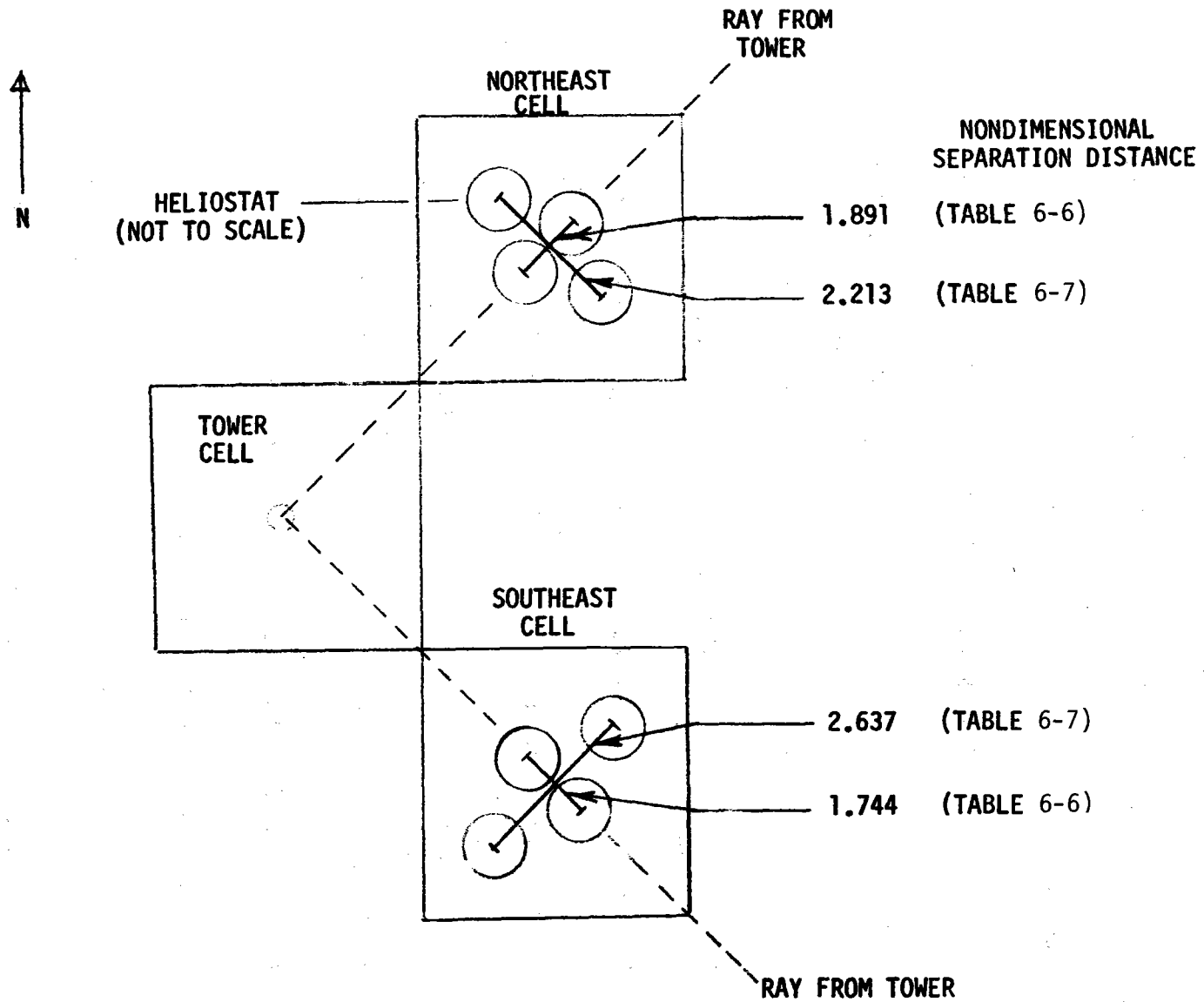
Figure 6-14. Utilization of Heliostat Spacing Data From Cell-by-Cell
(Tables 6-6 and 6-7)
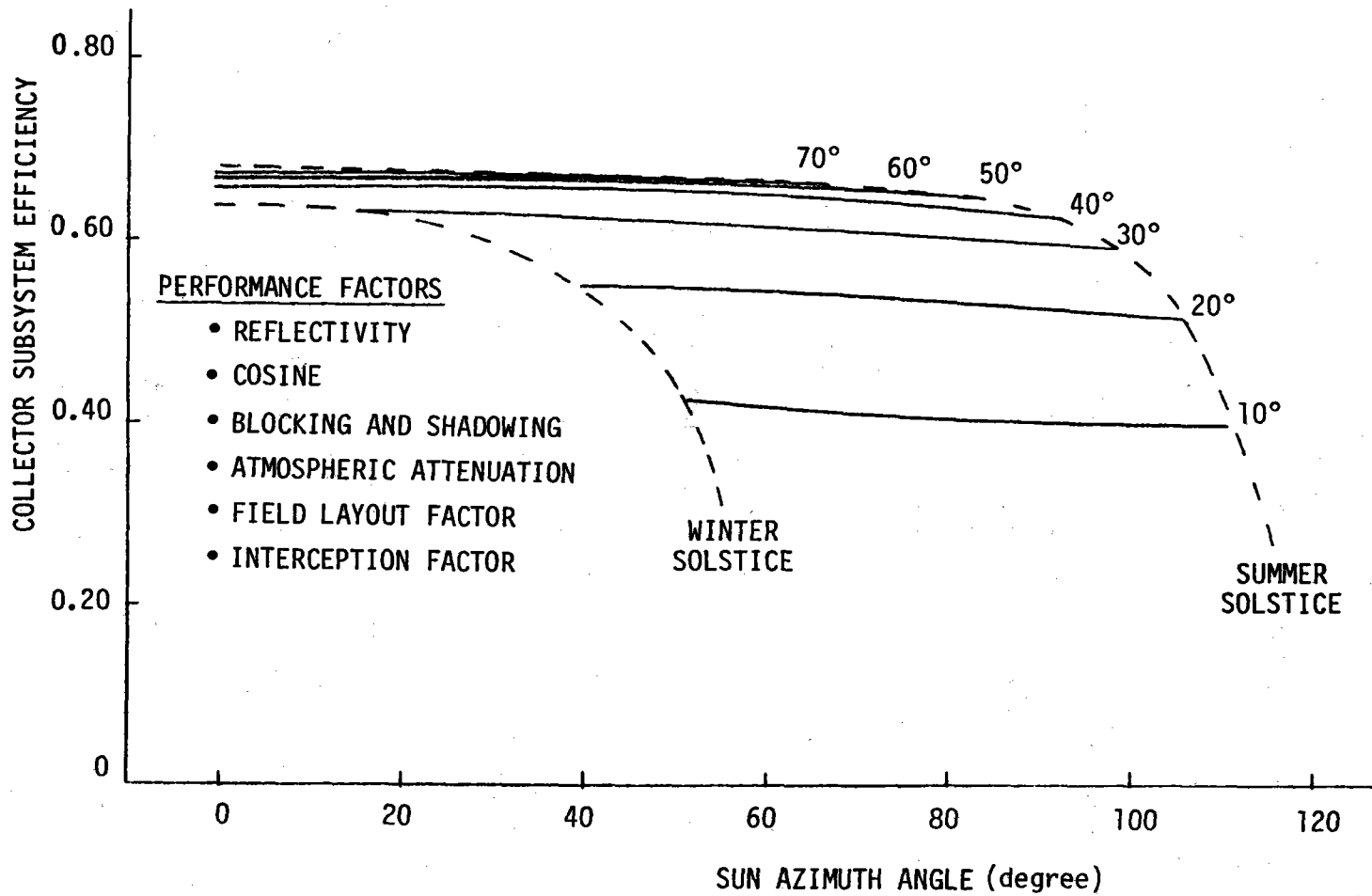
Figure 6-15. Baseline Collector Field Performance

(sun elevation angle >30°). A detailed tabulation of the corresponding receiver interception factor on a cell-by-cell basis is shown in Table 6-8. This table covers the complete 14 by 15 cell matrix. The interception data for cells outside the trim line should be ignored. Those immediately inside the trim line may represent fractional cells which have been retained as defined in Figure 6-13. For those remaining cells or fractions thereof, a glass-weighted average interception value of 0.966 exists over the complete field.

The impact of the collector field on the receiver operating environment is shown in Figures 6-16 and 6-17. Figure 6-16 shows the anticipated panel-by-panel power variations that occur at three representative times of the year which more or less bracket the operating environment for each panel. The peak power panels for the most part migrate around the surface of the receiver so that they are opposite from the sun side of the receiver. This effect is tempered somewhat by the overall shape of the field. Data of this type are useful in setting control limits for the individual panel control valves.

The design of the individual panel is governed by the heat transfer and thermal cyclic fatigue produced by the heat flux incident on the absorbing surface. Figure 6-17 shows a typical heat flux profile which is incident on the north facing receiver panel at equinox noon. The indicated peak of 1.37 MW/m^2 is significantly below the design limit of 1.7 MW/m^2.

Intuitively, it is felt that superior performance could be realized if the receiver was sized to produce a peak heat flux which approaches the 1.7 MW/m^2 design limit. This higher concentration ratio system should be superior because it reduces receiver size which in turn reduces heat loss and cost.

A closer evaluation, however, reveals that an unacceptable penalty is incurred in going to a small receiver. This is because of the finite size of the heliostat images which experience excessive spillage when the receiver size is reduced. Figure 6-18 illustrates the impact on the annual cost of energy in going to a smaller (or larger) receiver from the current 16.15 by 16.15 m cylindrical configuration. It also implicitly illustrates why the baseline dimension was selected. In going to the larger receiver, the increase in surface area, cost, and heat

TABLE 6-8
RECEIVER INTERCEPTION FACTOR

N ↑

(CELL-BY-CELL)

APPROXIMATE FIELD TRIM LINE
(FRACTIONAL CELLS INCLUDED INSIDE TRIM)
- SEE FIGURE 6-13 -

															Avg
0.655	0.693	0.727	0.758	0.782	0.800	0.812	0.815	0.812	0.800	0.782	0.753	0.727	0.693	0.655	0.806
0.699	0.742	0.780	0.812	0.839	0.858	0.870	0.873	0.870	0.858	0.839	0.812	0.780	0.742	0.699	0.853
0.743	0.788	0.829	0.863	0.890	0.909	0.920	0.923	0.920	0.909	0.890	0.863	0.829	0.788	0.743	0.891
0.782	0.830	0.872	0.907	0.932	0.950	0.959	0.962	0.959	0.950	0.932	0.907	0.872	0.830	0.782	0.925
0.816	0.866	0.908	0.940	0.964	0.978	0.985	0.987	0.985	0.978	0.964	0.940	0.908	0.866	0.816	0.951
0.845	0.894	0.935	0.965	0.983	0.993	0.997	0.997	0.997	0.993	0.983	0.965	0.935	0.894	0.845	0.969
0.864	0.914	0.954	0.979	0.993	0.998	1.000	1.000	1.000	0.998	0.993	0.979	0.954	0.914	0.864	0.978
0.878	0.927	0.964	0.987	0.997	1.000	1.000	1.008	1.000	1.000	0.997	0.987	0.964	0.927	0.873	0.983
0.883	0.932	0.968	0.989	0.998	1.000	0.994	TOWER	0.994	1.000	0.993	0.989	0.968	0.932	0.883	0.984
0.881	0.930	0.966	0.988	0.997	1.000	0.999	1.011	0.999	1.000	0.997	0.988	0.966	0.930	0.881	0.991
0.870	0.920	0.958	0.982	0.994	0.998	1.000	1.000	1.000	0.998	0.994	0.982	0.958	0.920	0.870	0.989
0.852	0.902	0.942	0.971	0.986	0.994	0.997	0.999	0.997	0.994	0.986	0.971	0.942	0.902	0.852	0.987
0.825	0.876	0.919	0.950	0.971	0.983	0.989	0.991	0.989	0.983	0.971	0.950	0.919	0.876	0.825	0.983
0.793	0.842	0.885	0.920	0.944	0.960	0.969	0.972	0.969	0.960	0.944	0.920	0.885	0.842	0.793	0.966
0.869	0.906	0.937	0.958	0.971	0.979	0.981	0.982	0.981	0.979	0.971	0.958	0.937	0.906	0.869	0.966*

*FIELD AVERAGE INCLUDING EFFECTS OF FIELD TRIM
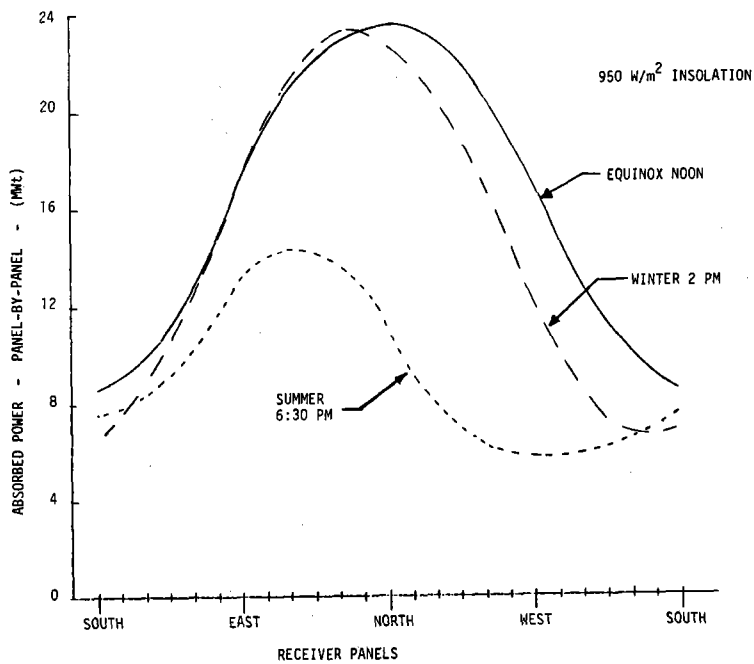
Figure 6-16. Circumferential Receiver Power Distribution

950 W/m^2 INSOLATION

EQUINOX NOON

WINTER 2 PM

SUMMER 6:30 PM

ABSORBED POWER - PANEL-BY-PANEL - (MWt)

SOUTH   EAST   NORTH   WEST   SOUTH

RECEIVER PANELS

9272-111

- EQUINOX NOON
- NORTH PANEL
- 950 W/m^2

INCIDENT HEAT FLUX (MW/m^2)

TOP
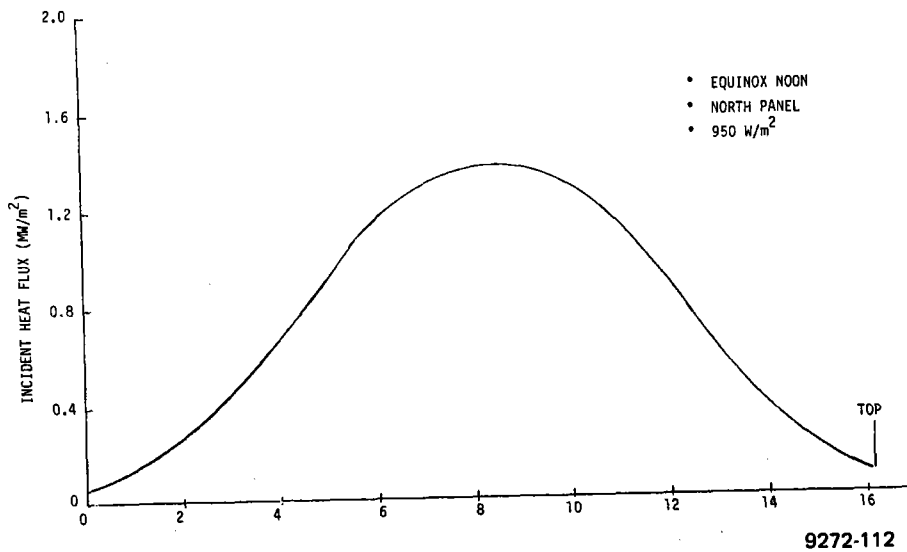
9272-112

Figure 6-17. Receiver Heat Flux Distribution Along "Worst" Panel

COST OF ENERGY ($/MWt-h-yr)

390 MWt ABSORBED INTO SODIUM

CYLINDER SIZE (HEIGHT = DIAMETER)
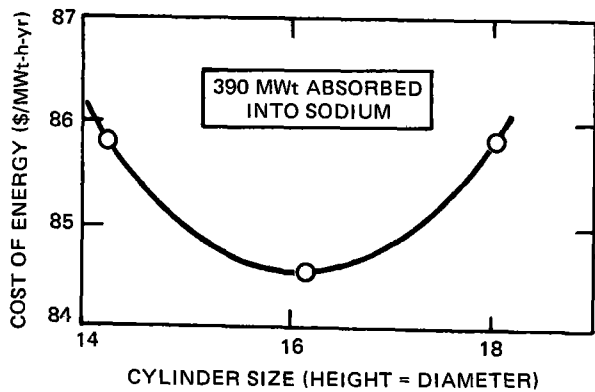
9272-113

Figure 6-18.   Impact of Receiver Size on Cost of Energy

loss more than offsets the increase in heliostat beam interception.   The large scale selected for the figure accentuates the difference in the cost of annual energy.   In reality, the difference is only slightly >1%.

6.3.2   Heliostat Assembly

The heliostat assembly is shown in Figures 6-19 and 6-20.   It consists of the reflective unit, the drive unit which orients the reflective unit, the foundation which supports the heliostat, and the heliostat electronics which controls the drive unit.

6.3.2.1   Reflective Unit

In order to facilitate handling and shipping from the manufacturing facility to the installation site, the reflective unit is made up of two reflector subassemblies.   Each reflector subassembly is comprised of six identical laminated mirror modules and a support frame.   The mirror modules are 1.22 m (48 in.) by 3.35 m (132 in.) and made of a 1.5 mm (0.060 in.) pane of fusion glass mirrored on its inner face and laminated to a 4.8 mm (0.1875 in.) float glass back-lite.   The clean reflectivity is estimated to be 0.92 at 0.05% iron and 0.945 at 0.01% iron.

The mirror modules are bonded to stringers which are, in turn, riveted to the cross beams.   The outer cross beam is supported by two diagonal beams.   All
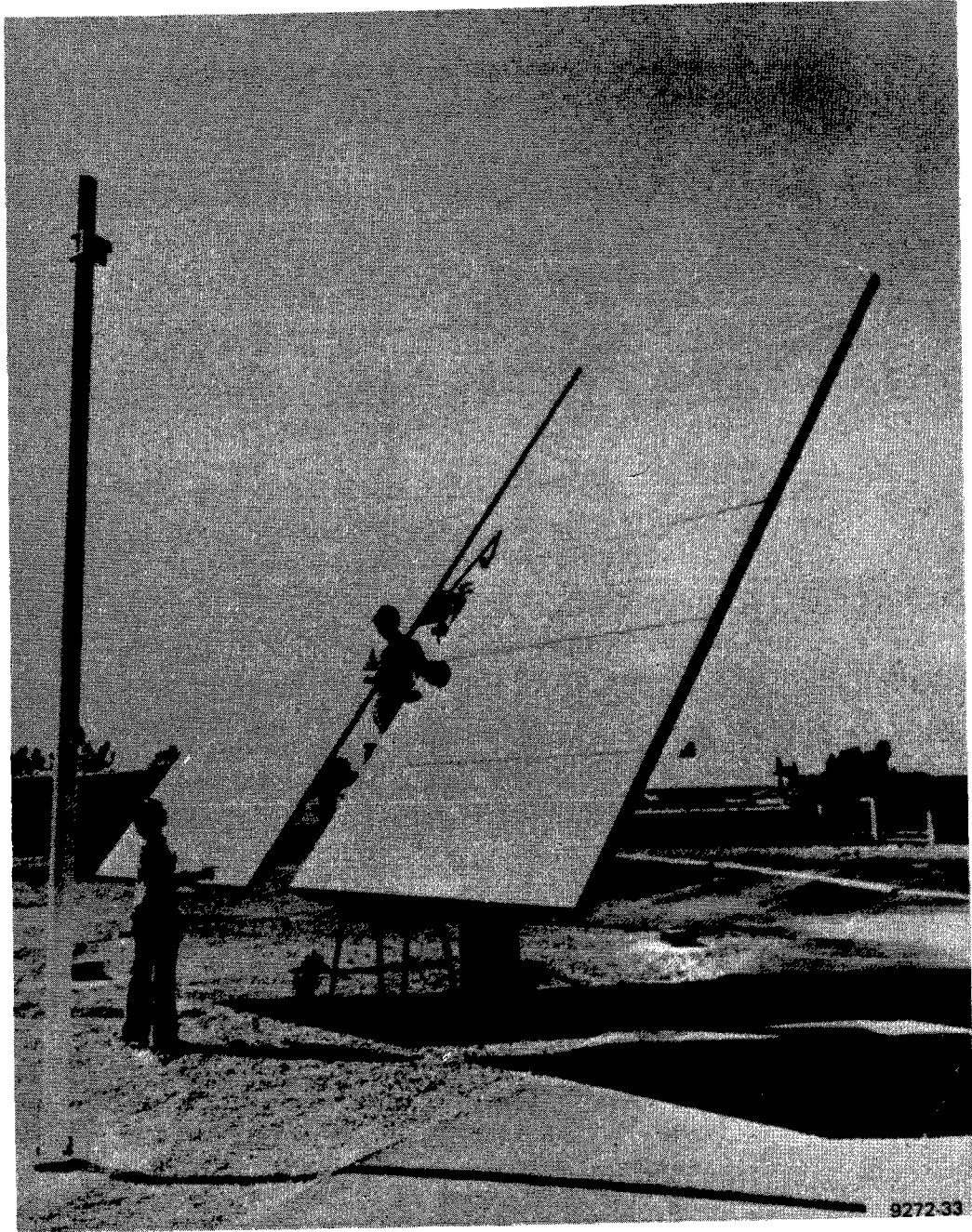
Figure 6-19. Primary Baseline Heliostat
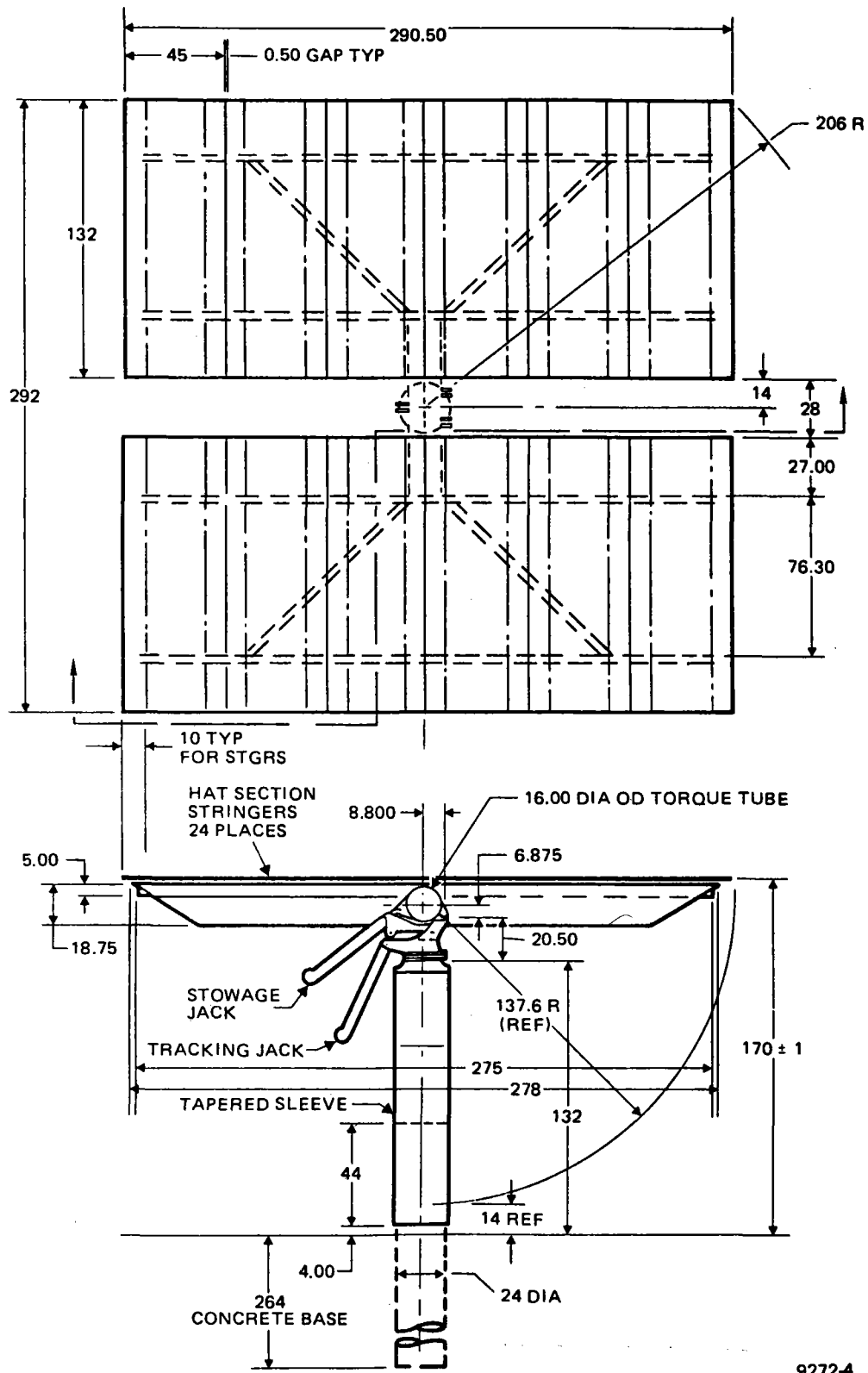
Figure 6-20.   Dimensions of Primary Baseline Heliostat

beams and stringers are made by continuous roll forming from coiled sheet stock. Each of the completed reflector subassemblies measures 3.35 m (132 in.) by 7.38 (290.5 in.).

The reflector subassemblies are assembled to the main beam at the top of the drive unit to produce a surface of 7.38 by 7.42 m (290.5 by 292 in.) with a slot of 0.71 m (28 in.) width down the middle. This gives a reflecting area of 49.0 m (528 ft^2).

In order to achieve high performance at low cost, glass with a high degree of flatness and with high transmission properties over the solar spectrum is required. Because of its high absorption characteristics, iron oxide content in the glass must be kept to a minimum. For these reasons, Corning fusion sheet glass (~0.05 wt % Fe), low iron float glass (~0.05 wt % Fe) and clear float glass (~0.08 wt % Fe), were investigated. Corning fusion glass was selected because of its high reflectance properties, its adequate flatness and reasonable costs. Although low iron float is flatter, and the extrapolated value of reflectance efficiency after silvering at a glass thickness of 1.5 mm (0.060 in.) approaches fusion glass, it cannot be made in that thickness. Currently, the thinnest float glass available is 2.1 mm (0.083 in.) thick which would lower the extrapolated reflectance efficiency to 92%.

6.3.2.2 Drive Unit

The function of the drive unit assembly is to rotate the heliostat reflective unit about the azimuth and elevation axes. The drive unit is operated for solar tracking, emergency slewing, stowage and for maintenance activities. The drive unit consists of an azimuth rotary drive assembly, two linear actuator assemblies for elevation drive, a drag link, a main beam, and the pedestal. The azimuth travel capacity of ±270° avoids the need for configurating the drive unit as a function of position in the field. The 180° of travel about the elevation axis is required to permit inverted mirror storage. Excessive operating loads are avoided by being able to stow the mirror in <15 min in rising wind conditions.

The calendar operating life of the drive unit is 30 years. The daily activity of the drive unit will consist of moving the mirror from a stowed position to acquire the sun, tracking the sun during the day and then returning the mirror to its stowed position at the end of the day. This life will be achieved without any scheduled maintenance activity.

6.3.2.3 Azimuth Drive Assembly

Movement of the heliostat assembly in azimuth is achieved with a harmonic drive train powered by a 480-V, 3-phase, 249-W (1/3 hp) bi-directional induction motor.

The major elements of the harmonic drive are the wave generator, the circular spline and the flexspline. The harmonic drive input is accomplished by rotation of the wave generator by the motor. The wave generator distorts the flexspline locally, so that some of the flexspline teeth engage circular spline teeth. Rotation of the points of engagement of the spline teeth cause relative motion of the flexspline to the circular spline. By attaching the circular spline to the pedestal and the flexspline to the aximuth housing, the output becomes rotation of the azimuth housing about the azimuth axis.

6.3.2.4 Elevation Actuators

Two linear actuators acting in conjunction with the drag link cause the main beam assembly to rotate about the elevation axis. Each actuator must have the capacity to rotate the torque tube 90°, to satisfy the requirement for a maximum travel of 180°. While the two actuators are identical, one is used daily as a tracking actuator, and the other, the stowing actuator, is used occasionally, possibly 30 times a year, when inverted storage may be required. The stowing actuator is preloaded into a structural stop, when the sun is being tracked, to eliminate its backlash from the system.

The elevation jacks each have identical 1/4-hp 480-V, 3-phase, 60 Hz bi-directional motors driving a helicon gear affixed to the nut of a ball screw.

6.3.2.5 Main Beam

The central torque tube type main beam connects the two reflector subassemblies together and ties the reflector unit to the elevation hinge and the elevating jacks at the top of the drive unit assembly. The main beam carries all the air loads and dead weight loads from the reflector unit to the pedestal as bending, torsion and shear. The main beam is 2.08 m (82.0 in.) long, of circular cross-section, 0.406 m (16 in.) in outside diameter (outside) formed of 12 gauge steel sheet, and hot-dip galvanized after fabrication. End plates are fusion welded to each end and machined flat and parallel to provide accurate location for the reflector subassemblies. Tapered holes in the reflector subassemblies and conical bolts provide accurate angular location of the subassemblies relative to each other.

In the slot between the two six-panel reflector subassemblies, the main beam has lugs of steel plate welded to it. Four of these lugs, in line, serve as the support and the elevation hinge line. They are attached to the drive housing at the top of the pedestal with two pins. The other two lugs are the mount for the elevating jack (actually, the stowing jack) through which the elevation rotational forces are applied to the reflector.

6.3.2.6 Pedestal

The support for the heliostat is provided by a pedestal 3.18 m (125 in.) high to provide clearance with the ground when the reflector is elevated at an angle. It is fabricated of 0.61 m (24 in.) diameter spiral welded steel pipe with a wall thickness of 2.66 mm (0.1046 in.). The lower 1.12 m (44 in.) of the length is expanded to produce a slight taper to obtain a wedged, slip-joint attachment with the foundation on installation. A recessed junction box is located in the pedestal 1.37 m (4.5 ft) above its lower end. Underground electrical lines are routed externally from the ground to the box, then through the box and up the inside of the pedestal. The drive unit housing is welded to the top of the pedestal.

A draw pressed dome is fusion welded to the top of the pedestal. A bolt circle in the dome provides a bolted interface to the circular spline in the azimuth drive unit.

The foundation is a concrete pier, 24 in. in diameter. The pier extends about 4 ft above grade and 20 ft below. A tapered steel shell establishes the mounting surface to the pedestal and serves as a form for the protruding end of the pier.

6.3.2.7 Heliostat Electronics

The heliostat electronics subassembly includes:

1) Pedestal Junction-Circuit Breaker Box — Located on the pedestal and interfaces with the field power and data network.

2) Cabling— A single cable takes power to and data to and from the heliostat controller box on the drive unit to and from the junction box. A second set of cables go from the controller box to the motors and sensors.

3) Heliostat Controller — A microprocessor in the heliostat controller does all command calculations. The microprocessor interfaces directly with motor switching network, sensor, and communication link.

4) Motors-Sensors — Incremental encoders and switching networks are mounted on the motor shaft.

The heliostat electronics receives signals from the data network and relays messages to the next heliostat in the chain. Open-loop tracking algorithms are used to determine the required heliostat position. The difference between the calculated position and actual position is used as an error signal for turning the motors on or off. The signal from the incremental encoder is used to determine the actual position by counting motor turns. The accumulated turns are stored in nonvolatile electrically erasable memory (EAROM); therefore, if power should be lost, the position reference of the heliostat will not be lost.

The electronic components are located at five different locations on the heliostat as shown in Figure 6-21. The Heliostat Controller is located in an electrical J-box on the drive unit. This location was selected over a ground location in order to give added protection from the environment and ground activity, and to minimize the heliostat wire required. A junction box is located on the pedestal which contains a circuit breaker, plug connectors, and terminators for the incoming power and communication fibers. Power to a heliostat can be controlled by activating the circuit breaker switch. A manual control box can be plugged into the pedestal junction box for local control of the heliostat. Local manual control isolates this heliostat without affecting the control of any other heliostat in the field.

6.3.2.8 Pedestal Junction-Circuit Breaker Box

The secondary feeder cable enters the heliostat pedestal and terminates in a junction box located on the side of the pedestal. The junction box is illustrated in Figure 6-21. The recessed box contains a circuit breaker which joins the incoming and outgoing cables and noninterchangeable fiber optic connectors. On the inside of the pedestal, the circuit breaker is wired directly into the cable leading to the heliostat controller.

An internal protective cover will be required to provide personnel protection from the 480-V terminations after the wire installations are made.

The cutout will also contain a cover for environmental protection. The cover will be designed to prevent water from flowing into it and will be sufficiently tight to exclude dust and prevent the formation of significant quantities of ice. The box will have a drain hole inside the pedestal to prevent the accumulation of significant quantities of water.

It is important that proper phasing be maintained in the power distribution network. Therefore, cables will be terminated in the factory with crimp or ring terminals which will only connect in one manner. Also, the fiber optic connectors will be male and female, with the male used for the incoming signal and the female for outgoing to prevent any possibility of reversing.
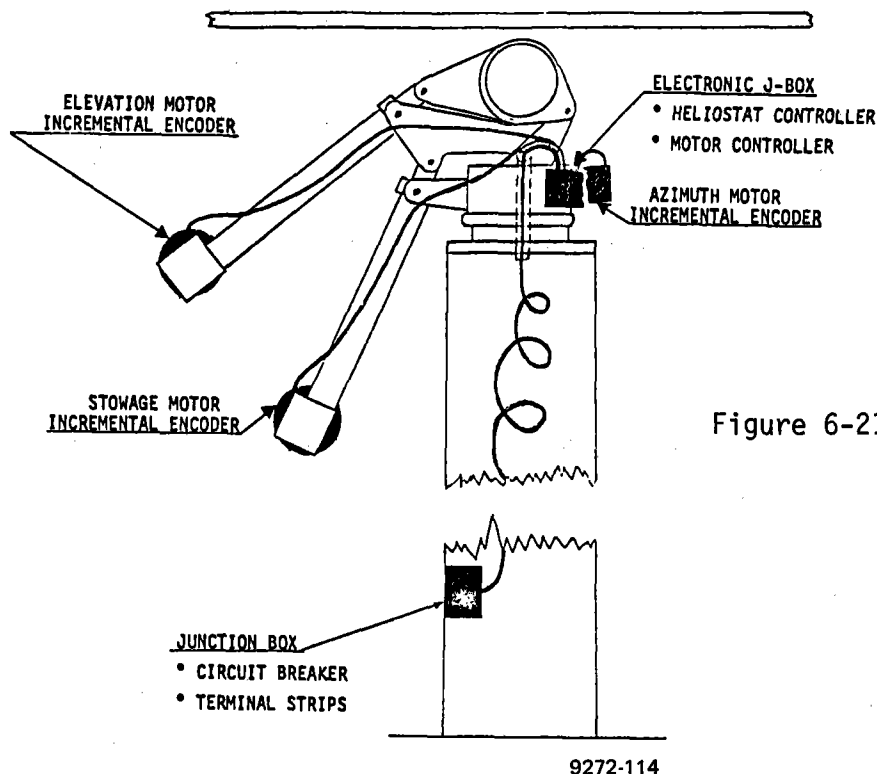
Figure 6-21. Heliostat Electronic Assembly

9272-114

6.3.2.9 Cabling

The heliostat pedestal wiring consists of 3 conductor, No. 16-AWG, 480-V, copper wire with aluminum sheath for power distribution and twin lead optical fiber cable for data transmission. The cable runs from the junction box in the pedestal to the heliostat controller mounted on the drive unit. In order to route the cable past the gimbal axis, a hollow shaft has been designed into the center of the azimuth axis. The cable will be routed through the shaft, thus allowing for rotation and elevation of the heliostat without putting stress on the power cable. To allow for 270° rotation of the azimuth gimbal, a section of cable is left slack inside the pedestal. The cable and other components are completely wired in the factory; hence, the only field wiring required is to connect the secondary feeder to the junction box.

6.3.2.10 Heliostat Controller

The Heliostat Controller is a microprocessor based unit which interfaces with the Heliostat Array Controller and the motor-sensor system.

The main functions of the Heliostat Controller are to respond to the commands from the Heliostat Array Controller, send information to the Heliostat Array Controller, calculate commands for moving the heliostat from one position to another position, and to keep track of heliostat orientation. Heliostat orientation is determined by counting the number of turns the motor makes. The processor contains a nonvolatile memory (EAROM) where the motor counts are kept. Even if the power should fail, the heliostat will not lose the number of motor turns or its reference position.

It is estimated that in the 1985 time period, the required capabilities of the Heliostat Controller will easily be available in a single chip microprocessor. The current trend and demand also indicate that microprocessors will be available with electrically erasable ROM's (EAROM) within the next year or two.

The communication interface consists of a differential line transceiver which receives serial data and transfers parallel data to the processor (the process is reversed for transmitting data). The address bits are decoded in the processor and, if they agree with the address of this heliostat, the message is decoded and executed.

Calculation of equations for control of the heliostats are done in the Heliostat Controller with inputs from the Heliostat Array Controller. Using a transmitted time signal, the Heliostat Controller updates its clock, calculates the sun angles, the gimbal angle required for reflecting the beam onto the target, the error signal between the actual gimbal angles and the commanded gimbal angles, and the motor command for reducing the error signal.

If the operating mode should be changed from tracking on the receiver to emergency slew off the receiver, a single command is transmitted to each Data Distribution Interface which transmits the message to each heliostat assigned to it. The Heliostat Controller then commands the reflected beam to move from the receiver to an aim point near the receiver. The Heliostat Controller maintains the beam at this aim point until the operating mode is changed by the Heliostat Array Controller. The Heliostat Controller will continue tracking even if the communication link with the heliostat array controller is lost.

6.3.2.11 Motor-Sensors

Besides the armature and field, the motor housing contains the motor control switching network and an incremental encoder.

The control (direction and on or off) of the 3Ø motors is accomplished by the heliostat controller switching the motors on and off to produce the required motion.

Incremental encoders are mounted at the base of each of the three drive motors to provide control feedback data. The encoder is designed to provide the controller with information concerning the direction and the number of revolutions of each motor.

The incremental encoder is designed with two Hall-effect transducers. A ferrous metal vane mounted on the motor shaft produces an interrupt in each of the transducer's magnetic fields at intervals slightly out of phase depending on the direction of rotation.

The encoder sensors are environmentally sealed in durable plastic casing. Dust and dirty atmospheric conditions do not produce damage or inaccuracy due to the magnetic operation of the units.

The encoder has an accuracy to within one motor revolution. This is equivalent to a deflection of 0.144 mrad in heliostat azimuth and approximately 0.144 mrad in elevation.

6.3.3 Field Electronics

The field electronics for the collector deliver power and control data to the heliostats and return information on the heliostat status to the master control.

6.3.3.1 Data Distribution Network

There are four basic electronic components that are used in controlling the heliostats in the collector field (Figure 6-22). They consist of a Heliostat Array Controller (HAC) located in the master control building which commands operating modes, transmits and coordinates reference time, and requests and receives data on heliostat performance. Information from the HAC is communicated via serial data transmission to the Heliostat Controllers (HC) which in turn provide the necessary calculations and tracking command signals to the drive motors. A Data Distribution Interface (DDI) between the HAC and the HC is used to distribute the commands down the appropriate line.
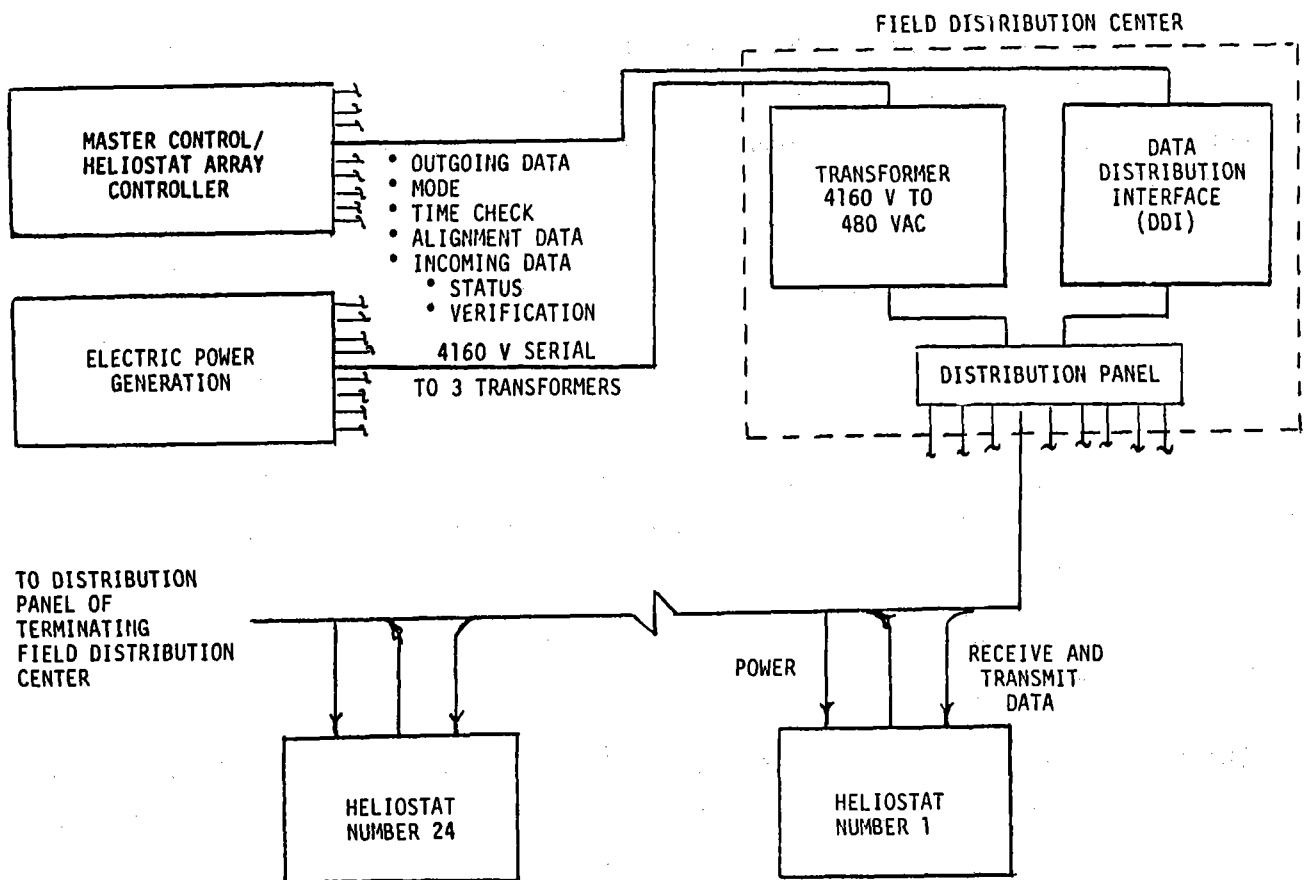
Figure 6-22. Collector Field Electronics

The data distribution interface receives data from the heliostat array controller via either of two redundant lines and logic networks. The redundancy provided should prevent loss of control of more than a few heliostats at a time. The logic network decodes the data and addresses it to the correct secondary data feeder and the intended heliostat.

The secondary data feeders from a DDI connect each heliostat on the line in a series hookup. Data received by a heliostat controller are decoded and, if addressed to the heliostat, the data are retained and a message relayed onto the next heliostat, and hence to a data distribution interface at the end of the line. If the data were not addressed to the heliostat, the message is relayed to the next heliostat.

If the operating mode should be changed from tracking on the receiver to emergency slew off the receiver, a single command is transmitted to each DDI which transmits the message to each heliostat assigned to it. The heliostat controller then commands the reflected beam to move from the receiver to an aim point near the receiver. The HC maintains the beam at this aim point until the operating mode is changed by HAC.

All data links use fiber optics. The communication link consists of an optical transmitter unit compatible in bandwidth to the heliostat array controller, a fiber optic communication line and a photo detector receiver for converting optical signals to their digital equivalents.

The unique advantages of optical transmission over electrical transmission make its use attractive in both performance and cost. Optical fiber transmission offers wider bandwidth and smaller cable cross-section than previously possible. In addition, since fiber optic cables neither pick up nor emit electron magnetic radiation and offer total electrical isolation, the problems of RFI, EMI, EMP, ground loops and sparking associated with electrical cables can be eliminated. These qualities of fiber cable allow the data transmission lines to be incorporated with existing power lines in a single cable, thus allowing for simplified routing and installation. The primary data link has, therefore, been designed

coincident with the primary field wiring (Figure 6-23). All cables are designed for direct burial to provide adequate protection at minimum cost.

6.3.3.2 Power Distribution Network

The power distribution network provides 480-V 60-Hz a-c power to the heliostat drive motors. The wiring configuration is designed to incorporate the lower cost of a radial configuration and the reliability of a network system. The field (Figure 6-23) consists of a primary distribution system originating from a central distribution point, each feeder of which provides power for two or three transformers collocated with the data distribution interfaces (DDI). The transformers are 225 kVA with a primary of 4160 V and a secondary of 480 V. Each transformer will supply power to 12 to 16 groups by a number of branch circuits, each of which feeds approximately 24 heliostats.

The continuous run from transformer to transformer permits the small gauge, low voltage branch circuit to operate as a secondary main in the case of a transformer failure. This hybrid radial system is not totally redundant since the heliostats normally supplied by a transformer which has failed are not supplied sufficiently for normal operation, but are available to drive into a stowage position or carry out emergency maneuvers which increase the operating safety of the field.

6.3.3.3 Heliostat Availability

The availability of a single heliostat was calculated by utilizing the MTBF and MTTR results from Table 6-9. The failures-per-day rate was calculated for each heliostat component by dividing the operational hours per day by the MTBF. A value of 10 h per day was used for the dynamic components (motors, actuators, electronics), 24 h per day for static components (pedestal, reflector), and 0.5 h per day for stowage elements. This value is then used to calculate the individual component availability and the heliostat availability.

BRANCH CIRCUITS (LOW VOLTAGE)

PRIMARY FEEDERS (HIGH VOLTAGE)

CENTRAL
DISTRIBUTION
POINT

TRANSFORMERS
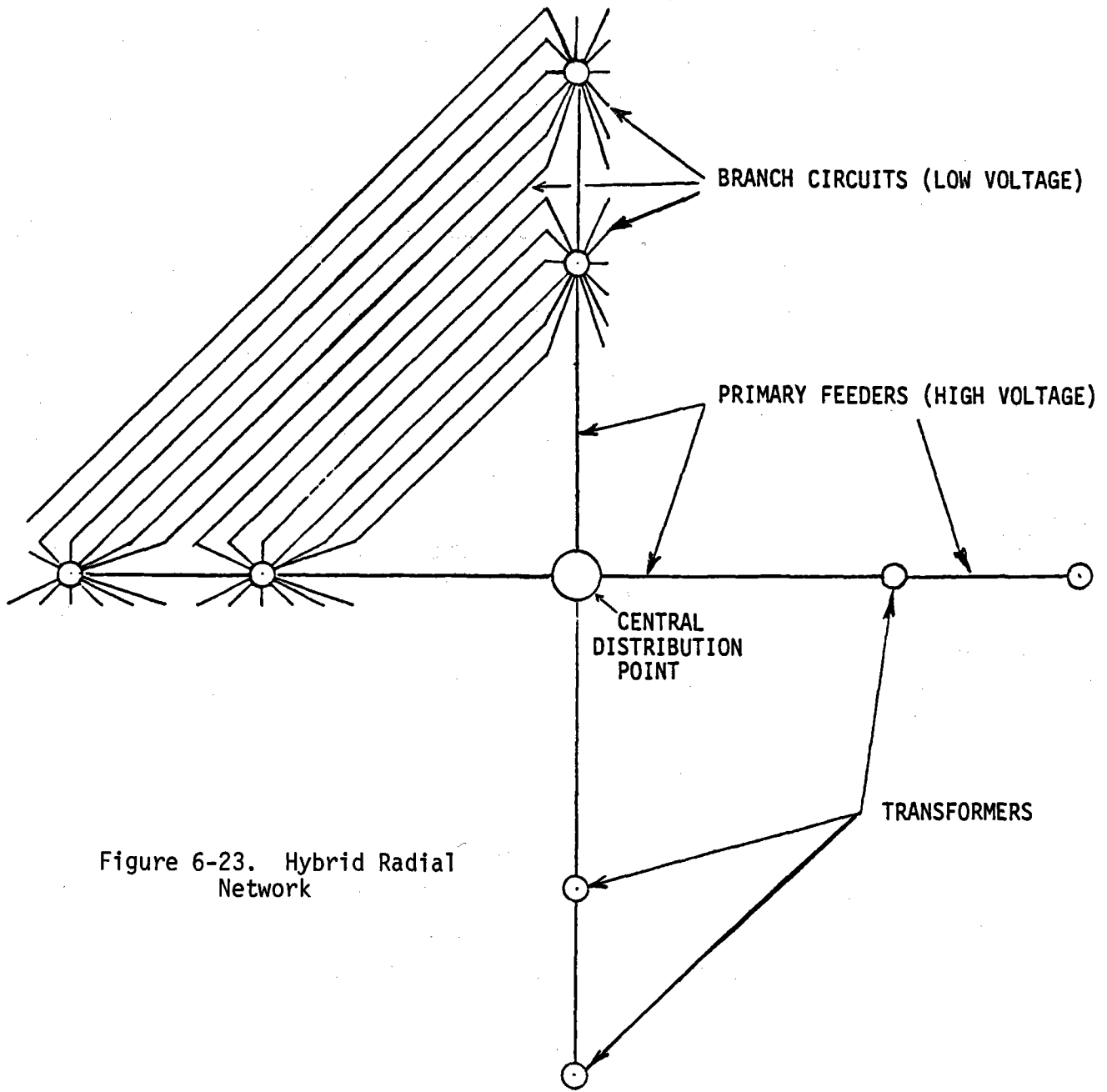
Figure 6-23. Hybrid Radial
Network

TABLE 6-9

COLLECTOR AVAILABILITY

	MTBF (h)	F/Day (10^{-6})	MTTR (h)	H/Day (10^{-6})
Drive Assembly, AZ	340,136	29.4	4.0	117.6
Jack Assembly, Track	366,300	27.3	2.2	60.6
Jack Assembly, Stowage	366,300	1.37	2.2	3.0
Drive Motor (2)	295,858	67.6	1.8	121.7
Stowage Motor	295,858	1.69	1.9	3.2
Heliostat Junction Box	862,069	11.6	1.6	18.6
Heliostat Control Electronics	606,060	16.5	1.3	21.5
Heliostat Cables (5)	9,090,909	5.5	1.8	9.9
Pedestal	9,090,909	2.64	1.0	2.6
Reflector Structure	8,333,333	2.88	1.5	4.3
Reflector Panel	10,000,000	2.4	2.0	4.8
Data Distribution Box	206,186	48.5	1.6	77.6
Power Transformer	(Redundant transformers - failure does not cause outage)			
Power Distribution Box	66,667	150.0	1.6	240.0
Field Cables	4,545,454	2.2	3.5	7.7

10-h Operating Day; 24-h Actual day; .5-h Stowage Day

The downtime of the heliostat due to field component failures is calculated in a similar manner. The results show that the heliostat will be "down" about 0.000368 h per day on the average due to heliostat component failures, and 0.000325 h per day on the average due to field component failures, or a total of 0.000693 h per day on the average. This converts to an availability of 0.999931.

7.0 ELECTRICAL POWER GENERATION SUBSYSTEM

7.1 REQUIREMENTS

Table 7-1 gives the requirements for the Electrical Power Generation Subsystem (EPGS). The EPGS must be capable of converting the thermal energy supplied by the Receiver Subsystem and the Thermal Storage Subsystem into electrical energy. The output from the EPGS shall be regulated for integration into existing electrical power system networks.

TABLE 7-1
EPGS DESIGN REQUIREMENTS

Electrical Power Output	
Day	100 MWe Net, 60 Cycle
Night (3 h)	100 MWe Net, 60 Cycle
Heat Rejection	Wet Cooling
Wet Bulb Temperature	$23^{o}C$ $(74^{o}F)$
Lifetime	30-yr Operating Life
Reference Site	Barstow, Calif.
Wing (Survival)	40 ms (90 mph)
Seismic (Survival)	Seismic Zone 3 Uniform Building Code (UBC)(0.25g Horizontal and Vertical ground acceleration)

The selected commercial turbine is of a standard design and type utilized in present day utility power generating plants and requires no new technical development.

7.2 DESIGN CHARACTERISTICS

The Commercial Plant EPGS conceptual design is based on the use of a standard tandum compound, double flow, reheat, condensing turbine.

The selected Commercial Plant cycle is shown in Figure 7-1 and utilizes single reheat and six stages of feedwater heating. The initial pressure is 12.5 MPa (1815 psia), initial temperature is 538°C (1000°F), and reheat temperature is 538°C (1000°F). Gross cycle efficiency is 43.1%. Two full capacity, motor-driven boiler feed pumps are provided. A mechanical draft, wet cooling tower is used for heat rejection.
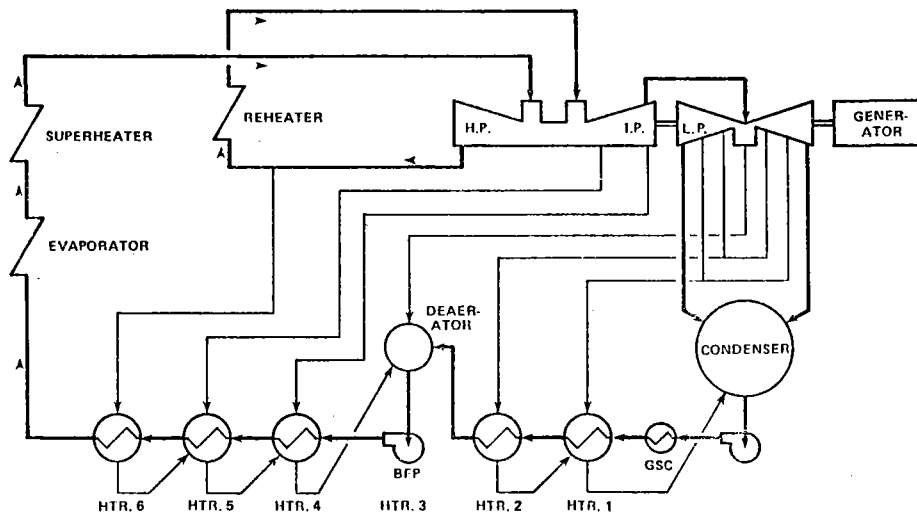
9272-116

Figure 7-1. Commercial Plant Turbine Cycle

A summary of the Commercial Plant EPGS design characteristics is given in Table 7-2.

7.3 COMMERCIAL TURBINE SELECTION

One of the attractive features of sodium as heat transport fluid in a central receiver concept is that it can permit the use of efficient, high-temperature,

TABLE 7-2

ADVANCED CENTRAL RECEIVER — ELECTRICAL POWER
GENERATION DESIGN CHARACTERISTICS

Gross Turbine-Generator Output	
Daytime (MWe)	112
Nighttime (MWe)	106
Net Turbine-Generator Output	
Daytime (MWe)	100
Nighttime (MWe)	100
Turbine Inlet Steam Conditions	
High Pressure (Throttle) Steam [^{O}C (^{O}F)]	538 (1000)
[MPa (psia)]	12.51 (1815)
Low Pressure (Reheat) Steam [^{O}C (^{O}F)]	538 (1000)
[MPa (psia)]	2.95 (428.2)
Rated Turbine Inlet Flow Rate [kg/h (lb/h)]	0.332×10^6 (0.732×10^6)
Heat Rejection	
Method	Wet Tower
Wet Bulb Temperature [^{O}C (^{O}F)]	23 (74)
Daytime [MWt (Btu/h)]	158 (540×10^6)
Nighttime [MWt (Btu/h)]	150 (511×10^6)
Turbine Exhaust Pressure [kPa (in. Hg)]	7.0 (2.0)
Generator Output	
Generator Rating (kVA)	135,000
Power Factor	0.90
Voltage (V)	13,800
Frequency (Cycles)	60
Main Transformer	
Rating (kVA)	130,000
Voltage (kV)	13.8/115
Feedwater Conditioning	
Dissolved Solids (ppb)	20-50
pH	9.5

TABLE 7-3
CONCEPTUAL DESIGN OF ADVANCED CENTRAL RECEIVER POWER SYSTEM
ESTIMATED TURBINE PERFORMANCE AND COSTS

	Turbine Type — Last Stage Blade Length						
	TC2F — 23 in.						
	Case 1	Case 2	Case 3	Case 4	Case 5	Case 6	Case 7
Gross Generation, VWO (kW)	117,520	117,520	117,520	117,520	117,520	117,520	117,520
Gross Turbine Heat Rate (Btu/kW-h)	8,077	7,919	7,982	8,038	8,102	7,766	7,828
Throttle Pressure (psig)	1,450	1,800	1,800	1,800	1,800	2,400	2,400
Throttle Temperature (°F)	1,000	1,000	1,000	950	950	1,000	1,000
Throttle Flow (lb/h)	776,417	765,396	785,296	796,840	817,557	762,350	782,482
Reheat Pressure (psia)	374.1	440.6	440.6	440.6	440.6	528.7	528.7
Reheat Temperature (°F)	1,000	1,000	950	950	900	1,000	950
Reheat Flow (lb/h)	681,474	668,601	685,984	696,068	714,165	671,385	689,109
Condenser Pressure (in. Hg abs)	2.0	2.0	2.0	2.0	2.0	2.0	2.0
Condenser Flow (lb/h)	557,203	544,620	551,155	563,997	577,138	530,724	543,089
Final Feedwater Temperature (°F)	433.1	449.7	449.7	449.7	449.7	467.5	467.5
Number of Heaters	5	6	6	6	6	7	7
Gross Cycle Efficiency (%)	42.25	43.09	42.75	42.45	42.12	43.94	43.59
Estimated Installed Cost ($)							
Turbine-Generator	9,493,000	9,581,000	9,581,000	9,581,000	9,581,000	10,355,000	10,355,000
Incremental Heater Cost Over Base (Base - 5 Heaters)	Base	100,000	100,000	100,000	100,000	200,000	200,000
Total Estimated Cost	9,493,000	9,681,000	9,681,000	9,681,000	9,681,000	10,555,000	10,555,000
	TC2F — 20 in.						
	Case 8	Case 9	Case 10	Case 11	Case 12	Case 13	Case 14
Gross Generation, VWO (kW)	117,520	117,520	117,520	117,520	117,520	117,520	
Gross Turbine Heat Rate (Btu/kW-h)	8,217	8,069	8,048	8,112	8,169	8,234	
Throttle Pressure (psig)	1,450	1,800	1,800	1,800	1,800	1,800	
Throttle Temperature (°F)	1,000	1,000	1,000	1,000	950	950	
Throttle Flow (lb/h)	781,205	796,873	777,161	797,367	809,088	830,124	
Reheat Pressure (psia)	376.0	497.8	436.4	436.4	436.4	436.4	
Reheat Temperature (°F)	1,000	1,000	1,000	950	950	900	
Reheat Flow (lb/h)	694,640	690,083	673,970	691,493	701,658	719,901	
Condenser Pressure (in. Hg abs)	2.0	2.0	2.0	2.0	2.0	2.0	
Condenser Flow (lb/h)	567,096	562,481	553,053	565,939	572,730	586,074	
Final Feedwater Temperature (°F)	433.5	461.8	448.1	448.1	448.1	448.1	
Number of Heaters	5	5	6	6	6	6	
Gross Cycle Efficiency (%)	41.53	42.29	42.40	42.06	41.77	41.44	
Estimated Installed Cost ($)							
Turbine-Generator	8,480,000	8,521,000	8,521,000	8,521,000	8,521,000	8,521,000	
Incremental Heater Cost Over Base (Base - 5 Heaters)	Base	Base	100,000	100,000	100,000	100,000	
Total Estimated Cost	8,480	8,521,000	8,621,000	8,621,000	8,621,000	8,621,000	

high-pressure steam turbines, turbines that represent current state-of-the-art technology. It also allows the use of reheat which increases cycle efficiency ~5% over a nonreheat cycle. Because of these features, the technical approach on the Electric Power Generation Subsystem was to select the most efficient and cost-effective turbine generator system and then to design the sodium heat transport systems to meet EPGS requirements.

A survey of turbine-generator costs and performances was conducted at the beginning of the program and resulted in the selection of 13 potentially viable systems that incorporated reheat and that could provide a net electrical output of 100 MWe. These 13 cases are delineated in Table 7-3. All of the selected turbines are of the tandem compound, two-flow type. Last-stage blade lengths of 58.4 cm (23 in.) and 50.8 (20 in.) were included. Three throttle pressures were considered: 10.0 MPa (1450 psig), 12.4 MPa (1800 psig), and 16.5 MPa (2400 psig), and two throttle temperatures were included: 510°C (950°F) and 538°C (1000°F). The condenser back pressure was assumed to be 6.7 kPa (2.0 in. Hg abs) in all cases. Gross cycle efficiencies varied from a low of 41.83% to a high of 43.9% for a 16.5 MPa (2400 psig), 538°C (1000°F) machine. In order to make a selection from among the 13 cases, a plot of the type shown in Figure 2-2 of Section 2 was prepared. In this figure, the gross cycle efficiency is plotted vs the turbine generator cost including feedwater heaters in excess of five but excluding heat rejection equipment, feedwater pumps, feedwater piping, etc. Also plotted on this graph is the cost effectiveness (breakeven) line which is based upon the assumption that the cost of the collector, receiver, and storage subsystems vary on the power ratio to the 0.8 power, i.e., $C \alpha (P/P_o)^{0.8}$ where C is the cost of the subsystem, P is the thermal power required from the receiver for a given case, and P_o is the baseline thermal power from the receiver. This line is arbitrarily normalized to the 42.29% gross efficiency value corresponding to the turbine in Case 9 and shows that the turbines in Cases 9, 10, 2, and 7 are about equivalent. There appears to be a slight advantage in the turbine-generator systems designated as Case 6. The data obtained from the survey clearly shows, for example, that Case 10 is to be preferred, from a cost effectiveness standpoint, relative to Cases 11, 12, and 13 in that order. Similarly, Case 2 has a distinct advantage over Cases 3, 4, and 5.

TABLE 7-4

ADVANCED CENTRAL RECEIVER POWER SYSTEM
COST AND POWER COMPARISON OF SELECTED TURBINE CYCLES

	Case 2	Case 6	Case 9	Case 10
Turbine Characteristics				
Turbine Type	TC2F - 23 in.	TC2F - 23 in.	TC2F - 20 in.	TC2F - 20 in.
No. of Heaters	6	7	5	6
Throttle Pressure (psig)	1,800	2,400	1,800	1,800
Throttle Temperature (°F)	1,000	1,000	1,000	1,000
Reheat Temperature (°F)	1,000	1,000	1,000	1,000
Exhaust Pressure (in.-Hg abs)	2.0	2.0	2.0	2.0
Gross Turbine Heat Rate (Btu/kW-h)	7,919	7,766	8,069	8,048
Generator Output (kW)	117,520	117,520	117,520	117,520
Gross Cycle Efficiency (%)	43.09	43.94	42.29	42.40
Comparative Costs ($)				
Turbine-Generator	9,581,000	10,355,000	8,521,000	8,521,000
Heat Rejection Equipment	20,000	Base	40,000	30,000
Main Steam Piping	0	15,000	Base	0
Hot and Cold Reheat Piping	0	0	Base	0
Feedwater Piping	0	0	Base	0
Feedwater Pumps and Motors	0	75,000	Base	0
Feedwater Heaters	100,000	200,000	Base	100,000
Total	9,701,000	10,675,000	8,561,000	8,651,000
Comparative Power Requirements (kW)				
Boiler Feed Pumps	Base	613	0	0
Cooling Tower Fans	12	Base	27	19
Circulating Water Pumps	42	Base	94	66
Hotwell and Heater Drain Pumps	Base	25	0	0
Total	54	638	121	85
Difference Over Base	Base	584	67	31
Cost Effectiveness ($)				
A. Capital Cost Difference	1,140,000	2,114,000	Base	90,000
B. Equalize Net Power Out	Base	523,000	60,000	28,000
C. Efficiency Effect on Cost	-6,030,000	-7,460,000	-4,690,000	-4,870,000
Relative New Worth (A+B+C)	-4,890,000	-4,830,000	-4,630,000	-4,750,000

From an evaluation of the data in Figure 2-2, it was concluded that Cases 2, 6, 9, and 10 should be studied in greater detail in order to make a final selection for an optimized system. This study included consideration of other costs on the EPGS side of the plant, including heat rejection equipment and auxiliary power requirements. The results of this study are summarized in Table 7-4. Although, in terms of total cost, the Case 9 turbine appears to be the most attractive, the Case 2 turbine-generator system is most cost effective overall, if power requirements and efficiency effects are factored into the selection process. The values for the equalized net power out shown in Table 2-4 are related to the power requirements and show that the overall system cost increases since the gross output must go up in order to maintain a net electrical output of 100 MWe. The power requirements are greatest for Case 6, for example. On the other hand, the improved efficiency of Case 6 results in an efficiency effect (or credit) on cost (-$7,460,000) that is substantially greater than for the other cases. The efficiency effect factor is essentially a measure of the reduction in overall plant cost resulting from the improved efficiency. The net effect of these two factors results, however, in slightly smaller relative net cost (-$4,830,000) for Case 6, for example, than for Case 2. In this evaluation, the larger the negative dollar value, the greater the cost effectiveness. Thus, the TC2F-23, 12.4 MPa (1800 psig) 530°C (1000°F) turbine with 538°C (1000°F) reheat and with a gross efficiency of 43.1% was chosen as the baseline concept for the solar central receiver.

Inherent in these cost tradeoff studies are the effects of turbine throttle pressure, among other factors, on the cost of the steam generators. In deriving the effect of efficiency on cost, the increase in the cost of the steam generator for operation at 16.5 MPa (2400 psig) was accounted for. This parametric analysis of steam generator cost vs pressure is discussed in Section 2. It is only to be noted here that, within the uncertainties of the parametric analyses, it appears that a 16.5 MPa (2400 psig) steam generator will cost somewhat more than would be justified by the improved efficiency derivable from the system. This conclusion could change during the Phase II program when a more detailed design, stress analysis, and manufacturing assessment can be made.
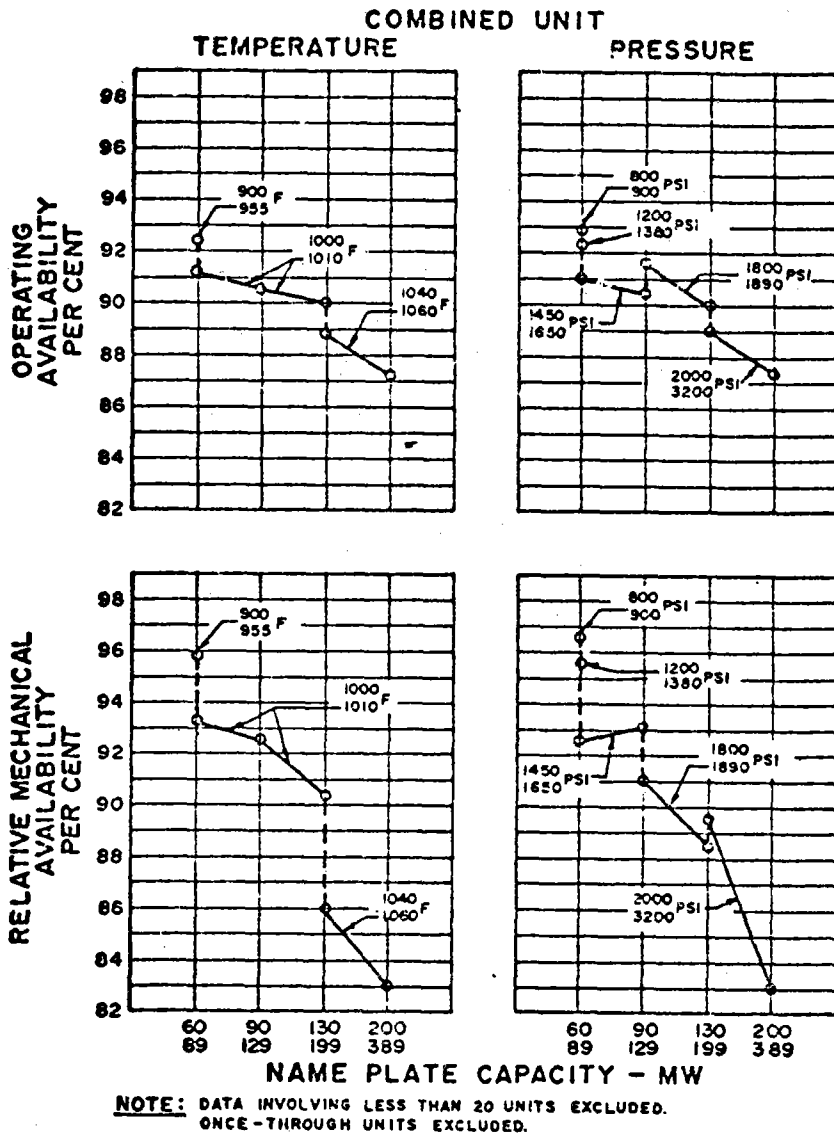
Figure 7-2. Effect of Initial Steam Temperature
and Pressure on Availability
(based on cumulative average 1960 - 64)

Another important consideration which supports the selection of 12.4 MPa (1800 psig) over 16.5 MPa (2400 psig) steam pressure for the 100-MWe Commercial Plant is turbine availability, particularly in cycling service. In general, lower steam pressures and temperatures reduce the detrimental effects of daily cycling. The effects of initial steam temperature and pressure on availability of fossil generating units have been studied by C. E. Richards and L. O. Beck in "Availability of Large Fossil Fuel Fired, Power Generating Units," ASME Paper 65-PRS-8, ASME-IEEE National Power Conference, September 19-22, 1965, among others, with the conclusion that increases in unit size and initial steam conditions have been accompanied by lower availability and higher forced-outage rates. Figure 7-2 from the Richards and Beck paper indicates the influence of both size and initial steam conditions on the availability of the overall unit. Forced outage experience with turbine and boiler components, shown in Figure 7-3, supports this trend. However, since it may be desirable from an overall system cost standpoint to operate at higher pressures and temperatures the turbine availability question will be given more consideration during the Phase II program.

7.4 REVISED BASELINE

In view of the above described surveys, tradeoff studies, and analyses, a revised baseline concept for the sodium-cooled central receiver has been adopted utilizing the TC2F23 Case 2 turbine. During the proposal stage, a turbine having a gross efficiency of 39.50% was assumed. The revised conditions applying to the turbine in Case 2 are compared with the initial values in Table 7-5. Two cycle heat balance diagrams, one applying to the valves wide open, rated pressure condition (116,741 kWe), and the other to maximum guaranteed conditions (112,000 kW) are shown in Figures 7-4 and 7-5, respectively, for the new baseline system. At the maximum guaranteed condition, the gross heat rate is 7918 Btu/kW-h and the boiler feed pump power is 2090 kW. The maximum turbine-generator capability (at the valves wide open, 5% overpressure condition) is estimated to be 122,505 kW with a gross heat rate of 7889 Btu/kW-h and a boiler feed pump power of 2310 kW. Under the latter circumstances, the throttle flow is 101.9 kg/s (808,400 lb/h) with a final feedwater temperature of 239.6°C (463.2°F).
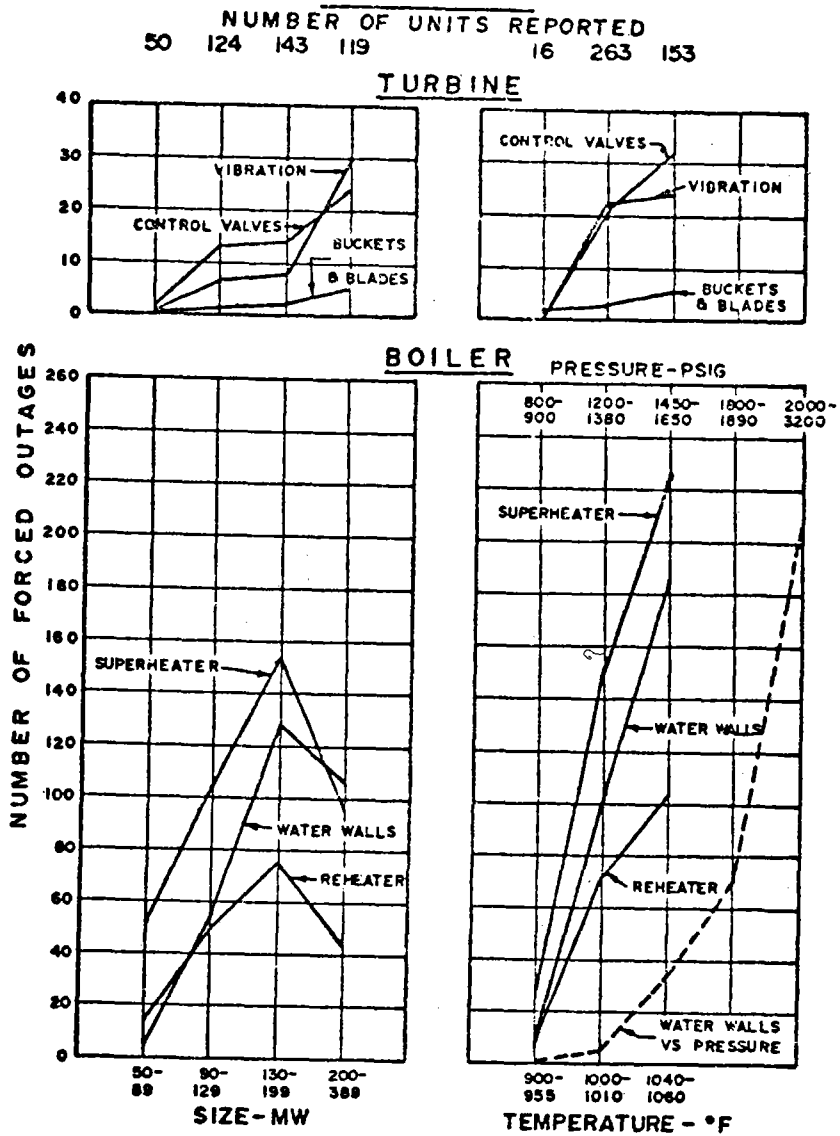
Figure 7-3. Forced-Outage Experience With Turbine and Boiler Components Based on 438 Units Reported in 1964

TABLE 7-5

REVISED BASELINE TURBINE DATA

	Previous Baseline	Revised Baseline
Turbine Type		
Last Stage Blade Length	TC2F-20 in.	TC2F-23 in.
Heater Extractions	5	6
Gross Generator Output		
Daytime	112 MW	112 MW
Night Time	106 MW	106 MW
Net Generator Output		
Daytime	100 MW	100 MW
Nighttime	100 MW	100 MW
Turbine Steam Conditions		
Inlet (Throttle) Steam	13.70 MPa (2000 psia) 538°C (1000°F)	12.51 MPa (1815 psia) 538°C (1000°F)
Reheat Steam	4.83 MPa (700 psia) 538°C (1000°F)	2.95 MPa (428.2 psia) 538°C (1000°F)
Turbine Exhaust Pressure	8.46 kPa (2.5 in. Hg abs)	8.46 kPa (2.0 in. Hg abs)
Final Feedwater Temperature	204.4°C (400°F)	234.2°C (453.6°F)
Gross Turbine Cycle Efficiency	39.50%	43.09%

A P&I diagram covering the reference EPGS system is included as Appendix C in Book 2. Details as to the flow rate, major equipment items, and state points can be found there.

7.5 COMMERCIAL TURBINE PERFORMANCE CHARACTERISTICS

The performance characteristics for the selected Commercial Plant turbine and heat rejection equipment was predicted during Phase I conceptual design in order to define EPGS performance during partial load and off-design turbine exhaust pressures. These data were also developed for use in the Solar Thermal Electric Annual Energy Calculator (STEAEC) computer model.

STEARNS – ROGER HEAT BALANCE NO. DAC-011 4/10/78

ADVANCED CENTRAL RECEIVER
DESIGN STUDY

VALVES WIDE OPEN-RATED PRESSURE
(2 IN. HGA CONDENSER PR.)

GENERATOR KV =	116,741	
FIXED LOSSES =	450	KW
GEN. LOSSES =	1411	KW
HEAT RATE =	7917	BTU

W-Flow-1b/h
P-Pressure-
T-Temp. -°F
H-Enthalpy-

768,400 W   1800 PSIG
1480.1 H   1000 F

670,692 W
4135 P
1000 F
1522.9 H

730 W   2872 W

5037 W

HP   4.57.4   27,019 W
1461.1 H   235.7 P   130.1 H   1384.3 H

IP   LP

1335.2 H

6363 W

2975 W

52.8 P   19.2 P   5.0 P

667,820 W
655.7 F
1335.2 H

3% ΔP   6% ΔP   6% ΔP

542,512 W   O W
MAKE-UP

TEP = 1035.4 H
ELEP = 1026.7 H
PCOND = 2.0"Hg

6% ΔP   6% ΔP   3% ΔP

69.1 H
607,296 W
101.1 F

16% ΔP

2 5 6   1200 W

SSR
1364.0 H

1400 W

6142 W

S   P E   180.2 H

58,559 W / 1335.2 H   29,835 W / 1452.4 H   30,901 W / 1384.3 H   135,444 W / 1293.3 H   35,675 W / 1207.2 H   20,371 W / 1117.2 H

768,400 W
440.6 H
458.3 F

445.6 P
-3F TD
10F DC

390.5 F
367.5 H

221.6 P
0F TD
10F DC

345.1 F
320.1 H

126.2 P
0F TD
10F DC

285.5 F
259.1 H

49.7 P
247.8 H
220.6 F

217.5 F
185.7 H

18.0 P
5F TD
10F DC   194.6 F   112.5 H

4.7 P
5F TD
10F DC

103.9 F
71.9 H

400.5 F
375.8 H

355.1 F
327.2 H

295.5 F
265.2 H

2265 P

164.6 F
132.6 H

113.9 F
81.9 H

η=75%
KW=2090

GROSS HEAT RATE = (768,400 (1480.1 - 440.6) + 667,820 (1523.0 - 3335.2)) / 116,741
= 7917 BTU/KWH

Figure 7-4.   Valves Wide Open, Rated Pressure
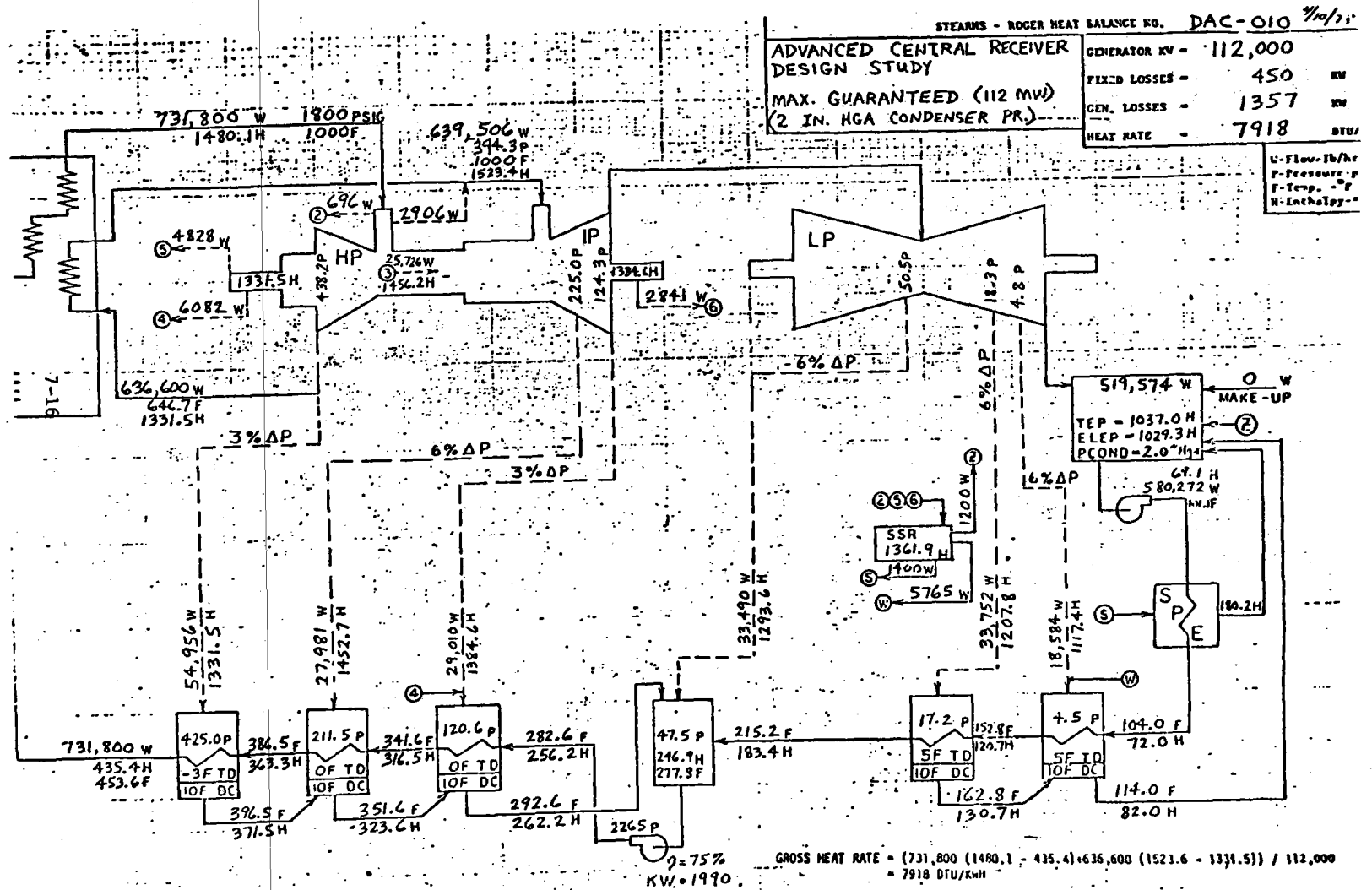
Figure 7-5.   Maximum Guaranteed Performance
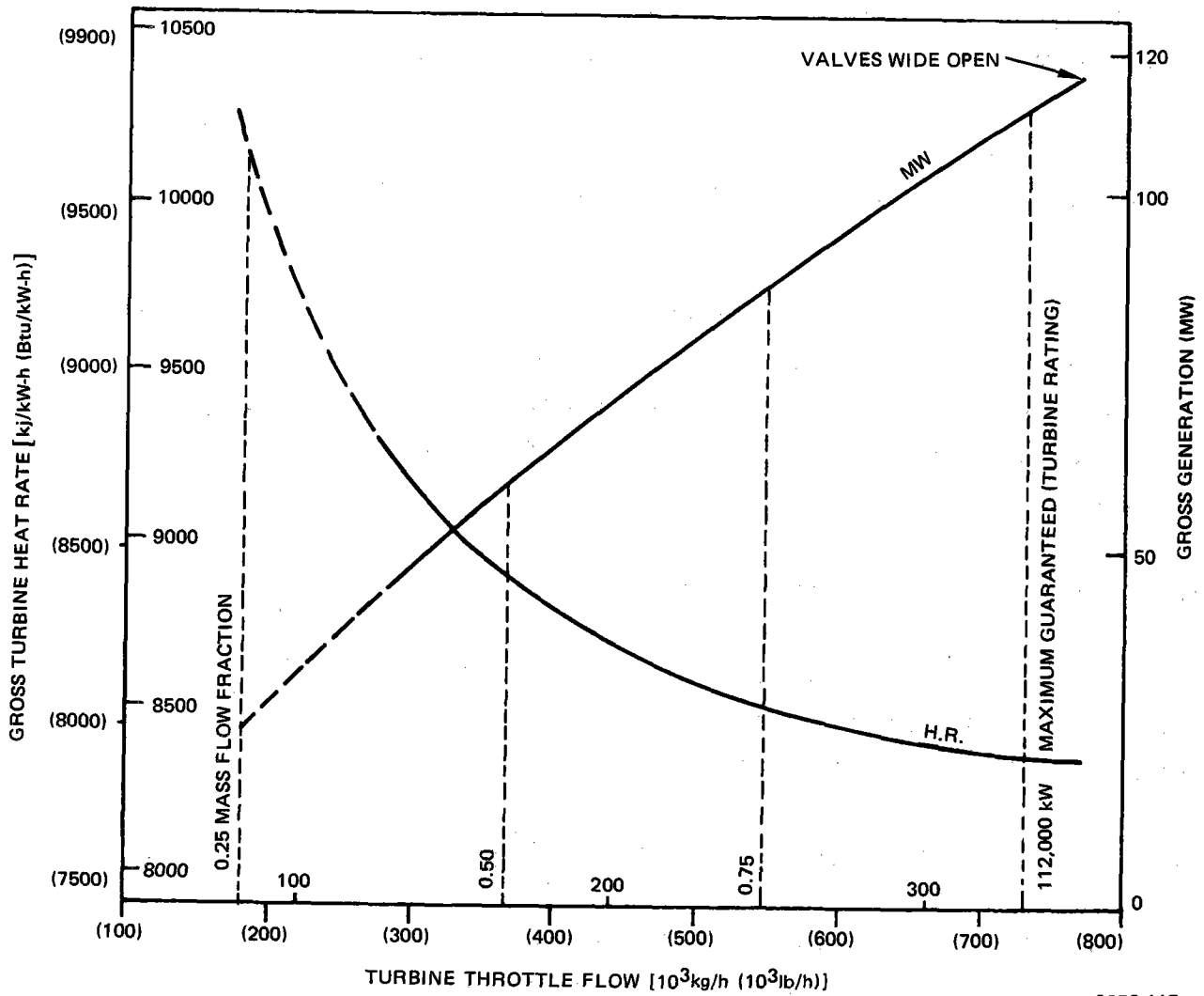
Figure 7-6.   Predicted Turbine Performance

The baseline heat balance for the selected Commercial Plant turbine cycle is shown in Figure 7-5.

7.5.1 Gross Turbine Heat Rate and Gross Generation vs Turbine Throttle Flow

Figure 7-6 shows the relationship between turbine heat rate and generation vs turbine throttle flow. These curves are based on a typical General Electric Company 100 MW TC2F-23 turbine rated as 12.4 MPa (1800 psig), $538^{\circ}C$ ($1000^{\circ}F$)/$538^{\circ}C$ ($1000^{\circ}F$) with a six heater cycle.

7.5.2 Condenser Pressure vs Ambient Wet Bulb Temperature and Inlet Water Temperature

Figure 7-7 shows condenser pressure (turbine exhaust pressure) vs ambient wet bulb temperature and inlet water temperature for various heat duties. This predicted condenser performance is based on Heat Exchange Institute Standards for Steam Surface Condensers (6th Edition) and the condenser design criteria noted in the figure.

7.5.3 Exhaust Pressure Correction to Heat Rate

Figure 7-8 shows the predicted change in turbine heat rate for various exhaust pressures and mass flow fractions for a typical 100 MW General Electric TC2F machine with 58.4 cm (23 in.) last stage blades.

7.5.4 Gross EPGS Efficiency vs Wet Bulb Temperature

Table 7-6 shows gross turbine efficiency as a function of wet bulb temperature and mass flow fraction. A plot of these data are shown in Figure 7-9.

7.6 COMMERCIAL TURBINE OPERATIONAL CHARACTERISTICS

An important consideration with respect to the selection of a turbine-generator for a solar application is the turbine operating limitations when constrained to cycling duty. The principal limitation will be the allowable temperature ramp
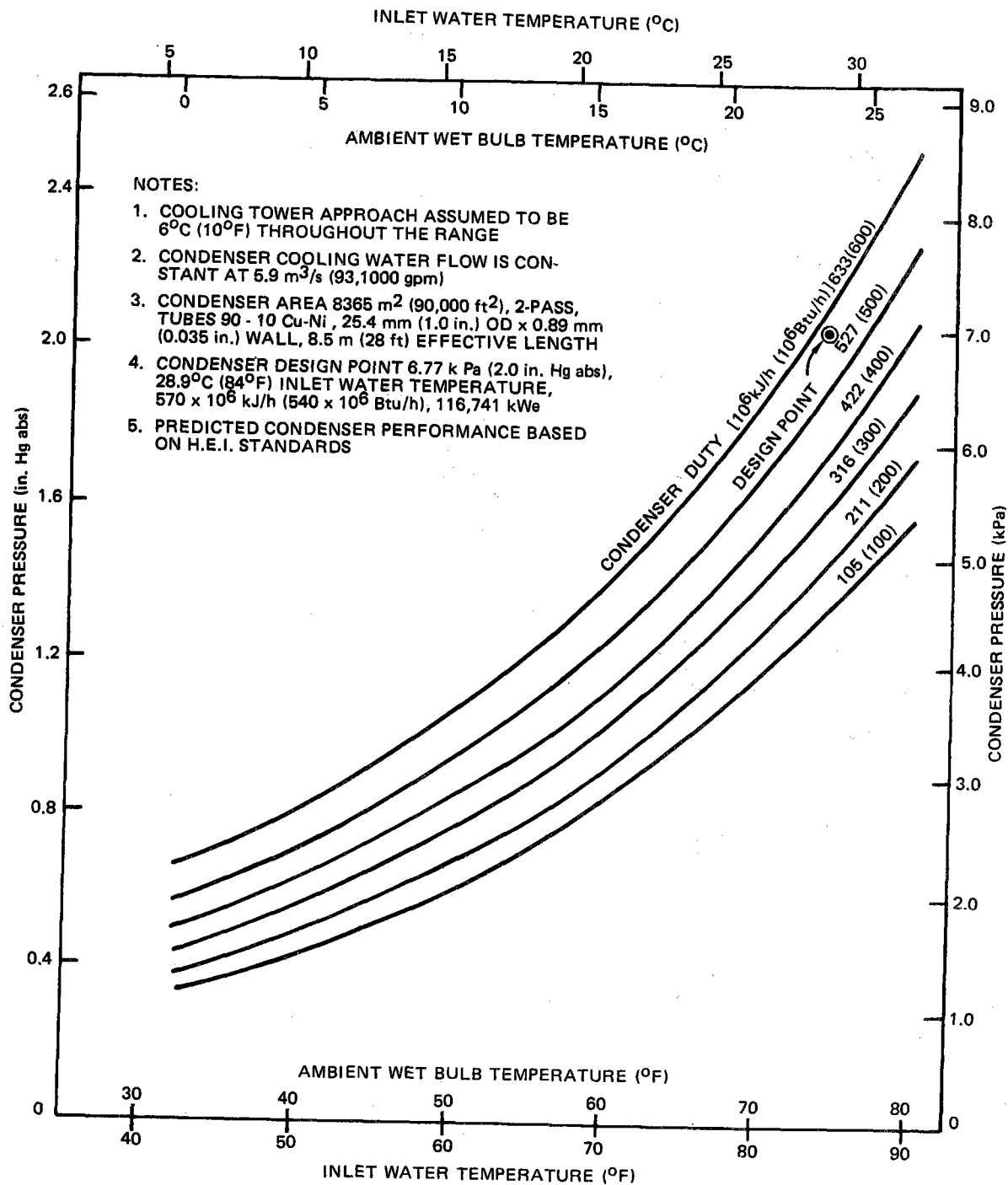
Figure 7-7. Condenser Performance

9272-118
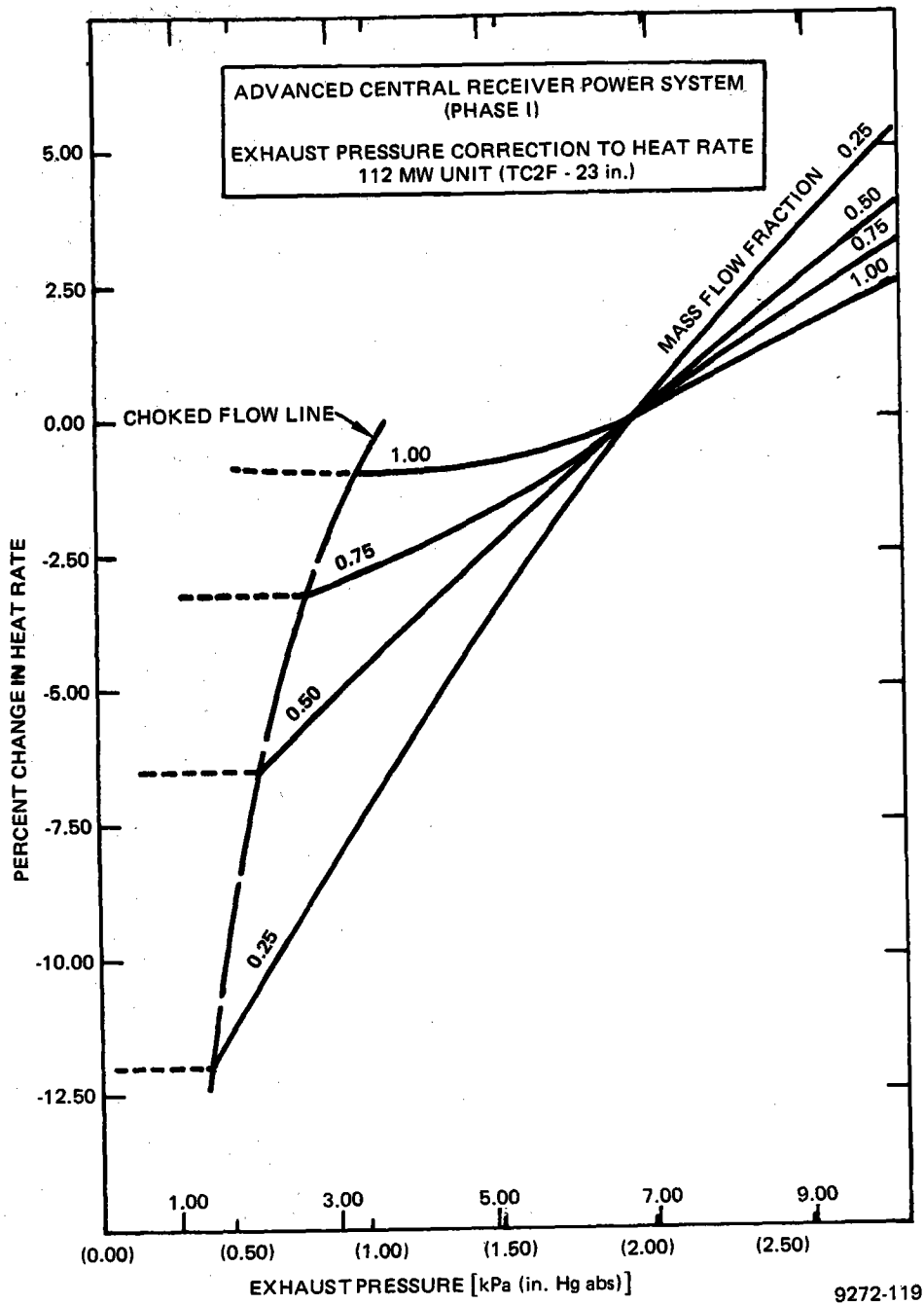
Figure 7-8. Predicted Change in Turbine Heat Rate

TABLE 7-6

GROSS EPGS EFFICIENCY
(Operating From Receiver or From Storage)

Wet Bulb Temperature (°C)	Mass Flow Fraction			
	0.25	0.50	0.75	1.00
0	0.404	0.433	0.437	0.435
5	0.401	0.433	0.437	0.435
10	0.396	0.430	0.436	0.435
15	0.388	0.424	0.434	0.435
20	0.378	0.418	0.431	0.434
25	0.367	0.410	0.424	0.430
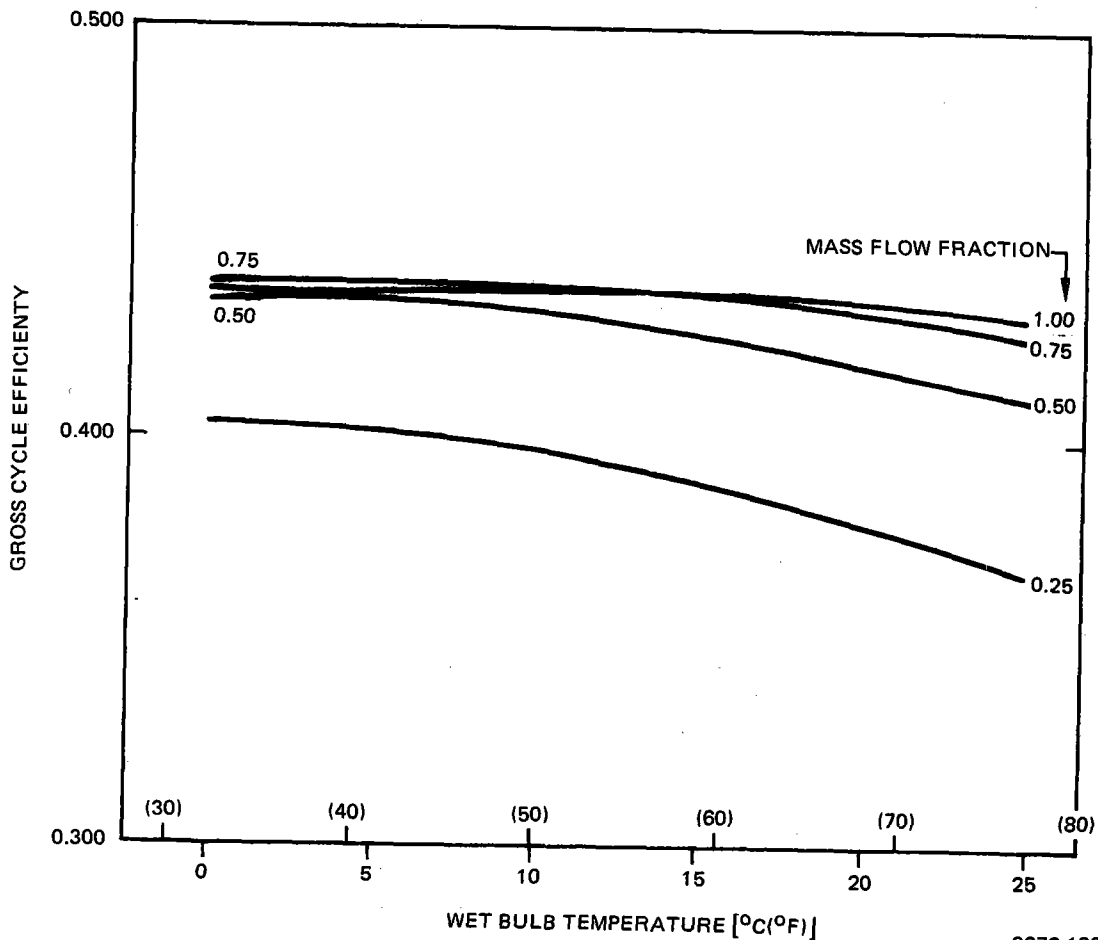
9272-120

Figure 7-9. Gross Cycle Efficiency vs Wet Bulb Temperature for Mass Flow Fractions 1.00, 0.75, 0.50, and 0.25

rate which is in turn determined by the nature of the duty. For the Commercial Plant turbine, it has been assumed that the turbine will cycle daily from no load to full load back to no load. For a 30-year operating life, this corresponds to approximately 10,000 cycle life, or a life expenditure of 0.01% per cycle.

The allowable temperature ramp rate is determined by the turbine manufacturer for a specific turbine and operating conditions. Typical cyclic life curves supplied by General Electric for this project are shown in Figures 7-10 and 7-11. Figure 7-10 indicates the temperature ramp rates for the high-pressure turbine section and Figure 7-11 shows the same for the reheat turbine. Using Figure 7-10 as an example, the 10,000 cycle curve indicates that a step change of ~94°C (170°F) or lower in metal temperature can be made instantaneously. Likewise, a ramp rate of ~161°C/h (290°F/h) or lower will have no effect on turbine life. The allowable temperature changes and ramp rates for the reheat turbine (Figure 7-11) are less than those for the high-pressure turbine (Figure 7-10).

7.6.1 Starting and Loading Procedures

Table 7-7 shows the recommended starting and loading procedures for a typical General Electric 100 MW (nominal) fossil-fired reheat turbine.

Actual starting and loading procedures for the solar turbine would depend on the allowable temperature ramp rate and probably would require longer starting and loading times than those shown in Table 7-7. However, the ability to match steam and metal temperatures (as in the case with a sodium-steam cycle) will have a considerable impact on starting and loading times.

7.6.2 Cooldown Curve

A cooldown curve for a typical fossil high-pressure turbine is depicted in Figure 7-12. The first-stage metal temperature decay curve was supplied by Westinghouse Electric Corp. (Curve CT-23784). The estimated shell metal temperature curve was added to satisfy the required STEAEC data. Generally, when the average shell metal temperature exceeds 400°C (750°F), it is considered a hot start; therefore, a startup following an overnight shutdown would normally be considered a hot start.

VALUES ON CURVES ARE LIFE
EXPENDITURE IN PERCENT PER
CYCLE. VALUES IN PARENTHESIS
ARE TOTAL NUMBER OF CYCLES
TO INITIATE A CRACK
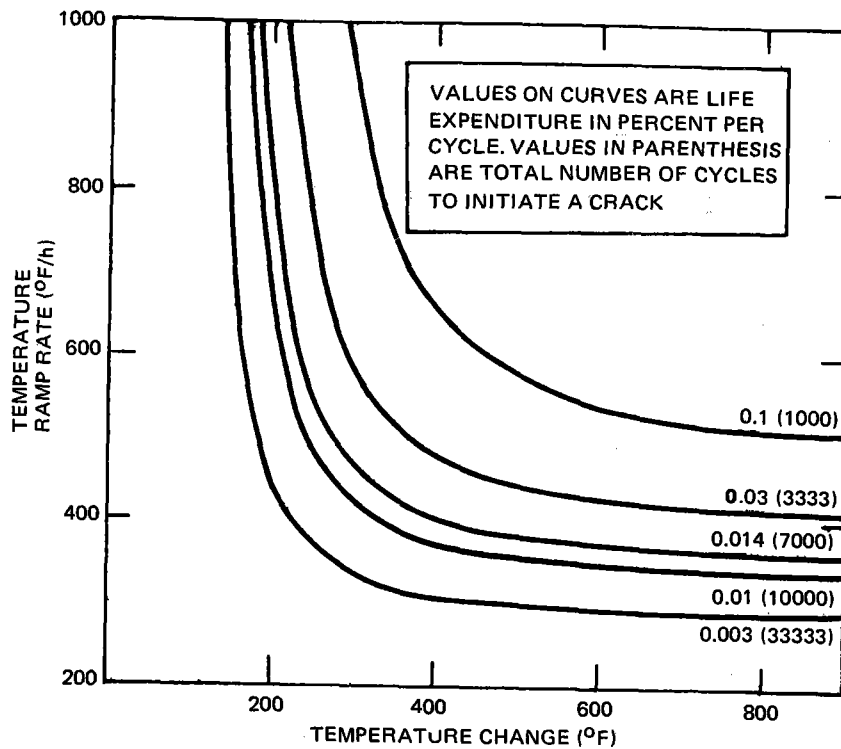
Figure 7-10.   High Pressure — Cyclic Life Curves

VALUES ON CURVES ARE LIFE
EXPENDITURE IN PERCENT PER
CYCLE. VALUES IN PARENTHESIS
ARE TOTAL NUMBER OF CYCLES
TO INITIATE A CRACK.
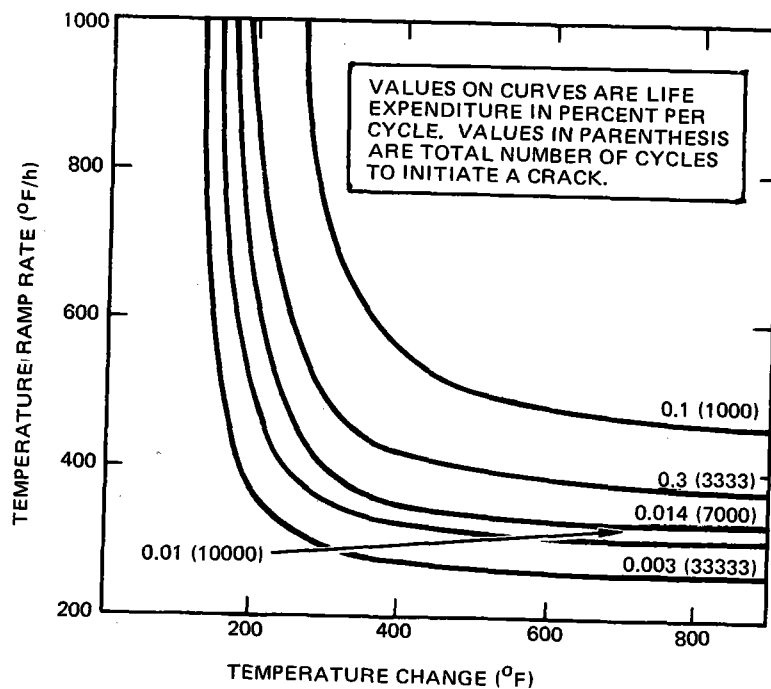
Figure 7-11.   Reheat — Cyclic Life Curves

TABLE 7-7

TYPICAL STARTING AND LOADING PROCEDURE

Type of Start	Cold Start	Warm Start	Hot Start
Initial Pressure	>40% Rated	>40% Rated	>40% Rated
Initial Temperature	371°C (700°F)	371°C (700°F)	Maximum Obtainable
Accelerate to 1000 rpm	(250 rpm/min) 4 min	(250 rpm/min) 4 min	(500 rpm/min) 2 min
Hold at 1000 rpm (Check Vibration)	10 min	10 min	5 min
Accelerate to 3550 rpm	(250 rpm/min) 10 min	(500 rpm/min) 5 min	(500 rpm/min) 5 min
Synchronize Generator and Apply 5 MW Load	—	—	—
Hold at 5 MW (to cool exhaust)	30 min	15 min	Not Applicable
Load Generator to Rated Load	(1/2%/min) 190 min	(1-1/2%/min) 63 min	(3%/min) 33 min
Total Time – Acceleration to Rated Load	244 min (4 h – 4 min)	97 min (1 h – 37 min)	45 min

Source: General Electric Co. (GEK - 27064A)

NOTE:

IF THE UNIT IS TRIPPED WITH THE TEMPERATURE AT A DIFFERENT VALUE THAN THAT GIVEN FOR TIME ZERO, SHIFT THE TIME SCALE SO THAT TIME ZERO STARTS AT THE TEMPERATURE WHEN TRIPPING OCCURRED.
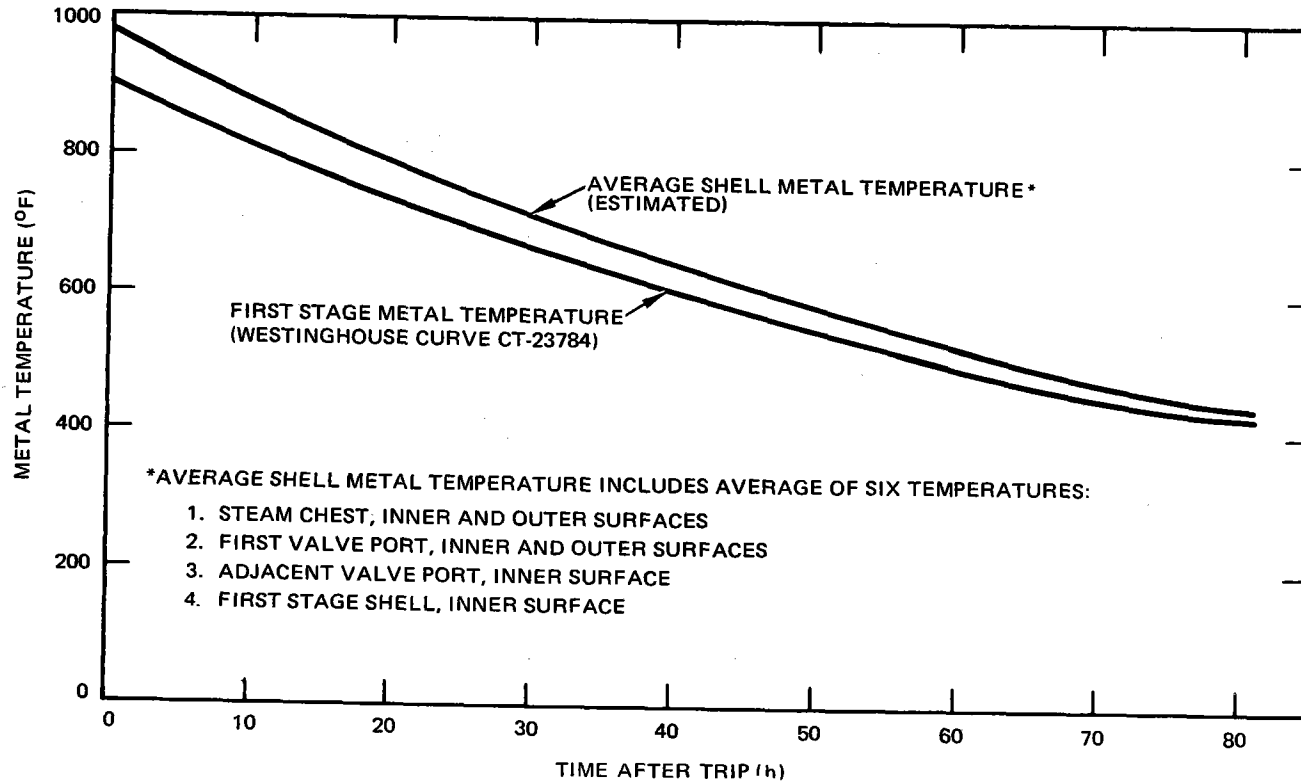
Figure 7-12. Cooldown Time for a Typical Fossil High Pressure Turbine

7.6.3 Variable Pressure Operation

In order to minimize the temperature change in major turbine components during a load reduction, variable pressure operation has been used on many intermediate and peaking load units. Figure 7-13 is a General Electric plot showing the advantage of variable pressure operation on a typical 12.4 MPa (1800 psig), 538°C (1000°F)/538°C (1000°F) unit. Below ~70% load, the main steam pressure is ramped downward from 12.4 MPa (1800 psig) to about 3.1 MPa (450 psig) at 10% load, while main steam and hot reheat temperatures are maintained as high as possible. This procedure results in higher first-stage shell inner metal temperature [400°C (750°F) vs 260°C (500°F) at no load] than would have been obtained using fixed pressure operation at lower loads. This procedure facilitates a faster restart or load increase with minimum loss in cyclic life. It is planned to implement variable pressure operation on this project.
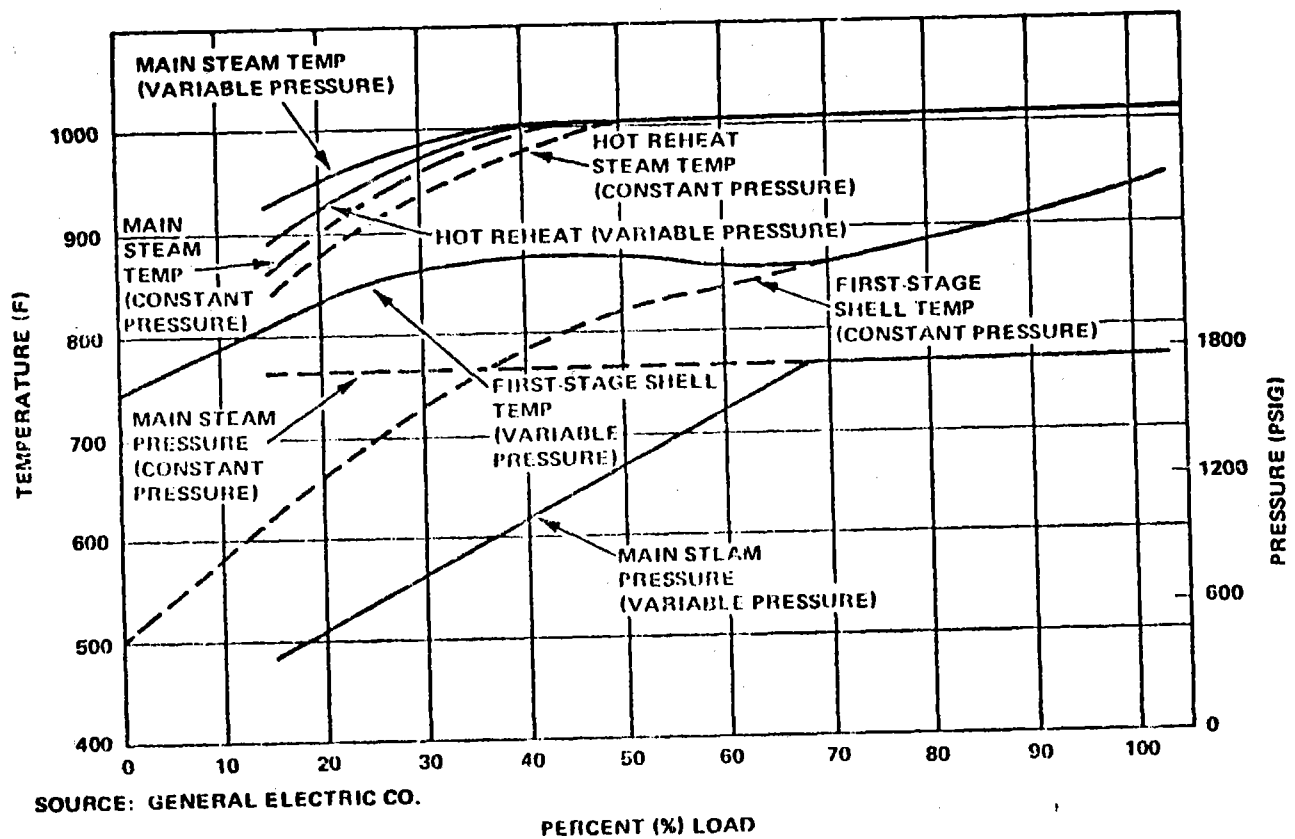
Figure 7-13. Variable Pressure Operation

TABLE 7-3

COMMERCIAL PLANT AUXILIARY
POWER REQUIREMENTS

Component	Receiver Operation Equinox (Design) 100 MW Net (kW)	Thermal Storage Operation 100 MW Net (kW)	Night Standby (kW)	Emergency Power ac (kW)	Emergency Power dc (kW)
Receiver Pump	3,360	-	-	-	-
Steam Generator Pump	560	560	-	-	-
Boiler Feed Pump	2,100	2,100	-	-	-
Hotwell Pump	150	150	140	-	-
Condenser Vacuum Pump	35	35	35	-	-
Condensate Trans Pump	-	-	24	-	-
Service Air Compressor	60	-	-	-	-
Instrument Air Compressor	30	30	30	-	-
Cooling Tower Fans	850	850	-	-	-
Circulation Water Pumps	1,870	1,870	1,030	-	-
Turbine ac Oil Pump	-	-	20	20	20
Lube Oil Filter Pump	1	1	1	-	-
Chemical Pumps	5	5	-	-	-
Motor-Operated Valves	-	-	-	5	-
Raw Water Pump	60	60	20	-	-
Clarified Water Pump	70	-	30	-	-
Water-Treating System	25	25	10	-	-
Jockey Pump (Fire Water)	5	5	5	-	-
Auxiliary Boiler	-	-	-	-	-
Turbine Turning Gear	-	-	5	5	-
Computer	15	15	7	15	-
Miscellaneous dc	-	-	-	-	20
Controls and Computer HVAC	50	50	30	30	-
Plant HVAC	175	175	175	-	-
Sewage Treatment Plant	2	2	2	-	-
Potable Water Pump	5	5	-	-	-
Receiver Tower Elevator	-	-	-	30	-
Heliostats and Controllers	350	-	-	600	600*
Lighting and Miscellaneous ac	100	100	100	30	-
Transformer Losses	450	450	-	-	-
Total	10,328	6,488	1,664	735	640

*Required for up to 30 s to defocus, stow position obtained with a-c emergency power.

7.6.4 Low Load Operation

From a utility viewpoint, it is desirable to operate the turbine-generator (and other major plant equipment) continuously and to avoid daily plant startups and shutdowns normally associated with a solar stand-alone plant. It was also necessary for the storage integration studies to determine the minimum load at which a turbine-generator can operate while connected to the line. This question was discussed with the major utility turbine manufacturers and the limitation seems to be excessive heating of the turbine exhaust hood structure and last stage blading associated with low load operation. It is recommended by both General Electric and Westinghouse that minimum load for normal online operation be 5% of rated load. The exhaust steam temperature at the 5% load point is generally less than 80°C (175°F) which is considered to be a maximum temperature for continuous operation. On many reheat turbine installations, exhaust hood water sprays are used to reduce or control the exhaust hood temperature. However, extended operation at low loads with the exhaust hood sprays in service is not recommended due to moisture erosion of the blades in the last few stages. We recommend therefore, that the minimum turbine load be considered to be about 10% of rated load, at which point exhaust hood sprays should not be required. Also, at ~10% load point, the exhaust hood temperature is 52°C (125°F) or less and the unit is available for rapid load increase.

7.7 AUXILIARY POWER REQUIREMENTS

Table 7-8 presents the auxiliary power requirements for the baseline commercial plant concept with an all-sodium storage system.

The maximum auxiliary power requirements occur at equinox noon when concurrently charging thermal storage and generating rated power. As seen from the table, the major power users are the receiver pump, steam generator pump, boiler feed pump, circulating water pumps, cooling tower fans, and the heliostats and controllers.

NOTE:

ALL 4.16 kV CIRCUIT BREAKERS
ARE 1,200 AMPERE, 250 MVA,

MCC=MOTOR CONTROL CENTER
LC=LOAD CENTER
XFMR=TRANSFORMER

115 kV
FROM
POWER
SYSTEM

115 kV
TO POWER
SYSTEM

CIRCUIT SWITCHER

OCB

STARTUP TRANSFORMER
115-4.16 kV
10.0/13.3/16.6 MVA
OA/FA/FA

MAIN POWER TRANSFORMER
115-13.2 kV
130 MVA FOA

UNIT AUXILIARY
TRANSFORMER
13.2 - 4.16 kV

GENERATOR
135 MVA
0.9 PF
13.8 kV

10.0/13.3/16.6 MVA
OA/FA/FA

4.16 kV BUS NO. 1A

4.16 kV BUS NO. 1B

EMERGENCY
d-c SYSTEM

EMERGENCY
d-c SYSTEM

MOTORS

NUMBER AS REQUIRED

NUMBER AS REQUIRED

EMERGENCY
GENERATOR 1A
625 kVA,
0.8 PF

EMERGENCY
GENERATOR
625 kVA, 0.8 PF

MOTORS

LC XFMR 1C
1250 kVA,
4160-480 V

LC XFMR 1D
1250 kVA,
4160-480 V

LC XFMR 1A
1250 kVA,
4160-480 V

LC XFMR 1B
1250 kVA,
4160-480 V

HELIOSTAT
FIELD

1600A 600A 600A 600A   600A 600A 1600A   1600A 600A 600A 600A   600A 600A 1600A

MOTORS

MOTORS

MOTORS

MOTORS

COOLING TOWER
LOAD CENTER

MCC 1A

MCC 1B

PLANT LOAD CENTER

9272-124

Figure 7-14. Commercial Plant Electrical One Line Diagram

During evening operation on thermal storage steam at rated load, the major auxiliary power users are the steam generator pump, boiler feed pump, cooling tower fans, and circulating water pumps.

During nighttime standby, auxiliary power is required for water treatment facilities, turbine turning gear, turbine a-c oil pumps, condenser vacuum pump, plant HVAC, lighting and miscellaneous a-c, and because steam is supplied to the turbine seals, the hot well pump and circulating water pump must also operate.

The heliostats and controllers required the major part of the emergency a-c power in order to move to a stow position in the event of a power loss. The d-c power required is currently identified as required to defocus the heliostats in the period between a power loss and the availability of the emergency a-c diesel generators. Rapid defocus is required to avoid overheating of the receiver panels.

7.8 EPGS ELECTRICAL SYSTEMS

7.8.1 Main Electrical System

The generator will be connected by isolated phase bus to the unit auxiliary transformer, surge protection, and voltage transformer cubicle, and the main power transformer, as shown in Figure 7-14, which is the electrical one-line diagram for the Commercial Plant.

The main power transformer will step up generator voltage to the voltage required by the power transmission system. For the purpose of this report, the transmission system was assumed to be 115 mV. The main power transformer will be rated 115-13.2 kV, 120 MVA, FOA. Transformer temperature rise will be reduced based on ambient temperature if ambient temperature exceeds 40°C. The 115 kV winding will be wye-grounded; the 13.2 kV winding will be delta.

The main power transformer will be connected to the transmission system by an overhead line or underground cable, oil circuit breaker, and disconnecting switches. The oil circuit breaker would be rated 115 kV, 1,200 A. The disconnecting switches

will be 115 mV, 1,200 A, 3-pole gang operated. The switches will be mounted on a steel structure. The 115-kV switching equipment will be as required by the utility.

The startup transformer will be connected to the transmission system by either an overhead line or underground cable and a circuit switcher. The circuit switcher will be rated 115 kV, 1,200 A. The startup transformer supply and switching equipment will be as required by the utility.

7.8.2 Auxiliary Systems

Auxiliary power will normally be supplied by the unit auxiliary transformer which will be rated 13,200-4, 160 V, 10.0/13.8/16.6 MVA, OA/FA/FA. Transformer temperature rise will be reduced based on ambient temperature if ambient exceeds 40°C. The primary will be connected delta. The secondary will be wye resistance-grounded. The unit auxiliary transformer will be connected to the generator isolated phase bus. The secondary of the transformer will feed two bus sections of metal-clad switchgear, operating at 4,160 V. The connection to the 4,160 V bus will be nonsegregated phase bus.

Startup power will be supplied from the transmission system by the startup transformer. The transformer will normally supply all auxiliary power when the generator is not operating. In addition, the transformer will be available for emergency service and to supply auxiliary power if the unit auxiliary transformer is not available (due to failure). The startup transformer will be rated 115 mV, 416 kV, 10.0/13.8/16.6 MVA, OA/FA/FA. The primary will be grounded wye, the secondary resistance-grounded wye. The transformer will have a tertiary. The final primary voltage will be determined by available transmission voltages. The transformer will be 550 mV BIL, and will be provided with surge arresters. Transformer temperature rise will be reduced based on ambient temperature if ambient exceeds 40°C.

Two bus sections of 4,160 V switchgear were selected to obtain greater reliability and substantially the same cost as a single bus section. The larger breaker required for a single bus section costs about twice as much as the smaller breakers required for two bus sections.

All motors larger than 200 hp will be served directly from the 4,160 V buses. Motors larger than 100 hp up to 200 hp will be served from load center circuit breakers. Where reversing motors are required, these will be served by motor control center. Motors of 100 hp and less will be served by motor control centers.

The plant load center (1A and 1B) will be double-ended with two 4,160-480 V, three-phase, 1250 kVA silicone oil-filled or dry-type transformers. The secondary main breakers will be 600 V, 1,600-A drawout power circuit breakers. A 600 V, 800-A drawout circuit breaker will be provided for the bus tie. Feeder circuit breakers will be 600 V, 600-A drawout power circuit breakers. The plant load center will be located indoors.

The cooling tower load center will be double-ended with two 4,160-480 V, three-phase, 1,250 kVA oil-filled transformers. The secondary main breakers will be 600 V, 1,600-A drawout power circuit breakers. A 600 V, 800-A drawout power circuit breaker will be provided for the bus tie. The feeder assembly will be a motor control center. The starters for cooling tower fans will be circuit-breaker combination, reversing (if reversing is required). Molded case breakers will supply lighting transformers and miscellaneous services. The cooling tower load center transformers will be located outdoors. The switchgear and motor control centers will be located indoors.

Two motor control centers will be served by the plant load centers, one from each bus section. Circuit-breaker combination starters will be provided for motors. Molded case breakers will be provided for lighting transformers, battery chargers, and miscellaneous service.

7.8.3 Emergency Generator

Two 500-kW emergency power diesel engine generators will provide a-c power for safe shutdown and emergency service. The generators will each be rated 625 kVA, 80% power factor, 4,160 V. Each generator will be connected to one of the 4,160 V bus sections by power cable. The diesels will be automatic starting.

7.8.4 Heliostat Field Feeders

The heliostat field will be served by four 4,160 V feeders, pad-mount transformers rated 4,160/240 V will supply the heliostat field. The feeders will be direct-burial power cable, with concrete cover. The number, size, and location of transformers will be defined under the Collector Subsystem.

7.8.5 Direct Current System

The direct current (d-c) system for the commercial plant will consist of a battery, two battery chargers, distribution panels, and two inverters. The battery will be a 60-cell lead acid, 400 A-h, pasted plate type. The battery chargers will be automatically regulated, 125 V dc float, 140 V dc-equalizing charge, 460 V ac supply. A main distribution panel will supply all loads over 100 A. There will be two small distribution panels. The small distribution panels will supply all loads of <100 A. All distribution panels will use switches and fuses. Two 15-kVA inverters will provide supply critical control requiring 120 or 208 V ac.

In addition to the standard plant d-c system, it is a requirement that emergency power for heliostat slewing be supplied immediately following loss of a-c power. A d-c/a-c inverter system is currently proposed to handle the emergency power requirements in the period between a power loss and the availability of the emergency a-c diesel generators. Alternate methods of supplying this interim emergency power will be investigated in Phase II of this program.

8.0 MASTER CONTROL SUBSYSTEM

8.1 REQUIREMENTS

The preliminary requirements for the Master Control Subsystem (MCS) for the Advanced System have been synthesized from analysis of the problem at hand; from Sandia Document SAND77-8035, October 1977 (and subsequent discussions); from Enclosure VIII, Attachment 5, Section 4 of RFP ET-78-R-03-1887, 10 MWe Solar Thermal Central Receiver Pilot Plant; several papers and articles, most notably Myers and Shultz, "A Computer Based Design of a Power Plant Control Center," IEE Transaction on Nuclear Science, Vol. NS-22, Feb. 1975, and DyLiacco and Bosa "Designing an Effective Man-Machine Interface for Power System Control," 1975 P.I.C.A.' and from discussions with various utility personnel.

The control system design philosophy includes these basic points:

1) MSC shall provide sensing, detection, monitor and control of all system and subsystem parameters necessary to ensure safe and proper operation of the plant.

2) Data display and/or recording shall be provided for those parameters pertinent to evaluation of plant performance, operation and safety.

3) Plant operation shall be essentially automatic with operator override capability provided.

4) Provide independent subsystem control for manual operation should the operator desire.

5) Provide for single console control with easily read displays during both automatic and manual operation.

6) Provide standard, proven, off-the-shelf control practices and simple, well-defined interfaces between MCS and subsystem controls.

7) Eliminate single point failure effects through redundancy where cost effective.

8) Provide supervisory subsystem control; i.e., set points, transfer functions, constants, biases, timing, sequencing.

TABLE 8-1

OPERATING MODE TRANSITION MATRIX

Transition

To ——→

From ↓

From \ To	Normal Solar	Low Solar	Intermittent Cloud	Extended	Thermal Storage Charge	Fully Charged Thermal Storage	Hot Shutdown	Cold Shutdown	Thermal Storage Hot Standby	Receiver Recirculation
Normal Solar		X			X	X	X		✓	
Low Solar	X		X	X						
Intermittent Cloud		X		X	X					
Extended		X	X				X			✓
Thermal Storage Charge	X		X				X	X	✓	
Fully Charged Thermal Storage		X	X				X		✓	
Hot Shutdown (TS Steam)				X	X			X	✓	✓
Hot Shutdown (Receiver Steam)	X				X	X		X		✓
Cold Shutdown (TS Steam Available)				X	X		X			
Cold Shutdown (Receiver Steam Only)	X				X		X			

X Possible transition
✓ Possible alternate condition

The duties of the MCS are:

1) Mode management - coordinated control
2) Integration of the independent subsystems for single operator, single console control
3) Acquire, manipulate, display, and record important plant data.

These are essentially the duties assigned to the MCS in the water-steam solar plant. However, the mode management is not as complex. The reasons for this lie in the fundamental control differences between the water-steam and the sodium plants, namely:

1) The sodium plant has series storage which:
   a) Effectively isolates the steam turbine from solar transients
   b) Eliminates the plant mode change duties of MCS except for startup and shutdown
   c) Since there is a single source and quality of steam, eliminates the need for MCS to manage an admission steam path
   d) Permits turbine response to grid demand changes without involving the receiver.

Table 8-1 indicates the various plant operating modes for a water steam plant. Each "X" on the chart indicates a transition from mode to mode that the control system must be capable of handling with MCS management. A mode change may involve changing the receiver operating point and control dynamics, changing the turbine from single to double steam input, varying the thermal storage operations. These changes can be required singly or in combinations. The MCS for a water-steam plant therefore has a large mode change repetoire for reaction to the sun brightness situation. The coordination and management of the subsystems involve much manipulation of subsystem controller set points, transfer function constants, and discrete signals for valve openings and closings, etc.

In the sodium system, the steam conditions are essentially decoupled from the solar conditions by the series storage. On the other hand, all plant energy

passes through the storage. While the steam reaction to the solar conditions are minimized, the series storage poses some new duties for MCS. Table 8-2 indicates the MCS subsystem coordination and management required for combinations of sun conditions (high insolation, low insolation), storage conditions (stored energy level high and low), and the demand from the network manager controlling the grid (high demand or low). There are two basic MCS duties that came out of these sets of conditions: management of power input to the system, and management of grid demand. Power input to the system, for a given solar condition, can only be controlled by controlling the number of heliostats that are active. MCS must accomplish this by communicating with the heliostat controllers. Grid demand can be controlled most effectively by giving the network controller the visibility of available plant operating time, computed by MCS, at the power level called for.

TABLE 8-2

MASTER CONTROL SUBSYSTEM COORDINATION AND MANAGEMENT

		Sun	Storage	Grid Demand	MCS Manages
Case 1	High	X	X	X	Power input to avoid over charge
Case 2	High	X	X		Power input to avoid over charge
	Low			X	
Case 3	High	X		X	Grid demand versus storage goals
	Low		X		
Case 4	High	X			Power input to coordinate storage goals
	Low		X	X	
Case 5	High		X	X	Grid demand to avoid under charge
	Low	X			
Case 6	High		X		Power input to avoid over charge
	Low	X		X	
Case 7	High			X	Grid demand to avoid under charge
	Low	X	X		
Case 8	Low	X	X	X	Grid demand to avoid under charge

Subsystem integration consists of the following MCS activities:

1) T-GS
    a) Turbine startup and shutdown in accordance with an optimum life algorithm, automatically and/or operator guidance menu.
    b) Coordinate grid demand signals with turbine throttle and steam generator.
    c) Monitor, display, and alarm appropriate data.

2) Receiver-Storage
    a) Startup and shutdown sequencing of valves, set points, motors, etc.
    b) Emergency sensing and shutdown coordination with collector.
    c) Controller transfer function and set point adjustment as required.
    d) Monitor, display, and alarm appropriate data.

3) Collector
    a) Startup and shutdown sequencing.
    b) Tracking management for modes, time, beam safety and alignment.
    c) Power modulation by partial field tracking.
    d) Emergency sensing, slew, and stow.
    e) Monitor, display, and alarm appropriate data.

4) Beam Characterization System
    a) Select, position, and acquire data for heliostats.
    b) Analyze data for mirror maintenance and beam alignment.
    c) Record and display data as appropriate.

8.2 MASTER CONTROL SUBSYSTEM DESIGN CHARACTERISTICS

8.2.1 Design Considerations

The design of the Master Control Subsystem for the Advanced Central Receiver Solar Power Plant must address objectives of high reliability, cost effectiveness and simplicity. To achieve these objectives the design must incorporate proven
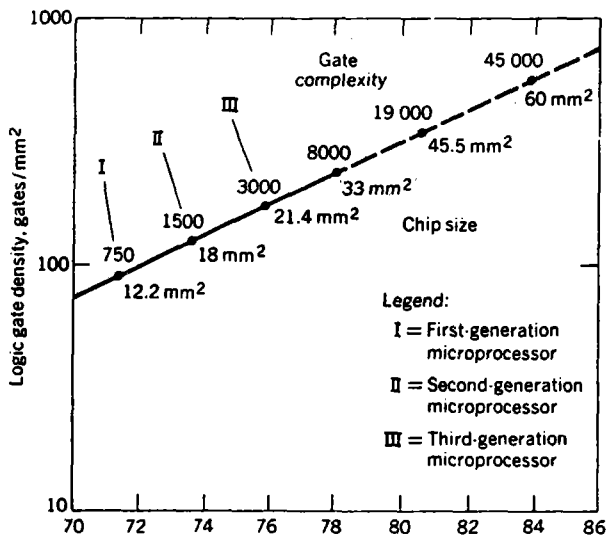
Figure 8-1. Logic Gate Microprocessor
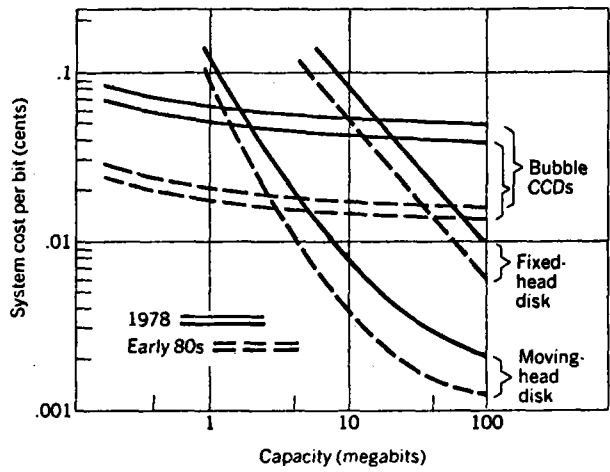
Figure 8-2. Secondary Information Storage Costs
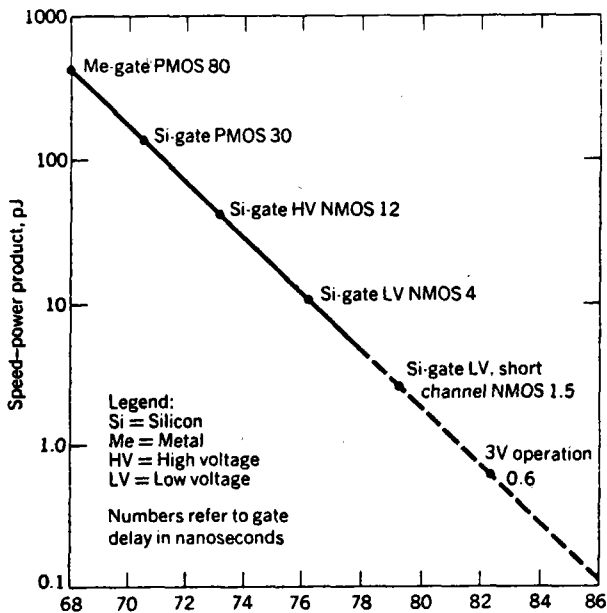
Figure 8-3. Speed Power Consumption Product Variation With Year
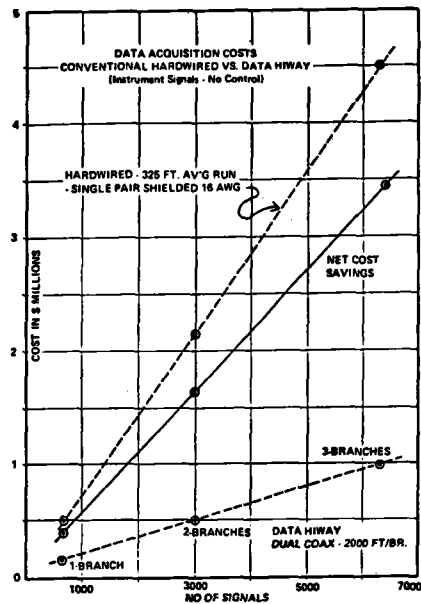
Figure 8-4. Data Acquisition Costs

hardware components; low cost hardware, software and interfaces; and a simple operational approach.

Looking ahead in the mid-1980 time frame when an advanced system would be consummated into a working plant, several opportunities will be available to the power plant control system designers that have a distinct advantage over present power plant control hardware techniques. These advantages include: (1) lower cost electronic products of all kinds, (2) high speed, very reliable information transmission techniques, (3) low power consuming electronic devices, and (4) high density electronic packaging. These opportunities are becoming prominent in all industries today and will see significant improvements and development in the years ahead.

Digital microprocessors today are proliferating in the control market. The computational power of these devices is approaching the minicomputer class at fractions of the cost and considerably smaller in size. Evidence of the present and projected improvements that dramatize the future for these devices is shown in Figures 8-1 through 8-3. A single microprocessor chip in 1980 will contian over two times as many logic gates with an increase of only 37% in size (see Figure 8-1). Secondary information storage costs are expected to decline significantly (Figure 8-2) and the speed and power consumption for these solid state devices is expected to improve dramatically (Figure 8-3).

The serial digital data transmission bus has been growing in popularity in the process industry because of: (1) reduced wiring costs (see Figure 8-4), (2) high immunity to external noise sources, and (3) the increased use of digital computers for process monitor and control applications. Fiber optic techniques are gradually replacing the coaxial and twisted pair serial data transmission buses. This technique retains the attributes of the conventional serial digital information transmission bus but has the capacity to handle transmission speeds approaching the speed of light. With the extremely wide frequency bandwidth of fiber optics (over 200 MHz) many individual signal paths can be accommodated on a single strand.
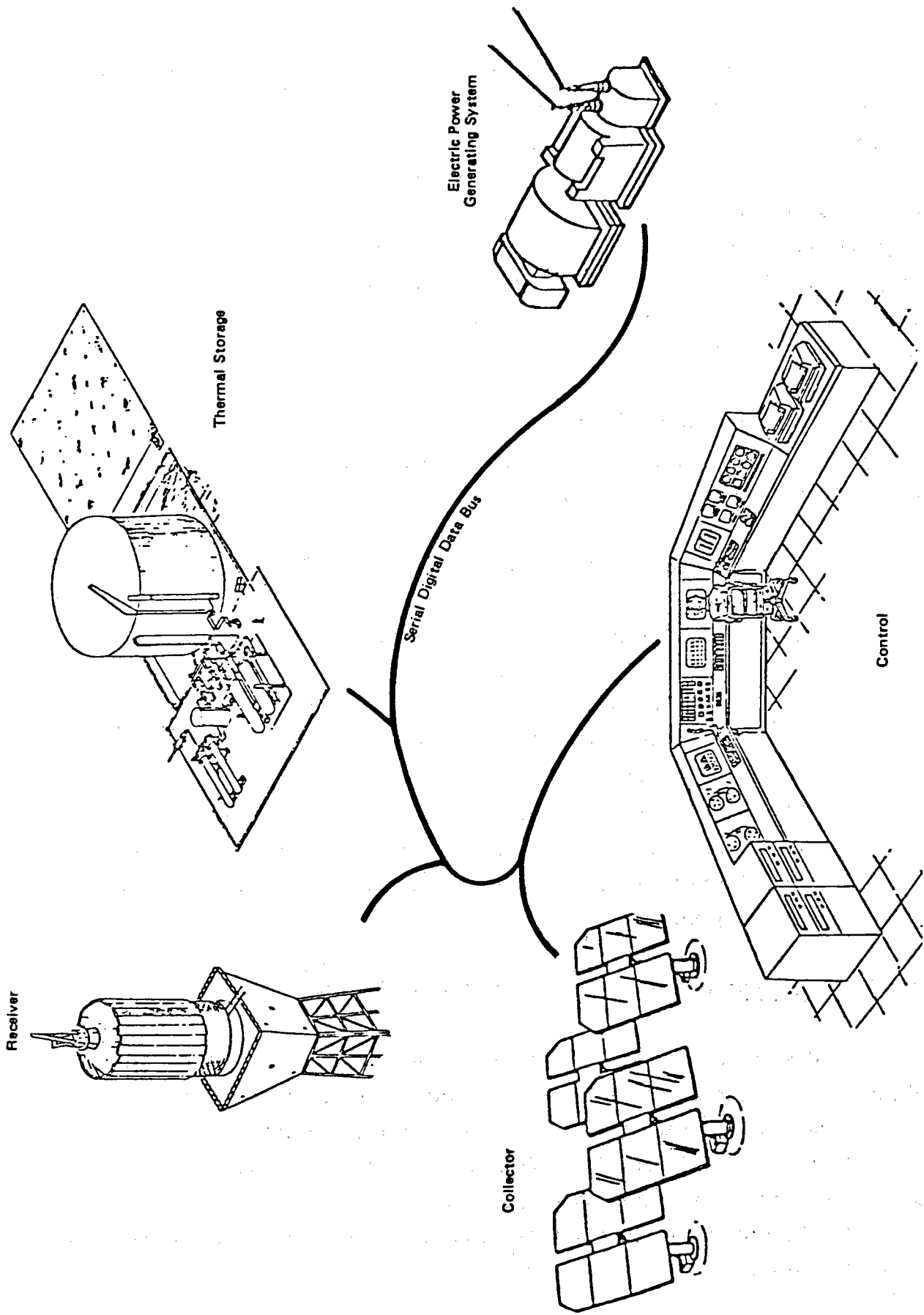
Figure 8-5. Distributed Control Concept

All of these devices and techniques mentioned heretofore utilize solid state integrated circuit technologies almost exclusively. This technology continues to show MTBF for components greater than fifty thousand hours (~5.5 years). Furthermore, the low power requirements to operate these devices coupled with the materials and packaging techniques used have extended the environmental limits of temperature, humidity and shock within which these components will operate. Consequently, sequence programmers, microprocessors, and digital converters do not have to be placed in stringently controlled environments. These devices will operate in many field environments.

All of these advantages have been implemented into the Master Control Design for the Advanced Central Receiver Power Plant Design. This design incorporates the following general features:

1) Distributed digital control of the power plant processes
2) Remotely located controllers
3) Serial redundant digital control and data communications between the control center and the subsystems
4) Single operator for plant and subsystem control and monitoring
5) Control processor terminals used for plant and subsystem control and monitoring
6) Microprocessor based controller hardware used throughout
7) Maximum use of CRT display devices for monitoring plant status
8) Three modes of operation: (1) automatic, (2) semiautomatic, and (3) manual.

8.2.2 Master Control Subsystem Design Commercial 100-MWe System

The Master Control Design for the Advanced Central Receiver Solar Power Plant incorporates a centralized plant control center that links via a serial digital data bus to remote subsystem controllers. An overview of this design concept is shown in Figure 8-5. This design employs a distributed control system concept whereby the individual controller functions are accomplished close to the process while the integrated plant control is performed in the control center.

A vital part of the control system concept is the man-machine interface with control displays located in the control center. At this station the operator monitors and commands the operations of the plant. Programmed command sequences are initiated from the control consoles and plant status and data are monitored, displayed, and recorded here.

The control center is linked to the remote subsystem controllers using a common and redundant serial communications scheme. This scheme will utilize optical isolated fiber optic transmission.

Control-Monitoring System Design

The design of control-monitoring system for the Advanced Central Receiver Solar Power Pilot Plant incorporates an integrated plant control center. This center connects master control and independent subsystem controls to the sub-system controllers, located remotely in the field, by a redundant serial fiber optic transmission scheme.

Features of the plant control center include:

1) Distributed control-monitoring functions with redundant failover capability

2) Single communication bus architecture interfacing all plant control facilities

3) Independent data acquisition and reduction system to accommodate pilot plant experimental instrumentation

4) Automatic and manual safing and protection systems

5) Recording, logging and hard copy capabilities that preserve significant plant operation events

6) Collector and beam characterization subsystems integrated into the plant control concept

7) Time of day, local weather, and grid demand coordination connected to the communications bus.

A block diagram of the plant control hardware is shown in Figure 8-6.

The control-monitoring system design employs a combination of hardware and software to achieve plant monitoring and control functions. Specific control-monitoring functions are distributed within six microprocessing systems that provide: (1) independent subsystem control and monitoring that supports automatic, semi-automatic and manual (cascade) modes of plant operation, and (2) a redundant failover capability for plant control functions to minimize single point failures of computational control hardware and peripherals.

This design approach distributes a common set of interfaces, hardware components, and software design disciplines across the subsystems, at the master control level, maintaining system integrity throughout. Significant cost, operational and benefits implementation are obtained through: (1) development of simpler stand-alone software packages for each subsystem processor in difference to development of software packages for a single processor which are complicated by limited single CPU and peripheral resources that each subsystem task must compete for, (2) use of multiprocessors to provide tailored subsystem throughput capacity for control, display and operator interaction without the need for high performance and costly mini or maxi computer systems, and (3) the adoption of the multiprocessor configuration to minimize system monitor-control failures at the control center interface by providing failover to a redundant "look-alike" system rather than a wire-by-wire large control board with a unique combination of manual control and monitoring appliances.

The control center philosophy assigns an independent processing capability to the subsystems with a reserve capacity to absorb the monitoring and control operations of a companion processor that has failed. The failover techniques and operation are discussed in Section 8.4. Five processors, each configured with memory, arithmetic, and mass storage peripherals, will provide the total capacity to monitor and control the plant operating functions exclusive of experimental data acquisition unique to test and development purposes.
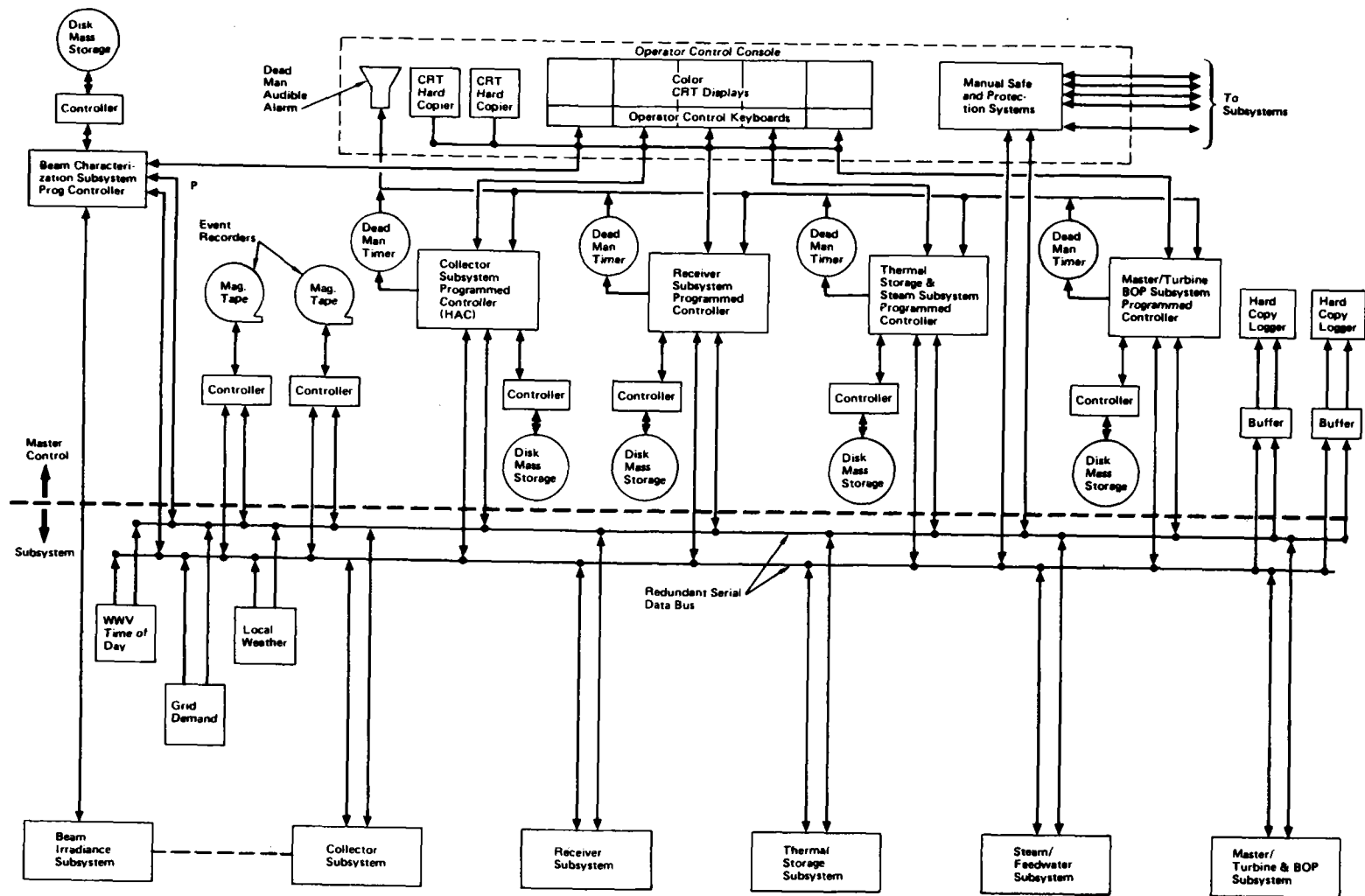
Figure 8-6. Master Control Subsystem — Block Diagram

One of the four processors will be configured with the software modules to control and monitor the operation of the heliostat array. The 100-MW plant which utilizes 14106 heliostats will require this processor, called the Heliostat Array Controller (HAC), to perform the following collector field tasks:

Heliostat Status — This major module will periodically request information about every heliostat in the field and maintain a status data base on a mass storage device (disk). This module can also be called as a subroutine to either store a status change in the data base or retrieve data about heliostat(s) from the disk for the requesting module. The operating mode will be represented as well as the last known azimuth and elevation angle positions.

Emergency Slew — A single command from either the MCS or the operator at the HAC can trigger emergency slew. Emergency slew is a rapid movement of all solar beams focused on the solar receiver away from the solar receiver to a standby position.

Mode Transition — This module will conduct all mode transitions, except for an emergency slew request, and ensure that they are executed without violating beam safety requirements.

Aim Point — This module shall calculate a trajectory of aim points across the heliostat field hemisphere to move these heliostats selected for special moves. The beam safety subroutine will be called to advise this module on avoiding areas where beams are not permitted.

Beam Safety — This module maintains a description of the topography of the heliostat field and surrounding air space where reflected solar beams are permitted and where they are not permitted. It will be necessary for this module to know the heliostat position (x, y, z) and the proposed beam path vector trajectory in order for the module to determine if the reflected beam will pass through a restricted zone.

Calibrate Heliostats — This module interfaces with the beam calibration-alignment. This module will calculate gimbal angles which will result in the selected heliostat hitting an active calibration target. After the calibration target has obtained several measurements of image centroid from several mirror positions, the correction algorithms can be executed and new alignment constraints determined.

Heliostat Reference Locate — If a heliostat or group of heliostats lose their reference points, this module will direct the heliostat(s) to move the shortest distance in order to get a reference update from the absolute encoders on the heliostat. This module will refer to the "status" information for the last known position and the beam safety module for authorization to command the movement.

Data Collection — This module will collect data from heliostats in accordance with several predetermined data collection formats. The collection module will collect data either from the HAC's global data base or request the required information from the heliostats.

Startup — This module will calculate the heliostat field to be used for cold and hot receiver startups. The determination of the requirements for startup will be obtained from data supplied by the receiver programmed monitor-controller.

A second programmed monitor-controller will be assigned to the receiver subsystem. This monitor-controller will perform the following tasks:

Startup Management — This module will determine the status of each receiver panel prior to a startup and solve the algorithms for the optimization of cold and hot receiver startups. Optimization data will be presented to the operator and used by the collector monitor-controller for the selection of the heliostats to be used for startup.

Receiver Shutdown — A module will be required for optimizing shutdown of the receiver to minimize thermal stresses and prevent the solidification of liquid sodium. This module will also provide: (1) set point command changes to the individual panel controllers initiated by the operator should they be required, (2) monitor tracking of panel status, and (3) formatting status change displays for alarm and operator interpretation.

Receiver Steady State Operation — The decoupling of the receiver subsystem from the steam-water and power generation subsystems removes interacting subsystem coordination requirements. Consequently, the steady-state module provides for the monitoring of receiver operating status and provides alarms and data to the operator. This module provides the capability for commanding controller setting changes if required.

Receiver Data Collection — This module acquires monitoring-control measurement and status data and formats these data for use by other monitor-control modules of the master control system.

Receiver Diagnostics — The available time remaining within the programmed controller will continually be filled running diagnostics on programmed controller hardware and interpreting the availability of monitor and control hardware in the field.

A third programmed controller monitors and controls the thermal storage and steam generation subsystems. This element of the power plant is, for the most part, typical of a conventional power plant. The thermal storage and steam generators will use local controllers to maintain steady-state operation. The tasks performed by this unit are:

Energy Management — This module calculates the status for operating the plant based on the available stored energy, the energy requirements to maintain grid demand and operating plan for the day, and the available energy storage replenishment. The data from these computations are formatted and displayed to the operator.

Data Acquisition — Operational data in the form of digitized analog measurements and binary status are collected and formatted for recording, operator display and use by other modules in master control.

Storage-Steam Control — This module provides the capability for the operator to command changes to control settings for the thermal storage and steam generators if required. Alarm and limit tests and display are performed by this module using data obtained from the data acquisition module.

The fourth program controller contains the modules that will coordinate the activities of all the program controllers as well as monitor and control, if required, specified functions of the balance of plant and turbine generator. Support systems (i.e., N_2 argon, compressed air, etc.) will be monitored by this unit. Monitor and control modules executed by the master, turbine, and BOP controller are:

Master Control Coordination — This module will manage the input and output traffic of the other programmed controllers when using the redundant serial data bus or the shared peripherals (i.e., event recorders and hard copy loggers). The plant operations sequencing for automatic operation will be provided in this module.

Master Data Base Manager — A master data base will be stored and updated in the master controller. These data bases will be a composite of the other data bases managed in the other three program controllers. The contents of the master data base will be used for the generation of plant reports and the display of graphic and tabular plant data to the operator.

Plant Report Generator — The generation of plant reports will be accomplished by this module, stored and output on the hardcopy loggers and visual operator display terminals. The report generator will obtain the information for reports from the master data base. Reports will be generated on a time basis or upon demand when requested by the operator.

<u>Redundant Bus Diagnostics</u> — A diagnostic module will be used to test the redundant data bus integrity with the other programmed controllers, shared peripherals, and remote subsystem interfaces. This module will automatically assign the programmed controllers to the functioning serial data bus. The failure of a serial data bus will post an alarm to the operation and the programmed controllers.

<u>Plant Startup</u> — The operator will be required to initiate the master control system startup following a power down incident or when required. A module will be required to initiate the program loading of the other programmed controllers and a functional test of master control when a system startup is required. This module will also report the startup status of master control upon request from the operator.

The fifth programmed controller provides the capability of calibrating the heliostats in the collector field. This controller interfaces to the redundant digital data bus or master control to communicate and transfer information to and from the collector subsystem programmed controller. This controller also interfaces to image digital radiometers remotely located in the field that measure the radiance patterns of the heliostat. A block diagram of this system is shown in Figure 8-7.

The programmed controller in the beam characterization system performs the following tasks:

<u>Data Collection</u> — This module will collect digitized video scanned irradiation data from a target reflection of a heliostat beam along with heliostat position and available light data. These data will be stored in raw form.

<u>Data Reduction and Analyses</u> — Beam reflectivity, irradiance, flux density comparisons, flux density distribution and beam centroid data reduction and analysis are performed by this module. Results of these analyses are used to determine the condition and alignment characteristics of each heliostat. These alignment and reflective characteristics are in turn transmitted to the collector
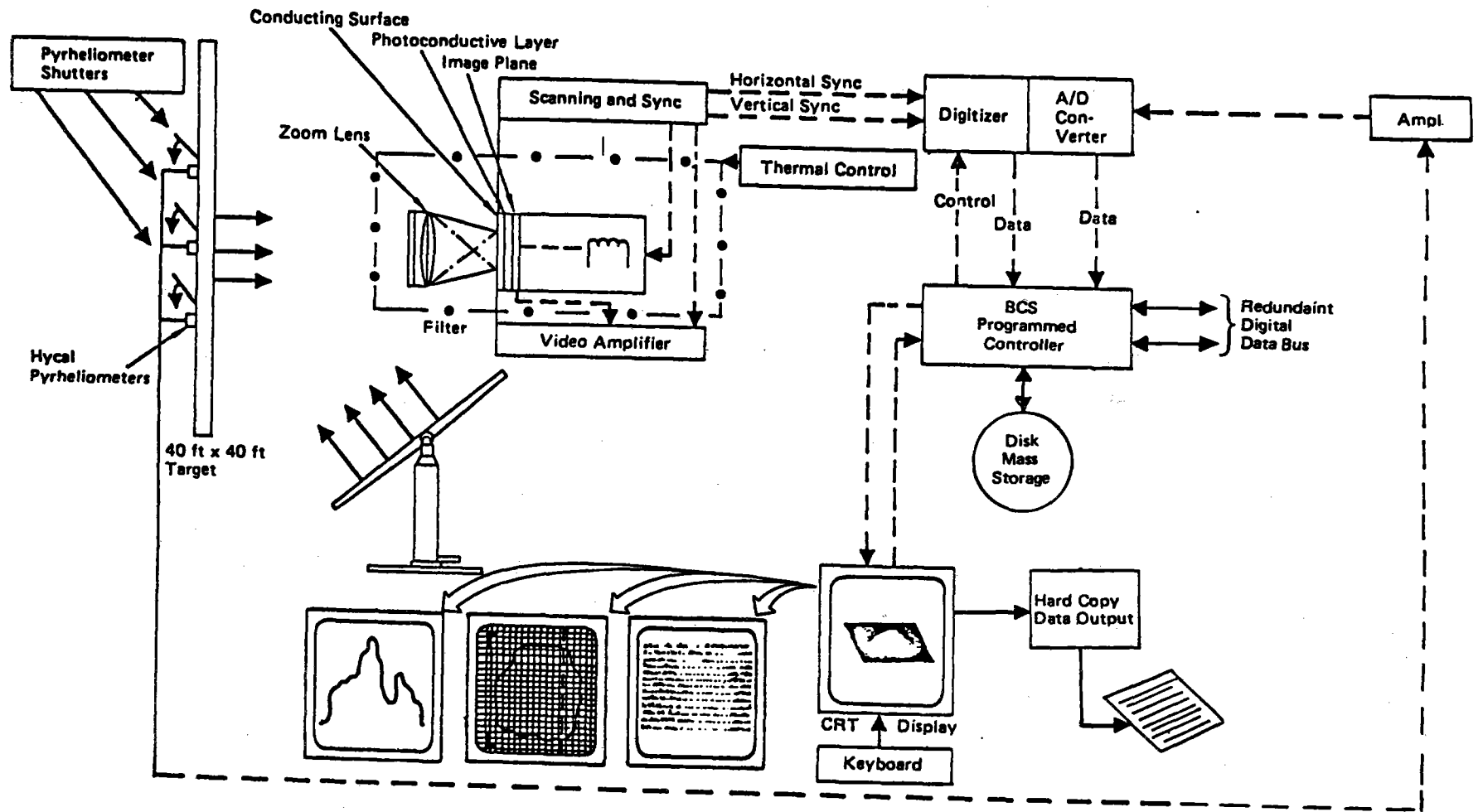
Figure 8-7. Beam Characterization System Block Diagram

subsystem programmed controller where heliostat alignment corrections and maintenance actions are programmed.

Data Display — The display of calibration data for a heliostat will be provided by this module. Tabular and graphical presentations can be commanded from the display terminal. An illustration of the type of display information is shown in Figure 8-8.

Diagnostics — This module will provide diagnostics that evaluate the programmed controller and irradiance system hardware. Hardware status and malfunction reports will be generated in this module.

The master control system design will accommodate the control and monitor elements of the commercial plant. An analysis summary of these parameters for master control is presented in Table 8-3.

8.2.3 Central Control Console Design

The central control console shown in Figure 8-9 is a unified control center designed for a single operator. The operator interfaces with the plant from this console through the use of color CRT displays and function keyboards. Recorders, printers, loggers and control processors support the plant monitoring and control functions. A safing control panel contains the plant emergency controls and the mode controls for switching from automatic to manual or vice versa.

The design of the control console connects four processor units to the common digital data bus and the processor control terminals. A block diagram of this arrangement is presented in Figure 8-5.

Each of the four processor control terminals can communicate with any of the processors. Thus the operator can command and monitor the plant from one CRT keyboard or command and monitor each subsystem through an independent CRT keyboard.

DATE-226 13 43 46 FILE 20
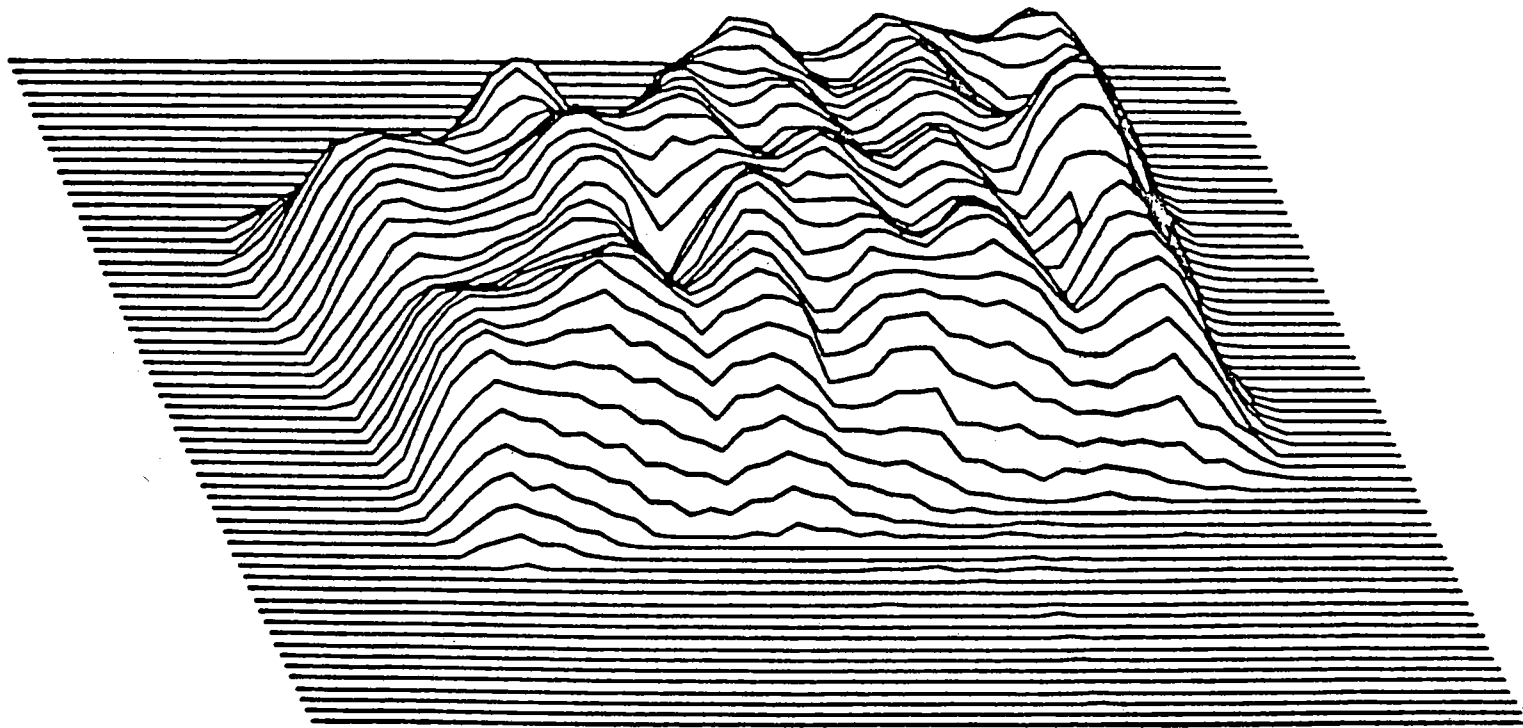
MAX VALUE — 253 MIN VALUE — 69 INTENSITY — 1.623 KWATTS

Figure 8-8. Data Display

Subsystem	Description	Control	Data	Alarm H	Alarm L
Sodium Cooled Receiver	Panel Controller	25	26	26	26
	High Temperature Sodium Tank	0	3	3	2
	Inert Gas and Support Services	2	6	6	2
	Drag Valve	1	1	0	0
	Receiver Pump Motor	3	9	3	2
	Cold Trap	0	1	1	1
	Panel Temperature	0	360	360	360
	Subtotal	31	405	398	392
Thermal Storage	Low Temperature Sodium Tank	0	2	2	2
	Low Temperature Tank Heater	1	4	2	0
	High Temperature Sodium Tank	0	2	2	2
	High Temperature Tank Heater	1	4	2	0
	Inert Gas and Support Services	2	8	4	0
	Subtotal	4	24	12	4
Steam Generator	Sodium Pump	2	13	4	4
	Sodium Mixing Tee	1	1	1	1
	Water-Steam Evaporator	1	4	3	1
	Feedwater Pump	1	1	1	1
	Moisture Separator	1	1	0	0
	Superheater	3	8	2	2
	Superheater Attemperator	1	5	0	0
	Superheater Condenser Bypass	1	1	1	1
	Reheater	1	1	1	1
	Reheater Steam	0	1	1	1
	Attemperator	1	2	1	1
	Reheat Sodium	1	1	1	1
	Inert Gas and Support Services	5	15	11	3
	Subtotal	19	54	27	17
	Total	54	537	437	413

TABLE 8-3

ANALYSIS SUMMARY OF MASTER CONTROL SYSTEM DESIGN
(Sheet 2 of 3)

Subsystem	Description	Control	Data	Alarm	
				H	L
Turbine Generator	Bearings	0	25	25	25
	Steam Chest	0	5	0	0
	Generator Cold Gas	0	1	1	1
	Reheat Steam	0	13	10	10
	Shaft	0	2	0	0
	Surface Temperatures	0	5	5	5
	Hydraulic Fluid	0	4	2	4
	Stator	0	6	6	6
	Generator Bus	0	2	1	1
	Generator Field	0	2	1	1
	Generator Phase	0	3	1	1
	Generator Cooling	1	2	1	0
	High Pressure Exhaust	0	2	1	2
	System Line Voltage	1	1	2	0
	Generator Output (MW)	1	1	0	0
	Lube Oil Cooler	0	1	1	0
	Turbine Speed	0	1	1	1
	Seal Steam	1	1	1	1
	Throttle	1	2	0	0
	Condenser Vacuum	0	1		
	Turbine Oil Trip	0	1	0	1
	Generator Armature (kV)	0	1	1	1
	Line-Generator Voltage Error	0	1	1	1
	Generator Fluid	0	5	5	5
	a-c Power	0	1	1	1
	Intercept Valves	2	4	4	4
	Generator Disconnect	1	2	0	0
	Generator Breaker Status	0	3	0	0
	Exciter System	1	5	1	0
	Pressure Limiting System	1	4	0	0
	Rate Select	3	3	3	3
	Auto Synch.	1	1	0	0
	Alternator Liquid	0	2	1	1
	Total	14	113	74	75

TABLE 8-3

ANALYSIS SUMMARY OF MASTER CONTROL SYSTEM DESIGN
(Sheet 3 of 3)

Subsystem	Description	Control	Data	Alarm	
				H	L
Collector and Beam Charac- terization	Heliostat Azimuth Position	0	14106	0	0
	Heliostat Elevation Position	0	14106	0	0
	Heliostat Controller Status	0	0	0	14106
	Communication Line Status	0	2	0	12
	Communication Line Control	2	0	0	0
	Wind Loading - 1% of Field	0	0	141	0
	Insolation Valve	0	12	0	12
	Heliostat Power Status	0	0	0	55
	Heliostat Power Control	55	0	0	0
	Calibration Camera Position	0	8	8	8
	Calibration Camera Temperature	4	4	4	4
	Remote Sensing Pyrheliometers	0	12	12	12
	Pyrheliometer Shutter	12	12	12	12
	Calibration Camera Zoom Lens	4	12	0	0
	Image Radiometer Power	4	0	0	4
	Total	81	28274	177	14215
	Grand Total	149	28924	688	14695
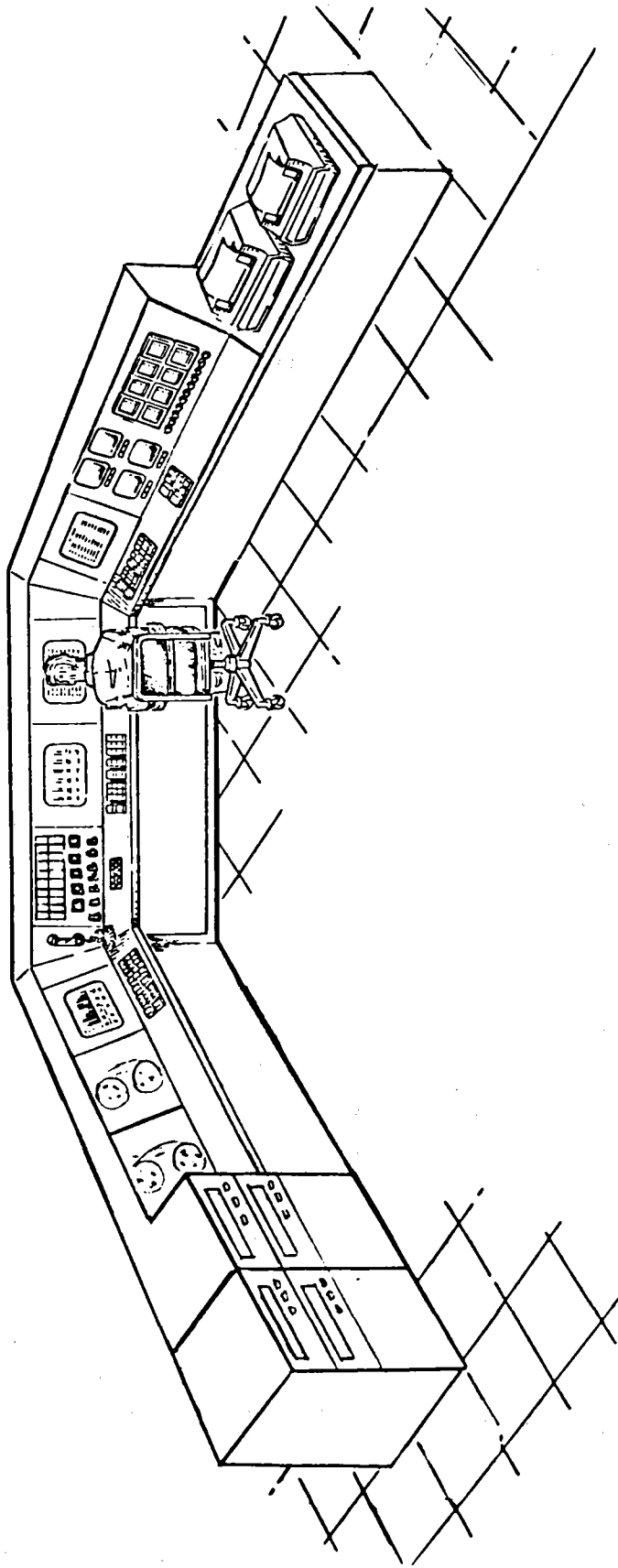
Figure 8-9. Central Control Console

Each processor contains the control and monitoring sequences for the entire plant. These programmed sequences are stored in separate secondary storage media and used by the processor as required. A program sequence exists for each subsystem. In addition, a master control program sequence provides overall plant control and arbitrates the use of perhipherals shared by all processor units.

The duplication of processor units, control units, and shared peripherals in the central control console provides a high degree of redundancy that minimizes single point failures.

8.2.4 <u>Data Communications Design</u>

The common communications link between the central control console and the subsystem controllers consists of a redundant fiber optics cable, or hardwire. A hardwire cable at present provides the most cost effective approach to the communications requirements. However, the high speed parallel transmission characteristics and superior electrical noise immunity available using fiber optics techniques are attractive. These techniques should be cost competitive with the hardwired approach in the 1980 and later time period.

The serial hardwired data link will transmit data between the central control console and subsystem controllers in a digital form. This technique is highly immune to external electrical noise perturbations and forms a totally compatible information interface with the central control console processors and the subsystem controllers.

Addressing schemes will be used to direct the data to the appropriate device and word bit patterns will accompany each transmission for the purpose of diagnosing single and multiple bit transmission errors. All information transfers will be sent over both the primary cable and the backup cable. A transmission line monitor continually tests the lines for loss of signal and, alarms the central control console if this happens. Each device reads both lines and accepts the primary line if found to be error free. Should an error occur or

Serial Digital Data Bus

To/From Plant Control

Redundant Serial Digital Data Bus

To/From Controllers

PID Controller

Interposing Logic

Digital Outputs

Inputs

Analog Outputs

Inputs

Xmtr

Xmtr

M

PID Controller

Xmtr

Xmtr

S
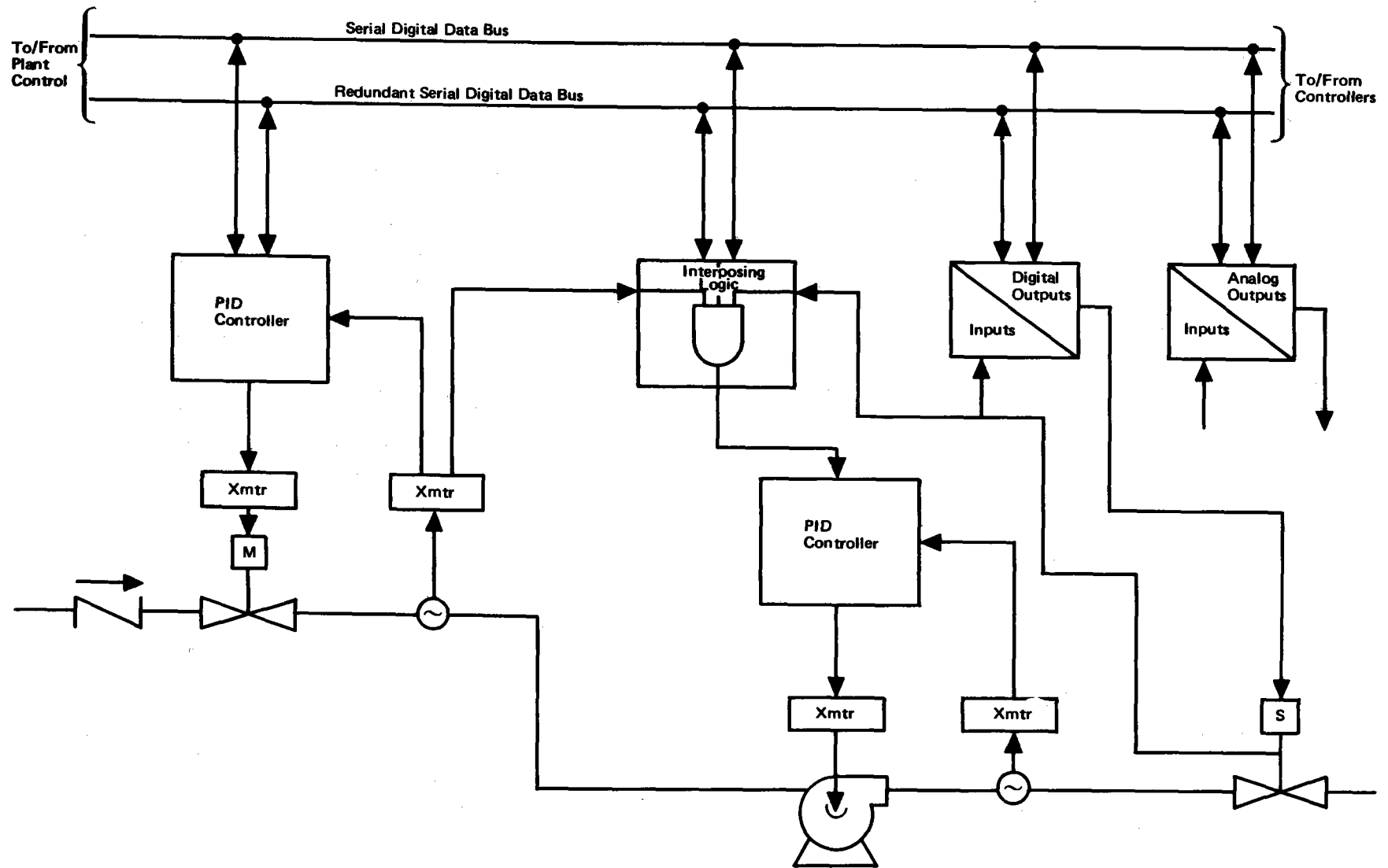
Figure 8-10.   Block Diagram Typical Controller Functions

loss of signal occur on the primary line, the device uses the data from the backup line providing it is error free. Error flags are used to inform the central control that a transmission error has occurred and retransmission of the message is required.

8.2.5 Subsystem Controller Design

Subsystem controllers used by the Advanced Central Receiver Solar Plant will consist of the following types of devices:

1) Proportional Integral Derivative (PID) Controllers
2) Interposing Logic Controllers
3) Discrete Controllers (digital output)
4) Discrete Monitors (digital input)
5) Analog Monitors (analog inputs)
6) Analog Controllers (analog outputs).

An example showing the use of many of these devices is shown in Figure 8-10. All of these devices connect to the serial data bus for communications with the central control console. In turn, they also link to the process monitor or control functions.

The conceptual design of the control system provides for the distribution of computational and logic functions within each controller device. This is implemented through the integration of microprocessors into the hardware. Consequently, the central control processor functions are not complicated with requirements for complex software and the need for very high performance equipment.

In addition to the computation and logic functions of the subsystem controllers, the microprocessor provides capabilities to diagnose the hardware on a time available basis, store data for use by the central control processors, and communicate with the backup controller to provide automatic failover independent of central control.

TABLE 8-4

TYPICAL PROCESSOR STORAGE AND THROUGHPUT SIZING REQUIREMENTS

Programmer Function	Total Storage Requirements		OPS/S Nonfloating Point	OPS/S Floating Point	Instructions Required to Spool (Words) out to Shared Peripherals
	Instructions	Data			
Operating System	12,000	—	—	—	—
Executive Functions	200	100	8,600	—	—
Data Acquisition and Central Control	1,950	15,200	18,325	—	—
Support S/W	10,000	1,000	—	—	—
Man-Machine S/W	3,200	6,720	73,400	—	—
Plant Subsystem Control	2,062	5,255	16,036	3,376	(1,450) 21,750
DDC Applications (60 loops)	3,385	3,852	37,363	4,812	—
On-Line Diagnostics	650	170	—	—	—
	33,447	32,297	143,724	8,188	21,750
Grand Total	65,744		173,662		

TABLE 8-5

SERIAL DIGITAL DATA BUS THROUGHPUT REQUIREMENTS

Functions	No.	Bits-Command (X2 Echo)	Read	Write	Update Rate	Bits/s
Analog Control	100	186	X	X	5	186,000
Discrete Control	125	186	X	X	5	232,500
Analog Monitoring	350	186	X		5	325,500
					Total	744,000

If a plant upset should occur, this hardware will automatically initiate an emergency monitor mode. At this time monitor and control data will be stored for a selected period of time or until the storage memory is full. Following the upset, central control can immediately interrogate these memories and log the data on a printer for analysis.

8.2.6 Results of Throughput Analyses

Analyses have been performed to project the throughput characteristics required for the central processor and the throughput required for the serial data bus. Results of these anlayses are shown in Tables 8-4 and 8-5.

The throughput requirement for the processor was based on analysis using experience estimates for the various operations required. The total number of operations required for the worse case condition (a single processor performing all plant control and subsystem control functions) is estimated to be 173,662 operations per second. To size the processor for cost effective program development and allow for expansion, this number should be multiplied by two. The preliminary estimates for the worst case processor thoroughput would approach 350,000 operations per seocnd.

Table 8-4 shows the preliminary estimate of the storage requirements for a typical central processor. The total resident and nonresident storage is estimated to be approximately 66,000 instructions.

The worst case throughput for the serial digital data bus is shown in Table 8-5. This throughput is based on reading and/or writing to or from each subsystem controller function five times a second. The total throughput estimate for the digital data bus is estimated to be 744 Kbits per second. This rate should be multiplied by two to obtain a throughput that supports a margin of safety for direct digital control applications.

8.2.7 Master Control Availability

The predicted number of failures of the major master control components listed in Table 8-6 are 6.23 per year. However, since all units are interconnected and redundant, there are, at the moment, no single failure items which would cause a system shutdown. Therefore, from a single failure analysis, the availability of the master control subsystem is 1.0. More detailed design and analysis considering multi-point failures will probably reduce this availability, but only slightly.

TABLE 8-6
MASTER CONTROL COMPONENTS LIST

	Number of Units	Failure Rate $(10^{-6}/h)$	MTBF (h)
Terminals (CRT)	4	20.0	50,000
Keyboard	4	4.0	250,000
Processor	4	125.7	8,000
Data Bus	2	27.5	36,364
Console	4	14.4	69,444

8.3 MASTER CONTROL SOFTWARE

The programmed controller inputs and outputs commands, performs information transfers, and provides monitor and control data for the operator and the subsystem. Programmed instructions in the controller are executed in a prescribed sequence to perform tasks associated with the command, communication and data functions. These tasks or modules will be organized in each of the programmed controllers to perform a series of functions needed to monitor and coordinate the control of the subsystems.

The software architecture shown in Figure 8-11 and used by all program controllers and processor systems utilizes an executive and scheduler to control the task priorities and task executions within the multi-asking foreground and background structure of the real time operating system.
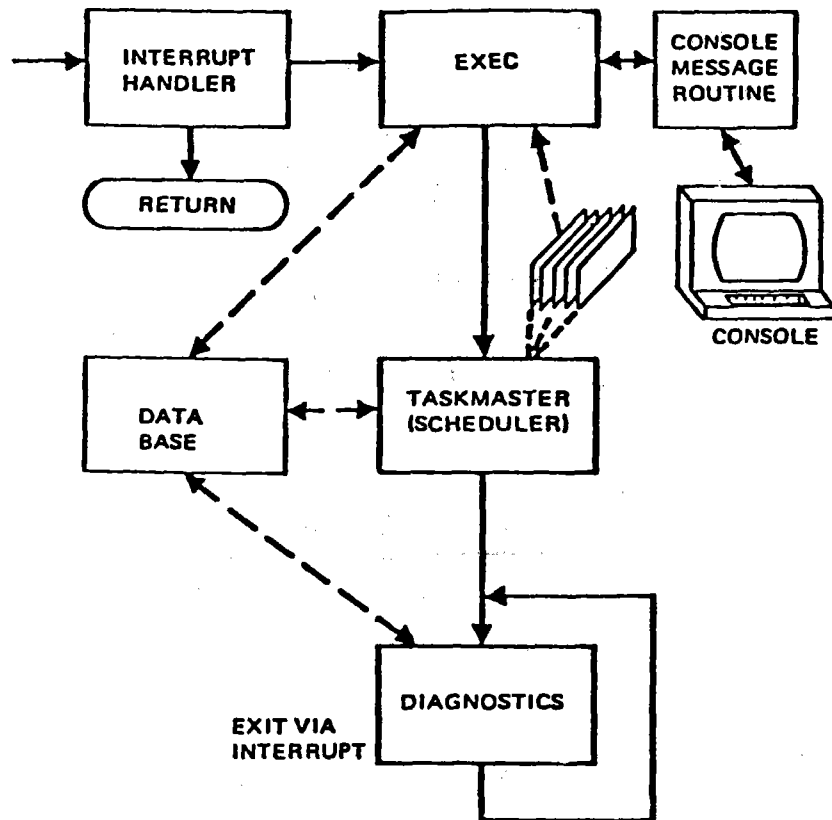
Figure 8-11. Master Control Software Architecture

The multi-asking approach to the software organization for the MCS real-time and nonreal-time software centers on a modular approach to design. The control applications code, data acquisition, and data reduction software are developed in small tasks or modules that run at the required time via a combination of interrupt and timed queues under control of the executive and scheduler. Only the applications software modules that are required to service MCS functions need to be memory resident. All others are stored on a disk mass storage device and called by the executive or scheduler to run when needed. The implementation of this design utilizes a common memory resident data base, shared by all of the applications modules within a program controller. Each module can extract data from this data base or alter and change specified data in the data base that is to be used by other modules. A global data base, composite of all the programmed controllers, is maintained by the programmed controller assigned to the master controller functions.

The application software will be written in Fortran IV. The operator interface with the software will be a conversational high level English language compiler that is easy to interpret. The executive, scheduler, interface device handling modules and those applications that required expediencies not capable in the Fortran compilation will be written in the assembly language code of the computer. This type of programming is expected to be a small percentage of the total programming task.

8.4 MASTER CONTROL OPERATION

Master control operates in any one of three modes from an integrated control console. These modes are:

Manual   - Subsystem Stand-Alone
Programmed-Auto   - Semi-Automatic Operation with Operator Inter-
                      vention required
Automatic   - Programmed Automatic Operation with Operator
                      Monitoring

The control console design provides the man-machine interfaces with which to control the plant and subsystems. Four individual terminals connected to the redundant serial data buses are used to control each of four subsystems independently (i.e., thermal storage, receiver and BOP/T-G, collector, and beam characterization system) or as an integrated plant system using master control.

The operator interface to the control console consists of color CRT displays and function keyboards. The keyboards and displays provide the mechanisms for control monitoring and communicating with the subsystems for automatic and manual modes of plant control.

The hierarchy of control for the semi-auto and automatic modes requires the operator to initiate a control or monitor request from a tabular conversational English language menu via the keyboard on any of the control console CRT displays. This menu consists of all the programmed operations modules that are available

to control, operate, monitor or diagnose the plant and subsystem controllers. Using a light pen or the keyboard, the operator selects the programmed operation module.

The selected module immediately enters into a conversational English language dialogue with the operator to establish the operating criteria for the operation or control the module represents. An example of the type of operator interaction that will take place between the operator and the OCS computer is shown in Figure 8-12. This interaction requires the operator to enter data or answer questions with a yes or no. The plant startup operation machine scenario may require many steps while mode change or requesting data may be from one to several steps.

Each color CRT terminal with keyboard can be configured to monitor and control a subsystem. In this manner the operator can perform the manual control operations of the plant in a cascade manner.

8.4.1 Automatic-Manual Transfer

Transferring from automatic or semi-auto modes of operation to the manual mode or vice-versa can be accomplished by one of the following methods:

Normal Auto-Manual Auto Transition Method
Emergency Auto-Manual Transition Method

Both methods are initiated by the operator via an independent set of back lighted function buttons provided on the control console.

At any time during manual or automatic operation of the plant, the operator can initiate a normal or emergency change of operation mode. Selecting and depressing the function button (manual or automatic) will cause the master processor to display a programmed menu on the CRT display for operations that are valid at the control sequence when the mode change action was initiated. The operator, for the normal mode change, will select the desired entry or exit point from the menu display.

OPERATOR:	RUN SOL-1	342108132124		
COMPUTER:	RECEIVER WARM START PROGRAM			

FACILITY STATUS

PARAMETER	E.U.	VARIATION NORMAL	TOLERANCE
TS-001	795 F	-325 F	+/- 100
TS-002	845 F	-275 F	+/- 100
TS-003	724 PSIA	-726 F	+/- 50
TS-004	849 F	-271 F	+/- 100

CONTROL STATUS

TSV-1	CLOSED
TSV-2	OPEN
TSV-3	CLOSED

ALL SYSTEMS GO

DO YOU WISH TO CHANGE A TOLERANCE VALUE?

OPERATOR:	YES
COMPUTER:	WHICH PARAMETER?
OPERATOR:	TS-003
COMPUTER:	OLD VALUE WAS +/- 50 PSIA
OPERATOR TYPES NEW VALUE:	NEW VALUE IS +/-100
COMPUTER:	DO YOU WISH TO CHANGE A TOLERANCE VALUE?
OPERATOR:	YES
COMPUTER:	WHICH PARAMETER?
OPERATOR:	TS-301
COMPUTER:	INVALID NUMBER
	DO YOU WISH TO CHANGE A TOLERANCE VALUE?

Figure 8-12. Sample Computer Conversational Dialogue

Depressing an "initiate" function button terminates the resident program sequence and directs the master processor to the selected control sequence.

The processor performs permissibility tests and checks for each normal mode request. This step is provided to prevent control upsets in the event a sequence step or information entry is incomplete.

Should a time critical emergency be present, the operator can ignore the CRT displayed menu and depress the emergency button after depressing the mode button. When the programmer detects this input, the program sequence is immediately suspended. Depressing the initiate function button terminates the resident program sequence and displays the appropriate message on the CRT. A time out audible alarm is also triggered at this event.

Along with providing the operator with the menu and conversational dialogue, the processor continuously tests each requested command input for correctness, completeness, and validity. If any of these criteria are not met, the processor acknowledges to the operator the error and initiates the dialogue that leads the operator to change, correct, or complete the request.

Upon completion of the dialogue between the operator and processor and upon initiation of the control sequence program, the operation is under processor control with capability for operator override. Plant monitor data are automatically displayed on the CRT as instructed by the program code or as requested by the operator.

The semi-auto control mode differs from the procedure described here in that the program provides for designated required operator entries into the programmed sequence. Typical of this mode, the processor displays a set of conditions on the CRT from which the operator makes a decision and responds with a command through the keyboard.

The manual mode of subsystem operation is performed by the operator from independent CRT keyboard consoles. Each of these consoles is connected to the data bus and communicates directly with the subsystem controllers.

The operator views the control operation of a subsystem via a CRT display using graphic and tabular data to interpret each control function. An overview display provides the operator with a scenario of all the controller functions for a subsystem. Scanning this color display, the operator quickly picks up color changes that show controllers which functions demand his assistance.

Using a keyboard or light pen entry, the operator can easily address the specific function display and interpret the cause of alarm. This display provides graphic and tabular information to the operator. Changes to the controller operation are accomplsihed via the operator through function keys on the keyboard.

Typical displays, that are designed to provide the operator with the usual appearances of standard controller displays, are shown in Figures 8-13 through 8-16.

8.4.2 Automatic Mode Operation

Automatic plant control operations do not require operator intervention. This mode of plant control will generally be utilized in the steady-state management modes of power generation that are sustained for relatively long periods of time. During this mode of operation, all control decisions are managed automatically by the master processor with the assistance from the subsystem controllers.

Reports and displays of control functions are produced at preprogrammed time intervals or when a programmed event (i.e., alarm limit exceeded, grid demand change, etc.) initiates a display process.

The operator, in this mode, interacts with the CRT displays, requesting a variety of monitor graphic and tabular summaries that state the plant and subsystem operation and control status. The operator overrides the automatic operation through a "request" and "grant" procedure initiated from the master processor function keyboard. This action can be taken to manually control a single function or to change the controlling parameters (i.e., set point, limits,

Plant operating
variables
of one group

Up to eight points in
each group

Deviation

Identifiers

Group number
Title

Operating target
(in analog units
and PIU); set
point (in basic
controller)

Desired deviation
range limits

"?" indicates
valid data
not acquired
due to hiway
(communication)
error

COLORS:
GREEN: Deviations, limits, set point or target
YELLOW: Titles and group numbers
RED: Titles and group numbers when Controller
alarms or overview limits are exceeded.

"R" indicates
controller
in reset

"A" denotes controller
alarm condition.

Figure 8-13.   Overview Display
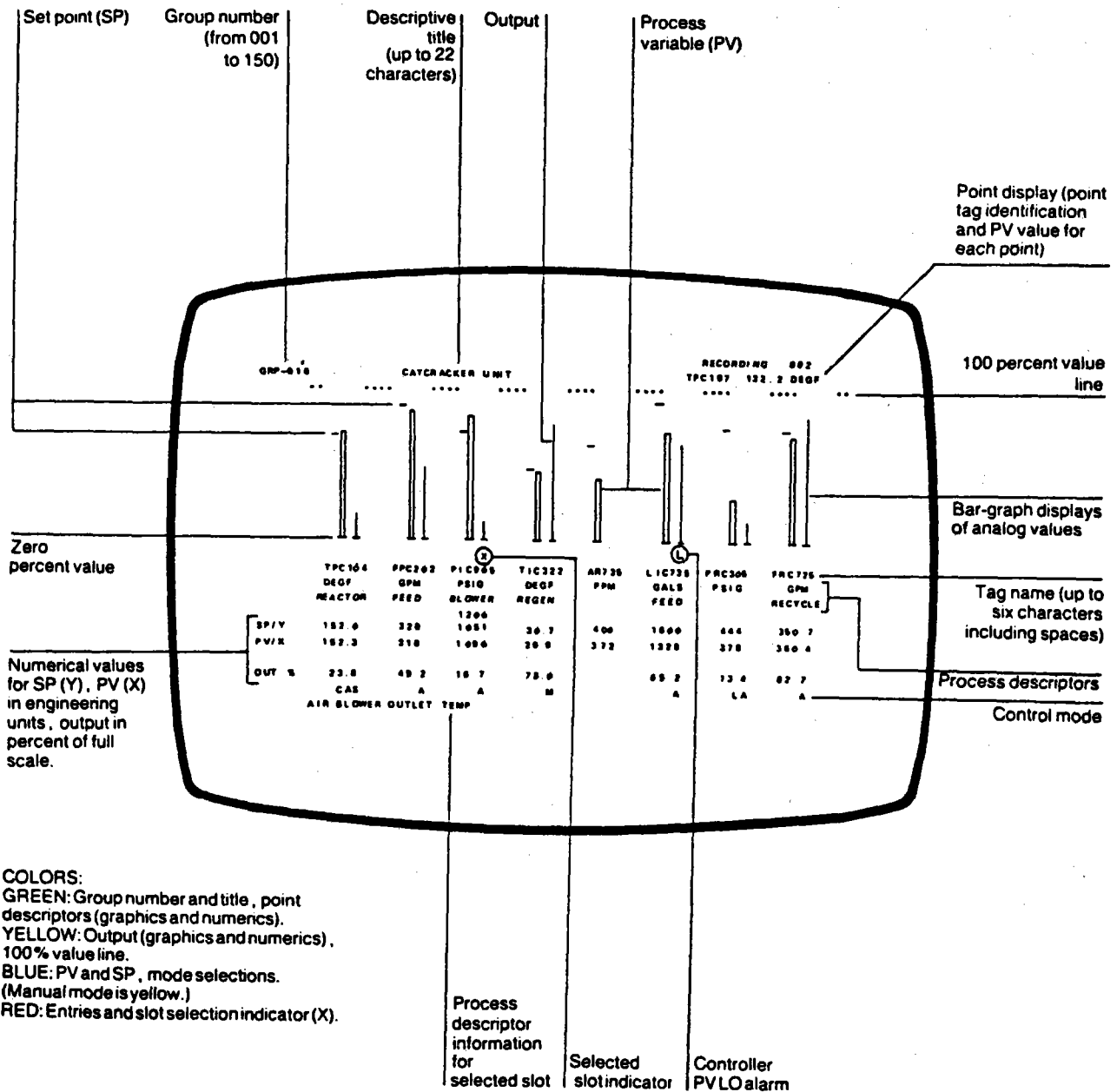
Figure 8-14. Group Display

```
                                          16:12  10/05/77

ACTIVE ALARMS  011        ALARM SUMMARY        PAGE-1


‡ 16:11:27  SFC-1234   DEV HI   INLET FLOW                          A23  011  ‡
‡ 16:10:55  MPA401     HI       COLUMN PRESSURE LIMIT TOP           A10  081  ‡
‡ 16:09:40  TFFC-167   PV LO    PREHEAT FUEL FLOW                   A17  005  ‡
‡ 16:05:20  AUX-55     OFF      REFLUX AUX-55 FEED PUMP             A13  013  ‡
‡ 16:05:12  SEA-003B   OPEN     BREAKER 13B120AC AREA.335 BLDG.22   A32       ‡
‡ 15:45:33  T-22-078   DEV HI   TANK-22 PRESSURE                    A31  088  ‡
‡ 15:19:45  MTI-413    PV HI    TRAY-8 TEMP                         A10  010  ‡
‡ 14:19:06  FC1072C    PV LO    REFLUX FLOW TOWER 2                 A09  015  ‡
‡ 14:02:27  TC1071B    DEV HI   REFLUX TEMP TOWER 2                 A09  015  ‡
‡ 13:55:47  SFC-2345   PV HI    OUTLET FLOW                         A33  024  ‡
‡ 12:33:40  MEA 402    OFF      BASE LEVEL PUMP-1                   A10  081  ‡
```

Figure 8-15. Active Alarm Display

GRP-007   S REBLRB DEETHANIZER   16 12 10/05/77 REC 001

7:00	106.6	650.0	139.1	70.3	103.5		660.6
8:00	106.1	660.9	137.8	68.4	104.1		663.2
9:00	106.2	661.6	136.5	69.0	100.6		658.6
10:00	105.9	661.2	137.0	70.4	104.4		660.9
11:00	106.4	670.7	134.1	71.2	104.0		657.8
12:00	106.1	661.0	136.2	69.3	106.1		660.6
13:00	106.3	671.0	137.5	70.4	107.4		661.7
14:00	105.7	632.1	130.6	71.8	108.5		660.4
15:00	105.0	567.4	137.4	72.1	107.7		662.8
16:00	106.1	556.0	137.2	70.0	108.2		664.2

	10TC-010	10FC-015	10TC-014	10FC-012	10FC-021	10LC-014	10PC-012	10FC-022
	DEGF	GPM	DEGF	KLB-HR A	KLB-HR B	INCHES	PSIG	GPM
	C2--FEED	REFLUX	TRAY 9	60LB STM	60LB STM	RBLR A:B	DEETH TP	DEPRD FD
SP/Y	98.0	675.0	136.0	70.0	100.0	52.2	300.0	665.0
PV/X	106.2	550.3	138.0	70.1	109.0	52.2	330.2	665.2
OUT %	54.1	94.9	70.4	48.6	63.2	74.8	54.0	72.4
	B	COH	COH	CAS	CAS	L(A)	A	A2
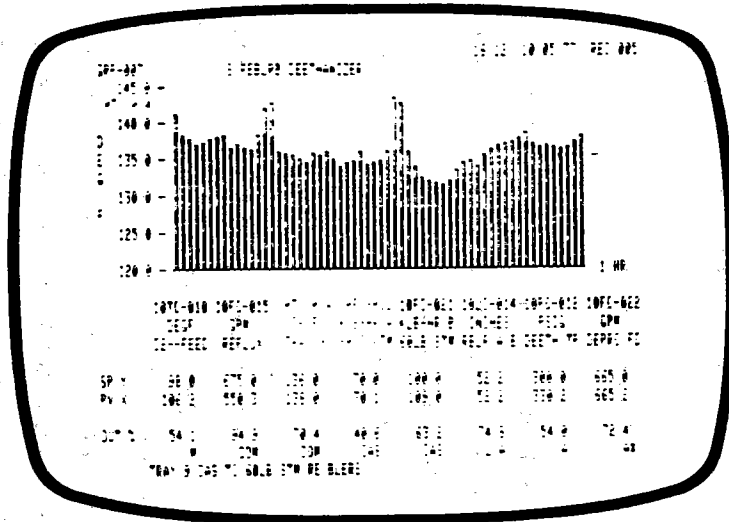
Hourly Averages

Trend – 1
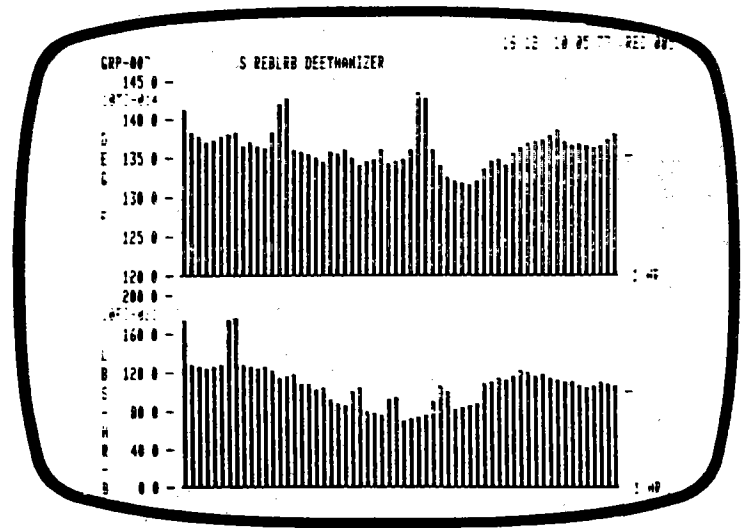
Trend – 2

Figure 8-16. CRT Display Hourly Averages and Trend Summaries

time constants, etc.) for one or a group of controlled elements. In all of these operator interventions with the plant control system, the communication is constructed using English language conversational statements from the programmer and brief operator actions through the function keyboard. The correctness and validity of each operator input is also checked and matched with permissible data.

8.4.3 Semi-Automatic Operation

Semi-automatic control operations provide the automatic operation but utilize preprogrammed and event programmed pauses to permit the operator to intervene. Decisions requiring operations or control parameter changes and verifications will be left to the operator in this mode. The control sequence will be suspended pending operator acknowledgement and action at the operator intervening places.

Like the automatic operations mode, the programmed-automatic operations mode permits the operator to "override" the automatic control process via the "request" and "grant" scenario.

8.4.4 Manual Operation

Manual operation of the plant requires the operator to initiate all pro-grammed control steps and change all of the control parameters for the receiver, thermal storage, and balance of plant subsystems. In this mode, the individual controllers of each subsystem must be manipulated by the operator to change control status.

The manual mode for the collector, beam characterization and turbine-generator subsystems will be quite different. Each of these subsystems will only operate with a high degree of automatic or sequence control at any time. Consequently, the manual mode of operation is highly constrained. In all three of these subsystems the manual mode consists of operator commands to initiate automatic or programmed functions within the subsystems.

The design of the plant control subsystem will provide the independent control and monitoring of each subsystem in the manual mode. Terminal displays will be available to service each subsystem, allowing the operator to cascade the control of the plant at the subsystem level.

The monitoring of plant control and performance data will be automatic upon request from the operator in manual mode control. Logging and report generation on the functions of the plant will also be output upon request from the operator.

8.4.5 Failover Operation

The plant control system will continuously run hardware diagnostic tests to evaluate the hardware availability. These diagnostics, under automatic processor control, run independent of the control operations and sequences on a time available basis. A failure within the plant control system hardware detected through diagnostics will (1) alarm the operator via the CRT display message and audible signal, (2) cause an automatic transfer of the failed function to pre-designated backup hardware, and (3) identify the failed component and describe the nature of the failure.

In addition, a watch dog timer will be provided with each of the four processor terminals to identify a hardware failure that would inhibit the diagnostics from running or alarming the operator. The watch dog timers will initiate an alarm signal in the event the processor does not initiate a timer reset within a prescribed time interval. Control transfer will be automatic to the designated backup console and in parallel with an audible operator alarm.

The automatic failover of control and monitor functions will be available using a plant control design that provides the following failover features:

1) Each control processer terminal will contain the program sequence for all plant operations. Thus, any terminal can be selected to be master plant control, subsystem control, or a combination master and subsystem control.

2) All control processor terminals will have a common path with which to communicate with the other terminals.

3) The operator can configure any terminal as a backup to another terminal at any time.

4) Each control processor terminal will periodically transfer pertinent control criteria (i.e., limits, set points, program sequence number, etc.) to the backup.

This design minimizes the operator intervention to handle plant control processor terminal upsets that could take the plant off line.

8.5 MASTER CONTROL 300-MWe COMMERCIAL POWER PLANT

The MCS for the 300-MW commercial power plant will incorporate the design concepts defined for the 100-MWe commercial power plant in Sections 8.2 through 8.4. The Master Control Subsystem will require the identical hardware and software configurations as set forth for the 100-MWe plant with the exception of the collector subsystem. The following concept changes for the collector subsystem will be integrated into MCS to accommodate the increase in the collector field size from 14,106 heliostats (100 MW) to approximately 43,000 heliostats (300 MW):

1) One additional programmed controller will be used in the collector subsystem. This controller will provide the computational nonreal time functions associated with aim points, beam safety, calibrate, startup, and status report generation.

2) One programmed controller will perform the real time functions of commanding heliostats, collecting heliostat status information, and interacting with the operator.

3) The communications type and throughput requirements will need an independent communications bus for the collector subsystem that will not be shared with the other subsystems.

4) In the event of a programmed controller failure in the collector subsystem, the functions of the failed unit will only be delegated to the companion controller.

5) The common redundant data bus supporting the programmed controllers of subsystems other than the collector field will interface to the collector subsystem programmed controllers through independent I/O ports.

Figure 8-17 shows a block diagram of the collector field controller configuration.
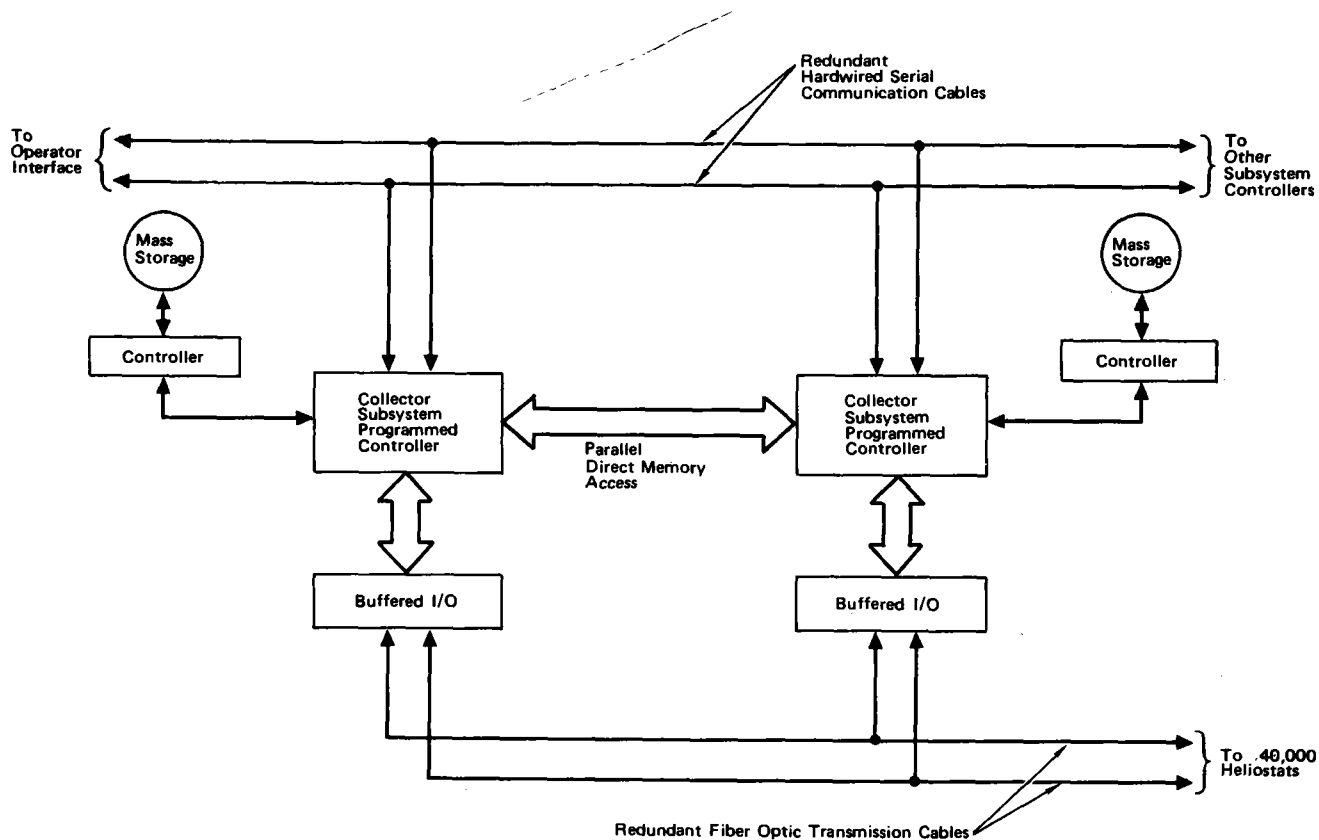
Figure 8-17. Collector Field Controller Configuration — Commercial 300-MW Power Plant

9272-133

9.0 ASSESSMENT OF COMMERCIAL-SIZE ADVANCED CENTRAL POWER SYSTEM

9.1 COMMERCIAL PLANT COST SUMMARY

9.1.1 Capital Costs

This section presents the results of the cost estimating effort for the 100-MWe commercial plant and the 300-MWe plant. Tables 9-1 and -2 give costs according to the cost breakdown schedule as given in the Preliminary Specification, Reference 1. Cost details and backup information are presented in Volume IV.

All cost estimates are presented in terms of 1978 dollars. The first commercial plant is assumed to be preceded by a commercial-scale demonstration plant and a pilot plant. The cost of the heliostat field is strongly affected by the heliostat production capability, which is influenced by the number of water-steam plants that are built or under construction. By the late 1980's, it is assumed that the water-steam pilot plant is complete and several larger-sized plants are under construction such that a heliostat production rate of 25,000 units per year is available. The first commercial plant reflects first-year production in these facilities. Nth plant estimates are for the tenth year of production at the above rate for heliostats or for other components, at the rate of two solar plants per year.

The cost estimates for the Collector Subsystem and the Master Control Subsystem were developed by MDAC. MDAC's estimates for these subsystems have benefited from the extensive work they have performed on water-steam systems. The cost estimates for the Electric Power Generating (EPG) subsystem were developed by Stearns-Roger (SR). SR also has made similar estimates for water-steam systems as well as using their extensive experience on fossil-fueled power plants. The estimates on the subsystem containing sodium (Receiver and Thermal Storage) are made by ESG using 25 years of experience with sodium system, both in design and construction of sodium system. Special consideration has been given to develop estimates for sodium components based on commercial practice rather than nuclear requirements.

TABLE 9-1
100-MWe COMMERCIAL PLANT — ALL-SODIUM STORAGE

CBS	Subsystem	First Commercial ($000)	Nth Plant ($000)
4100	Site, Structures, etc.	5,381	5,271
4200	Turbine Plant Equipment	19,424	19,424
4300	Electric Plant Equipment	4,834	4,301
4400	Collector Equipment	60,596	45,820
4500	Receiver Equipment	23,305	19,852
4600	Thermal Storage Equipment	12,086	11,460
4800	Distributables and Indirect	26,988	17,565
	Total	152,614	123,693

TABLE 9-2
281-MWe COMMERCIAL PLANT — ALL-SODIUM STORAGE

CBS	Subsystem	First Commercial ($000)	Nth Plant ($000)
4100	Site Structures, etc.		11,239
4200	Turbine Plant Equipment		38,759
4300	Electric Plant Equipment		6,865
4400	Collector Equipment		131,820
4500	Receiver Equipment		42,077
4600	Thermal Storage Equipment		30,490
4800	Distributables and Indirect		44,784
	Total		306,034

The sub-items in CBS 4100 (Site, Structures and Miscellaneous Equipment) include estimates by both SR and ESG based on construction experience.

For CBS 4800, Table 9-3 identifies the costing method for each of the sub-items. CBS 4820 is based on information from the Salt River Project indicating that 1/2% of capital cost items is a reasonable estimate, but can vary based on utility philosophy.

CBS 4830, 4840, and 4850 are based on ESG experience on both sodium and nonsodium systems. Contingency, CBS 4860 is variable depending on the cost category. CBS 4100 through 4400 is estimated at 10% since these items are either relatively standard utility items (turbine generators, for example) or have received extensive consideration on other programs (heliostats, for example). Sodium system at the conceptual design phase are typically estimated with 30% contingency at the conceptual design stage, but reduced to 15% for the Nth plant.

9.1.2 Operating and Maintenance Costs

Operating and maintenance costs are estimated for the 100-MWe commercial plant and the Nth plant as shown in Table 9-4. These costs are based on operating staff and material estimates by Stearns-Roger and on actual operating expenses and staffing used by the Salt River Project for their Agua Fria Station. The Agua Fria costs were for a single 100-MWe unit of a six-unit station. The costs are then projected to a single unit of a one-unit plant. The costs shown include maintenance materials. O&M costs for the 300-MWe unit are shown in Table 9-5.

The Nth plant O&M costs are substantially reduced, based primarily on the assumption that several plants would be grouped at the same site so that the economics of a multi-unit station such as indicated in Table 9-5 can be obtained.

9.2 POTENTIAL IMPROVEMENTS AND 281-MWe PLANT STUDIES

The potential improvements considered in this section are alternatives that were considered during the 100-MWe conceptual design but not included or are the result of broader scoping studies to determine minimum cost conditions due to scale effects.

TABLE 9-3
SUMMARY 4800

4810	Temporary Facilities — See Breakdown Sheet, Vol IV
4820	Spare Parts 1/2% of 4200 through 4600
4830	A&E Services 5% of 4100 through 4300
4840	Construction Management 5% of 4100 through 4300; 4400, 50, and 60; 4514, 15, 20, 40, 50, and 60; 4610 through 4660
4850	Startup and Checkout — 20 Man-Years at $50K/yr
4860	Contingency - 10% of 4100 through 4400; 30% of 4500 and 4600

TABLE 9-4
ADVANCED CENTRAL RECEIVER O&M COSTS

O&M Items	First Commercial (1,000/yr)			Nth Plant		
OM100 Operations Supervision			693			301
OM200 Maintenance Materials			581			253
OM210 Spare Parts		581			253	
OM211 Turbine and Electric Plant	320			139		
OM212 Collector Equipment	195			85		
OM212 Receiver Equipment						
OM214 Thermal Storage Equipment	66			29		
OM220 Material for Repair						
OM230 Other						
OM300 Maintenance Labor			1,112			810
OM310 Scheduled Maintenance	1,112			810		
OM320 Corrective Maintenance						
Total			2,386			1,364

TABLE 9-5
ADVANCED CENTRAL RECEIVER — 281 MWe O&M Costs

O&M Items	First Commercial ($1,000/yr)			Nth Plant		
OM100 Operations Supervision			843			376
OM200 Maintenance Materials			1,078			469
OM210 Spare Parts		1,078			469	
OM211 Turbine and Electric Plant	593			258		
OM212 Collector Equipment	363			158		
OM212 Receiver Equipment						
OM214 Thermal Storage Equipment	122			54		
OM220 Material for Repair						
OM230 Other						
OM300 Maintenance Labor			2,539			1,800
OM310 Scheduled Maintenance	2,539			1,650		
OM320 Corrective Maintenance						
Total			4,460			2,645

9.2.1 Potential Improvements

The potential improvement items that have been identified are as follows:

1) Air-rock storage concept for long duration storage
2) Increase plant size to ~300 MWe
3) Increase storage capacity to 13 h at 100% power.

The air-rock storage concept was evaluated during the Task 3 effort with the result that the design as then envisioned was not cost competitive with the all-sodium storage except at the large storage capacities. Also considered were the uncertainties in rock durability. A greatly simplified design has since been developed under company funding which reduces the storage costs. In addition, scoping laboratory tests of rock subjected to a limited number of thermal transients have tended to establish the suitability of the rocks selected.

The current system concept using air-rock storage includes a small amount of all-sodium storage to provide a short duration of buffering between the receiver and the steam generator.

The air-rock storage offers a promising potential improvement in reducing capital costs for storage durations greater than about 6 h. The discussion here shows the advantage of longer storage durations in reducing bus bar energy costs. The air-rock storage concept is discussed extensively in Section 5.

The increase in plant size reduces bus bar energy cost both due to the effects of scale on many plant components and the optimized field costs as discussed in Subsection 9.2.2.

Increased storage capacity as presented in Subsection 9.2.2 also reduces bus bar energy costs (BBEC) until plant operation reaches 24 h a day. In the simplified analytic study below with uniformly distributed outages, the minimum BBEC occurs at 13.4 h of storage (at 100% power). Operation 24 h a day is initially reached in the summertime and covers more of the year as storage capacity increases.
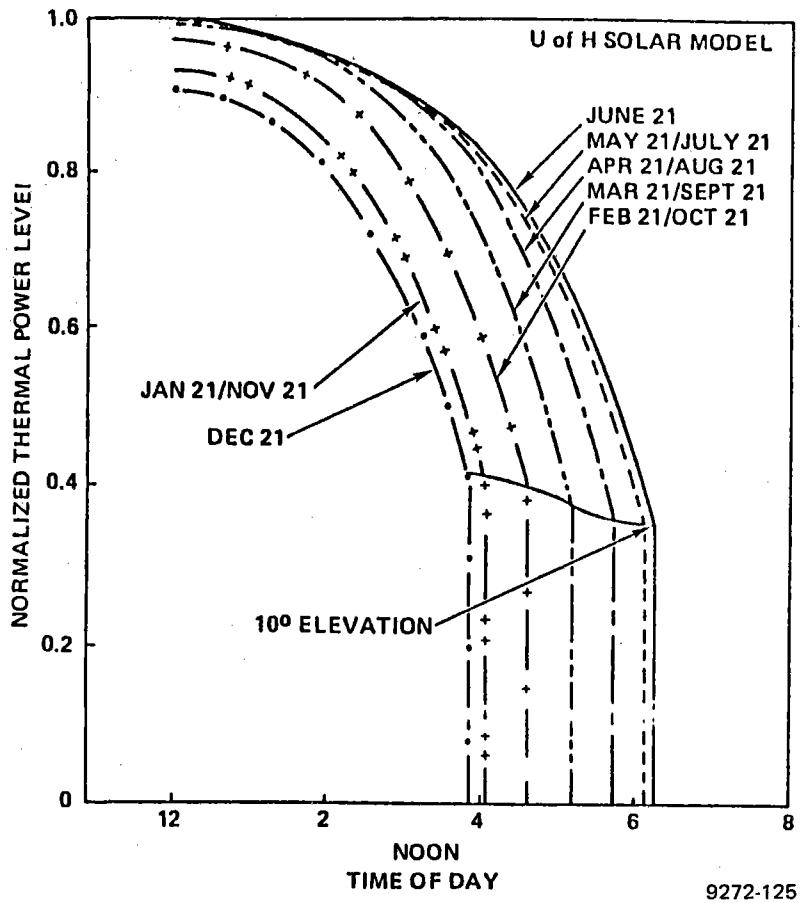
Figure 9-1.   Normalized Receiver Power
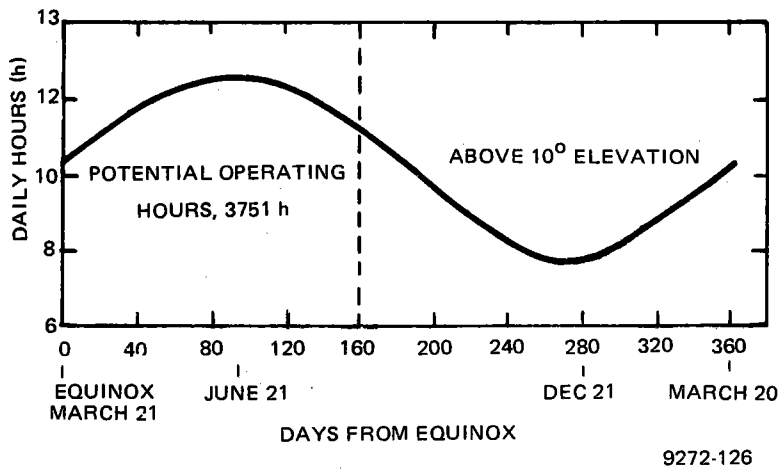
Figure 9-2.   Number of Operating Hours With
Sun at >10⁰ Elevation

Hence, total operating hours over the year increase slowly, producing the minimum point in the BBEC curve. A more realistic (random) weather outage model, the minimum point in BBEC would be less well defined, with the minimum somewhat beyond the 13.4 h of this study.

9.2.2 System Analysis

9.2.2.1 Operating Hours and Storage Capacity

Figure 9-1 shows the normalized profile for power absorbed by the receiver for one day each month of the year. Useful insolation is considered to be available when the sun reaches an elevation 10°. The number of operating hours with the sun at an elevation $>10^o$ is shown in Figure 9-2. Integration of the area under the curves of Figure 9-1 gives the daily thermal energy collected in units of (MWt-h)/MWt. For a peak power of 390 MWt, the daily energy collected is shown in Figure 9-3. The area under this curve is integrated to give the yearly collectable energy of 1.2×10^6 MWt-h/yr. The net collectable energy from the University of Houston computer model is 0.955×10^6 MWt-h. This model includes atmospheric disturbances such as turbulence, cloud cover, and other weather effects representative of high desert conditions. These weather conditions reduce the annual collectable energy by 17%.*

In the following analysis to determine annual full power operating hours as a function storage capacity, a weather outage of 17% is used, a forced outage of 5% due to mechanical problems is assumed, with 20 days per year maintenance scheduled for December. The total insolation operating time per year (Figure 9-4) is 3,751 h. Hence, weather outage is limited to 638 h (17% of 3,751 h). It is assumed that weather conditions do not affect operation from storage. This simple operating model assumes that the weather outage is uniformly distributed throughout the year; hence, in the summer months, with excess solar energy available over what is required to fill the storage, storage operation can be used to compensate for the weather outage.

---

*Based on a net collectable energy of 0.995×10^6 MWt-h which was later corrected to 0.955×10^6 MWt-h. The weather outage should be 20%; however, the results of the study are unaffected.
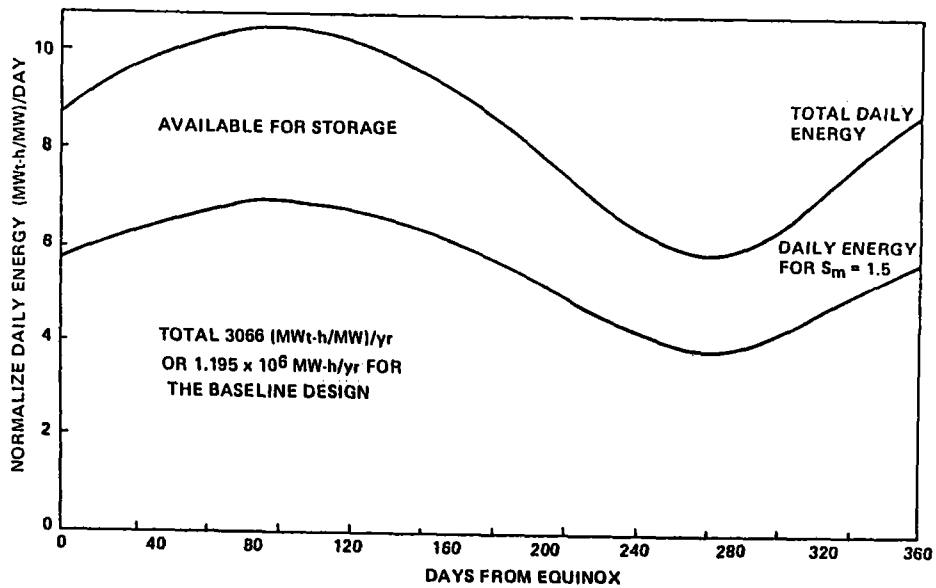
9272-127

Figure 9-3. Daily Energy
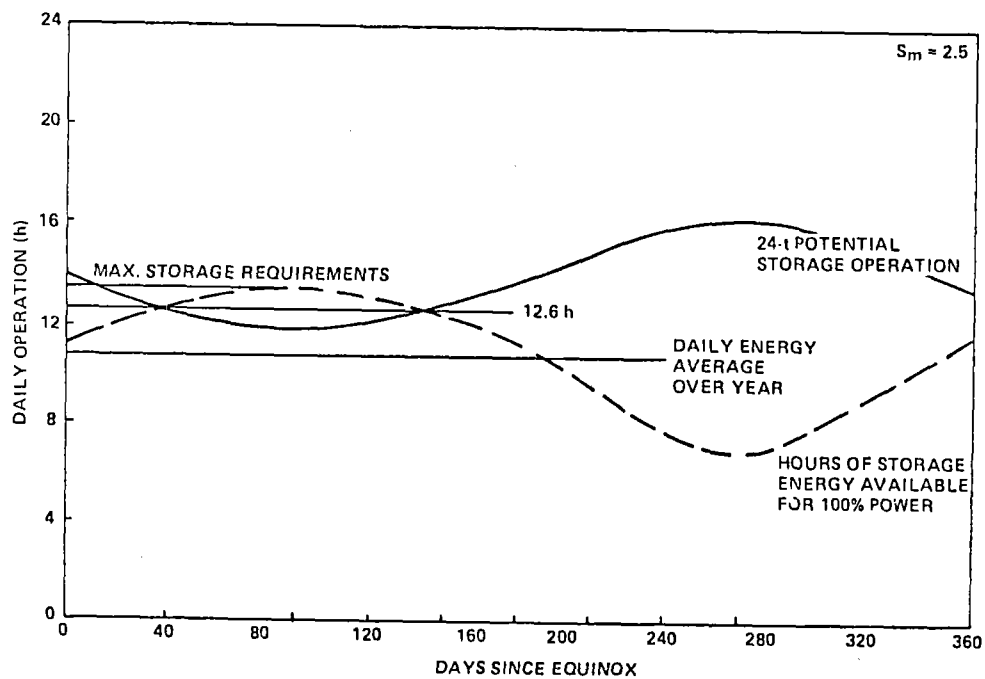
9272-128

Figure 9-4. Storage Characteristics for SM = 2.5

For a given power level and solar multiple, the storage capacity is selected to be equal to the average daily excess energy available over that required for direct operation. Figure 9-4 shows a typical graph (for a solar multiple of 2.5) showing storage energy available in hours at 100% power, the average daily energy, and the hours of storage required for full-time operation at 100% power. The daily average storage capacity is 10.7 h. However, depending on the criteria used, the storage capacity could vary from a minimum of 7 h to a maximum of 13.5 h. The equivalent full power operating hours of Figure 9-5 are based on the average daily storage capacity. For a storage capacity somewhat over 13 h, the total yearly plant operating hours became limited by the 24-h day. The 24-h day limit is reached during June initially, and plant operating hours increase only slowly thereafter as increasing storage capacity permits more and more around-the-clock operating and tends to mitigate the weather outage (Figure 9-5).

Figure 9-6 shows storage capacity in hours (MWt-h)/MWt as a function of solar multiplier for two different criteria. The upper curve is the storage capacity for the maximum storage energy available on June 21, and the lower curve is based on the average daily energy available. These results are general and not identified with a specific power level as long as the insolation profile of Figure 9-1 is unchanged.

The optimum storage capacity for a solar thermal plant is difficult to assess, with the results dependent on the assumptions made and the characteristics of the using utility. In this simple analytic approach, the operating hours determined here are used together with the plant costs as a function of solar multiplier to calculate bus bar energy costs using the techniques found in JPL 5040-29, "The Cost of Energy From Utility-Owned Solar Electric Systems," June 1976. Plant costs are estimated for a net electrical generating capacity of 100 MWe, scaled from the reference baseline costs (with 3 h of storage). Figure 9-7 shows plant cost estimates obtained as shown in Tables 9-6 and 9-7. These values are for the purposes of this study comparison, and the base cost may not be identical with the more recent estimates. Operating hours are obtained from Figure 9-5. Figure 9-8 shows bus bar energy cost $\overline{BBEC}$ as a function of solar multiplier which also dictates the thermal storage capacity. This curve shows a minimum $\overline{BBEC}$ energy cost for a solar multiple of 2.8 with a storage capacity of
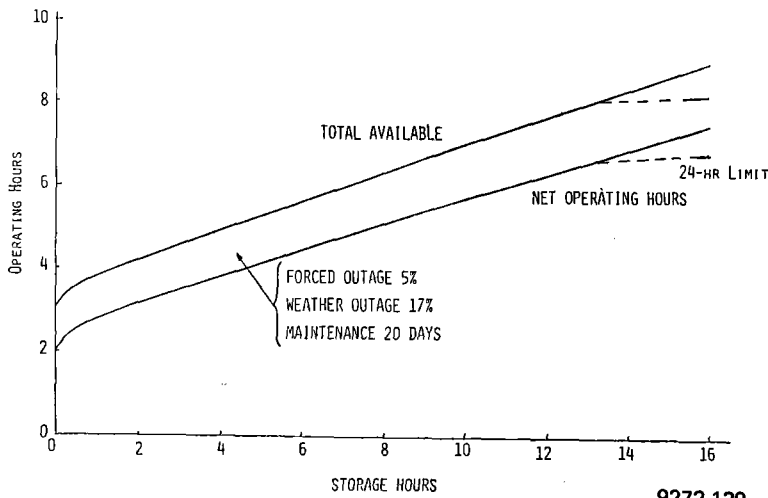
Figure 9-5. Storage Study —
Operating Hours

Figure 9-6. Storage Capacity
vs Solar Multiplier
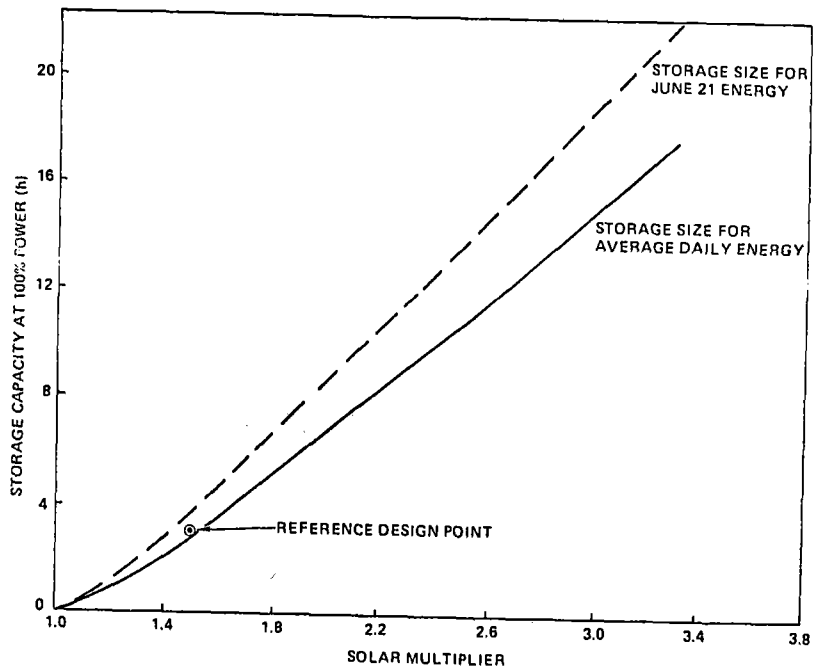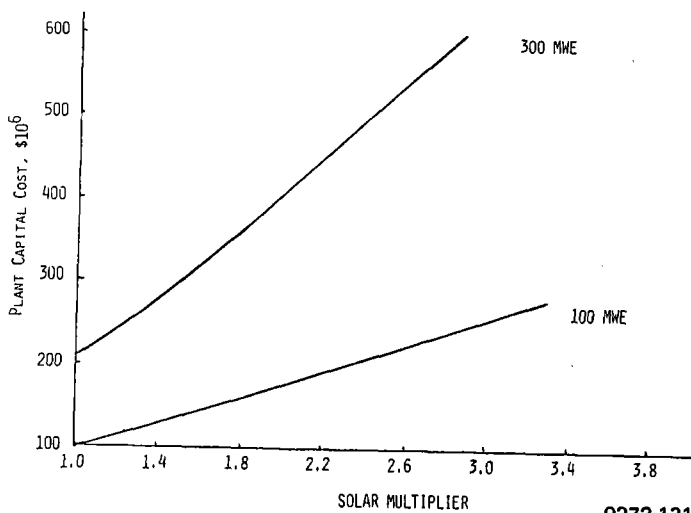
Figure 9-7. Storage Study —
Plant Capital Cost —
All-Sodium Storage

TABLE 9-6

100-MWe STORAGE CAPACITY STUDY — Nth PLANT COST SCALING

CBS	Subsystem	Power (MWt)				
		390	260	499	629	780
		Storage (h)				
		3	0	6	10	15
		SM = 1.5 Base*	SM = 1.0	SM = 1.92	SM = 2.42	SM = 3.0
4100	Site[1]	8.0	7.0	8.7	9.6	10.5
4200	Turbine-Generator	19.5	19.5	19.5	19.5	19.5
4300	Electric Plant	6.4	6.4	6.4	6.4	6.4
4400	Collector[2]	45.8	32.0	56.2	70.1	86.1
4500	Receiver[3]	19.7	15.3	23.1	27.0	31.3
4600	Thermal Storage[4]	11.1	0	22.2	37.0	55.5
4800	Distributables and Indirect (22%)	24.3	17.4	29.9	37.2	45.8
		134.8	96.1	166.0	206.8	255.1

*Midterm Preliminary Estimate
(1) Scale Improvements $6.5(SM/1.5)^{0.2}$ + land $1.5(SM/1.5)$
(2) Scale using figure of merit curve vs thermal power
(3) Scale with $(SM/1.5)^{0.8}$ (base cost less steam generator)
(4) Scale linearly with storage capacity

TABLE 9-7

281-MWe STORAGE CAPACITY STUDY — Nth PLANT COST SCALING

CBS	Subsystem	Power (MWt)				
		723	1084	1388	1749	2082
		Storage (h)				
		0	3	6	10	14
		SM = 1.0	SM = 1.5	SM = 1.92	SM = 2.42	SM = 2.88
4100	Site[1]	10.1	12.3	13.7	15.5	17.1
4200	Turbine-Generator	36.8	36.8	36.8	36.8	36.8
4300	Electric Plant	8.0	8.0	8.0	8.0	8.0
4400	Collector[2]	87.8	120.0	151.0	190.0	225.0
4500	Receiver[3]	27.4	35.0	40.5	46.6	51.3
4600	Thermal Storage[4]	0	31.6	63.4	105.3	147.5
4800	Distributables and Indirect (22%)	37.2	53.8	69.7	89.8	108.7
		207.3	297.5	383.1	492.0	594.4

(1) Scale from 100-MWe base. Improvements $6.5(P_1/P_0)^{0.2}$ + land $1.5(P_1/P_0$
(2) Scale using figure of merit curve vs thermal power
(3) Scale with $(P_1/P_0)^{0.8}$ from 100-MWe base and with $(SM/1.5)^{0.8}$ (less steam generator).
(4) Scale linearly with storage capacity
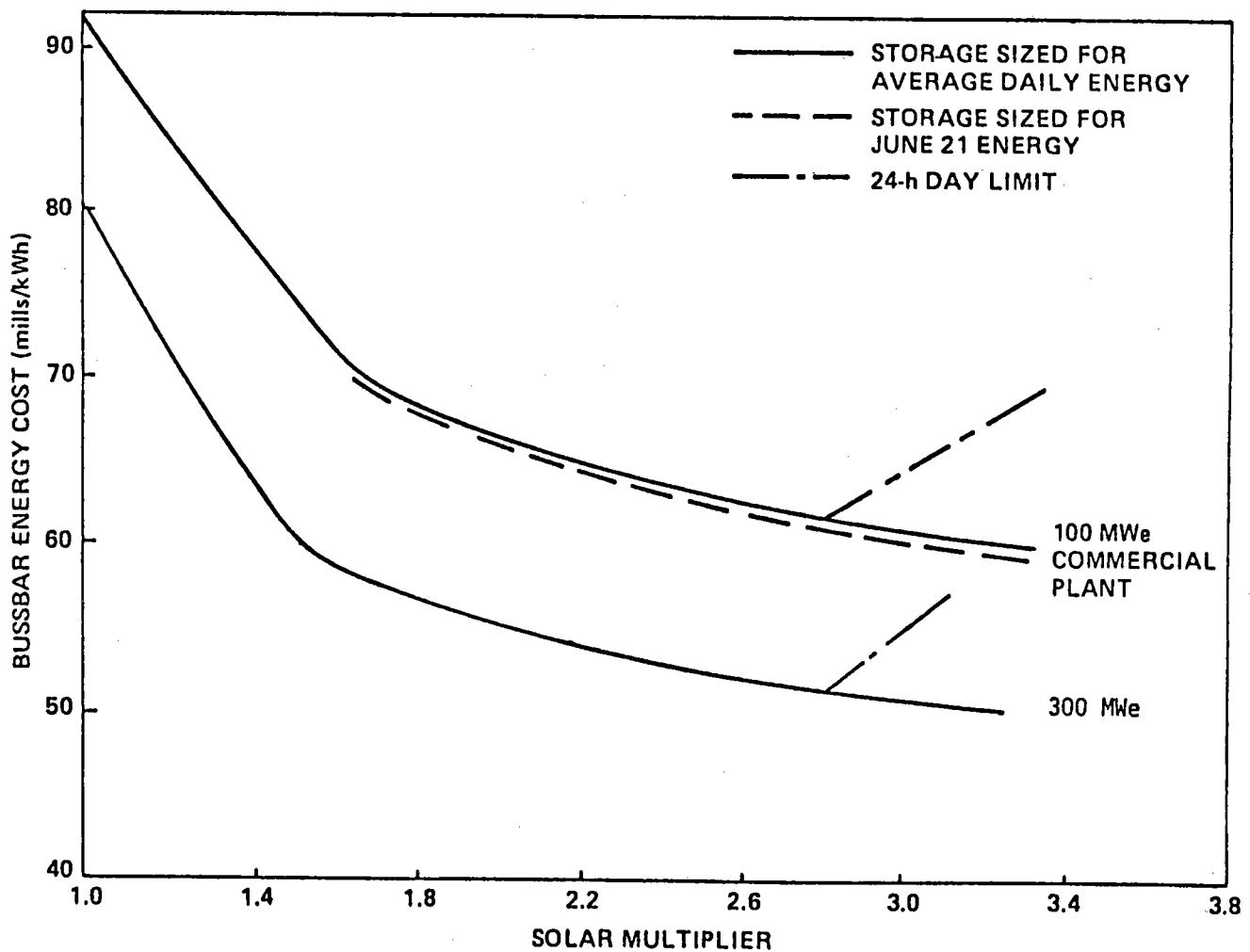
Figure 9-8. Storage Capacity Study — Busbar Energy Costs as a
Function of Solar Multiplier

12.4 (based on average yearly storage capacity). This minimum for $\overline{\text{BBEC}}$ is due to
the break in the operating hour curve when storage capacity is such that 24-h
operation is attained during at least part of the year.

9.2.2.2 Reduced Power Operation at Night

Reduced power operation at night was examined in order to avoid the daily
start and stop cycle on the steam turbine. Some utilities consider that repeated
start cycles are detrimental to turbine life, even for conditions that satisfy

hot start requirements. An alternative is to operate around the clock but at reduced power conditions to minimize the added storage requirements. The minimum power level for long duration operation is generally considered to be about 20%.

For the 100 MWe plant, the added storage capacity required is 818 MW-h to provide the 14.9 h on December 21 to operate all night at 20% power. The equivalent capacity in 100% power operation is 4.4 h. A solar multiplier of 2.05 is required to fill this storage capacity on December 21. On the basis of average daily capacity, this solar multiple corresponds to a storage of 7.2 h. Table 9-8 summarizes the cost and performance for storage capacities increased to 4.4 and 7.2 h. For the baseline configuration with a nominal 3 h of storage and a solar multiple of 1.5, only 1.4 h of 100% power operation is available on December 21. Table 9-8 shows that it is more cost effective to match the solar multiple and the storage capacity to reduce BBEC. A utility network analysis would be required to determine the worth of the added capital expense.

9.2.2.3 Optimum Collector Subsystem Capacity

One of the primary objectives of this study was to determine the optimum thermal capacity for the energy collection portion of the advanced central receiver system. In order to develop meaningful results, it was necessary to start the analysis with reasonable assumptions related to hardware cost and performance.

The basic cost assumptions used in the analysis are shown in Table 9-9. These models reflect the latest estimates that were developed midway through the contract period. In many cases, these models reflect a greater level of design understanding than was available when the initial cost models presented in Table 6-1 were developed. However, these changes are in no way significant enough to alter the conclusions related to the conceptual design analysis presented in Section 6.2.1.

The error budget assumed for the heliostat, which can significantly influence the optimization analysis, is made up of two components. The beam pointing error represents gross reflector point errors and was assigned a value of 1.5 mr (1σ)

TABLE 9-8
COST OF 20% POWER OPERATION AT NIGHT

CBS	Power (MWt)		
	390	533	533
	Storage (h)		
	3	4.4	7.2
	SM = 1.5	SM = 2.05	SM = 2.05
	Base (10^6)	Option 1 (10^6)	Option 2 (10^6)
4100　Site	8.0	8.5	8.5
4200　Turbine-Generator	19.5	19.5	19.5
4300　Electric Plant	6.4	6.4	6.4
4400　Collector	45.8	59.0	59.0
4500　Receiver	19.7	23.9	23.9
4600　Thermal Storage	11.1	15.5	26.6
4800　Distributables and Indirect	24.3	29.2	31.7
	134.8	162.0	175.6
Operating Hours	3,484	4,187	4,886
BBEC mills/kW-h	72.9	75.6	68.8
December 21 Operation h - 100%	1.4	1.4	1.4
- 20%	—	Remaining Night	Remaining Night
June 21 Operation h - 100%	3.0	2.4	6.0
- 20%	—	Remaining Night	Remaining Night

based on current heliostat error budget analysis. The beam quality error represents the combined influence of surface waviness, thermal distortion, wind distortion, and gravity effects. A value of 2.2 mr (1σ) was assumed for this error mode.

The results of the optimization analysis, carried out with the aid of the University of Houston optimization codes, are shown in Figure 9-9. This figure shows the cost of annual thermal energy delivered at the base of the tower for

TABLE 9-9

COST MODELS

Fixed	$5.25 M	Constant based on water-steam study
Heliostat	$65.67/m^2	Excluding land and wiring
Land	$1.66/m^2	$6,717/acre - including rough site preparation
Wiring	0.0412 R	Cost per heliostat
Trenching	0.4237 ΔR	R = distance from tower to computational cell
Electrical Distribution	5.72 Waz	ΔR = radial spacing in cell Waz = azimuthal spacing in cell (distances in M)
Sodium Pump	40.7 P (H-66 m)	Cost of approximately $1000/hp H = receiver centerline elevation (M) P = absorbed power (MW)
Receiver	$10.4 M (L D/260.8 m^2)$^{0.8}$	From previous sodium study
	$8.3 M (L D/260.8 m^2)$^{0.8}$	Alternate model developed late in study. L = receiver length (m) D = receiver diameter (m)
Tower	Cost = $109 (FL - 22 m)$^{2.1}$ FL = Rec Equator Elev - 4 m	Based on water-steam study
Piping Network		
Piping	55 . D (in.) 30 . D (in.)	$/ft (stainless steel) $/ft (carbon steel)
Valves	$2,000 . D (in.) $3,000 . D (in.)	6-in. - 17-in. Valves 17-in. - 24-in. Valves
Expansion and Bends	X (1.5)	Adjustment to pipe length
Vertical Factor		5% increase per 60 ft
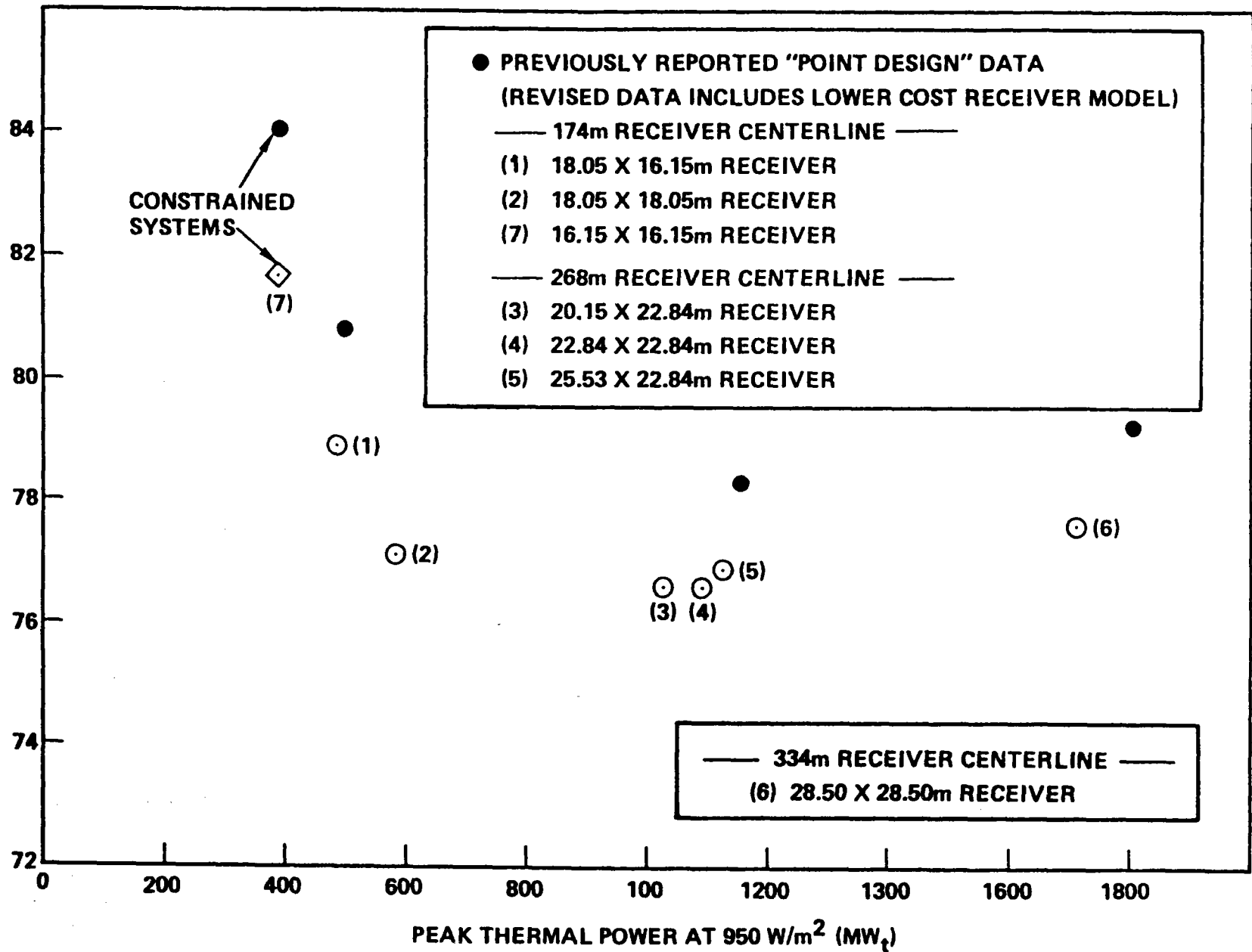
Figure 9-9. Thermal Capacity Optimization Analysis

systems rated from 390 MWt to 1800 MWt peak absorbed power. The solid data points were developed assuming the first receiver cost model shown in Table 9-4 while the open data points reflect the second, lower cost receiver model.

The results indicate that some cost advantage can be realized in designing energy collection systems which have peak power capacities in the range of approximately 600 to 1200 MWt. Since the optimization indicates that a broad, minimum-cost valley exists, systems anywhere in this range would have approximately the same level of cost effectiveness. The slight rise experienced at the right side of the figure reflects the lower optical performance experienced by the larger systems, specifically in the areas of atmospheric attenuation and receiver interception.

The increase in cost of energy indicated at the left side of the figure can be explained by considering the definition of the figure of merit parameter. On a simplistic basis, the figure of merit can be expressed as FOM = $(F_c + \Sigma H_c)/\Sigma E$, where F_c reflects fixed or nearly fixed costs, ΣH_c is heliostat dependent costs summed over the entire field, and ΣE is the summation of energy delivered to the receiver from the individual heliostats. The F_c parameter includes consideration of the receiver, tower, piping, pumps which all have some but not, in general, an overwhelming cost dependence on power. In addition, the F_c parameter contains truly fixed cost items such as indirects, installation facilities and equipment, A&E services, etc. The other parameters related to heliostat dependent costs and energy are, in general, directly related to power level.

As smaller plant sizes are considered, the heliostat cost and energy terms decrease in a nearly direct proportion to the reduction in plant power. The fixed cost term also decreases due to reductions primarily in receiver and tower cost. However, the reduction for the entire fixed cost term is less than the corresponding reductions experienced by the heliostat cost and energy terms. The net effect of going to a smaller system (assuming the same economic models apply) is to increase the figure of merit parameter because of the relative constancy of the fixed cost parameter.

Based on the data presented in this figure, a reference large commercial system configuration was selected for further definition. The selected case corresponds to the (4) data point shown on the figure.

9.2.3 281-MWe Commercial Plant

Based on the preceding collector field studies, an alternate, larger size commercial sized plan was established with a nominal size of 300 MWe (net 281 MWe). The thermal rating is 1,084 MWt, which is near the collector field minimum. Storage capacity was retained at 3 h for ease of comparison with the 100-MWe plant, even though a larger storage duration was shown in the previous study to reduce bus bar energy cost. A 281-MWe plant with 13.4 h of storage would require a solar multiple of 2.8 and a peak thermal power of about 2,000 MWt. While this power level is well beyond the minimum point of Figure 9-9, the figure-of-merit cost has not increased greatly and could represent a future design point.

9.2.3.1 281-MWe Plant Description

The 281-MWe plant flow schematic is shown in Figure 9-10. The concept is identical with that for the 100-MWe plant with two exceptions. Two evaporator units are used in parallel, and an additional feedwater heater is inserted on the suction side of the feedwater pump, giving a total of seven heaters. Table 9-10 provides a summary of basic 281-MWe plant data. The design data sheets of Appendix D provide a list of system and component performance and design data.

9.2.4 300-MWe EPG Subsystem

The eight turbine-generator systems shown in Table 9-6 were considered for use in the 281-MWe commercial power plant. These configurations were evaluated to determine the system cost effective combination of performance and subsystem cost. Since the collector field, receiver, and thermal storage subsystems represent most of the plant cost, achieving high combine cycle efficiently is important. The cost effectiveness criteria, developed to aid in the selection of the turbine configuration, were determined to be a $5 x 10^6 decrease in collector, receiver, and thermal storage subsystem cost for a one percentage point gross cycle efficiency charge.
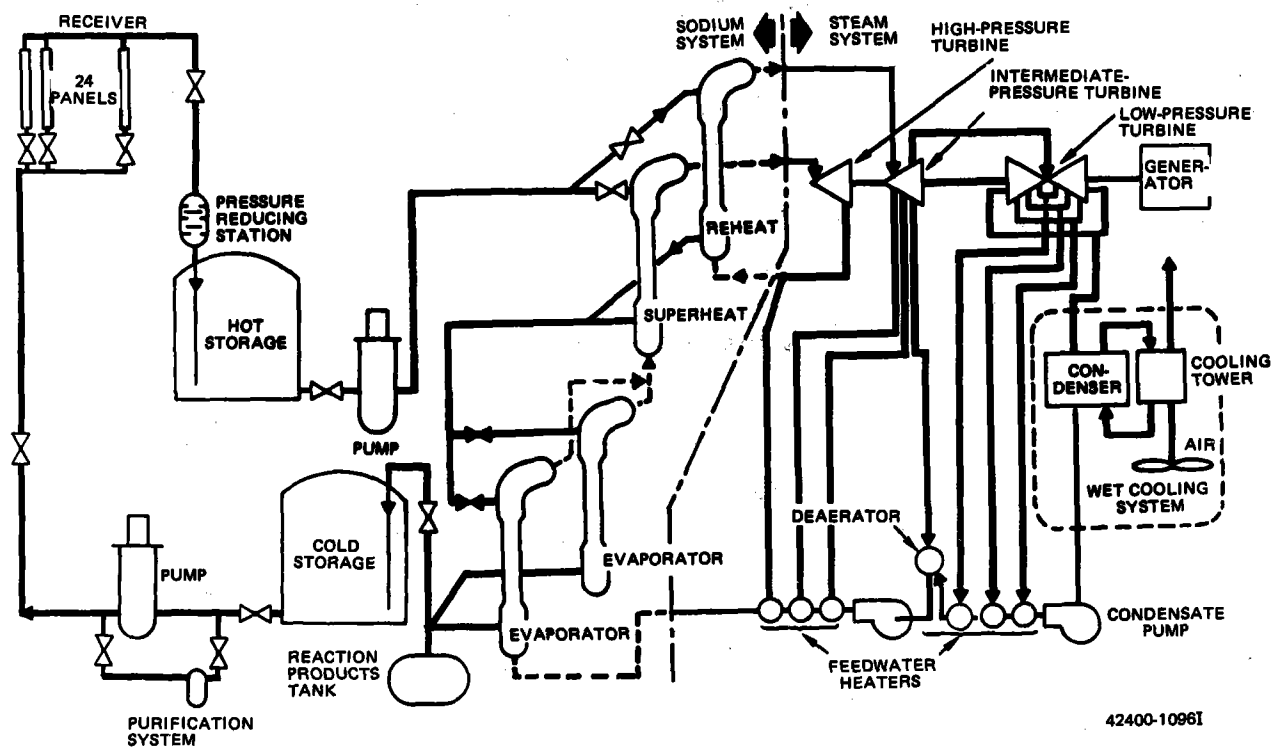
Figure 9-10. Advanced Central Receiver System —
300-MWe Commercial Plant

By inspection of the configurations in Table 9-11, Cases 5, 6, and 7 represented the most promising. Case 5 was selected as a base for cost comparisons.

Case	Turbine	T/G Δ Cost $\$10^6$	η Δ Points	Equivalent System Cost Increment $\Delta\$10^6$	Cost Effectiveness $\Delta\$10^6$
5	TC2F-30	Base	Base	--	--
6	TC2F-33.5	+1.41	+0.48	-2.4	Yes -0.99
7	TC4F-26	+3.07	+0.77	-3.85	Yes -0.78

Case 6 is the more cost effective on the above criteria and is selected as the turbine-generator configuration with seven feedwater heaters for the 281-MWe conceptual design.

TABLE 9-10

ADVANCED CENTRAL RECEIVER BASELINE DATA SUMMARY — OPTIMUM PLANT

System	Parameter	Optimum Plant
Electric	Net Power (MWe)	281
	Gross Power (MWe)	312
	Cycle Efficiency (%)	43.2
Receiver	SM	1.5
	Nominal Thermal Power (MWt)	723
	Maximum Thermal Power (MWt)	1084
	Receiver Temperature - in [$^{\circ}$C ($^{\circ}$F)]	288 (550)
	Receiver temperature - out [$^{\circ}$C ($^{\circ}$F)]	593 (1100)
	Flow Rate [(10^6 kg/h) 10^6 lb/h]	10.2 (22.6)
	Receiver Midpoint Elevation in (ft)	268 (879)
Storage (100% Power)	Operating Time (h)	3
	Energy (MWt-h)	2400*
	Quantity [(10^6 kg (10^6 lb)]	23 (50.4)
	Volume [10^3 m^3 (10^3 ft^3)]	28.2 (1010)
EPG	Turbine in Pressure [MN/m^2 (psig)]	16.5 (2400)
	Superheater Temperature [$^{\circ}$C ($^{\circ}$F)]	538 (1000)
	Reheater Temperature [$^{\circ}$C ($^{\circ}$F)]	538 (1000)
Collector	Mirror Area [km^2 (ft^2)]	1.99 (21.4 x 10^6)
	No. of Heliostats	40,660

*Includes reduction in night parasitic power of 18 MWe

TABLE 9-11

ADVANCED CENTRAL RECEIVER — 300-MWe TURBINE-GENERATOR COST AND PERFORMANCE

	Steam Conditions							
	1800 lb, 1000/1000°F, 2 in. Hg abs				2400 lb, 1000/1000°F, 2 in. Hg abs			
	Case 1	Case 2	Case 3	Case 4	Case 5	Case 6	Case 7	Case 8
	Turbine Type — LSB							
	TC2F-30	TC2F-33.5	TC4F-26	TC4F-30	TC2F-30	TC2F-33.5	TC4F-26	TC4F-30
VWO kW	312,200	312,200	312,200	312,200	312,200	312,200	312,200	312,200
GTHR Btu kWh	8,181	8,081	8,018	8,001	7,995	7,907	7,855	7,858
Gross Cycle Efficiency, %	41.71	42.23	42.56	42.65	42.68	43.16	43.45	43.43
No. of Heaters	6	6	6	6	7	7	7	7
List Price(1/76)	$15.92(10^6)$	$17.00(10^6)$	$18.32(10^6)$	$20.81(10^6)$	$15.80(10^6)$	$16.90(10^6)$	$18.20(10^6)$	$20.69(10^6)$
Escalation 6/78(16%)	2.55	2.72	2.93	3.33	2.52	2.70	2.91	3.31
Sell Price 6/78	$18.47(10^6)$	$19.72(10^6)$	$21.25(10^6)$	$24.14(10^6)$	$18.32(10^6)$	$19.60(10^6)$	$21.11(10^6)$	$24.00(10^6)$
Installation 10%	1.85	1.97	2.12	2.41	1.83	1.96	2.11	2.40
Installation Cost (T-G only)	$20.32(10^6)$	$21.69(10^6)$	$23.37(10^6)$	$26.55(10^6)$	$20.15(10^6)$	$21.56(10^6)$	$23.22(10^6)$	$26.40(10^6)$
$/kWe	65.08	69.47	74.85	85.04	64.54	69.06	74.37	84.56

The advantages of increased unit size on cost (scale effect) are shown in Table 9-12 for the turbine plant equipment (CBS 4200) and for the electric plant equipment (CBS 4300). For a factor of 2.8 in net power output, the cost per kilowatt decreases 40% for both the turbine equipment and the electric plant equipment.

TABLE 9-12

ADVANCED CENTRAL RECEIVER PRELIMINARY EPGS COST ESTIMATE
(100 MWe vs 300 MWe)

Plant Size (Net Output)	100 MWe (10^3)	281 MWe (10^3)
4200 - Turbine Plant Equipment		
4210 - Turbine, Generator, and Access	10,856	21,560
4200 - Heat Rejection System	4,215	6,275
4230 - Condensing Systems	320	577
4240 - Feed Heating Systems	1,655	3,203
4250 - Working Fluid Circulation, Treatment	2,378	3,544
Total 4200	19,424	35,159
$/kWe	194	117
4300 - Electric Plant Equipment		
4310 - Switchgear	860	1,502
4320 - Station Service Equipment	1,302	2,163
4330 - Protective Equipment	253	300
4340 - Power Wiring, Electrical Structures and Containers	938	2,231
Total 4300	3,353	6,196
Total $/kWe	34	21
Total 4200 + 4300	22,777	41,335
Total $/kWe	228	138

9.2.5 281-MWe Receiver

Collector and receiver optimization studies on the 281-MWe power plant indicated that a receiver height and diameter of 22.8 m (74.8 ft) was the optimum size. The peak heat flux on this receiver was increased from 1.37 MWt/m^2 in the 100-MWe baseline receiver to 1.85 MWt/m^2. It was felt that the receiver state-of-the-art would be sufficiently advanced in later generation plants to warrant such a heat flux increase.

The configuration of the 281-MWe (1084-MWt) receiver is considered to be a scaled-up version of the 100-MWe baseline receiver, using 24 absorber panels as before. In order to maintain approximately the same tube pressure drop, the tubes have been increased in outside diameter from 1.91 cm (0.075 in.) to 3.18 cm (1.25 in.) with the wall thickness remaining at 0.124 cm (0.049 in.).

This increase in tube diameter will cause a decrease in the sodium heat transfer coefficient. Since the total ΔT between the external surface of the tubes and the sodium is dominated by the tube wall thermal resistance, the overall ΔT is only moderately larger. Since the average heat flux has increased from 0.485 MWt/m^2 to 0.664 MWt/m^2 — an increase of 37% — the larger receiver will definitely have a higher outer surface temperature and, hence, greater thermal losses per unit area. However, the surface area per unit incident thermal power is so much less, the overall thermal effectiveness of the receiver is improved.

The lower panel manifolds will be fixed and the upper manifolds will be free floating as before. Six additional sliding attachment brackets will be employed — spaced vertically along each group of tubes. The total thermal expansion of the panels will be about 17.8 cm (7.0 in.).

The remainder of the receiver is scaled-up from the 100-MWe baseline receiver. The details are given in Table 9-13.

TABLE 9-13

100-MWe AND 281-MWe RECEIVER COMPARISON

	100 MWe	281 MWe
Receiver Dimensions		
Panel Height (m)	16.1	22.8
Diameter (m)	16.1	22.8
Panel Width (m)	2.1	3.0
Tube OD (cm)	1.91	3.18
Wall Thickness (cm)	0.124	0.124
Mid-Point Elevation (m)	174	268
Substructure Height (m)	7.0	10.0
Manifold OD (cm)	20	32
Expansion Tank Overall Diameter (m)	8.0	12.0
Antisiphon Pipe OD (cm)	76	127
Strongback Box Beams (cm)	15/0.95	15/0.95
Insulation Thickness (cm)	7.6	7.6
Thermal Data		
Maximum Abosrbed Thermal Power (MWt)	390	1084
Normal Abosrbed Thermal Power (MWt)	260	723
Maximum Flow Rate (kg/h)	3.66×10^6	10.2×10^6
Normal Flow Rate (kg/h)	2.44×10^6	6.80×10^6
Inlet Temperature (°C)	288	288
Outlet Temperature (°C)	593	593
Peak Heat Flux (MWt/m²)	1.37	1.85
Average Heat Flux (MWt/m²)	0.49	0.66
Typical Sodium Velocities (m/s)	1-6	1-6
Maximum Tube Temperature (°C)	625	640
Maximum Tube ΔP (kPa)	80	80

Estimated Receiver Weights (including sodium)	kg	lb	kg	lb
Twenty-Four Panels	39,300	86,500	91,400	201,000
Piping and Expansion Tank	20,900	46,000	58,600	129,000
Insulation	26,900	59,200	61,800	136,000
Structure	158,200	348,000	300,500	661,000
Roof	10,000	22,000	19,100	42,000
Crane	20,200	44,500	43,600	96,000
Dry Total	275,500	606,200	575,000	1,265,000
Sodium	66,400	146,000	186,400	410,000
Wet Total	341,900	752,000	761,400	1,675,000

9.2.5.1 281-MWe Receiver Subsystem

The receiver subsystem for the 281-MWe commercial plant is identical in concept to tnat for the 100-MWe plant. All components and piping are substantially larger in size as is indicated by the details given on the Design Data Sheets of Appendix D, Volume II, Book 2. The steam generator arrangement requires duty as follows:

Evaporator	412 MWt	(2 units)
Superheater	213 MWt	
Reheat	98 MWt	
Total	723 MWt	

In order to keep the evaporator units in a size range compatible with current design experience, two units are used with a duty of 206 MWt each. The two units operate in parallel with inlet control valves used to obtain flow balance as shown in Figure 9-10. These two half-size evaporator units and the superheater unit would be designed to be physically identical in size though the superheat unit would be constructed using Type 316 stainless steel rather than the 2-1/2 Cr - 1 Mo used for the evaporator units. The reheat unit would be similar in size to the current CRBRP steam generator design.

The receiver pump flow capacity is required to be 3.8 m/s (60,000 gpm) which is somewhat beyond current flow capacity experience for sodium pumps in this country, but the French have pumps of this size. Two pumps in parallel of the size for CRBRP (1.9 m/s - 33,000 gpm) provide a potentially attractive alternative.

The design data sheets of Appendix D provide additional 281-MWe plant details.

9.2.5.2 Thermal Storage Subsystem for 281-MWe Commercial Plant

The thermal storage subsystem design proposed for the 281-MWe commercial plant is the all-sodium hot and cold tank system similar to the 100-MWe plant design baseline. The thermal storage system contains the hot and cold storage

liquid sodium tanks, the P-2 pump which pumps sodium to the steam generator system and a pressure reducing device which permits low pressure design (atmospheric) for the storage tanks. The thermal storage subsystem can be charged (flow into the hot tank) at energy rates up to 100% of the receiver thermal power (1084 MWt). This maximum charging rate corresponds to 10.2×10^6 kg/h (22.6×10^6 lb/h). Sodium is pumped from the hot storage tank at energy rates to a maximum of 723 MWt corresponding to 6.82×10^6 kg/h (15.0×10^6 lb/h) to generate steam for the electric power generating system. After flowing through the steam generators, the sodium flows to the cold sodium storage tank. During normal daytime operation, hot sodium in excess of what is needed for normal direct operation is stored in the hot storage tank. The receiver and collector subsystems are sized such that a sufficient quantity is stored to provide up to 3.25-h operation at 100% rated power (or any combination of hours x percent rated power which totals 325). With the all-sodium thermal storage subsystem, plant operation is always from storage. The steam conditions provided are the same regardless of whether or not the receiver loop is in operation.

The storage tanks are 42.7 m (140 ft) in diameter with a height of 21.3 m (70 ft). The hot tank operating at 593°C (1100°F) is made of stainless steel; the cold tank at 288°C (550°F) is made of carbon steel. The tanks operate at static head pressures only in order to minimize cost. This requires a pressure-reducing device to dissipate the tower static head. There is a total of 22.16×10^6 kg (48.7×10^6 lb) of sodium in the thermal storage subsystem.

The pressure-reducing device for the baseline configuration consists of a nominal 22-in. drag valve. A steam generator pump in this system moves the hot sodium through the steam generator units to the cold storage tank. The receiver pump identified in the receiver subsystem description charges the hot storage tank. The steam generator pump is similar to the FFTF pump with approximately the same head and flow requirements. The developed head for this pump is 76 m (250 ft) at 2.65 m^3/s (42,000 gpm).

The thermal storage system functional requirements are presented in Table 9-14. The design characteristics of the all-sodium 281-MWe ACR Thermal Storage Subsystem are presented in the Design Data Sheets of Appendix D, Volume II, Book 2.

TABLE 9-14

281-MWe ADVANCED CENTRAL RECEIVER THERMAL STORAGE SUBSYSTEM FUNCTIONAL REQUIREMENTS

Parameter	Requirement
Thermal Storage Capacity	
Capacity (MWt-h)	2170
Additional Capacity for Shutdown, 12-h Hold and Restart (MWt-h)	180
Total Capacity (MWt-h)	2350
Maximum Charging Rate (MWt)	1084
Maximum Extraction Rate (MWt)	723
Time at Maximum Extraction Rate (h)	3
Temperature Conditions	Generate Steam Including Reheat at $1000^{\circ}F^{+10}_{-50}$
Reduced Power Operation (%)	10 to 100
Transient Operation (Power)	
10% to 100% or 100% to 10%	90
30% Charge to 100% Extraction or 100% Extraction to 30% Charge	2 min

9.2.5.3 281-MWe Air-Rock Storage System

The requirements for an air-rock storage system for the 281-MWe plant are essentially the same as those for the 100-MWt plant except that the maximum plant absorbed power is 1084 MWt instead of 390 MWt. In the 100-MWe design, there are nine storage modules each a square 28.8 m (94.6 ft) on a side and each containing six fan-HX units. The nine modules form the overall active storage region — a square 86.4 m (283 ft) on a side and 11 m (36 ft) high.

The 281-MWe storage system consists of 25 modules forming a 5 x 5 square that is 144 m (472 ft) on a side. The overall storage system height remaining at 11 m (36 ft) and the active rockbed height remains at 6.1 m (20 ft).

N

T = TOWER

CELL SIZE

228.6 X 228.6 m

RECEIVER ₵ ELEV
268 m

RECEIVER SIZE
22.84 X 22.84 m
(CYLINDER)

NUMBER HELIOSTATS
40591

GROUND COVERAGE
21.4%

FIELD TRIM LINE

1943.1 m

1257.3 m

1714.5 m
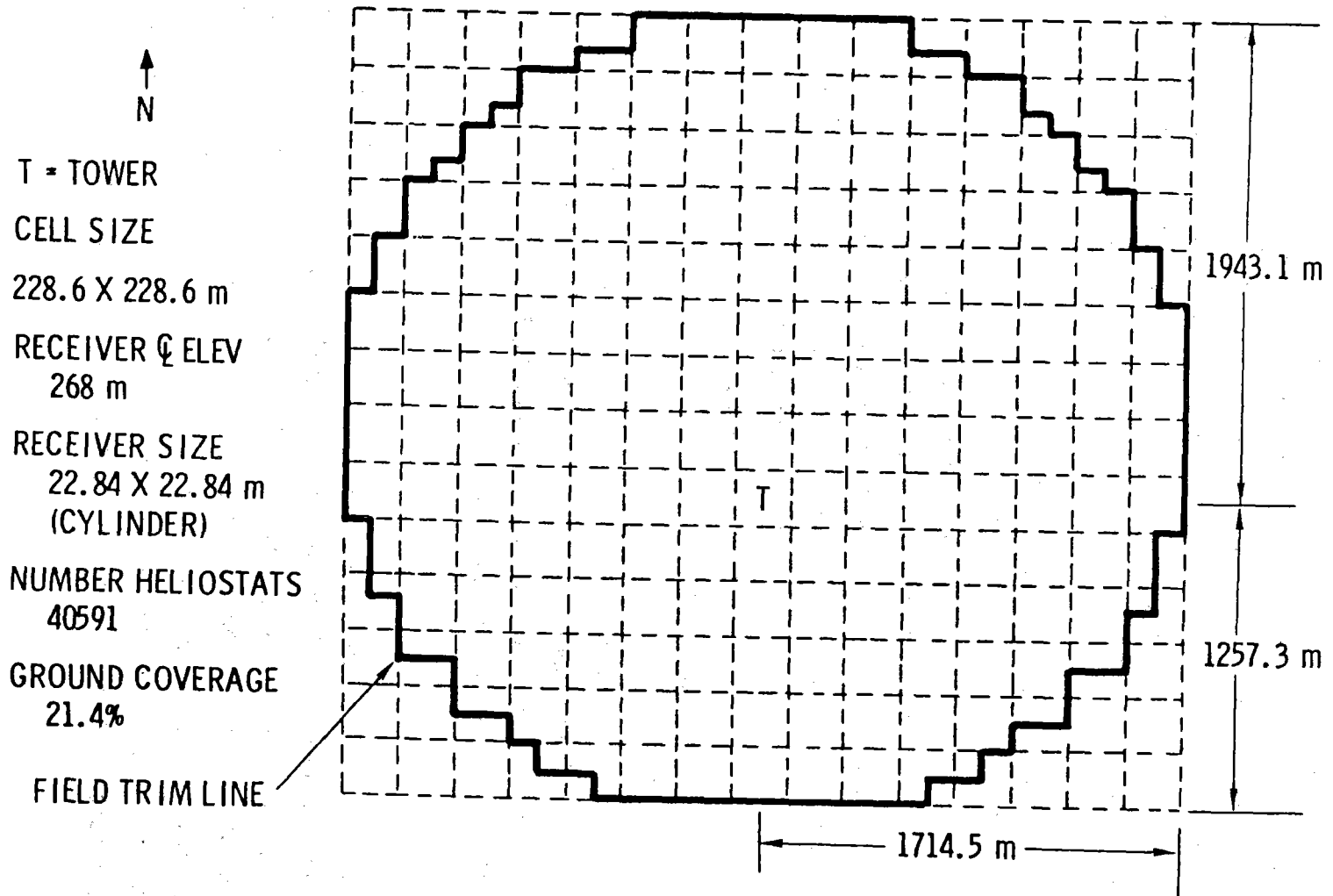
Figure 9-11.   Collector Field Characteristics for Large (1087 MWt) System

The storage capacity is the same as the 100 MWe design — a nominal 3 h of storage with an actual capacity of about 12 h if a small performance penalty is accepted. The number of fan-HX units is now 150. The HX dimensions remain at 2.44 x 2.44 x 0.85 m (8 x 8 x 2.8 ft), and the fan size is still 1.52 m (5 ft). All concrete duct sizes are the same except that there are more of them. The cost of this storage system would be very nearly 25/9 times the cost of the 100-MWe unit. The sodium piping would increase by a factor somewhat greater than this, while the earth-fill containment would increase more slowly than this.

9.2.5.4 281-MWe Commercial Plant Collector Field

The characteristics of the collector field, receiver, and tower for the large commercial system (1087 MWt → ~300 MWe) are summarized in Figure 9-11 along with a definition of the computational cells used to carry out the analysis. The fact that the field trim line coincides with the edge of the computational cell matrix on all sides indicates that the optimum field would extend slightly beyond the computational cell matrix considered. This is, however, an insignificant perturbation to the result presented.

The 22.84 x 22.84 m cylindrical receiver would experience a peak heat flux of ~1.94 MW/m^2 if all beams were directed toward the equator of the receiver. Because of the size of the receiver, a vertical aim strategy can be employed for the "small image" heliostats which will reduce the peak heat flux to a value <1.6 MW/m^2.

Detailed information related to numbers of heliostats of heliostats located throughout the field is shown on a cell-by-cell basis in Table 9-15. These data are for the east half of the field and the group of cells which make up the east-west line of symmetry. The mirror image of these data (except the left-hand column) would exist for the west side of the field. The heliostat assumed for this system is identical to the design described in Volume II, Section 6.3 except that zero canting is assigned for the individual heliostat panels.

TABLE 9-15

NUMBER OF HELIOSTATS BY CELL
(East Side Only — Symmetric East-West —
1087 MWt System)

134	132	130	62	0	0	0	0
155	156	150	142	134	31	0	0
183	183	174	163	151	137	31	0
220	218	206	188	172	153	138	0
270	267	248	220	196	169	150	65
341	328	300	256	220	189	163	139
448	420	358	295	243	202	171	146
479	452	423	328	265	214	178	152
TOWER	466	451	344	271	219	182	154
459	415	437	329	266	215	179	75
409	411	370	297	244	202	171	36
355	344	303	259	218	186	79	0
272	267	247	220	190	82	0	0
212	212	200	137	41	0	0	0

Detailed heliostat spacing for this large capacity commercial system is presented in nondimensional form in Tables 9-16 and 9-17 for radial and azimuthal separations, respectively. As in the previous table, these data are presented for the east half of the field only with symmetry assumed for the data pertaining to the west side of the field. The proper interpretation of these data is illustrated in Figure 9-12 for two typical cells in the vicinity of the tower.

The average performance characteristics for the collector field are summarized in Table 9-18. This table includes the effects of all optical performance factors including heliostat reflectivity, field cosine, heliostat blocking and shadowing, atmospheric attenuation, receiver interception factor, and a field layout factor. This latter quantity represents an adjustment factor which must be applied in converting the field from an ideal cell-by-cell description to a real layout with non-interfering heliostats which could occur at cell boundaries and access roads for the central area.

TABLE 9-16
NONDIMENSIONAL* RADIAL SPACING

```
┌                  ┐
│   CELL BY CELL   │
│  EAST HALF ONLY  │
└                  ┘
```

6.865 6.934 7.089 7.369 7.756 8.266 8.884 9.660

5.975 6.009 6.218 6.533 6.916 7.446 8.049 8.801

5.121 5.170 5.399 5.740 6.161 6.716 7.348 8.069

4.301 4.374 4.617 4.988 5.451 6.055 6.701 7.459

3.533 3.600 3.856 4.305 4.820 5.485 6.182 6.995

2.774 2.887 3.184 3.704 4.298 4.968 5.721 6.584

2.041 2.218 2.632 3.207 3.839 4.645 5.449 6.301

1.679 1.996 2.178 2.854 3.583 4.411 5.249 6.111

TOWER 1.778 2.049 2.748 3.512 4.316 5.148 6.022

1.697 1.744 2.222 2.906 3.608 4.392 5.205 6.120

2.416 2.444 2.602 3.189 3.877 4.637 5.429 6.315

2.662 2.812 3.155 3.661 4.296 4.991 5.795 6.637

3.321 3.453 3.785 4.262 4.855 5.529 6.299 7.132

4.150 4.237 4.506 4.948 5.504 6.160 6.899 7.805

*DIMENSIONAL VALUE = (NONDIMENSIONAL VALUE) (7.39773 m)

TABLE 9-17
NONDIMENSIONAL* AZIMUTHAL SPACING

$$\begin{bmatrix} \text{CELL BY CELL} \\ \text{EAST HALF ONLY} \end{bmatrix}$$

2.079 2.082 2.066 2.078 2.093 2.112 2.181 2.420

2.060 2.041 2.049 2.063 2.059 2.080 2.104 2.201

2.040 2.021 2.031 2.048 2.047 2.071 2.099 2.127

2.019 2.002 2.014 2.032 2.035 2.063 2.071 2.103

2.006 1.988 2.000 2.019 2.025 2.057 2.069 2.104

2.021 2.018 1.998 2.013 2.019 2.032 2.048 2.086

2.089 2.052 2.026 2.019 2.021 2.035 2.053 2.072

2.378 2.119 2.074 2.039 2.010 2.023 2.043 2.063

TOWER 2.304 2.067 2.021 2.006 2.019 2.040 2.060

2.451 2.637 1.966 1.997 1.988 2.023 2.043 2.086

1.935 1.901 1.984 2.019 2.021 2.035 2.053 2.094

2.021 1.976 1.998 2.013 2.041 2.054 2.092 2.131

2.112 2.073 2.042 2.041 2.068 2.101 2.159 2.219

2.170 2.131 2.122 2.120 2.123 2.175 2.231 2.381

*DIMENSIONAL VALUE = (NONDIMENSIONAL VALUE) (7.39773 m)
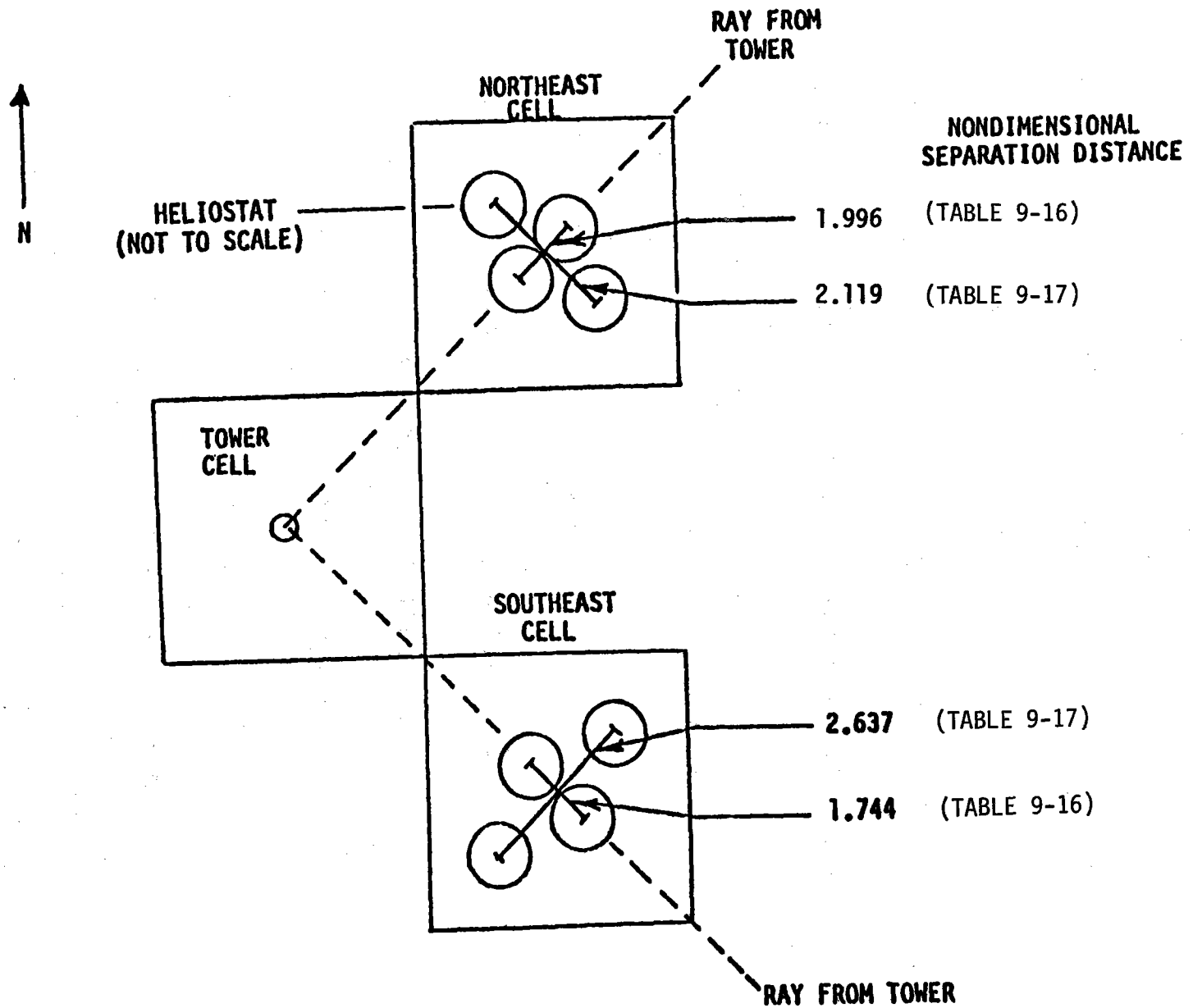
Figure 9-12.   Utilization of Heliostat Spacing Data from Cell-by-Cell Tables
(Tables 9-16 and 9-17)

TABLE 9-18
COLLECTOR FIELD EFFICIENCY MATRIX

Sun Elevation Angle (deg)	Sun Azimuth Angle (deg)						
	0	30	60	75	90	110	130
5	NE	NE	0.290	0.281	0.279	0.280	NE
15	NE	NE	0.457	0.447	0.448	NE	NE
25	NE	0.573	0.560	0.552	0.543	NE	NE
45	0.641	0.639	0.636	0.624	0.611	NE	NE
65	0.651	0.646	0.639	NE	NE	NE	NE
89.5	0.656	NE	NE	NE	NE	NE	NE

NE - Nonexistent

*Field Efficiency $\equiv$ (Helo Reflect) (cosine) (Block and Shadow) (atm Attn) X

$$0.91 \qquad\qquad\qquad\qquad\qquad\qquad 0.94$$

$$0.98 \qquad\qquad\qquad\qquad 0.954$$

(Field Layout Factor) (Interception Factor)

As indicated at the bottom of the table in the defining equation, many of the parameters are assumed to be a constant on the average over the entire year. The tabular values then reflect the variations in field cosine and heliostat blocking and shadowing which occur over the year. The values indicated in the table correspond to possible combinations of sun elevation and azimuth angle. The "non-existent" entries are used to indicate impossible sun location conditions.

9.2.6 System Power Flow — 281-MWe Plant

A system power flow chart is given in Figure 9-13 for the 281-MWe net system for equinox noon with 3 h of storage. The incident power for direct operation at 281-MWe net is 1238 MWt. The overall plant efficiency is 22.7%.
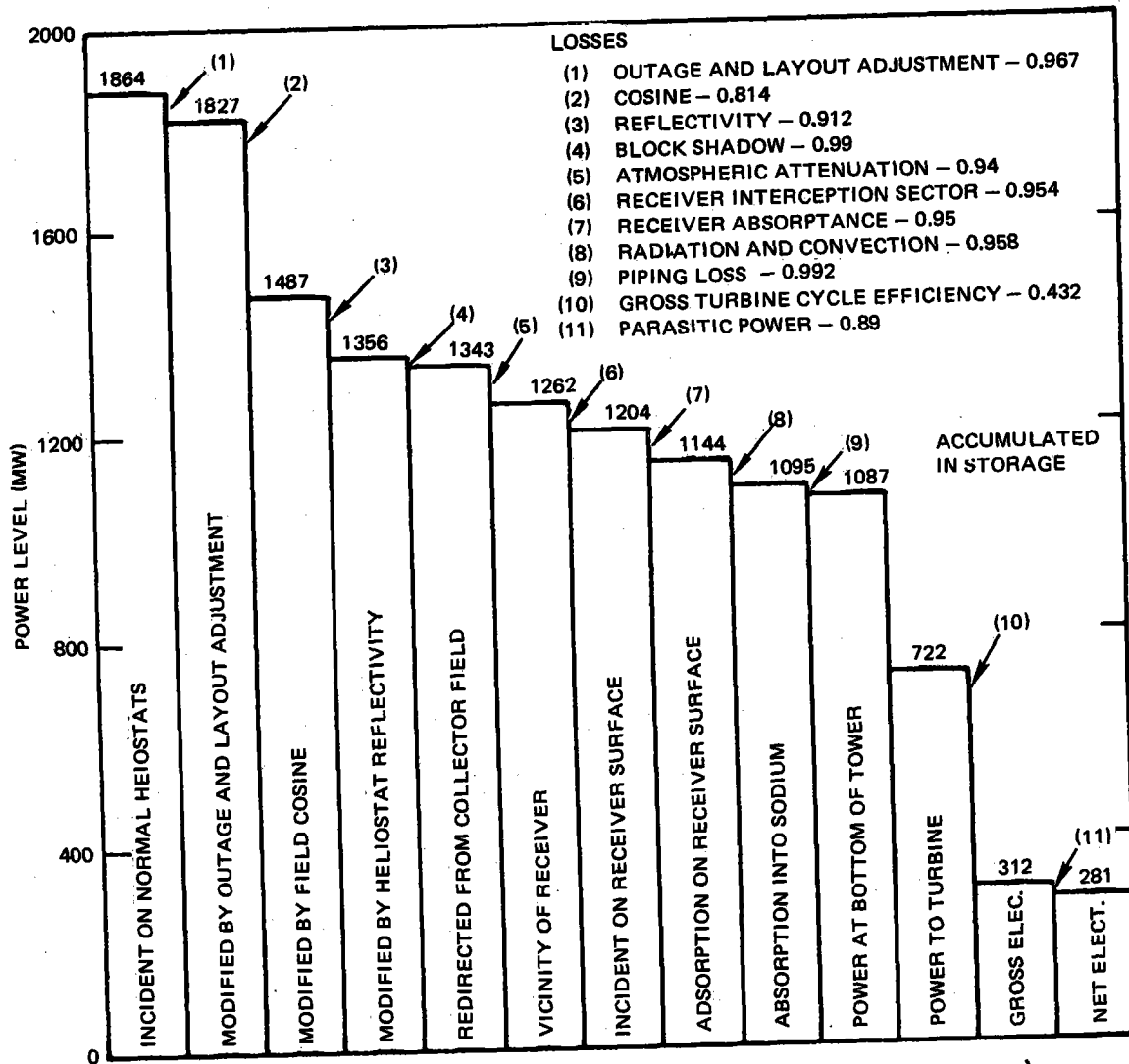
Figure 9-13.   281-MWe System Power Flow (Equinox Noon)

9.3 POTENTIAL IMPLEMENTATION LIMITATIONS

9.3.1 Environment

One of the potential limitations to the implementation of the sodium-cooled, central-receiver, solar-thermal power plant concerns its environmental effects. General environmental impacts have been studied in some detail in the past using water-steam as a baseline concept. Examples of such work are contained in References 9-1 through 9-5, inclusive. Even though the baseline considered was generally water-steam, most of the information is generic in nature, and therefore applies to all central receiver concepts, including the sodium system. Insofar as plant operation is concerned, the conclusions reached on the environmental impacts of the water - steam-cooled concept are identical in kind, but somewhat more severe than those on the sodium concept, except for one item: the heat transport fluid (sodium) in the latter will burn if it is exposed to air to form oxide, hydroxide, and carbonate aerosols that could potentially pose a hazard to plant personnel, the general public, or the surrounding flora and fauna.

A reasonably detailed series of calculations was performed on the Phase I program to predict the aerosol concentration and fallout within and outside the plant boundary. The calculational techniques and results are discussed in Section 10 below. The calculations have shown that the threshold limit value for 24-h/day inhalation [2 mg/m^3 of $Na(OH)_2$] by human beings would be reached at the plant perimeter (assumed to be 1600 m from the base of the tower) if a continuous jet of sodium at 0.5 kg/s (1 lb/s) were released to the environment at the 174 m elevation. This release rate corresponds to a release through about a 0.95 cm diameter hole in the receiver, a hole which is considered to be about as large a puncture or crack as is likely to ever occur. Moreover, the calculated concentration values correspond to the most adverse weather types, they neglect such naturally occuring phenomena as agglomeration and they disregard conversion of the hydroxide to carbonate. For short term releases, where 80 mg/m^3 is allowed, release rates can be substantially greater (20 kg/s). Thus, assuming that human inhalation limits are the most sensitive environmental criterion, the presence of sodium does not appear to present an unreasonable risk to the environment outside

of the plant perimeter. It is also to be noted that, although the oxide and hydroxide forms of sodium are of concern insofar as their effects on humans, flora, and fauna are concerned, these compounds are not toxic and they readily convert to carbonates after exposure to air for a few minutes or hours, depending upon the amount of water in the air in the vicinity of the release. The carbonate is generally considered to be reasonably innocuous. One other mitigating circumstance is the fact that the release and subsequent burning of a jet of sodium is readily visible; consequently, action can be initiated to drain sodium away from the failed area. This procedure will further limit the amount of sodium released in an accident situation.

Additional calculations were performed to predict the aerosol concentration values and the deposition in the vicinity of a ground-level, pool-type fire that could be postulated to occur as a result of a sodium spill. Under the most adverse weather circumstances, the long-term, threshold-limit value is reached at the outer boundary of the plant if the burning area of the pool is about 15 m^2. For short term releases, which are the more likely events since corrective action can be taken,* a pool fire area of 160 m^2 can occur without the aerosol concentration exceeding the 80 mg/m^3 criterion. Fallout rates and concentrations just downwind from the pool fire but within the plant boundary are, however, high. A deleterious effect on plant life, if there is any, within this boundary could be anticipated. Outside the boundary, however, there does not appear to be a serious environmental concern.

Although the calculations, which are reasonably conservative, predict an acceptable environmental effect if a release of hot sodium should occur, the likelihood of such an event is very small insofar as large quantities are concerned. Since the early 1950's when sodium and NaK loops of significant sizes were first put into operation, no major release or spill above several hundred pounds has occurred, yet millions of hours of operating time have been accumulated in both sodium loops and operating nuclear power plants in the U.S. and abroad.

---

*Sodium can be drained from all parts of the loop into either or both of the large storage tanks

TABLE 9-19

SOLAR THERMAL POWER SYSTEM ENVIRONMENTAL ISSUES AND RESPECTIVE IMPACT AREAS*

ISSUE	AIR QUALITY	WATER QUALITY	LAND USE / SOLID WASTE	ECOLOGICAL IMPACTS	HEALTH & SAFETY	ESTHETICS	SOCIAL / INSTITUTIONAL	RESOURCES
HANDLING AND DISPOSAL OF SYSTEM FLUIDS AND WASTES (u)	X	X	X	X	X			
COOLING TOWER IMPACTS (u)	X			X				
COLLECTOR GLASS BREAKAGE (u,m)					X	X		X
ECOLOGICAL IMPACTS OF THE HELIOSTAT FIELD (u)		X	X	X		X		
AUXILIARY UNIT EMISSIONS/RESIDUALS (u)	X	X	X	X				
POTABLE WATER CONTAMINATION (u)		X			X			
SYSTEM MAINTENANCE (u)		X		X	X			
HELIOSTAT REFLECTION (u)				X	X	X		
WATER USE (u)				X				X
ALTERATION OF THE MICROCLIMATE (u)	X			X				
SYSTEM COMPONENTS MANUFACTURE (m)						X	X	
RECEIVER TOWER IMPACTS (u)				X	X	X		X
BOOM TOWN EFFECTS (u)	X	X	X				X	X
LAND DISPLACEMENT (u)			X	X		X	X	X
CONSUMER-UTILITY INTERFACE (u)							X	
ZONING/BUILDING CODES (u)						X	X	
SITE RECOVERY AFTER PLANT SHUTDOWN (u)			X	X		X	X	
COMPONENT QUALITY ASSURANCE AND REGULATION (u,m)					X		X	
NOISE (TURBINES - COOLING TOWERS) (u)						X		

*This table extracted from Reference 9-3

KEY

X = DENOTES IMPACT AREA

M = IMPACT ARISING FROM MANUFACTURING PROCESS

U = IMPACT OCCURRING AS A RESULT OF SYSTEM USE

As noted above, other environmental issues (see Table 9-19 for a comprehensive listing as taken from Reference 9-3) are approximately the same for the sodium-cooled central receiver concept as for the water-steam. However, since the sodium-cooled concept has a higher efficiency, the collector area and field sizes are substantially smaller (0.692 km^2 vs about 0.8 for 100 MWe for plants with comparable solar multiples) and the land area required per 100 MWe plant is less (3.062 km^2 vs about 3.6 km^2). The first factor can potentially mollify effects from the heliostat canopy, and the second can reduce the total land area required per plant, although neither of these is a major factor insofar as the environment is concerned. The tower height for a 100-MWe sodium-cooled plant is also somewhat shorter (174 m vs about 188 m) than that for a comparably sized water-steam system; therefore, it represents somewhat less of a collision hazard to birds and airplanes. Finally, the improved efficiency results in somewhat less water usage for cooling water makeup for the sodium system; therefore, the water vapor discharge into the air is reduced. It follows also that the heat discharge into the air is somewhat lower.

The overall conclusion that has been reached at this point in the development of the sodium concept is that it does not pose any new environmental concern other than that discussed above relative to the accidental release of sodium coolant to the atmosphere. No study performed to date indicates a deviation from the general conclusion reached, for example, by the authors of Reference 9-2 (Page 106) to the effect that:

> "Solar energy conversion is generally considered to be more benign enviromentally and more labor intensive than fossil fuel conversion."

9.3.2 Land Use Constraints

On balance, the land use requirements for the sodium-cooled concept can be expected to be substantially less than that for water-steam concept. As specified above, the total area occupied by heliostats (the field area) for the 100-MWe baseline concept is 3.062 km^2. For the 300-MWe concept, it is 8.86 km^2. Thus the concerns for displacement of agriculture, grazing, and recreational land seem to be somewhat smaller for the sodium concept than for certain other central

receiver concepts. "The land-intensiveness of STE (solar thermal electric) is balanced by a number of factors. Among these are: (1) the fact that STE does not generate radioactive wastes which require long-term isolated storage either above or below ground, (2) STE does not typically generate the solid wastes associated with fossil fuel-fired power plants (i.e., ash) which require on- or off-site disposal, and (3) STE is relatively nonpolluting in terms of air, water, and thermal pollution."[9-1]

9.3.3 Water Requirements

The water requirements for heat rejection for the 100 MWe and 300 MWe sodium-cooled concepts are 93,000 gal/min and 280,000 gal/min, respectively. Cooling water makeup, which is a more definitive measure of water requirements, is 1,350 gal/min (0.085 m^3s) and 3600 gal/min (0.227 m^3/s) for the 100- and 300-MWe plants, respectively. Water requirements for wet-cooling towers with mechanical draft are therefore expected to be somewhat less for the sodium-cooled system. This difference can be significant if wet cooling is to be used for solar central receivers in the southwest regions since, according to Reference 9-2, Page 53, the Rio Grande, California, Great Basin, Upper Colorado, and Lower Colorado water resource regions are expected to experience shortages by the Year 2000.

Water requirements for mirror washing are expected to be significantly less for a sodium-cooled plant just on the basis of fewer, smaller reflector area. However, this water requirement is not significant relative to that needed for heat rejection. Water needed for general plant facilities and human needs is expected to be essentially the same for all central receiver concepts, and is also very small relative to heat rejection needs.

9.3.4 Use of Scarce or Imported Materials

The only material that may be of concern with regard to the sodium-cooled concept is chromium. In the current baseline design, all components and piping

---
[1]See Page 43 of Reference 9-1

that hold sodium at temperatures above about $400^\circ C$ ($750^\circ F$) are to be fabricated out of one of the austenitic stainless steels (typically Type 304 stainless steel) or out of 2-1/4 Cr - 1 Mo steel. Type 304 stainless steel contains about 18% chromium; consequently, there is a significant amount of chromium required in each plant.* Relative to the annual production of stainless steel in the U.S., however, the quantities required in a 100-MWe-sized sodium-cooled concept are very small.

The large quantities of sodium required in an all-sodium storage solar plant are frequently thought to be of some concern. However, the annual production of sodium has been as high as 1.6×10^8 Kg (177,000 tons/year) (1973). The quantity of sodium required for 3 hours of storage is about 14.5×10^6 Kg (32×10^6 lb), a value that is about 9% of annual production. The demand for metallic sodium in the U.S. has been declining in recent years because its main use has been in the production of anti-knock compounds in automotive gasolines (tetra ethyl lead, for example). The EPA has dictated that the amounts of lead in automotive gasolines shall be reduced significantly over the next few years. Thus, the need for sodium in sodium-cooled central receivers can, in fact, have the effect of maintaining the sodium production rate at or close to current capabilities, although the time phasing would be important.

9.3.5 State of Technology

About 127 sodium and NaK test loops, with thermal power levels up to 70 MW, have been designed, built, and operated over the last 20 to 25 years. A representative listing of these is shown in Table 9-20. Many hundreds of thousands of hours of operating time have been successfully accumulated. Over one-half of these loops are still in operation, and additional ones are being built. In addition to a large number of sodium loops, about 21 liquid-metal-cooled (sodium and NaK) nuclear reactors have been designed, constructed, and operated. Some of these systems (see Figure 9-14 have or had power levels as low as 100 kWt, others as high as 1000 MWt. The first of these reactors was built in 1951, and 7 of

---

*If a steel-sodium, thermocline storage system is used in the sodium-cooled concept, the amount of stainless steel needed may increase substantially although, from a metallurgical viewpoint, low-carbon steel may be suitable in this case.

TABLE 9-20
NON-NUCLEAR SODIUM TEST RIGS IN USA

Site	Test Rig	Temperature (°F)	Inventory (gal)	Flow (gpm)	Status
LMEC	SCTI (70 MWt)	1050	25,000	8,700	Design
	SCTL	1200	13,000	3,500	Operating
	SPTF	1100	20,000	20,000	Operating
	LLTR	900	2,000	—	Construction
	B/057-2	1300	500	—	Operating
	B/006-2	1350	200	—	Operating
	B/032-9	1200	6,000	—	Operating
HEDL	CRCTA	1200	39,000	500	Operating
	TTL	1200	850	600	Operating
GE	SGTR	1000	3,000	200	Operating
	DNB Loop	1000	2,000	100	Operating
	3-Sodium Pots	1300	1,000	—	Operating
W̲	GPL-1	1200	500	200	Operating
	GPL-2	1200	2,000	2,000	Operating
	3-Sweater	1200	20	3	Operating
ANL	CCTL	1200	1,000	800	Operating
	SFSCF	800	100	100	Operating
	Camel	1200	30	200	Operating
	FFDL	1200	30.2	30	Operating
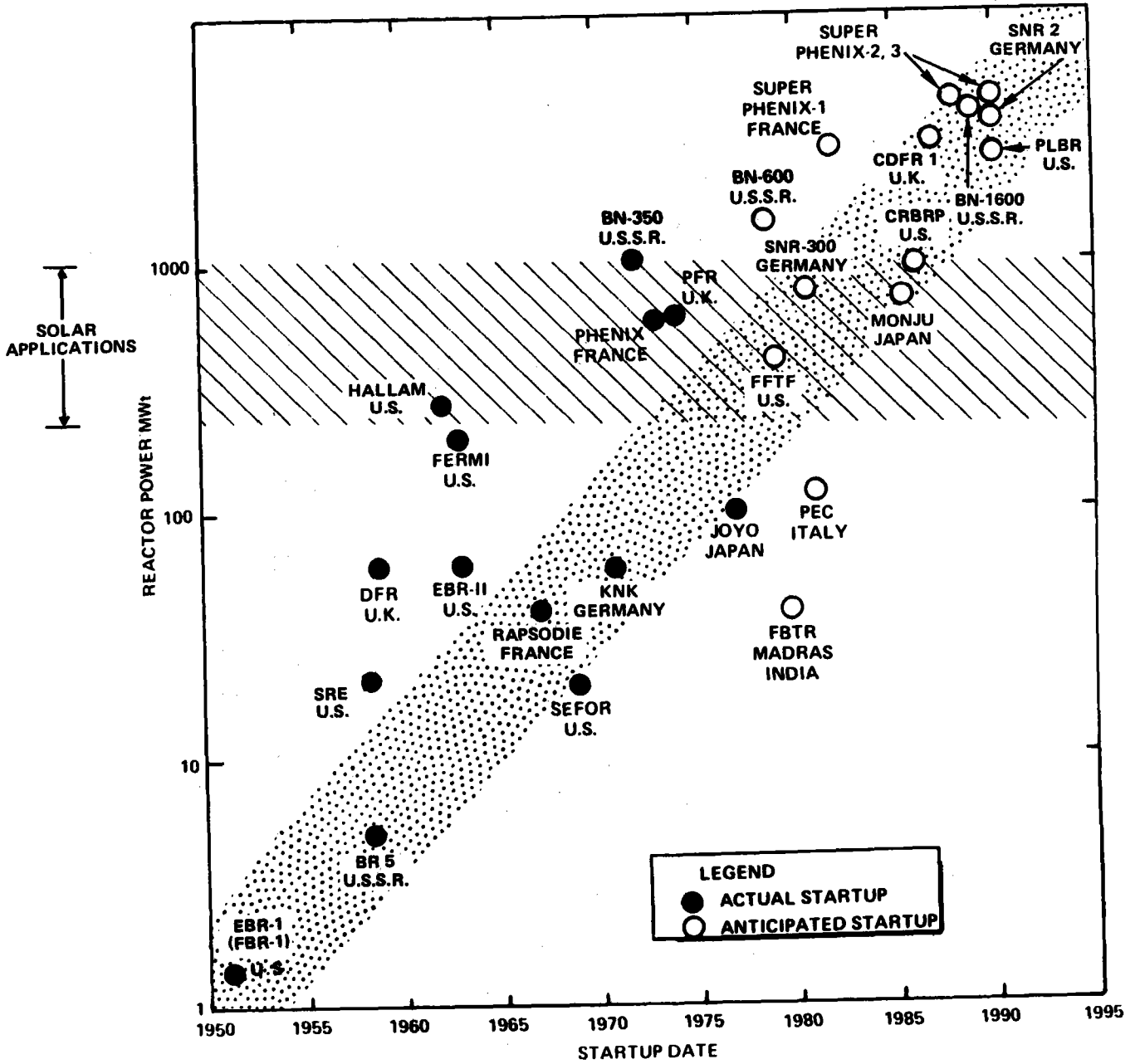
Figure 9-14.   World LMFBR Plant (Progress Growth)

78-J26-16-4

them are still operating. About 14 new sodium-cooled power reactors, with power levels up to 1300 MWe (3500 MWt), are under construction or in design in the U.S. and abroad. In the process of building the liquid metal loops, and particularly in the development and operation of sodium-cooled nuclear power plants, components such as pumps, valves, tanks, heat exchangers, and steam generators have been designed, fabricated, extensively tested, and operated. For example, in the U.S. alone, over 322,000 h of successful operation have been accumulated to date on various types of sodium pumps with capacities in the range of 2,700 to 14,500 gpm (0.17 to 0.9 m^3/s). Thus, the current state of sodium technology is more than adequate to justify its application to solar electric systems. Furthermore, sodium components in the size range for solar pilot plants (i.e., 50 to 20 MWe) have already been developed and tested, and are essentially available, in terms of required pressure, temperature, and capacity ranges. Components of the sizes that would be applicable to full-scale commercial solar plants (i.e., 100 MWe) are currently in the design and test stage for use in liquid-metal-cooled, nuclear power plants in the U.S., and are expected to be available within the time frame projected for solar electric commercialization. Components of the size needed in the optimized (~300 MWe) solar plant have already been built, tested, and operated in other countries.

9.3.6 Production Capability and Capacity

The only mass-production type item required in the sodium-cooled concept is the heliostat. This production capability and capacity are very limited at the present time, but the problems associated with meeting the forecasted demand have been dealt with in detail on a number of other programs. The assumption has been made on this program that heliostat production capability will grow to meet the power production requirements for the solar central receiver plant. Since the number of heliostats per plant of the same capacity is less in the sodium system than in the water-steam plant, the production capability could be met more easily or sooner in time. The production capability for the steam side of the sodium-cooled concept (i.e., steam turbines, generators, cooling towers, condensers, etc.) already exists since the sodium-cooled system utilizes "off the shelf," modern-steam-plant, turbine technology and systems. No specialized turbine types would be required over and above those normally ordered by utilities who procure

new Rankine cycle steam plants. The assumption is made that the solar central receiver becomes economically viable, steam turbines for the solar plant would be procured in place of steam turbines for fossil-fuel plants. Thus, the demand would only follow the projected demand for new capacity in the most economical mode of operation (i.e., peaking plants or intermediate load plants), and therefore, the required capacity has probably already been accounted for by current manufacturers. This hypothesis is valid as long as the solar plant penetration does not require a significant increase in backup capacity.

The production capacity and capability for sodium has been discussed here. At the present time, the capacity is more than adequate and the capability probably exceeded the actual production during 1977. The production of sodium in 1977 was 1.6×10^8 Kg (177,000 T), but capacity was 1.72×10^8 Kg (190,500 T). As the demand for sodium decreases in the area of the production of anti-knock compounds (tetraethyl lead, etc.), the need for sodium in the central receiver system might be expected to rise in such a way as to match production capability, depending upon the economical viability of the concept and the timing for its introduction.

Although virtually every sodium component, except the receiver, has been built on a large scale both in the U.S. and worldwide, these components are not being produced in large quantities at the present time. Large quantities in the sense of mass production are, however, not required. The sodium-component manufacturing requirements would be similar to those for steam turbines and generators. Assuming, for example, that the annual growth rate in the demand for electrical energy in the U.S. is 5.5% and that approximately 25% of that new capacity is in the intermediate load demand category, one finds that on the average about 15-MWe per year would be required between 1985 and 1995.* If all of this demand were optimistically met by solar central receivers of the 300-MWe size, a total of 50 plants a year would have to be installed. In terms of U.S. heavy machining manufacturing capability, this market does not represent a large number of components, although the components are of large size. The Energy Systems Group has already made preparations, for example, to produce 10 steam generators each in the 100-MWt size category for the Clinch River Breeder Reactor. Within the

---

*1975 total capacity is taken to be 500 MWe

TABLE 9-21
SODIUM COMPONENT RELIABILITY ASSESSMENT

Component	Operating (h/Yr)	Failures/h (λ)	Failure Rate/Yr (λ')	MTTR (h)	Outage/Yr Unavailability (h)
Receiver	3,750	49×10^{-6}	1.8×10^{-1}	20	3.6
24 - Receiver Valves	3,750	240×10^{-6}	0.9	10	10
Surge Tank	3,750	Negligible			
Drag Valve	3,750	125×10^{-6}	0.47	20	10
3 - Large Valves	3,750	375×10^{-6}	1.4	20	28
Pipe	3,750	Negligible			
Tanks	8,760	Negligible			
P-1 Pump	3,750	26×10^{-6}	9.75×10^{-2}	100	9.7
P-2 Pump	4,680	46×10^{-6}	0.21	100	21
3 - Large Valves	4,680	375×10^{-6}	1.75	20	35
Evaporator	4,680	1.7×10^{-6}	0.008	200	1.6
Superheater	4,680	0.5×10^{-6}	0.002	200	0.4
Reheater	4,680	0.6×10^{-6}	0.003	200	0.6

TABLE 9-22
TOTAL SYSTEM AVAILABILITY RESULTS (%)

	Forced Outage	Planned Outage
Collector	0.01	
Receiver	2.2	0.6*
Thermal Storage	0.6	
Master Control	0.05	
EPG	2.46	4.5
Total Unavailability	5.32 +	5.1 = 10.42
Total Availability = 89.6		

*The amount which may not coincide with the 4.5% of the EPG outage

time frame postulated for economic viability for solar central receivers, it is anticipated that the production requirements for sodium components could readily be met.

9.4 RELIABILITY

The reliability assessment of the sodium system is given in Table 9-21. The summary for the overall system is given in Table 9-22.

The unavailability values for the electric power generation equipment (EPG), the collector, and the master control systems were taken from Reference 9-6.

The values for the receiver and the thermal storage system were calculated using standard methodology. Mean time to repair (MTTR) was estimated from experience with similar equipment and assumes that spares are available. For the MTTR time estimates, credit was taken for the fact that there are ~12 h per day for repair at night. No credit was taken for the independently operated sodium loops and, therefore, the unavailabilities of the components are not strictly in series. The actual energy loss should be less than we calculate.

The receiver and steam generator failure rate estimates were based on the observation that tube failures occur primarily in the welds. The failure rate of 4×10^{-10} failures per hour per 2.54 cm (1.0 in.) of weld used in this study is reported in Reference 9-7.

The value of the failure rate used for the receiver control valves is based on experience with valves of a similar type used in the Sodium Pump Test Facility (SPTF) of the Energy Technology Engineering Center (ETEC).[9-8] These values use a free convectively cooled sodium freeze seal blanketed with argon gas. The seal is a rotating seal which has an extremely high success ratio. There is no flow leak-tightness requirements on the valve. The valve body is a cylindrical extension of the pipe, which minimizes valve pipe stress distortions. It is for these reasons, combined with excellent experience with this valve type, that the failure rate used for this valve is lower than that used for the large sodium valves.

Large sodium valve failure rates were taken from Reference 9-9.

The pump failure rate data were taken from Reference 9-10, and take into account the fact that the advanced central receiver pumps have bearings which will be pressurized before the pump is started.

Our experience shows that multipass welds made to code welding requirements do not leak. Therefore, the failure rate of the tanks and piping system is considered to be negligible relative to the total of the components.

The plant reliability assessment is consistent with our experience with sodium plants of similar complexity and size (i.e., the sodium reactor experiment,[9-11] and the Hallam Nuclear Power Facility[9-12]).

10.0 PRELIMINARY SAFETY ANALYSIS

The specific safety requirements for the Advanced Central Receiver Power System - Sodium-Cooled Concept, include the conventional occupational safety requirements and requirements peculiar to a sodium-cooled solar power plant. The conventional safety requirements include the applicable Occupational Safety and Health Administration (OSHA) regulations of the Federal Government (Title 29 Chapter XVII, Part 1910 for operations and Part 1926 for construction) and/or the OSHA regulations for the state in which the site is located. Other specific requirements will include the American National Standards Institute (ANSI) requirements (ANSI C2-1973 National Electrical Safety Code); the National Fire Protection Association (NEMA) requirements (NFPA 70-1978 National Electrical Code, National Fire Codes, Vol. 1-15); standards of the National Electrical Manufacturers Association (NEMA); ASME Boiler and Pressure Vessel Code, Sections I, II, V, VIII, Division 1 and IX; Standards of the American Institute of Steel Construction and the American Concrete Institute; applicable liquid metal safety criteria; and the building codes, air pollution and water quality regulations of the local governmental agency. The System Safety Program Requirements Specification for Solar Thermal Power Systems[10-1] and System Safety Design Criteria for the Central Receiver Solar Thermal Power System[10-2] will be used as guidelines.

10.1 PUBLIC SAFETY

The three recognized potential hazards which can impact the areas beyond the site boundary are: (1) brush fires from coincident beams, (2) damage to eye tissue from excessive irradiance, and (3) sodium combustion products aerosols from a leak in the exposed receiver tubes or from a ground level fire. The first two items are controlled by providing a brush-free fenced exclusion area of 1,000 m from the edge of the field.[10-3]

The third concern, sodium combustion products dispersed to the site boundary from leaks in the receiver or from pool fires at ground level, has been examined in detail both analytically[10-4] and experimentally.[10-5]

TABLE 10-1

SODIUM RELEASE WHICH PRODUCES LIMITING AEROSOL CONCENTRATIONS AT PLANT BOUNDARY OF 1600 m (1 mile)

Type of Release	Amount of Release [kg/s (lb/s)]	Pasquill Weather Type	Reference Wind Speed [m/s (mi/h)]	Aerosol Particle Size [(μm) AED]	Aerosol Concentration Limit (mg/m^3)
Jet from 174 in (570 ft^2) Elevation	0.5 (1)	B*	1 (2)	20	2†
Pool on Ground	15 m^2 (150 ft^2)	F*	2 (4-1/2)	1	2
Jet from 174 m (570 ft) Elevation	20 (40)	B*	1 (2)	20	80§
Pool on Ground	160 m^2 (1600 ft^2)	F*	2 (4-1/2)	1	80

*Weather conditions which maximize the delivery of aerosols downwind
†Long-term limit (continuous exposure)
§Short-term limit (1/2 h to 1 h)

TABLE 10-2

CALCULATED MAXIMUM SODIUM AEROSOL CONCENTRATIONS

Type of Release	Downwind Distance [m (miles)]	Concentration (mg/m^3)	Pasquill Weather Type	Reference Wind Speed [m/s (mi/h)]	Aerosol Particle Size [(μm) AED]
Jet from 174 m (570 ft) Elevation	700 (0.4)	3.5	A*	1 (2)	20
Pool on Ground	<100 (0.06)	<50.0	F*	2 (4.5)	1

NOTE: Maximum concentrations inside plant boundary for releases which produced limiting concentrations at assumed plant boundary of 1600 m (1 mile)

*Weather condition which maximizes the delivery of aerosols downwind

The largest leak expected to occur in the receiver is postulated to be caused by a rifle bullet piercing one of the receiver tubes. The resulting 1 cm (3/8 in.) hole releases a jet of sodium which catches fire and forms a plume of sodium, and sodium combustion products. The plume develops into a white cloud of Na, Na_2O_2, $N_2(OH)$, and Na_2CO_3 aerosols and is carried toward the site boundary by the wind. A computer code,[10-6] based on test data, has been developed which calculates the sodium and sodium combustion product distribution as a function of time and distance from the sodium release. A summary of the significant results of these calculations is given in Tables 10-1 and 10-2.

Table 10-1 gives the maximum allowed release rates to produce acceptable long-term and emergency aerosol concentrations at the site boundary assuming meteorological conditions which maximize the aerosol concentrations downwind. The concentration limit for long-term exposure is 2 mg/m^3. The limit for emergency release is 80 mg/m^3.

The estimated release rate from the postulated accident at the top of the tower is ~1 kg/s (2 lb/s) or factor of 20 below the limiting value.

The exposed surface area of a burning sodium pool at ground level which will give the emergency limit at the side boundary is 160 m^2 (1600 ft^2). The free surface area for combustion in the catch pans (described under Plant Protection) will be limited to less than 1/20 this value by compartmentalization and by the use of vented covers on the pans.

It may be concluded from these results that the combustion of sodium at the installation will not represent a hazard to the public. In addition, it is planned to limit the burning rate or the total amount of sodium combustion by the following means: (1) the tower will be monitored by closed-loop television with a fixed image reference. At the initiation of a plume, which will change the image, an alarm signal in the control room will alert the operator and shutdown procedures will be implemented thus limiting the amount of sodium release. An alternate plan is to use acoustic emission techniques to detect leaks.

Table 10-2 gives the maximum concentration and the location where it occurs. It is seen that the maximum occurs well within the site boundary. The maximum surface concentration corresponding to the postulated leak rate continuing for 25 min is expected to be ~40 mg/m^2). Preliminary studies indicate that this concentration is not deleterious to the mirror surfaces.

10.2 PERSONNEL SAFETY

Personnel safety is adequately covered by the Occupational Safety and Health Administration (OSHA). For design purposes, the provisions of Title 8, California Administrative Code, will also be invoked (assuming a California site). In case of conflict between the two, the Federal Standards will govern.

Particular emphasis will be placed on preventing coincident multiple beam irradiance anywhere but at the receiver. In addition, personnel will wear flame-proof clothing, appropriate hard hats, PVC gloves, and eye protection when they are outside of the protection of the buildings or when they are working on open sodium systems.

Plant features which enhance plant safety aspects are:

1) Location of the elevator inside of the tower.

2) Railed catwalks at the elevations of the horizontal pipe runs and caged ladders for the vertical runs of the riser and downcomer will be provided.

3) Exit doors at the catwalk levels every 30 m (100 ft) will lead to a protected exterior ladder. (Personnel will be excluded from the upper one-half of the tower during operation.)

4) At least two exits will be provided at the tower base.

5) Oxygen meters will be installed in all pits subject to potential argon flooding.

6) Sodium-sensitive aerosol detectors will be located in enclosed spaces.

7) Emergency safety showers and eyewash fountains will be placed at strategic locations.

8) Approved fire suppressant extinguishers (Nax) will be placed throughout the facility.

9) Provision will be made for the programmed draining of systems or components which are suspected of leaking.

10) Sodium catch pans will be provided under major components to confine the consequences of sodium leaks to a local controlled area until the component can be drained. The steam generator catch pans will be provided with a sump and pump to assure the catch pan remains dry.

11) Nitrogen gas will be supplied for the purpose of flooding the catch pans if Na combustion is initiated.

10.3 PLANT PROTECTION FEATURES

Protecting the plant integrity is considered to be an important first step in protecting the public and operating personnel. The identified events which can potentially damage the plant are given in Table 10-3 together with plant features and actions planned to prevent or mitigate the damage. There are two independently operating sodium loops, the Energy Absorption Loop (EAL), consisting of the cold tank, the receiver pump (P-1), the receiver and the drag valve, and the Power Generation Loop (PGL), consisting of the hot tank, the steam generator pump (P-2), and the steam generator. The plant protective features respond in accordance with which loop is affected.

10.4 CONCLUSION

The plant safety features incorporated in the design provide a wide margin of safety for the public, personnel, and the plant.

TABLE 10-3
PLANT PROTECTION — SUMMARY FEATURES

Initiating Event	Plant Protective Features to Limit Consequences	Action Taken
Loss of Load	Alarm and P-2 pump speed reduction to condenser power capacity	Steam dumped to condenser.
Turbine and Steam Equipment Failure	Turbine trip circuits	Turbine trip PGL* shutdown.
Steam Generator to Sodium Leak	Rupture disk in steam generator shell; reaction products tank; isolation valves; antisyphon on T-1 inlet	Turbine trip and PGL tripped and secured.
Faulting in PGL	PGL trip circuits	Turbine and PGL trip.
Sodium-to-Air Leak in PGL Components	Sodium aerosol detectors; catch pans; N$_2$ supply for catch pans	PGL shutdown N$_2$ flood affected pan.
Leak in T-2 Tank	Sodium aerosol detectors; catch pans; pump connection to the T-1 tank	Plant shutdown.
Leak in T-1 tank	Sodium aerosol detector; catch pans; pump connection to T-2 tank	Plant shutdown.
Loss of Flow in the EAL	Check valve; syphon break in riser and downcomer lines; emergency slew circuits	Emergency slew mirror field. Shut down and secure the EAL loop.
Sodium Leak in Riser or Downcomer Lines	Sodium aerosol detectors; catch pans with N$_2$; drain lines	Defocus mirror field. Shut down EAL. Drain the affected lines.
Sodium Leak in the Receiver Headers	Sodium aerosol detectors; catch pans with N$_2$; receiver drain line; steel cover on top of tower	Defocus mirror field. Shut down EAL. Drain receiver.
Sodium Leak in Receiver	Television surveillance loop (or acoustic emission monitor); receiver drain line; top 30 m (100 ft) of tower insulated and steel capped; receiver support structure insulated	Slew mirror filed. Shut down EAL loop. Drain receiver.
Focusing Error at Tower	Temperature sensors on structures; receiver structure insulated	Slew mirror field.

*Power generation loop - hot tank, P-2 pump, and steam generator
†Energy absorption loop - cold tank, P-1 pump, and receiver assembly.

REFERENCES

2-1. Advanced Central Receiver Program Requirements, Sandia Laboratories, A-10270, March 16, 1978

5-1. D. Kunii and O. Levenspiel, Fluidization Engineering, Wiley, 1969, Pages 67, 211

5-2. J. Perry, Chemical Engineer's Handbook, 4th Edition, McGraw-Hill, 1963, Page 5:49

5-3. W. Kays and A. London, Compact Heat Exchangers, National Press, 1955, Page 123

5-4. G. Lof and R. Hawley, "Unsteady-State Heat Transfer Between Air and Loose Solids," Industrial and Engineering Chemistry, Vol. 40, No. 6, June 1948, Pages 1067-1070

5-5. E. Alanis, L. Saravia, and L. Rouetta, "Measurement of Rock Pile Heat Transfer Coefficients," Solar Energy, Peragon Press, Vol. 40, 1977, Pages 571-572

5-6. W. McAdams, Heat Transmission, McGraw-Hill, 3rd Edition, 1954, Page 295

5-7. E. Mouradian, Personal Notes on Thermal Properties of Gases

5-8. 77AT-9195, "Revised Management Plan for the Program entitled 'Conceptual Design of Advanced Central Receiver Power Systems,'" Contract EG-77-C-03-1483, October 14, 1977

9-1. ERDA 77-47/4, "Solar Program Assessment: Environmental Factors," ERDA, Division of Solar Energy, March 1977

9-2. LBL-6329 (UC-62), "The Central Receiver Power Plant: An Environmental, Ecological, and Socioeconomic Analysis," M. Davidson and D. Grether, Lawrence Berkeley Laboratory, June 1977

9-3. DOE/EDD-0004, "Environmental Development Plan (EDP), Solar Thermal Power Systems, 1977," DOE, March 1978

9-4. COO/4339-1, "Solar Energy Conversion: An Analysis of Impacts on Desert Econosystems," D. T. Patten, Arizona State University, September 1977

9-5. EPA 600/7-77-086, "Preliminary Environmental Assessment of Solar Energy Systems," D. R. Sears, et al, Lockheed Missiles and Space Company, August 1977

9-6. SAN 1107-76-8, MOC G 6776, "Central Receiver Solar Thermal Power System, Phase I, CDRL, Item 2, Pilot Plant Preliminary Design Report, Volume II, System Description and System Analysis," McDonnell Douglas Astronautics Company, October 1977, pp 4-146, Table 4-15

9-7. Newburn, F. A., Editor, "Commercial LMFBR Steam Generator Design Comparison," AI Technical Document N254TI30001, September 30, 1977

9-8. Personal Communication, Bruce Pilling, Manager, Energy Collection Loop (ECL) - Energy Technology Engineering Center

9-9. AI Internal Letter dated February 25, 1976, W. Vaughn to E. Baumeister, "LMFBR-PLBR Reactor Outlet Temperature Effects on Plant Reliability and Availability"

9-10. L. D. Felten, "Reliability of Large Sodium Pumps," AI Document N147TI240-003 dated November 6, 1975

9-11. L. E. Glasgow, "Assessment of Sodium Reactor Experiment Reliability," AI Document TDR-12224 dated October 31, 1966

9-12. S. Berger, et al, "Hallam Nuclear Power Facility Reactor Operations Analysis Program Semiannual Progress Report 3, September 1, 1963-February 29, 1964, AI Document NAA-SR-9799 issued September 15, 1964, Page 4

10-1. System Safety Program Requirements Specification for Solar Thermal Power System, MCR-77-162, Martin Marietta Corporation, April 1977

10-2. System Safety Design Criteria for the Central Receiver Solar Thermal Power System, MCR-77-161, Martin Marietta Corporation, April 1977

10-3. "Central Receiver Solar Thermal Power System, Phase 1, CDRL Item 2, Pilot Plant Preliminary Design Report, Volume II, System Description and System Analysis, SAN 1108-76-8, MDC G 6776, McDonnell Douglas Astronautics Company, October 1977, pp 4-164, 4-192

10-4. J. M. Otter, "Scoping Analysis for Sodium Release Experiments," AI Document N001TI130086, To be issued

10-5. R. P. Johnson, "Summary of Characterization of Released Airborne Particle Tests Conducted at INEL, AI Document N707TI30053, August 7, 1978

10-6. J. M. Otter, D. K. Chang, "COMRADEX Code Development," AI Document N707TI130047, September 26, 1977